UNIVERSIDAD COMPLUTENSE DE MADRID
FACULTAD DE CIENCIAS QUÍMICAS
Departamento de Química-Física I

TESIS DOCTORAL

Nucleación de sólidos cristalinos por simulación

Nucleation of crystalline solids by simulation

MEMORIA PARA OPTAR AL GRADO DE DOCTOR

PRESENTADA POR

Jorge Reñé Espinosa

Directores

Eduardo Sanz García
Carlos Vega de las Heras

Madrid 2019

Universidad Complutense de Madrid
Facultad de Ciencias Químicas
Departamento de Química Física I

Nucleación de sólidos cristalinos por simulación

Memoria para optar
al grado de Doctor en Ciencias Químicas
realizada por

Jorge Reñé Espinosa

Directores:
Prof. Eduardo Sanz García
Prof. Carlos Vega de las Heras

Dpto. Química-Física I

Madrid, 2017

A mi abuelo Mariano.

The work in this thesis is based on the following publications:

Results: Chapter 1
Homogeneous ice nucleation at moderate supercooling from molecular simulation.
E. Sanz, C. Vega, J. R. Espinosa, R. Caballero-Bernal, J. L. F. Abascal and C. Valeriani.
J. Am. Chem. Soc., **135**, 15008, (2013).
Results: Chapter 2
Homogeneous ice nucleation evaluated for several water models.
J. R. Espinosa, E. Sanz, C. Valeriani and C. Vega
J. Chem. Phys., **141**, 18C529, (2014).
Results: Chapter 3
The mold integration method for the calculation of the crystal-fluid interfacial free energy from simulations.
J. R. Espinosa, C. Vega and E. Sanz
J. Chem. Phys., **141**, 044715, (2014).
Results: Chapter 4
The crystal-fluid interfacial free energy and nucleation rate of NaCl from different simulation methods.
Jorge R. Espinosa, Carlos Vega, Chantal Valeriani, and Eduardo Sanz.
J. Chem. Phys., **142**, 194709, (2015).
Results: Chapter 5
Seeding approach to crystal nucleation.
Jorge R. Espinosa, Carlos Vega, Chantal Valeriani, Eduardo Sanz.
J. Chem. Phys., **144**, 034501, (2016).
Results: Chapter 6
Ice-Water Interfacial Free Energy for the TIP4P, TIP4P/2005, TIP4P/Ice and mW Models as Obtained from the Mold Integration Technique.
Jorge R. Espinosa, Carlos Vega and Eduardo Sanz.
J. Phys. Chem. C, **120**, 8068, (2016).
Results: Chapter 7
On the time required to freeze water.
J. R. Espinosa, C.Navarro, E.Sanz, C.Valeriani and C.Vega.
J. Chem. Phys., **145**, 211922, (2016).
Results: Chapter 8
Interfacial free energy as the key to the pressure-induced deceleration of ice nucleation.
Jorge R. Espinosa, Alberto Zaragoza, Pablo Rosales-Pelaez, Caridad Navarro, Chantal Valeriani, Carlos Vega and Eduardo Sanz.
Phys. Rev. Lett., **145**, 211922, (2016).
Results: Chapter 9
Lattice Mold technique for the calculation of crystal nucleation rates.

Jorge R. Espinosa, Pablo Sampedro, Chantal Valeriani, Carlos Vega and Eduardo Sanz. *Faraday discussions* **195**, 569-582 (2017).

Results: Chapter 10

A simulation study of homogeneous ice nucleation in supercooled salty water.
Guiomar D. Soria, Jorge R. Espinosa, Jorge Ramirez, Chantal Valeriani, Carlos Vega and Eduardo Sanz.
under review in J. Chem. Phys. (2017).

Results: Chapter 11

On the Role of Salt, Pressure and Water Activity on Homogeneous Ice Nucleation.
Jorge R. Espinosa, Guiomar D. Soria, Jorge Ramirez, Chantal Valeriani, Carlos Vega and Eduardo Sanz.
J. Phys. Chem. Lett. **8**, 4486-4491, (2017).

Other publications not in the thesis:

On fluid-solid direct coexistence simulations: The pseudo-hard sphere model.
J. R. Espinosa and E. Sanz and C. Valeriani and C. Vega.
J. Chem. Phys., **139**, 144502, (2013).

Competition between ice Ih and Ic in homogeneous water freezing.
Alberto Zaragoza, Maria M. Conde, Jorge R. Espinosa, Chantal Valeriani, Carlos Vega and Eduardo Sanz.
J. Chem. Phys., **143**, 134504 (2015).

On the calculation of solubilities via direct coexistence simulations: Investigation of NaCl aqueous solutions and Lennard-Jones binary mixtures.
J. R. Espinosa, J. M. Young, H. Jiang, D. Gupta, C. Vega, E. Sanz, P. G. Debenedetti and A. Z. Panagiotopoulos.
J. Chem. Phys. **145**, 154111, (2016).

A potential model for sodium chloride solutions based on the TIP4P/2005 water model.
A. L. Benavides, M. A. Portillo, V. C. Chamorro, J. R. Espinosa, J. L. F. Abascal, and C. Vega.
J. Chem. Phys. **147**, 104501, (2017).

Índice general

Capítulo 1
Resumen

1.1. Introducción

Cuando un líquido se enfría por debajo de su temperatura de fusión, este debería congelarse. Generalmente la presencia de impurezas o de las paredes que lo contienen pueden ayudar a la formación de la fase sólida. Sin embargo, incluso en ausencia de impurezas, se pueden formar pequeños núcleos de la nueva fase en el seno del líquido metaestable. Este mecanismo que origina la formación de una fase sólida se denomina nucleación homogénea[1,2]. La nucleación homogénea es un proceso activado ya que para que se forme un núcleo crítico, el sistema debe superar una barrera de energía libre. Ese es el motivo por el cual muchos líquidos puros pueden mantenerse subenfriados durante mucho tiempo, hasta que aparece una fluctuación de orden local que forma una región de la fase estable más grande que un cierto tamaño crítico que provoca que todo el sistema cristalice.

Un sistema de gran interés es el agua, dado que es una de las más comunes e importantes moléculas para la vida. Comprender la formación de hielo a partir de agua subenfriada es muy relevante en ciencias del clima[3–5] (a menudo en las nubes se encuentran pequeñas gotas de agua subenfriada que si se transforman en hielo pueden reflejar la radiación UV disminuyendo el calentamiento global), microbiología[6], en la industria alimenticia[7,8], ciencia de materiales[9] y geología[10]. También poder controlar la formación de hielo tendría un gran impacto en criopreservación y en ciencias del alimento[11,12]. Sin embargo, esto todavía es un gran reto.

La simulación puede ser una herramienta útil para estudiar la nucleación ya que los núcleos que se forman son muy pequeños ($\sim nm$), tienen un periódo de vida muy breve ($\sim ns$) y no se puede predecir donde van a aparecer. Todo esto provoca que experimentalmente sea muy complicado estudiarla y comprenderla en profundidad. En ese sentido, la simulación molecular es muy útil para investigar este fenómeno[13,14] ya que puede proporcionar una visión microscópica del proceso. Sin embargo, el principal problema de estudiar la nucleación por simulación es el largo tiempo que puede llevar

observar la formación de un núcleo de manera espontánea en los volumenes accesibles. Por este motivo, es necesario recurrir a técnicas especiales para observarla. Esto es por lo que durante esta tesis doctoral se ha dedicado un gran esfuerzo a desarrollar y validar técnicas nuevas y más sencillas que las existentes para estudiar la nucleación por simulación. Para el desarrollo y la validación de las nuevas técnicas se han estudiado sistemas sencillos que habían sido caracterizados anteriormente con técnicas alternativas. Una vez alcanzado este objetivo, emplearemos las nuevas técnicas para entender mejor la física de la nucleación de hielo en diferentes condiciones como a presión ambiente, a altas presiones y en disoluciones acuosas.

1.2. Objetivos

Los objetivos de esta tesis doctoral son los siguientes:

1. Desarrollar nuevas técnicas alternativas para medir tasas de nucleación líquido-sólido, J, y energías interfaciales, γ, basadas en ideas más simples y eficientes que las técnicas propuestas en la literatura. Demostrar que estas técnicas son capaces de proporcionar resultados fiables tanto para J como γ en un amplio intervalo de metaestabilidad.

2. Implementar estos métodos para caracterizar en detalle la nucleación de hielo en agua pura a presión ambiente. Para ello, se utilizarán varios modelos de agua y se evaluarán los factores determinantes de este fenómeno, como son J y γ, y se compararán con las medidas experimentales de estas magnitudes.

3. Por último, extender estas técnicas al estudio de sistemas más complejos. En primer lugar, investigando la nucleación de hielo a altas presiones y comparando nuestras predicciones con datos experimentales[15]. Y en segundo lugar, midiendo tasas de nucleación de hielo en disoluciones acuosas de electrolitos. El objetivo de este punto es también entender el efecto que se produce al aplicar presión y/o añadir sal al agua y comprobar si se puede obtener una expresión general que relacione ambos efectos[16].

1.3. Resultados

En base a los objetivos mencionados previamente, ahora se van a comentar los resultados principales que se obtuvieron punto por punto.

A. **Nuevas técnicas para el estudio de la nucleación líquido-cristal.**

Inicialmente se desarrolló el Seeding[17–19], una técnica que por primera vez permitió calcular tasas de nucleación de hielo y energías interfaciales hielo-fluido para subenfriamientos moderados. Para demostrar que el Seeding, a pesar de ser una técnica aproximada, podía proporcionar resultados razonables, calculamos J y γ para cuatro sistemas arquetipo bien conocidos en un amplio rango de condiciones. Obtuvimos en todos los casos buena concordancia para ambas magnitudes con otros cálculos independientes realizados con técnicas más costosas. También se desarrolló la técnica que denominaremos Mold Integration[20], la cual sirve para calcular energías libres interfaciales en condiciones de coexistencia. Para validar esta técnica, medimos γ para diferentes sistemas (incluidos los previamente comentados) y planos cristalinos obteniendo en todos los casos resultados excelentes. Por último, siguiendo este mismo enfoque, desarrollamos otra nueva metodología llamada Lattice Mold[21], para calcular tasas de nucleación que no depende de parametros de orden ni de Teoría Clásica de Nucleación como es el caso del Seeding. Esta técnica también fue validada obteniendo resultados satisfactorios.

B. **Entendiendo la nucleación de hielo**

En este bloque, evaluamos tasas de nucleación de hielo mediante Seeding para varios modelos de agua[19,22]. Observamos que aunque algunos modelos describían mejor que otros las propiedades experimentales del agua, todos ellos predecían tendencias similares. Se propuso un ajuste basado en la Teoría Clásica de Nucleación[23,24] para los datos calculados por Seeding, que permitió estimar tasas de nucleación desde condiciones de coexistencia hasta subenfriamientos muy elevados, basándose en una dependencia lineal negativa de γ con el subenfriamiento observada en todos los modelos. Se calculó γ a coexistencia para el hielo cúbico y el hielo hexagonal con el fluido, observándose que eran muy similares y sugiriendo por tanto que la fase responsable de la nucleación de hielo a presión normal debía ser una mezcla de ambas fases intercaladas. Finalmente se propuso una hipótesis para explicar unos controvertidos resultados de medidas experimentales de J recientemente publicados[25] que discrepaban de todas las medidas anteriores.

C. **Agua bajo presión vs. agua salada**

Combinando la experiencia ganada al aplicar Seeding y Mold Integration en diferentes sistemas, y sobre todo en agua, se decidió medir tasas de nucleación a altas presiones. Las medidas experimentales[15], demuestran que la nucleación de hielo se ve dificultada al aplicar presión al agua, pero la razón por la cual esto sucedía era desconocida hasta este trabajo. Mediante nuestras simulaciones descubrimos que el factor principal que produce este deceleración en J es el incremento de γ con la presión. Esto también ocurre cuando añadimos sal al agua, J disminuye y por tanto la nucleación se decelera. Calculamos tasas de nucleación para una disolución

de NaCl observando un comportamiento cualitativamante similar al del agua bajo presión. Finalmente evaluamos si este efecto se podía relacionar mediante la variación que sufre la actividad del agua en presencia de sal o presión, como propone una regla ampliamente utilizada en la literatura[16]. Nuestros resultados muestran que no es posible relacionar los efectos de la presión y la sal en la nucleación de hielo únicamente mediante esta magnitud.

1.4. Conclusiones

Nuestro principal objetivo de esta tesis ha sido estudiar la nucleación homogénea de hielo. Para ese propósito se han desarrollado diferentes técnicas basadas en ideas simples pero eficientes para medir tanto tasas de nucleación como energías interfaciales, que son los parámetros más importantes para describir el fenómeno de la nucleación. Una vez que validamos estas técnicas para "fluidos simples", las aplicamos para el complicado y anómalo caso del agua, donde estudiamos diferentes modelos de potencial, para los cuales evaluamos J, γ y otras muchas propiedades relevantes para caracterizar la nucleación. Debido a la buena concordancia que obtuvimos entre las predicciones de algunos modelos y los resultados experimentales para agua pura a presión ambiente, decidimos ir más allá investigando la nucleación a altas presiones y en disolución. Observamos que aunque cualitativamente en ambos casos la nucleación se dificulta principalmente debido a un incremento de la energía interfacial, no es posible obtener una expresión general que relacione cuantitativamente el efecto de la presión y las sales en agua. Por último, como conclusión final de este trabajo, se puede afirmar que la Teoría Clásica de Nucleación es una teoría que ha permitido calcular tasas de nucleación en combinación con el Seeding para una gran variedad de sistemas en buena concordancia con medidas no sujetas a ninguna teoría, lo cual sugiere la validez y la generalidad que posee esta teoría al describir la nucleación.

Bibliografía

1. Debenedetti, P. G., *Metastable liquids: Concepts and Principles* (Princeton University Press, 1996).

2. Kashchiev, D., *Nucleation: Basic Theory with Applications* (Butterworth-Heinemann, Oxford, 2000).

3. Cantrell, W. & Heymsfield, A., Production of ice in tropospheric clouds. *Bull. Amer. Meteor. Soc.* **86**, 795 (2005).

4. Baker, M. B., Cloud microphysics and climate. *Science* **276**, 1072–1078 (1997).

5. DeMott, P. J., Prenni, A. J., Liu, X., Kreidenweis, S. M., Petters, M. D., Twohy, C. H., Richardson, M. S., Eidhammer, T. & Rogers, D. C., Predicting global atmospheric ice nuclei distributions and their impacts on climate. *Proc. Natl. Acad. Sci.* **107**, 11217–11222 (2010).

6. Hirano, S. S. & Upper, C. D., Bacteria in the leaf ecosystem with emphasis on pseudomonas syringae - a pathogen, ice nucleus, and epiphyte. *Microbiol. Molec. Biol. Rev.* **64**, 624 (2000).

7. Maki, L. R., Galyan, E. L., M.M., C. & Caldwell, D. R., Ice nucleation induced by pseudomonas-syringae. *Appl. Microbiol.* **28**, 456–459 (1974).

8. Li, J. K. & Lee, T. C., Bacterial ice nucleation and its potential application in the food-industry. *Trends in Food Sci. & Tech.* **6**, 259–265 (1995).

9. Michaelides, A. & Morgenstern, K., Ice nanoclusters at hydrophobic metal surfaces. *Nature Materials* **6**, 597–601 (2007).

10. Gerrard, A. G., *Rocks and Landforms* (Springer Netherlands, 1988).

11. Morris, G. J. & Acton, E., Controlled ice nucleation in cryopreservation–a review. *Cryobiology* **66**, 85 (2013).

12. Studer, D., High-pressure freezing system (2001), US Patent 6,269,649.

13. ten Wolde, P. R. & Frenkel., D. .

14. Auer, S. & Frenkel, D., Prediction of absolute crystal-nucleation rate in hard-sphere colloids. *Nature* **409**, 1020 (2001).

15. Kanno, H., Speedy, R. J. & Angell, C. A., Supercooling of water to -92^{o}c under pressure. *Science* **189**, 880–881 (1975).

16. Koop, T., Luo, B., Tsias, A. & Peter, T., Water activity as the determinant for homogeneous ice nucleation in aqueous solutions. *Nature* **406**, 611–614 (2000).

17. Bai, X.-M. & Li, M., Calculation of solid-liquid interfacial free energy: A classical nucleation theory based approach. *J. Chem. Phys.* **124**, 124707 (2006).

18. Knott, B. C., Molinero, V., Doherty, M. F. & Peters, B., Homogeneous nucleation of methane hydrates: Unrealistic under realistic conditions. *J. Am. Chem. Soc.* **134**, 19544–19547 (2012).

19. Sanz, E., Vega, C., Espinosa, J. R., Caballero-Bernal, R., Abascal, J. L. F. & Valeriani, C., Homogeneous ice nucleation at moderate supercooling from molecular simulation. *Journal of the American Chemical Society* **135**, 15008–15017 (2013).

20. Espinosa, J. R., Vega, C. & Sanz, E., The mold integration method for the calculation of the crystal-fluid interfacial free energy from simulations. *J Chem. Phys.* **141**, 134709 (2014).

21. Espinosa, J. R., Sampedro, P., Valeriani, C., C., V. & E., S., Lattice mold technique for the calculation of crystal nucleation rates. *Faraday Discussions* **195**, 569 (2016).

22. Espinosa, J. R., Sanz, E., Valeriani, C. & Vega, C., Homogeneous ice nucleation evaluated for several water models. *J. Chem. Phys.* **141**, 18C529 (2014).

23. Becker, R. & Doring, W., Kinetische behandlung der keimbildung in ubersattigten dampfen. *Ann. Phys.* **416**, 719–752 (1935).

24. Volmer, M. & Weber, A., Keimbildung in ubersattigten gebilden. *Z. Phys. Chem.* **119**, 277 (1926).

25. Laksmono, H., McQueen, T. A., Sellberg, J. A., Loh, N. D., Huang, C., Schlesinger, D., Sierra, R. G., Hampton, C. Y., Nordlund, D., Beye, M., Martin, A. V., Barty, A., Seibert, M. M., Messerschmidt, M., Williams, G. J., Boutet, S., Amann-Winkel, K., Loerting, T., Pettersson, L. G. M., Bogan, M. J. & Nilsson, A., Anomalous behavior

of the homogeneous ice nucleation rate in no-man's land. *The Journal of Physical Chemistry Letters* **6**, 2826–2832 (2015).

Capítulo 2
Summary

2.1. Introduction

When a liquid is cooled below its freezing point it is supposed to freeze. Usually, the presence of impurities or the solid boundaries of the liquid provide preferential sites for the formation of the solid phase. However, even in the absence of impurities, small nuclei of the new phase may be formed within the bulk metastable liquid. This mechanism of formation of the solid phase is called homogeneous nucleation[1,2]. Homogeneous nucleation is an activated process since the formation of a critical nucleus requires the overcoming of a free energy barrier. That is the reason why many purified liquids can be maintained in a metastable state for a long time until a spatially and temporally localised density fluctuation of the new stable phase is larger than a *critical size* an the whole system transforms into the new phase.

A system of particular interest is water given that is one of the most common and important molecules for life. Understanding the freezing of water from the supercooled liquid is of great interest in climate science[3–5] (often small droplets of supercooled water in the clouds can crystallize into ice and reflect the UV radiation reducing the global warming), microbiology[6], the food industry[7,8], materials science[9] and geology[10]. Also, controlling the freezing of water would have an impact in cryopreservation and food science[11,12]. However this still constitutes a great challenge.

Computer simulations can be a useful tool for studying nucleation given that the nuclei are rather small ($\sim nm$), short-lived ($\sim ns$) and it is unpredictible to know where they will appear. All these facts provoke that is very challenging to study it experimentally. In that sense computer simulations are a valuable tool to investigate nucleation[13,14] since they provide a microscopic description of the process. The main drawback when studying nucleation by simulations is the extremely long lag times needed to observe a nucleus in the accesible volumes. For this reason, is necessary to resort to special techniques to observe it. A big effort has been devoted during this thesis to develop and to validate new and easier techniques to investigate nucleation. For the develo-

ping and validating these new techniques, we have studied simple systems which have been well-characterized in the past by means of other alternative techniques. Once that was accomplished, we employed them to understand the physics behind ice nucleation at different conditions such as ambient pressure, high pressures and from electrolyte solutions.

2.2. Objectives

When we started this predoctoral work the objectives were the following:

1. Develop new alternative techniques to measure crystal nucleation rates, J, and fluid-crystal interfacial free energies γ based on simpler and more efficient approaches than the current available techniques in literature. Demonstrate that our techniques are capable of providing reliable results for J and γ in a wide range of metastabilty

2. Implement these techniques for studying homogeneous ice nucleation at normal pressure. For that purpose, we will employ several water model potentials and we will evaluate the main factors involved in this phenomenon, J and γ, for characterizing the process in detail. A comparison of our results with the experimental measurements will be made.

3. Extend our techniques to study more complex and demanding problems. Firstly, by investigating ice nucleation at high pressures and comparing our predictions with the experimental results[15]. Secondly, computing ice nucleation rates from NaCl aqueous solutions. The aim of this item is also to understand the physics behind the effects of adding pressure and salt in water, and verify if a general expression can relate both effects[16].

2.3. Results

Based on the objectives mentioned before, we will now discuss the main results obtained for each aim.

A. **Novel techniques for studying liquid-to-crystal nucleation.**

Firstly we developed the Seeding technique[17–19], a new method that allowed for the first time to estimate ice nucleation rates and ice-water interfacial free energies at moderate supercooling. To demonstrate that Seeding, despite of being an approximate technique, could provide reliable results, we computed J and γ for

four different archetypal systems in a broad range of conditions. We obtained in all cases good agreement for both magnitudes with other independent more expensive calculations. We also present Mold Integration[20], a novel technique for calculating interfacial free energies at coexistence conditions. To validate this technique, we applied it for different systems (including the previous ones) and crystal orientations obtaining excellent results. Finally, following a similar approach to that in which is based Mold Integration, we develop a new methodology, called Lattice Mold[21], for estimating nucleation rates without depending on any local order parameter nor Classical Nucleation Theory as Seeding does. We also validate it getting good agreement with previously reported values.

B. **Understanding ice nucleation**

In this block we evaluated ice nucleation rates for several water models[19,22], via Seeding. Although the performance of some models was more accurate in predicting experimental properties of water than some others, we observed similar trends in all cases. We present a Classical Nucleation Theory[23,24] fit for the data from Seeding, that allows to estimate nucleation rates from the melting line to very deep supercoolings, which is based on a linear negative dependence of γ along supercooling observed in every model. We also estimated γ at coexistence between the fluid and the cubic and hexagonal ices obtaining similar values for both polymorphs, and hence suggesting that the involved phase on ice nucleation at normal pressure might be a stacking disordered mix of hexagonal and cubic ices. Finally, we propose an hypothesis to explain some controversial results of experimental measurements of J recently published[25].

C. **Water under pressure vs. salty water**

By combining the gained experience of applying Seeding and Mold Integration in many systems, and mainly in pure water, we decided to measure ice nucleation rates at high pressures. The experimental measurements[15] showed that ice nucleation is hindered when applying pressure on water, but the physical basis behind that remained still unknown. By means of our simulations we discovered that the main factor that produces the decceleration of the nucleation rate at high pressures was the increase of γ. Also when one adds salt into water, a decceleration of J occurs. We computed ice nucleation rates from a NaCl solution noticing the same qualitative behavior as in compressed water. Finally, we examined the widely-accepted proposal by Koop *et al*[16] that the ice nucleation rate for different pressures and solute concentrations can be mapped through the variation of the water activity when adding salts or applying pressure. Our results suggest that it is not possible to relate both effects only by using this magnitude.

2.4. Conclusions

Our main aim of this thesis was to study homogeneous ice nucleation, for that purpose, we developed different techniques based on simple and efficient ideas to measure nucleation rates and interfacial free energies, two of the most important parameters to quantificate the nucleation phenomenon. Once we validated them for "simple fluids", we applied them for the case of water, where we evaluated for several water models J, γ and many other relevant properties to characterize properly ice nucleation. Due to the nice agreement obtained between the predictions of our models and the experimental results for pure water at normal pressure, we decided to go further by studying ice nucleation at high pressures and from aqueous solutions. Although qualitatively we observed that in both cases nucleation was hindered, mainly due to an increase of the interfacial free energy, we found that is not possible to propose a general expression for relating quantitatively compressed and salty water. Finally, as a main conclusion of this work, we can state that Classical Nucleation Theory have allowed us to evaluate in combination with the Seeding technique nucleation rates for a wide variety a systems in good agreement with independent measurements not based in any theory, which clearly suggests the validity of this theory when describing the nucleation phenomenon.

Bibliography

1. Debenedetti, P. G., *Metastable liquids: Concepts and Principles* (Princeton University Press, 1996).

2. Kashchiev, D., *Nucleation: Basic Theory with Applications* (Butterworth-Heinemann, Oxford, 2000).

3. Cantrell, W. & Heymsfield, A., Production of ice in tropospheric clouds. *Bull. Amer. Meteor. Soc.* **86**, 795 (2005).

4. Baker, M. B., Cloud microphysics and climate. *Science* **276**, 1072–1078 (1997).

5. DeMott, P. J., Prenni, A. J., Liu, X., Kreidenweis, S. M., Petters, M. D., Twohy, C. H., Richardson, M. S., Eidhammer, T. & Rogers, D. C., Predicting global atmospheric ice nuclei distributions and their impacts on climate. *Proc. Natl. Acad. Sci.* **107**, 11217–11222 (2010).

6. Hirano, S. S. & Upper, C. D., Bacteria in the leaf ecosystem with emphasis on pseudomonas syringae - a pathogen, ice nucleus, and epiphyte. *Microbiol. Molec. Biol. Rev.* **64**, 624 (2000).

7. Maki, L. R., Galyan, E. L., M.M., C. & Caldwell, D. R., Ice nucleation induced by pseudomonas-syringae. *Appl. Microbiol.* **28**, 456–459 (1974).

8. Li, J. K. & Lee, T. C., Bacterial ice nucleation and its potential application in the food-industry. *Trends in Food Sci. & Tech.* **6**, 259–265 (1995).

9. Michaelides, A. & Morgenstern, K., Ice nanoclusters at hydrophobic metal surfaces. *Nature Materials* **6**, 597–601 (2007).

10. Gerrard, A. G., *Rocks and Landforms* (Springer Netherlands, 1988).

11. Morris, G. J. & Acton, E., Controlled ice nucleation in cryopreservation–a review. *Cryobiology* **66**, 85 (2013).

12. Studer, D., High-pressure freezing system (2001), US Patent 6,269,649.

13. ten Wolde, P. R. & Frenkel., D. .

14. Auer, S. & Frenkel, D., Prediction of absolute crystal-nucleation rate in hard-sphere colloids. *Nature* **409**, 1020 (2001).

15. Kanno, H., Speedy, R. J. & Angell, C. A., Supercooling of water to -92^{o}c under pressure. *Science* **189**, 880–881 (1975).

16. Koop, T., Luo, B., Tsias, A. & Peter, T., Water activity as the determinant for homogeneous ice nucleation in aqueous solutions. *Nature* **406**, 611–614 (2000).

17. Bai, X.-M. & Li, M., Calculation of solid-liquid interfacial free energy: A classical nucleation theory based approach. *J. Chem. Phys.* **124**, 124707 (2006).

18. Knott, B. C., Molinero, V., Doherty, M. F. & Peters, B., Homogeneous nucleation of methane hydrates: Unrealistic under realistic conditions. *J. Am. Chem. Soc.* **134**, 19544–19547 (2012).

19. Sanz, E., Vega, C., Espinosa, J. R., Caballero-Bernal, R., Abascal, J. L. F. & Valeriani, C., Homogeneous ice nucleation at moderate supercooling from molecular simulation. *Journal of the American Chemical Society* **135**, 15008–15017 (2013).

20. Espinosa, J. R., Vega, C. & Sanz, E., The mold integration method for the calculation of the crystal-fluid interfacial free energy from simulations. *J Chem. Phys.* **141**, 134709 (2014).

21. Espinosa, J. R., Sampedro, P., Valeriani, C., C., V. & E., S., Lattice mold technique for the calculation of crystal nucleation rates. *Faraday Discussions* **195**, 569 (2016).

22. Espinosa, J. R., Sanz, E., Valeriani, C. & Vega, C., Homogeneous ice nucleation evaluated for several water models. *J. Chem. Phys.* **141**, 18C529 (2014).

23. Becker, R. & Doring, W., Kinetische behandlung der keimbildung in ubersattigten dampfen. *Ann. Phys.* **416**, 719–752 (1935).

24. Volmer, M. & Weber, A., Keimbildung in ubersattigten gebilden. *Z. Phys. Chem.* **119**, 277 (1926).

25. Laksmono, H., McQueen, T. A., Sellberg, J. A., Loh, N. D., Huang, C., Schlesinger, D., Sierra, R. G., Hampton, C. Y., Nordlund, D., Beye, M., Martin, A. V., Barty, A., Seibert, M. M., Messerschmidt, M., Williams, G. J., Boutet, S., Amann-Winkel, K., Loerting, T., Pettersson, L. G. M., Bogan, M. J. & Nilsson, A., Anomalous behavior

of the homogeneous ice nucleation rate in no-man's land. *The Journal of Physical Chemistry Letters* **6**, 2826–2832 (2015).

Capítulo 3
Discusión Integradora

El objetivo de este apartado es realizar una breve descripción de las partes y capítulos de la memoria y presentar la conexión entre los artículos utilizados dentro del bloque de resultados además de especificar cuáles han sido las contribuciones más relevantes en los artículos.

Durante este periódo de investigación en el Grupo de Termodinámica Estadística de Fluidos Moleculares fundamentalmente se ha estudiado el fenómeno de la nucleación desde un fluido metaestable hasta un sólido cristalino por medio de simulación molecular. Esto lo hemos estudiado para un buen número de sistemas, desde el fluido más simple que presenta transición sólido-líquido como son las esferas duras, hasta fluidos tan anómalos y complejos como el agua y disoluciones acuosas de electrolitos.

La simulación molecular es una herramienta muy útil para estudiar este fenómeno debido a que los tamaños y tiempos de vida de los núcleos ($\sim nm \sim ns$ respectivamente) se adecuan muy bien a las escalas de volumen y tiempo accesibles en simulación, a las cuales experimentalmente es muy difícil tener acceso.

Pero desgraciadamente, observar nucleación de manera espontánea en simulación solo sucede en condiciones de metaestabilidad muy alta donde los núcleos críticos son muy pequeños y los sistemas muy difíciles de equilibrar porque el subenfriamiento es muy elevado. De forma que si queremos estudiar la nucleación en regímenes de metaestabilidad moderada, que es donde típicamente los experimentales pueden medir, hemos de recurrir a técnicas especiales que nos permitan observarla.

Estas técnicas especiales, a menudo se denominan *técnicas de eventos raros* ya que la nucleación es un proceso activado y por eso es "raro" observarla. Estas técnicas nos permiten mediante diferentes mecanismos cruzar la barrera de energía libre. Algunas de estas técnicas, las cuales están bien establecidas, son Umbrella Sampling (US)[1,2], Forward Flux Sampling (FFS)[3,4], Metadynamics[5,6] o Transition Path Sampling (TPS)[7,8]. El problema de estas técnicas es que además de ser bastante costosas desde un punto de vista computacional, habitualmente solo pueden ser empleadas en condiciones de mayor metaestabilidad que la de los experimentos. También aplicarlas a modelos de agua[9,10] supone un problema adicional dado que la dinámica de esta molécula es mucho más lenta

comparada con los modelos de partículas monoatómicas (Esferas Duras, Lennard-Jones, NaCl) donde estas técnicas se han aplicado típicamente hasta la fecha[2,4,11].

Por este motivo, dado que el principal objetivo de esta tesis es estudiar la nucleación de hielo, hemos tenido que desarrollar diferentes técnicas alternativas para estudiar la nucleación desde un punto de vista computacional más eficiente y en regiones de metaestabilidad donde sí se puede comparar con los experimentos. Las técnicas que se han desarrollado durante este trabajo han sido "Seeding"[12–14] (capítulos I, V), "Mold Integration"[15] (capítulo III) y "Lattice Mold"[16] (capítulo IX). Estas técnicas son las que se han empleado fundamentalmente en este trabajo para estudiar la nucleación de sistemas simples como esferas duras o más complejos como el agua.

Antes de aplicar estas técnicas a problemas muy novedosos, como puede ser la formación de hielo a partir de disoluciones, las hemos validado[15–17] (Capítulos III, V y IX) para sistemas en los que se conocían bien magnitudes relevantes en la nucleación como son la tasa de nucleación o la energía interfacial[2,4,11,18,19]. Una vez cumplido el objetivo inicial de tener a nuestra disposición diferentes técnicas para estudiar este fenómeno, las hemos aplicado para caracterizar en profundidad la nucleación de hielo a presión atmosférica (Capítulos I, II y VII), y posteriormente para estudiar la formación de hielo en sistemas más complejos como disoluciones acuosas de NaCl (Capítulos X y XI) o en agua pura en condiciones extremas de alta presión (Capítulo VIII).

De modo que después de esta breve introducción al problema y a los objetivos de esta tesis, vamos a realizar una descripción de las partes y capítulos de esta memoria, la cual se divide en tres bloques: fundamento teórico, resultados y conclusiones.

En la primera parte de la memoria se va a discutir el fenómeno de la nucleación, la cual puede producirse de manera homogénea a través de fluctuaciones de orden local en el líquido puro, o de manera heterogénea asistida por la presencia de impurezas o paredes externas. También se va a describir este fenómeno desde un punto de vista teórico a través de la Teoría Clásica de Nucleación[20,21], CNT, que combina un esquema cinético[20,21] con un enfoque termodinámico[22,23] para evaluar las magnitudes más relevantes involucradas en este proceso. En la CNT la nucleación se describe como una competición entre dos términos, uno que la favorece que es el menor potencial químico de la fase naciente y otra que la dificulta que es la energía que cuesta formar la interfase entre la fase naciente y la fase metaestable. También en este bloque se explica la ley de Avrami[24], una ley que permite evaluar el tiempo necesario para que un porcentaje de una muestra cristalice a partir de la tasa de nucleación (el número de núcleos que aparecen por unidad de tiempo y volumen) y la velocidad de crecimiento de estos núcleos.

Finalmente en este bloque se discuten de manera breve (ya que en detalle se hará en los capítulos de resultados) las tres técnicas de simulación que se han utilizado para la obtención de todos nuestros resultados, junto con un apéndice que contiene detalles técnicos sobre los parámetros de orden que se han usado en el Seeding.

En la segunda parte de la memoria se encuentran los diferentes **capítulos de resultados**. En este caso se sigue el orden cronológico y continuo que hemos seguido a lo largo de este trabajo. Ahora procederemos a describir brevemente algunos de los aspectos más relevantes de los capítulos de resultados.

En el primer capítulo, **Cap. I**, estudiamos la nucleación de hielo a presión atmosférica. La importancia de entender en profundidad este fenómeno se debe a que la formación de hielo en la nubes es un factor clave que puede aliviar en gran medida el calentamiento global[25–28]. Además comprender bien este proceso tiene gran relevancia en otras áreas como la criopreservación de alimentos, células o tejidos[29], o incluso en microbiología[30] e industria alimenticia[31,32]. En este capítulo se calculan por primera vez tasas de nucleación para los modelos de agua TIP4P/2005[9] y TIP4P/Ice[10], dos de los modelos que mejor reproducen muchas de las propiedades del agua real sobre todo para fases condensadas. Para ello usamos la técnica de Seeding (sembrado). Insertamos clústeres de hielo de diferentes tamaños en agua subenfriada y acotamos las temperaturas a las cuales los núcleos insertados eran críticos. Esto en combinación con la Teoría Clásica de Nucleación[20,21], nos permitió obtener tasas de nucleación a varios subenfriamientos moderados. Estas tasas comparaban sorprendentemente bien con las medidas experimentales y nos permitieron determinar el comportamiento de la tasa de nucleación frente al subenfriamiento. Adicionalmente observamos que la energía interfacial γ entre el hielo y el agua líquida no era constante con la temperatura y que a medida que subenfriamos el agua esta disminuye.

En el segundo capítulo, **Cap. II**, decidimos ampliar el estudio anterior incluyendo otros dos modelos de agua, el TIP4P[33] y el mW[34] para ver la comparativa y la generalidad de las predicciones de varios modelos de agua en el ámbito de la nucleación. Se observó que en todos los modelos de agua estudiados, γ disminuía al aumentar el subenfriamiento con una dependencia razonablemente lineal, la cual es una información muy valiosa para los experimentales. Esto permitió además utilizar nuestros datos de Seeding para hacer ajustes basados en las ecuaciones de la CNT, obteniendo así predicciones continuas para la tasa de nucleación desde subenfriamientos muy bajos hasta condiciones de muy alta metaestabilidad. Poder conocer la tasa a cualquier temperatura nos permitió comparar con datos de otros autores[18,35,36] medidos por otras técnicas más rigurosas (FFS, US) obteniendose una buena concordancia. También se observó que aunque todos los modelos de agua estudiados predecían cualitativamente tendencias similares, los que mejor concordaban cuantitativamente con los valores experimentales eran el TIP4P/2005 y el TIP4P/Ice. Finalmente, para el modelo TIP4P/2005 estimamos la velocidad de crecimiento del hielo, u, para diferentes subenfriamientos que en combinación con la tasa de nucleación J y mediante una fórmula propuesta en el año 1939 por Avrami[24] nos permitió hallar el tiempo necesario para que un porcentaje de una muestra cristalice.

Con esta estimación además se puede hallar cuál ha de ser la velocidad de subenfriamiento para formar el vidrio evitando así que la muestra cristalice durante el proceso de enfriamiento, la cual es extremadamente alta en el caso del agua.

Experimentalmente es extremadamente complicado medir la energía interfacial para las interfases líquido-cristal, a diferencia del caso del líquido-vapor donde sí es sencillo medirla. Por ese motivo, poder evaluar γ mediante simulación es muy útil. En el tercer capítulo **Cap. III** se presenta y valida la técnica de Mold Integration (MI), la cual tiene como objetivo calcular γ en condiciones de coexistencia y además tener una precisión tal que permita distinguir entre la anisotropía de diferentes planos cristalinos. En este primer artículo se valida la técnica para diferentes planos cristalinos de tres sistemas monoatómicos diferentes que fueron esferas duras, argón (Lennard-Jones) y esferas pseudo-duras[37]. Para los dos primeros sistemas, γ había sido determinada con anterioridad por otros autores[19,38–40] para diferentes planos cristalinos utilizando otras técnicas como Cleaving[40] y Capillary Wave Fluctuations[41,42]. Los resultados obtenidos por MI para estos dos sistemas fueron muy satisfactorios y en muy buena concordancia con los valores previos de la literatura[19,38–40] para los diferentes planos cristalinos. En cuanto al sistema de esferas pseudo-duras, resultó tener una energía interfacial muy similar a la de las esferas duras originales, lo cual fue muy positivo para completar la validación de este nuevo modelo como un firme candidato de versión continua y derivable que permite simular esferas duras en Dinámica Molecular.

En el siguiente capítulo **Cap. IV**, investigamos la nucleación de cristales de NaCl a partir de su fundido para el modelo Tosi-Fumi[43,44]. Sobre este tema, había una discrepancia en la literatura para las predicciones de γ de este modelo entre las Referencias[4,45] y la Ref.[46] donde se postulaba que γ valía $\sim 80-100 mJ/m^2$ y $\sim 35 mJ/m^2$ respectivamente. Debido a estas diferencias decidimos estudiar este caso por medio de MI y Seeding. En primer lugar estudiamos la energía interfacial a coexistencia por medio de MI para cuatro orientaciones cristalográficas diferentes obteniendo una γ promedio de $\sim 100 mJ/m^2$. En segundo lugar, insertamos varios clústeres de NaCl cristalino de diferentes tamaños en el fundido y evaluamos tanto la tasa como la energía interfacial. Lo que observamos es que apenas había una dependencia de γ con la temperatura oscilando todos los valores en un amplio rango de subenfriamiento en torno a $100 mJ/m^2$. Por último hicimos un cálculo de Umbrella Sampling a coexistencia para verificar este valor por una tercera ruta y también obtuvimos un valor similar al de las dos rutas anteriores. Se observó que la geometría de los clústeres en el máximo de la barrera era esférica, lo cual nos ayudó a entender las discrepancias de nuestros valores con los de las Referencias[4,45] donde si se consideraba una simetría esférica para los núcleos críticos γ era de aproximadamente $100 mJ/m^2$, también en concordacia con nuestros resultados. Por otro lado, no se consiguió entender el origen de las discrepancias entre nuestros valores y los de la Ref.[46].

El siguiente capítulo **Cap. V** es un capítulo fundamental de esta memoria donde se aplica Seeding a cuatro sistemas arquetipo para los cuales las tasas de nucleación y las energías interfaciales se conocen bien. El objetivo de este trabajo era convencer al lector que a pesar de que el Seeding es una técnica aproximada que está sujeta al uso de un parámetro de orden que distingue entre las partículas tipo-sólido y tipo-líquido de nuestras simulaciones, puede dar resultados muy coherentes y en buena concordancia con otras técnicas independientes en un amplio intervalo de metaestabilidad. También se pretendía demostrar que la CNT es una teoría general que funciona y que mediante su uso acoplado al Seeding proporciona estimaciones de tasas de nucleación compatibles con medidas en las que no se asume ninguna teoría. Para ello se estudiaron los siguientes sistemas: Esferas duras (HS), Lennard-Jones (LJ), NaCl (Tosi-Fumi) y el modelo de agua "coarse grained" mW. Tanto la energía interfacial a coexistencia como las tasas de nucleación a alta sobresaturación previamente estimadas ya en la literatura por otras vías[2,4,11,18,36,40,47,48], coincidieron razonablemente bien para todos los sistemas a los que aplicamos Seeding. Esto demuestró la validez de las curvas halladas por el Seeding a pesar de ser una técnica aproximada y también que la CNT es capaz de predecir correctamente tasas de nucleación para diferentes sistemas.

En el sexto capítulo, **Cap. VI**, vamos a aplicar la técnica de Mold Integration para un caso particularmente más complejo que para los modelos con los que inicialmente se validó la técnica, el agua. Medir la tensión interfacial del agua hielo-líquido a coexistencia experimentalmente es muy complicado y por ese motivo, las predicciones hasta la fecha son muy dispares[49]. Por lo que poder evaluarla por simulación para modelos realistas de agua aporta información que experimentalmente es inaccesible y muy relevante. El objetivo era evaluar para varios modelos de la familia TIP4P (TIP4P,TIP4P/2005 Y TIP4P/Ice) y para el modelo monoatómico de agua mW la energía interfacial entre el hielo Ih y el agua líquida. Los modelos de agua de la familia TIP4P al ser poliatómicos tienen grados de libertad orientacionales, lo cual añade una dificultad extra al cálculo. Este fue un trabajo costoso que llevó mucho tiempo ponerlo a punto, y que en primera instancia se realizó para los modelos TIP4P, TIP4P/2005 y mW para los cuales ya había valores de γ a coexistencia[50–52]. Una vez validada la extensión del método para moléculas con grado orientacional con los modelos TIP4P y TIP4P/2005, se lo aplicamos también al TIP4P/Ice para el cual calculamos para diferentes planos tanto la γ entre el hielo Ih-fluido como la del Ic-fluido. De este estudio se concluyó que ambos polimorfos tenían la misma energía interfacial promedio sobre todos los planos estudiados con el agua líquida, sosteniendo aún más la hipótesis de que la formación de hielo en el agua es mediante un apilamiento alternado de ambas fases cristalinas[53–55]. Además todos los valores que se hallaron para los cuatro modelos de agua estaban en buena concordancia con nuestras prediciones de γ a coexistencia a partir del Seeding[17,53,56].

En el séptimo capítulo, **Cap. VII**, se pretendía entender una discrepencia recientemente publicada[57] entre medidas experimentales de tasas de nucleación de hielo. Este nuevo artículo contradecía un gran número de medidas publicadas hasta la fecha[58–61]. Para ello evaluamos con más precisión la tasa de nucleación para el modelo TIP4P/Ice, el cual había sido el modelo que mejor reproducía los valores experimentales. También calculamos las velocidades de crecimiento en función del subenfriamiento, lo cual combinado con las tasas de nucleación, nos permitió evaluar las curvas de Avrami[35,56], es decir, el tiempo requerido para cristalizar un cierto porcentaje de la muestra en función de la temperatura. Representando las curvas de tiempo de Avrami junto al tiempo requerido para observar nucleación en un volumen dado, se discutió el "cross-over" entre dos regímenes: un régimen de nucleación donde el sistema permanece como un fluido metaestable hasta que después de un tiempo nuclea, y otro régimen donde antes de que el sistema pueda equilibrar ya aparecen pequeños núcleos que van creciendo poco a poco y que evitan que el sistema pueda estar en "equilibrio" ni tan siquiera durante un periódo breve y que impide medir tasas de nucleación correctamente. Esta discusión sobre estos dos regímenes nos permitió postular una hipótesis sobre el origen de la reciente discrepancia[57] en las tasas de nucleación respecto a las diferentes grupos experimentales[58–61] previamente publicadas. A su vez como conclusión de este trabajo pudimos afirmar que el modelo TIP4P/Ice reproduce fielmente tanto las velocidades de crecimiento del hielo, las tasas de nucleación experimentales y las propiedades anómalas del agua subenfriada, lo cual para el modelo mW que también se estudió no fue así.

En el siguiente capítulo **Cap. VIII** se estudia el efecto de la presión sobre la nucleación de hielo. En el año 1975 Speedy, Kanno y Angell[62] consiguieron tener microgotas de agua líquida hasta -92 C aplicando presiones de hasta 2000 bares. Este experimento demostró como la nucleación de hielo se ve dificultada al comprimir el agua, lo cual es muy importante en criopreservación de células, tejidos y alimentos donde no interesa que se forme hielo[29]. De hecho algunos congeladores usan esta estrategia para mejorar la preservación de estos sistemas[63]. Nuestro objetivo de este capítulo fue comprobar si el modelo TIP4P/Ice que a presión normal reprodujo muy bien las tasas de nucleación experimentales era capaz también de dar resultados satisfactorios a 2000 bares. Mediante una combinación de técnicas, Seeding+MI, evaluamos la curva de nucleación a 2000 bares y observamos que al igual que en el experimento la nucleación sufría una deceleración notable. Evaluando los parámetros termodinámicos implicados en este fenómeno, pudimos concluir que el responsable mayoritario de esta deceleración era el incremento de la energía interfacial hielo-líquido. Además otra vez la predicción del modelo respecto al experimento fue muy razonable. Por último mencionar que como estudio colateral a este trabajo también se estudió la nucleación del modelo mW a altas presiones. Esto fue motivado por un trabajo publicado en 2014[48] que afirmaba que la deceleración en

la tasa de nucleación a medida que aumentaba la presión indicaba la existencia de una nueva fase de hielo, hielo 0, la cual daba origen a la formación posterior de hielo Ih o Ic. Como este trabajo originalmente se propuso con el modelo de agua mW, estudiamos la nucleación bajo presión también para este modelo y observamos la misma tendencia cualitativa que en el TIP4P/Ice aunque cuantitavamente los resultados comparaban significativamente peor con el experimento. No obstante, este estudio nos ayudó a entender que el origen de la proposición del hielo 0, residía en una incorrecta interpretación de las partículas interfaciales del hielo-líquido en la Referencia [48] y que también en este modelo la deceleración de la tasa al aumentar la presión se producía por un incremento en γ y no debido a una nueva fase implicada en la nucleación de hielo.

En el noveno capítulo, **Cap. IX**, dada la extrema importancia de poder medir tasas de nucleación por simulación y siendo esta la magnitud que mejor define la nucleación y la cual se puede medir experimentalmente, propusimos una nueva técnica para evaluarla. Esta técnica se basa en una idea similar al Mold Integration y no depende de parámetros de orden ni de la CNT para estimar tasas de nucleación. La llamamos "Lattice Mold" [16]. Para validar este método calculamos la tasa para tres estados diferentes de esferas duras y para un estado de cloruro sódico. Los resultados que obtuvimos estaban en buena concordancia con valores previos procedentes de otras técnicas como Umbrella Sampling [2], Forward Flux Sampling [4,11] y Seeding [17]. De hecho la primera aplicación que tuvo este método fue corregir una de las tasas calculadas por FFS para el cloruro sódico en la literatura [4]. Esta nueva técnica puede ser utilizada de manera complementaria al Seeding dado que no depende de parámetros de orden siendo útil para verficar si los resultados aproximados del Seeding son coherentes con estos. Además si la estructura de interés que se desea estudiar es muy compleja y no hay parámetros de orden que permitan detectarla, con esta técnica se puede imponer dicha estructura y evaluar la tasa sin necesidad de recurrir a ningún parámetro de orden.

En el capítulo décimo, **Cap. X**, vamos a estudiar la nucleación de hielo a partir de una disolución de cloruro sódico. Entender los factores implicados en este proceso es muy relevante, dado que en las nubes de la atmósfera la formación de hielo también se produce a partir de gotas que poseen solutos [25,64]. Para ello vamos a evaluar como afecta a la tasa de nucleación del hielo añadir sal al agua, en este caso concreto NaCl a concentración 1.85 molal y presión ambiente. Para este estudio aplicamos las técnicas de Seeding y MI. Lo que observamos, fue un incremento muy significativo de la energía interfacial entre el hielo y la disolución respecto a la del hielo con el agua pura para la misma presión y subenfriamiento. Analizando los diferentes factores implicados en la nucleación, concluimos que γ era el factor determinante que producía el descenso considerable de la tasa de nucleación observada en nuestras simulaciones y experimentalmente [65,66]. Esto es un efecto análogo al que se consigue cuando se presuriza el agua [67,68]. Por este motivo

el siguiente paso va a ser comprobar si añadir sal al agua o presión causa efectos que cuantitativamente son similares y se puede establecer una concentración de sal que cause el mismo efecto que una presión determinada.

Y ya en el último capítulo, **Cap. XI**, vamos a estudiar si efectivamente existe una presión que cause un efecto similar al de la concentración de una sal dada. Esto ya se había postulado en la literatura en la Ref.[66] donde se propone una regla empírica que mediante la actividad del agua se puede obtener una curva de nucleación universal tanto para disoluciones acouosas de sales como para agua a altas presiones. Esto es algo que podría ser muy útil para la comunidad científica dado que medir la actividad del agua es sencillo, mientras que medir J resulta más complicado, por lo que si a partir de la actividad se pudiera inferir de manera directa y fiable la tasa, esto sería muy importante. La idea[66] consiste en representar las tasas de nucleación en función de la diferencia de actividad del agua líquida a coexistencia con el hielo y la actividad del agua líquida a un subenfriamiento dado tanto para las diferentes disoluciones a presión normal como para el agua pura o las disoluciones bajo presión, tomando como estado de referencia el agua pura a 1 bar. Aunque en la Ref.[66] los autores consiguen representar todos los resultados de tasas experimentales en una línea de J universal, cuando nosotros aplicamos este mismo tratamiento para nuestros modelos de agua no observamos que la curva de nucleación de alta presión y la de la disolución acuosa de NaCl confluyan en una única curva. Aunque en la región donde es posbile medir las tasas de nucleación experimentalmente (desde $J = 10m^{-3}s^{-1}$ hasta $J = 10^{16}m^{-3}s^{-1}$) las tasas para ambos sistemas son similares, observamos que las tasas de estos discrepan significativamente para subenfriamientos menores donde J es más baja (i. e. menor que $J = 10m^{-3}s^{-1}$). Esto nos sugiere que esta regla puede funcionar de manera fortuita únicamente cuando para una diferencia de actividad dada, γ es similar en disoluciones y en agua bajo presión como es el caso en la región experimental accesible. Cuando esto no sucede esta regla no se cumple, y gracias al Seeding que permite medir en un amplio intervalo de subenfriamientos hemos podido testar esta regla concluyendo que no es general a diferencia de lo que ocurre con la Teoría Clásica de Nucleación que parece dar buenos resultados para todos los sistemas considerados en este trabajo.

Finalmente la memoria termina con unas conclusiones, donde se hace una retrospectiva de los resultados obtenidos durante estos últimos años.

Bibliografía

1. Torrie, G. & Valleau, J., Nonphysical sampling distributions in Monte Carlo free-energy estimation: Umbrella sampling. *Journal of Computational Physics* **23**, 187–199 (1977).

2. Auer, S. & Frenkel, D., Prediction of absolute crystal-nucleation rate in hard-sphere colloids. *Nature* **409**, 1020 (2001).

3. Allen, R. J., Warren, P. B. & ten Wolde, P. R., Sampling rare switching events in biochemical networks. *Phys. Rev. Lett.* **94**, 018104 (2005).

4. Valeriani, C., Sanz, E. & Frenkel, D., Rate of homogeneous crystal nucleation in molten NaCl. *J. Chem. Phys.* **122**, 194501 (2005).

5. Laio, A. & Parrinello, M., Escaping free-energy minima. *Proc. Natl. Acad. Sci.* **99**, 12562 (2002).

6. Trudu, F., Donadio, D. & Parrinello, M., Freezing of a Lennard-Jones fluid: From nucleation to spinodal regime. *Phys. Rev. Lett.* **97**, 105701 (2006).

7. Bolhuis, P. G., Chandler, D., Dellago, C. & Geissler, P. L., Transition path sampling: Throwing ropes over rough mountain passes, in the dark. *Ann. Rev. Physical Chem.* **53**, 291 (2002).

8. Moroni, D., ten Wolde, P. R. & Bolhuis, P. G., Interplay between structure and size in a critical crystal nucleus. *Phys. Rev. Lett.* **94**, 235703 (2005).

9. Abascal, J. L. F. & Vega, C., A general purpose model for the condensed phases of water: TIP4P/2005. *J. Chem. Phys.* **123**, 234505 (2005).

10. Abascal, J. L. F., Sanz, E., Fernandez, R. G. & Vega, C., A potential model for the study of ices and amorphous water: TIP4P/Ice. *J. Chem. Phys.* **122**, 234511 (2005).

11. Filion, L., Hermes, M., Ni, R. & Dijkstra, M., Crystal nucleation of hard spheres using molecular dynamics, umbrella sampling, and forward flux sampling: A comparison of simulation techniques. *J. Chem. Phys.* **133**, 244115 (2010).

12. Bai, X.-M. & Li, M., Calculation of solid-liquid interfacial free energy: A classical nucleation theory based approach. *J. Chem. Phys.* **124**, 124707 (2006).

13. Sanz, E., Vega, C., Espinosa, J. R., Caballero-Bernal, R., Abascal, J. L. F. & Valeriani, C., Homogeneous ice nucleation at moderate supercooling from molecular simulation. *Journal of the American Chemical Society* **135**, 15008–15017 (2013).

14. Knott, B. C., Molinero, V., Doherty, M. F. & Peters, B., Homogeneous nucleation of methane hydrates: Unrealistic under realistic conditions. *J. Am. Chem. Soc.* **134**, 19544–19547 (2012).

15. Espinosa, J. R., Vega, C. & Sanz, E., The mold integration method for the calculation of the crystal-fluid interfacial free energy from simulations. *J Chem. Phys.* **141**, 134709 (2014).

16. Espinosa, J. R., Sampedro, P., Valeriani, C., C., V. & E., S., Lattice mold technique for the calculation of crystal nucleation rates. *Faraday Discussions* **195**, 569 (2016).

17. Espinosa, J. R., Vega, C., Valeriani, C. & Sanz, E., Seeding approach to crystal nucleation. *J. Chem. Phys.* **144**, 034501 (2016).

18. Li, T., Donadio, D., Russo, G. & Galli, G., Homogeneous ice nucleation from supercooled water. *Phys. Chem. Chem. Phys.* **13**, 19807–19813 (2011).

19. Davidchack, R. L., Morris, J. R. & Laird, B. B., The anisotropic hard-sphere crystal-melt interfacial free energy from fluctuations. *J. Chem. Phys.* **125**, 094710 (2006).

20. Becker, R. & Doring, W., Kinetische behandlung der keimbildung in ubersattigten dampfen. *Ann. Phys.* **416**, 719–752 (1935).

21. Volmer, M. & Weber, A., Keimbildung in ubersattigten gebilden. *Z. Phys. Chem.* **119**, 277 (1926).

22. Gibbs, J. W., On the equilibrium of heterogeneous substances. *Trans. Connect. Acad. Sci.* **3**, 108–248 (1876).

23. Gibbs, J. W., On the equilibrium of heterogeneous substances. *Trans. Connect. Acad. Sci.* **16**, 343–524 (1878).

24. Avrami, M. *J. Chem. Phys* **7**, 1103 (1939).

25. Cantrell, W. & Heymsfield, A., Production of ice in tropospheric clouds. *Bull. Amer. Meteor. Soc.* **86**, 795 (2005).

26. Baker, M. B., Cloud microphysics and climate. *Science* **276**, 1072–1078 (1997).

27. DeMott, P. J., Prenni, A. J., Liu, X., Kreidenweis, S. M., Petters, M. D., Twohy, C. H., Richardson, M. S., Eidhammer, T. & Rogers, D. C., Predicting global atmospheric ice nuclei distributions and their impacts on climate. *Proc. Natl. Acad. Sci.* **107**, 11217–11222 (2010).

28. Michaelides, A. & Morgenstern, K., Ice nanoclusters at hydrophobic metal surfaces. *Nature Materials* **6**, 597–601 (2007).

29. Morris, G. J. & Acton, E., Controlled ice nucleation in cryopreservation–a review. *Cryobiology* **66**, 85 (2013).

30. Hirano, S. S. & Upper, C. D., Bacteria in the leaf ecosystem with emphasis on pseudomonas syringae - a pathogen, ice nucleus, and epiphyte. *Microbiol. Molec. Biol. Rev.* **64**, 624 (2000).

31. Maki, L. R., Galyan, E. L., M.M., C. & Caldwell, D. R., Ice nucleation induced by pseudomonas-syringae. *Appl. Microbiol.* **28**, 456–459 (1974).

32. Li, J. K. & Lee, T. C., Bacterial ice nucleation and its potential application in the food-industry. *Trends in Food Sci. & Tech.* **6**, 259–265 (1995).

33. Jorgensen, W. L., Chandrasekhar, J., Madura, J. D., Impey, R. W. & Klein, M. L., Comparison of simple potential functions for simulating liquid water. *J. Chem. Phys.* **79**, 926 (1983).

34. V. Molinero, and E. B. Moore, Water modeled as an intermediate element between carbon and silicon. *The Journal of Physical Chemistry B* **113**, 4008–4016 (2009).

35. Moore, E. B. & Molinero, V., Structural transformation in supercooled water controls the crystallization rate of ice. *Nature* **479**, 506–508 (2011).

36. Haji-Akbari, A., DeFever, R. S., Sarupria, S. & Debenedetti, P. G., Suppression of sub-surface freezing in free-standing thin films of a coarse-grained model of water. *Phys. Chem. Chem. Phys.* **16**, 25916–25927 (2014).

37. Jover, J., Haslam, A. J., Galindo, A., Jackson, G. & Muller, E. A., Pseudo hard-sphere potential for use in continuous molecular-dynamics simulation of spherical and chain molecules. *The Journal of Chemical Physics* **137**, 144505 (2012).

38. Davidchack, R. L. & Laird, B. B., Direct calculation of the hard-sphere crystal /melt interfacial free energy. *Phys. Rev. Lett.* **85**, 4751–4754 (2000).

39. Davidchack, R. L., Hard spheres revisited: Accurate calculation of the solid–liquid interfacial free energy. *J. Chem. Phys.* **133**, 234701 (2010).

40. Davidchack, R. L. & Laird, B. B., Direct calculation of the crystal–melt interfacial free energies for continuous potentials: Application to the Lennard-Jones system. *J. Chem. Phys.* **118**, 7651–7657 (2003).

41. Hoyt, J. J., Asta, M. & Karma, A., Method for computing the anisotropy of the solid-liquid interfacial free energy. *Phys. Rev. Lett.* **86**, 5530–5533 (2001).

42. Sun, D. Y., Mendelev, M. I., Becker, C. A., Kudin, K., Haxhimali, T., Asta, M., Hoyt, J. J., Karma, A. & Srolovitz, D. J., Crystal-melt interfacial free energies in hcp metals: A molecular dynamics study of mg. *Phys. Rev. B* **73**, 024116 (2006).

43. Fumi, F. & Tosi, M., Ionic sizes and born repulsive parameters in the NaCl-type alkali halides I. *Journal of Physics and Chemistry of Solids* **25**, 31–43 (1964).

44. Tosi, M. & Fumi, F., Ionic sizes and born repulsive parameters in the NaCl-type alkali halides II. *Journal of Physics and Chemistry of Solids* **25**, 45–52 (1964).

45. Zykova-Timan, T., Valeriani, C., Sanz, E., Frenkel, D. & Tosatti, E., Irreducible finite-size effects in the surface free energy of NaCl crystals from crystal-nucleation data. *Phys. Rev. Lett.* **100**, 036103 (2008).

46. Zykova-Timan, T., Ceresoli, D., Tartaglino, U. & Tosatti, E., Why are alkali halide surfaces not wetted by their own melt? *Phys. Rev. Lett.* **94**, 176105 (2005).

47. Benet, J., MacDowell, L. G. & Sanz, E., Interfacial free energy of the NaCl crystal-melt interface from capillary wave fluctuations. *The Journal of Chemical Physics* **142**, 134706 (2015).

48. Russo, J., Romano, F. & Tanaka, H., New metastable form of ice and its role in the homogeneous crystallization of water. *Nature Materials* **13**, 733 (2014).

49. Ickes, L., Welti, A., Hoose, C. & Lohmann, U., Classical nucleation theory of homogeneous freezing of water: thermodynamic and kinetic parameters. *Phys. Chem. Chem. Phys.* **17**, 5514–5537 (2015).

50. Davidchack, R. L., Handel, R., Anwar, J. & Brukhno, A. V., Ice ih-water interfacial free energy of simple water models with full electrostatic interactions. *Journal of Chemical Theory and Computation* **8**, 2383–2390 (2012).

51. Benet, J., MacDowell, L. G. & Sanz, E., A study of the ice-water interface using the TIP4P/2005 water model. *Phys. Chem. Chem. Phys.* **16**, 22159–22166 (2014).

52. Limmer, D. T. & Chandler, D., Premelting, fluctuations, and coarse-graining of water-ice interfaces. *The Journal of Chemical Physics* **141**, 18C505 (2014).

53. Zaragoza, A., Conde, M. M., Espinosa, J. R., Valeriani, C., Vega, C. & Sanz, E., Competition between ices ih and ic in homogeneous water freezing. *The Journal of Chemical Physics* **143**, 134504 (2015).

54. Malkin, T. L., Murray, B. J., Brukhno, A. V., Anwar, J. & Salzmann, C. G., Structure of ice crystallized from supercooled water. *Proceedings of the National Academy of Sciences* **109**, 1041–1045 (2012).

55. Malkin, T. L., Murray, B. J., Salzmann, C. G., Molinero, V., Pickering, S. J. & Whale, T. F., Stacking disorder in ice i. *Phys. Chem. Chem. Phys.* **17**, 60–76 (2015).

56. Espinosa, J. R., Sanz, E., Valeriani, C. & Vega, C., Homogeneous ice nucleation evaluated for several water models. *J. Chem. Phys.* **141**, 18C529 (2014).

57. Laksmono, H., McQueen, T. A., Sellberg, J. A., Loh, N. D., Huang, C., Schlesinger, D., Sierra, R. G., Hampton, C. Y., Nordlund, D., Beye, M., Martin, A. V., Barty, A., Seibert, M. M., Messerschmidt, M., Williams, G. J., Boutet, S., Amann-Winkel, K., Loerting, T., Pettersson, L. G. M., Bogan, M. J. & Nilsson, A., Anomalous behavior of the homogeneous ice nucleation rate in no-man's land. *The Journal of Physical Chemistry Letters* **6**, 2826–2832 (2015).

58. Murray, B. J., Broadley, S. L., Wilson, T. W., Bull, S. J., Wills, R. H., Christenson, H. K. & Murray, E. J., Kinetics of the homogeneous freezing of water. *Phys. Chem. Chem. Phys.* **12**, 10380 (2010).

59. Manka, A., Pathak, H., Tanimura, S., Wolk, J., Strey, R. & Wyslouzil, B. E., Freezing water in no man's land. *Phys. Chem. Chem. Phys.* **14**, 4505–4516 (2012).

60. Pruppacher, H. R., A new look at homogeneous ice nucleation in supercooled water drops. *J. Atmosph. Sci.* **52**, 1924 (1995).

61. Taborek, P., Nucleation in emulsified supercooled water. *Phys. Rev. B* **32**, 5902–5906 (1985).

62. Kanno, H., Speedy, R. J. & Angell, C. A., Supercooling of water to -92^{o}c under pressure. *Science* **189**, 880–881 (1975).

63. Studer, D., High-pressure freezing system (2001), US Patent 6,269,649.

64. Koop, T., Homogeneous ice nucleation in water and aqueous solutions. *Zeitschrift für Physikalische Chemie* **218**, 1231 (2004).

65. Alpert, P. A., Aller, J. Y. & Knopf, D. A., Ice nucleation from aqueous nacl droplets with and without marine diatoms. *Atmos. Chem. Phys.* **11**, 5539 (2011).

66. Koop, T., Luo, B., Tsias, A. & Peter, T., Water activity as the determinant for homogeneous ice nucleation in aqueous solutions. *Nature* **406**, 611–614 (2000).

67. Espinosa, J. R., Zaragoza, A., Rosales-Pelaez, P., Navarro, C., Valeriani, C., Vega, C. & Sanz, E., Interfacial free energy as the key to the pressure-induced deceleration of ice nucleation. *Phys. Rev. Lett.* **117**, 135702 (2016).

68. Kanno, H. & Angell, C. A., Homogeneous nucleation and glass formation in aqueous alkali halide solutions at high pressures. *The Journal of Physical Chemistry* **81**, 2639–2643 (1977).

Parte I

Fundamento teórico

Fundamento Teórico: Capítulo 1

Nucleación: El inicio de la estabilidad

En este capítulo se va a explicar el fenómeno de la nucleación, la teoría física que mejor la describe y las técnicas de simulación mediante las cuales se ha estudiado la nucleación en esta tesis doctoral.

En la sección 1.1 vamos a introducir el fenómeno de la nucleación y a distinguir entre nucleación homogénea y heterogénea, además de explicar la importancia de comprender bien este proceso cuando sucede de manera homogénea. En la sección 1.2 se va a ilustrar la Teoría Clásica de Nucleación, la cual es una teoría empírica macroscópica que nos permite interpretar el fenómeno físico de la nucleación. Esta teoría permite evaluar la energía libre de formación de un agregado de la fase estable en el seno de la fase metaestable y la tasa de nucleación correspondiente al estado termodinámico de la fase metaestable, que es el número de clústeres de tamaño crítico que aparecen por unidad de volumen y tiempo. La tasa de nucleación es una magnitud muy relevante que define la nucleación y que se puede medir tanto por simulación como por experimento. En algunas condiciones, para caracterizar la nucleación es más relevante conocer el tiempo necesario para cristalizar un sistema que la propia tasa de nucleación, por lo tanto, en la sección 1.3 explicaremos cómo se puede evaluar este tiempo requerido para cristalizar una muestra a partir de la tasa de nucleación y la velocidad de crecimiento cristalino. Por último en la sección 1.4 se van a mencionar las diferentes técnicas disponibles en simulación para estudiar eventos raros tales como la nucleación y dentro de las cuales se va a hacer especial hincapié en aquellas que se han utlizado/desarrollado durante esta tesis doctoral.

1.1. El fenómeno físico de la nucleación

El proceso de transformación de una fase metaestable en una estable, sucede por medio de la formación de un pequeño embrión de la fase estable el cual cuando alcanza un cierto tamaño crítico, crece de manera irreversible hasta transformar por completo la fase metaestable en la estable. Por lo tanto, la nucleación es el primer paso necesario

para que se produzca una transición de fase de primer orden[1].

El fenómeno de la nucleación es un proceso activado, que implica que para proceder a la transformación de la fase metaestable en la estable es necesario sobrepasar una barrera de energía libre. La altura de esta barrera va a depender de cuán alejadas estén las condiciones en las que se encuentra la fase metaestable de la línea de coexistencia. Cuando nos situamos sobre esta línea de coexistencia la altura de la barrera tiende a infinito, así como el tamaño del clúster crítico necesario para cruzarla. Pero a medida que nos alejamos de la línea de coexistencia, la fuerza motriz para promover la nucleación y la transformación total del sistema se va incrementando, provocando que la altura de la barrera de energía libre y el tamaño de los embriones disminuyan dramáticamente.

Existen dos mecanismos por los cuales se puede observar nucleación:

1. **Nucleación homogénea**, cuando ésta se produce a partir de una sola fase a través de fluctuaciones espontáneas de orden local que conducen a la formación de un clúster suficientemente grande como para sobrepasar la barrera de energía libre y generar la transformación de fase completa.

2. **Nucleación heterogénea**, similar a la homogénea, pero facilitada por la presencia de impurezas o paredes que ayudan a la formación del núcleo sobre la superficie de estos "cuerpos extraños" disminuyendo considerablemente la barrera de energía libre.

Un ejemplo sencillo es el caso de la formación de hielo. Cuando nosotros introducimos un vaso de agua en el congelador a unos quince grados bajo cero, en pocas horas al sacarlo el agua se habrá transformado en hielo. El mecanismo por el cual se ha formado el hielo es mediante nucleación heterogénea. En esta tesis hemos demostrado que si quisieramos congelar este mismo volumen de agua ultrapura (en ausencia de impurezas) y sin ayuda del recipiente que lo contiene ni esperando toda la edad del universo seriámos capaces de observar el hielo. De hecho, sin ayuda de impurezas o recipientes ni esperando toda la edad del universo y con un volumen tal como todo el agua de la hidrosfera seriámos capaces de observar la formación de hielo a -20 grados bajo cero[2].

Aunque a priori uno puede pensar que la mayoría de los fenómenos de nucleación en la naturaleza suceden mediante nucleación heterogénea, la nucleación homogénea tiene mucha importancia en la naturaleza (un ejemplo es la congelación de microgotas en la nubes) incluso más allá de la idea física de simplificar esta transición de fase para entenderla mejor. De hecho, el primer paso para entender correctamente la nucleación heterogénea, es comprender ampliamente el mecanismo y las variables termodinámicas involucradas en el proceso homogéneo el cual todavía posee muchas incógnitas.

Ya por lo tanto una vez habiendo enmarcado nuestro proceso a estudiar, estamos en condiciones de abordar el problema desde un punto de vista teórico.

1.2. Teoría Clásica de Nucleación

La teoría más utilizada para describir la nucleación homogénea es la Teoría Clásica de Nucleación, en inglés denominada *Classical Nucleation Theory* , de ahí sus siglas CNT. Esta teoría que ha sido ampliamente utilizada hasta la fecha tanto por experimentales como por simuladores, es una teoría macroscópica que fue formulada originalmente por Volmer and Weber[3], y posteriormente modificada por Becker y Doring[4]. Para formular esta teoría, Volmer and Weber en el año 1926 se ayudaron de las ecuaciones de Gibbs[5,6] que describían el trabajo reversible de formación de un clúster de una nueva fase naciente, y de esta manera pudieron proponer una teoría de nucleación de la cual se podían obtener tasas de nucleación.

Años más tarde, en el 1935, en el trabajo de Becker y Doring[4], se propone la utilización de la distribución del estado estacionario (*steady state*) en sustitución a la formulación original de la distribución de núcleos en equilibrio propuesta por Volmer y Weber. Esta contribución además permitió obtener una ecuación para la tasa de nucleación que no dependía del número de partículas. En el año 1949, Turnbull y Fisher[7] fueron los primeros que aplicaron estas ecuaciones para el estudio de materia condensanda.

En las siguientes secciones explicaremos como a través de la Teoría Clásica de Nucleación podemos obtener la tasa de nucleación y la altura de la barrera de energía libre que un sistema debe sobrepasar para nuclear.

1.2.1. Tasa de nucleación según la CNT

Por definición la tasa de nucleación es el número de núcleos críticos formados por unidad de volumen y de tiempo. Esta magnitud que vamos a representar con la letra J a lo largo de toda esta tesis doctoral es la que mejor representa y define este fenómeno. Generalmente las medidas experimentales de tasas de nucleación se interpretan a posteriori mediante una teoría fenomenológica que típicamente es la CNT, originalmente propuesta por Volmer y Weber[3]

La condición inicial de este planteamiento es que el proceso de crecimento y redisolución del núcleo la fase S debe ser mediante la adición y eliminación de monómeros sobre el núcleo crítico naciente de la nueva fase. Para ello se tiene que cumplir que la población de monómeros sea predominante frente a dímeros, trímeros... y que no haya colisiones entre núcleos. Con estas premisas podemos escribir las siguientes reacciones de formación y desaparición del núcleo.

$$(N-1)_S + 1 \underset{k_{-,N_S}}{\overset{k_{+,(N-1)_S}}{\rightleftharpoons}} N_S \tag{1.1}$$

$$N_S + 1 \underset{k_{-,(N+1)_S}}{\overset{k_{+,N_S}}{\rightleftharpoons}} (N+1)_S \tag{1.2}$$

donde $(N-1)_S$ es un núcleo con $N-1$ partículas, $k_{+,(N-1)_S}$ es la tasa de adición de un monómero $N=1$ a un núcleo $(N-1)_S$ y k_{-,N_S} la tasa de eleminación de un núcleo N_S. Este enfoque fue inicialmente propuesto para el caso de la nucleación vapor-líquido donde la concentración de monoméros es muy superior a la de dímeros, trímeros, etc ... y donde además las colisiones entres diferentes núcleos es extremadamente improbable.

La tasa de nucleación neta para un clúster de tamaño N_S se puede considerar como el flujo a lo largo del tiempo de los clústeres que alcanzan ese tamaño N_S, lo cual es equivalente a hallar la velocidad neta con la que un clúster gana una partícula:

$$J(N_S,t) = n_{N_S}(t)k_{+,N_S} - n_{(N+1)_S}(t)k_{-,(N+1)_S}, \tag{1.3}$$

donde n_{N_S} representa la concentración de clústeres de tamaño N_S. Para calcular la tasa mediante la ec. (1.3) Volmer y Weber hicieron las siguientes suposiciones:

1. El flujo de retorno de un núcleo más grande que el núcleo crítico, $N_S > N_S^*$, hacia el estado inicial es cero.

2. Para $N_S < N_S^*$, podemos tomar $n_{N_S}(t)$ como la distribución de núcleos en equilibrio n_{N_S}, y calcular así la probabilidad de encontrar un clúster crítico en equilibrio con el sistema como $e^{-\beta\Delta G(N_S^*)}$, donde $\beta = 1/k_BT$ y suponiendo a su vez que $n1 \sim n$, siendo n la densidad global.

   Utilizando estas aproximaciones en la ec. (1.3) obtenemos:

$$J(N_S) = n_{N_S}k_{+,N_S^*} = n_1 k_{+,N_S^*}e^{-\beta\Delta G(N_S^*)}, \tag{1.4}$$

siendo k_{+,N_S^*} y $\Delta G(N_S^*)$ la tasa de adición de una partícula o monómero al clúster crítico y la barrera de energía libre del núcleo crítico, respectivamente.

La tasa de nucleación que se calcula mediante la ec. 1.4 es dependiente del número de partículas del clúster, y esto la hace complicada de evaluar. Es por este hecho por lo que años más tarde Becker y Doring[4] reeemplazan la distribución de clústeres en equilibrio n_{N_S} por la distribución del estado estacionario $n_{N_S}^e$ y así eliminar esta dependencia.

Para ello en la ec. (1.3) introducen la distribución del estado estacionario $n_{N_S}^e$, quedando

$$J = n_{N_S}^e k_{+,N_S} - n_{N_S+1}^e k_{-,N_S+1}. \tag{1.5}$$

Con esta expresión y considerando que para los estados estacionarios el flujo es el mismo, llegamos a la siguiente ecuación:[8]

$$J = n_1 \left[\sum_{N_S=1}^{\infty} \frac{1}{k_{+,N_S}\zeta_{N_S}} \right]^{-1}, \tag{1.6}$$

siendo

$$\zeta_{N_S} = \prod_{N_S=1}^{N_S-1} \frac{k_{+,N_S}}{k_{-,N_S+1}} \tag{1.7}$$

para $N_S > 1$.

La utilización de esta constante englobadora ζ_{N_S} equivale a aproximar las semi-reacciones a una reacción global de formación del núcleo n_{N_S}.

$$N_S n_1 \rightleftharpoons^{\zeta_{N_S}} n_{N_S}. \tag{1.8}$$

Considerando que ζ_{N_S} se puede expresar como $\zeta_{N_S} = \left(\frac{n_{N_S}}{n_1}\right) = e^{-\beta\Delta G(N_S)}$, podemos hallar una fórmula para la tasa nucleación que ya no depende de N_S:

$$J = n_1 \left[\sum_{N_S=1}^{\infty} \frac{1}{k_{+,N_S} e^{-\beta\Delta G(N_S)}}\right]^{-1}. \tag{1.9}$$

Finalmente Becker y Doring para obtener una expresión que tuviera contacto con el mundo experimental hicieron una serie de simplificaciones y aproximaciones para la ec. 1.9:

1. Los términos del sumatorio que corresponden a los clústeres cercanos al máximo de la barrera de energía libre $\Delta G(N_S^*)$ dominan en la ec. 1.9.

2. $\Delta G(N_S)$ se reemplaza por los dos primeros términos diferentes de cero en la expansión de Taylor alrededor de N_S^*

3. k_{+,N_S} se sustituye por k_{+,N_S^*}

4. El sumatorio se sustituye por una integral desde $N_S - N_S^* = -\infty$ hasta $N_S - N_S^* = \infty$ haciendo que n_{N_S} sea una función continua de N_S.

En definitiva esta serie de simplificaciones implican realizar el cálculo de J en la región del top de la barrera y además limitan el cálculo hasta el tamaño del núcleo crítico N_S*. Pero de este modo podemos reescribir la ecuación anterior de la siguiente manera:

$$J = n_1 k_{+,N_S^*} \left(\frac{|\Delta G''(N_S)|_{N_S^*}}{2\pi k_B T}\right)^{1/2} e^{-\beta\Delta G(N_S^*)}, \tag{1.10}$$

siendo n_1 la concentración de monómeros de la fase metaestable, k_{+,N_S^*} la frecuencia con la que se incorporan moléculas al núcleo crítico, $|\Delta G''(N_S)|_{N_S^*}$ la segunda derivada de la energía libre de Gibbs en función de N_S calculada en el núcleo crítico y $\Delta G(N_S^*)$

la altura de la barrera para el clúster crítico. El término entre paréntesis se denomina factor de Zeldovich[9], Z,

$$Z = \left(\frac{|\Delta G''(N_S)|_{N_S^*}}{2\pi k_B T} \right)^{1/2} \tag{1.11}$$

que en la práctica sirve para considerar que durante el estado estacionario, la concentración de clústeres críticos no es realmente una concentración de equilibrio. Z es un número entre 0 y 1 que representa la probabilidad que tiene un clúster que está en la cumbre de la barrera de cruzarla. El inverso del factor de Zeldovich también representa la anchura de la barrera. Cuando $N_S - N_S^* > 1/(2Z)$ el núcleo será poscrítico y la concentración de clústeres será $n = 0$, por el contrario si $N_S - N_S^* < -1/(2Z)$ la concentración de clústeres será la de equilibrio $n = n_{equi}$. Por lo tanto solo serán núcleos críticos aquellos que $|N_S - N_S^*| < 1/(2Z)$.

Para calcular la frecuencia con la que nuevas partículas se incorporan al núcleo crítico, k_{+,N_S^*}, vamos a utilizar la expresión que Turnbull y Fischer[7] proponen para el estudio de sistemas condensados,

$$k_{+,N_S^*} = \frac{24 D (N_S^*)^{2/3}}{\lambda^2}. \tag{1.12}$$

Esta expresión depende de D, el coeficiente de difusión de los monómeros de la fase metaestable, λ, la longitud que ha de recorrer una partícula para adherirse o eliminarse del clúster crítico y finalmente del término $(N_S^*)^{2/3}$ que corresponde con el número de sitios disponibles en la superficie de un clúster esférico para que se adhiera o elimine una partícula.

Esta frecuencia de adhesión de nuevas partículas al clúster también se puede evaluar mediante la fórmula propuesta por Auer y Frenkel[10]:

$$k_{+,N_S^*} = \frac{< (N_S(t) - N_S^*)^2 >}{2t} \tag{1.13}$$

la cual se calcula como un coeficiente difusivo del número de partículas del clúster crítico en el máximo de la barrera en función del tiempo t.

De modo que combinando la Ec. 1.13 con la Ec. 1.10 podemos llegar a una expresión final para la tasa de nucleación que es:

$$J = n_1 \frac{< (N_S(t) - N_S^*)^2 >}{2t} \left(\frac{|\Delta G''(N_S)|_{N_S^*}}{2\pi k_B T} \right)^{1/2} e^{-\beta \Delta G(N_S^*)}, \tag{1.14}$$

Llegados a este punto, mediante la Ec. 1.14 ya somos capaces de evaluar la tasa de nucleación mediante Teoría Clásica de Nucleación, siempre y cuando conozcamos los diferentes parámetros de los que depende esta ecuación. Estos parámetros son los siguientes:

1. La concentración de monómeros de la fase metaestable n_1, que en un líquido esto sería la densidad.

2. La frecuencia con la que adhieren nuevas partículas al núcleo crítico en el máximo de la barrera k_{+,N_S^*}.

3. La altura de barrera del clúster crítico $\Delta G(N_S^*)$.

4. La segunda derivada de la energía libre de Gibbs en función del tamaño del núcleo, $|\Delta G''(N_S)|_{N_S^*}$.

En la siguiente sección vamos a explicar como se puede evaluar la dependencia $\Delta G(N_S)$ mediante las ecuaciones de Gibbs[5,6] para calcular el trabajo reversible de formación de un núcleo de la fase estable en el seno de la fase metaestable.

1.2.2. Barrera de nucleación según Gibbs

Como ya se ha comentado anteriormente, la nucleación es un proceso activado y para que este fenómeno suceda, el sistema deberá traspasar una barrera de energía libre denominada barrera de nucleación $\Delta G(N_S^*)$. Para calcular esta barrera partiremos de dos sistemas I y II en condiciones termodinámicas de presión (p_L) y temperatura (T_L) constantes. El sistema I está compuesto por la fase metaestable L y el sistema II está constituido por esa misma fase metaestable y un embrión de la nueva fase S (Figura 1.1). También vamos a considerar que el núcleo de S es muy pequeño frente a la fase metaestable L. Nuestro objetivo va a ser calcular el trabajo reversible de formación del

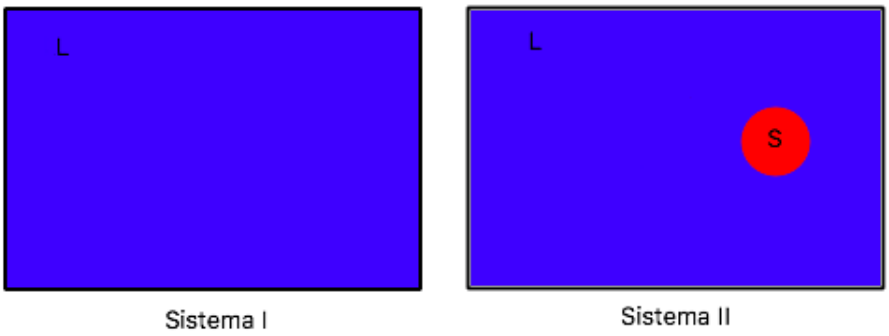

Figura 1.1: Representación esquemática de los dos sistemas, inicial (Sistema I) y final (Sistema II), para los cuales vamos a calcular el trabajo reversible de formación del clúster de la nueva fase S. El sistema I está constituido por la fase metaestable L, y el sistema II por esa misma fase metaestable más un embrión de la nueva fase S. Ambos sistemas se encuentran en condiciones termodinámicas de presión p_L y temperatura T_L constantes.

clúster de la nueva fase S en la fase metaestable L. Para ello vamos a empezar calculando la energía libre de Gibbs, G, de los dos sistemas I y II. La energía libre de Gibbs para el primer sistema que solo contiene la fase metaestable L es:

$$G_I = N\mu_L, \tag{1.15}$$

donde N es el número total de partículas del sistema y μ_L el potencial químico de la fase metaestable L a la presión p_L. Para calcular esto mismo también para el sistema II lo haremos de la siguiente manera:

$$G_{II} = F_{II} + p_L(V_L + V_S), \tag{1.16}$$

donde F_{II} es la energía libre de Helmhotz del sistema II, V_L es el volumen de la fase metaestable, V_S el volumen del núcleo de la fase estable naciente y p_L va a ser la presión global del sistema. Si desarrollamos el término F_{II} obtendremos la siguiente expresión:

$$G_{II} = (N_L\mu_L - p_LV_L) + (N_S\mu_S(p_S) - p_SV_S) + \mathbf{A}\gamma + p_L(V_L + V_S), \tag{1.17}$$

donde N_L es el número de partículas de la fase metaestable, N_S el número de partículas de la fase estable naciente y $\mu_S(p_S)$ el potencial químico de la fase estable a su presión correspondiente (p_S), que va a ser distinta de p_L debido al incremento de presión de Laplace. Dado que para este sistema aparece una nueva fase S, el trabajo que tenemos que realizar para crear la interfase que las separa, viene determinado por el área de la propia interfase, A y por la energía libre interfacial, γ. El número total de partículas de nuestro sistema vendrá dado por $N = N_L + N_S$ y aproximaremos los volúmenes como aditivos $V = V_L + V_S$.

Si desarrollamos la ecuación 1.17 algunos términos se cancelan y obtenemos:

$$G_{II} = N_L\mu_L + N_S\mu_S(p_S) + V_S(p_L + p_S) + \mathbf{A}\gamma \tag{1.18}$$

El siguiente paso va a ser calcular la diferencia de energía libre de Gibbs, ΔG entre nuestros dos sistemas:

$$\Delta G = G_{II} - G_I, \tag{1.19}$$

para ello vamos a restar las ecuaciones 1.18 y 1.15, para obtener:

$$\Delta G = N_L\mu_L + N_S\mu_S(p_S) + V_S(p_L - p_S) + \mathbf{A}\gamma - N\mu_L, \tag{1.20}$$

la cual podemos reescribirla de la siguiente manera:

$$\Delta G = -(N - N_L)\mu_L + N_S\mu_S(p_S) + V_S(p_L - p_S) + \mathbf{A}\gamma, \tag{1.21}$$

donde $(N - N_L)$ es N_S.

Una vez llegado a este punto, para calcular la barrera de nucleación, la CNT necesita de las dos siguientes suposiciones:

1. El clúster que crece posee la misma estructura cristalina que la fase sólida estable S.

2. El núcleo ha de ser incompresible, por lo que su densidad debe permanecer practicamente constante.

Derivando la expresión para la energía libre de Gibbs respecto a la presión a $T = cte$:

$$\left(\frac{\partial G}{\partial p}\right)_T = V. \tag{1.22}$$

obtenemos V el volumen. Si integramos esta ecuación a lo largo de la presión suponiendo el volumen constante porque consideramos que el sólido es incompresible, obtenemos la siguiente relación termodinámica que nos permite definir $\mu_S(p_S) = \mu_S(p_L) + V_S/N_S(p_S - p_L)$. De este modo podemos entonces reescribir la ecuación 1.21 como:

$$\Delta G = -N_S\mu_L + N_S\left(\mu_S(p_L) + V_S/N_S(p_S - p_L)\right) + V_S(p_L - p_S) + \mathbf{A}\gamma \tag{1.23}$$

de donde reorganizando términos obtendremos,

$$\Delta G = N_S(\mu_S(p_L) - \mu_L) + \mathbf{A}\gamma. \tag{1.24}$$

Esta ecuación la podemos reescribir de la siguiente manera,

$$\Delta G = -N_S|\Delta\mu| + \mathbf{A}\gamma. \tag{1.25}$$

De este modo tenemos una función de ΔG que depende de dos términos, el número de partículas que forman parte de la nueva fase estable S (N_S) por la diferencia de potenciales químicos entre ambas fases $\Delta\mu = \mu_S(p_L) - \mu_L$, y la energía libre interfacial γ por el área de la interfase que hay entre las dos fases $\mathbf{A}$.

- El primer término de esta ecuación es un término de *bulk* que depende del grado de metaestabilidad de la fase L con respecto a la fase termodinámicamente estable S. Este término es de signo negativo y es la fuerza motriz que favorece que suceda el proceso de nucleación.

- El segundo término es el término de superficie y viene dado por la energía interfacial γ que representa el coste necesario para crear la interfase entre la nueva fase S y la metaestable L que multiplica el area $\mathbf{A}$ que el clúster expone a la interfase. Este término de superficie que es positivo, representa el coste energético que impide que la nucleación sea espontánea.

En la expresión 1.25, **A** va a depender de la geometría que posea el clúster, si suponemos que la geometría del clúster naciente es esférica podemos obtener una expresión dependiente del radio del clúster R.

Tomando $\mathbf{A} = 4\pi R^2$, área de una esfera y N_S el número de partículas de esa esfera de volumen $V = (4/3)\pi R^3$, la barrera en la Ec. (1.25) queda:

$$\Delta G = -\rho_S(4/3)\pi R^3|\Delta\mu| + 4\pi R^2\gamma \tag{1.26}$$

Como podemos observar ΔG en ambas expresiones (1.25) y (1.26) tiene dos términos, uno que induce la nucleación y que depende de $\Delta\mu$ y otro que la dificulta que depende de γ.

Si representamos la ecuación 1.26, así como los dos términos que la componen podemos observar un máximo en la función ΔG (Figura 1.2).

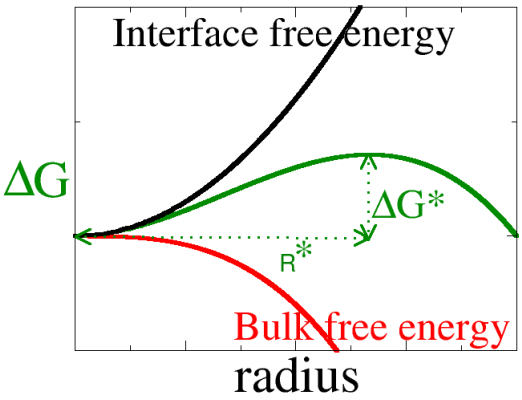

Figura 1.2: Representación esquemática de la barrera de energía libre (ΔG) en el proceso de nucleación en función del radio del clúster (R). La curva negra corresponde al coste energético debido a la contribución de la energía interfacial por el área del núcleo ($\gamma\mathbf{A}$), la curva roja corresponde al término $N_S\Delta\mu$, fuerza motriz del proceso y la curva verde representa ΔG, la barrera de nucleación, que es la suma de los dos términos anteriores.

El punto más alto de la barrera se conoce como *top o máximo de la barrera*. Está caracterizado por el valor de un radio concreto, **radio crítico** R^*, al cual corresponde el valor máximo de la energía libre, ΔG^*. El núcleo que corresponde al máximo de la función se denomina **núcleo crítico**, N_S^*, y se define como el *clúster* que tiene una probabilidad del 50 % de continuar creciendo irremediablemente hasta que la transformación hacia la fase estable es completa y el otro 50 % de probabilidad de volverse a disolver en la fase

metaestable L. El radio crítico viene definido por la siguiente expresión:

$$R^* = \frac{2\gamma}{\rho_S \left|\Delta\mu\right|} \tag{1.27}$$

y la energía libre en el máximo de la barrera:

$$\Delta G^* = \frac{16\pi\gamma^3}{3(\rho_S \left|\Delta\mu\right|)^2} \tag{1.28}$$

Las expresiones anteriores se han obtenido al obtener el máximo de la ecuación 1.26 respecto de R. Cabe destacar el hecho de que la barrera de nucleación es directamente proporcional a la energía interfacial al cubo e inversamente proporcional tanto al cuadrado de la densidad de la fase estable ρ_S y a la diferencia de potencial químico entre las dos fases $\Delta\mu$. En vista de esto se puede inferir que en condiciones de coexistencia termodinámica donde $\Delta\mu = 0$, la altura de la barrera ha de tender a infinito.

Por otro lado, la ecuación 1.26 también la podemos expresar en función del número de partículas del clúster que crece de la siguiente manera:

$$\Delta G = (36\pi)^{1/3}(N_S/\rho_S)^{2/3}\gamma - N_S \left|\Delta\mu\right| \tag{1.29}$$

y si esta ecuación la maximizamos con respecto a N_S obtendremos la expresión que nos relaciona el número de partículas en el clúster crítico con la energía interfacial γ y el grado de supersaturación $\Delta\mu$:

$$N_S^* = \frac{32\pi\gamma^3}{3\rho_S^2 \left|\Delta\mu\right|^3} \tag{1.30}$$

donde N_S^* es el número de partículas del clúster crítico.

Es conveniente recalcar que estas expresiones 1.28 y 1.30 para la altura de la barrera y para el tamaño del clúster crítico respectivamente dependen de la geometría que se considere y que en este caso ha sido la esfera dado que es la geometría que minimiza el área de contacto entre ambas fases y por tanto el esfuerzo energético que ha de sobrepasar el sistema al nuclear.

Si combinamos las ecuaciones 1.28 y 1.30 podemos despejar la altura de barrera del clúster crítico como:

$$\Delta G^* = N_S^* \frac{\left|\Delta\mu\right|}{2}, \tag{1.31}$$

lo cual indica que la altura de barrera del clúster crítico (que puntualmente denominaremos como A) es 1/2 del término $N_S^* \left|\Delta\mu\right|$, la fuerza motriz que hace que el sistema nuclee (que puntualmente denominaremos como B). Así por tanto,

$$A = \frac{B}{2}. \tag{1.32}$$

Si el término $\mathbf{A}\gamma$ lo llamamos C, podemos reescribir la ecuación 1.24 de la siguiente forma,

$$A = C - B. \tag{1.33}$$

De manera que si combinamos las ecuaciones 1.32 y 1.33 podemos despejar C en función de A obteniendo que $C = 3A$. Esto implica que la altura de la barrera para el clúster crítico también la podemos calcular mediante la siguiente expresión:

$$A = \Delta G^* = \frac{\gamma \mathbf{A}^*}{3} \tag{1.34}$$

donde A^* se refiere al área del clúster crítico.

Otra modo de deducir la dependencia de la barrera de nucleación con N_S es considerar que en el equilibrio (inestable) del clúster crítico con la fase metaestable, los potenciales químicos de ambas fases son iguales:

$$\mu_S(p_S) = \mu_L, \tag{1.35}$$

en la cual, por medio de la misma relación termodinámica que usamos previamente en la ecuación 1.23 donde $\mu_S(p_S) = \mu_S(p_L) + V_S/N_S(p_S - p_L)$, llegamos a la siguente expresión,

$$\mu_S(p_L) + \frac{V_S}{N_S}(p_S - p_L) = \mu_L. \tag{1.36}$$

Si aplicamos la expresión de Laplace, $\Delta P = p_S - p_L = 2\gamma/R$ en la ecuación 1.36, esta la podemos reescribir:

$$\mu_S(p_L) + \frac{1}{\rho_S}\frac{2\gamma}{R} = \mu_L, \tag{1.37}$$

y despejando términos llegar a la siguiente ecuación

$$\frac{2\gamma}{\rho_S R} = \mu_L - \mu_S(p_L). \tag{1.38}$$

Despejando R en esta ecuación obtenemos una expresión idéntica a la Ec. 1.27 previamente obtenida. También de esta deducción se puede observar que si la ecuación 1.36 la reordenamos

$$\mu_L - \mu_S(p_L) = \frac{V_S}{N_S}(p_S - p_L) \tag{1.39}$$

y multiplicamos en ambos lados por N_S,

$$N_S(\mu_L - \mu_S(p_L)) = \frac{(p_S - p_L)}{\rho_S} N_S \tag{1.40}$$

llegamos a una ecuación análoga a la Ec. 1.24 pero que depende de la diferencia de presiones entre ambas fases en vez de la diferencia de potencial químico.

$$\Delta G = -N_S \frac{(p_S - p_L)}{\rho_S} + \mathbf{A}\gamma. \tag{1.41}$$

Una vez hallado el máximo de la función $\Delta G(N_S)$, para poder calcular la tasa de nucleación mediante la ecuación 1.14 necesitamos evaluar la segunda derivada de $\Delta G(N_S)$ en el máximo de la barrera. Para calcular Z, vamos a combinar la Ec. 1.11, con la segunda derivada de la Ec. 1.24 para estimarlo mediante la siguiente relación:

$$Z = \left(\frac{|\Delta\mu|}{6\pi k_B T N_S^*} \right)^{1/2}. \tag{1.42}$$

Así por tanto, mediante este enfoque termodinámico, podemos reescribir la Ec. 1.14 para obtener la expresión de final de tasa de nucleación que se ha utilizado generalmente a lo largo de esta tesis doctoral:

$$J = n_1 \frac{< (N_S(t) - N_S^*)^2 >}{2t} \left(\frac{|\Delta\mu|}{6\pi k_B T N_S^*} \right)^{1/2} e^{-\beta \Delta G(N_S^*)}. \tag{1.43}$$

1.3. Ley de Avrami

Experimentalmente a veces se mide la fracción de volumen que ha cristalizado en una muestra en lugar de la tasa de nucleación. Dicha fracción está relacionada, por supuesto, con la tasa de nucleación, que da cuenta del número de núcleos cristalinos nuevos que aparecen por unidad de tiempo en la muestra. Pero también hay que tener en cuenta la velocidad con la que crecen los cristales nucleados. La expresión propuesta por Avrami combina ambos factores para dar cuenta de la fracción de muestra que ha cristalizado a lo largo del tiempo. Podemos calcular la fracción de volumen (ϕ) que ha cristalizado a un tiempo τ a través de la siguiente expresión,

$$\phi(\tau) = \int_0^\tau J \frac{4\pi}{3} \Big[\int_0^{t'} u dt'' \Big]^3 dt' \tag{1.44}$$

donde u es la velocidad de crecimiento cristalino de los núcleos. En condiciones de T_L=cte y suponiendo que u y J también son constantes, esta integral da:

$$\phi = \frac{\pi}{3} J u^3 \tau^4. \tag{1.45}$$

Esta expresión fue propuesta por Avrami, Mehl, Johnson y Kolgomorov a finales de los años 30 de manera independiente pero simultánea[11–13] y ha sido ampliamente aplicada en

problemas de metalurgia[14,15]. A partir de la Ecuación 1.45 podemos calcular el tiempo τ necesario para cristalizar un fracción de volumen del sistema si conocemos la velocidad de crecimiento u y J. La funcionalidad de u respecto al subenfriamiento no es monotónica, a medida que nos alejamos de la línea de coexistencia aumenta hasta llegar a un máximo, donde a partir de él disminuye. Esto se debe a que hay una competición entre dos factores, la fuerza motriz para pasar de una fase metaestable a la estable $\Delta\mu$ y la disminución de la difusión de las moléculas debida al descenso de T. Este hecho produce que la funcionalidad de τ tampoco sea monotónica sufriendo en primer lugar un descenso a medida que bajamos la temperatura hasta llegar a un mínimo a partir del cual vuelve a crecer según seguimos enfriando. El comportamiento no monotónico de τ, se debe a la competición entre la fuerza motriz termodinámica que favorece la nucleación en contraposición a la cinética del crecimiento cristalino.

En la Figura 1.3 se muestra un ejemplo de una curva del tiempo necesario para cristalizar una fracción del sistema en función del subenfriamiento. Como se puede observar la curva alcanza un mínimo a partir del cual se vuelve a incrementar el tiempo necesario para cristalizar un porcentaje del sistema.

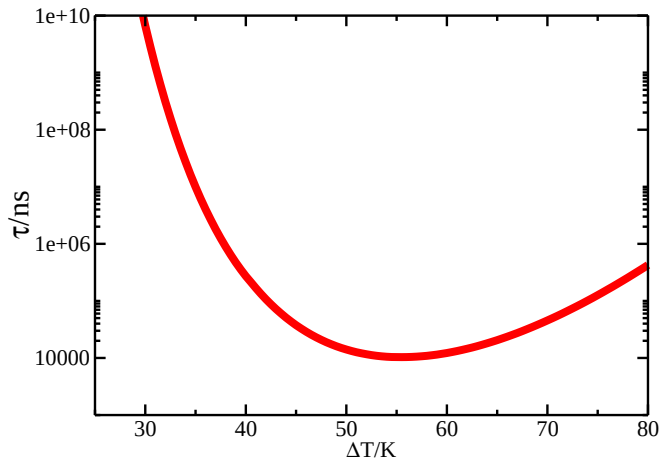

Figura 1.3: Tiempo requerido para cristalizar un porcentaje del 70 % de una muestra de agua en función del subenfriamiento $\Delta T/K$, el cual se define como $T_f - T$. Esta curva ha sido calculada para el modelo TIP4P/Ice[16]. Para más detalles consultar la Referencia[17].

Una vez descritas las principales ecuaciones de la Teoría Clásica de Nucleación para caracterizar este fenómeno así como la Ley de Avrami que nos relaciona la tasa de nucleación y la velocidad de crecimiento cristalina para obtener el tiempo necesario para observar cristalización, vamos a describir las técnicas de simulación que se han empleado durante esta tesis doctoral para la obtención de la mayoría de resultados.

1.4. Técnicas de simulación para estudiar la nucleación

La simulación molecular es una herramienta extremadamente útil que es capaz de explicar procesos macroscópicos permitiendonos entender los mecanismos microscópicos que los generan.

En el caso concreto de la nucleación, la simulación es una herramienta especialmente útil dado el pequeño tamaño de los núcleos que aparecen, que suelen ser del orden de los nanometros, y de su escasa duración, que es del orden de los nanosegundos. Estas dos escalas de tamaños y tiempos se adaptan muy bien a los volúmenes y tiempos accesibles en simulación.

Aunque por otro lado, como la nucleación es un proceso activado en el cual se necesita sobrepasar una barrera de energía libre, cuando el grado de sobresaturación no es muy elevado, a menudo el tiempo necesario para observar la formación de un núcleo de manera espontánea en un volumen típico de simulación es inaccesible.

Esto provoca que para poder estudiar la nucleación se necesitan usar técnicas de eventos raros que nos permiten observar la formación de los núcleos en ventanas de tiempo accesibles desde el punto de vista computacional.

Algunas de estas técnicas han sido muy utilizadas en las dos últimas décadas para el cálculo tanto de barreras como de tasas de nucleación. Algunos ejemplos de estas técnicas son Umbrella Sampling (US)[18–21], Forward Flux Sampling (FFS)[22–26] , Metadynamics[27,28] o Transition Path Sampling (TPS)[29–31].

Aunque estos métodos aceleran artificialmente de diferentes maneras la aparición del núcleo de la fase estable, en principio no modifican el verdadero mecanismo del sistema en la cristalización. En contraposición tienen el problema de que son técnicas extremadamente costosas desde un punto de vista computacional y que restringe la mayoría de los estudios a fluidos altamente metaestables donde el tamaño de los núcleos son pequeños (del orden de 100-150 partículas) y las barreras de nucleación también (del orden de 30-40 k_BT). Esto impide que se pueda hacer una comparación en las mismas condiciones termodinámicas entre tasas halladas por simulación y mediante experimentos, lo cuales típicamente se realizan en condiciones de metaestabilidad más moderada.

Por este motivo en esta tesis doctoral, en vez de emplear estas técnicas de eventos raros ahora mencionadas, hemos utilizado principalmente Seeding[2,32–34], que a pesar de ser aproximada, nos permite evaluar tasas de nucleación en un amplio intervalo de metaestabilidad pudiendo comparar así tanto con experimentos como con resultados de otras técnicas de simulación en sus regiones correspondientes. También en esta tesis se han utilizado otras técnicas como Lattice Mold[35] y puntualmente Umbrella Sampling. En las siguientes secciones procederemos a explicar en que consisten.

1.4.1. Seeding method

El "Seeding" [2,32–34] ha sido la piedra angular de esta tesis, y es la técnica que se ha utilizado generalmente para evaluar tasas de nucleación, barreras de nucleación y energías interfaciales para muchos sistemas (Esferas duras, Lennard-Jones, NaCl, agua y disoluciones acuosas de NaCl) en un amplio rango de condiciones.

Esta técnica consiste en insertar un clúster de la fase estable en el seno de la fase metaestable y determinar qué condiciones termodinámicas hacen que este clúster sea crítico. En la Figura 1.4 se muestra una configuración donde se puede observar un clúster cristalino de la fase estable embebido en la fase metaestable para así ilustrar gráficamente en que consiste esta técnica.

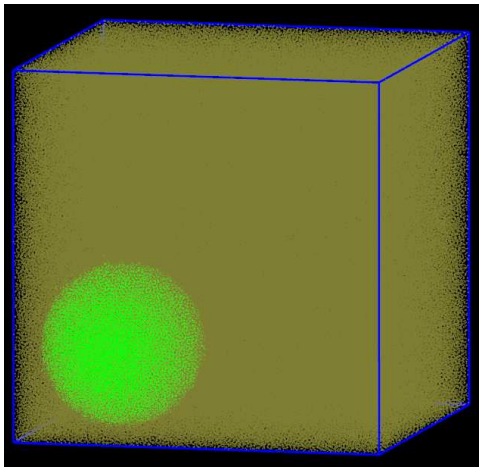

Figura 1.4: Cluster cristalino insertado de $\sim$ 40000 esferas duras (HS) en un fluido sobrepresurizado de un millón de esferas duras empleado para realizar un cálculo de Seeding de HS perteneciente a la Ref.[34]

El Seeding es un técnica basada en la CNT que nos permite calcular los parámetros necesarios de la Ec. 1.43 para hallar J mediante simulación. En primer lugar, mediante simulación vamos a calcular el número de partículas del núcleo crítico N_S^* y en qué condiciones de metaestabilidad (T_L y p_L) éste es crítico. Conociendo las condiciones de p y T que hacen el clúster crítico y el diagrama de fases de nuestro sistema podemos evaluar mediante simulación utilizando integración termodinámica el valor de $\Delta\mu$ para esas condiciones y así estimar la barrera y la energía interfacial mediante las Ec. 1.28 y 1.30. También por simulación se va a estimar la frecuencia con la que nuevas partículas se adhieren al clúster crítico en el máximo de la barrera, k_{+,N_S^*}, lo cual lo vamos a hacer mediante la Ec. 1.13 como anteriormente ha sido descrito. Para el cálculo del factor de Zeldovich, vamos a utilizar la expresión 1.42 que también va a depender de N_S^* y

de $\Delta\mu$. Y por último evaluaremos la densidad del fluido metaestable en la condiciones termodinámicas en las que el clúster insertado ha sido crítico.

Una vez habiendo calculado estos parámetros por simulación para un tamaño de clúster, si este mismo procedimiento lo realizamos para otros tamaños de clúster, podemos medir la dependencia de los factores que acabamos de mencionar a lo largo de la supersaturación, y por tanto evaluar J (véase Figura 1.5) para un amplio rango de metaestabilidad y también otros parámetros termodinámicos de gran relevancia en la nucleación como es la energía interfacial (Figura 1.6).

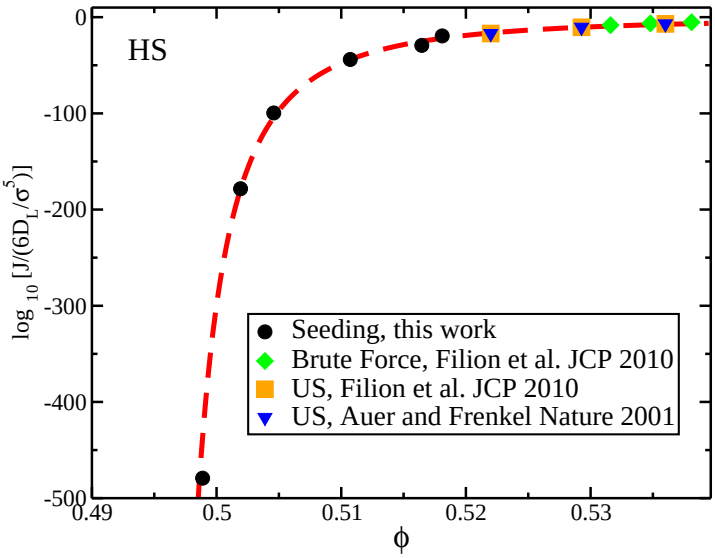

Figura 1.5: Curva de nucleación estimada para esferas duras (línea roja discontinua) mediante un ajuste Seeding+CNT, los círculos negros son las tasas calculadas por medio del Seeding y los demás símbolos representan cálculos independendientes mediante otras técnicas indicadas en la leyenda. Figura tomada de la Ref.[34].

Es importante comentar que el Seeding es una técnica aproximada porque sus resultados dependen del parametro de orden local (ver Apéndice) que se utiliza para determinar el número de partículas/moléculas del clúster insertado y esto tiene una cierta arbitrariedad a la hora de etiquetar las partículas/moléculas de la interfase. No obstante, siguiendo un criterio que denominamos "mislabelling"[34,36,37] (descrito en detalle en los capítulos 2 y 5 y en el Apéndice) se pueden optimizar los parámetros de orden[38] para obtener un etiquetado equitativo tanto de las partículas/moléculas del sólido como las del líquido. Este criterio en todos los casos en los que se ha aplicado Seeding ha funcionado correctamente dando tasas de nucleación en buena concordancia con las evaluadas mediante otras técnicas independientes. Además, cuanto mayor sean los tamaños de clúster insertados, la proporción de las moléculas de la interfase respecto a las del

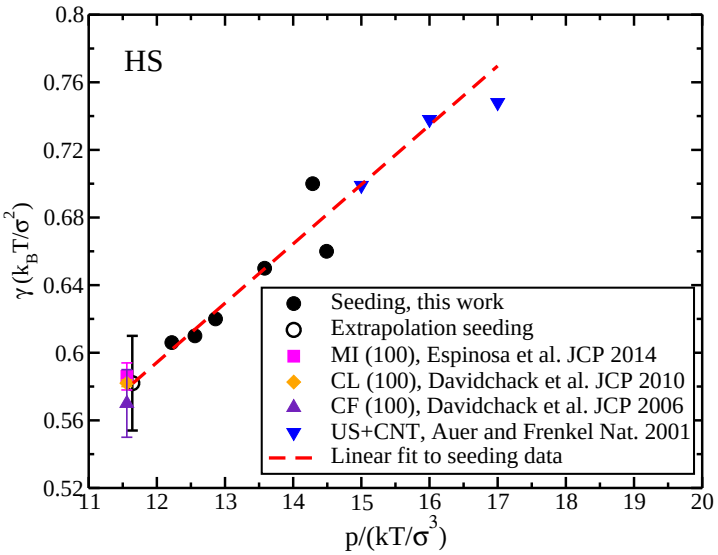

Figura 1.6: Energía libre interfacial estimada para esferas duras (línea roja discontinua) mediante un ajuste Seeding+CNT, los círculos negros representan los valores obtenidos para los diferentes clústeres insertados y los restantes símbolos son los valores hallados por diferentes técnicas independientes indicadas en la leyenda. Figura tomada de la Ref.[34].

interior baja y eso reduce considerablemente la arbitrariedad de esta técnica introducida por el parámetro de orden.

1.4.2. Lattice Mold technique

La siguiente técnica que vamos a describir es una técnica también desarrollada durante este periodo predoctoral por la cual se pueden estimar tasas de nucleación sin necesidad de recurrir a parámetros de orden locales ni a la CNT. Esta técnica se llama Lattice Mold[35] (LM) y se basa en una idea muy similar a la de Mold Integration (técnica para evaluar γ que posteriormente describiremos en la sección 1.5.1)

La idea principal del método se esquematiza en la figura 1.7 y consiste en usar un molde con las posiciones de red de la fase cristalina estable para provocar la cristalización del fluido metaestable. La formación del clúster se ve inducida por el molde cristalino de pozos de energía potencial. Cuando la interacción pozo-partícula del molde está apagada las partículas no sienten la presencia del molde, por el contrario cuando activamos la interacción pozo-partícula, las partículas se introducen dentro los pozos del molde dando lugar a un clúster cristalino.

Si gradualmente vamos encendiendo la interacción del molde con las partículas,

podemos calcular el trabajo reversible de formación del clúster ΔG. La probabilidad por unidad de volumen de encontrar un clúster cristalino tal como se ha generado en el fluido por medio del molde será:

$$P = \rho_f e^{-\Delta G/(k_b T)} \tag{1.46}$$

donde ρ_f representa la densidad del fluido.

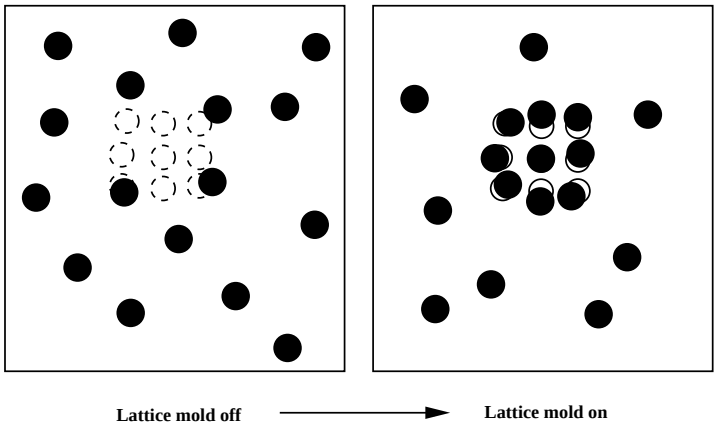

Figura 1.7: Representación esquemática de cómo un molde con la estructura cristalina de la fase estable (círculos vacíos) puede inducir la formación de un clúster cristalino.

Para que esta relación se cumpla es estrictamente necesario que la formación del clúster sea reversible, es decir, que sea pre-crítico. Para ello, hemos de utilizar un molde que posea un número de pozos y una anchura de pozo que no haga que el sistema cruce inmediatamente la barrera de nucleación.

Si cuando encendemos el molde cristalino, al sistema le lleva un cierto periodo de inducción cruzar la barrera de nucleación y cristalizar por completo eso significa que nuestro clúster es pre-crítico. En esas condiciones, si medimos el tiempo promedio $< t >$ que le lleva al sistema cruzar la barrera una vez que el molde está encendido, lanzando varias simulaciones de una misma configuración inicial con el clúster formado pero con diferentes velocidades iniciales en las partículas, podemos evaluar $< t >$ y mediante la siguiente fórmula 1.47, J, la tasa de nucleación:

$$J = P/ < t > . \tag{1.47}$$

En la figura 1.8 se muestran los tres estados de esferas duras para los que se evaluó la tasa de nucleación usando LM. Como se puede observar, para los tres estados en los que se midió J, se obtuvieron resultados coherentes con los procedentes de otras técnicas independientes.

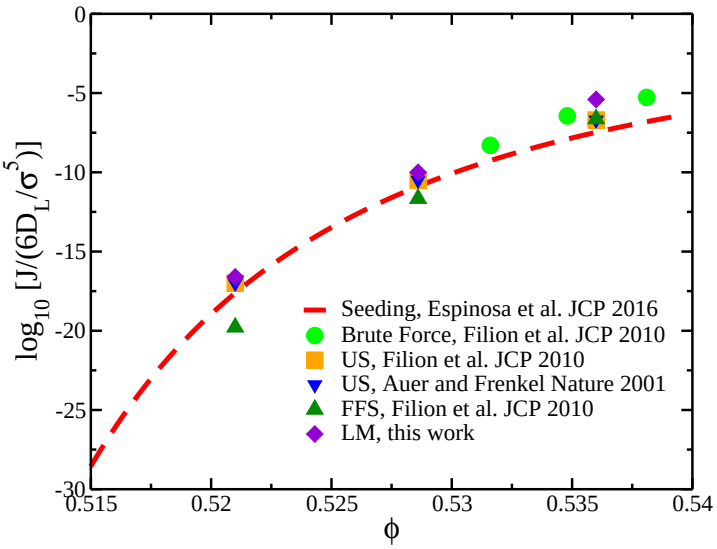

Figura 1.8: Tasa de nucleación de esferas duras en función de la fracción empaquetamiento ϕ evaluada mediante diferentes técnicas como se indica en la leyenda. Los rombos morados representan los valores hallados por Lattice Mold. Esta figura pertenece a la Ref.[35].

En el capítulo dedicado a esta técnica (Cap. 9), se darán más detalles sobre cómo implementarla y se validará para dos sistemas arquetipo diferentes, esferas duras y cloruro sódico.

1.4.3. Umbrella Sampling

La técnica de Umbrella Sampling ha sido ampliamente utilizada para estudiar la nucleación por simulación[18–21] en las últimas dos décadas. Esta técnica se inspira en la Teoría Clásica de Nucleación (solo en el enfoque cinético, dado que la parte termodinámica se evalua rigurosamente sin recurrir a la formulación de Gibbs) y permite evaluar tanto barreras como tasas de nucleación. En primer lugar nos vamos a centrar en el cálculo de la barrera de energía libre por simulación.

Dado que los clústeres sólidos están a bajas concentraciones podemos considerar que éstos forman una mezcla ideal en la que no interaccionan. El potencial químico de una especie con N_S moléculas en dicha mezcla a presión p_L, $\mu_{N_S}(p_L)$, viene dado por la expresión del potencial químico de un gas en una mezcla de gases ideales:

$$\mu_{N_S}(p_L) = \mu^*_{N_S}(p_L) + k_B T \ln(x_{N_S}) \tag{1.48}$$

donde $\mu^*_{N_S}(p_L)$ es el potencial químico del gas puro a la presión de la mezcla (un gas de

clústeres con N_s moléculas en este caso) y x_{N_S} es la fracción molar de clústeres con N_S moléculas.

Imaginemos ahora que convertimos, a presión p_L, el sistema de monómeros puros en un sistema puro de clústeres con N_S moléculas. El trabajo o barrera de energía libre de Gibbs por clúster de N_S moléculas formado será:

$$\Delta G(N_S) = \mu^*_{N_S}(p_L) - N_S\mu^*_{N_1}(p_L) \tag{1.49}$$

donde $\mu^*_{N_1}(p_L)$ es el potencial químico de un sistema de monómeros puros, que es igual al potencial químico de monómeros en la mezcla, $\mu_{N_1}(p_L)$, dado que la fracción molar de monómeros es prácticamente 1. Restando $\mu^*_{N_S}(p_L)$ y $N_S\mu_{N_1}(p_L)$ tenemos:

$$\Delta G(N_S) = \mu_{N_S}(p_L) - k_BT\ln(x_{N_S}) - N_S\mu_{N_1}(p_L) \tag{1.50}$$

Dado que todas las especies en la mezcla están en equilibrio entre sí, el potencial químico de un clúster con N_S moléculas es N_S veces el de un monómero, por lo que el primer y el tercer término del miembro de la derecha en la expresión de arriba se anulan:

$$\Delta G(N_S) = -k_BT\ln(x_{N_S}) \tag{1.51}$$

La fracción molar de clústeres con N_S partículas es el número de dichos clústeres, n_{N_S}, dividido por el número de todas las especies, que se puede aproximar por el número de monómeros, n_{N_1}:

$$\Delta G(N_S) = -k_BT\ln\left(\frac{n_{N_S}}{n_{N_1}}\right) \tag{1.52}$$

Esta expresión nos proporciona la barrera de energía libre mediante simulación para un primer tramo de la barrera. A partir de simulaciones NpT de fuerza bruta se pueden evaluar las probabilidades de tener diferentes tamaños de núcleos espontáneamente en el sistema. Pero de manera espontánea solo es posible estimar la altura de barrera $\Delta G(N_S)$ hasta un cierto tamaño de núcleo (N_S^{ref}). Más allá de éste tamaño para calcular la barrera necesitamos recurrir a la técnica Umbrella Sampling [18–21] porque la probabilidad de tener núcleos más grandes que N_S^{ref} es muy baja como para evaluarla mediante una simulación estándar. Cuando un núcleo $N_S > N_S^{ref}$ es muy probable que este sea el más grande de todo el sistema N_S^b. Con este técnica vamos a sesgar el muestreo de configuraciones que contienen un clúster de tamaño N_S^b entorno a un tamaño de clúster que fijaremos como N_S^0. Esto se consigue añadiendo un término harmónico a nuestro potencial de la siguiente forma:

$$\omega[N_S^b(r^n), N_S^0] = \frac{1}{2}k[N_S^b(r^n) - N_S^0]^2, \tag{1.53}$$

donde $N_S^b(r^n)$ es el número de partículas del núcleo más grande de nuestro sistema, el cual depende de las coordenadas de todas las partículas r^n, y k y N_S^0 controlan la

anchura y el tamaño en torno al cual centramos nuestro muestreo respectivamente. La energía libre a partir de estas simulaciones se extrae de la siguiente manera,

$$\beta\Delta G(N_S^b) = -ln\langle\frac{\delta(N_S^b(r^n) - N_S^0)}{e^{-\beta\omega[N_S^b(r^n),N_S^0]}}\rangle + constante \tag{1.54}$$

donde β es $1/k_BT_L$ siendo k_B la constante de Boltzmann y T_L la temperatura del sistema. Así de este modo, mediante simulaciones de US podemos hallar $\Delta G(N_S^b)$ más una constante para diferentes intervalos de N_S^0. Juntando los diferentes intervalos desde N_S^{ref} hasta el tamaño del clúster crítico N_S^* podemos reconstruir la segunda parte de la barrera $\Delta G(N_S^b)$ calculada mendiante US. Combinando el primer tramo estimado mediante la Ec. 1.52 a partir de una simulación de fuerza bruta junto con el segundo tramo, evaluado mediante US, se obtiene todo el perfil de energía libre de la formación de un núcleo en función del número de partículas que lo componen.

Para calcular la barrera mediante esta técnica necesitaremos un parámetro de orden local[38] que nos evalue el clúster más grande de nuestro sistema, que va a ser nuestra coordenada de reacción. En el caso de US, la elección del parámetro de orden local para evaluar el número de partículas del clúster no influye en la altura de la barrera que se obtiene, como sí sucede en el caso del Seeding. En la Figura 1.9 se muestra cómo en función del criterio utilizado para separar las partículas con entorno tipo-líquido de las tipo-sólido (ξ_c), el tamaño del núcleo crítico varía sensiblemente pero no así la barrera de nucleación obtenida mediante US.

En el Apéndice se describirán los dos parámetros de orden local utilizados durante esta tesis doctoral para distinguir entre partículas tipo-sólido y tipo-líquido para evaluar el número de partículas de los clústeres en nuestros sistemas.

Una vez hemos hallado mediante simulación $\Delta G(N_S)$, podemos hallar facilmente $\Delta G''(N_S)$ y por lo tanto así el factor de Zeldovich mediante la Ec. 1.11. De modo que el último término necesario para calcular el pre-factor cinético κ y la tasa J mediante la Ec. 1.14 es k_{+,N_S^*}, que se calcula siguiendo la fórmula propuesta por Auer y Frenkel[10] como un coeficiente difusivo del número de partículas del clúster crítico en el máximo de la barrera en función de t, cuya expresión se da en la Ec. 1.13.

1.5. Técnicas de simulación para evaluar energías libres interfaciales

Experimentalmente medir energías interfaciales para interfases líquido-cristal es muy complejo, incluso para un caso tan común como la del hielo con el agua líquida todavía hay muchas discrepencias entre las medidas procedentes de diferentes grupos experimentales[39]. La simulación molecular puede ser de gran ayuda en este aspecto.

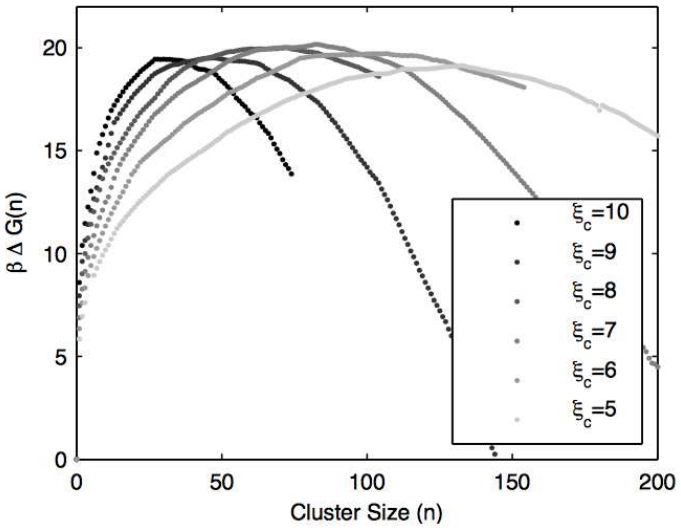

Figura 1.9: Barreras de nucleación en función del número de partículas del clúster más grande estimadas mediante US para el estado termodinámico $p* = 17$ de esferas duras. Aunque las barreras han sido evaluadas con diferentes criterios para separar las partículas del sólido de las del líquido, ξ_c, aproximadamente todas ellas conducen al mismo resultado para $\beta\Delta G(N_S^*)$. Esta figura ha sido tomada de la Ref.[25] para ejemplificar este hecho.

Aunque no es una tarea sencilla evaluar la tensión interfacial entre un sólido y un líquido tampoco por simulación, existen diferentes metodologías en la literatura que permiten calcular γ en condiciones de coexistencia. Algunas de ellas son Cleaving Method[40], Capillary Wave Fluctuations[41], Tethered MonteCarlo[42] y Metadynamics[27]. Aunque todas estas metodologías han permitido evaluar γ mediante diferentes rutas termodinámicas en muchos sistemas[27,43–46], no todas son igualmente buenas en términos de precisión, simplicidad y coste computacional. Generalmente todas estas técnicas son bastantes complejas de implementar y conllevan un coste computacional muy elevado. Es por tanto, por lo que durante este trabajo predoctoral, se decidió desarrollar una nueva metodología para evaluar γ de manera sencilla y con una precisión tal que permitiera medir la anisotropía entre los diferentes planos cristalinos de un sólido.

A esta nueva técnica le hemos denominado Mold Integration, y le hemos utilizado para evaluar γ para sistemas tales como Esferas Duras, Lennard-Jones, NaCl y agua. Adicionalmente esta técnica nos ha sido de gran utilidad para complementar nuestros estudios de nucleación mediante Seeding, contrastando las predicciones del Seeding para la energía interfacial a coexistencia con los valores hallados mediante esta técnica independiente, que no depende de parámetros de orden ni está basada en la CNT. A pesar

de que este técnica se describe en detalle en capítulos posteriores (III y VI), vamos a dar en la siguiente sección una ligera descripción de la idea principal en la que se basa.

1.5.1. Mold Integration

Esta técnica se propuso en el 2014 en la Ref.[47] y permite calcular energías interfaciales cristal-fluido γ en condiciones de coexistencia termodinámica entre ambas fases. La idea principal de la metodología consiste en inducir de manera reversible la formación de una fina capa cristalina en un fluido (como se esquematiza en la figura 1.10).

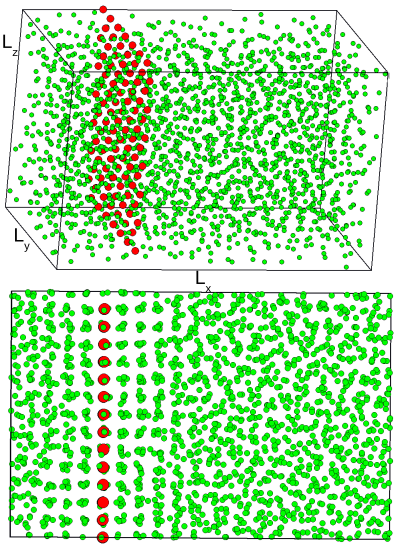

Figura 1.10: Parte superior: instantánea de una configuración de un fluido de esferas duras a coexistencia (partículas verdes). Parte inferior: instantánea de un fluido que contiene una fina capa cristalina en condiciones de coexistencia también. El diámetro de las partículas verdes ha sido reducido a 1/4 de su tamaño original para mejorar la visualización. El molde que induce la formación de la capa cristalina está formado por un conjunto de pozos de energía potencial (esferas rojas) cuyas posiciones son las posiciones de red de un plano cristalino de un cristal en condiciones de coexistencia. La interacción entre el molde y las partículas está apagada en la configuración de la parte superior y encendida en la de abajo.

El trabajo necesario para generar la capa cristalina ΔG^s está relacionado únicamente con γ porque al formarse en condiciones de coexistencia el potencial químico entre el fluido y el cristal es el mismo. Un esquema del perfil de energía libre que separa el líquido del sólido se muestra en la Figura 1.11.

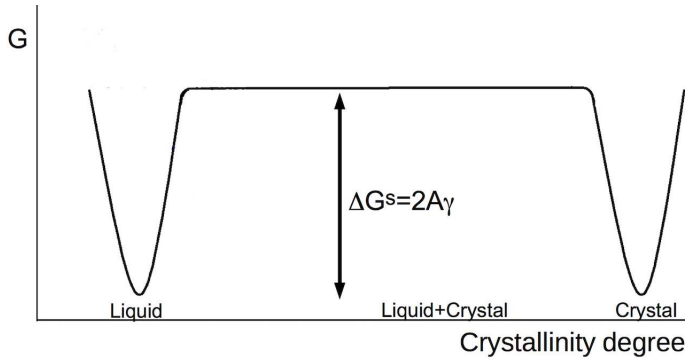

Figura 1.11: Esquema del perfil de energía libre que conecta el sólido y el líquido a través del grado de cristalinidad en condiciones de coexistencia. El perfil de energía libre es plano porque las dos fases poseen el mismo potencial químico y porque además estamos considerando que el área de contacto entre las dos fases permanece contante, como sucede en la técnica de Mold Integration.

Como la capa cristalina que vamos a inducir expone dos interfases a la fase fluida, ΔG^s será simplemente la energía interfacial por el área de las dos interfases en contacto con el fluido:

$$\gamma = \frac{\Delta G^s}{2A}. \tag{1.55}$$

Para inducir la formación de la capa cristalina vamos a utilizar un molde compuesto por pozos de energía potencial. Las posiciones de estos pozos vienen dadas por las posiciones de las partículas de un plano cristalino en las condiciones termodinámicas de coexistencia con el fluido. Cuando el molde está apagado (es decir, cuando en el potencial de interacción del sistema no se incluyen términos pozo-partícula), las partículas del fluido difunden libremente y no sienten la presencia del molde (ver figura superior 1.10). Por el contrario, cuando el molde se enciende (es decir cuando se incluyen en el sistema interacciones pozo-partícula), cada pozo del molde contendrá una partícula y si los pozos son suficientemente estrechos se formará la capa cristalina (ver figura inferior 1.10).

De modo que si encendemos gradualmente la interacción entre el molde y las partículas y formamos una capa cristalina de manera reversible, que cuando apagamos el molde se desvanece, podemos obetener el trabajo de formación de la capa por medio de integración termodinámica.

Poder calcular γ en condiciones de coexistencia con un método que no depende de parámetros de orden como es el caso de MI, nos permite comparar con nuestros resultados de Seeding y evaluar la concordancia entre la predicción de la energía interfacial del Seeding a coexistencia y el valor hallado por Mold integration. Como se puede ver en

la Figura 1.6 los resultados de MI (cuadrados rosas) concuerdan tanto con valores procedentes de otras técnicas para interfase plana[48,49] como con los obtenidos por Seeding extrapolados a coexistencia[34].

Esta técnica además permite evaluar la anisotropía cristalina de los diferentes planos dado que su resolución típicamente permite distinguir entre valores razonablemente cercanos de γ. Los detalles técnicos y una descripción en profundidad del método se explicarán más adelante en los capítulos de resultados donde se ha utilizado (Capítulos 3,4 y 6).

Bibliografía

1. Chaikin, P. M. & Lubensky, T. C., *Principles of Condensed Matter Physics* (Cambridge University Press, 1995).

2. Sanz, E., Vega, C., Espinosa, J. R., Caballero-Bernal, R., Abascal, J. L. F. & Valeriani, C., Homogeneous ice nucleation at moderate supercooling from molecular simulation. *Journal of the American Chemical Society* **135**, 15008–15017 (2013).

3. Volmer, M. & Weber, A., Keimbildung in ubersattigten gebilden. *Z. Phys. Chem.* **119**, 277 (1926).

4. Becker, R. & Doring, W., Kinetische behandlung der keimbildung in ubersattigten dampfen. *Ann. Phys.* **416**, 719–752 (1935).

5. Gibbs, J. W., On the equilibrium of heterogeneous substances. *Trans. Connect. Acad. Sci.* **3**, 108–248 (1876).

6. Gibbs, J. W., On the equilibrium of heterogeneous substances. *Trans. Connect. Acad. Sci.* **16**, 343–524 (1878).

7. Turnbull, D. & Fisher, J. C., Rate of nucleation in condensed systems. *The Journal of Chemical Physics* **17**, 71–73 (1949).

8. Oxtoby, D. W., Homogeneous nucleation: theory and experiment. *J. Phys.:Condens. Matter* **4**, 7627 (1992).

9. Zeldovich, J., On the theory of new phase formation, cavitation. *acta physicochimica urss* **18**, 1–22 (1943).

10. Auer, S. & Frenkel, D., Numerical prediction of absolute crystallization rates in hard-sphere colloids. *J. Chem. Phys.* **120**, 3015–3029 (2004).

11. Avrami, M. *J. Chem. Phys* **7**, 1103 (1939).

12. Johnson, W. A. & Mehl, P. A. *Trans. Am. Inst. Mining and Metallurgical Engineers* **135**, 416 (1939).

13. Kolgomorov, A. N. *Bull. Acad. Sci. USSR, Phys. Ser.* **1**, 355 (1937).

14. Turnbull, D., Kinetics of solidification of supercooled liquid mercury droplets. *J. Chem. Phys.* **20**, 411 (1952).

15. Rappaz, M., Modelling of microstructure formation in solidification processes. *International Materials Reviews* **34**, 93–124 (1989).

16. Abascal, J. L. F., Sanz, E., Fernandez, R. G. & Vega, C., A potential model for the study of ices and amorphous water: TIP4P/Ice. *J. Chem. Phys.* **122**, 234511 (2005).

17. Espinosa, J. R., Navarro, C., Sanz, E., Valeriani, C. & Vega, C., On the time required to freeze water. *The Journal of Chemical Physics* **145**, 211922 (2016).

18. Torrie, G. & Valleau, J., Nonphysical sampling distributions in Monte Carlo free-energy estimation: Umbrella sampling. *Journal of Computational Physics* **23**, 187–199 (1977).

19. van Duijneveld, J. S. & Frenkel, D., Computer simulation study of free energy barriers in crystal nucleation. *J. Chem. Phys.* **96**, 4655 (1992).

20. ten Wolde, P. R., Ruiz-Montero, M. J. & Frenkel, D., Numerical calculation of the rate of crystal nucleation in a Lennard-Jones system at moderate undercooling. *J. Chem. Phys.* **104**, 9932 (1996).

21. Auer, S. & Frenkel, D., Prediction of absolute crystal-nucleation rate in hard-sphere colloids. *Nature* **409**, 1020 (2001).

22. Allen, R. J., Warren, P. B. & ten Wolde, P. R., Sampling rare switching events in biochemical networks. *Phys. Rev. Lett.* **94**, 018104 (2005).

23. Valeriani, C., Sanz, E. & Frenkel, D., Rate of homogeneous crystal nucleation in molten NaCl. *J. Chem. Phys.* **122**, 194501 (2005).

24. Sanz, E., Valeriani, C., Frenkel, D. & Dijkstra, M., Evidence for out-of-equilibrium crystal nucleation in suspensions of oppositely charged colloids. *Phys. Rev. Lett.* **99**, 055501 (2007).

25. Filion, L., Hermes, M., Ni, R. & Dijkstra, M., Crystal nucleation of hard spheres using molecular dynamics, umbrella sampling, and forward flux sampling: A comparison of simulation techniques. *J. Chem. Phys.* **133**, 244115 (2010).

26. Haji-Akbari, A. & Debenedetti, P. G., Direct calculation of ice homogeneous nucleation rate for a molecular model of water. *Proceedings of the National Academy of Sciences* **112**, 10582–10588 (2015).

27. Laio, A. & Parrinello, M., Escaping free-energy minima. *Proc. Natl. Acad. Sci.* **99**, 12562 (2002).

28. Trudu, F., Donadio, D. & Parrinello, M., Freezing of a Lennard-Jones fluid: From nucleation to spinodal regime. *Phys. Rev. Lett.* **97**, 105701 (2006).

29. Bolhuis, P. G., Chandler, D., Dellago, C. & Geissler, P. L., Transition path sampling: Throwing ropes over rough mountain passes, in the dark. *Ann. Rev. Physical Chem.* **53**, 291 (2002).

30. Moroni, D., ten Wolde, P. R. & Bolhuis, P. G., Interplay between structure and size in a critical crystal nucleus. *Phys. Rev. Lett.* **94**, 235703 (2005).

31. Lechner, W., Dellago, C. & Bolhuis, P. G., Role of the prestructured surface cloud in crystal nucleation. *Phys. Rev. Lett.* **106**, 085701 (2011).

32. Bai, X. M. & Li, M., Differences between solid superheating and liquid supercooling. *J. Chem. Phys.* **123**, 151102 (2005).

33. Knott, B. C., Molinero, V., Doherty, M. F. & Peters, B., Homogeneous nucleation of methane hydrates: Unrealistic under realistic conditions. *J. Am. Chem. Soc.* **134**, 19544–19547 (2012).

34. Espinosa, J. R., Vega, C., Valeriani, C. & Sanz, E., Seeding approach to crystal nucleation. *J. Chem. Phys.* **144**, 034501 (2016).

35. Espinosa, J. R., Sampedro, P., Valeriani, C., C., V. & E., S., Lattice mold technique for the calculation of crystal nucleation rates. *Faraday Discussions* **195**, 569 (2016).

36. Espinosa, J. R., Sanz, E., Valeriani, C. & Vega, C., Homogeneous ice nucleation evaluated for several water models. *J. Chem. Phys.* **141**, 18C529 (2014).

37. Zaragoza, A., Conde, M. M., Espinosa, J. R., Valeriani, C., Vega, C. & Sanz, E., Competition between ices ih and ic in homogeneous water freezing. *The Journal of Chemical Physics* **143**, 134504 (2015).

38. Lechner, W. & Dellago, C., Accurate determination of crystal structures based on averaged local bond order parameters. *J. Chem. Phys.* **129**, 114707 (2008).

39. Ickes, L., Welti, A., Hoose, C. & Lohmann, U., Classical nucleation theory of homogeneous freezing of water: thermodynamic and kinetic parameters. *Phys. Chem. Chem. Phys.* **17**, 5514–5537 (2015).

40. Broughton, J. Q. & Gilmer, G. H., Molecular dynamics investigation of the crystal–fluid interface. VI. Excess surface free energies of crystal–liquid systems. *J. Chem. Phys.* **84**, 5759–5768 (1986).

41. Hoyt, J. J., Asta, M. & Karma, A., Method for computing the anisotropy of the solid-liquid interfacial free energy. *Phys. Rev. Lett.* **86**, 5530–5533 (2001).

42. Fernandez, L. A., Martin-Mayor, V., Seoane, B. & Verrocchio, P., Equilibrium fluid-solid coexistence of hard spheres. *Phys. Rev. Lett.* **108**, 165701 (2012).

43. Handel, R., Davidchack, R. L., Anwar, J. & Brukhno, A., Direct calculation of solid-liquid interfacial free energy for molecular systems: Tip4p ice-water interface. *Phys. Rev. Lett.* **100**, 036104 (2008).

44. Angioletti-Uberti, S., Ceriotti, M., Lee, P. D. & Finnis, M. W., Solid-liquid interface free energy through metadynamics simulations. *Phys. Rev. B* **81**, 125416 (2010).

45. Benjamin, R. & Horbach, J., Crystal-liquid interfacial free energy via thermodynamic integration. *The Journal of Chemical Physics* **141**, 044715 (2014).

46. Benet, J., MacDowell, L. G. & Sanz, E., A study of the ice-water interface using the TIP4P/2005 water model. *Phys. Chem. Chem. Phys.* **16**, 22159–22166 (2014).

47. Espinosa, J. R., Vega, C. & Sanz, E., The mold integration method for the calculation of the crystal-fluid interfacial free energy from simulations. *J Chem. Phys.* **141**, 134709 (2014).

48. Davidchack, R. L., Morris, J. R. & Laird, B. B., The anisotropic hard-sphere crystal-melt interfacial free energy from fluctuations. *J. Chem. Phys.* **125**, 094710 (2006).

49. Davidchack, R. L. & Laird, B. B., Direct calculation of the hard-sphere crystal /melt interfacial free energy. *Phys. Rev. Lett.* **85**, 4751–4754 (2000).

Parte II

Results

Results: Chapter 1

Homogeneous ice nucleation at moderate supercooling from molecular simulation

E. Sanz, C. Vega, **J. R. Espinosa**, *R. Caballero-Bernal, J. L. F. Abascal and C. Valeriani*

Departamento de Química Física, Facultad de Ciencias Químicas, Universidad Complutense de Madrid, 28040 Madrid, Spain

1.1. Abstract

Among all the freezing transitions, that of water into ice is probably the most relevant to biology, physics, geology or atmospheric science. In this work we investigate homogeneous ice nucleation by means of computer simulations. We evaluate the size of the critical cluster and the nucleation rate for temperatures ranging between 15 K and 35 K below melting. We use the TIP4P/2005 and the TIP4P/Ice water models. Both give similar results when compared at the same temperature difference with the model's melting temperature. The size of the critical cluster varies from ∼8000 molecules (radius= 4 nm) at 15 K below melting to ∼600 molecules (radius= 1,7 nm) at 35 K below melting. We use Classical Nucleation Theory (CNT) to estimate the ice-water interfacial free energy and the nucleation free energy barrier. We obtain an interfacial free energy of 29(3) mN/m from an extrapolation of our results to the melting temperature. This value is in good agreement both with experimental measurements and with previous estimates from computer simulations of TIP4P-like models. Moreover, we obtain estimates of the nucleation rate from simulations of the critical cluster at the barrier top. The values we get for both models agree within statistical error with experimental measurements.

At temperatures higher than 20 K below melting we get nucleation rates slower than the appearance of a critical cluster in all the water of the hydrosphere in the age of the universe. Therefore, our simulations predict that water freezing above this temperature must necessarily be heterogeneous.

1.2. Introduction

When a liquid is cooled below its freezing point it is supposed to freeze. Usually, impurities or the solid boundaries of the liquid provide preferential sites for the formation of the solid phase. However, even in the absence of impurities, small nuclei of the new phase may be formed within the bulk metastable liquid. This mechanism of formation of the solid phase is called homogeneous nucleation.[1,2] Homogeneous nucleation is an activated process since the formation of a critical nucleus requires the surmounting of a free energy barrier. After that, the crystalline nucleus can grow (nucleation-and-growth mechanism). In general, at moderate supercooling, the limiting step is the formation of the critical cluster rather than the crystal growth. The most relevant quantity to characterize nucleation is the nucleation rate, *i.e.* the number of nucleating clusters per unit time and volume.

Water freezing is arguably the most important liquid-to-solid transition. For example, ice formation in atmospheric clouds is a key factor to the global radiation budget and to climate change.[3–5] Water freezing is also a big issue, for instance, in the cryopreservation of cells and tissues.[6] Moreover, ice formation is relevant to microbiology[7], food industry[8,9], materials science[10], geology[11] or physics.[1,12–17]

Despite its great importance, our understanding of water freezing is far from complete. Not even homogeneous nucleation, the simplest conceivable mechanism by which ice can be formed, is fully understood. One of the reasons for this is the need to perform experiments with small droplets (10-100 μm) to avoid heterogeneous nucleation.[18–21] This, and the time that the droplets can be stabilized, sets the order of magnitude that can be probed for the nucleation rate, J. Thus, experimental measurements for $\log_{10}(J/(\mathrm{m}^{-3}\mathrm{s}^{-1}))$ typically range between 4 and and 14 . This corresponds to a temperature window spanning from 239 K to 233 K, the latter often referred to as "homogeneous nucleation temperature".[22] Our knowledge of the nucleation rate outside this temperature window is limited to extrapolations based on CNT. Such extrapolations must be taken with care since the uncertainties in the nucleation rate and the narrow range of temperatures for which J can be measured lead to important differences in the estimated value of the interfacial free energy and/or the kinetic prefactor.[20] Moreover, it has not been possible so far to observe a critical ice nucleus in experiments because critical nuclei are relatively small and short-lived. Therefore, we only have estimates of the critical cluster size based on experimental measurements of J.[12,18,23–26] The purpose

of this paper is to fill these gaps by obtaining the first estimate of the size of the critical cluster and of the nucleation rate at high temperatures which is not entirely based on theoretical extrapolations from measurements at low temperatures. We will make use of computer simulations to achieve these goals.

Computer simulations are a valuable tool to investigate nucleation[27,28] since they provide a microscopic description of the process. It is therefore somehow surprising that the number of simulation studies dealing with ice nucleation is rather small.[29] On the one hand, it has been shown that ice nucleation can occur spontaneously (without the aid of special simulation techniques) when an electric field is applied[30], when crystallization is assisted by a substrate[31,32] or by an interface[33], when coarse-grained models with accelerated dynamics are simulated at high supercoolings,[15,34,35] or when small systems are simulated[36–38]. On the other hand, if nucleation does not happen spontaneously, rare event techniques must be used. The number of such works is limited and the agreement between different groups is not entirely satisfactory. Radhakrishnan and Trout[39,40], Quigley and Rodger[41] and Brukhno et al.[42] determined the free energy barrier for the formation of ice critical clusters with the TIP4P water model at 180 K (50 degrees below the model's melting temperature), but mutually consistent results were not found. Reinhardt and Doye[43] and Li *et al.*[16] evaluated the nucleation rate of the mW model at 55 K below freezing finding a discrepancy of six orders of magnitude. Very recently, Reinhardt *et al.* investigated ice nucleation at moderate supercoolings,[44] to estimate the free energy of formation of small pre-critical clusters. It is almost certain that more ice nucleation studies are on the way and, hopefully, the discrepancies will become smaller.

None of the studies mentioned in the previous paragraph deal with large systems at moderate supercoolings like the present investigation does. By supercooling, ΔT, we mean the difference between the melting temperature and the temperature of interest. Note that the melting temperature of a model does not necessarily coincide with the experimental melting temperature or with the melting temperature of other models. In this work we determine, by means of computer simulations, the size of critical ice clusters and the nucleation rate for ΔT ranging from 15 to 35 K. In this way we provide, for the first time, nucleation rates for ΔT lower than 35 K, where experimental measurements are not currently feasible (CNT based estimates of J can in principle be made for any supercooling but, to the best of our knowledge, there are no such estimates available for $\Delta T < 30K$).[2,12,20] Our simulations predict that for $\Delta T < 20$ K it is impossible that homogeneous ice nucleation takes place. Therefore, ice must necessarily nucleate heterogeneously for supercoolings lower than 20 K. Moreover, we can directly compare our results for the largest studied supercoolings to the experimental measurements. We find, within uncertainty, a good agreement with experimental nucleation rates. We predict that the radius of the critical cluster goes from $\sim$40 Å(8000 molecules) at ΔT *ca.* 15 K to $\sim$17 Å(600 molecules) at ΔT *ca.* 35 K. We also estimate the surface free energy via CNT.

We obtain, in agreement with predictions based on experimental measurements,[12,45,46] that the surface free energy decreases with temperature. An extrapolation of the interfacial free energy to the melting temperature gives a value of ∼29 mN/m, in reasonable agreement with experimental results[47], and with calculations by simulation.[48]

We use two simple, yet realistic, water models; namely TIP4P/2005[49] and TIP4P/Ice[50]. The melting temperature[49,50] and the ability of these models to predict properties of real water has already been well established.[51] The results obtained for both water models are quite similar provided that they are compared at the same ΔT.

1.3. Methodology

To evaluate the size of critical ice clusters we follow a similar approach to that proposed by Bai and Li[52] to calculate the solid-liquid interfacial energy for a Lennard-Jones system. They employ spherical crystal nuclei embedded in the supercooled liquid and determine the temperature at which the solid neither grows nor melts. The key issue of this methodology is that determining the melting temperature of a solid cluster embedded in its corresponding supercooled liquid water is equivalent to the determination of the critical size of the cluster for a certain given temperature. Thus, in a sense, this methodology can be regarded as the extension to nucleation phenomena of the well known direct coexistence technique.[53] A similar method was applied to water by Pereyra et al.[54] They inserted an infinitely long (through periodical boundary conditions) ice cylinder in water and determined the melting temperature of the cylinder. Recently, the approach of Bai and Li has been used to investigate the nucleation of clathrate hydrates.[55,56]

Here we shall implement this methodology to study a three-dimensional spherical ice cluster embedded in supercooled water. This follows closely the experimental situation where the incipient ice embryo is fully immersed into liquid water. Such *brute force* approach requires very large systems (containing up to $2{\times}10^5$ water molecules). However, molecular dynamics simulations can be efficiently parallelised so that it is nowadays possible to deal with such system size. The methodology can then be implemented in a rather straightforward way, and is particularly useful at moderate supercooling, where other techniques (such as umbrella sampling[57,58], Forward Flux Sampling[59] or Transition Path Sampling[60]) may become numerically too expensive.

Once we calculate the critical cluster size we make use of CNT[61–63] in its version for spherical clusters to estimate the surface free energy, γ:

$$\gamma = \left(\frac{3 N_c \rho_s^2 |\Delta\mu|^3}{32\pi} \right)^{1/3} \tag{1.1}$$

where ρ_s is the number density of the solid and $\Delta\mu$ is the chemical potential difference

between the metastable liquid and the solid at the temperature under consideration. This expression allows us to obtain a value for γ associated to each cluster. CNT can also be used to estimate the height of the nucleation free-energy barrier, ΔG_c:

$$\Delta G_c = \frac{16\pi\gamma^3}{3\rho_s^2|\Delta\mu|^2}. \tag{1.2}$$

Once ΔG_c is known, we can use the following CNT-based expression to evaluate the nucleation rate[64]:

$$J = Zf^+\rho_f \exp(-\Delta G_c/(k_B T)) \tag{1.3}$$

where Z is the Zeldovich factor, $Z = \sqrt{(|\Delta G''|_{N_c}/(2\pi k_B T))}$, and f^+ is the attachment rate of particles to the critical cluster. The CNT form of the Zeldovich factor is

$$Z = \sqrt{|\Delta\mu|/(6\pi k_B T N_c)}, \tag{1.4}$$

which can be obtained from our calculations of N_c. We follow Ref. 64 to calculate f^+ as a diffusion coefficient of the cluster at the top of the barrier:

$$f^+ = \frac{< (N(t) - N_c)^2 >}{2t}. \tag{1.5}$$

Therefore, in order to obtain nucleation rates we combine CNT predictions with simulations of the critical clusters.

By using the methodology here described, the nucleation rate of clathrate hydrates has been recently calculated.[56] The validity of this approach relies on the ability of CNT to make good estimates of the free energy barrier from measured values of the critical cluster size. CNT is expected to work well for big critical clusters. We are confident that the cluster sizes we deal with in this work are big enough for CNT to produce meaningful predictions. We discuss why in Sec. 1.6.1.

1.4. Technical details

1.4.1. Simulation details

We carry out NpT GROMACS[65] molecular dynamics simulations (MD) of a system that consists of one spherical ice-Ih cluster surrounded by supercooled water molecules. We use two different rigid non-polarizable models of water: TIP4P/2005[49] and TIP4P/Ice.[50] TIP4P/2005 is a model that provides a quantitative account of many water properties[51,66] including not only the well known thermodynamic anomalies but also the dynamical ones.[67,68] TIP4P/Ice was designed to reproduce the melting temperature,

the densities and the coexistence curves of several ice phases. One of the main differences between the two models is their ice Ih melting temperature at 1 bar: $T_m = 252$ K for TIP4P/2005 and $T_m = 272$ K for TIP4P/Ice. We evaluate long range electrostatic interactions using the smooth Particle Mesh Ewald method[69] and truncate both the LJ and real part of the Coulombic interactions at 9 Å. We preserve the rigid geometry of the water model by using constraints. All simulations are run at the constant pressure of $p = 1$ bar, using an isotropic Parrinello-Rahman barostat[70] and at constant temperature, using the velocity-rescaling thermostat.[71] We set the MD time-step to 3 fs.

1.4.2. Order parameter

To determine the time evolution of the cluster size, we use the rotationally invariant order parameters proposed by Lechner and Dellago, $\bar{q}_i$.[72] In Fig. 2.1 we show the $\bar{q}_4, \bar{q}_6$ values for 5000 molecules of either liquid water, ice Ih or ice Ic at 1 bar and 237 K for TIP4P/2005. The cut-off distance to identify neighbors for the calculation of $\bar{q}_i$ is 3,5 Å between the oxygen atoms. This approximately corresponds to the position of the first minimum of the oxygen-oxygen pair correlation function in the liquid phase.

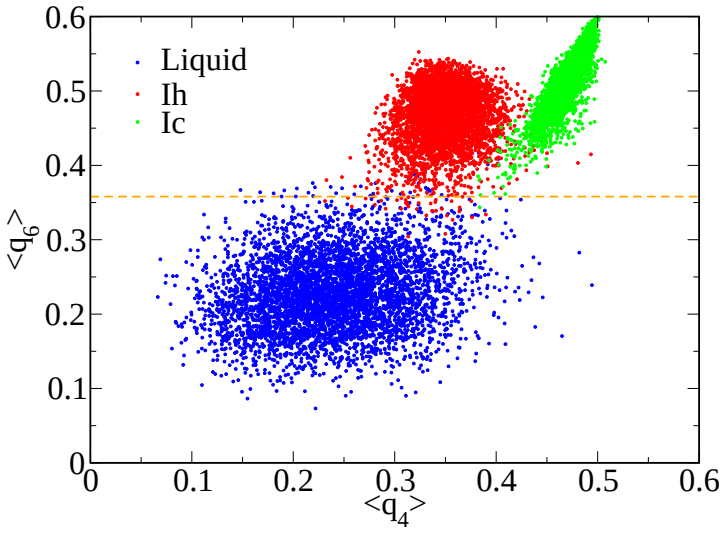

Figure 1.1: Values of $\bar{q}_6$ and $\bar{q}_4$[72] for 5000 molecules of the liquid phase (blue), of ice-Ih (red), and of ice-Ic (green) at 237 K for the TIP4P/2005 model.

From Fig. 2.1 it is clear that $\bar{q}_6$ alone is enough to discriminate between solid-like and fluid-like molecules, as already suggested in Ref. 73. As a threshold to separate the liquid from the solid clouds in Fig. 2.1 we choose $\bar{q}_{6,t} = 0{,}358$, represented as a horizontal dashed line in the figure. This threshold separates the liquid from both ice Ih and Ic. Therefore, even though we prepare the clusters with ice-Ih structure, ice-Ic molecules

would be detected as solid-like should they appear as the clusters grow. Unlike Refs. 74 and 75 we do not consider as solid-like particles on the surface which are neighbor to solid-like particles. Once molecules are labelled either as solid or liquid-like, the solid cluster is found by means of a clustering algorithm that uses a cut-off of 3.5 Å to find neighbors of the same cluster.

1.4.3. Initial configuration

We prepare the initial configuration by inserting a spherical ice-Ih cluster (see Fig. 1.2 for a cluster of 4648 molecules) into a configuration of supercooled water with $\sim$ 20 times as many molecules as the cluster. To obtain the cluster, we simply cut a

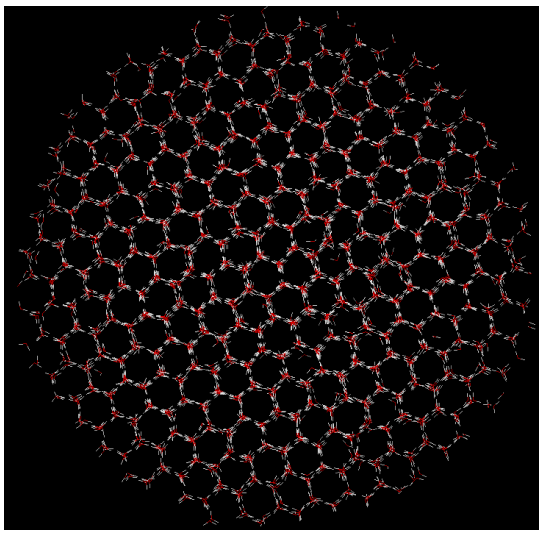

Figure 1.2: Snapshot of a spherical ice-Ih cluster of 4648 molecules.

spherical portion of a large equilibrated ice Ih crystal. Next, we insert the ice cluster in the supercooled liquid removing the liquid molecules that overlap with the cluster. Finally, we equilibrate the system for about 0.2 ns at 200 K. This time is long enough to equilibrate the cluster-liquid interface (see Supporting Information). We then perform simulations for three different system/cluster sizes labeled as H (Huge), L (Large) and B (Big) (see Table 1.1). As far as we are aware, the studied system size are beyond any previous numerical study of ice nucleation. Calculations were performed in the Spanish super-computer Tirant. For system H we use 150 nodes yielding 0.72 ns/day; for system L, 50 nodes at 1.5 ns/day and, for system B, 32 nodes at 4.7 ns/day.

Our order parameter allows us to correctly identify as solid-like the great majority of the molecules belonging to the cluster shown in Fig. 1.2 (4498 out of 4648). Fig. 1.3(a) shows that indeed most molecules of the inserted ice cluster are detected as solid-like

(red) as opposed to liquid-like (blue). Notice that most blue particles in Fig. 1.3(a) are located at the interface. This is not surprising giving that our order parameter was tuned to distinguish between liquid-like and solid-like particles in the bulk. Fig. 1.3(a) corresponds to the cluster *just* inserted in the liquid. After 0.2 ns of equilibration our order parameter detects that the number of molecules in the cluster drops down to 3170. To explain the origin of this drop we show in Fig. 1.3(b) a snapshot of the 4648 inserted molecules after the 0.2 ns equilibration period. Clearly, the drop comes from the fact that the outermost layer of molecules of the inserted cluster becomes liquid-like during equilibration. By removing the liquid-like molecules from Fig. 1.3(b) one can easily identify again the hexagonal channels typical of ice (Fig. 1.3(c)). Therefore, the drop from 4648 to 3170 molecules in the ice cluster is due to the equilibration of the ice-water interface. The size of the equilibrated clusters, N_c, is given in Table 1.1.

Table 1.1: Total number of molecules in the system, N_t (ice cluster + surrounding liquid water molecules) and number of molecules of the inserted spherical ice cluster, N_i for the three configurations prepared. N_c is the number of molecules in the ice cluster after equilibration of the interface. The radius of the equilibrated clusters r_c in Å is also presented.

System	N_t	N_i	N_c^{2005}	N_c^{Ice}	r_c^{2005}	r_c^{Ice}
B	22712	1089	600	600	16.7	16.8
L	76781	4648	3170	3167	29.1	29.2
H	182585	9998	7931	7926	39.5	39.7

Once the interface is equilibrated for 0,2 ns, the number of molecules in the cluster grows or shrinks (depending on the temperature) at a much slower rate (typically requiring several nanoseconds as it is shown in Fig. 1.4). The initial time in our simulations corresponds to the configuration equilibrated after 0.2 ns. We run MD simulations of the system with the equilibrated interface at several temperatures below the bulk melting temperature of the model. The objective is to find a temperature range within which the cluster can be considered to be critical. The temperature range is comprised between the lowest temperature at which the solid cluster melts and the highest at which it grows. We monitor the number of molecules in the cluster and the global potential energy to find whether the cluster melts or grows.

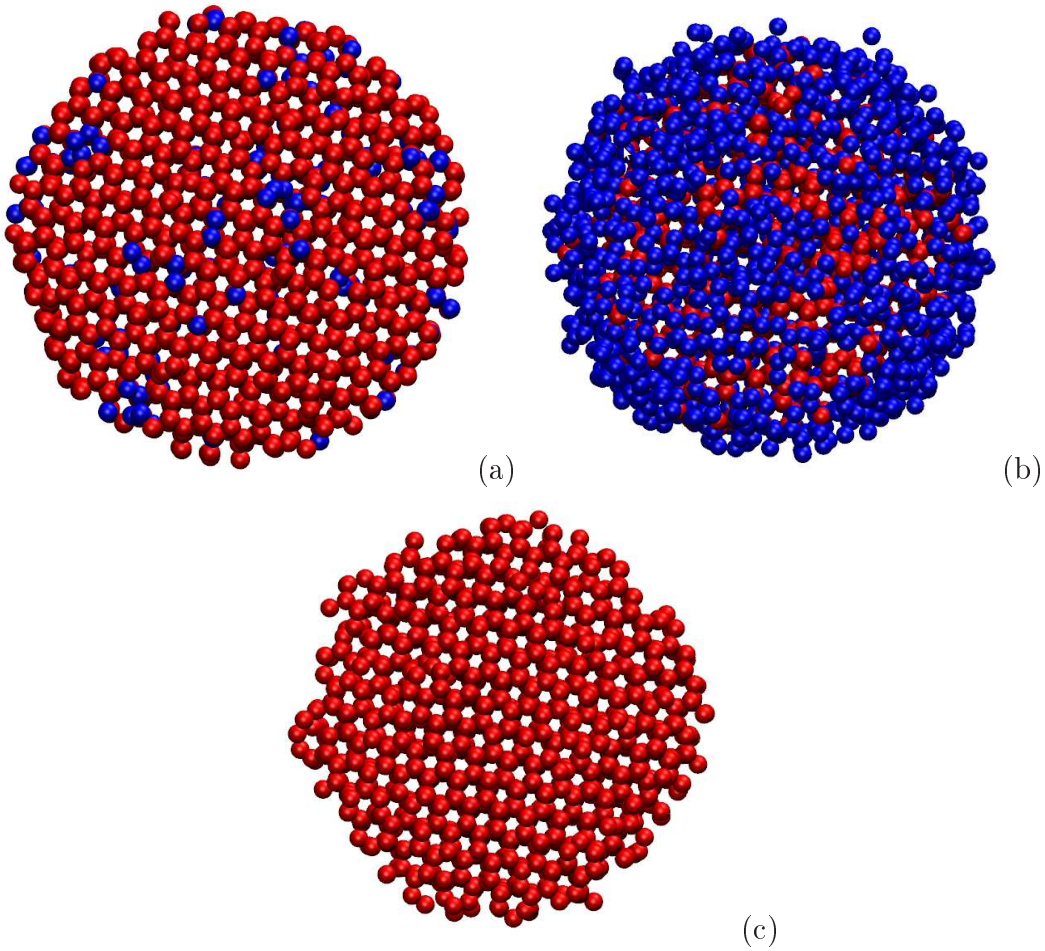

Figure 1.3: Snapshot of the 4648 molecules inserted as an ice cluster just after insertion (a), and after 0.2 ns equilibration (b). Molecules are colored in red if detected as solid-like and in blue if detected as liquid-like. In (c) only solid-like molecules of snapshot (b) are shown.

1.5. Results

1.5.1. Size of the critical clusters

In Fig. 1.4 we represent the number of molecules in the ice cluster versus time for system H, TIP4P/2005. Depending on the temperature the cluster either grows (230 K and 235 K) or shrinks (240 K). The highest temperature at which the cluster grows is 235 K and the lowest temperature at which it melts is 240 K. Hence, a cluster of $\sim$7900 molecules (as detected by our order parameter) is critical at 237,5 $\pm$ 2,5 K. An

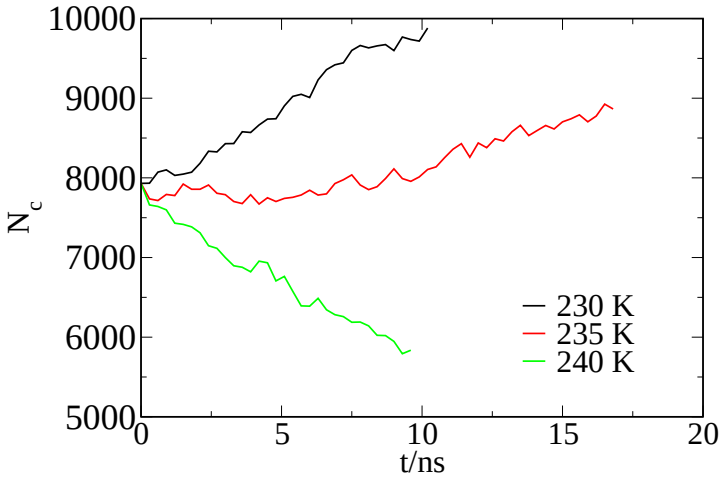

Figure 1.4: Number of molecules in the ice cluster versus time for system H and the TIP4P/2005 potential. Results are shown for different temperatures as indicated in the legend.

analogous result can be obtained by monitoring the potential energy of the system as a function of time. (see Supporting Information). A decrease in the energy corresponds to the cluster's growth whereas an increase in the energy corresponds to its melting. By doing this analysis for both models (TIP4P/2005 and TIP4P/Ice) and for the three cluster sizes (H, L, and B), we obtain the results summarized in Table 1.2.

Table 1.2: We report the temperature (T in K) for which the prepared ice clusters are found to be critical, the supercooling (ΔT in K) for the corresponding water model, the chemical potential difference between the fluid and the solid ($\Delta\mu$ in kcal/mol), the liquid-solid surface free energy (γ in mN/m) estimated from Eq. 4.6, and the nucleation free energy barrier height (ΔG_c in k_BT) estimated from Eq. 7.8.

Model	System	N_c	T	ΔT	$\Delta\mu$	γ	ΔG_c
TIP4P/2005	B	600	222.5	29.5	0.114	20.4	77
TIP4P/2005	L	3170	232.5	19.5	0.080	24.9	275
TIP4P/2005	H	7931	237.5	14.5	0.061	25.9	515
TIP4P/Ice	B	600	237.5	34.5	0.133	23.6	85
TIP4P/Ice	L	3167	252.5	19.5	0.083	25.4	261
TIP4P/Ice	H	7926	257.5	14.5	0.063	26.3	487

For the temperatures explored in this work (from about 15 K to 35 K below the melting temperature of both TIP4P/2005 and TIP4P/Ice) the size of the ice critical cluster ranges from nearly 8000 (radius of 4 nm) to about 600 molecules (radius of 1.7

nm). This compares reasonably well with a critical cluster radius of $\sim$ 1.3 nm obtained by applying CNT to experimental measurements at a supercooling of about 40 K.[25,26] Our results are also consistent with CNT based estimates of the critical size at lower supersaturations.[2,76] For instance, in Fig. 15.7 of Ref.[2], a critical cluster size ranging from 1000 to 300 molecules is predicted for 25 K $< \Delta T <$ 30 K. An interesting remark is that the temperatures of the TIP4P/Ice are basically shifted 20 K above the the corresponding ones for TIP4P/2005 with the same nucleus size. This is precisely the difference between the melting temperatures of both models and, thus, the supercoolings are very similar for a given ice cluster size in both models. This is more clearly shown in Fig. 1.5 where the size of the critical cluster is plotted as a function of the the difference between the melting temperature of the model and the temperature of interest $\Delta T = T_m - T$. We observe that, within our error bar, the critical cluster size of both models scales in the same way with respect to their melting temperatures. This is not so surprising since TIP4P/2005 and TIP4P/Ice present a similar charge distribution and mainly differ in the choice of the potential parameters.

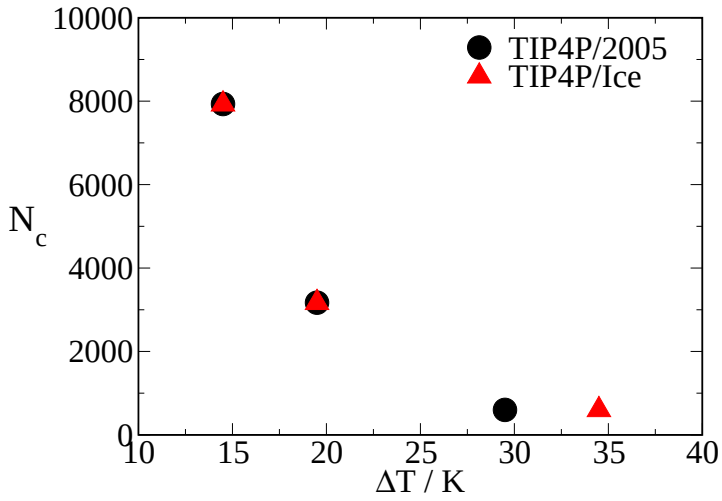

Figure 1.5: Critical cluster size versus ΔT for the studied water models. Notice that the points corresponding to both models at low supercooling are essentially on top of each other.

In previous works[51,66,77] we observed that, for a number of properties, the values of TIP4P/2005 lie in the middle of the values obtained for TIP4P and TIP4P/Ice. Therefore, it is expected that TIP4P gives similar results to TIP4P/2005 and TIP4P/Ice regarding the dependence of N_c with ΔT. Matsumoto et al.[36] studied ice nucleation at 230 K and a density of 0.96 g/cm^3 using the TIP4P model. This thermodynamic state point corresponds to a pressure of about -1000 bar and ΔT 5 K.[78] By extrapolating the data of Fig. 1.5 to $\Delta T = 5K$ one gets a critical cluster of the order of hundreds

of thousand molecules. Therefore, it is likely that the results obtained by Matsumoto et al.[36], although pioneering and useful to learn about the ice nucleation pathway, may suffer from system size effects and may not be valid to estimate either the size of the critical cluster or the nucleation rate.

In an important paper, Koop et al.[79] showed that the homogeneous nucleation rate (and therefore the temperature of homogeneous nucleation) of pure water and of water solutions can be described quite well by a function that depends only on the water activity. This conclusion has been confirmed in more recent experiments.[14] Although the nucleation rate for an aqueous solution is the same as for pure water, the freezing points are different. One is then tempted to suggest that the size of the critical cluster at the homogeneous nucleation temperature could be the same for pure water and for aqueous solutions. Moreover, the fact that thermodynamics is sufficient to predict the rate seems to indicate that the water mobility is also determined by the free energy of water. A microscopic study of the relationship between crystallization rates, structure and thermodynamics of water which may explain the empirical findings of Koop and coworkers has recently been presented in Ref. 15.

1.5.2. Interfacial free energy and free energy barrier

Once the size of the critical cluster is known, one can use Eq. 4.6 to estimate the solid-liquid interfacial free energy. Since ice density changes little with temperature[80], the density at coexistence is used in our calculations ($\rho_{m,TIP4P/Ice}$=0.906 g/cm^3 and $\rho_{m,TIP4P/2005}$=0.921 g/cm^3). For most substances it is possible to approximate $\Delta\mu$ by $\Delta h_m(T_m-T)/T_m$, where Δh_m is the melting enthalpy and T_m is the melting temperature. For water, however, this may not be a good approximation because Δh significantly changes with temperature as a manifestation of the anomalous sharp increase of the heat capacity of water as temperature decreases.[24,81] Hence, one needs to do a proper evaluation of the chemical potential difference between both phases to get the surface free energy from Eq. 4.6. We have calculated $\Delta\mu$ at every temperature by means of standard thermodynamic integration[82] from the coexistence temperature, at which $\Delta\mu = 0$. In Table 1.2 we report the values we obtain for $\Delta\mu$ and γ.

First of all we note that γ decreases with temperature for both models. This is in qualitative agreement with experimental estimates of the behavior of γ with T.[12,45,46] A more quantitative comparison is not possible in view of the large discrepancies between different estimates (see Fig. 10 in Ref. 12). Motivated by the fact that the interfacial free energy can only be measured at coexistence, we extrapolate our results to the melting temperature. To do that, we take the two largest clusters and evaluate the slope of $\gamma(T)$. We get a value for the slope of $\sim$0.18 mN/(m K) for both models, in very good agreement with a recent calculation for the TIP4P/2005 model.[44] With a linear extrapolation we get a value for γ at T_m of $\sim$28.7 mN/m for both models, which can be compared to

experimental measurements. In contrast with the vapor-liquid surface tension, the value of γ for the solid-fluid interface is not well established. Experimental values range from 25 to 35 mN/m.[83] Our calculated data for γ at coexistence lies in the middle of that range, so our models predict a surface free energy which is consistent with current experimental data. We now compare our estimated γ to direct calculations from simulations using a planar interface. The value of γ depends on the plane in contact with the liquid. Since the cluster used here is spherical we shall compare with the average of the values obtained for the basal and prismatic planes. Davidchak et al. computed γ for a planar fluid-solid interface using two models similar to those used in this work: TIP4P and TIP4P-Ew. For TIP4P, in an initial publication the authors reported a value of $\gamma = 23{,}9$ mN/m[84] that was later on modified (after improving their methodology) to $\gamma = 26{,}5$ mN/m.[48] For the TIP4P-Ew[85] Davidchak et al. reported (using the improved methodology) a value of 27,6 mN/m.[48] TIP4P-Ew is known to predict water properties in relatively close agreement to those of TIP4P/2005. Therefore, our results are also consistent with the calculations reported in the literature for similar models. To conclude, our values of γ seem to be reasonable estimates of the interfacial free-energy of the planar ice-water interface.

To estimate the height of the nucleation free-energy barrier we make use of Eq. 7.8. Our results are summarized in Table 1.2. In view of the height of the nucleation barrier for the clusters of systems L and H, around 250 and 500 k_BT respectively, it seems virtually impossible to observe homogeneous nucleation of ice for supercoolings lower than 20 K. The height of the nucleation barrier provides an estimate of the concentration of critical clusters in the metastable fluid as $\rho_f \exp(-\Delta G_c/(k_BT))$, where ρ_f is the number density of the fluid. For $\Delta G_c = 250\ k_BT$, one critical cluster would appear on average in a volume $\sim 10^{60}$ times larger than the volume of the whole hydrosphere. From the values of ΔG_c of Table 1.2 we may infer why spontaneous ice nucleation has never been observed in previous studies of supercooled water with the TIP4P/2005 model[86–88]. Our results show that the free energy barrier for nucleation even for temperatures as low as 35 K below melting is still of about 80 k_BT. This is much larger than the typical barrier found in studies where spontaneous crystallization occurs in brute force simulations[89,90] (about $18k_BT$). It is worth mentioning that neither Shevchuk and Rao[91] nor Overduin and Patey[92] find any evidence of ice nucleation in TIP4P models after runs of several microseconds which is consistent with the results of this work. Our results may be of great interest to studies in which the competition between the crystallization time and the equilibration time of water is crucial[93–95].

1.5.3. Nucleation rate

Although the free energy barriers alone provide a strong indication that ice can not appear on our planet via homogeneous nucleation at moderate supercoolings ($\Delta T <$

20 K), it is worth calculating the nucleation rate, J, to confirm such statement. The nucleation rate takes into account not only the concentration of the clusters but also the speed at which these are formed. Moreover, the supercoolings for the smallest clusters we investigate are comparable to those where most experimental measurements of J have been made ($\Delta T \sim 35$ K).[12–14,17,96]

To calculate the nucleation rate we use Eq. 4.8. First, we compute f^+ from Eq. 4.10 by running 30 simulations of the cluster at the temperature at which it was determined to be critical. We monitor $(N(t) - N_c)^2$ and average it over all the runs. In Fig. 1.6 we plot $< (N(t) - N_c)^2 >$ versus time for the system L, TIP4P/2005. From the slope at long times we can infer f^+.[64] We get $f^+ = 70 \cdot 10^9\ s^{-1}$. The Zeldovich factor for this particular case is $1{,}77 \cdot 10^{-3}$, and the density of the liquid is 0.977 g/cm^3. With this, we have all the ingredients needed to calculate the nucleation rate via Eq. 4.8. The final result for this case is $\log_{10}(J/(\mathrm{m}^{-3}\mathrm{s}^{-1}))$=-83.

The same procedure is used to calculate the nucleation rate for the rest of the systems described in Table 1.1. The results for the nucleation rate as a function of the supercooling are presented in Fig. 9.4 and compared to the experimental measurements of Pruppacher[12] and Taborek[13]. The horizontal dashed line corresponds to the nucleation rate required for the appearance of one critical cluster in the volume of Earth's hydrosphere in the age of the universe, which we call "impossible nucleation rate". The vertical line shows at which temperature the impossible nucleation rate line intercepts the upper limit of our error bars (grey and orange shadows for TIP4P/2005 and TIP4P/Ice respectively). In view of this figure we can confidently claim what the free energy barriers previously hinted: it is impossible that ice nucleates homogeneously in our planet for $\Delta T < 20$ K. In other words, heterogeneous nucleation must take place in order for water to freeze for supercoolings lower than 20 K. This is consistent with the fact that, when heterogeneous nucleation is suppressed, moderately supercooled water can remain metastable long enough for its thermodynamic properties to be measured.[21,22,97–99] From our results it is also clear that ice formation should not be expected in brute force molecular dynamics simulations at moderate supercoolings (provided that the system is large enough not to be affected by finite size effects).[36] To observe ice formation in brute force simulations the nucleation rate should be higher than $\log_{10}(J/(\mathrm{m}^{-3}\mathrm{s}^{-1})) = 32$ (this number is obtained assuming the formation of ice after running about 100 ns in a system of about 50nm^3, which are typical values in computer simulations of supercooled water). Notice also that the maximum in the isothermal compressibility at room pressure[86,87] found at about $\Delta T = 20$ K for the TIP4P/2005 model can not be the ascribed to the transient formation of ice as the nucleation rate of ice at this temperature is negligible.

Another interesting aspect of Fig. 9.4 is the comparison with experiment. Both models give nucleation rates that reproduce the experimental measurements within the uncertainty of our method. This excellent result brings confidence in the ability of the selected models to predict relevant quantities for the nucleation of ice such as the nu-

cleation rate, the critical cluster size, and the surface free energy.

We also include in Fig. 9.4 a green dashed line that corresponds to the CNT based estimates of J shown in Fig. 13.6 of Ref.[2] The agreement between CNT, simulations and experiments is quite satisfactory. To the best of our knowledge, there are no CNT estimates of J available for supersaturations lower than 30 K to compare our results with.[2,12,20]

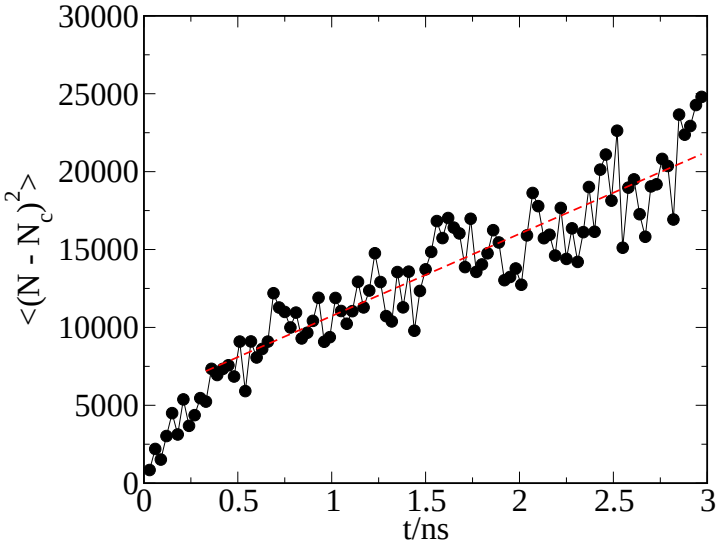

Figure 1.6: $< (N(t) - N_c)^2 >$ versus time for configuration L, TIP4P/2005. The attachment rate f^+ is obtained as half the value of the slope. The curve above is obtained as an average over 30 trajectories. In approximately half of these trajectories the critical cluster ended up growing, whereas it eventually melted in the other half.

By using Forward Flux Sampling[59], Li *et al.* determined J for the mW model of water for temperatures between 35 and 55 K below the model's melting temperature.[16] Since we are interested in ice nucleation at moderate supersaturation, our study deals with lower supercoolings (14,5 K$< \Delta T <$ 34,5 K). Nonetheless, our highest supercooling (34.5 K) is very close to the lowest one of Li *et al.* (35 K) so we can compare both results. The values of Li *et al.* for J are 5-8 orders of magnitude below the experimental ones when compared at the same absolute temperature (the deviation increases when the comparison is made at the same degree of supercooling). The nucleation rates calculated in this work for TIP4P/2005 and TIP4P/ice are similar (although slightly larger) to those for the mW model. Initially this may appear surprising as the mW model is a coarse grained model of water with no hydrogens, which makes its dynamics faster than that of both real water and TIP4P-like models.[100] However the free energy barrier of mW may be larger, compensating this kinetic effect. In fact the interfacial free energy of

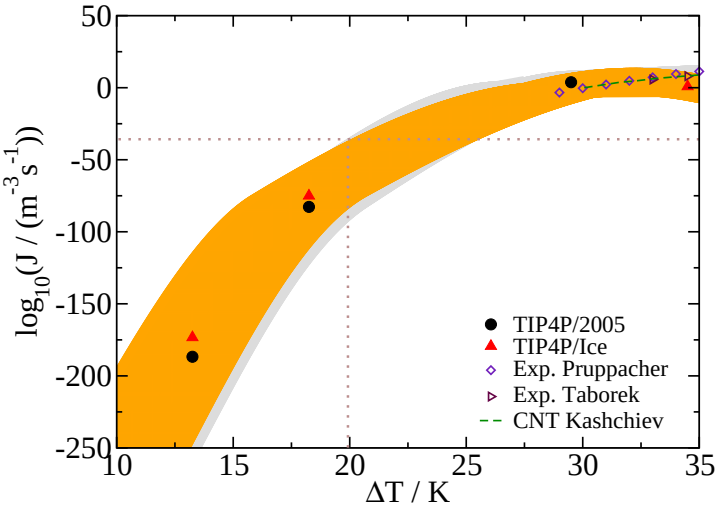

Figure 1.7: Nucleation rate as a function of the supercooling. Symbols correspond to our simulation results and to experimental measurements as indicated in the legend. The green dashed line corresponds to CNT estimates of J.[2] The grey and orange shadows represent the estimated error bars for TIP4P/2005 and TIP4P/Ice respectively interpolated by splines. The horizontal dotted line indicates the rate given by the growth of one cluster in the age of the universe in all the water of the Earth's hydrosphere. The vertical dotted line indicates the supercooling below which homogeneous nucleation is impossible.

mW has been found[16] to be $\gamma = 31$ mN/m (larger than the values found in this work for TIP4P/2005 and TIP4P/Ice). This high value of γ may be partially compensated by a significant overestimate of the ice density of this model (0.978 g/cm^3 to be compared to the experimental result 0.91 g/cm^3). The net balance is that the values of J of the mW model are similar, although somewhat lower, than those for TIP4P/2005 and TIP4P/ice.

As for the size of the critical cluster, we find that it is of about 600 water molecules for TIP4P/Ice at 237.5 K ($\Delta T = 34{,}5$ K). Li *et al.* have reported a critical cluster size of about 850 molecules for the mW model at 240 K ($\Delta T = 35$ K). Both results are compatible since Li *et al.* include in the ice cluster molecules which are neighbor to the solid cluster, and we do not. In summary, our results for TIP4P/2005 and TIP4P/Ice are consistent with Li's *et al.* for mW.

1.6. Discussion

1.6.1. Validity and possible sources of error

The methodology we have used is subject to two main error sources: the determination of the cluster size and the location of the temperature at which the clusters are found to be critical. Moreover, our approach relies on the validity of CNT. In the following paragraphs we discuss the extent to which our results may be affected by these issues.

In nucleation studies, the size of the largest solid cluster is usually considered a good reaction coordinate. To identify the cluster, we first need to distinguish between liquid-like and solid-like molecules. The chosen criterion should be able to identify the majority of molecules of the bulk solid as solid-like, and the majority of molecules of the bulk fluid as liquid-like. One could in principle find several criteria that successfully perform this task. However, when interfaces are present in the system (as in the case of a solid-liquid[89] or a solid-vapor[101,102] interface) depending on the chosen criterion one might assign differently the interfacial molecules (see for instance References 43 and 16 for an illustration of this problem for the mW water model).

How does the choice of a criterion to distinguish liquid from solid-like molecules affect our results? Whether the cluster grows or shrinks for a given temperature does not depend on the particular choice of the order parameter (see Supporting Information). The same trend can be obtained by monitoring global thermodynamic properties of the system, such as the total potential energy (see Supporting Ingormation). Therefore, the fact that the cluster shown in Fig. 1.3 is critical at 232.5 K is independent on the particular choice of the criterion to distinguish liquid from solid-like molecules.

A different problem arises if one asks the question: how many ice molecules are present in Fig.3b? Different criteria provide different answers even though the configuration presented in Fig.3b is unique. Since the origin of this arbitrarity is due to the interfacial region, it is expected that the arbitrarity will become smaller as the ice cluster becomes larger. However, for the system sizes considered in this work the interface region still matters. To take this effect into account we have estimated the error bars in Fig. 9.4 considering an arbitrarity of 60 % in the labeling of *interfacial* molecules. This would affect the value of γ by 7 %, and the free-energy barriers height by up to 20 %. Although this estimated error seems large, it is worth pointing out that differences between the free-energy barrier estimated by different groups may be, in the case of water, much larger than that.[39–42] In summary we conclude that the liquid/solid criterion chosen in this work provides reasonable estimates of γ, and when used within the CNT framework allows to interpret our simulations results in a rather straightforward way.

Another important error source in the calculation of J is the location of the temperature at which a cluster is critical. As we show in Fig. 1.4, by performing runs at

different temperatures we identify, within a certain range, the temperature that makes critical a given ice cluster. We assign the temperature in the middle of the range to the corresponding cluster, but the temperature that really makes the cluster critical could in principle be any other within the range. This uncertainty has a strong contribution to the error bars in Fig 9.4, particularly at low supercoolings, where the variation of J with T is very steep. This error could, in principle, be easier to reduce than that coming from the arbitrarity in the determination of the number of particles in the cluster. One simply has to do more runs to narrow the temperature range. However, these simulations are very expensive given the large system sizes we are dealing with. It is interesting to point out that temperature control is also seen as a major error source in experiments.[17]

Our results for γ, ΔG_c, and J rely on the validity of CNT. Classical Nucleation Theory is expected to break down for small clusters, when the view of nucleation as a competition between bulk and surface free energies starts to be questionable (in clusters of a few hundred particles most molecules are placed at the surface). However, for the large cluster sizes investigated in this work it seems reasonable to assume that CNT works well. The satisfactory comparison of our estimate of γ with that obtained in simulations of a flat interface[48] is certainly encouraging in this respect. Moreover, we have applied the methodology described in this paper to calculate the nucleation rate of the mW water model and we get, within error, the same nucleation rate as in Ref.[16] This is a very stringent test to our approach, given that in Ref[16] a method that relies neither on CNT nor on the definition of the cluster size was used (Forward Flux Sampling). This comparison is made for a supercooling of 35 K, the deepest investigated in this work. For lower supercoolings, where the critical cluster is larger, the methodology is expected to be even more robust. The advantage of the approach used here is that it allows to estimate (at a reasonable computational cost) critical cluster sizes and nucleation rates at low and moderate supercooling.

1.6.2. Novelty

In this paper we provide values for the homogeneous nucleation rate of ice at moderate supercoolings ($\Delta T < 33$ K). For the first time, this is done without extrapolating from measurements at high supercoolings. The experimental determination of J is limited to a narrow temperature window at high supercoolings (between 233 K and 239 K). In that window, J can be directly measured without introducing any type of approximation. It only requires the knowledge of the droplet volume, the cooling rate and the fraction of freezing events. Differences in the value of J between different experimental groups are relatively small (between one and two orders of magnitude). Therefore, the experimental value of J is well established for the narrow range of temperatures in which the current experimental techniques can probe the nucleation rate.[12–14,17,96] To obtain values of J outside that temperature window one can either extrapolate the data or

make an estimate via CNT. An extrapolation from such a narrow temperature window would not be very reliable because J changes sharply with T. In turn, an estimate of J based on CNT relies in the knowledge of the interfacial free energy. Unfortunately, our current knowledge of γ for the water-ice interface is far from satisfactory in at least three respects. Firstly, the calculated values of different groups using CNT differ significantly (see for instance Tables I and II in Ref 20). Secondly, the values obtained for γ from CNT seem to be different from those determined for a planar ice-water interface at the melting point (see for instance Fig. 8 in Ref 103). Finally, there is even no consensus about the value of γ for a planar interface at the melting point of water, a magnitude that in principle could be obtained from direct experiments without invoking CNT (values between 25 and 35 mN/m have been reported). A look to Fig. 10 of the classic paper of Pruppacher[12] is particularly useful. It shows the enormous uncertainty that exists at any temperature about the value of γ for the ice-water interface. Since γ enters in the estimation of J as a power of three in an exponential term, the enormous scatter implies that, at this moment, there is no reliable estimate of the value of J for moderately supercooled water arising from CNT. In other words, you can get many different estimates of J from the different estimates of γ shown in the paper by Pruppacher. In addition, to the best of our knowledge, no one has estimated J using CNT for supersaturations lower than 30 K.[2,12,20]

Regarding the critical nucleus size, it is not possible at the moment to measure it experimentally by direct observation. Therefore, the prediction of the critical cluster at moderate and experimentally accessible supercoolings is a novel result. Since the TIP4P/2005 has been quite successful in describing a number of properties of water (notably including the surface tension for the vapor-liquid equilibrium) we believe that the values reported here for γ and J from our analysis of the critical cluster are a reasonable estimate for the corresponding values for real water.

1.6.3. Summary and outlook

We have studied homogeneous ice nucleation by means of computer simulations using the TIP4P/2005 and TIP4P/Ice water models. This is the first calculation of the size of the critical cluster and the nucleation rate at moderate supercoolings (14.5-35 K). Both models give similar results when compared at the same supercooling.

To determine the size of the critical cluster, we use a numerical approach in the spirit of direct coexistence methods. We prepare an initial configuration by inserting a large ice cluster (about 10000, 4600 and 1000 molecules) in an equilibrated sample of liquid water. Then, we let the interface equilibrate for 0.2 ns at 200 K. Finally, we perform molecular dynamic runs at several temperatures to detect either the melting or the growth of the inserted cluster by monitoring its size. We find that the size of the critical cluster varies from ∼8000 molecules (radius= 4 nm) at 15 K below melting to

$\sim$600 molecules (radius= 1,7 nm) at 35 K below melting.

We use CNT to estimate the interfacial free energy and the nucleation free energy barrier. Our predictions show that the interfacial free energy decreases as the supercooling increases, in agreement with experimental predictions. An extrapolation of the interfacial free energy to the melting temperature gives a value of 29(3) mN/m, which is in reasonable agreement with experimental measurements and with estimates obtained from computer simulations for TIP4P-like models. We get free energy barriers higher than 250 kT for supercoolings lower than 20 K. This strongly suggests that homogeneous ice nucleation for supercoolings lower than 20 K is virtually impossible. We confirm this by calculating the nucleation rate. To do that we compute, by means of molecular dynamics simulations, the rate at which particles attach to the critical clusters. These calculations show that, indeed, for supercoolings lower than 20 K it is impossible that ice nucleates homogeneously. According to this prediction, ice nucleation must necessarily be heterogeneous for supercoolings lower than 20 K. The nucleation rate we obtain at higher supercoolings (30-35 K) agrees, within the statistical uncertainty of our methodology, with experimental measurements.

It would be interesting to extend this work in several directions. Modifying the shape of the inserted cluster (inserting for instance a small crystal with planar faces) or even inserting a block of cubic ice Ic to analyse whether this cluster may be more stable as suggested by some studies[20,104] are interesting issues that deserve further studies. Secondly, it would be of interest to consider other water models, to analyse the possible similarities/differences with respect to nucleation of different potential models varying significantly either in the charge distribution as TIP5P[105] or in the way the tetrahedral order is induced as in the mW model.[100] Analyzing the behaviour at higher degrees of supercooling than those presented here is another interesting problem as well as the determination of the growth rate of ice.[106] We foresee that all these issues will be the centre of significant activity in the near future.

Acknowledgments

E. Sanz acknowledges financial support from the EU grant 322326-COSAAC-FP7-PEOPLE-2012-CIG and from the Spanish grant Ramon y Cajal. C. Valeriani acknowledges financial support from the EU grant 303941-ANISOKINEQ-FP7-PEOPLE-2011-CIG and from the Spanish grant Juan de la Cierva. Fundings also come from MECD Project FIS2010-16159 and from CAM MODELICO P2009/ESP/1691. All authors acknowledge the use of the super-computational facility Tirant at Valencia from the Spanish Supercomputing Network (RES), along with the technical support and the generous allocation of CPU time to carry out this project (through projects QCM-2012-2-0017, QCM-2012-3-0038 and QCM-2013-1-0047). One of us (C. Vega) would like to dedicate this paper to the memory of Prof. Tomas Boublik. We thank A. Reinhardt and J.P.K. Doye for sending us a preprint of their work prior to publication.

Bibliography

1. Debenedetti, P. G., *Metastable liquids: Concepts and Principles* (Princeton University Press, 1996).

2. Kashchiev, D., *Nucleation: Basic Theory with Applications* (Butterworth-Heinemann, Oxford, 2000).

3. Cantrell, W. & Heymsfield, A., Production of ice in tropospheric clouds. *Bull. Amer. Meteor. Soc.* **86**, 795 (2005).

4. Baker, M. B., Cloud microphysics and climate. *Science* **276**, 1072–1078 (1997).

5. DeMott, P. J., Prenni, A. J., Liu, X., Kreidenweis, S. M., Petters, M. D., Twohy, C. H., Richardson, M. S., Eidhammer, T. & Rogers, D. C., Predicting global atmospheric ice nuclei distributions and their impacts on climate **107**, 11217–11222 (2010).

6. Morris, G. J. & Acton, E., Controlled ice nucleation in cryopreservation–a review. *Cryobiology* **66**, 85 (2013).

7. Hirano, S. S. & Upper, C. D., Bacteria in the leaf ecosystem with emphasis on pseudomonas syringae - a pathogen, ice nucleus, and epiphyte. *Microbiol. Molec. Biol. Rev.* **64**, 624 (2000).

8. Maki, L. R., Galyan, E. L., M.M., C. & Caldwell, D. R., Ice nucleation induced by pseudomonas-syringae. *Appl. Microbiol.* **28**, 456–459 (1974).

9. Li, J. K. & Lee, T. C., Bacterial ice nucleation and its potential application in the food-industry. *Trends in Food Sci. & Tech.* **6**, 259–265 (1995).

10. Michaelides, A. & Morgenstern, K., Ice nanoclusters at hydrophobic metal surfaces. *Nature Materials* **6**, 597–601 (2007).

11. Gerrard, A. G., *Rocks and Landforms* (Springer Netherlands, 1988).

12. Pruppacher, H. R., A new look at homogeneous ice nucleation in supercooled water drops. *J. Atmosph. Sci.* **52**, 1924 (1995).

13. Taborek, P., Nucleation in emulsified supercooled water. *Phys. Rev. B* **32**, 5902–5906 (1985).

14. Knopf, D. A. & Rigg, Y. J., Homogeneous ice nucleation from aqueous inorganic/organic particles representative of biomass burning: Water activity, freezing temperatures, nucleation rates. *J. Phys. Chem. A* **115**, 762–773 (2011).

15. Moore, E. B. & Molinero, V., Structural transformation in supercooled water controls the crystallization rate of ice. *Nature* **479**, 506 (2011).

16. Li, T., Donadio, D., Russo, G. & Galli, G., Homogeneous ice nucleation from supercooled water. *Phys. Chem. Chem. Phys.* **13**, 19807–19813 (2011).

17. Riechers, B., Wittbracht, F., Hutten, A. & Koop, T., The homogeneous ice nucleation rate of water droplets produced in a microfluidic device and the role of temperature uncertainty. *Phys. Chem. Chem. Phys.* **15**, 5873–5887 (2013).

18. Kramer, B., Hubner, O., Vortisch, H., Woste, L., Leisner, T., Schwell, M., Ruhl, E. & Baumgartel, H., Homogeneous nucleation rates of supercooled water in single levitated microdroplets. *J. Chem. Phys.* **111**, 6521 (1999).

19. Stockel, P., Weldinger, I. M., Baumgartel, H. & Leisner, T., Rates of homogeneous ice nucleation in levitated h2o and d2o droplets. *J. Phys. Chem. A* **109**, 2540 (2005).

20. Murray, B. J., Broadley, S. L., Wilson, T. W., Bull, S. J., Wills, R. H., Christenson, H. K. & Murray, E. J., Kinetics of the homogeneous freezing of water. *Phys. Chem. Chem. Phys.* **12**, 10380 (2010).

21. Mishima, O., Volume of supercooled water under pressure and the liquid-liquid critical point. *J. Chem. Phys.* **133**, 144503 (2010).

22. Debenedetti, P. G., Supercooled and glassy water. *J. Phys. Condens. Matter* **15**, R1669–R1726 (2003).

23. Mori, A., Maruyama, M. & Furukawa, Y., Second order expansion of gibbs thomson equation and melting point depression of ice crystallite. *J. Phys. Soc. Japan* **65**, 2742 (1996).

24. Jeffery, C. A. & Austin, P. H., Homogeneous nucleation of supercooled water: Results from a new equation of state. *J. Geophys. Research* **102**, 25269 (1997).

25. Kiselev, S. B., Physical limit of stability in supercooled liquids. *Int. J. Thermophys.* **22**, 1421–1433 (2001).

26. Liu, J., Nicholson, C. E. & Cooper, S. J., Direct measurement of critical nucleus size in confined volumes. *Langmuir* **23**, 7286–7292 (2007).

27. ten Wolde, P. R. & Frenkel., D., Enhancement of protein crystal nucleation by critical density fluctuations. *Science* **277**, 1975 (1997).

28. Auer, S. & Frenkel, D., Prediction of absolute crystal-nucleation rate in hard-sphere colloids. *Nature* **409**, 1020 (2001).

29. Sear, R. P., The non classical nucleation of crystals: microscopic mechanisms and applications to molecular crystals, ice and calcium carbonate. *Internat. Materials Rev.* **57**, 328 (2012).

30. Svishchev, I. & Kusalik, P. G., Crystallization of liquid water in a molecular dynamics simulation. *Phys. Rev. Lett.* **73**, 975–978 (1994).

31. Koga, K., Gao, G. T., Tanaka, H. & Zeng, X. C., Formation of ordered ice nanotubes inside carbon nanotubes. *Nature* **412**, 802–805 (2001).

32. Moore, E. B., de la Llave, E., Welke, K., Scherlis, D. A. & Molinero, V., Freezing, melting and structure of ice in a hydrophilic nanopore. *Phys. Chem. Chem. Phys.* **12**, 4124–4134 (2010).

33. Vrbka, L. & Jungwirth, P., Homogeneous freezing of water starts in the subsurface. *J. Phys. Chem. B* **110**, 18126 (2006).

34. Moore, E. B. & Molinero, V., Ice crystallization in water no man land. *J. Chem. Phys.* **132**, 244504 (2010).

35. Moore, E. B. & Molinero, V., Is it cubic? ice crystallization from deeply supercooled water. *Phys. Chem. Chem. Phys.* **13**, 20008 (2011).

36. Matsumoto, M., Saito, S. & Ohmine, I., Molecular dynamics simulation of the ice nucleation and growth process leading to water freezing. *Nature* **416**, 409–413 (2002).

37. Yamada, M., Mossa, S., Stanley, H. E. & Sciortino, F., Interplay between time-temperature transformation and the liquid-liquid phase transition in water. *Phys. Rev. Lett.* **88**, 195701 (2002).

38. Kesselring, T. A., Lascaris, E., Franzese, G., Buldyrev, S. V., Hermann, H. J. & Stanley, H. E. *J. Chem. Phys.* **138**, 244506 (2013).

39. Radhakrishnan, R. & Trout, B., Nucleation of hexagonal ice (Ih) in liquid water. *J. Am. Chem. Soc* **125**, 7743–7747 (2003).

40. Radhakrishnan, R. & Trout, B. L., Nucleation of crystalline phases of water in homogeneous and inhomogeneous enviroments. *Phys. Rev. Lett.* **90**, 158301 (2003).

41. Quigley, D. & Rodger, P. M., Metadynamics simulations of ice nucleation and growth. *J. Chem. Phys.* **128**, 154518 (2008).

42. Brukhno, A. V., Anwar, J., Davidchack, R. & Handel, R. *J. Phys. Condens. Matter* **20**, 494243 (2008).

43. Reinhardt, A. & Doye, J. P. K. *J. Chem. Phys.* **136**, 054501 (2012).

44. Reinhardt, A. & Doye, J. P. K., Note: Homogeneous tip4p/2005 ice nucleation at low supercooling. *The Journal of Chemical Physics* **139**, 096102 (2013).

45. Zobrist, B., Koop, T., Luo, B. P., Marcolli, C. & Peter, T., Heterogeneous ice nucleation rate coefficient of water droplets coated by a nonadecanol monolayer. *J. Phys. Chem. C* **111**, 2149–2155 (2007).

46. Alpert, P. A., Aller, J. Y. & Knopf, D. A., Initiation of the ice phase by marine biogenic surfaces in supersaturated gas and supercooled aqueous phases. *Phys. Chem. Chem. Phys.* **13**, 19882–19894 (2011).

47. Hardy, S. C. *Philos. Mag.* **35**, 471 (1977).

48. Davidchack, R. L., Handel, R., Anwar, J. & Brukhno, A. V. *J. Chem. Theory Comput.* **8**, 2383 (2012).

49. Abascal, J. L. F. & Vega, C. *J. Chem. Phys.* **123**, 234505 (2005).

50. Abascal, J. L. F., Sanz, E., Fernandez, R. G. & Vega, C. *J. Chem. Phys.* **122**, 234511 (2005).

51. Vega, C. & Abascal, J. L. F., Simulating water with rigid non-polarizable models: a general perspective. *Phys. Chem. Chem. Phys* **13**, 19663–19688 (2011).

52. Bai, X. M. & Li, M., Calculation of solid-liquid interfacial free energy: A classical nucleation theory based approach. *J. Chem. Phys.* **124**, 124707 (2006).

53. Ladd, A. J. C. & Woodcock, L., Interfacial and co-existence properties of the lennard-jones system at the triple point. *Molec. Phys.* **36**, 611 (1978).

54. Pereyra, R. G., Szleifer, I. & Carignano, M. A. *J. Chem. Phys.* **135**, 034508 (2011).

55. Jacobson, L. C. & Molinero, V., Can amorphous nuclei grow crystalline clathrates? the size and crystallinity of critical clathrate nuclei. *J. Am. Chem. Soc* **133**, 6458–6463 (2011).

56. Knott, B. C., Molinero, V., Doherty, M. F. & Peters, B., Homogeneous nucleation of methane hydrates: Unrealistic under realistic conditions. *J. Am. Chem. Soc.* **134**, 19544–19547 (2012).

57. Auer, S. & Frenkel, D., Quantitative prediction of crystal-nucleation rates for spherical colloids: A computational approach. *Ann. Rev. Phys. Chem.* **55**, 333 (2004).

58. Auer, S. & Frenkel, D., Prediction of absolute crystal-nucleation rate in hard-sphere colloids. *Nature* **409**, 1020 (2001).

59. Allen, R. J., Warren, P. B. & ten Wolde, P. R., Sampling rare switching events in biochemical networks. *Phys. Rev. Lett.* **94**, 018104 (2005).

60. Bolhuis, P. G., Chandler, D., Dellago, C. & Geissler, P. L., Transition path sampling: Throwing ropes over rough mountain passes, in the dark. *Ann. Rev. Phys. Chem.* **53**, 291 (2002).

61. Volmer, M. & Weber, A. *Z. Phys. Chem.* **119**, 277 (1926).

62. Becker, R. & Doring, W. *Ann. Phys.* **24**, 719–752 (1935).

63. Kelton, K. F., *Crystal Nucleation in Liquids and Glasses*, vol. 45 (Academic Press, Boston, 1991).

64. Auer, S. & Frenkel, D., Numerical prediction of absolute crystallization rates in hard-sphere colloids. *J. Chem. Phys.* **120**, 3015–3029 (2004).

65. Hess, B., Kutzner, C., van der Spoel, D. & Lindahl, E., Algorithms for highly efficient, load-balanced, and scalable molecular simulation. *J. Chem. Theory Comput.* **4**, 435–447 (2008).

66. Vega, C., Abascal, J. L. F., Conde, M. M. & Aragones, J. L., What ice can teach us about water interactions: a critical comparison of the performance of different water models. *Faraday Discuss.* **141**, 251–276 (2009).

67. Pi, H. L., Aragones, J. L., Vega, C., Noya, E. G., Abascal, J. L. F., Gonzalez, M. A. & McBride, C., Anomalies in water as obtained from computer simulations of the tip4p/2005 model: density maxima, and density, isothermal compressibility and heat capacity minima. *Molec. Phys.* **107**, 365–374 (2009).

68. Gonzalez, M. A. & Abascal, J. L. F., The shear viscosity of rigid water models. *J. Chem. Phys.* **132**, 096101 (2010).

69. Essmann, U., Perera, L., Berkowitz, M. L., Darden, T., Lee, H. & Pedersen, L. G., A smooth particle mesh ewald method. *J. Chem. Phys.* **103**, 8577–8593 (1995).

70. Parrinello, M. & Rahman, A., Polymorphic transitions in single crystals: A new Molecular Dynamics method. *J. Appl. Phys.* **52**, 7182–7190 (1981).

71. Bussi, G., Donadio, D. & Parrinello, M., Canonical sampling through velocity rescaling. *J. Chem. Phys.* **126**, 014101 (2007).

72. Lechner, W. & Dellago, C. *J. Chem. Phys.* **129**, 114707 (2008).

73. Reinhardt, A., Doye, J. P. K., Noya, E. G. & Vega, C. *J. Chem. Phys.* **137**, 194504 (2012).

74. Ghiringhelli, L. M., Valeriani, C., Los, J. H., Meijer, E. J., Fasolino, A. & Frenkel, D., State-of-the-art models for the phase diagram of carbon and diamond nucleation. *Molec. Phys.* **106**, 2011–2038 (2008).

75. Li, T., Donadio, D., Ghiringhelli, L. M. & Galli, G., Surface-induced crystallization in supercooled tetrahedral liquids. *Nature Mat.* **8**, 726–730 (2009).

76. Bogdan, A., Thermodynamics of the curvature effect on ice surface tension and nucleation theory. *The Journal of Chemical Physics* **106**, 1921–1929 (1997).

77. Vega, C. & de Miguel, E., Surface tension of the most popular models of water by using the test-area simulation method. *J. Chem. Phys.* **126**, 154707 (2007).

78. Sanz, E., Vega, C., Abascal, J. L. F. & MacDowell, L. G., Phase diagram of water from computer simulation. *Phys. Rev. Lett.* **92**, 255701 (2004).

79. Koop, T., Luo, B., Tslas, A. & Peter, T., Water activiy as the determinant for homogeneous ice nucleation in aqueous solutions. *Nature* **406**, 611 (2000).

80. Noya, E. G., Menduina, C., Aragones, J. L. & Vega, C., Equation of state, thermal expansion coefficient, and isothermal compressibility for ices ih, ii, iii, v, and vi, as obtained from computer simulation. *J. Phys. Chem. C* **111**, 15877 (2007).

81. Kumar, P., Buldyrev, S. V., Becker, S. R., Poole, P. H., Starr, F. W. & Stanley, H. E., Relation between the widom line and the breakdown of the stokes-einstein relation in supercooled water. *Proc. Nat. Acad. Sci.* **104**, 9575–9579 (2007).

82. Frenkel, D. & Smit, B., *Understanding Molecular Simulation* (Academic Press, London, 1996).

83. Granasy, L., Pusztai, T. & James, P. F., Interfacial properties deduced from nucleation experiments: A cahn hilliard analysis. *J. Chem. Phys.* **117**, 6157 (2002).

84. Handel, R., Davidchack, R. L., Anwar, J. & Brukhno, A. *Phys. Rev. Lett.* **100**, 036104 (2008).

85. Horn, H. W., Swope, W. C., Pitera, J. W., Madura, J. D., Dick, T. J., Hura, G. L. & Head-Gordon, T., Development of an improved four-site water model for biomolecular simulations: TIP4P-Ew. *J. Chem. Phys.* **120**, 9665 (2004).

86. Abascal, J. L. F. & Vega, C., Widom line and the liquid-liquid critical point for the tip4p/2005 water model. *J. Chem. Phys.* **133**, 234502 (2010).

87. Abascal, J. L. F. & Vega, C., Eos supercooled. *J. Chem. Phys.* **134**, 186101 (2011).

88. Wikfeldt, K. T., Huang, C., Nilsson, A. & Pettersson, L. G. M., Enhanced small-angle scattering connected to the widom line in simulations of supercooled water. *J. Chem. Phys.* **134**, 214506 (2011).

89. Filion, L., Hermes, M., Ni, R. & Dijkstra, M., Crystal nucleation of hard spheres using md umbrella sampling and forward flux sampling: A comparison of simulation techniques. *J. Chem. Phys.* **133**, 244115 (2010).

90. Lundrigan, S. E. M. & Saika-Voivod, I., Test of classical nucleation theory and mean first-passage time formalism on crystallization in the lennard-jones liquid. *J. Chem. Phys.* **131**, 104503 (2009).

91. Shevchuk, R. & Rao, F., Microsecond long atomistic simulation of supercooled water. *J. Chem. Phys.* **137**, 036101 (2012).

92. Overduin, S. D. & Patey, G. N. *J. Chem. Phys.* **138**, 184502 (2013).

93. Limmer, D. T. & Chandler, D., The putative liquid-liquid transition is a liquid-solid transition in atomistic models of water. ii. *J. Chem. Phys.* **138**, 214504 (2013).

94. Poole, P. H., Bowles, R. K., Saika-Voivod, I. & Sciortino, F., Free energy surface of st2 water near the liquid-liquid phase transition. *J. Chem. Phys.* **138**, 034505 (2013).

95. Liu, Y., Palmer, J. C., Panagiotopoulos, A. Z. & Debenedetti, P. G., Liquid-liquid transition in st2 water. *J. Chem. Phys.* **137**, 214505 (2012).

96. Pruppacher, R. & Klett, J. D., *Microphysics of Clouds and Precipitation* (Kluwer Academic Publishers, 1997).

97. Speedy, R. J. & Angell, C. A., Isothermal compressibility of supercooled water and evidence for a thermodynamic singularity at -45 degrees c. *J. Chem. Phys.* **65**, 851–858 (1976).

98. Hare, D. E. & Sorensen, C. M., The density of supercooled water. ii. bulk samples cooled to the homogeneous nucleation limit. *J. Chem. Phys.* **87**, 4840 (1987).

99. Holten, V., Bertrand, C. E., Anisimov, M. A. & Sengers, J. V., Thermodynamics of supercooled water. *J. Chem. Phys.* **136**, 094507 (2012).

100. Molinero, V. & Moore, E. B., Water modeled as an intermediate element between carbon and silicon. *J. Phys. Chem. B* **113**, 4008–4016 (2009).

101. Vega, C., Martin-Conde, M. & Patrykiejew, A., Absence of superheating for ice ih with a free surface: a new method for determining the melting point of different water models. *Mol. Phys.* **104**, 3583 (2006).

102. Conde, M. M., Vega, C. & Patrykiejew, A., The thickness of a liquid layer on the free surface of ice as obtained from computer simulation. *J. Chem. Phys.* **129**, 014702 (2008).

103. Bartell, L. S. & Huang, J. F., Supercooling of water below the anomalous range near 226 k **98**, 7455–7457 (1994).

104. Huang, J. F. & Bartell, L. S., Kinetics of homogeneous nucleation in the freezing of large clusters. *J. Phys. Chem.* **99**, 3924 (1995).

105. Mahoney, M. W. & Jorgensen, W. L., A five-site model for liquid water and the reproduction of the density anomaly by rigid, nonpolarizable potential functions. *J. Chem. Phys.* **112**, 8910–8922 (2000).

106. Razul, M. S. G. & Kusalik, P. G., Crystal growth investigations of ice/water interfaces from molecular dynamics simulations: Profile functions and average properties. *J. Chem. Phys.* **134**, 014710 (2011).

Results: Chapter 2

Homogeneous ice nucleation evaluated for several water models

J. R. Espinosa , *E. Sanz, C. Valeriani and C. Vega*

Departamento de Química Física, Facultad de Ciencias Químicas, Universidad Complutense de Madrid, 28040 Madrid, Spain

2.1. Abstract

In this work we evaluate by means of computer simulations the rate for ice homogeneous nucleation for several water models such as TIP4P, TIP4P/2005,TIP4P/ICE and mW (following the same procedure as in Sanz *et al* J.A.C.S. **135** 15008 (2013)) in a broad temperature range. We estimate the ice-liquid interfacial free-energy, and conclude that for all water models γ decreases as the temperature decreases. Extrapolating our results to the melting temperature, we obtain a value of the interfacial free-energy between 25 and 32 mN/m in reasonable agreement with the reported experimental values. Moreover, we observe that the values of γ depend on the chosen water model and this is a key factor when numerically evaluating nucleation rates, given that the kinetic prefactor is quite similar for all water models with the exception of the mW (due to the absence of hydrogens). Somewhat surprisingly the estimates of the nucleation rates found in this work for TIP4P/2005 are slightly higher than those of the mW model, even though the former has explicit hydrogens. Our results suggest that it may be possible to observe spontaneous crystallization of TIP4P/2005 at about 60K below the melting point.

2.2. Introduction

When liquid water is super-cooled to below its melting point, it becomes metastable and eventually freezes into its thermodynamically stable phase (ice). On the one hand, in the presence of impurities, this phase transition occurs quite easily (this is the reason why ice will appear in your refrigerator only after few hours). On the other hand, in the absence of impurities, metastable liquid water can survive even at temperatures well below the melting point, until homogeneous nucleation takes place and water is transformed into ice. Homogeneous nucleation is an activated process, given that the system has to overcome a nucleation free-energy barrier and to form a critical ice cluster in order to crystallize[1].

By performing experiments with micrometer-size water droplets, it has been possible to prepare metastable liquid water at temperatures down to 235K[2–5]. Below this temperature (known as the homogeneous nucleation temperature) water freezes in a few seconds. Such experiments permits one to experimentally determine the nucleation rate J (i.e the number of ice critical clusters per unit of volume and time) for temperatures between 235K and 242K, with values of J defined within less than three orders of magnitude. Outside this range, it has not been possible to experimentally determine the nucleation rate, either because it is too large (below 235K) or too small (above 242K). Given that J is known only in a narrow temperature range, to estimate its values outside such range[5] classical nucleation theory (CNT)[1] could provide reasonable predictions, since the main ingredients needed are the interfacial free-energy of the liquid-ice interface at coexistence (γ) and the kinetic prefactor. However, on the one hand, even though γ could in principle be experimentally measured, its reported values (so far) range from 25 to 35 mN/m[6]; on the other hand, the kinetic prefactor is not known experimentally.

For these reasons, we believe that computer simulation could give a reasonable contribution in this context, since they could help both in determining the value of γ and evaluating the homogeneous nucleation rate over a broader temperature range. As far as we are aware, little work has been devoted numerically to compute γ for the ice-water interface: the only exception being Ref.[7,8], where γ was calculated at the melting point for several water models.

Moreover, work still needs to be done to estimate ice nucleation rates by means of numerical simulations. First of all, in order to know the amount of supercooling of liquid water (which determines the nucleation rate) one needs to know the melting temperature. However, until 2005[9], the melting point of most water models had not been calculated. The first pioneering numerical paper on ice nucleation was that of Matsumoto et al[10], where spontaneous crystallization was observed at 230K for a system of 500 molecules at a pressure of about -1000 bar using the TIP4P model[11]. Later on, for the same water model, the nucleation free-energy barrier had been calculated at

180K in Ref.[12],[13] and[14]. The nucleation rate has been also recently computed for the mW water model[15] by Li et al[16] using forward flux sampling between 240K and 220K, by Reinhardt and Doye[17] using umbrella sampling at 220K. At 220K the value of J computed for mW by both groups differs by 5 orders of magnitude. This difference is somewhat larger than the expected statistical uncertainty for nucleation rates (which is expected to be of 1-2 orders of magnitude). Although both groups used different rare-events techniques the origin of the discrepancy it is not clear as for other systems the values of J computed from forward flux sampling and umbrella sampling seems to be in better agreement[18]. For the mW model using brute force simulations at 208K Moore and Molinero[19] were able to nucleate ice spontaneously in about 100ns in a system of 5000 molecules, leading to a rate of about $10^{32}m^{-3}s^{-1}$. In 2013, our group estimated the value of J and γ for other two water models, TIP4P/2005[20] and TIP4P/ICE[21], at low/moderate supercooling using the "seeding technique"[22,23] together with CNT[24]. Even though the main advantage of the seeding technique is that it allows one to estimate the nucleation free-energy barrier even at moderate supercooling (differently from more rigorous numerical techniques such as umbrella sampling or forward flux sampling that might be CPU-time consuming at such temperatures), its main disadvantage is that it combines precise simulation results with an approximate theoretical formalism. The nucleation rates evaluated for both TIP4P/2005 and TIP4P/ICE water models[24] were in reasonable agreement with experiments. However, this agreement may have been due to a fortuitous cancellation of errors, occurring when an approximate water model is used in combination with an approximate technique. Therefore, in this work we will apply the same technique as in Ref.[24] to estimate ice nucleation rate using other water models, such as TIP4P[11] and mW[15].

In what follows, we will first provide more technical details about our previous work[24]. Next, we will analyze the differences in the estimates of γ for several water models, and observe that values of γ change significantly from a water model to another: even though for all water models γ decreases as the temperature decreases. We then compute the kinetic prefactor, and conclude that it is quite similar for all water models, with the exception of mW for which it is about three orders of magnitude larger: this is certainly due to the lack of hydrogens in the model. However, being this difference significant, it is γ that plays the central role in determining the nucleation rates. To conclude, we evaluate J and compare the results obtained for each water model. In particular we will focus on the mW model potential to determine whether the nucleation rate can be enhanced compared to other water models. We first observe that J estimated with the seeding technique compares nicely to the values of J reported for the same mW model in the literature (to within 5-6 orders of magnitude which is the expected uncertainty at high supercooling). Somewhat surprisingly, estimates of the nucleation rates for TIP4P/2005 are slightly higher than those for the mW model (even though the former has explicit hydrogens). The results of this work suggest that it may be possible

to observe spontaneous crystallization of TIP4P/2005 at about 57K below the melting point (i.e. 195K). Given that nucleation rate at 230K is very small, nucleation is not likely to be observed in computer simulations for TIP4P/2005. At such low temperature (and room pressure) a maximum in the compressibility has been found for this model by Abascal and Vega[25,26] and Bresme et al.[27] thus providing a point of the Widom line. The results of this work support the existence of the Widom line for TIP4P/2005, and that this line is not due to the transient formation of ice[28].

2.3. Methodology

2.3.1. The "seeding"technique

The technique first proposed by Bai et al.[22,23] consisted of inserting a solid cluster in a supercooled Lennard-Jones fluid, determining the temperature at which the cluster was critical (i.e where it can freeze or melt with equal probability). We shall denote this technique as "seeding", as it can be regarded as the insertion of a seed of the stable phase (i.e the solid) in the supercooled liquid.

By assuming that classical nucleation theory can be used to describe and interpret the results obtained for the critical cluster size, then the technique allows one to estimate of the interfacial free energy γ at the given thermodynamic conditions. According to CNT the critical cluster size N_c is

$$N_c = \frac{32\pi\gamma^3}{3\rho_s^2|\Delta\mu|^3} \tag{2.1}$$

where ρ_s is the number density of the solid phase (i.e ice Ih), $\Delta\mu$ the chemical potential difference between the solid and the fluid phase at the temperature at which the cluster is critical.

Once the value of γ has been determined via Eq. 4.6 one can estimate (once again using CNT) the free energy barrier for nucleation from the expression :

$$\Delta G_c = \frac{16\pi\gamma^3}{3\rho_s^2|\Delta\mu|^2}. \tag{2.2}$$

Finally, one can estimate nucleation rates. Following the approach described in detail by Auer and Frenkel[1,29,30], J can be obtained from the expression :

$$J = \rho_f Z f^+ \exp(-\Delta G_c/(k_B T)) \tag{2.3}$$

where $(\rho_f Z f^+)$ is the kinetic prefactor, with f^+ the attachment rate of particles to the critical cluster, ρ_f the number density of the fluid and Z the Zeldovich factor[1]. The

CNT form of the Zeldovich factor is

$$Z = \sqrt{(|\Delta G''|_{N_c}/(2\pi k_B T))} = \sqrt{|\Delta\mu|/(6\pi k_B T N_c)} \tag{2.4}$$

so that Z can be easily computed, once the size of the critical cluster N_c, the temperature at which it is critical T and the chemical potential difference between the solid and the liquid are known. According to Ref.[29–31], f^+ can be computed as a diffusion coefficient of the cluster size at the top of the barrier (at the temperature at which the cluster is critical):

$$f^+ = \frac{< (N(t) - N_c)^2 >}{2t}. \tag{2.5}$$

The seeding technique can be particularly useful at moderate supercooling, where estimating the critical cluster size, the free-energy barrier height and the rate by more rigorous numerical techniques would be very CPU-time consuming.

A similar approach has been recently used by Pereyra et al[32], where the authors determined the temperature at which a cylindrical ice slab would melt or grow, in Ref.[33], by Knott et al determined the critical cluster size in a nucleation study of methane hydrate, and in Ref.[24], where Sanz et al studied ice nucleation from supercooled water.

Drawbacks in the estimate of γ

Admittedly, the way presented in Eq.(4.6) to estimate γ is quite approximate, since it assumes that CNT is correct. The justification of this approach can be provided only a posteriori by comparison with more rigorous calculations.

First of all, different crystal planes will have different values of γ, whereas γ computed according to Eq.(4.6) does not take into account the different crystal planes and only corresponds to an average among them. On the one hand, it has been shown for several systems such as hard spheres, Lennard Jones and water[7,8,14,34–36] that comparing γ computed for different planes results in differences smaller than about five per cent. On the other hand, one may assume that the spherical interface will represent the average value of γ over different planes. In any case the relation between the value of γ of a spherical cluster with that computed for a planar interface is not completely clear.

To conclude, our calculations of γ rely on the assumption that the shape of the cluster is spherical. Visual inspection of our molecular dynamics trajectories suggests that this is indeed a reasonable approximation.

2.3.2. Distinguishing between liquid and ice-like molecules

As in our previous work[24], in order to identify molecules as liquid or ice Ih-like, we have used the $\bar{q}_6$ order parameter proposed in Ref.[37]: molecules with $\bar{q}_6$ larger than 0.358 will be classified as solid (ice Ih) and those with smaller values of as liquid-like.

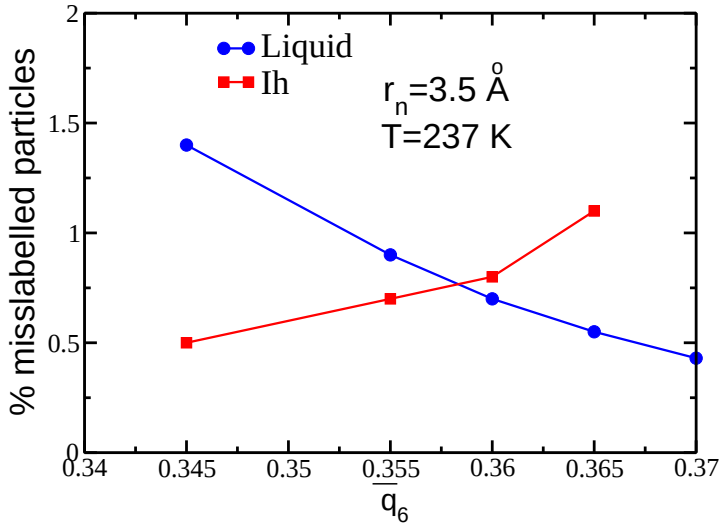

Figure 2.1: Percentage of mislabelled particles according to $\bar{q}_6$, evaluated for bulk ice Ih and bulk liquid water at 237K and 1bar (for TIP4P/2005), using the first minimum of the $g(r)$ as a cutoff for the calculation of $\bar{q}_6$. For ice Ih mislabelled particles are those with a value of the order parameter smaller than $\bar{q}_6$. For liquid water mislabelled particles are those with a value of the order parameter larger than $\bar{q}_6$.

Following this criterion, we conclude that only about 0,7 per cent of bulk ice Ih molecules are wrongly identified as liquid-like, and vice versa 0,7 per cent of bulk liquid molecules identified as solid-like (see Fig. 2.1) . Since ice Ih and supercooled water have a quite similar structure, one may neglect this small mislabelling (furthermore it is very difficult to find order parameters with smaller mislabelling).

Drawbacks in the estimate of N_c

The solid-fluid interface at the nucleus is not sharp, and we implicitly assume that the width of the interfacial region is very small relative to the size of the nucleus. This is of course, an approximation. Order parameters are very useful to distinguish between bulk ice and bulk liquid, but it is by far more difficult to distinguish between liquid and solid molecules in the interfacial region.[16–18] This constitutes a systematic source of error.

Therefore, determining N_c entails an uncertainty due to the interfacial molecules. Of course, the larger the clusters the smaller the amount of uncertainty in N_c, since the ratio of the number of molecules at the interface to those in the cluster's core decreases with the system size. Whether the approach used in this work is reasonable or not can only be tested at posteriori, by comparing the results of this work with those found in

the literature.

2.3.3. Our setup for the seeding technique

In this work, by means of the seeding technique, we determine the temperature at which three clusters of different sizes are critical. Three initial systems were obtained by inserting spherical ice Ih clusters of different sizes in supercooled water (molecules overlapping with the cluster were removed). After inserting the cluster, we equilibrated its interface for about 0.2ns at 200 K, enough to equilibrate the interface but not to observe melting or growing of the cluster (which typically requires 2-20ns). After this 0.2ns the sizes of the ice cluster were of about 7930, 3170 and 600 respectively for the three clusters sizes considered in this work. In each system, the total number of water molecules was about 20 times larger than the inserted cluster to avoid interactions between the cluster and its periodic images. Thus, the total number of molecules of water (considering both the ice Ih cluster and the molecules of the supercooled liquid) were 182585, 76781 and 22712 respectively. In order to be able to simulate such rather large systems, we had to recur to supercomputer facilities.

Once the cluster is equilibrated, we performed MD runs at different temperatures and monitor the cluster size to determine the temperature at which each cluster is critical.

There is an additional point worthy of comment concerning our initial setup. When implementing the seeding technique we use a starting cluster with Ih crystal structure. Yet in recent work, both experimental and numerical, have been strongly suggested that initial ice nuclei contain stacking faults. This has resulted in recent papers referring to stacking disordered ice I[38–43]. One may wonder about the consequences of this on the present study as it could have some impact on some relevant quantities such as the chemical potential difference, the interfacial free energy, and kinetic factors. This is an interesting point that deserves an independent study on its own. However there is some indication that the impact of the presence of stacking faults in ice I on the final results may be rather small. Free energy calculations (obtained from the Einstein crystal calculations) for ices Ih and Ic using the TIP4P/2005 model indicate that the free energy difference between these two solid phases is quite small[44]. In addition, preliminary calculations similar to those performed in this work, but inserting a cluster of pure Ic, reveal little differences with those obtained using a cluster of ice Ih[44] (suggesting that both the interfacial energy and the kinetic factors are quite similar for ices Ih and Ic).

2.3.4. The chosen water model potentials

In Ref.[24], we have studied both TIP4P/ICE and TIP4P/2005 water models, where MD runs were performed with Gromacs[45] using a velocity-rescaling[46] thermostat and

an istropic Parrinello-Rahman barostat[47] with a relaxation time of about 2ps. The LJ term of the potential was truncated at 9 Å and long range corrections were added to account for the truncation of the LJ part. Ewald sums (with the PME technique[48]) were used to deal with the electrostatic interactions. The real part of the electrostatic potential was also truncated at 9 Å. In this work we shall extend our previous study to the TIP4P model[11]. The details of the simulations are similar to those used in our previous work. In addition we have also performed simulations for the mW model of water[49]. Simulations for the mW model were performed using the LAMMPS package[50] In the mW water model hydrogens are not present, and tetrahedral ordering is induced by using three body forces. The model has no charges, and due to the short range of the two and three body forces it is computationally very fast.

The comparison between the results of TIP4P family models is of interest, as these models present the same charge distribution (with one LJ center on the oxygen, two positive charges on each H and a negative charge on the H-O-H bisector) but differ in the strength of the hydrogen bond (increasing as TIP4P, TIP4P/2005 and TIP4P/ICE) and thus in their melting points (increasing in the same order).

The mW model has recently become quite popular in nucleation studies (either brute force[19] or using umbrella sampling or forward flux sampling techniques[16,17]. Therefore, we will use this model to test the validity of the seeding technique and to analyze whether the absence of hydrogens speeds up the nucleation rate compared to other models where hydrogen atoms are explicit.

Let us finish this section with a final comment. In this work we are using classical statistical mechanics (i.e standard molecular dynamics simulations). Since nucleation of ice occurs at low temperatures, where nuclear quantum effects gain importance, one may wonder about possible impact of such effects on nucleation studies of water. The parameters of empirical potentials are typically obtained by forcing the model to reproduce experimental properties within the framework of classical statistical mechanics. Thus the parameters of empirical potentials incorporate to some extend nuclear quantum effects in an effective way. That may explain the success of models like TIP4P/2005 to describe interfacial free energies and dynamic properties of real water. As will be shown in this work this strategy seems to also be successful when estimating nucleation rates of water. However, the properties of deuterated water (melting point, temperature of the maximum in density) differ significantly from those of water indicating that nuclear quantum effects are important and this effect can not be captured by classical statistical mechanics (i.e within this framework the melting point does not depend on the mass associated with the hydrogen atom). To capture isotopic effects in nucleation studies of water, it is necessary to have an accurate potential energy surface of water (obtained from accurate electronic structure calculations) , and to incorporate nuclear quantum effects. However we have shown recently that by using a modified version of TIP4P/2005 (TIP4PQ/2005) in combination with path integral simulations, it is to describe reaso-

nably well isotopic effects in water[51–54]. It would be interesting in the future to pursue a study similar to that performed in this work, where TIP4PQ/2005 is used in combination with path integral calculations to analyze isotopic effects on the nucleation of ice (although this calculations would be at least one order of magnitude more expensive than those performed in this work). In any case the results of this work seem to indicate, that TIP4P/2005, in combination with classical simulations, seems to be reasonably successful in describing experimental values of the nucleation rates. Therefore the strategy of incorporating nuclear quantum effects via effective potentials does not seem too bad for this problem.

2.4. Results

Before presenting our main results, we summarize a few properties at the melting point of the chosen water potentials (Table 2.1).

Table 2.1: Melting temperature, ice Ih density[55,56], melting enthalpy and γ at coexistence (extrapolated from the results for the finite size clusters) for TIP4P, TIP4P/2005, TIP4P/ICE, mW and experiments.

model	T_m/K	$\rho_s/(gcm^{-3})$	ΔH_m/(kcal/mol)	γ/(mN/m)
TIP4P	230	0.94	1.05	25.6
TIP4P/ICE	272	0.906	1.29	30.8
TIP4P/2005	252	0.921	1.16	29.0
mW	274.6	0.978	1.26	29.6
Experiment	273.15	0.917	1.44	29

All chosen water models differ in their properties at the melting point. No water model is able to simultaneously reproduce the coexistence density, the melting temperature and the melting enthalpy (even though TIP4P/ICE nicely reproduces the melting temperature and the solid density, it underestimates the melting enthalpy by about ten per cent). The experimental density of ice Ih at the melting point is $0{,}92 g/cm^3$[57]. It is clear from the results of Table 2.1 that the density of ice Ih is very well reproduced by TIP4P/2005 and TIP4P/ICE, and reasonably well by TIP4P, whereas for mW the density of ice Ih is too high. Given that mW reproduces reasonably well the density of water at the melting point (i.e 1 g/cm^3) it turns out that for this water model the density change from ice Ih to liquid water is only of about 2 per cent, considerably smaller than that found in experiments where the density change is about 10 per cent. In other words, for mW , freezing is a weakly first order phase transition.

Our main results for all water models are summarized in Table 2.2. The runs used to determine the temperature at which each of the studied clusters becomes critical are

Table 2.2: Reported for a given cluster size and water model are the corresponding supercooling, ΔT/K, ice-Ih density, $\rho_s/(\mathrm{g/cm^3})$, chemical potential difference between the liquid and the solid, $\Delta\mu(kcal/mol)$, number of particles in the cluster, N_c, attachment rate, f^+/s^{-1}, Zeldovich factor, Z, diffusion coefficient, $\mathrm{D}/(\mathrm{m^2/s})$, λ/Å, interfacial free energy, $\gamma/(\mathrm{mN/m})$, height of the nucleation free energy barrier, $\Delta G_c/(\mathrm{k}_B\mathrm{T})$, and decimal logarithm of the nucleation rate, $log_{10}(\mathrm{J}/(\mathrm{m}^{-3}\mathrm{s}^{-1}))$. Statistical errors for ΔG_c and $log_{10}(J)$ are shown in parenthesis. The uncertainty in ΔT is of about 2.5K, so that the errors in $\Delta\mu$, γ and ΔG_c are of about 7 per cent. As discussed in the main text, if systematic errors are included, the error in γ does not increase much, but the error in ΔG_c and $log_{10}J$ presented in this Table should be multiplied by two. For the medium clusters we have also included (in parenthesis) the value of the attachment rate and λ obtained using only times larger than 1.5 ns in the determination of the attachment rate.

Model	ΔT	ρ_s	$\Delta\mu$	N_c	f^+	Z	D	λ	γ	ΔG_c	$log_{10}J$
Tip4p/ICE	14.5	0.908	0.0629	7926	$6.9\cdot10^{12}$	$9.07\cdot10^{-4}$	$1.80\cdot10^{-10}$	5.0	26.3	487(34)	-173(16)
Tip4p/ICE	19.5	0.909	0.0826	3167	$2.9(2.6)\cdot10^{12}$	$1.66\cdot10^{-3}$	$9.63\cdot10^{-11}$	4.1(4.4)	25.4	261(18)	-75(9)
Tip4p/ICE	34.5	0.911	0.1335	600	$3.0\cdot10^{11}$	$5.00\cdot10^{-3}$	$1.10\cdot10^{-11}$	2.2	23.7	85(6)	1(4)
Tip4p/2005	14.5	0.923	0.0612	7931	$1.9\cdot10^{12}$	$9.31\cdot10^{-4}$	$1.48\cdot10^{-10}$	6.4	25.9	515(36)	-186(17)
Tip4p/2005	19.5	0.924	0.0801	3170	$1.2(1.3)\cdot10^{12}$	$1.70\cdot10^{-3}$	$9.69\cdot10^{-11}$	6.4	25.0	275(19)	-83(9)
Tip4p/2005	29.5	0.925	0.1137	600	$1.8\cdot10^{11}$	$4.76\cdot10^{-3}$	$3.31\cdot10^{-11}$	6.5	20.4	77(5)	3(3)
Tip4p	12.5	0.942	0.0515	7931	$3.4\cdot10^{13}$	$8.92\cdot10^{-4}$	$1.44\cdot10^{-10}$	2.0	22.0	472(33)	-166(15)
Tip4p	17.5	0.943	0.0696	3170	$4.0(5.6)\cdot10^{12}$	$1.66\cdot10^{-3}$	$4.90\cdot10^{-11}$	2.5	21.9	261(18)	-75(9)
Tip4p	27.5	0.944	0.1018	600	$1.8\cdot10^{11}$	$4.73\cdot10^{-3}$	$1.06\cdot10^{-11}$	3.1	18.5	76(5)	4(3)
mW	14.6	0.980	0.0669	7926	$9.0\cdot10^{14}$	$9.32\cdot10^{-4}$	$4.50\cdot10^{-9}$	2.2	29.5	514(36)	-183(17)
mW	19.6	0.981	0.0895	3167	$2.3(2.5)\cdot10^{14}$	$1.72\cdot10^{-3}$	$2.33\cdot10^{-9}$	2.7	29.0	280(20)	-81(9)
mW	34.6	0.983	0.1553	600	$1.1\cdot10^{14}$	$5.36\cdot10^{-3}$	$2.69\cdot10^{-9}$	2.0	28.9	98(7)	-2(4)

provided as Supplementary Material[58].

2.4.1. Ice Ih density

As shown in Table 2.2, the density of ice Ih increases as the temperature decreases and this is also found in experiments (at least up to 125K). Below this temperature the experimental density of ice Ih is approximately constant. This is a consequence of the third law of thermodynamics which implies that certain quantities such as the heat capacity or the the coefficient of thermal expansion tends to zero when the temperature goes to zero. Since the coefficient of thermal expansion goes to zero at low temperatures that implies that the density of solid phases do not change much with temperature at low temperatures (at constant pressure). These effects can not be reproduced by classical simulations since their description would require the incorporation of nuclear quantum

effects[51,59]).

2.4.2. The chemical potential difference between the fluid and the solid, $\Delta\mu$

In order to determine the chemical potential difference between the liquid and the solid, we perform NpT simulations below melting for bulk ice Ih and liquid water. Next, we compute the enthalpy in both systems and perform thermodynamic integration to determine $\Delta\mu$ (at coexistence, the chemical potential of the solid and liquid are the same).

As shown in Fig.2.2, the value of $\Delta\mu$ is quite different for different models. $\Delta\mu$ can often be approximated using the enthalpy change at melting[1]:

$$\Delta\mu = \Delta H_m \left(1 - \frac{T}{T_m}\right) \tag{2.6}$$

As shown in Table 2.1, the enthalpy change at melting depends on the chosen model and at the same supercooling $\Delta\mu$ increases when using TIP4P, TIP4P/2005, TIP4P/ICE and mW, respectively. Even though Eq. 2.6 allows one to explain the results of Fig. 2.2 for low supercoolings (where it becomes basically exact), it cannot be safely used for large supercoolings where the value of $\Delta\mu$ rigorously obtained from thermodynamic integration visibly differs from that obtained via Eq. 2.6. The reason for this difference is that the enthalpy of liquid water changes dramatically when water is supercooled, as shown by the increase in the heat capacity (which reaches a maximum at the so called Widom line[60]). The only water model where the approximation works is the mW. For this model, the maximum in density is located at 250K, and the maximum in the heat capacity is displaced to lower temperatures. To conclude, the value of $\Delta\mu$ at large supercooling is sensitive to the thermodynamic behavior of supercooled water, and in particular to the location of the maximum in the heat capacity (if any) with respect to the melting temperature.

2.4.3. Determining N_c

To illustrate how the temperature at which the cluster is critical is determined we shall present one example for the mW model. In Fig.2.3, the time evolution of the cluster containing 600 ice molecules is shown for the mW model, at 1 bar and T=240K. At this temperature the cluster is critical and in approximately half of the trajectories it melts, whereas in the other half it grows.

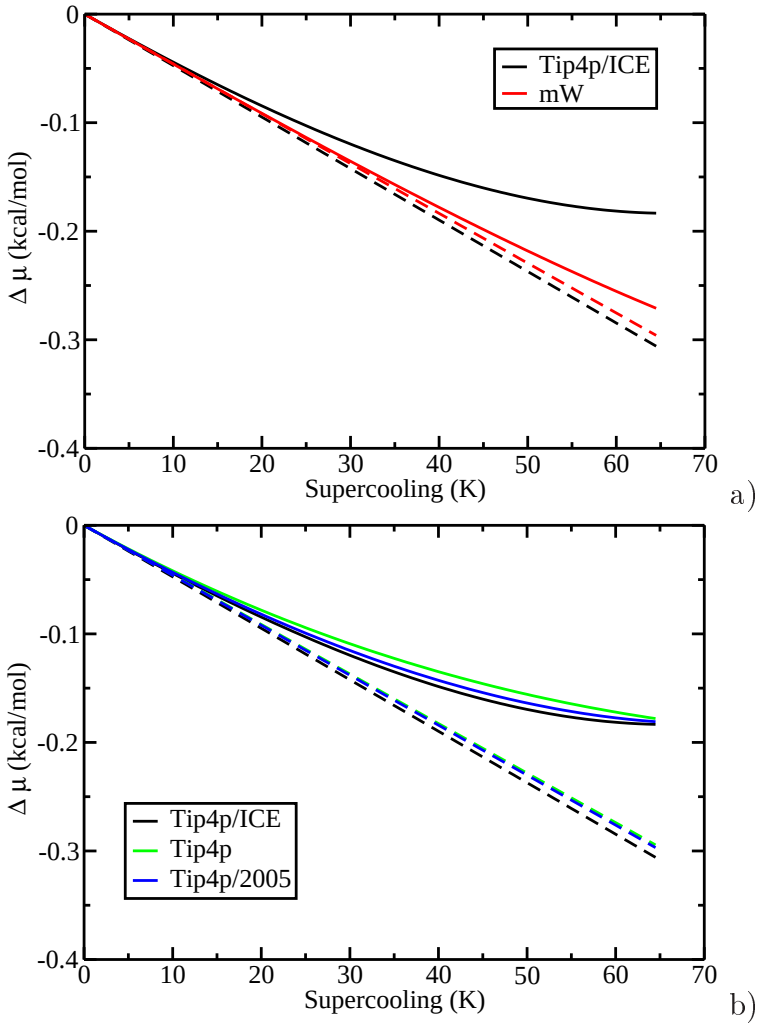

Figure 2.2: $\Delta\mu$ obtained from thermodynamic integration (solid lines) and from Eq. 2.6 (dashed lines) as a function of the supercooling ΔT. a) Results for mW and TIP4P/ICE. b) Results for TIP4P, TIP4P/2005 and TIP4P/ICE.

2.4.4. The interfacial free energy, γ

By means of Eq.4.6, we have estimated γ for each cluster size. In Fig.2.4 the value of γ is plotted as a function of the supercooling. As can be seen for all models γ decreases with the temperature (i.e decreases as one increases the supercooling). Our results are compatible with a possible linear decrease of γ with T although a faster (than linear) decreases of γ with T cannot be discarded. The derivate of γ with ΔT is the surface excess entropy. We obtained a slope of -0.13, -0.25 and -0.38 mN/(K.m) for TIP4P/ICE,

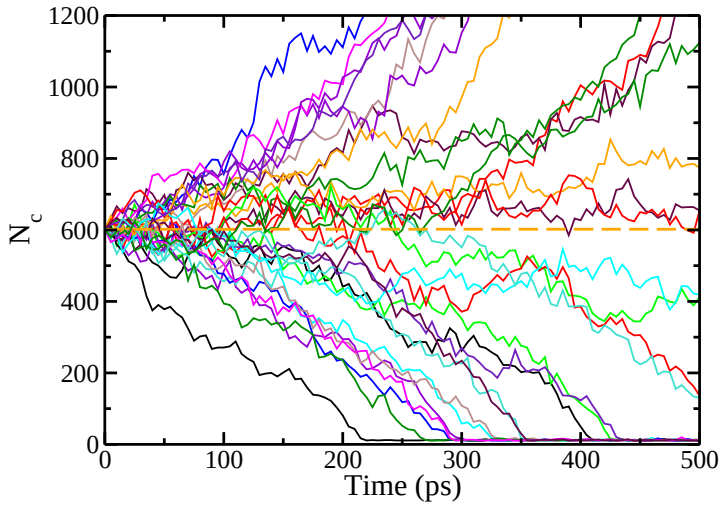

Figure 2.3: Time evolution of the cluster size for the mW at T=240K and 1bar. The size of the initial cluster was about 600 molecules. Results obtained for 30 independent trajectories are shown.

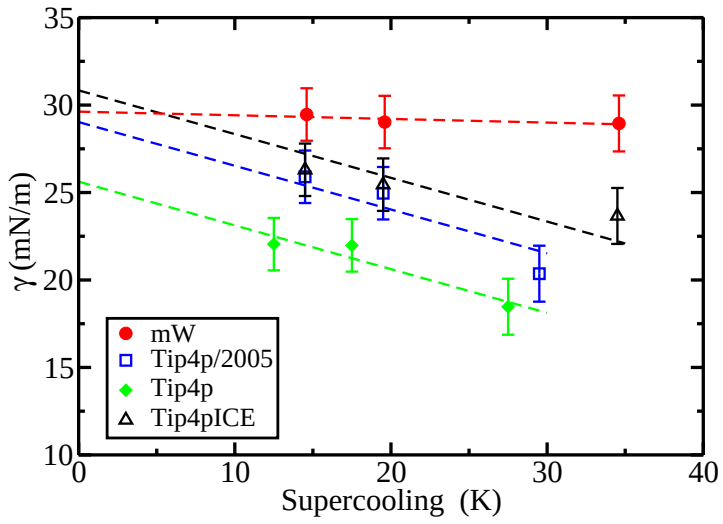

Figure 2.4: Interfacial free energy between ice Ih and liquid water as a function of the degree of supercooling as obtained from the seeding technique in combination with CNT for TIP4P, TIP4P/2005, TIP4P/ICE and mW.

TIP4P and TIP4P/2005 models. These slopes have large error bars arising from our uncertainty in the determination of γ. To reduce such error bars we use the fact that all TIP4P-like models seem to display similar behavior, so we shall adopt the average slope,

namely -0.25 mN/(K.m), for the three models. Such slope is in good agreement with the slope calculated in Ref.[61] for the TIP4P/2005 ($-0{,}18$ mN/(K.m)). Experimentally there is no consensus neither on the value of γ for the planar interface nor on the change of γ with the degree of supercooling (see fig.10 in the paper of Pruppacher[2]). In any case the slope reported here, namely $-0{,}25 mN/(K.m)$, is roughly consistent with the slopes presented in fig.10 of Ref.[2].

To estimate the value of γ at the melting point we extrapolate our data to $\Delta T = 0$ (using the averaged slope of -0.25mN/(Km) for the TIP4 family models). The extrapolations are shown in Fig. 2.4 and the values of γ at coexistence thus obtained are reported in Table 2.1.

Within the TIP4P family the value of γ increases with the strength of the hydrogen bond. Therefore within this family one could state that γ increases with the melting enthalpy or with the melting point. The correlation between γ and the melting enthalpy was first proposed by Turnbull[1,62]. Another correlation between γ and the melting point has been proposed by Laird[63]. We indeed confirm that for the TIP4P family both the correlation of Turnbull[62] and Laird[63] could be useful to predict the trends in γ. In fact, mW and TIP4P/ICE both have the same melting point and melting enthalpy. According to the Turnbull recipe, or the Laird recipe, they should have a quite similar value of γ. This seems to be consistent with the results of this work.

Moreover the results presented in Table 2.1 are in reasonable agreement with results obtained by other authors. Using the cleavage method and averaging over the basal, primary prismatic and secondary prismatic planes, the value of γ for TIP4P , TIP4P-Ew[64] (a model with similar properties to TIP4P/2005) has been reported to be 26,5(4), 27,6(5) mJ/m^2 respectively[7]. Using the mW, Ref.[16] estimated γ to be $31 mN/m$, in reasonable agreement with our estimate. Experimentally, the value of γ for the ice Ih-water interface has been reported to be between 27 and 35 mN/m. The most cited work is that of Ref.[65] which reports a value of $29{,}1 mN/m$. In the absence of better criteria, we shall assume this to be the most reliable value. According to that, TIP4P/2005 provides estimates of γ in agreement with experiments, TIP4P being slightly smaller than the experimental one, and the value of the mW and TIP4P/ICE slightly higher.

2.4.5. The attachment rate, f^+

When computing the attachment rate via Eq. 4.10, we observe that the results obtained for TIP4P, TIP4P/2005 and TIP4P/ICE are quite similar. The attachment rate is obtained after running 10 molecular dynamics trajectories at the temperature that makes the cluster critical (30 trajectories were performed in the case of the mW model). In Fig. 2.5 we show (for the TIP4P model) the mean squared displacement (as obtained from the average of the 10 trajectories) of the cluster size as a function of time for the ice cluster of 3170 molecules (see also the Supplementary material[58]). All trajectories

start from the same configuration and differ in the initial set of Maxwellian momenta. The results of Fig.2.5 were fitted to a straight line and the attachment rate is just half the value of the slope. The fact that we are starting all runs from the same configuration (although with different momenta) may have some impact on the computed slopes as pointed out recently by Rozmanov and Kusalik[66]. This can be minimized by excluding the short-time behaviour from the calculation of the attachment rate. In Table II , we have determined the attachment rate for the medium cluster using both the entire window time and times larger than 1.5ns (results in parenthesis). As it can be seen, the impact on the attachment rate is small.

From the slope of the curve shown in Fig. 2.6 one can obtain f^+ via Eq. 4.10. For the smallest cluster , f^+ is of the order of $10^{11}s^{-1}$ whereas for the largest cluster is of the order of $10^{12} - 10^{13}s^{-1}$. The results for the attachment rate f^+ are shown in Table 2.2. Notice that there was a misprint in the main text in our previous work[24] where we stated that the attachment rate for TIP4P/2005 of the medium cluster was 70 $10^9 s^{-1}$. The correct value (shown in Table 2.2) is 1.2 $\cdot 10^{12}s^{-1}$ and this correct value was used in the calculations of our previous work[24] leading to a value of $log_{10}J$ of -83 which is the same as that reported here in Table 2.2).

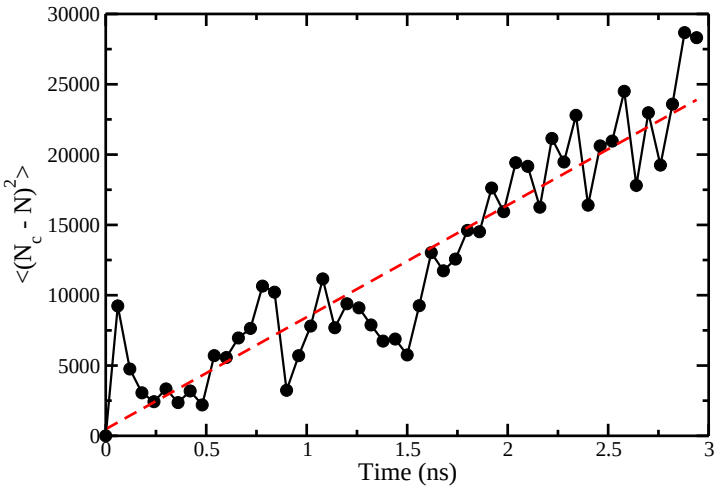

Figure 2.5: Attachment rate for the cluster of 3170 molecules of the TIP4P model. Results obtained from the average of 10 different trajectories. Simulations were performed at 212.5K and 1 bar. Notice that in Fig.6 of our previous work[24], the results were obtained for the medium cluster of TIP4P/ICE and not for the medium cluster of the TIP4P/2005 model as stated in the caption.

According to Ref.[1], since the attachment rate f^+, is related to the time required

for a molecule to attach to the solid cluster, one could express it as

$$f^{+} = \frac{24D(N_c)^{2/3}}{\lambda^2} \tag{2.7}$$

$N_c^{2/3}$ is the number of molecules at the cluster's surface and λ^2/D is the time required for a molecule to diffuse a given length λ (D being the diffusion coefficient of the supercooled liquid phase). Having numerically computed D at few temperatures, one could use an Arrhenius-like expression to estimate the diffusion coefficient as a function of temperature below melting:

$$\ln D = \ln D_0 - \frac{E_a}{RT} \tag{2.8}$$

whose coefficients for each model are presented in Table 2.3.

Table 2.3: Coefficients of the fit of Eq.2.8 to the diffusion coefficient of supercooled water for the TIP4P, TIP4P/2005, TIP4P/ICE and mW water models.

Model	$\ln(D_0/(m^2/s))$	$E_a/(kJ/mol)$
TIP4P	-1.30	39.526
TIP4P/2005	2.88	50.803
TIP4P/ICE	-1.84	44.709
mW	-13.46	12.890

Figure 2.6 clearly shows that an Arrhenius-like expression is sufficient to describe the variation of D with T for the temperature range considered in this work (i.e from the melting point up to temperatures of about 60K below melting).

It is interesting to point out that D does not decrease much with temperature in the case of the mW model. The decrease of D with T is more pronounced in the case of the TIP4P potentials. In the figure we have also included experimental results[68]. As can be seen, the TIP4P/2005 model is able to describe the experimental values reasonably well. As shown in Fig.6 our values of D for TIP4P/2005 are entirely consistent with those determined previously (for temperatures up to 210K) by Rozmanov and Kusalik[67].

Having determined the value of D, we can estimate the value of λ required to reproduce the results of f^{+} obtained in this work using Eq. 7.5 (reported in Table 2.2). The value of λ (see Table 2.2) is of about one molecule diameter (i.e 3.5) and does not depend strongly neither on temperature nor on the water model. This means that in order to obtain fast and reasonable estimates of f^{+} over a broad range of temperatures, one could in principle only need to determine D, without having to recur to the expensive calculations needed to compute f^{+} using Eq.7.5.

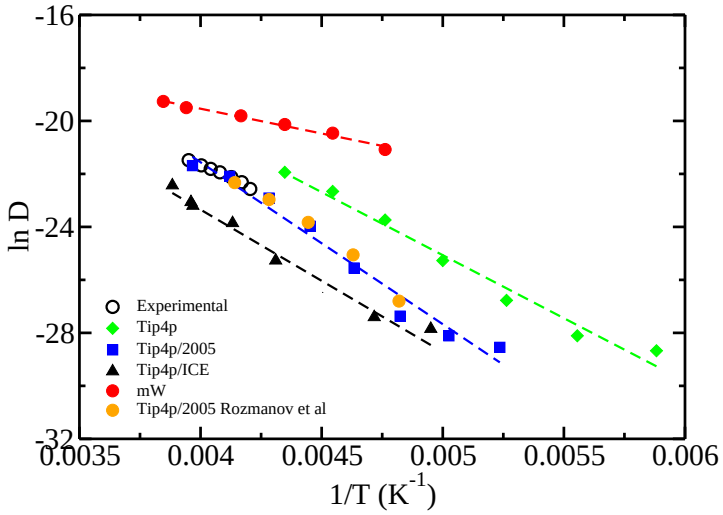

Figure 2.6: The diffusion coefficients for TIP4P/2005, TIP4P/ICE, TIP4P and mW models. Symbols correspond to simulation results of this work. Lines were obtained from an Arrhenius fit. For the TIP4P/2005 model we have also included the results from Rozmanov and Kusalik[67] (orange circles) for temperatures up to 210K. Experimental values: open circles[68].

The attachment rate for the mW is about 2-3 orders of magnitude larger than that for the other models. Once again λ is of the order of a molecular diameter. The larger value of f^+ for the mW can be explained by taking into account the fact that for this model D is much larger than for the rest of the models (and for real water) corresponding to an enhanced dynamics. Therefore we should point out that both f^+ and D decreases with T much less in the mW model than in other models. The absence of explicit hydrogens provokes higher values of D, f^+ and faster dynamics. If the nucleation free-energy barrier of this model is similar to that of the other models considered in this work, then by considering the kinetic prefactor one should expect the kinetics of this model being three orders of magnitude faster than that of the other models.

2.4.6. The kinetic prefactor

The kinetic prefactor required to estimate J is given by the product of ρ_f, Z and f^+. The number density of the liquid, of the order of 10^{28} molecules/m^3, does not change much with temperature. The product Zf^+ does not have a strong temperature dependence either given that as the temperature decreases Z increases and f^+ decreases. Thus, we find that Zf^+ is of the order of 10^9 s^{-1} for the TIP4P family of models. Hence, the kinetic prefactor for TIP4P-like models is of the order of 10^{37} m^{-3}s^{-1}.

As TIP4P/2005 describes quite well the diffusion coefficient of water at different temperatures, we believe that this is the order of magnitude of the kinetic prefactor of real water. Notice that for the mW model the kinetic prefactor is 2-3 orders of magnitude larger that for the TIP4P models. Therefore for the mW model the kinetic prefactor is of the order of 10^{40} $m^{-3}s^{-1}$.

2.4.7. The free-energy barrier, ΔG_c

The free-energy barriers for all clusters considered in this work are reported in Table 2.2.

For the largest clusters the free energy barrier is about $500k_B$T , for the medium clusters about $250k_B$T and for the smallest clusters about $80k_B$T and the differences among models are not particularly large. The lowest value of the free-energy barrier corresponds to TIP4P and the largest to mW although the differences are not too large. For the mW model, which has a somewhat larger value of γ, one would expect the largest free-energy barriers. However, this is not the case given that both the ice density and $\Delta\mu$ are very large, partially compensating this effect.

For TIP4P/ICE our results differ from those of Ref.[69], where by means of umbrella sampling, a free-energy barrier of $35k_BT$ and a critical cluster of 300 molecules at a temperature of 235K was reported. Our estimate is of $80k_BT$ and 600 molecules at the same temperature. Performing 10 independent runs starting from an initial configuration of a 300 molecule cluster, we observed that the cluster always melted after 30-50ns. These results suggest that a cluster of 300 ice molecules is most likely sub-critical for these thermodynamic conditions. Although the order parameter used in Ref.[69] is different from that used in this work we found that both criteria differ only in about ten per cent in identifying the size of a given cluster.

We have included in Table 2.2 the statistical error in ΔG_c. Once the order parameter is chosen then we can determine N_c accurately (so that there is practically no statistical error in the determination of N_c). We have an uncertainty of about 2.5K in ΔT , and that provokes an uncertainty of about 7 % in both $\Delta\mu$ and γ. Notice that these two errors are not independent since we are obtaining γ from Eq. 4.6. Therefore if $\Delta\mu$ is underestimated by 7 % then γ will be underestimated by 7 % also. According to this the statistical error in ΔG_c is also about 7 %. The statistical error for ΔG_c is shown in Table 2.2. This statistical error can be reduced by performing more trajectories. In principle, this statistical error can be reduced at the expense of using a huge amount of CPU time.

There is however an additional source of uncertainty which is systematic and can not be reduced by performing more trajectories. Different order parameters will yield somewhat different values of N_c (mainly due to the interfacial region). It is difficult to evaluate the impact of this systematic error (in fact if you know exactly the magnitude

and sign of the systematic error you can always correct your results to the exact value !) and for this reason we shall just provide a rough estimate. Different (reasonable) order parameters gave differences of up to $N_c^{2/3}$ molecules for N_c. This gives a systematic error in N_c of about 5 %, 7 % and 12 % for the large, the medium and the small cluster respectively. of about 10 %. It follows then, that this systematic source of error would affect the values of γ 4.6 by about 5/3 %,7/3 % and 4 % respectively. These systematic errors are smaller than the statistical error for γ (of about 7 %). Since ΔG_c scales with γ^3 (see Eq. 7.8)then the systematic error would affect the values of ΔG_c by about 5 % 7 % and 12 % respectively. We mentioned previously that the stochastic error in ΔG_c is of about 7 %. It seems that the systematic error for ΔG_c is similar to the stochastic error. In Table 2.2 we have included only the statistical errors in ΔG_c . If one wishes to estimate the total error (i.e including the systematic error) one can roughly multiply the error of Table 2.2 by two.

2.4.8. The nucleation rate, J

The homogeneous nucleation rate J is defined as the number of critical nuclei per unit of volume and time. Results of the nucleation rate are also reported in Table 2.2, where we conclude that the order of magnitude changes from $10^{-180}\mathrm{m}^{-3}\mathrm{s}^{-1}$ for the temperatures around 15 degrees below melting to about $10^{0}\mathrm{m}^{-3}\mathrm{s}^{-1}$ for temperatures about 35K below.

Due to the number of approximations we used to determine these numbers one might wonder whether our predictions for the nucleation rate J are reliable or not. The statistical error in $log_{10}J$ is presented in Table 2.2. The error in the kinetic prefactor in the expression of J has an error of about one order of magnitude. From the error in ΔG_c it is easy to obtain its contribution to the error in $log_{10}J$ simply by dividing by 2.3 (from the conversion natural to decimal logarithms). Therefore the total statistical error in $log_{10}J$ is obtained after adding these two terms. As discussed previously , if systematic errors were also included then the error in $log_{10}J$ presented in Table 2.2 should be (roughly) multiplied by two. From this it follows that the total error in $log_{10}J$ (stochastic and systematic) is of about 40, 20 and 6 for the largest, medium and smallest clusters considered in this work.

We use the results obtained at three different temperatures to estimate J over a broad range of temperatures. For this purpose we need to calculate the height of the nucleation free energy barrier, ΔG_c, and the kinetic prefactor, $Z\rho_f f^+$, for any temperature and obtain the rate with Eq. 4.8. To obtain $\Delta G_c(T)$ we use Eq. 7.8, where the functions $\gamma(T)$, $\Delta\mu(T)$ and $\rho_s(T)$ are required. For γ, we assume that it changes linearly with T in the way shown by the fits in Fig. 2.4 (dashed lines). The chemical potential difference as a function of temperature is calculated by thermodynamic integration (see Fig. 2.2). The density of the solid as a function of temperature is taken from a linear fit

to the results of Table 2.2. To obtain the kinetic prefactor as a function of temperature we need $\rho_f(T)$, Z(T) and $f^+(T)$. The density of the fluid changes smoothly with temperature and we have considered a constant value of 0.94 g/cm^3 for all models. By using Eqs. 4.9 and 4.6 and with the functions $\gamma(T)$ and $\Delta\mu(T)$ above described one can easily obtain Z(T). Finally, we use Eq. 7.5 to obtain $f^+(T)$. Eq. 7.5 requires, in turn, D(T) and $\lambda(T)$. For D(T) we use the fit given by Eq. 2.8. For λ we take a value independent of temperature and equal to an average between the values found for the three clusters (for all cases λ is of the order of a molecular diameter). With these approximations (which appear quite reasonable after the results presented so far) we can obtain J for any value of ΔT (supercooling).

In fig.2.7, we present the results of the logarithm of J as a function of the degree of supercooling for different water models. In figure 2.7 (a) we show our results for the mW model and compare it with previous calculations of J. At 240K our value of J is about 4 orders of magnitude higher that the value reported by Li et al.[16], whereas at 220K , 215K and 208K our value is about 4-6 orders of magnitude lower than the values reported by Li et al.[16] (220K using forward flux sampling), Russo et al.[70] (215K using umbrella sampling) and Moore and Molinero[19] (at 208K using brute force simulations). From this, we conclude that our predictions of the nucleation rate for the mW model are in reasonably good agreement with results previously reported in the literature, taking into account that the approach used here is an approximate one and that the uncertainty in J from our technique is about 6 orders of magnitude at high supercooling (coming from the uncertainty in determining the temperature at which the cluster is critical and the procedure used to distinguish solid from liquid-like molecules). We estimated the size of the critical cluster to be of 86 molecules at 205K for the mW model, in excellent agreement with the value reported by Moore and Molinero for the same model and temperature which was of about 90 molecules[19]. Since Russo et al.[70] have determined not only nucleation rates but also, f^+ , N_c and the free energy barrier it is interesting to have a closer comparison term by term. This is done in Table 2.4. As can be seen, the agreement for all individual terms is quite good. For $log_{10}(J)$ is reasonable taking into account that, as discussed previously, our uncertainty in $log_{10}(J)$ at high supercoolings, when all possible sources of error are considered, is of about 6 orders of magnitude.

Let us now describe the results for TIP4P like models. As it can be observed in figure 2.7 b), the values of homogeneous nucleation rates for TIP4P/2005 almost coincide (to within the error bars) with those computed for TIP4P/ICE, whereas the ones for TIP4P are slightly higher. In Fig. 2.7 c) the values of homogeneous nucleation rates for TIP4P/2005 are compared to experimental ones at the temperatures where most experiments are available (i.e between 235K and 240K). From the data we conclude that the results of TIP4P/2005 are consistent with the experimental ones (taking into account the combined uncertainty of both experimental and simulation results). Thus it seems that TIP4P/2005 is able to reproduce not only the ice density, the ice-water

Table 2.4: Contributions (term by term) to J for the mW model as obtained in this work and as obtained by Russo et al.[70]. Results of this work were obtained at $p = 1bar$ whereas those of Russo et al.[70] were obtained at $p = 0bar$. This small difference of pressure is not expected to affect any of the terms of the table. f^+ is given in s^{-1}, ΔG_c in k_BT units and J in $(m^{-3}s^{-1})$

Source	T(K)	N_c	f^+	Z	ΔG_c	$log_{10}(J)$
This work	215.1	128	1.0×10^{13}	0.016	38.2	23.2
Russo et al	215.1	81	0.8×10^{13}	0.018	23.5	29.4
This work	225	213	2.0×10^{13}	0.0109	51.5	17.5
Russo et al	225	180	2.6×10^{13}	0.0115	40.1	22.58
This work	235	405	4.1×10^{13}	0.0070	76.3	6.8
Russo et al	235	400	4.7×10^{13}	0.0077	72.0	8.7

interfacial free-energy and the diffusion coefficient, but also the nucleation rate J of real water. We also compare our results with recent experimental work where homogeneous ice nucleation was measured in nanoscopic water droplets[72]. By using such small droplets in Ref.[72] homogeneous ice nucleation was probed at an extremely high supercooling (59 K below melting). Notably, the agreement between the TIP4P/2005 model and the experiments of Ref.[72] is also very good. As can be seen in fig. 2.7 c) , for the mW model, the values of J obtained in previous works[16,19,70] seem to be in good agreement with the experimental results when the supercooling is large. In fact the agreement with the recent results of Manka et al.[72] is quite good. However for moderate supercooling J of the mW model seems to be lower than those found in experiments, this is most likely due to the high value of the interfacial free energy γ of the model.

Another interesting feature is that for the TIP4P model the nucleation rate reaches a maximum value and after that it decreases slightly (see Fig. 2.7 c) . For the other TIP4P models one may expect similar behavior but at lower temperatures. The maximum is caused by the fact that the thermodynamic driving force for nucleation increases as the temperature decreases (i.e the free-energy barrier decreases) and at the same time the kinetic prefactor decreases dramatically with temperature and at very low temperatures becomes the dominant factor. The fact that J may reach a maximum has been already suggested by Jeffery and Austin[73] and is consistent with the experimental results of Refs.[74,75] when studying the freezing of water clusters at very low temperatures (i.e 72K below melting), although is not entirely clear if at this high supercooling the formation of ice is limited by ice nucleation or by growth (see discussion below) .

2.4.9. Homogeneous nucleation temperature

The homogeneous nucleation temperature T_H is a kinetic concept. T_H is the temperature below which water does not exist in its liquid phase (because it freezes). However, to properly define T_H, we need to specify both the sample size and the duration of the experiment. The experimental value of homogeneous nucleation temperature ($T_H^{exp} = 235K$) can be approximated by the temperature at which one critical ice cluster is formed in a spherical micrometer-size water droplet and for one minute:

$$J = \frac{1}{\frac{4}{3}\pi(2\ \ 10^{-6})^3 60} = 10^{14}/(m^3 s). \tag{2.9}$$

This experimental rate is represented by a dashed line in figure 2.7. As can be seen in figure 2.7 b) in the case of TIP4P/ICE and TIP4P/2005, T_H^{exp} is located about 37K below melting, in reasonable agreement with the experimental value. In the case of TIP4P T_H^{exp} is slightly lower (around 30K below melting).

Let us now estimate the free-energy barrier height when $J = 10^{14}/(m^3 s)$. For the TIP4P models it is of the order of $53k_B$T (given that the kinetic prefactor is about $10^{37}\ m^{-3}s^{-1}$) whereas for the mW model it is of the order of $60k_B$T. Since the values of J for TIP4P/2005 agree quite well with experiments, this strongly suggest that at the experimental value of T_H^{exp} (i.e 235K) the free energy barrier for nucleation is about $53k_B$T. It is interesting to point out that the attachment rate f^+, of the mW model, is of the same order of magnitude of that found for LJ systems. Therefore for systems formed by atoms/ions , f^+ seems to be of the same order magnitude. Obviously for these systems the free energy barrier must be about $60k_B$T at T_H^{exp}[1]. However, for water, f^+ is three orders of magnitude smaller and the free energy barrier at T_H^{exp} must be about $53k_B$T. In other words as a rule of thumb one can state that the experimental homogeneous nucleation of water in micrometric droplets is the temperature at which the free energy barrier becomes of about $53k_BT$. It is interesting to point out that both the value of the homogeneous nucleation temperature and of associated free energy barrier depend on the volume of the droplets with which the experiments are performed. The considerations above are all for micrometric water droplets, which is the most widespread experimental set up for the study of homogeneous ice nucleation. But this is not always the case. In fact, in a recent work, by using nanoscopic droplets much higher nucleation rates, and smaller nucleation barriers, were probed[72]. Therefore, the so called "homogeneous nucleation line" depends on the volume of the water droplets and should not be taken as a definite limit for the existence of supercooled liquid water.

When dealing with computer simulations, both length and time-scales are quite different. The simulation value of the homogeneous nucleation temperature (T_H^{sim}) can be estimated as the temperature at which one critical ice cluster is formed in a simulation with a box side of 40 (corresponding to a typical supercooled water density of about

$0{,}94 g/cm^3$ in a system of 2000 molecules) for 1 microsecond. At these conditions, the nucleation rate takes the value:

$$J = \frac{1}{(40\ 10^{-10})^3 10^{-6}} = 10^{31}/(m^3 s) \tag{2.10}$$

as represented by a dashed line in figure 2.7. As can be seen in figure 2.7 b) in the case of TIP4P/ICE and TIP4P/2005, T_H^{sim} is located about 60-65K below melting. Whereas once more in the case of TIP4P T_H^{exp} is slightly lower (around 50 below melting). Again, knowing the nucleation rate, one could estimate the free-energy barrier height at T_H^{sim} for TIP4P/ICE, TIP4P/2005 and TIP4P to be of the order of $13 k_B$T. Whereas the free-energy barrier height at T_H^{sim} for mW is of the order of $19 k_B$T (given that the kinetic prefactor for this water model is three orders of magnitude larger). When simulating simple/atomic fluids (such as hard spheres[18], Lennard-Jones[76] or NaCl[31]), spontaneous nucleation within reasonable time-scale can be observed with brute force simulations when the free-energy barrier height is of the order of $18 k_B$T.

2.4.10. Growth rate and Avrami's law

Rozmanov and Kusalik[77] have determined the growth rate of TIP4P/2005 for temperatures between the melting point and 210K and fitted their results to a Wilson-Frenkel like expression[78–80]. To estimate the ice growth rate at lower temperatures we have performed direct coexistence simulations for the TIP4P/2005 at 1bar and temperatures below 210K. The system consists of 2048 molecules. In the initial configuration half of the molecules are forming ice and the other half supercooled water (i.e approximately we have a 35 Å layer of ice and a 35 Å layer of water). The evolution of the potential energy with time is shown in fig.2.8. For all considered temperatures the system freezes completely (as shown from the final plateau of the energy, from visual inspection of the final configuration and from the analysis of the sample using order parameters). Obviously the time required to form ice is much longer at 200K (1500ns) than at 220K (80ns). To estimate the growth rate we simply divided 35 Å (i.e the thickness of the liquid slab) by the time required to freeze the system. Notice that this is used just to provide a rough estimate of the growth rate of ice. A rigorous determination of the growth rate requires performing the analysis over a larger number of independent trajectories. For the three highest temperatures 220K, 215K and 210K the growth rate estimated in this work is fully consistent with that obtained previously by Rozmanov and Kusalik.[77,81] For the two lowest temperatures, the growth rate estimated in this work , 0.049 Å /ns at 205K and 0.025 Å /ns at 200K , should be compared to the values 0.056 Å/ns and 0.040 Å/ns obtained from the fit of Rozmanov and Kusalik (for the average of the different planes).[81] Since the agreement is satisfactory we shall assume that the fit of Rozmanov and Kusalik for the ice growth rate, can be used for temperatures below 210K.

In general, nucleation is the limiting step for supercooled liquid water to transform into ice. Therefore, once a critical cluster is formed, ice crystal growth tends to occur quite rapidly. However, at low temperatures this might not be the case, since the ice growth rate , u , might be very small. When the growth rate is small, one should introduce a new parameter, τ_x (which is the time required to crystallize a certain volume fraction of the sample ϕ). τ_x depends on two properties, the value of J,and the value of the growth rate of ice , u. The Avrami's equation has been considered for obtaining τ_x [19,82,83]. In Debenedetti's book the expression for τ_x is provided and it is given by :

$$\tau_x^{Avrami} = ((3\phi)/(\pi J u^3))^{1/4} \tag{2.11}$$

By using Avrami's expression we have plotted τ_x^{Avrami} in fig. 2.9 as a function of the degree of supercooling for the TIP4P/2005 model. Although we used $\phi = 0{,}7$, τ_x^{Avrami} is practically the same for any value between 0.6 and 0.9 chosen for ϕ, as τ_x changes as $\phi^{1/4}$. As can be seen the minimum τ_x is of the order of several microseconds. The minimum in τ_x occurs at smaller values of supercooling that the maximum in J. In any case it is important to recall the fact that τ_x rather than J is the relevant magnitude at large supercoolings as the growth rate of ice can be the limiting factor. There is still a subtle issue with respect to the application of Avrami's expression. Notice that Avrami's expression contains only the intensive parameters ϕ, J, and u, so τ_x does not depend on the size of the system. However, as pointed out by Berg[84], there are important system size effects on τ_x specially when one goes down to the system size typical of computer simulations. When the nucleation time τ_{nu} (i.e the time required to form a critical nucleus) :

$$\tau_{nu} = 1/(JV) \tag{2.12}$$

is larger than the diffusive time one can not find a critical cluster growing in the system until the nucleation time has elapsed. In such regime, Avrami's traditional expression can not be applied and the crystallization time is dominated by the nucleation time, that is inversely proportional to the system's volume. Following Berg[84], let us define a parameter q as the ratio of two times, the growth time τ_{growth} (i.e the time required to crystallize completely the simulation box after a post-critical nucleus has been formed) and τ_{nu} as :

$$\tau_{growth} = L/u \tag{2.13}$$

$$q = \tau_{growth}/\tau_{nu} \tag{2.14}$$

where L is the dimension of one of the sizes of the cubic simulation box. Notice that q depends on the system size so it is not an intensive property. In fact for any

temperature q tends to ∞ as one increases the system size to the thermodynamic limit (the numerator scales as L whereas the denominator scales as L^{-3}). According to Berg[84] τ_x can be expressed as :

$$\tau_x = \tau_{nu}(1 + f_d(q)) \tag{2.15}$$

The function $f_d(q)$ behaves as $A_d q$ for values of q smaller than one (i.e when the growth time is smaller than the nucleation time) and behaves as $B_d q^{3/4}$ for values of q larger than 64 (i.e when the growth time is larger than the nucleation time). Between these two values one has a crossover behavior. According to this for values of q larger than 64 , one recovers the traditional Avrami's expression. However for small values of q τ_x can be approximated quite well by τ_{nu}. Since τ_{nu} depends on the system size, so does τ_x. In fig. 2.9 we have also plotted the value of τ_{nu} for system sizes of 2000, 20000, 200000 and 2000000 molecules of water. For each system size τ_x is given by τ_{nu} up to the temperature at which τ_{nu} intersects Avrami's expression. Obviously as one moves to larger system sizes the intersect moves to lower supercooling (i.e higher temperatures) and in the thermodynamic limit, Avrami's expression is valid for all temperatures. However this is certainly not the case for finite size systems. Notice also that due to the finite size effects small systems gain an extra stability with respect to freezing (i.e more time is needed to freeze the system). One could state that crystallization is controlled by nucleation when τ_{nu} is much larger than τ_{growth} , and by ice growth when the opposite is true. This behavior is sensitive to the system size used in the simulations.

After the previous discussion it is clear that the conditions where spontaneous crystallization of TIP4P/2005 water could be most affordable in terms of CPU time would be a system of about 20000 molecules at about 195K (i.e 57K below the melting point). Under these conditions Avrami's expression is valid and from our estimates it should take about 6 microseconds to freeze the system. That may explain why no ice formation was observed in runs of about one microsecond in previous work[27,85].

Regarding the possible existence of a liquid-liquid critical point, a key question is to know if the liquid can be equilibrated before it freezes[19,86–89]. In the case of the TIP4P/2005 model this is equivalent studiying whether 6 microseconds are enough to obtain the properties of metastable water at high supercoolings (i.e in the range of 50 to 65K at 1 bar below the melting temperature). Obviously the 6 microseconds refers to the study of this work (i.e at p=1bar). Further work is needed to analyze how τ_x changes with pressure.

In fig.2.9 the free energy barrier and size of the critical cluster are shown for TIP4P/2005 as a function of the supercooling. Under the conditions where the crystallization time from Avrami's expression is at a minimum we estimate a free energy barrier of 14 $k_B T$ and a size of the critical cluster of about 60 molecules.

2.5. Conclusions

In this work we have determined the temperature at which several clusters become critical for both TIP4P and mW water models. In our previous work[24] we performed similar calculations for TIP4P/2005 and TIP4P/ICE. By assuming that CNT can be used to describe the critical cluster size, the value of the interfacial Ih-water free energy γ was obtained. We performed runs of the time evolution of the cluster size with time from its critical value and at the temperature at which it is critical to determine the attachment rate f^+. Finally the value of the nucleation rate was estimated as a function of the supercooling, by using CNT to estimate the free energy barrier, and the attachment rate to obtain the kinetic prefactor. The main conclusions of our work are:

1. γ was found to decrease with temperature with a slope (related to the excess interfacial entropy) of about -0.25 mN/(K.m) in reasonable agreement with the previous estimate of Reinhard and Doye for the TIP4P/2005 model (i.e -0.18 mN/(K.m)). For the mW the temperature dependence was found to be weaker.

2. By extrapolating to the melting temperature an estimate of the interfacial free energy for the planar interface was obtained for several water models. The values of γ for the planar interface decrease in the order TIP4P/ICE, mW, TIP4P/2005 and TIP4P. The values obtained of γ for the planar interface are in reasonable agreement with the reported experimental values $25 - 35$ mN/m.

3. The attachment rate can be estimated quite well by using the diffusion coefficient, and assuming a typical attachment length of about one molecular diameter (i.e 3.5 Å). For the mW model , the decrease of D with T is weak, certainly accelerating significantly the dynamics at very low temperatures.

4. By fitting the diffusion coefficient to an Arrhenius expression and assuming a linear variation of γ with temperature we have estimated J for a wide range of temperatures. For the mW the values obtained for J are in reasonable agreement with previous estimates. The predictions of the TIP4P/2005 for J are consistent (taking into account the uncertainties) with the experimental values. The model predicts a homogeneous nucleation temperature of about 37K , in agreement with experiments.

5. At T_H^{exp} the kinetic prefactor to be used in CNT should be of the order of $10^{37}(m^{-3}s^{-1})$ whereas the free energy barrier ΔG_c is of about 53 k_BT. At T_H^{sim}, ΔG_c is of about 14 k_BT.

6. The growth of ice is not arrested at least for temperatures up to 50K below the melting point. By using Avrami's equation we estimated that for large systems (i.e

large enough to have at least one critical cluster in the simulation box) about 6 microseconds would be required to have a significant fraction of ice for a supercooling of about 60K. For smaller systems the time would be larger as one needs to wait until a critical cluster is formed. Thus, for small systems, the liquid phase gains kinetic stability so it becomes possible to have the liquid as metastable phase for longer times.

We recognize that the picture provided in this work is far from complete, since we are using a number of approximations in the entire formulation. However it provides an initial framework for forthcoming studies possibly using more sophisticated methods such as umbrella sampling, forward flux sampling or transition path sampling.[90] These calculations will be of much interest, but certainly not cheap from a computational point of view. Although nucleation studies of ice from simulation are still in its infancy we hope our work will encourage further interest in this area, highly relevant for cryopreservation[91], the food industry[92] and climate prediction[93–95].

Acknowledgements

This work was funded by grants FIS2013/43209-P of the MEC, and by the Marie Curie Integration Grants 303941-ANISOKINEQ-FP7-PEOPLE-2011-CIG and 322326-COSAAC-FP7-PEOPLE-2012-CIG . C.Valeriani acknowledges financial support from a Juan de La Cierva and E.S. from a Ramon y Cajal Fellowship, respectively. Calculations were carried out thank to the supercomputer facility Tirant from the Spanish Supercomputing Network (RES) (through project QCM-2014-1-0021). The authors thank Dr. Philip Geiger and Prof. Christoph Dellago for having kindly shared with them configurations of the TIP4P/ICE. We thank Prof. Molinero for providing us the input files to perform runs of the mW model of water using LAMMPS. We thank the two reviewers of this paper for their helpful comments. We thank Dr. Carl McBride for a critical reading of the manuscript.

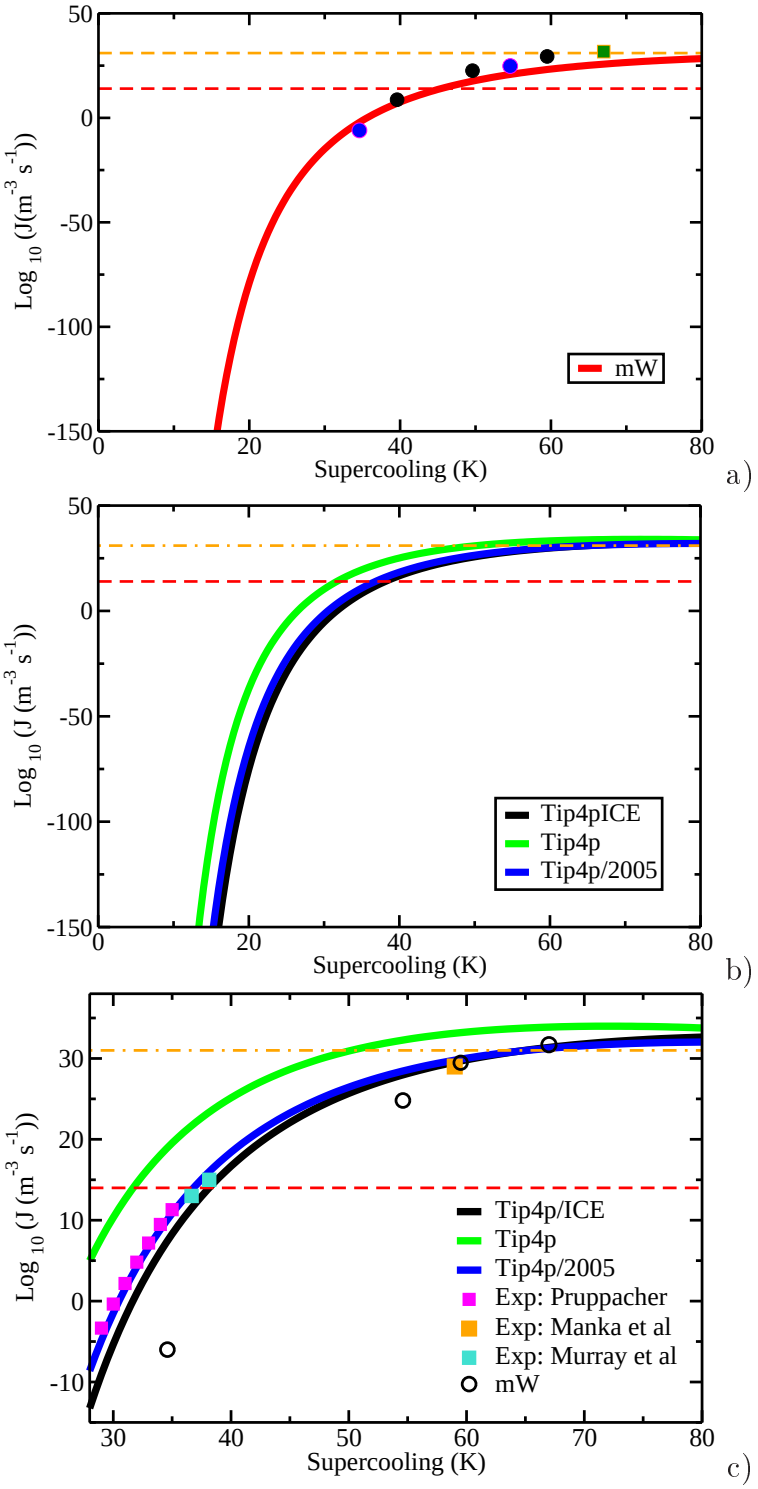

Figure 2.7: Values of J for several water models, as obtained in this work, from experiment, and in previous work (in the case of the mW model). The horizontal lines correspond to $log_{10}J/(m^{-3}s^{-1}) = 14$ and $log_{10}J/(m^{-3}s^{-1}) = 31$ which are the approximate values of J at the homogeneous nucleation temperature in experiments and in simulations respectively. a) J for the mW model as obtained in this work (red solid line) . Blue circles are results at 240K and 220K from Ref.[16], black circles are the results from Russo et al.[70] and green square at 208K from Ref.[19]. b) J for the TIP4P , TIP4P/ICE and TIP4P/2005 models. c) J of the models studied in this work (solid lines) compared to experiments (filled squares) of Pruppacher[2], Murray et al.[71] and Manka et al[72]. Empty circles are estimates of J for the mW model as reported in References[16,19,70]. Notice that, in the c panel, both x and y-axis differ from the other two panels.

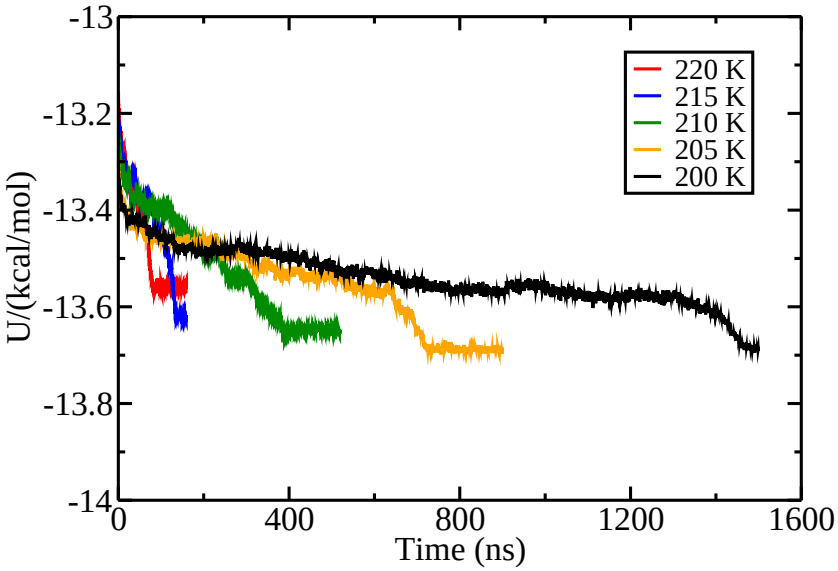

Figure 2.8: Evolution of the potential energy with time in direct coexistence runs of the TIP4P/2005 model using a slab with 2048 molecules (half ice Ih and half liquid water) at the temperatures, from the left to the right, of 220K, 215K, 210K, 205K and 200K.

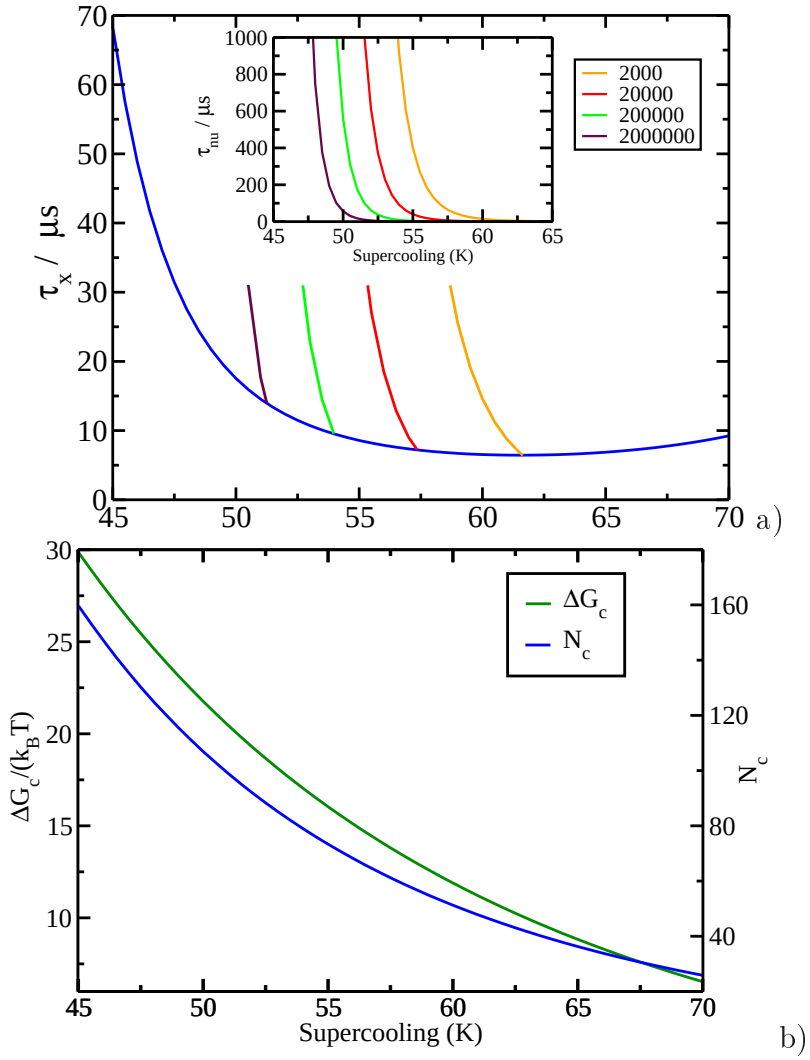

Figure 2.9: (a): τ_x for $\phi = 0{,}7$ for the TIP4P/2005 model as a function of the supercooling. τ_x is the time necessary to crystallize 70 % of the system. Inset: plot of the nucleation time, τ_{nu}, versus the supercooling. (b): Free energy barrier for nucleation and size of the critical cluster for TIP4P/2005 as a function of the supercooling.

Bibliography

1. Kelton, K. F., *Crystal Nucleation in Liquids and Glasses*, vol. 45 (Academic Press, Boston, 1991).

2. Pruppacher, H. R., A new look at homogeneous ice nucleation in supercooled water drops. *J. Atmosph. Sci.* **52**, 1924 (1995).

3. Taborek, P., Nucleation in emulsified supercooled water. *Phys. Rev. B* **32**, 5902–5906 (1985).

4. Stockel, P., Weldinger, I. M., Baumgartel, H. & Leisner, T., Rates of homogeneous ice nucleation in levitated h2o and d2o droplets. *J. Phys. Chem. A* **109**, 2540 (2005).

5. Murray, B. J., Broadley, S. L., Wilson, T. W., Bull, S. J., Wills, R. H., Christenson, H. K. & Murray, E. J., Kinetics of the homogeneous freezing of water. *Phys. Chem. Chem. Phys.* **12**, 10380 (2010).

6. Granasy, L., Pusztai, T. & James, P. F., Interfacial properties deduced from nucleation experiments: A cahn hilliard analysis. *J. Chem. Phys.* **117**, 6157 (2002).

7. Davidchack, R. L., Handel, R., Anwar, J. & Brukhno, A. V. *J. Chem. Theory Comput.* **8**, 2383 (2012).

8. Handel, R., Davidchack, R. L., Anwar, J. & Brukhno, A. *Phys. Rev. Lett.* **100**, 036104 (2008).

9. Vega, C., Sanz, E. & Abascal, J. L. F., The melting temperature of the most common models of water. *J. Chem. Phys.* **122**, 114507 (2005).

10. Matsumoto, M., Saito, S. & Ohmine, I., Molecular dynamics simulation of the ice nucleation and growth process leading to water freezing. *Nature* **416**, 409 (2002).

11. Jorgensen, W. L., Chandrasekhar, J., Madura, J. D., Impey, R. W. & Klein, M. L., Comparison of simple potential functions for simulating liquid water. *J. Chem. Phys.* **79**, 926 (1983).

12. Radhakrishnan, R. & Trout, B. L., Nucleation of crystalline phases of water in homogeneous and inhomogeneous environments. *Phys. Rev. Lett.* **90**, 158301 (2003).

13. Quigley, D. & Rodger, P. M., Metadynamics simulations of ice nucleation and growth. *J. Chem. Phys.* **128**, 154518 (2008).

14. Brukhno, A. V., Anwar, J., Davidchack, R. & Handel, R. *J. Phys. Condens. Matter* **20**, 494243 (2008).

15. Molinero, V. & Moore, E. B., Water modeled as an intermediate element between carbon and silicon. *The Journal of Physical Chemistry B* **113**, 4008–4016 (2009).

16. Li, T., Donadio, D., Russo, G. & Galli, G., Homogeneous ice nucleation from supercooled water. *Phys. Chem. Chem. Phys.* **13**, 19807–19813 (2011).

17. Reinhardt, A. & Doye, J. P. K. *J. Chem. Phys.* **136**, 054501 (2012).

18. Filion, L., Hermes, M., Ni, R. & Dijkstra, M., Crystal nucleation of hard spheres using md umbrella sampling and forward flux sampling: A comparison of simulation techniques. *J. Chem. Phys.* **133**, 244115 (2010).

19. Moore, E. B. & Molinero, V., Structural transformation in supercooled water controls the crystallization rate of ice. *Nature* **479**, 506 (2011).

20. Abascal, J. L. F. & Vega, C. *J. Chem. Phys.* **123**, 234505 (2005).

21. Abascal, J. L. F., Sanz, E., Fernandez, R. G. & Vega, C. *J. Chem. Phys.* **122**, 234511 (2005).

22. Bai, X.-M. & Li, M., Test of classical nucleation theory via molecular-dynamics simulation. *J. Chem. Phys.* **122**, 224510 (2005).

23. Bai, X.-M. & Li, M., Calculation of solid-liquid interfacial free energy: A classical nuclea tion theory based approach. *J. Chem. Phys.* **124**, 124707 (2006).

24. Sanz, E., Vega, C., Espinosa, J. R., Caballero-Bernal, R., Abascal, J. L. F. & Valeriani, C., Homogeneous ice nucleation at moderate supercooling from molecular simulation. *J. Am. Chem. Soc.* **135**, 15008–15017 (2013).

25. Abascal, J. L. F. & Vega, C., Widom line and the liquid-liquid critical point for the tip4p/2005 water model. *J. Chem. Phys.* **133**, 234502 (2010).

26. Abascal, J. L. F. & Vega, C., Eos supercooled. *J. Chem. Phys.* **134**, 186101 (2011).

27. Bresme, F., Biddle, J. W., Sengers, J. V. & Anisimov, M. A., Minimum in the thermal conductivity of supercooled water: A computer simulation study. *J. Chem. Phys.* **140**, 161104 (2014).

28. Limmer, D. T. & Chandler, D., The putative liquid-liquid transition is a liquid-solid transition in atomistic. *J. Chem. Phys.* **138**, 214504 (2013).

29. Auer, S. & Frenkel, D., Numerical prediction of absolute crystallization rates in hard-sphere colloids. *J. Chem. Phys.* **120**, 3015–3029 (2004).

30. Auer, S. & Frenkel, D., Prediction of absolute crystal-nucleation rate in hard-sphere colloids. *Nature* **409**, 1020 (2001).

31. Valeriani, C., Sanz, E. & Frenkel, D., Rate of homogeneous crystal nucleation in molten nacl. *J. Chem. Phys.* **122**, 194501 (2005).

32. Pereyra, R. G., Szleifer, I. & Carignano, M. A. *J. Chem. Phys.* **135**, 034508 (2011).

33. Knott, B. C., Molinero, V., Doherty, M. F. & Peters, B., Homogeneous nucleation of methane hydrates: Unrealistic under realistic conditions. *J. Am. Chem. Soc.* **134**, 19544–19547 (2012).

34. Davidchack, R. L., Morris, J. R. & Laird, B. B., The anisotropic hard-sphere crystal-melt interfacial free energy from fluctuations. *J. Chem. Phys.* **125**, 094710 (2006).

35. Davidchack, R. L., Hard spheres revisited: Accurate calculation of the solid–liquid interfacial free energy. *J. Chem. Phys.* **133**, 234701 (2010).

36. Davidchack, R. L. & Laird, B. B., Direct calculation of the crystal–melt interfacial free energies for continuous potentials: Application to the lennard-jones system. *J. Chem. Phys.* **118**, 7651–7657 (2003).

37. Lechner, W. & Dellago, C. *J. Chem. Phys.* **129**, 114707 (2008).

38. Carignano, M. A., Formation of stacking faults during ice growth ... *J. Phys. Chem. C* **111**, 501 (2007).

39. Seo, M., Yang, E., Kim, K., Choi, S. & Kim, J. S., Undertanding anistropic .... *J. Chem. Phys.* **137**, 154503 (2012).

40. Moore, E. B. & Molinero, V., Is it cubic? ice crystallization from deeply supercooled water. *Phys. Chem. Chem. Phys.* **13**, 20008 (2011).

41. Kuhs, W. F., Sippel, C., Falenty, A. & Hansen, T. C., Extent and relevance of stacking disorder in ice ic. *Proceedings of the National Academy of Sciences* **109**, 21259 (2012).

42. Malkin, T. L., Murray, B. J., Brukhno, A. V., Anwar, J. & Salzmann, C. G., Structure of ice crystallized from supercooled water. *Proceedings of the National Academy of Sciences* **109**, 1041 (2012).

43. Benet, J., MacDowell, L. G. & Sanz, E., Undertanding anistropic .... *Phys. Chem. Chem. Phys.* **in press**, DOI: 10.1039/C4CP03398A (2014).

44. Zaragoza, A., Conde, M. M., Espinosa, J. R., Valeriani, C., Vega, C. & Sanz, E., Competition between ices ih and ic in homogeneous water freezing. *The Journal of Chemical Physics* **143**, 134504 (2015).

45. Lindahl, E., Hess, B. & van der Spoel, D., Gromacs 3.0: a package for molecular simulation and trajectory analysis. *J. Mol. Model.* **7**, 306 (2001).

46. Bussi, G., Donadio, D. & Parrinello, M., Canonical sampling through velocity rescaling. *J. Chem. Phys.* **126**, 014101 (2007).

47. Parrinello, M. & Rahman, A., Polymorphic transitions in single crystals: A new molecular dynamics method. *J. App. Phys.* **52**, 7182 (1981).

48. Wheeler, D. R. & Newman, J., A less expensive ewald lattice sum. *Chem. Phys. Lett.* **366**, 537 (2002).

49. Molinero, V. & Moore, E. B., Water modeled as an intermediate element between carbon and silicon. *J. Phys. Chem. B* **113**, 4008–4016 (2009).

50. Plimpton, S., no se. *J. Comput. Phys.* **117**, 1 (1995).

51. McBride, C., Vega, C., Noya, E. G., Ramirez, R. & Sese, L. M., Quantum contributions in the ice phases: The path to a new empirical model for water-tip4pq/2005. *J. Chem. Phys.* **131**, 024506 (2009).

52. Vega, C., Conde, M. M., McBride, C., Abascal, J. L. F., Noya, E. G., Ramirez, R. & Sese, L. M., Heat capacity of water: A signature of nuclear quantum effects. *J. Chem. Phys.* **132**, 046101 (2010).

53. McBride, C., Noya, E., J.L.Aragones, Conde, M. & C.Vega, The phase diagram of water from quantum simulations. *Phys. Chem. Chem. Phys.* **14**, 10140 (2012).

54. McBride, C., Aragones, J., E.G.Noya & Vega, C., A study of the influence of isotopic substitution on the melting point and temperature of maximum density of water by means of path integral simulations of rigid models. *Phys. Chem. Chem. Phys.* **14**, 15199 (2012).

55. Vega, C., Abascal, J. L. F., Conde, M. M. & Aragones, J. L., What ice can teach us about water interactions: a critical comparison of the performance of different water models. *Faraday Discuss.* **141**, 251–276 (2009).

56. Vega, C. & Abascal, J. L. F., Simulating water with rigid non-polarizable models: a general perspective. *Phys. Chem. Chem. Phys* **13**, 19663–19688 (2011).

57. Feistel, R. & Wagner, W., A new equation of state for H2O ice ih. *J. Phys. Chem. Reference Data* **35**, 1021–1047 (2006).

58. **See EPAPS Document No. E-JCPS for further details about the runs used to determine N_c and the attachement rate f^+.**

59. Herrero, C. P. & Ramirez, R., Path-integral simulation of solids. *J. Phys. Condens. Matter* **26**, 233201 (2014).

60. Kumar, P., Buldyrev, S. V., Becker, S. R., Poole, P. H., Starr, F. W. & Stanley, H. E., Relation between the widom line and the breakdown of the stokes-einstein relation in supercooled water. *Proc. Nat. Acad. Sci.* **104**, 9575–9579 (2007).

61. Reinhardt, A. & Doye, J. P. K., Note: Homogeneous tip4p/2005 ice nucleation at low supercooling. *J. Chem. Phys.* **139**, 096102 (2013).

62. Turnbull, D., Kinetics of solidification of supercooled liquid mercury droplets. *Appl. Phys.* **21**, 1022–1028 (1950).

63. Laird, B. B. *J. Chem. Phys.* **115**, 2887 (2001).

64. Horn, H. W., Swope, W. C., Pitera, J. W., Madura, J. D., Dick, T. J., Hura, G. L. & Head-Gordon, T., Development of an improved four-site water model for biomolecular simulations: TIP4P-Ew. *J. Chem. Phys.* **120**, 9665 (2004).

65. Hardy, S. C. *Philos. Mag.* **35**, 471 (1977).

66. Rozmanov, D. & Kusalik, P. G., Isoconfigurational molecular dynamics study of the kinetics of ice crystal growth. *Phys. Chem. Chem. Phys.* **14**, 13010 (2012).

67. Rozmanov, D. & Kusalik, P. G., Transport coefficients of the tip4p-2005 water model. *J. Chem. Phys.* **136**, 044507 (2012).

68. Price, W. S., Ide, H. & Arata, Y. *J. Phys. Chem.* **103**, 448–450 (1999).

69. Geiger, P. & Dellago, C. *J. Chem. Phys.* **139**, 164105 (2013).

70. Russo, J., Romano, F. & Tanaka, H., New metastable form of ice and its role in the homogeneous crystallization of water. *Nature Materials* **13**, 733 (2014).

71. Murray, B. J., Broadley, S. L., Wilson, T. W., Bull, S. J., Wills, R. H., Christenson, H. K. & Murray, E. J., Kinetics of the homogeneous freezing of water. *Phys. Chem. Chem. Phys* **12**, 10380–10387 (2010).

72. Manka, A., Pathak, H., Tanimura, S., Wolk, J., Strey, R. & Wyslouzil, B. E., Freezing water in no man's land. *Phys. Chem. Chem. Phys* **14**, 4505–4516 (2012).

73. Jeffery, C. A. & Austin, P. H., Homogeneous nucleation of supercooled water: Results from a new equation of state. *J. Geophys. Research* **102**, 25269 (1997).

74. Huang, J. F. & Bartell, L. S., Kinetics of homogeneous nucleation in the freezing of large clusters. *J. Phys. Chem.* **99**, 3924 (1995).

75. Bartell, L. S. & Huang, J. F., Supercooling of water below the anomalous range near 226 k **98**, 7455–7457 (1994).

76. Baidakov, V. G., Tipeev, A. O., Bobrov, K. S. & Ionov, G. V., Crystal nucleation rate isotherms in lennard-jones liquids. *J. Chem. Phys.* **132**, 234505 (2010).

77. Rozmanov, D. & Kusalik, P. G., Temperature dependence of crystal grwth of hexagonal ice (ih). *Phys. Chem. Chem. Phys* **13**, 15501–15511 (2011).

78. Wilson, H. A. *Philos. Mag.* **50**, 238 (1900).

79. Frenkel, J. *Phys. Z. Sowjetunion* **1**, 498 (1932).

80. Broughton, J. Q., Gilmer, G. H. & Jackson, K. A., Crystallization rates of a lennard-jones liquid. *Phys. Rev. Lett.* **49**, 1496–1500 (1982).

81. Rozmanov, D. & Kusalik, P. G., Anisotropy in the crystal growth of hexagonal ice, ih. *J. Chem. Phys.* **137**, 094702 (2012).

82. Avrami, M., Kinetics of phase change. i general theory. *J. Chem. Phys.* **7**, 1103–1112 (1939).

83. Debenedetti, P. G., *Metastable liquids: Concepts and Principles* (Princeton University Press, 1996).

84. Berg, B. A. & Dubey, S., Finite volume kolmogorov-johnson-mehl-avrami theory. *Phys. Rev. Lett.* **100**, 165702 (2008).

85. Shevchuk, R. & Rao, F., Note: Microsecond long atomistic simulation of supercooled water. *J. Chem. Phys.* **137**, 036101 (2012).

86. Poole, P. H., Sciortino, F., Essmann, U. & Stanley, H. E., Phase behavior of metastable water. *Nature* **360**, 324 (1992).

87. Liu, Y., Palmer, J. C., Panagiotopoulos, A. Z. & Debenedetti, P. G., Liquid-liquid transition in st2 water. *J. Chem. Phys.* **137**, 214505 (2012).

88. Limmer, D. T. & Chandler, D., The putative liquid-liquid transition is a liquid-solid transition in atomistic models of water. *J. Chem. Phys.* **135**, 134503 (2011).

89. Palmer, J., Martelli, F., Liu, Y., Car, R., Panagiotopoulos, A. Z. & Debenedetti, P. G., Metastable liquid-iquid transition in a molecular model of water. *Nature* **510**, 385 (2014).

90. Bolhuis, P. G., Dellago, C., Geissler, P. L. & Chandler, D., Transition path sampling: throwing ropes over mountains in the dark. *J. Phys.:Condens. Matter* **12**, A147 (2000).

91. Morris, G. J. & Acton, E., Controlled ice nucleation in cryopreservation–a review. *Cryobiology* **66**, 85 (2013).

92. Maki, L. R., Galyan, E. L., M.M., C. & Caldwell, D. R., Ice nucleation induced by pseudomonas-syringae. *Appl. Microbiol.* **28**, 456–459 (1974).

93. Cantrell, W. & Heymsfield, A., Production of ice in tropospheric clouds. *Bull. Amer. Meteor. Soc.* **86**, 795 (2005).

94. Baker, M. B., Cloud microphysics and climate. *Science* **276**, 1072–1078 (1997).

95. DeMott, P. J., Prenni, A. J., Liu, X., Kreidenweis, S. M., Petters, M. D., Twohy, C. H., Richardson, M. S., Eidhammer, T. & Rogers, D. C., Predicting global atmospheric ice nuclei distributions and their impacts on climate **107**, 11217–11222 (2010).

Results: Chapter 3

The mold integration method for the calculation of the crystal-fluid interfacial free energy from simulations.

J. R. Espinosa, *C. Vega and E. Sanz*

Departamento de Química Física, Facultad de Ciencias Químicas, Universidad Complutense de Madrid, 28040 Madrid, Spain

3.1. Abstract

The interfacial free energy between a crystal and a fluid, γ_{cf}, is a highly relevant parameter in phenomena such as wetting or crystal nucleation and growth. Due to the difficulty of measuring γ_{cf} experimentally, computer simulations are often used to study the crystal-fluid interface. Here, we present a novel simulation methodology for the calculation of γ_{cf}. The methodology consists in using a mold composed of potential energy wells to induce the formation of a crystal slab in the fluid at coexistence conditions. This induction is done along a reversible pathway along which the free energy difference between the initial and the final states is obtained by means of thermodynamic integration. The structure of the mold is given by that of the crystal lattice planes, which allows to easily obtain the free energy for different crystal orientations. The method is validated by calculating γ_{cf} for previously studied systems, namely the hard spheres and the Lennard-Jones systems. Our results for the latter show that the method is accurate enough to deal the anisotropy of γ_{cf} with respect to the crystal orientation. We also calculate γ_{cf} for a recently proposed continuous version of the hard sphere potential and

obtain the same γ_{cf} as for the pure hard sphere system. The method can be implemented both in Monte Carlo and Molecular Dynamics. In fact, we show that it can be easily used in combination with the popular Molecular Dynamics package GROMACS.

3.2. Introduction

A fluid and a crystal at coexistence are divided by a flat interface. The work needed to create such interface per unit area is known as the interfacial free energy. The crystal-fluid interfacial free energy, γ_{cf}, is a highly relevant quantity due to its central role in important phenomena such as wetting or crystal nucleation and growth[1–3]. Despite its importance, γ_{cf} is still unknown for many substances given that there is not an easy and reliable way of measuring γ_{cf} experimentally[4]. This difficulty contrasts with the determination of the fluid-fluid interfacial free energy, a task for which there are well established experimental and computational techniques[5,6]. Unfortunately, these techniques are not easy to implement when one of the phases involved in the coexistence has an infinitely large viscosity, as the crystal phase has. Moreover, γ_{cf} is anisotropic and depends on the orientation of the crystal with respect to the fluid. The situation for water, arguably the most important substance on earth, is a good example of the difficulty of measuring γ_{cf}: while it is well known that the interfacial tension of liquid water at ambient conditions is 72 mN/m, the reported values for the ice-water interfacial free energy at ambient pressure range from to 25 to 35 mN/m[7].

Computer simulations can be used to assess experimental measurements of γ_{cf} and to improve our understanding on the crystal-fluid interface at a molecular scale. An important effort has been devoted to develop simulation methodologies to calculate the crystal-fluid interfacial free energy. To the best of our knowledge, these are the existing computational methods for the calculation of the crystal-fluid interfacial free energy: the cleaving method, the capillary fluctuation method, the methadynamics method, the tethered Monte Carlo method, and the Classical Nucleation Theory method. The cleaving method, proposed by Broughton and Gilmer in 1986[8], was the first method devised to directly compute γ_{cf} in a simulation. In this scheme the reversible work needed to cleave and re-combine the crystal and the fluid is calculated by thermodynamic integration. This method is still in use and an improved version of it has been recently employed to calculate γ_{cf} for several water models[9,10], hard particles[11,12], Lennard Jones[13] and dipolar fluids[14]. The cleaving method has recently been further improved by sorting out some hysteresis issues[15]. In the tethered Monte Carlo scheme[16] a complex order parameter is used to allow for a continuous transition between the fluid and the solid. This method has been applied to the hard sphere system[16]. The Metadynamics method[17] uses the rare event simulation technique Metadynamics[18] to obtain the work of formation of the interface from a fluid at coexistence. This methodology was originally applied to a

Lennard-Jones system[17] and has also been used to assess experimental measurements of γ_{cf} for Pb[19]. The crystal-fluid interfacial free energy can also be indirectly estimated by combining simulation measurements of the size of critical nuclei with classical nucleation theory[20]. This approach has been used, e. g., to estimate γ_{cf} for chlatrates[21] or water[22].

All the aforementioned methods have proved successful in the calculation of γ_{cf} for a number of systems. However, not all methods are equally good in terms of accuracy, simplicity and computational cost. The anisotropy of γ_{cf} for different crystal orientations is easy to study with the capillary fluctuation and with the cleaving methods, whereas dealing with the orientation of the crystal with respect to the fluid is not so trivial for the other methods. On the other hand, while the Metadynamics and the tethered Monte Carlo methods converge well for relatively small system sizes, the capillary fluctuation and the classical nucleation methods require large system sizes. From a practical point of view there are methods simple to implement, like that based on classical nucleation theory, or more cumbersome ones like the cleaving method that requires following a multi-step thermodynamic route. Moreover, all methods but the cleaving require a local-bond order parameter in order to either detect the interface or induce its formation. Such order parameter, used to distinguish liquid-like from solid-like molecules, may be difficult to conceive if the structure of the crystal lattice is complex. In this work we present a simple method for the direct calculation of γ_{cf} that gives accurate results even for relatively small system sizes. The calculation of γ_{cf} for different crystal orientations is trivial with this methodology. The method can be easily implemented in a bespoke Monte Carlo (MC) code or even in open access Molecular Dynamics (MD) packages as GROMACS[23]. In brief, we use a mold of potential energy wells placed at the positions of the atoms in a lattice plane to induce the formation of a crystal slab in the fluid at coexistence conditions. The work of formation of the crystal slab, obtained via thermodynamic integration, is directly related to the interfacial free energy.

We test the method by calculating the interfacial free energy of hard spheres (HS) and Lennard-Jones (LJ) (for several orientations of the crystal) and by comparing the results with values published in the literature[11,13,17,24,25]. Moreover, we compute γ_{cf} for the pseudo hard-sphere potential recently proposed in Ref.[26].

3.3. The mold integration method

3.3.1. Description of the method

In this section we describe a new methodology to compute the interfacial free energy between a crystal and a fluid, γ_{cf}, by means of computer simulations. The basic idea is to reversibly induce the formation of a thin crystalline slab in the fluid (see Fig. 9.1 for snapshots of a fluid and a fluid with a crystal slab). The work needed to form

such crystalline slab, ΔG^s, is related to γ_{cf}. Because the formation of the crystal slab is performed at coexistence conditions the fluid and the fluid plus the crystal slab have the same chemical potential. Then, ΔG^s is just the interfacial free energy times the area of the interface times 2. The factor of 2 is due to the fact that when the crystal slab is formed two crystal-fluid interfaces are created (see Fig. 9.1, bottom). Thus, γ_{cf} can be simply obtained as:

$$\gamma_{cf} = \frac{\Delta G^s}{2A}. \tag{3.1}$$

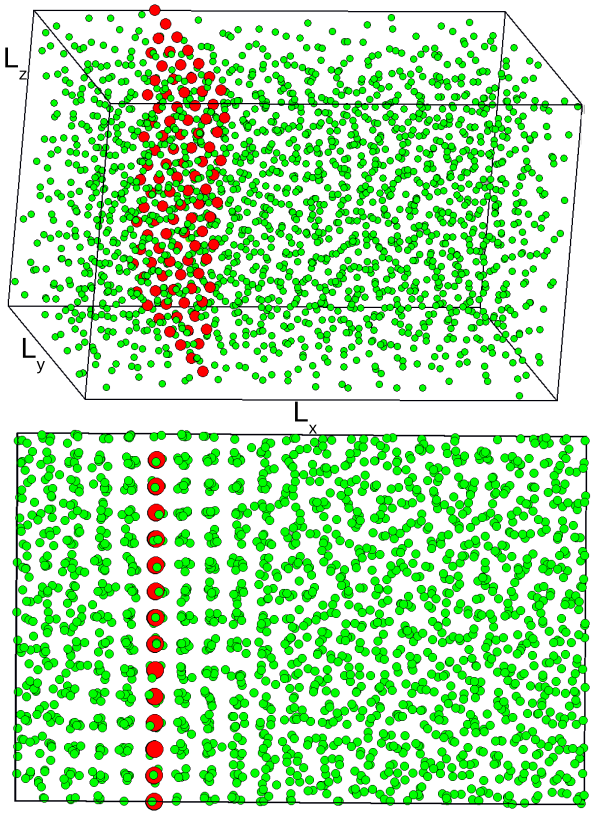

Figure 3.1: Top: snapshot of a hard-sphere fluid at coexistence (green particles). Bottom: snapshot of a fluid with a thin crystal slab at coexistence conditions (a projection on the $x-z$ plane is shown). The diameter of green particles has been reduced to 1/4 of its original size. The mold that induces the formation of the crystal slab is conformed by a set of potential energy wells (red spheres) whose positions are given by the lattice sites of the selected crystal plane at coexistence conditions. The interaction between the mold and the hard-spheres is switched off in the top configuration and on in the bottom one.

In order to induce the formation of the crystal slab we use a mold composed of potential energy wells. The location of the wells is given by that of the particles in the lattice plane whose γ_{cf} is calculated. In Fig. 9.1 we show a snapshot of the mold used for the calculation of γ_{cf} for the 100 plane of hard spheres (red spheres). Each potential well must be small enough so that it can only accommodate one particle. When the mold is switched off, particles freely diffuse in the fluid (Fig. 9.1, top). On the contrary, when the mold is switched on, every well contains a particle and, if the wells are sufficiently narrow, a crystal slab is formed at coexistence conditions (Fig. 9.1, bottom). Typically, the mold consists of 1 or 2 crystalline planes. In Fig. 9.1 we show a mold composed of a single plane. When filled with particles, the mold induces the formation of crystalline planes in either side (Fig. 9.1, bottom) thus giving rise to two crystal-fluid interfaces. By gradually switching the interaction between the mold and the particles the work of formation of the crystal slab at coexistence conditions can be obtained by means of thermodynamic integration.

To perform thermodynamic integration we define the following potential energy:

$$U(\lambda) = U_{pp}(\mathbf{r_1}, ..., \mathbf{r_N}) + \lambda U_{pm}(\mathbf{r_1}, ..., \mathbf{r_N}; \mathbf{r_{w_1}}, ..., \mathbf{r_{w_{N_w}}}) \tag{3.2}$$

where N is the number of particles and N_w the number of wells; $\mathbf{r_1}, ..., \mathbf{r_N}$ denotes the positions of all particles and $\mathbf{r_{w_1}}, ..., \mathbf{r_{w_{N_w}}}$ the position of the wells (which are kept fixed during the simulation); U_{pp} is the potential energy given by the interaction between all particles and U_{pm} is the potential energy given by the interaction between the mold and the particles. λ is a parameter that varies from 0 to 1 connecting the initial state (mold switched off, Fig. 9.1, top) with the final state (mold switched on, Fig. 9.1, bottom). The interaction between the mold and the particles, U_{pm}, is pair additive:

$$U_{pm}(\mathbf{r_1}, ..., \mathbf{r_N}; \mathbf{r_{w_1}}, ..., \mathbf{r_{w_{N_w}}}) = \sum_{i=1}^{i=N} \sum_{w_j=1}^{w_j=N_w} u_{pw}(r_{iw_j}), \tag{3.3}$$

where $u_{pw}(r_{iw_j})$ is a square-well interaction between the i^{th} particle and the j^{th} well that depends on the distance between their centers, r_{iw_j}:

$$u_{pw}(r_{iw_j}) = \begin{cases} -\varepsilon, & \text{if } r_{iw_j} \leq r_w \\ 0, & \text{if } r_{iw_j} > r_w \end{cases}. \tag{3.4}$$

Where r_w and ε are the radius and the depth of the wells respectively. These are the only adjustable parameters of the method. Below we explain how to deal with the tuning of these parameters. In any case, r_w can not be larger than the particle radius to avoid multiple filling of a single well.

By performing thermodynamic integration in λ[27] one can obtain the free energy difference between the fluid and the fluid plus the filled mold, ΔG^m:

$$\begin{aligned} \Delta G^m &= \int_{\lambda=0}^{\lambda=1} d\lambda \left\langle \frac{\partial U(\lambda)}{\partial \lambda} \right\rangle_{\lambda,N,p_x,T} \\ &= \int_{\lambda=0}^{\lambda=1} d\lambda \left\langle U_{pm} \right\rangle_{\lambda,N,p_x,T} \end{aligned} \tag{3.5}$$

where p_x and T are the coexistence pressure and temperature respectively. The mold coordinates and the edges of the simulation box parallel to the mold are kept fixed throughout the simulation. For that purpose, the pressure is exerted only along the axis perpendicular to the mold, the x axis in our case. Thus, the x edge is allowed to fluctuate to keep the pressure constant, while the y and z edges do not change. The mold coordinates are not rescaled when a volume move is performed. The integrand, $\langle U_w \rangle_{\lambda,N,p_x,T}$, is evaluated in Np_xT simulations for various values of λ and then integrated numerically to get ΔG^m. ΔG^m is the free energy change due to the appearance of the crystal slab plus that due to the interaction between the particles and the mold. The latter is simply given by $-N_w\varepsilon$ (recall that the well-particle interaction is just a square well of depth ε). To calculate the interfacial free energy we are just interested in the free energy change due to the generation of the crystal slab:

$$\Delta G^s = \Delta G^m + N_w\varepsilon. \tag{3.6}$$

This equation, combined with Eq. 7.9, allows in principle for the calculation of γ_{cf} in a straightforward manner.

There is one open issue, though: the value of ΔG^s, and hence that of γ_{cf}, depends on r_w. Therefore, one has to find a priori which value of r_w gives the right value for γ_{cf}. We shall refer to this radius as r_w^o (optimal well radius). In order to chose r_w^o it is important to understand the way in which the mold affects the free energy landscape. In Fig. 3.2 we show a sketch of the free energy profile that separates the fluid from the crystal as a function of the crystallinity degree (XD). The latter can be measured, for instance, with the aid of a local bond order parameter that quantifies the number of crystal-like particles in the system[28,29]. The black curve in Fig. 3.2 corresponds to the free energy profile in the absence of any mold. The liquid and the crystal have the same free energy given that the simulations are carried out at coexistence conditions. In between both phases there is a free energy plateau corresponding to the presence of a crystal slab in the fluid at coexistence conditions. Given that when a crystal slab is present there are two interfaces of the same area A (see Fig. 9.1, bottom), the free energy difference between the plateau and the minima is $2A\gamma_{cf}$. For $r_w > r_w^o$ the free energy profile at low crystallinity degrees changes to that sketched by the blue curve. In this

case, the free energy gap between the plateau and the fluid's minimum is reduced by the mold, but there is still a free energy cost to form a crystal slab. Therefore, a fluid where a mold with $r_w > r_w^o$ is switched on can remain stable for a long time before any crystal slab arises. If the minimum given by the blue curve is shallow (values of r_w larger than r_w^o but close to r_w^o) a fluid slab can form after some induction period due to thermal fluctuations. For $r_w < r_w^o$ the free energy profile changes to that schematically shown by the red curve in Fig. 3.2. Accordingly, as soon as the mold is switched on a crystal slab will quickly develop in order to minimize the free energy. Therefore, the evolution of XD depends on whether r_w is larger or smaller than r_w^o. Exploiting this difference r_w^o can be enclosed within a certain range by running simulations for different values of r_w and monitoring the behaviour of XD.

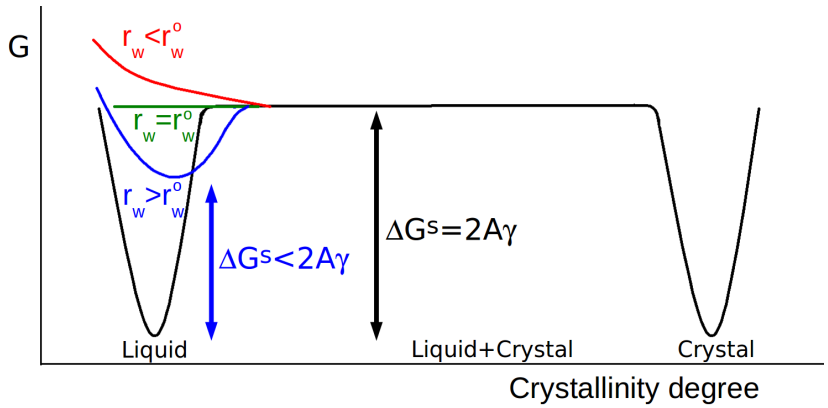

Figure 3.2: Sketch of the free energy profile versus the crsystallinity degree for various potential well radius, r_w, at coexistence conditions. The black curve corresponds to the free energy profile in the absence of any mold. The free energy is flat in between both phases because the emerging crystal slab has the same chemical potential as the fluid and it grows with constant crystal-fluid interfacial area.

Once r_w^o is identified, one could in principle perform thermodynamic integration for $r_w = r_w^o$ to obtain γ_{cf}. However, in a flat landscape as that given by $r_w = r_w^o$ (green curve in Fig. 3.2), XD can freely grow and may eventually fall into the crystal's basin. Therefore, it is not advisable to perform thermodynamic integration for $r_w = r_w^o$. Instead, it is safe to integrate to states with $r_w > r_w^o$ (blue profile in Fig. 3.2) for which there is a well defined minimum in the free energy profile. Although these integrations yield underestimates of γ_{cf}, they provide a function $\gamma_{cf}(r_w)$ that can be extrapolated to r_w^o in order to obtain the right value of γ_{cf}.

In summary, the method, which we call *mold integration method*, consists of the following steps: i) Preparation: The mold coordinates are obtained and an initial configuration of the fluid at coexistence conditions is prepared. The simulation box dimensions

must be compatible with those of the mold. ii) Choice of r_w^o: The mold is switched on and several simulations are run starting from the fluid configuration previously prepared. Simulations are repeated for different values of r_w. By monitoring XD a range within which r_w^o is enclosed is identified. iii) Calculation of $\gamma_{cf}(r_w)$: Thermodynamic integration is performed by gradually switching the mold on. By repeating this for several values of $r_w > r_w^o$ a $\gamma_{cf}(r_w)$ function is obtained. iv) The extrapolation of $\gamma_{cf}(r_w)$ to r_w^o provides the definite value of γ_{cf}.

Being the method above described completely novel, our approach shares some features with existing methodologies. For example, in the Metadynamics method[17] the work needed to create a crystal slab in a fluid at coexistence is also calculated, although in a different way (via Metadynamics as opposed to thermodynamic integration) and with the aid of local-bond order parameters that may be difficult to find for complex crystal structures. This difficulty is bypassed in our method with the use of an *ad hoc* mold In some recent implementations of the cleaving method a cleaving potential based on the location of the particles in the crystal plane is used[9], in resemblance to our mold of potential energy wells. However, whereas in our method the mold is used as a platform for the growth of a crystal slab in the fluid, in the cleaving method the cleaving potential is used to cleave both phases in order to subsequently recombine them. Therefore our route to a system at coexistence is more direct than that proposed in the cleaving framework. The use of potential wells is not exclusive of methods for the calculation of γ_{cf}. Potential wells have also been used in the calculation of the free energy of amorphous and crystalline solids via thermodynamic integration[30].

3.3.2. Implementation

The implementation of the mold integration technique in MC is rather straightforward. A routine to evaluate the interaction between the particles and the mold, U_{pm}, via Eq. 3.3 has to be incorporated to a standard Np_xT MC code. U_{pm} is evaluated every time a move is attempted and the change of λU_{pm} associated to the move is added to the energy change according to which the trial move is accepted or rejected. To perform thermodynamic integration via Eq. 3.5 the average value of U_{pm} must be evaluated in the course of the simulation.

It is also possible to implement the mold integration technique in MD. We briefly discuss here how to do it for the popular MD package GROMACS[23]. The trick is to consider the wells as a special kind of atom. The interaction between the wells and the particles, Eq. 3.4, can be approximated by the following equation:

$$u_{pw}(r_{iw_j}) = -\frac{1}{2}\varepsilon\left[1 - \quad \tanh\left(\frac{r_{iw_j} - r_w}{\alpha}\right)\right] \tag{3.7}$$

where r_{iw_j}, r_w and ε have the same meaning as in Eq. 3.4 and α controls the steepness of

the well's walls. This potential is continuous and differentiable and can therefore be used in MD. In Fig. 3.3 we compare $u_{wp}(r_{riw_j})$ given by Eq. 3.4 (black) with that given by Eq. 9.5 (red) for $\alpha = 0{,}005\sigma$. It is evident that a square-well interaction is well approximated by Eq. 9.5. In GROMACS it is possible to define the well-particle interaction given by Eq. 9.5 in a tabular form, so there is no need to modify the source code to program the interaction between the wells and the particles. The interaction between different wells has to be also defined in GROMACS in a tabular form. Such interaction is simply 0. In order to fix the position of the wells we use the 'frozen'GROMACS option. To perform thermodynamic integration via Eq. 3.5 we need to be able evaluate $< U_{pm} >$ for a given value of $\lambda \in [0:1]$. To do that we run the simulation with a well-particle interaction given by λu_{wp}. Since GROMACS provides average values of the potential energy for any kind of pair interaction, one can obtain $\lambda < U_{pm} >$ as the average particle-well potential energy, and, in turn, $< U_{pm} >$. Finally, GROMACS also allows that the pressure is exerted only in one specific direction of the simulation box. Therefore, GROMACS includes all required tools for an easy implementation of the mold integration method in MD.

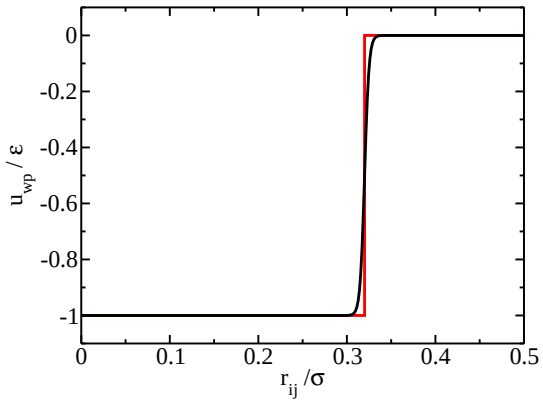

Figure 3.3: Well-particle interaction potential for $r_w = 0{,}32\sigma$. We use a square-well potential for the well-particle interaction in MC simulations (red curve). In order to perform MD simulations we approximate the square-well interaction by the continuous potential given by Eq. 9.5 (black curve). In this particular example α in Eq. 9.5 is $0{,}005\sigma$.

3.4. Results and discussion

3.4.1. A worked example: γ_{cf} of hard spheres

Preparation

The first step is obtaining the mold coordinates and a fluid configuration at coexistence conditions. The dimensions of the simulation box must be consistent with those of the mold. The mold coordinates are obtained by replicating the unit cell and taking a plane of the resulting lattice. In our case we replicate 1x7x7 times the fcc unit cell and take a plane of atoms parallel to the $y-z$ plane. The resulting coordinates are shown by the red spheres in Fig. 9.1, top. Under periodic boundary conditions the mold is just a 100 plane of an fcc lattice. A configuration of the fluid at coexistence conditions (pressure = 11.54 $k_BT/\sigma^{3\,31}$) is then prepared in a box whose y and z edges have the same length as the y and z sides of the mold. To achieve this we equilibrate the fluid in an NpT simulation where pressure is exerted only along the x axis (we refer to this as Np_xT ensemble). In this way the length of the x axis, L_x, is allowed to fluctuate, while L_y and L_z are kept fixed to the desired value (7 times the unit cell side in this particular example). The resulting simulation box, that contains 1960 particles, is shown in Fig. 9.1, top, alongside the corresponding mold. We summarize the system size used for the study of the HS system in the top row of Table 3.1.

System	ST	hkl	$(L_y\text{x}L_z)/(\sigma^2)$	N_w	N_L	N	r_w^o/σ	$\gamma_{cf}/(\frac{k_BT}{\sigma^2})$
HS	MC	100	10.978x10.978	98	1	1960	0.315	0.586 (8)
PHS	MD	100	12.531x12.531	256	2	5632	0.375	0.588 (8)

Table 3.1: Summary of the system size used for the calculation of γ_{cf} for the HS and PHS models. ST stands for simulation type, hkl for the Miller indices of the crystal plane whose γ_{cf} is calculated, N_w for number of wells, N for number of particles and N_L for number of layers (in the mold). The optimal well radius, r_w^o, and the estimated value of γ_{cf} are also reported in the table.

Choice of r_w^o

Once the fluid is equilibrated we proceed to run Np_xT simulations starting from a fluid configuration. The mold is switched on at the beginning of the simulations. If the interaction between the mold and the particles is sufficiently large all wells are quickly filled when the mold is switched on. We find this to be the case when ε in Eq. 3.4 is larger than $\sim 7k_BT$. We monitor XD in the course of our simulations. As a measure of

XD we use the following parameter, ξ:

$$\xi = \frac{\rho - \rho_f}{\rho_s - \rho_f} \tag{3.8}$$

where ρ is the actual density of the system and ρ_f and ρ_s are the coexistence densities of the fluid and the solid respectively. Thus, ξ fluctuates around 0 when the whole system is fluid, and around 1 when the whole system is crystalline. As a crystal slab grows in the fluid ξ should take intermediate values between the typical ones for the fluid and the crystal. In the appendix 3.6.1 we show that this simple way of quantifying XD is totally equivalent to a more sophisticated one based in counting the the number of particles in the largest cluster of solid-like particles.

In Fig. 3.4 we show the evolution of ξ for several values of r_w. For a given value of r_w we run 10 trajectories starting from the same initial configuration in order to have a statistical picture of the behaviour of the system upon switching the mold on. The trajectories differ in the seed for the random number generator. Each Np_xT MC simulation consists of a million sweeps. A sweep, in turn, consists of a displacement attempt per particle plus a volume move. The displacement shifts for volume and displacement moves are tuned so that an average acceptance of 30-40 per cent is attained.

Three different types of behaviour can be seen when the trajectories are inspected for each r_w: (a) Behaviour consistent with the presence of a deep minimum in the free energy-XD profile: in plots e) and f) of Fig. 3.4 XD stays low and fluctuates around a certain equilibrium value for all trajectories. This is consistent with the situation sketched by the blue curve in Fig. 3.2: r_w is larger than r_w^o and XD fluctuates around the minimum given by the blue curve. (b) Behaviour not consistent with the presence of a minimum the free energy-XD profile: in plots a) and b) of Fig. 3.4 XD readily grows as the mold is switched on and each trajectory evolves differently from the others. This corresponds to the situation illustrated by the red curve in Fig. 3.2: r_w is smaller than r_w^o and, due to the presence of the mold, there is no free energy penalty for the growth of XD. (c) Behaviour consistent with the presence of a shallow minimum in the free energy-XD profile: In plots c) and d) of Fig. 3.4 XD fluctuates around an equilibrium value for some trajectories although, stochastically, there are trajectories that visit high values of XD. For instance, for $r_w = 0{,}33\sigma$ the trajectory given by the orange curve stays at low XD until it jumps around $7 \cdot 10^5$ MC sweeps. This phenomenology suggests that there is a minimum in the free energy profile as indicated in Fig. 3.2 by the blue curve. However, the gap between the minimum and the horizontal plateau is not high and can be stochastically overcome by thermal activation.

Since the optimal radius, r_w^o, must be in between the highest r_w that shows no hint of a minimum ($r_w = 0{,}31\sigma$) and the lowest that does show it ($r_w = 0{,}32\sigma$) we take $r_w^o = 0{,}315 \pm 0{,}005\sigma$.

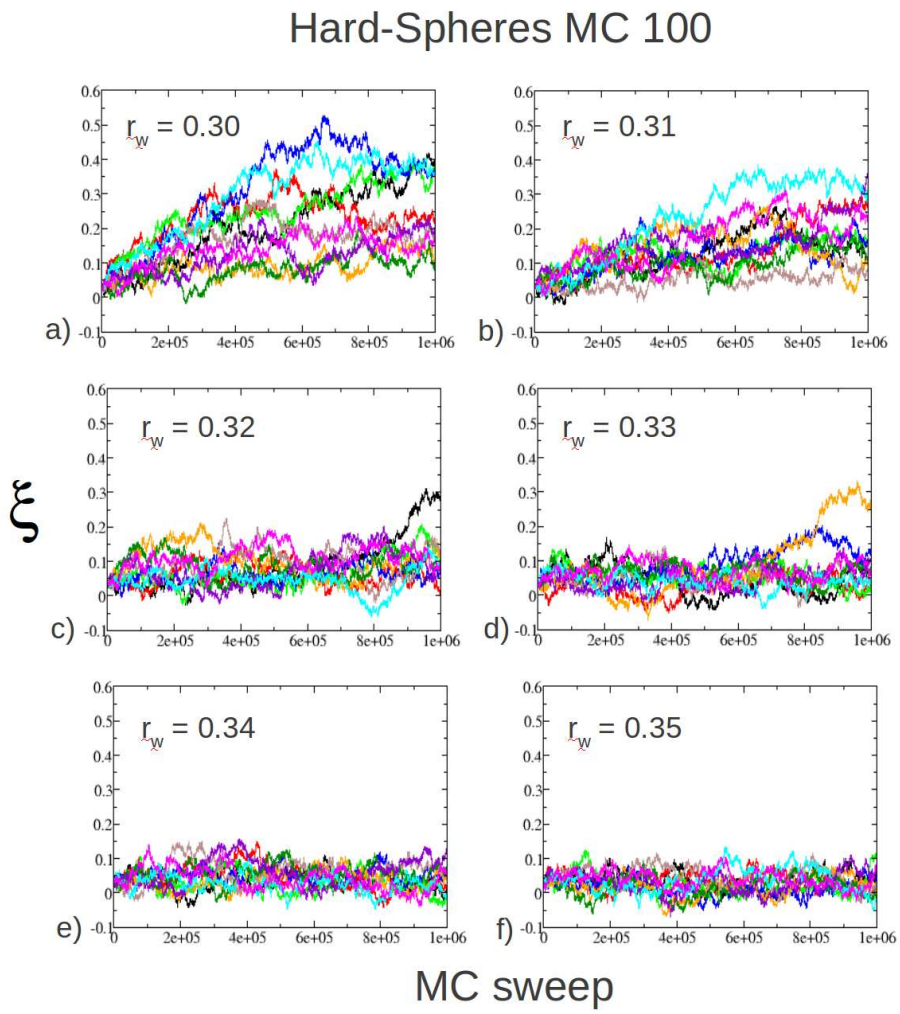

Figure 3.4: Crystallinity degree, XD, as measured by the parameter ξ (see main text) as a function of simulation time for several values of the radius of the potential wells, r_w/σ, as indicated inside each plot. The well depth is in all cases $7.5k_BT$. For a given r_w 10 trajectories differing in the seed for the random number generator are started from a fluid configuration. The mold is switched on at the beginning of the simulation. The plot corresponds to the HS potential and the 100 crystal orientation.

In summary, the recipe to find r_w^o is to look for a value of r_w that is comprised in between the largest one that shows no indication of the presence of a minimum in the free energy-XD profile and the smallest one that does show it. A given r_w shows no indication of a minimum if XD can grow and evolves in a different way for different

trajectories. By contrast, a given r_w shows indication of a minimum if some trajectories show that XD fluctuates around a low constant value. In Appendix 3.6.2 we show how the free energy profile along the XD coordinate can be estimated for each well radius using the information contained in Fig. 3.4. This is quite helpful to identify which radii generate a free energy profile with a minimum and which ones do not.

Calculation of $\gamma_{cf}(r_w)$

Once we get a value for r_w^o we proceed to calculate $\gamma_{cf}(r_w)$ for $r_w > r_w^o$ by means of thermodynamic integration (Eq. 3.5). Thermodynamic integration is performed by gradually switching the mold on in such way that all wells are filled with particles when the upper integration limit is reached (*i.e.* when $\lambda = 1$ in Eq. 3.5). In Fig. 3.5 (a) we plot the average number of filled wells versus the parameter $\lambda \in [0:1]$ that controls the strength of the interaction between the particles and the mold via Eq. 3.2. Each point in Fig. 3.5 is obtained in an Np_xT MC simulation consisting of $3{,}3 \cdot 10^5$ equilibration sweeps and $6{,}7 \cdot 10^5$ production sweeps. The plot in Fig. 3.5 corresponds to a well-particle interaction parameter $\varepsilon = 7{,}5\ k_BT$ (Eq. 3.4) and to an $r_w = 0{,}34\sigma$. The value of ε must guarantee that every well contains a particle for $\lambda = 1$. Provided that this condition is fulfilled, ε can take any value. However, it is convenient that ε is not too large so that the integrand varies smoothly as λ increases. In the particular case study we present here the mold is conformed by 98 wells (see Fig. 9.1, top) As shown in Fig. 3.5 (a) all 98 wells are filled when λ approaches 1. On average, about 17 wells are occupied when the mold is switched off. The curve that is actually integrated in Eq. 3.5 is shown in Fig. 3.5 (b). The integrand, U_{pm}, is simply given by the product between the average number of filled wells and $-\varepsilon$. The integral of the curve shown in Fig. 3.5 (b) is $\Delta G^m = -600{,}123\ k_BT$, which gives the free energy difference between the system with the mold on and the system with the mold off. To simply get the free energy difference between the fluid and the fluid having the structure induced by the mold, ΔG^s, we need to subtract to ΔG^m the interaction between the mold and the fluid: $\Delta G^s = \Delta G^m + \varepsilon N_w = -600{,}123 + 7{,}5 \cdot 98 = 134{,}88 k_BT$. ΔG^s divided by two times the area L_yL_z gives an (under)estimate of the interfacial free energy (Eq. 7.9): $\gamma_{cf}(r_w = 0{,}34\sigma) = 0{,}560 k_BT/\sigma^2$. In this step γ_{cf} is evaluated for some other values of $r_w > r_w^o$ in order to extrapolate $\gamma_{cf}(r_w)$ to r_w^o in the following step.

As previously discussed, in order for thermodynamic integration to be reversible we must avoid integrating at values of r_w that entail any risk that the system crystallizes. Clearly, Fig. 3.4 shows that such risk is negligible for $r_w = 0{,}34$ and $0{,}35\sigma$, since XD fluctuates around a low, equilibrium value for all trajectories. The situation is not so clear for $r_w = 0{,}33\sigma$, where the trajectory given by the orange curve appears to have jumped to the free energy plateau from where the system could evolve towards the crystalline state. Therefore, by performing thermodynamic integration at $r_w = 0{,}33\sigma$ there is a

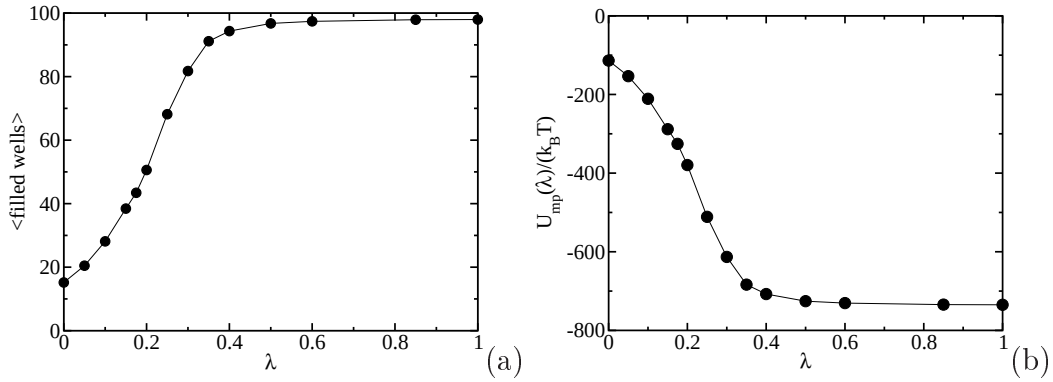

Figure 3.5: (a) average number of filled wells as a function of the parameter λ that controls the strength of the interaction between the mold and the particles. (b) the integrand of eq. 3.5 is plotted against λ. both plots correspond to the 100 face of HS and to a 98-well mold with $r_w = 0{,}34\sigma$ and $\varepsilon = 7{,}5k_BT$.

small chance that the system crystallizes in the typical simulation time required to perform thermodynamic integration. Hence, according to the study shown in Fig. 3.4, it is safe to perform thermodynamic integration only for $r_w \geq 0{,}34\sigma$. However, one can also try doing thermodynamic integration for r_w's closer to r_w^o and validate the integration *a posteriori* by checking that the system did not crystallize for any integration point. One of these checks is shown in Fig. 6.5, where we plot XD for the runs used to compute each integration point in Fig. 3.5. XD stays low for all integration points, which guarantees that the integration is reversible. It is important to do this check after performing thermodynamic integration, specially for r_w's close to r_w^o.

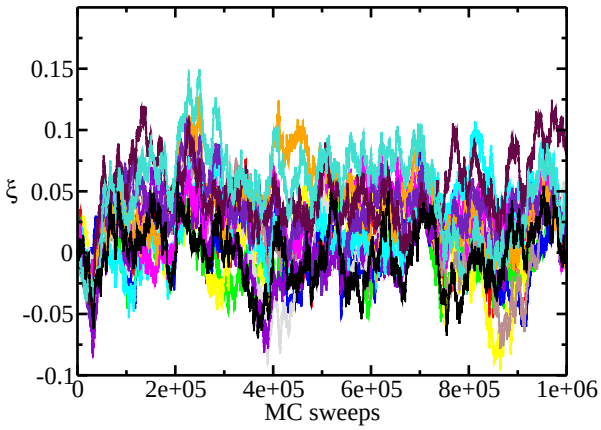

Figure 3.6: Crystallinity degree as measured by the parameter ξ for the simulations corresponding to each integration point in Fig. 3.5.

Extrapolation of $\gamma_{cf}(r_w)$

Above we have discussed in detail the calculation of $\gamma_{cf}(r_w)$ for $r_w = 0{,}34\sigma$. The same calculation has to be repeated for other values of r_w in order to get a function $\gamma_{cf}(r_w)$ that can be extrapolated to the radius previously identified as the optimal one: $r_w^o = 0{,}315\sigma$. In Fig. 3.7 we show $\gamma_{cf}(r_w)$ for the HS system. The dependency of γ_{cf} on r_w looks rather linear, which allows to easily extrapolate $\gamma_{cf}(r_w)$ to r_w^o. The extrapolation is given by the open symbol with the error bar in Fig. 3.7. Thus, our estimated value for γ_{cf} for the 100 plane of HS is $\gamma_{cf} = 0{,}586(8)k_BT/\sigma^2$. The main error source in our calculation comes from the uncertainty in determining r_w^o. The uncertainty in the thermodynamic integration also contributes, although to a lesser extent, to our final error bar. Our value is in very good agreement with the most recent estimate of $\gamma_{cf} = 0{,}582(2)k_BT/\sigma^2$ [11] (horizontal dashed lines in Fig. 3.7), obtained via the cleaving method[8]. Our value is also in agreement with the latest estimate of γ_{cf} for the 100 plane of HS from capillary wave fluctuations: $0{,}57(2)kT/\sigma^2$ [24].

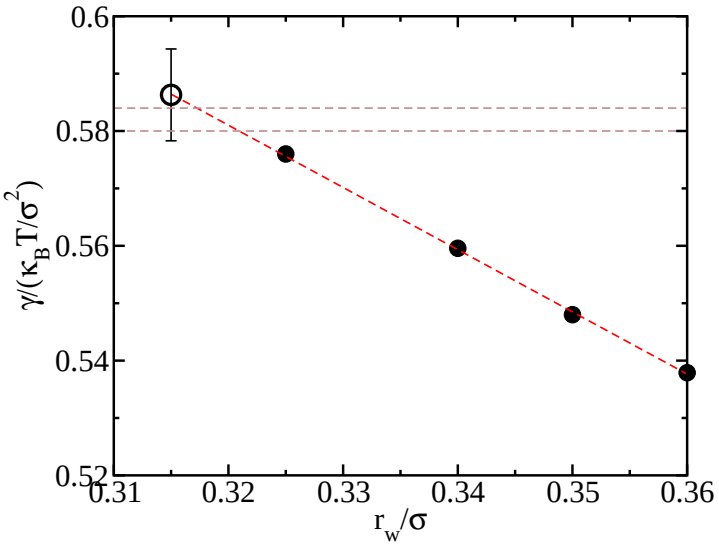

Figure 3.7: Solid symbols: interfacial free energy versus the radius of the potential wells for the 100 face of HS. The red dashed line is a linear fit to our data. The value of the fit at $r_w = r_w^o = 0{,}315\sigma$ gives our estimate for the interfacial free energy $\gamma_{cf} = 0{,}586\ k_BT/\sigma^2$, indicated by the open symbol. The horizontal dashed lines indicate the value of γ_{cf} given in Ref.[11].

This excellent result proves the ability of our mold integration method to evaluate the crystal-fluid interfacial free energy. The method is simple conceptually and easy to implement. With a 10 processors machine and our bespoke MC algorithm the calculation of the crystal-fluid interfacial free energy for the 100 plane of HS took us about two days.

To further validate the methodology in the following section we show results for the LJ system, for which we compute the interfacial free energy not only for the 100 plane but also for the 111 plane.

3.4.2. γ_{cf} for the LJ system

In this section we report the calculation of γ_{cf} for the LJ model as modified by Broughton and Gilmer[32]. We perform the calculation at the triple point of the model, which was determined in Ref.[33] to be at $T = 0{,}617\epsilon/k_B$, corresponding to a pressure $p = -0{,}02\epsilon/\sigma^3$ (ϵ and σ are the interaction parameters of the LJ system[32]). At these thermodynamic conditions the density of the fluid is 0.828 σ^{-3} and that of the crystal 0.945 σ^{-3}[13].

To illustrate the suitability of our methodology to deal with the anisotropy of the crystal-fluid interfacial free energy we calculate γ_{cf} for two different crystal orientations. The orientation of the crystal with respect to the fluid is indicated by the Miller indices of the plane parallel to the interface. In this work we calculate γ_{cf} for the 100 and the 111 orientations. Obtaining γ_{cf} for a given crystal orientation with the mold integration method just requires using a mold coming from the lattice plane that defines such orientation. In Fig. 3.8 we show the molds used for the calculation of the 100 (left) and the 111 (right) interfacial free energies.

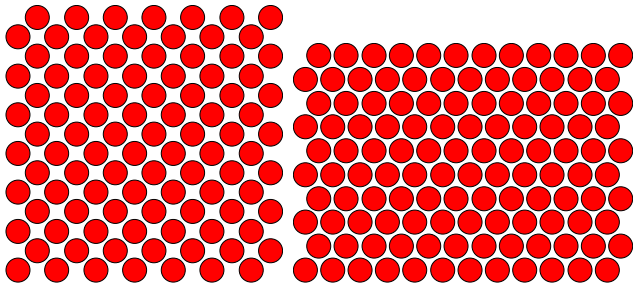

Figure 3.8: Molds used for the calculation of γ_{cf} for the 100 (left) and the 111 (right) crystal orientations of the LJ system. Note the more compact packing of wells in the 111 mold.

In the previous section, where we describe the calculation of γ_{cf} for the HS system, we use a single layer mold. However, the mold can be composed of more than a single layer. We prove in this section that using molds composed of two layers (bilayer mold) one obtains results which are consistent with those obtained by using a single layer (monolayer mold). Moreover, we also compare in this section MC with MD. In the implementation section above we describe the way the mold integration method can be

easily implemented in the popular MD simulation package GROMACS, which we use to calculate γ_{cf} for the LJ system.

The first step is to prepare the mold and a fluid configuration at equilibrium in a simulation box compatible with the mold. We give details on how to do this for the HS system in the previous section. In Table 3.2 we list the simulations used for the calculation of γ_{cf} for the 100 and 111 crystal orientations for the LJ system. We indicate the area of the simulation box side parallel to the mold (L_yxL_z), the number of wells that conform the mold, the number of layers of the mold and the number of particles of the system.

Once the initial set up is ready we run a number of trajectories (about 10) for different values of r_w in order to find r_w^o. As previously described for the HS system, r_w^o can be found by looking at the behaviour of XD as a function of the simulation time for different r_w's. The values of r_w^o thus obtained are shown in Table 3.2. It is interesting to realize that r_w^o changes from one crystal orientation to another. r_w^o is always smaller for the 111 plane. This shows that it is necessary to adjust the value of r_w^o for every crystal orientation separately. We also show in Table 3.2 that r_w^o also depends on the number of layers that conform the mold. Monolayer molds need smaller values of r_w^o to induce the formation of a crystal slab than bilayer ones. The work required to fill a well increases as its radius decreases since the smaller the well's volume the more unfavourable it becomes confining a particle inside. Therefore, one has to supply more energy per well to a monolayer mold in order to get the same energy per unit area as in a bilayer mold. This seems reasonable since a bilayer mold has twice as many wells per unit area. Finally, from our analysis it also turns out that MD r_w^os are slightly larger than MC ones (when compared for the same crystal orientation and the same number of layers in the mold). This may be due to the fact that, although the continuous potential given by Eq. 9.5 closely follows a square-well interaction (see Fig. 3.3), the equivalence is not perfect. Nevertheless, as we show below, the small difference in r_w^o between MC and MD is not reflected in the estimated value of γ_{cf}.

Once r_w^o is identified for each system the next step is to perform thermodynamic integration for at least a couple of values of $r_w > r_w^o$ in order to obtain a function $\gamma_{cf}(r_w)$ that can be extrapolated to r_w^o. In Fig. 3.9 we show $\gamma_{cf}(r_w)$ for all systems investigated. Red symbols correspond to the results for the 100 orientation and black ones to the 111 orientation. Let us start by discussing the results for the 100 orientation. Filled symbols correspond to the calculation of $\gamma_{cf}(r_w)$ via thermodynamic integration and empty ones to the extrapolation of $\gamma_{cf}(r_w)$ to r_w^o. The black squares correspond to MC and the black circles to MD simulations, both with a monolayer mold. It is clear from Fig. 3.9 that both MC and MD yield consistent results for the calculation of $\gamma_{cf}(r_w)$ via thermodynamic integration. A linear extrapolation of the MC and MD data to their corresponding values of r_w^o (see Table 3.2) provides an estimate for γ_{cf}, indicated by the open symbols in Fig. 3.9 and reported in Table 3.2. Within the error of the method both MC and MD give

ST	hkl	$(L_y \text{x} L_z)/(\sigma^2)$	N_w	N_L	N	r_w^o/σ	$\gamma_{cf}/(\frac{\epsilon}{\sigma^2})$
MC	100	11.323x11.323	98	1	1960	0.305	0.372(8)
MD	100	11.323x11.323	98	1	1960	0.315	0.372(8)
MD	100	14.543x14.543	324	2	6480	0.385	0.373(8)
MC	111	13.726x9.906	120	1	2160	0.285	0.350(8)
MD	111	13.726x9.906	120	1	2160	0.295	0.354(8)
MD	111	13.726x9.906	240	2	2160	0.385	0.348(8)
	100				12158		0.371(3) [13]
	100				38740		0.369(8) [34]
	100				2352		0.370(2) [17]
	100				1790		0.34(2) [35]
	111				8916		0.347(3) [13]
	111				38740		0.355(8) [34]
	111				1674		0.35(2) [35]

Table 3.2: Summary of the size of the systems used for the calculation of γ_{cf} for the LJ system. The meaning of ST, hkl, N_w, N_L and N is the same as in Table 3.1. For comparison, in the bottom frame of the table we give values for γ_{cf} obtained in previous works, alongside the number of particles used for their calculation.

the same γ_{cf} for the 100 orientation. By using a bilayer mold (black diamonds) we get also, within error, the same value for γ_{cf}. Red squares and circles correspond to the results for a 111 monolayer mold as obtained from MC and MD respectively. Again, a good agreement between both simulation techniques is obtained. Moreover, the results for the bilayer (red diamonds) give the same γ_{cf} as the monolayer mold. In summary, in Fig. 3.9 we show that the mold integration technique gives consistent results regardless the simulation technique (MC or MD), or the number of layers in the mold (1 or 2). The accuracy of the technique is sufficient to distinguish between the interfacial free energy of two different crystal orientations (100 and 111).

As discussed above, in order to compute γ_{cf} we recommend to obtain first two or three under-estimates of γ_{cf} for $r_w > r_w^o$, where thermodynamic integration is reversible, and then extrapolate the results to r_w^o. A close inspection of Fig. 3.9 shows that the MC estimate of γ_{cf} for the 100 orientation was directly performed at $r_w = r_w^o$. This allows to directly estimate γ_{cf} without the need of any extrapolation, but apparently contradicts the advice of performing thermodynamic integration for $r_w > r_w^o$. In fact, we had to resort to a tailored type of MC move in order to perform thermodynamic integration for $r_w = r_w^o$, where the reversibility of thermodynamic integration is compromised by the possibility that the system fully crystallizes. Such move consisted in performing blocks

of thousands of MC sweeps that are accepted or rejected according to the final value of XD. If XD increases beyond the point at which the system is committed to fully crystallize, the whole block of MC sweeps is rejected and re-started with a different seed for the random number generator. Otherwise, the MC simulation continues normally. In order to set both the length of the simulation blocks and the XD threshold it is necessary to get some experience first by examining several unbiased runs at $r_w = r_w^o$. In this way we have two MC estimates of γ_{cf} for the 100 interface: one coming from the 'direct'calculation of γ_{cf} at $r_w = r_w^o$ (as described in this paragraph), and another coming from the extrapolation of estimates for $r_w > r_w^o$. As shown in Fig. 3.9 both estimates coincide pretty well, which gives us confidence in the extrapolation procedure described in previous sections. Although both ways of estimating $\gamma_{cf}(r_w^o)$ are equally valid, we recommend the use of the extrapolation method because it is more general as it does not require the implementation of the MC-block moves described in this paragraph.

In Table 3.2 we show that one can obtain consistent results for molds with one or two layers. In principle any number of layers can be used. However, one must take into account that r_w^o increases as the number of layers increases (see table 3.2) and that r_w^o can not be larger than 0.5 σ in order to avoid multiple filling of the wells. For this reason, in practise, we could not use a mold with more than two layers to compute γ_{cf}. In any case, there is no practical advantage in using bi-layer over mono-layer molds. In fact, with a mono-layer mold the number of well-particle interactions is half as many and the code runs faster.

The interfacial free energy for the LJ model at the triple point has been directly determined by Broughton and Gilmer in 1986 using the cleaving method[35], by Laird and Davidchack using a more accurate variant of the same methodology[13], by Morris and Song using a capillary fluctuation approach[34] and by Angioletti-Uberti *et al.* using a Metadynamics-based approach[17]. In the bottom part of table 3.2 we report the values of γ_{cf} obtained in these works. The agreement between our data and those obtained in Refs.[13,34] is very good. The comparison with Ref.[35] is not bad either, particularly taking into account that in 1986 the computational resources did not allow for accurate enough calculations to distinguish between different crystal orientations. In Ref.[20] γ_{cf} was indirectly estimated via classical nucleation theory ($\gamma_{cf} = 0{,}302(2)\epsilon/k_BT$). The discrepancy with our data may be partly due to the fact that in Ref.[20] a value of γ_{cf} averaged over several crystal orientations is provided. In summary, in Table 3.2 we show that the values obtained from our method are in good agreement with the general consensus reached for the γ_{cf} of LJ for two different crystal orientations.

The extensive work done on the LJ system allows for a comparison between different simulation methods. In table 3.2 we report the number of molecules used for the calculation of γ_{cf} for each simulation method. The number we report for Ref.[34], where the capillary fluctuation method was used, is an average over all systems employed. In terms of computational cost, the capillary fluctuation method is expensive. Moreover

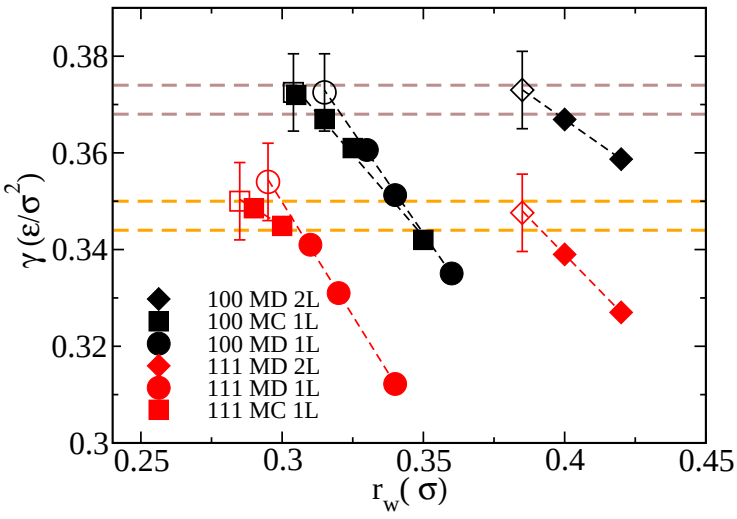

Figure 3.9: Interfacial free energy as a function of the well radius for the LJ-like potential proposed in Ref.[32]. Results are shown for two different crystal orientations (111, red symbols, and 100, black symbols), two simulation techniques (MC, squares, and MD, other symbols), and two thicknesses of the mold (bilayer, 2L, diamonds, and monolayer, 1L, other symbols). Filled symbols are simulation data and empty symbols with error bars correspond to the extrapolation to r_w^o. Brown and orange dashed horizontal lines correspond to the value of $\gamma_c f$ reported in Ref.[13] for the 100 and 111 orientations respectively. Black and red dashed lines are linear fits to the different sets of solid symbols.

it requires the evaluation of the spectrum of capillary waves for at least three different crystal orientations in order to provide a value of γ_{cf}. The method based on Classical Nucleation Theory also requires a large number of particles because such theory works best for large cluster sizes[20]. The cleaving method used in Ref.[35] used relatively small systems, but the results were not accurate enough to distinguish between different crystal orientations. Many more particles were used in Ref.[13] in order to gain accuracy. Both the Metadynamics method and our mold integration method are capable of producing accurate results for systems of less than 2000 particles. We have checked that there are no significant system size effects present in our simulations. In Table 3.2 we show that a calculation with 6480 particles gives the same result as one with 1960. Therefore, the possibility of using small systems is a positive aspect of our method.

Another advantage is the simplicity with which it deals with different crystal orientations (one simply has to use a mold coming from the corresponding lattice plane). Also the cleaving and the capillary fluctuation methods easily deal with the anisotropy of γ_{cf}. In both methods the fluid is brought into contact with the crystal at the desired orienta-

tion. For the capillary fluctuation method the problem is not so straightforward, though. What is obtained from the analysis of the capillary waves spectrum is the interfacial stiffness, and several orientations must be combined with a cubic harmonic expansion in order to obtain estimates of γ_{cf}. The way to deal with the anisotropy of γ_{cf} is more complex for the other methods. In the Metadynamics method, for instance, an order parameter has to be devised in order to induce the growth of the crystal. Finding a good order parameter may be a non-trivial task for crystal structures whose complexity goes beyond that of simple fcc or bcc lattices[36]. The classical nucleation method also requires an order parameter to measure the size of the embedded clusters.

3.4.3. γ_{cf} for the pseudo hard-sphere potential

A system composed of hard spheres (HS) is arguably the simplest non-trivial model having fluid, crystal and glass phases[37,38]. Therefore, this model is widely used by researchers on a diverse range of problems like the glass transition[39], crystal nucleation[40], or granular matter[41]. There is great interest in finding a continuous potential whose kinetic and thermodynamic behaviour reproduces that of the discontinuous potential of pure HS. Finding such potential would allow to explore the physics of the HS system with simple MD simulations. This is important because MD simulation packages like GROMACS are nowadays accessible to a large scientific community. For instance, having a continuous version of the HS potential would be of great help for the investigation the crystallization of hard spheres, where large discrepancies between experimental and simulation measures of the nucleation rate have been reported (see Ref.[42] and references therein).

Quite recently, Jover *et al.* have proposed a continuous potential that at reduced temperature 1.5 behaves very much alike a system of pure HS in terms of the equation of state and the diffusion coefficient[26]. We refer to the potential proposed by Jover *et al.* at reduced temperature 1.5 as the pseudo hard-sphere potential, PHS. Later on, Espinosa *et al.* showed that the coexistence pressure and densities for the PHS model are also very similar to those of the pure HS system[43].

The PHS potential is a good candidate for the investigation of the crystal nucleation rate of HS given that, as mentioned before, both models have a very similar thermodynamic coexistence, diffusion coefficient, and equation of state. Nothing is known, however, about the γ_{cf} of the PHS potential, a crucial parameter in crystal nucleation[3]. If γ_{cf} was also similar to that of pure HS then the PHS model could be reliably used in MD simulations to obtain predictions about the crystallization behaviour of HS. Here, we use the mold integration method to obtain γ_{cf} for the PHS model.

We evaluate the interfacial free energy for the 100 crystal orientation in order to compare with our results for the pure HS model. We use a two-layer mold with 128 particles in each layer. The system size is summarized in the bottom row of table 3.1.

All simulations are performed with the GROMACS MD package.

To determine r_w^o we monitor the XD as a function of time for several trajectories and for several r_w's. To monitor XD we use the parameter ξ defined in Eq. 4.2. The results are shown in Fig. 3.10. As explained above for the HS and LJ cases r_w^o will be comprised in between the largest value of r_w that shows no indication of the presence of a minimum in the free energy-XD profile and the smallest r_w that does show it. In Fig. 3.10 $r_w/\sigma = 0{,}42$ clearly corresponds to the presence of a deep minimum (one that can not be overcome by thermal activation for any of the 10 trajectories). By contrast, $r_w/\sigma = 0.36$ and 0.37 show no presence of a minimum because XD can grow and evolves in a different way for different trajectories. $r_w/\sigma = 0{,}38 - 41$ correspond to a shallow minimum because in all cases there are trajectories for which XD fluctuates for a significant period around typical values for the deep minimum case (XD$\approx$ 0,05). Therefore we set $r_w^o/\sigma = 0{,}375(5)$.

Once we get r_w^o we perform thermodynamic integration for values of $r_w > r_w^o$ and obtain the solid points shown in Fig. 3.11. The extrapolation of these data to r_w^o gives $\gamma_{cf} = 0{,}588(8) k_B T/\sigma^2$ that is, within the error bar, the same value we find for the pure HS system. This result implies that the PHS model can be used with confidence for the study of the behaviour of HS. The simulation details and results for the HS and PHS models are compared in Table 3.1.

3.5. Summary and conclusions

We propose a novel simulation methodology for the calculation of the crystal-fluid interfacial free energy. The main idea of the method is the use of a mold of potential energy wells to induce the formation of a crystal slab in a fluid at coexistence conditions. The coordinates of the mold's wells are given by the lattice positions of the crystal plane whose interfacial free energy is evaluated. The interaction between the wells and the fluid particles is square-well like. The free energy difference between the fluid and the fluid having the crystal slab induced by the mold is obtained by means of thermodynamic integration along a reversible path in which the wells are gradually filled. The method consists in four basic steps: (i) preparation of the mold and of the initial configuration of the fluid; (ii) estimation of the optimal radius of the wells; (iii) calculation of the interfacial free energy as a function of the well radius by thermodynamic integration; (iv) extrapolation of the function obtained in step (iii) to the optimal radius to get the final estimate of the interfacial free energy.

We validate our methodology by calculating the interfacial free energy of systems composed of hard spheres and Lennard-Jones particles. In both cases we find a very good agreement with previous estimates. Moreover, we show that our methodology is accurate enough to discriminate between different crystal orientations of the Lennard-

Jones system. We also use the new method to calculate the interfacial free energy for a continuous version of the hard sphere model for which, to the best of our knowledge, the interfacial free energy had not been previously calculated. Within the statistical uncertainty of our calculations we obtain the same interfacial free energy for both the continuous and the discontinuous potentials.

One of the main advantanges of our method with respect to existing ones is that no local-bond order parameter is required to either detect the interface or induce the growth of the solid[16,17,20,44]. The cleaving method does not require an order parameter either[35], but it entails following a rather cumbersome thermodynamic route. Our method, gives accurate results even for relatively small systems (about 2000 particles), which can not be achieved with the capillary fluctuation[44] or the classical nucleation[20] methods. Moreover, it can potentially deal with complex crystal lattices with no extra methodological complexity. The method can be easily implemented either in Monte Carlo or in standard Molecular Dynamics packages such as GROMACS. Therefore, we hope it will be appealing to the scientific community interested in investigating the properties of the crystal-melt interface.

Acknowledgements

All authors thank the Spanish Ministry of Economy and Competitiviness for the financial support through the project FIS2013-43209-P. E. Sanz and J. R. Espinosa acknowledge financial support from the EU grant 322326-COSAAC-FP7-PEOPLE-2012-CIG and E. Sanz from a Spanish grant Ramon y Cajal.

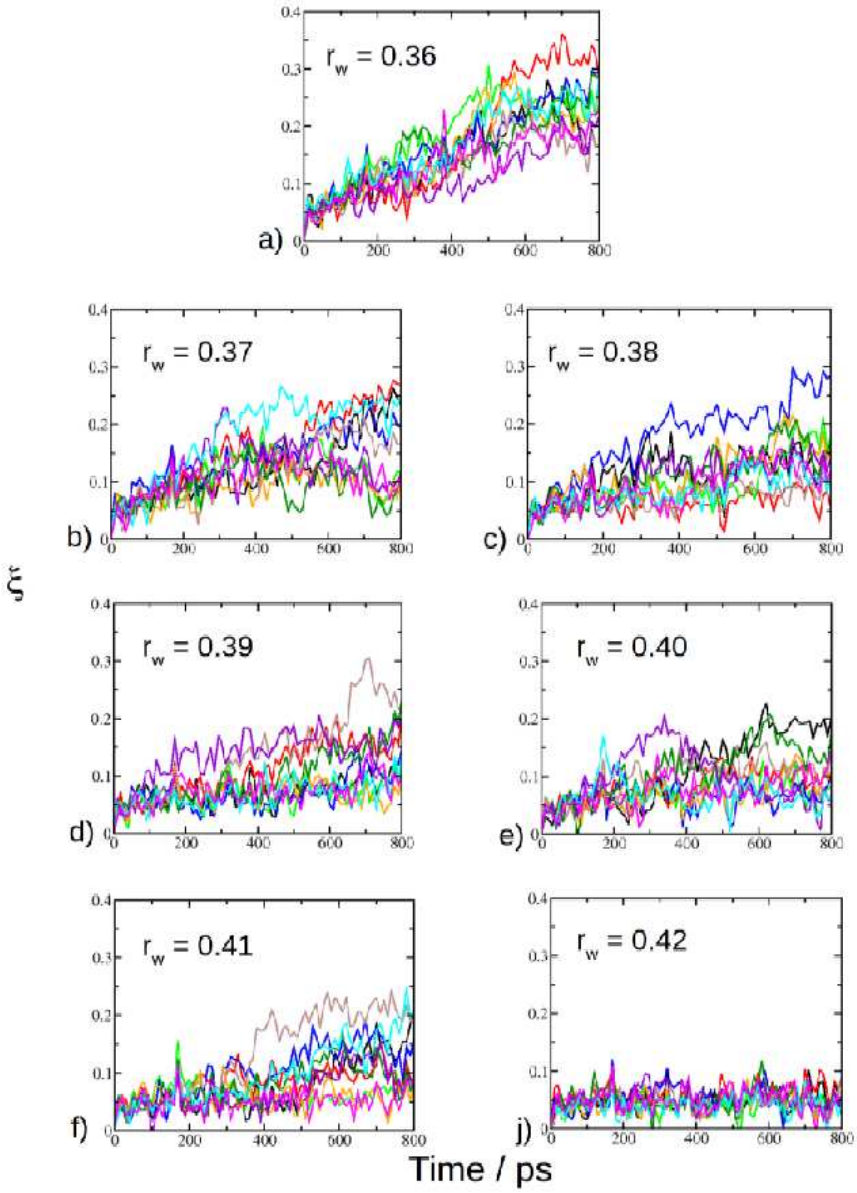

Figure 3.10: Crystallinity degree, XD, as measured by the parameter ξ (see main text) as a function of simulation time for several values of the radius of the mold potential wells, r_w/σ, as indicated inside each plot. The well depth is in all cases $7.5k_BT$. For a given r_w 10 trajectories differing in the seed for the random number generator are started from a fluid configuration. The mold is switched on at the beginning of the simulation. The plot corresponds to the PHS potential and the 100 crystal orientation.

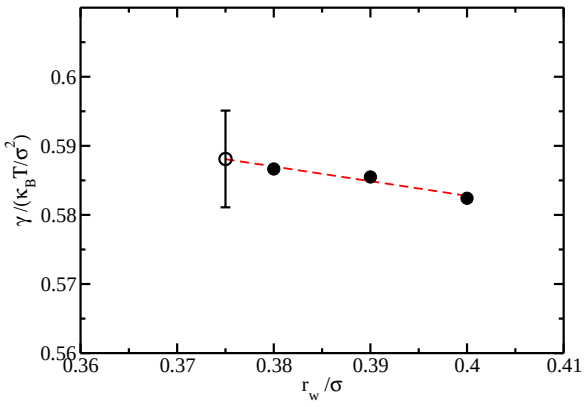

Figure 3.11: Solid symbols: interfacial free energy versus the well radius for the PHS model. Dashed line: linear fit to the solid symbols. Empty symbol: extrapolation of the linear fit to r_w^o.

Bibliography

1. Boettinger, W., Coriell, S., Greer, A., Karma, A., Kurz, W., Rappaz, M. & Trivedi, R., Solidification microstructures: recent developments, future directions. *Acta Materialia* **48**, 43 – 70 (2000).

2. Woodruff, D. P., *The solid-liquid interface* (Cambridge University Press, Cambridge, 1973).

3. Kelton, K. F., *Crystal Nucleation in Liquids and Glasses* (Academic, Boston, 1991).

4. Kelton, K. F., *Solid State Physics* (Academic Press, Dordrecht, 1991).

5. Rowlinson, J. S. & Widsom, B., *Molecular theory of capillarity* (Clarendon Press, Oxford, 1982).

6. Gloor, G., Jackson, G., Blas, F. & de Miguel, E., Test-area simulation method for the direct determination of the interfacial tension of systems with continuous or discontinuous potentials. *J. Chem. Phys.* **123**, 134703 (2005).

7. Pruppacher, H. R., A new look at homogeneous ice nucleation in supercooled water drops. *J. Atmosph. Sci.* **52**, 1924 (1995).

8. Broughton, J. Q. & Gilmer, G. H., Molecular dynamics investigation of the crystal–fluid interface. vi. e xcess surface free energies of crystal–liquid systems. *J. Chem. Phys.* **84**, 5759–5768 (1986).

9. Handel, R., Davidchack, R. L., Anwar, J. & Brukhno, A., Direct calculation of solid-liquid interfacial free energy for molecular systems: Tip4p ice-water interface. *Phys. Rev. Lett.* **100**, 036104 (2008).

10. Davidchack, R. L., Handel, R., Anwar, J. & Brukhno, A. V., Ice ih-water interfacial free energy of simple water models with full electrostatic interactions. *Journal of Chemical Theory and Computation* **8**, 2383–2390 (2012).

11. Davidchack, R. L., Hard spheres revisited: Accurate calculation of the solid–liquid interfacial free energy. *J. Chem. Phys.* **133**, 234701 (2010).

12. Mu, Y. & Song, X., Crystal-melt interfacial free energies of hard-dumbbell systems. *Phys. Rev. E* **74**, 031611 (2006).

13. Davidchack, R. L. & Laird, B. B., Direct calculation of the crystal–melt interfacial free energies for continuous potentials: Application to the lennard-jones system. *J. Chem. Phys.* **118**, 7651–7657 (2003).

14. Wang, J., Apte, P. A., Morris, J. R. & Zeng, X. C., Freezing point and solid-liquid interfacial free energy of stockmayer dipolar fluids: A molecular dynamics simulation study. *The Journal of Chemical Physics* **139**, 114705 (2013).

15. Benjamin, R. & Horbach, J., Crystal-liquid interfacial free energy via thermodynamic integration. *The Journal of Chemical Physics* **141**, 044715 (2014).

16. Fernandez, L. A., Martin-Mayor, V., Seoane, B. & Verrocchio, P., Equilibrium fluid-solid coexistence of hard spheres. *Phys. Rev. Lett.* **108**, 165701 (2012).

17. Angioletti Uberti, S., Ceriotti, M., Lee, P. D. & Finnis, M. W., Solid liquid interface free energy through metadynamics simulations. *Phys. Rev. B* **81**, 125416 (2010).

18. Laio, A. & Parrinello, M., Escaping free-energy minima. *Proc. Natl. Acad. Sci.* **99**, 12562 (2002).

19. Angioletti-Uberti, S., The solid-liquid interface free-energy of pb: comparison of theory and experiments. *Journal of Physics: Condensed Matter* **23**, 435008 (2011).

20. Bai, X.-M. & Li, M., Calculation of solid-liquid interfacial free energy: A classical nuclea tion theory based approach. *J. Chem. Phys.* **124**, 124707 (2006).

21. Knott, B. C., Molinero, V., Doherty, M. F. & Peters, B., Homogeneous nucleation of methane hydrates: Unrealistic under realistic conditions. *J. Am. Chem. Soc.* **134**, 19544–19547 (2012).

22. Sanz, E., Vega, C., Espinosa, J. R., Caballero-Bernal, R., Abascal, J. L. F. & Valeriani, C., Homogeneous ice nucleation at moderate supercooling from molecular simulation. *Journal of the American Chemical Society* **135**, 15008–15017 (2013).

23. Hess, B., Kutzner, C., van der Spoel, D. & Lindahl, E., Algorithms for highly efficient, load-balanced, and scalable molecular simulation. *J. Chem. Theory Comput.* **4**, 435–447 (2008).

24. Davidchack, R. L., Morris, J. R. & Laird, B. B., The anisotropic hard-sphere crystal-melt interfacial free energy from fluctuations. *J. Chem. Phys.* **125**, 094710 (2006).

25. Davidchack, R. L., Morris, J. R. & Laird, B. B., The anisotropic hard-sphere crystal-melt interfacial free energy from fluctuations. *The Journal of Chemical Physics* **125**, 094710 (2006).

26. Jover, J., Haslam, A. J., Galindo, A., Jackson, G. & Muller, E. A., Pseudo hard-sphere potential for use in continuous molecular-dynamics simulation of spherical and chain molecules. *The Journal of Chemical Physics* **137**, 144505 (2012).

27. Frenkel, D. & Smit, B., *Understanding Molecular Simulation*, chap. 7.1 (Academic Press, 2002).

28. ten Wolde, P. R., Ruiz-Montero, M. J. & Frenkel, D., Numerical calculation of the rate of crystal nucleation in a Lennard-Jones system at moderate undercooling. *J. Chem. Phys.* **104**, 9932 (1996).

29. Lechner, W. & Dellago, C., Accurate determination of crystal structures based on averaged local bond order parameters. *The Journal of Chemical Physics* **129**, 114707 (2008).

30. Schilling, T. & Schmid, F., Computing absolute free energies of disordered structures by molecular simulation. *The Journal of Chemical Physics* **131**, 231102 (2009).

31. Noya, E. G., Vega, C. & de Miguel, E., Determination of the melting point of hard spheres from direct coexistence simulation methods. *The Journal of Chemical Physics* **128**, 154507 (2008).

32. Broughton, J. Q. & Gilmer, G. H., Molecular dynamics investigation of the crystal-fluid interface. i. bulk properties. *The Journal of Chemical Physics* **79**, 5095–5104 (1983).

33. Broughton, J. Q. & Gilmer, G. H., Molecular dynamics investigation of the crystal-fluid interface. iv. free energies of crystal-vapor systems. *The Journal of Chemical Physics* **84**, 5741–5748 (1986).

34. Morris, J. R. & Song, X., The anisotropic free energy of the lennard-jones crystal-melt interface. *J. Chem. Phys.* **119**, 3920–3925 (2003).

35. Broughton, J. Q. & Gimer, G. H., Molecular dynamics investigation of the crystal-fluid interface. vi. excess surface free energies of crystal-liquid systems. *The Journal of Chemical Physics* **84**, 5759 (1986).

36. Santiso, E. E. & Trout, B. L., A general set of order parameters for molecular crystals. *J. Chem. Phys.* **134**, 064109 (2011).

37. Alder, B. J. & Wainwright, T. E., Phase transition for a hard sphere system. *J. Chem. Phys.* **27**, 1208–1209 (1957).

38. Pusey, P. N. & van Megen, W., Phase behaviour of concentrated suspensions of nearly hard colloidal spheres. *Nature* **320**, 340 (1986).

39. Pham, K. N., Puertas, A. M., Bergenholtz, J., Egelhaaf, S. U., Moussaid, A., Pusey, P. N., Schofield, A. B., Cates, M. E., Fuchs, M. & Poon, W. C. K., Multiple glassy states in a simple model system. *Science* **296**, 104 (2002).

40. Auer, S. & Frenkel, D., Prediction of absolute crystal-nucleation rate in hard-sphere colloids. *Nature* **409**, 1020 (2001).

41. Song, C., Wang, P. & Makse, H. A., A phase diagram for jammed matter. *Nature* **453**, 629–632 (2008).

42. Filion, L., Ni, R., Frenkel, D. & Dijkstra, M., Simulation of nucleation in almost hard-sphere colloids: The discrepancy between experiment and simulation persists. *The Journal of Chemical Physics* **134**, 134901 (2011).

43. Espinosa, J. R., Sanz, E., Valeriani, C. & Vega, C., On fluid-solid direct coexistence simulations: The pseudo-hard sphere model. *The Journal of Chemical Physics* **139**, 144502 (2013).

44. Hoyt, J. J., Asta, M. & Karma, A., Method for computing the anisotropy of the solid-liquid interfacial free energy. *Phys. Rev. Lett.* **86**, 5530–5533 (2001).

45. Pusey, P. N., Zaccarelli, E., Valeriani, C., Sanz, E., Poon, W. C. K. & Cates, M. E., Hard spheres: crystallization and glass formation. *Phyl. Trans. Roy. Soc. A* **367**, 4993–5011 (2009).

3.6. Appendix

3.6.1. Measure of XD

Here we show that the simple order parameter ξ used to quantify XD is totally equivalent to a more sophisticated one based on counting the the number of particles in the largest cluster of solid-like particles. Solid-like particles can be identified by means of a local-bond order parameter based on the local coordination of the particles[28]. The specific parameters we use in this work are those given in Ref.[45]. The largest cluster of solid-like particles corresponds to the crystal slab induced by the mold at coexistence conditions (e. g., the 6-7 crystal planes that can be seen around the mold in Fig. 9.1, bottom). In Fig. 3.12 we show the equivalent to Fig. 3.4 but using the number of particles in the biggest cluster of solid-like particles, n_s, instead of ξ as the parameter to follow the formation of the crystal. By comparing both figures it is clear that the simple parameter ξ provides the same information as the more sophisticated n_s.

3.6.2. Free energy profiles.

By analysing the trajectories where XD is monitored (e.g. Figs. 3.4 or 3.12) the free energy profile along the XD coordinate can be estimated as:

$$\Delta G/(k_B T) = -\ln P(XD) + constant \tag{3.9}$$

where $P(XD)$ is the probability that the system takes a certain value of the order parameter, XD. Then, by simply making a histogram of XD for all trajectories performed for a given well radius it is possible to get an estimate of the corresponding free energy profile. In Fig. 3.13 we show the free energy profile thus calculated for the 111 plane of the LJ system using both ξ and n_s as measures for XD. The conclusions that can be drawn by examining either order parameter are the same: for $r_w \geq 0{,}29\sigma$ there is a minimum whereas for $r_w \leq 0{,}28\sigma$ there is not. Consequently, we set the optimal radius r_w^o for this system to $0{,}285 \pm 0{,}005\sigma$.

Eq. 4.3 does not give absolute free energies (there is a missing constant) but allows to determine whether there is a minimum present or not. In any case, in order to compare all curves in the same free energy scale we have shifted each minimum to the work needed to fill the wells for the corresponding well radius (calculated by thermodynamic integration via Eq. 3.6). For the cases where the minimum is absent ($r_w = 0{,}28$) we have shifted the plateau of the curves to the work needed to fill a mold of wells with $r_w = r_w^o = 0{,}285\sigma$, given by the dashed horizontal line. The statistics of the free energy given by Eq. 4.3 are reasonably good when the system repeatedly samples configurations in the vicinity of a free energy minimum but become poor when it quickly moves along

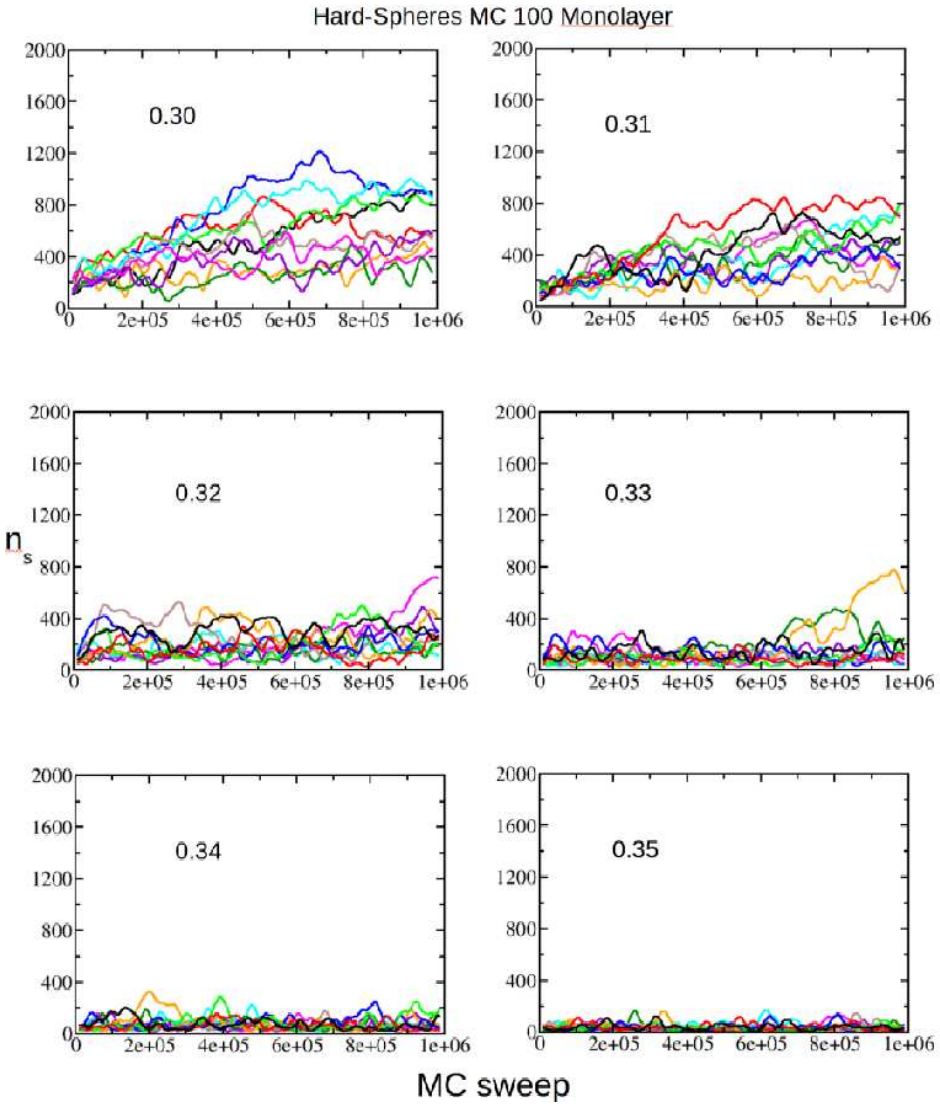

Figure 3.12: Crystallinity degree as measured by the number of particles in the biggest cluster of solid-like particles, n_s as a function of simulation time for several values of the radius of the potential wells, r_w/σ, as indicated inside each plot. The well depth is in all cases $7.5k_BT$. For a given r_w 10 trajectories differing in the seed for the random number generator are started from a fluid configuration. The mold is switched on at the beginning of the simulation. The plot corresponds to the HS system and the 100 crystal orientation.

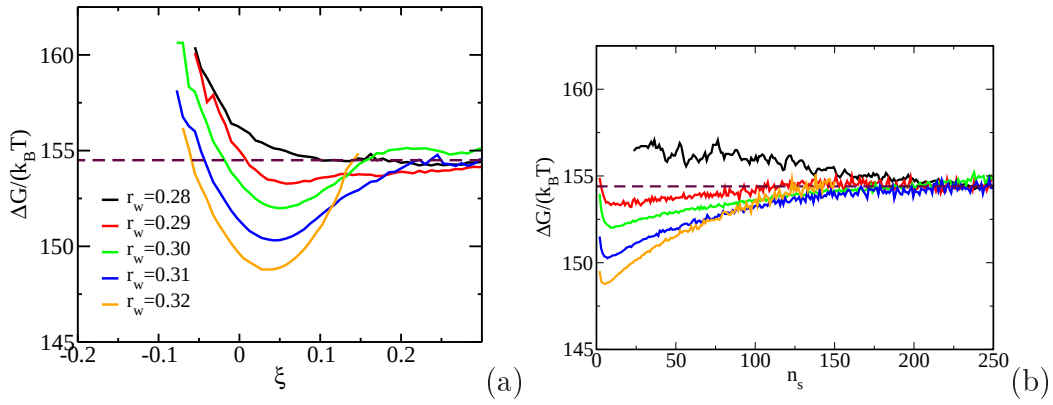

Figure 3.13: Free energy profile as a function of XD for the 111 plane of the LJ system as measured by ξ, (a), and by n_s, (b) for different well radii (as indicated in the legend in σ units).

the free energy plateau. Therefore, one has to be cautious and restrict the use of Eq. 4.3 to small values of XD.

With the degree of accuracy we got in the present study we were able to distinguish the anisotropy between the 111 and 100 faces of the LJ system. One could in principle try to further improve the accuracy by decreasing the range within which r_w^o is enclosed (by launching trajectories for more values of r_w). This is certainly a possibility worth exploring. However, it may require a substantial amount of trajectories to detect a mininum shallower than $1k_BT$, which is the depth of the shallowest minimum we could probe (curve corresponding to $r_w = 0{,}29$ in Fig. 3.13).

Results: Chapter 4

The crystal-fluid interfacial free energy and nucleation rate of NaCl from different simulation methods

Jorge R. Espinosa[†], *Carlos Vega*[†], *Chantal Valeriani*[‡] *and Eduardo Sanz*[†]

[†]Departamento de Quimica Fisica I, Facultad de Ciencias Quimicas, Universidad Complutense de Madrid, 28040 Madrid, Spain.
[‡]Departamento de Fisica Aplicada I, Facultad de Ciencias Fisicas, Universidad Complutense de Madrid, 28040 Madrid, Spain.

4.1. Abstract

In this work we calculate the crystal-fluid interfacial free energy, γ_{cf}, for the Tosi-Fumi model of NaCl using three different simulation techniques: Seeding, Umbrella Sampling and Mold Integration. The three techniques give an orientationaly averaged γ_{cf} of about 100 mJ/m^2. Moreover we observe that the shape of crystalline clusters embedded in the supercooled fluid is spherical. Using the Mold Integration technique we compute γ_{cf} for four different crystal orientations. The obtained interfacial free energies range from 100 to 114 mJ/m^2, being (100) and (111) the crystal planes with the lowest and highest γ_{cf}, respectively. Within the accuracy of our calculations, the interfacial free energy either does not depend on temperature or changes very smothly with it. Combining the Seeding technique with Classical Nucleation Theory, we also estimate nucleation free energy barriers and nucleation rates for a wide temperature range (800-1040K). The obtained results compare quite well with brute force calculations and with previous results obtained with Umbrella Sampling [C. Valeriani, E. Sanz and D. Frenkel, J. Chem. Phys, **122**, 194501 (2005)].

4.2. Introduction

The crystal-fluid interfacial free energy, γ_{cf}, is a crucial parameter in crystal nucleation and growth, as well as in wetting phenomena[1–3]. Unfortunately, it is quite difficult to measure γ_{cf} experimentally[4]. Typically, experimental measurements of the crystal nucleation rate are combined with Classical Nucleation Theory (CNT)[3] to estimate both the height of the nucleation barrier and the interfacial free energy[5–8].

Computer simulations are a useful tool to estimate crystal-fluid interfacial free energies. Several simulation methods have been implemented for that purpose: the cleaving method[9], the capillary fluctuation technique[10], metadynamics[11,12], tethered Monte Carlo[13], the contact angle approach[14,15], the seeding method[16–18], umbrella sampling[19], and the mold integration technique[20]. For systems like Lennard Jones[12,20–22], hard spheres[13,20,23–25] or water[17,18,26–28] some of these techniques have been used by different groups and a reasonable consensus on γ_{cf} has been reached. However, this is not the case for Sodium Chloride.

In 2005 two different values of γ_{cf} for the Tosi-Fumi model[29,30] of NaCl were reported: 36 mJ/m^2, based on measures of the contact angle of a liquid drop on top of its solid[14,31]; and 99 mJ/m^2, based on calculations of the nucleation free energy barrier combined with Classical Nucleation Theory[32]. These discrepancies were ascribed to finite size effects in small crystal clusters in a combined effort by both groups later on in 2008[33].

In our present work we calculate γ_{cf} for the Tosi-Fumi NaCl by three different techniques, namely, mold integration, seeding and umbrella sampling. The Mold Integration (MI) method consists in calculating the work needed to reversibly induce the formation of a crystal slab in the fluid under coexistence conditions. The seeding technique consists in inserting large crystalline clusters in the supercooled fluid and determining the temperature at which such clusters are critical. Then, CNT is used to provide estimates of the interfacial free energy. By means of the umbrella sampling (US) method it is possible to compute the free energy needed to form crystal clusters and then CNT is used to derive the interfacial free energy. Contrary to both umbrella sampling and seeding methods, the mold integration technique does not rely on CNT and and provides direct measures of γ_{cf}.

We find that the three techniques give a γ_{cf} averaged over crystal orientations of about 100 mJ/m^2. This good agreement is obtained assuming a spherical shape for the clusters both in seeding and in umbrella sampling. This assumption is justified by our analysis of the shape of the clusters in the seeding technique that confirms their spherical shape. The seeding technique also allows us to evaluate the dependence of γ_{cf} with temperature and to conclude that γ_{cf} does not depend on temperature.

Even more relevant to crystal nucleation than the interfacial free energy is the nucleation rate (i.e. the number of critical clusters formed per unit of time and volume).

Contrary to γ_{cf}, the nucleation rate can be directly measured experimentally[34–36]. By means of our seeding simulations, CNT, and calculations of the attachment rate of particles to the critical cluster we estimate the nucleation rate and find a good agreement between numerical simulations and experiments.

4.3. NaCl Model

Several model potentials have been implemented to simulate alkali halides such as those proposed by Smith and Dang[37], by Joung and Cheatham[38] or by Tosi and Fumi[29,30]. We opt for the Tosi-Fumi potential, whose properties are quite close to those of real NaCl[29,30,39], in order to be able to compare with previous studies[14,31,32]. Tosi-Fumi[29] is a two-body and non-polarizable potential:

$$U(r_{ij}) = A_{ij}e^{B(\sigma_{ij}-r_{ij})} - \frac{C_{ij}}{r_{ij}^6} - \frac{D_{ij}}{r_{ij}^8} + \frac{q_i q_j}{r_{ij}}, \tag{4.1}$$

where r_{ij} is the distance between two ions with charge $q_{i,j}$. The first term is the Born-Mayer repulsive term, $-\frac{C_{ij}}{r_{ij}^6}$ and $-\frac{D_{ij}}{r_{ij}^8}$ are the van der Waals attractive interaction terms and the last one corresponds to the Coulomb interaction. The parameters A_{ij}, B, C_{ij}, D_{ij} and σ_{ij} are given in table 4.1.

	A_{ij}	B	C_{ij}	D_{ij}	σ_{ij}
Na-Na	25.4435	3.1546	101.1719	48.1771	2.340
Na-Cl	20.3548	3.1546	674.4793	837.0.770	2.755
Cl-Cl	15.2661	3.1546	6985.6786	14031.5785	3.170

Table 4.1: Parameters for the Tosi-Fumi NaCl[29], A_{ij} in kJ/mol, B in $Å^{-1}$, C_{ij} in $Å^6 kJ/mol$, D_{ij} in $Å^8 kJ/mol$ and σ_{ij} in Å.

In this work we have truncated the non-Coulomb part of the potential at $r_c = 14$ Å and added long range tail corrections to the energy (when simulating the system with Monte Carlo (MC) and Molecular Dynamics (MD)) and pressure (in MD). We have used Ewald sums (in MC) to deal with Coulomb interactions, truncating the real part of the sums at the same cut-off. For MD calculations we have used PME (Particle-Mesh Ewald method)[40] truncating at the same cut-off.

4.4. Simulation Details

We have used the GROMACS 4.5.5 package[41,42] to perform Molecular Dynamics simulations in the NpT ensemble. The Tosi-Fumi NaCl potential has been implemented in GROMACS in a tabulated form. The time step for the Velocity-Verlet algorithm was set to 0.002 ps and a velocity-rescale thermostat with a relaxation time of 0.5 ps was used to keep the selected temperature[43]. All our simulations are carried out at 1 bar using the Parrinello-Rahman barostat[44] with a relaxation time of 0.5 ps.

4.5. Mold Integration Method

This methodology has been recently proposed by Espinosa et al.[20] and allows to calculate the crystal-fluid interfacial free energy for a flat interface (at coexistence). The method has been validated with the calculation of γ_{cf} for hard spheres and Lennard-Jones[20].

The basic idea of this methodology is to reversibly induce the formation of a thin crystalline slab in the fluid with the aid of a mold of potential energy wells placed in the sites of a lattice plane. By switching on a square-well-like interaction between the wells and the fluid particles, the latter remain confined in the mold inducing the appearance of a thin crystal slab as sketched in Fig. 4.1[45]. In Fig. 4.1 (a) the mold (orange and gray spheres) is switched off and the fluid (small particles) does not feel its presence. In (b) the mold is switched on and each well is filled with a fluid particle, which creates a crystal slab around the mold. The work needed to go from (a) to (b) is related to the work required to create two crystal-fluid interfaces[20].

The only difference from the present work and reference[20] in terms of methodology is that here we use two different types of wells that selectively attract either Na^+ or Cl^- ions. (The systems studied in Ref.[20] were mono-component, so every well interacted with every particle.) In the following section we describe how the interfacial free energy is calculated for the 100 plane of NaCl with the MI method and give the results for other orientations.

4.5.1. Calculation of γ_{cf} with the MI method

In this section we report the calculation of γ_{cf} for four different crystal orientations using the MI method. We will start with explaining in more detail the calculations for the 100 plane and then give the results for all other orientations.

The first step is obtaining the mold coordinates and a fluid configuration at coexistence conditions. The dimensions of the mold have to be coherent with the unit cell

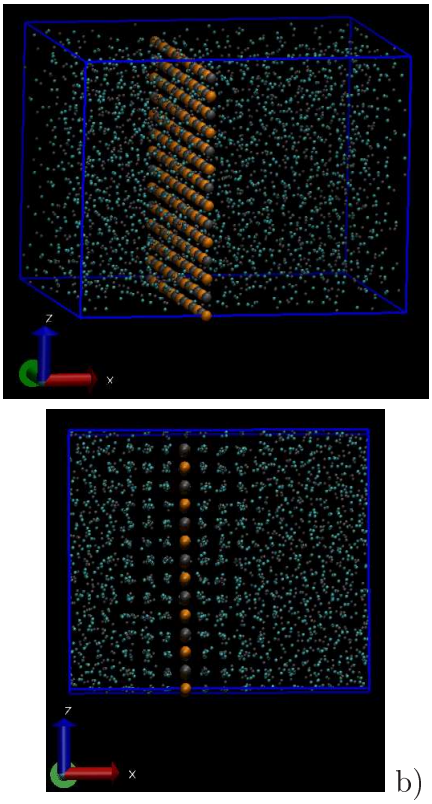

Figure 4.1: Top: Snapshot of a sodium chloride fluid at coexistence (green and black ions). Bottom: Snapshot of a fluid with a thin crystal slab at coexistence conditions. The diameter of the ions has been reduced to 1/4 of its original size. The mold that induces the formation of the crystal slab is conformed by a set of potential energy wells (in orange the ones for sodium ions and in grey the ones for chloride ions) whose positions are given by the lattice sites of the selected crystal plane (100) at coexistence conditions. The interaction between the mold and the ions is switched off in a) and on in b).

parameters at coexistence conditions. In Figs. 4.1 and 4.2 we show a representation of the mold used to induce the appearance of different crystal-fluid interfaces.

The mold for the (100) orientation has 196 wells, half for sodium and half for chloride ions. The fluid consists of 2744 ions equilibrated at coexistence conditions. The simulation box where the fluid is equilibrated is prepared in such way that the area of one of its sides coincides with that of the mold (see Fig. 4.1 (a)). This side is kept fixed and to maintain the pressure constant variations of the volume are made through changes in the direction perpendicular to it, which in our case is the x direction (we refer to this type of simulations as Np_xT[46]). The mold is kept fixed throughout the simulation.

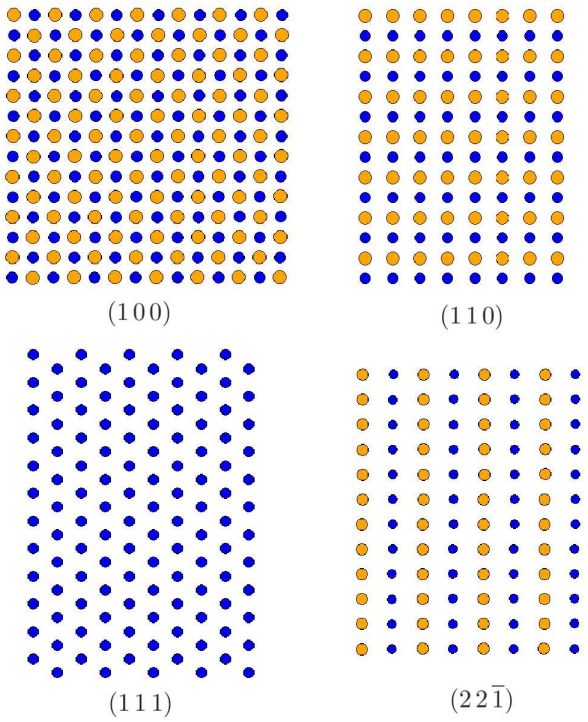

Figure 4.2: Molds used to induce the formation of crystal slabs for the different crystal orientations.

Once a fluid-mold configuration is prepared, we need to find the potential well radius that gives the correct value for γ_{cf}, r_w^o (the work needed to fill the mold depends on the well radius and there is only one radius for which the correct interfacial free energy is obtained[20]). To find r_w^o we run, for different values r_w of the well radius, several Np_xT trajectories starting from a fluid configuration where we switch on the mold at the beginning of the simulation. In the present paper we launch 8 trajectories of 1ns for each r_w. We set the depth of the square-well-like interaction between wells and particles to $\epsilon_m = 7{,}5k_BT$. This ensures that the mold is permanently filled (195.6 out of 196 wells are filled on average). Along each trajectory we monitor a parameter that accounts for the global degree of crystallinity, ξ:

$$\xi = \frac{\rho - \rho_f}{\rho_s - \rho_f} \tag{4.2}$$

where ρ is the actual density of the system and ρ_f and ρ_s are the coexistence densities of the fluid and the solid, respectively. Therefore, ξ fluctuates around 0 when the whole system is fluid and around 1 when is crystalline. As a crystal slab grows in the fluid, ξ

takes intermediate values. This is just a simple way to quantify the crystallinity degree, but one can also use a method based on counting the number of ions in the largest cluster of solid-like ions, using the same local order parameter as the one we will use in the "seeding" technique (see below). By means of the trajectories launched for each r_w we obtain a probability distribution $P(\xi)$ needed to estimate the free energy profile associated to the order parameter ξ.

$$G(\xi)/(k_B T) = -\ln P(\xi) + constant, \tag{4.3}$$

The constant is, in principle, unknown and we are just interested in the shape of the profile. As discussed in Ref.[20], if r_w is too large the system is in the free energy basin corresponding to the fluid (low values of ξ give a minimum in $G(\xi)$) and the mold is not able to induce the formation of a stable crystal slab. If, on the contrary, r_w is too small, the mold provides more energy than that required for the formation of the crystal slab and the $G(\xi)$ profile does not show a basin corresponding to the fluid phase. Accordingly, the free energy profile where the minimum first disappears gives r_w^o. In Fig. 4.3 we represent the free energy profiles for four different values of r_w.

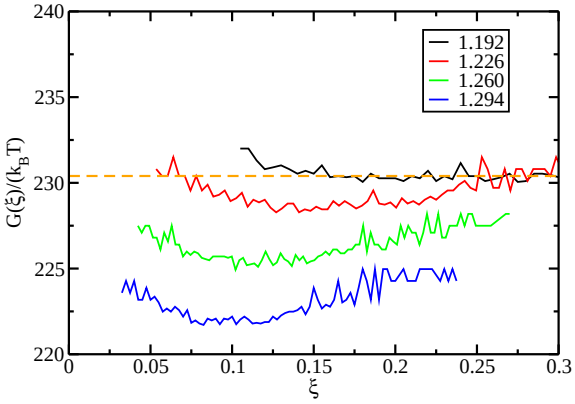

Figure 4.3: Free energy profile as a function of the crystallinity degree, ξ, for the 100 plane and for different well radii as indicated in the legend (in Å). In order to compare all curves in the same free energy reference we have shifted each minimum to the work needed to fill the mold for the corresponding well radius (calculated via thermodynamic integration). For the case where the minimum is absent (black curve) we have shifted the plateau to the work needed to fill a mold of wells with $r_w = r_w^o$, given by the dashed horizontal line.

$G(\xi)$ for r_w = 1.294, 1.260 and 1.226 Å clearly shows a minimum whereas for r_w = 1.192 Åit does not. Therefore, $r_w^o \in$ [1,192, 1,226Å]. Taking the mid point of the interval: r_w^o= 1.21 Å. The statistics of the free energy given by Eq. 4.3 is reasonably good only when the system repeatedly samples configurations in the vicinity of a free

energy minimum. Therefore, the use of Eq. 4.3 must be restricted to small values of crystallinity. An alternative approach to determine r_w^o, based on the inspection of $\xi(t)$ for various trajectories, is discussed in Ref.[20].

Once r_w^0 is obtained, the next step is to calculate $\gamma_{cf}(r_w)$ for $r_w > r_w^0$ by means of thermodynamic integration (thermodynamic integration can only be performed for $r_w > r_w^0$, where the system is still in the fluid basin and the integration is reversible[20]):

$$\gamma_{cf}(r_w) = \frac{1}{2A}\left(\epsilon_m N_w - \int_0^{\epsilon_m} d\epsilon < N_{fw} >\right) \tag{4.4}$$

where ϵ is the well depth and ϵ_m is the maximum well depth, A is the area of the interface (or the area of the mold), N_w is the total number of wells, and N_{fw} is the number of filled wells. To calculate the integral in Eq. 6.2 Np_xT simulations are performed for several well depths between $\epsilon = 0$ and $\epsilon = \epsilon_m$. The average number of filled wells ($< N_{fw} >$) is computed in each simulation. In Fig. 4.4 we plot $< N_{fw} >$ versus ϵ for $r_w = 1{,}26$Å.

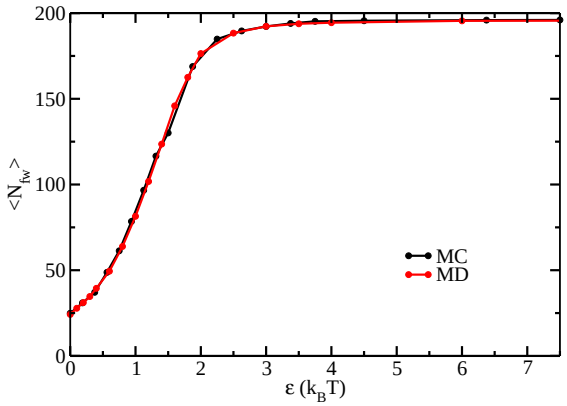

Figure 4.4: Average number of filled wells, $< N_{fw} >$, as a function of the depth of the well, ϵ. The plot corresponds to the (100) face and to a 196-well mold with $r_w = 1{,}26$Å. The red and black curves correspond to MD and MC simulations respectively.

Beyond $\epsilon \approx 5k_BT$ all wells are almost permanently filled. Note that the result of Eq. 6.2 does not depend on the value of ϵ_m as long as all wells are filled when $\epsilon = \epsilon_m$. Therefore, to avoid performing useless calculations, it is not convenient that ϵ_m largely exceeds the value of ϵ beyond which the wells are permanently filled. By integrating the curve shown in Fig. 4.4 we obtain $\gamma_{cf}(r_w = 1{,}26\text{Å}) = 97{,}5 mJ/m^2$. We made sure that the integration was reversible by switching off the mold at the end of the calculation and checking that the crystallinity degree ξ readily goes to 0 for all values of ϵ. The closer r_w to r_w^o the shallower the fluid basin and the more likely the integration is not reversible. Therefore, large values of r_w are preferred in this respect. However, one can

not increase r_w beyond the point where more than one particle fits in each well. As we show in Fig. 4.4 the simulations can be either performed with a bespoke MC code or with an MD package, such as GROMACS (in Ref.[20] some hints on how to implement the MI method in GROMACS are given). MD simulations to obtain each of the points in Fig. 4.4 are 800 ps long (50 ps for equilibration and 750 for production) and MC are 100000 cycles (10000 for equilibration and 90000 for production).

The calculations described in the previous paragraph for $r_w = 1{,}26$Å are repeated for several $r_w > r_w^o$ in order to obtain a $\gamma_{cf}(r_w)$ curve that can then be extrapolated to r_w^o (shown in Fig. 4.5).

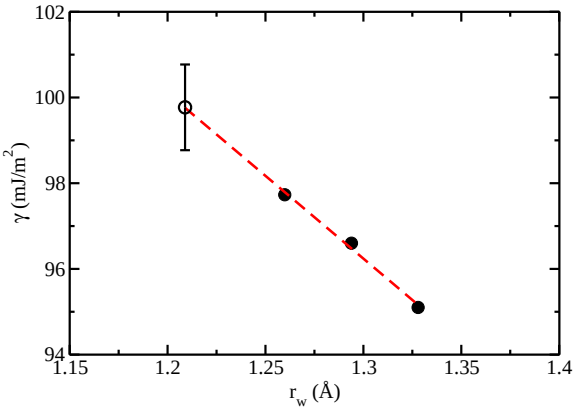

Figure 4.5: The solid filled symbols represent the interfacial free energy versus the potential well radius for the (100) plane. The red dashed line is a linear fit to the solid symbols. The empty symbol is an extrapolation of the fit to r_w^o, that gives our estimate for the interfacial free energy.

By performing a linear extrapolation to r_w^o we obtain a γ_{cf} for the 100 crystal plane of $(100\pm1)mJ/m^2$. Using the molds shown in Fig. 4.2 we repeat the same calculation for other crystal orientations. In Table 4.2 we report, for each orientation, the system size, the number of wells, the optimal radius, and the calculated γ_{cf}.

All crystal planes have a γ_{cf} of about 100 mJ/m^2 except the (111) plane, whose γ_{cf} is 15 % higher. This is perhaps not totally unexpected since the (111) plane, contrary to all other planes, is constituted of ions of the same chemical identity, therefore it is not electro-neutral. In principle, one could suspect that the (111) interface is unstable because of the dipolar moment coming from the stacking of charged planes parallel to the interface[47]. However, this dipolar interaction can be efficiently screened by the melt, a dense fluid of charged particles. In fact, it has been recently shown that the 111 crystal-melt interface of NaCl is rough and shows no signs of being unstable or undergoing surface reconstruction[48].

hkl	$(L_y \mathrm{x} L_z)/(\mathrm{\AA}^2)$	N_w	N_{Tot}	$r_w^o/\mathrm{\AA}$	$\gamma_{cf}/(\frac{mJ}{m^2})$
(1 0 0)	41.40x41.40	196	2744	1.21	100 ± 1
(1 1 0)	33.45x41.40	112	2688	1.07	103 ± 1
(1 1 1)	36.21x50.18	120	2880	0.87	114 ± 1
(2 2 $\overline{1}$)	36.21x40.97	120	2880	1.07	105 ± 1

Table 4.2: Interfacial area ($L_y \mathrm{x} L_z$), number of wells (N_w), number of particles (N_{Tot}), optimal well radius (r_w^o), and interfacial free energy (γ_{cf}) for all crystal orientations studied with the MI method.

4.6. Seeding

4.6.1. The seeding technique

This technique has been first proposed by Bai and Li[16,49] for the calculation of the crystal-fluid interfacial free energy of the Lennard-Jones system. Later on, it was used to determine γ_{cf} for clathrates[17] and for several water models[18,28]. In brief, it consists in inserting a crystalline cluster in a supercooled fluid and performing simulations at several temperatures while monitoring the size of the cluster. If the chosen temperature is below the temperature at which the cluster is critical, the cluster will grow, whereas if it is above the cluster will melt. So the temperature at which the cluster is critical is enclosed in between the highest temperature at which the cluster grows and the lowest at which it melts. This approach is similar to the one used by Pereyra et al.[50] to determine the temperature at which a cylindrical crystalline slab of ice melts or grows.

Once the temperature at which the cluster is critical is known, the seeding approach makes use of Classical Nucleation Theory (CNT) to obtain estimates of the interfacial free energy. According to CNT[3], the free energy required for the formation of a crystalline cluster in the supercooled fluid is:

$$\Delta G(N) = -N|\Delta\mu| + A\gamma_{cf} \tag{4.5}$$

where $\Delta\mu$ is the chemical potential difference between the crystal and the supercooled fluid, N is the number of particles in the crystal cluster and A is the cluster's surface area. Assuming that the crystalline cluster has a spherical shape, the value of N that maximizes ΔG (N_c) is given by:

$$N_c = \frac{32\pi\gamma_{cf}^3}{3\rho_s^2|\Delta\mu|^3} \tag{4.6}$$

where ρ_s is the density of the solid phase. This equation allows to estimate γ_{cf}. There are two ways of calculating $\Delta\mu$. The first one is by means of thermodynamic integration

from the coexistence temperature, where $\Delta\mu = 0$. The other is by approximating $\Delta\mu$ by $\Delta H_m(1 - T/T_m)$, where ΔH_m is the enthalpy change at melting and T_m is the melting temperature. We have checked that the approximation works well and gives the same result as the rigorous thermodynamic integration.

Apart from obtaining estimates of γ_{cf} via Eq. 4.6 one can estimate the nucleation free energy barrier (ΔG_c) and the nucleation rate (J) with CNT. The free energy barrier for nucleation is given by:

$$\Delta G_c = \frac{N_c}{2}|\Delta\mu|. \tag{4.7}$$

Following the approach described by Auer and Frenkel[3,19,51], the nucleation rate J can be obtained from the expression :

$$J = \rho_f Z f^+ \exp(-\Delta G_c/(k_B T_c)) \tag{4.8}$$

where the product $\rho_f Z f^+$ is the kinetic prefactor, κ_p, where f^+ the attachment rate of particles to the critical cluster, ρ_f the fluid density and Z the Zeldovich factor[3]. The CNT form of the Zeldovich factor is

$$Z = \sqrt{(|\Delta G''|_{N_c}/(2\pi k_B T_c))} = \sqrt{|\Delta\mu|/(6\pi k_B T_c N_c)} \tag{4.9}$$

so that Z can be computed once the size of the critical cluster, N_c, the temperature at which it is critical, T_c, and the chemical potential difference between the solid and the liquid are known. According to Ref.[19,32,51], f^+ can be computed as a diffusion coefficient of the cluster size at the top of the barrier (which requires launching about 10 runs at the temperature at which the cluster is critical):

$$f^+ = \frac{< (N(t) - N_c)^2 >}{2t}. \tag{4.10}$$

Alternatively, f^+ can be approximated in a way that does not require running simulations of the critical cluster[3]. According to Ref[3] since the attachment rate f^+ is related to the time required for a particle to attach to the crystal cluster, it can be estimated as:

$$f^+ = \frac{24D(N_c)^{2/3}}{\lambda^2} \tag{4.11}$$

where λ^2/D is the time needed for a molecule to diffuse the typical distance required to attach to the cluster λ and D is the diffusion coefficient of the supercooled liquid.

The seeding technique can be particularly useful at low and moderate supercooling, where estimating the critical cluster size, the free-energy barrier height and the rate by more rigorous numerical techniques would be very expensive (from a computational point of view).

4.6.2. Approximations in the seeding approach

The seeding technique is an approximate approach to calculate γ_{cf}. First of all, it relies on the validity of CNT. Next, the inserted clusters have a defined shape. The expressions above for the CNT correspond to the assumption that the clusters are spherical. We will discuss later on that this is actually a good approximation for NaCl. The interfacial free energy thus obtained corresponds to an average over all possible crystal orientations, so the technique does not provide information about the anisotropy of γ_{cf} with the orientation of the crystal. Finally, the method heavily relies on the way the number of particles in the cluster (N_c) is determined. This is typically evaluated with the aid of local bond-order parameters able to discriminate between liquid-like and solid-like particles[52]. Therefore, N_c depends on the specific choice of the order parameter. Of course, reasonable choices of order parameter give similar values for N_c, but differences of about 30 % in the number of particles can be found between different order parameters. According to Eq. 4.6, a 30 % error in N_c results in an uncertainty of 10 % in γ_{cf}. Therefore, the ambiguity in the determination of N_c substantially affects the accuracy with which γ_{cf} is determined via the seeding technique.

In this work we use the same order parameter as in Ref.[32] to measure N_c. In Ref.[32] the order parameter was tuned so that the percentage of particles wrongly labelled as liquid-like in the bulk solid was the same as that of particles wrongly labelled as solid-like in the bulk liquid. The same criterion was used to tune the order parameter when studying the ice-water interface and led to reasonable values for γ_{cf}[18,28].

We can also check if our choice of the order parameter is reasonable by visually inspecting the clusters.

In Fig. 4.6(a) we show the top view of a cluster as detected by our order parameter. The crystalline features of the cluster can be clearly appreciated. In Figs. 4.6(b), (c) and (d) we show the snapshots resulting from adding 1, 2 and 3 extra layers of particles to the cluster originally detected by our order parameter. These extra layers do not perfectly fit on top of the underlying solid lattice. Therefore, the order parameter employed seems to be a good one because it does not add a fluid-like layer to the cluster (neither removes a solid-like layer from it).

4.6.3. Setup for the seeding technique

To prepare the initial configuration we insert a crystalline cluster in the supercooled fluid and remove the fluid molecules that overlap with the cluster. Then, the fluid-crystal interface is equilibrated for 8 ps keeping the positions of the ions of the inserted cluster fixed. In this way the cluster does not loose particles and the interface is equilibrated by the attachment of new particles to the cluster. At last, the constraint is released and the system is further equilibrated for 8 ps until N varies smoothly with time. Following

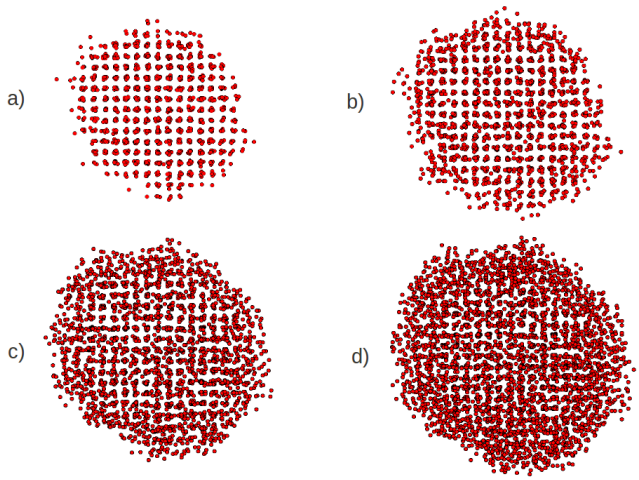

Figure 4.6: a) Snapshot of a solid cluster as detected by the local order parameter used in this work (same as in Ref.[32]). b) Same cluster as in a) but with an extra layer of particles attached to it. c) Same cluster as in a) but with two extra layers of particles attached to it. d) Same cluster as in a) but with three extra layers of particles attached to it. The crystalline character of the cluster fades as extra layers are added.

equilibration, we launch trajectories at different temperatures to find the temperature at which the equilibrated cluster is critical.

In Fig. 4.7 we show the evolution of N with time during equilibration and during production, when trajectories are launched at different temperatures from the equilibrated cluster. The equilibration is typically performed at low temperatures (925 K in this particular case) to avoid the cluster loosing particles during the second stage of equilibration.

A list of all cluster sizes after equilibration is given in table 4.3.

In each system the total number of ions is approximately 20 times larger than the inserted cluster to avoid interactions between the cluster and its periodic images. The total number of ions, N_{Tot} for each system (considering the solid cluster and the supercooled fluid) is also given in table 4.3: in order to be able to simulate such large systems, we had to recur to supercomputing facilities.

4.6.4. Cluster shape

The CNT expressions given above correspond to the assumption that the critical cluster adopts a spherical shape. In principle this is a reasonable assumption because

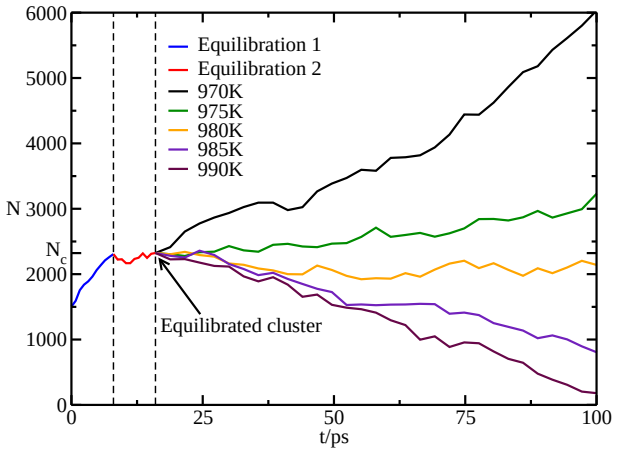

Figure 4.7: Number of particles in the cluster (N) versus time. During the first stage of equilibration (8 ps, blue curve) the cluster is kept frozen and it grows as the interface equilibrates. In the second stage (red curve) the constraint is released and the system is equilibrated for another 8ps. These two equilibration runs are performed at 925 K. Finally, several simulations starting from the configuration of the equilibrated cluster are run at different temperatures to locate the temperature at which such cluster is critical.

Nc	N_{Tot}	T_c	ρ_s	γ_{cf}
284	21724	857.5	1.95	113
1152	46522	962.5	1.92	97
2322	46396	980.0	1.91	104
8084	110248	1007.5	1.90	114
11164	194920	1022.5	1.89	102

Table 4.3: Number of ions in the critical cluster (N_c), total number of ions in the system (N_{Tot}), temperature at which the cluster is found to be critical (T_c[K]), density of the solid at that temperature ($\rho_s[g/cm^3]$) and the interfacial free energy from Eq. 4.6 in mJ/m^2.

a sphere is the shape with the lowest surface area. However, in Ref.[32] it was suggested that the cluster could be cubic rather than spherical. This is a plausible possibility for the cluster's shape, given that NaCl has a cubic unit cell. To investigate if the shape of the cluster is spherical or cubic we equilibrate both a cubic and a spherical cluster and compare the shape of the resulting clusters. In Fig. 4.8(a) we show a snapshot of both clusters just after being inserted and in Fig. 4.8(b) after the equilibration of the interface.

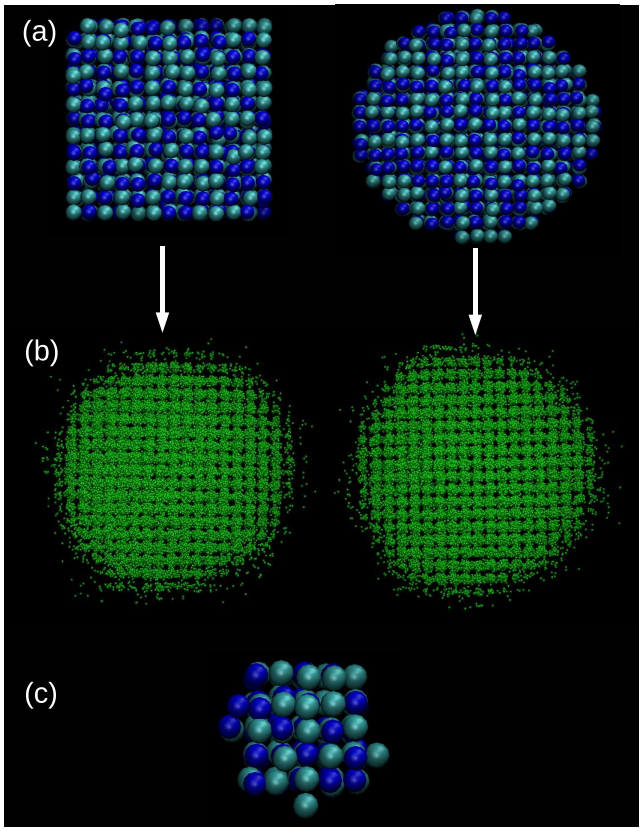

Figure 4.8: Snapshots of different crystalline NaCl clusters. (a) A cubic (left) and a spherical (right) cluster of about 2000 particles obtained from the bulk solid lattice. (b) A superimposition of 60 clusters equilibrated as described in the main text from the clusters in (a). (c) A sphere of 130 particles obtained from the bulk solid lattice. The shape of the cluster looks cubic rather than spherical due to the limited number of particles.

In Fig. 4.8(b) 60 independent equilibrated clusters are superimposed (with the same orientation) in order to get a statistical representation of the average cluster shape. Both equilibrated clusters have a very similar average shape that clearly looks more spherical than cubic. Some faceting is present that makes the average shape different from that of a perfect sphere. But such faceting is also present in the spherical cluster originally inserted (Fig. 4.8(a), right) and is a consequence of discretizing a sphere with a cubic lattice. To quantify the degree of sphericity of the clusters we expanded their density with respect to their center of mass in rank four spherical harmonics and calculated the quadratic invariant S_4[53]. The 60 clusters equilibrated from a sphere give an average S_4 of 0.03 while those coming from a cube give $S_4 = 0{,}034$. S_4 for a perfect sphere is 0.003 and for a perfect cube 0.115. Therefore, both cubic and spherical clusters equilibrate to a shape which is closer to a sphere. In summary, we can consider our clusters spherical and confidently use the CNT expressions above.

4.6.5. Interfacial free energy

Once the cluster is equilibrated, we perform MD runs at different temperatures and monitor the cluster size to determine the temperature at which each cluster is critical, as shown in Fig. 4.7 for one of the clusters. In the example of Fig. 4.7 the size of the cluster does not change during the simulation at T=980 K, so we consider this as the temperature at which a cluster with $N_c = 2322$ particles is critical. Once we know T_c we obtain $\Delta\mu$ as $\Delta H_m(1 - T_c/T_m)$. Next we measure in an NpT simulation ρ_s at T_c: in this way, we obtain all variables needed to obtain γ_{cf} via Eq. 4.6. For this model, $\Delta H_m = 3{,}36 kcal$ per mol of ions and $T_m = 1082K$[39]. The results obtained for all clusters are reported in Table 4.3.

In Fig. 4.9 we show that, within the accuracy of our data, the interfacial free energy does not change with the supercooling (the difference between the melting temperature and the temperature of interest). This implies, according to the thermodynamic relation $-S_{cf} = (\partial\gamma_{cf}/\partial T)_p$, that the entropic cost of forming the crystal-fluid interface for NaCl is either zero or very small. In Fig. 4.9 we also show the $\gamma(T)$ dependence predicted by Turnbull's rule[54] ($\gamma_{cf} = C_T\rho_s^{2/3}\Delta H(T)/N_A$, where N_A is Avogadro's number, $\Delta H(T)$ is the enthalpy difference between the liquid and the solid, and C_T=0.394 is the Turnbull's constant obtained from the calculated γ_{cf} at coexistence (105 mJ/m^2)). Turnbull's rule has been successfully used to predict nucleation times for Al and Lennard-Jones systems[55,56]. The mild decrease of γ as the supercooling increases predicted by Turnbull is consistent with our data. Since our data do not show a clear temperature dependence we obtain γ_{cf} at the melting temperature simply by averaging γ_{cf} for all supercoolings studied. This average is indicated in Fig. 4.9 with a dashed line and corresponds to 105 mJ/m^2. As discussed above, this value is subject to a systematic error of about 10 % due to the arbitrariness of the order parameter. The statistical error of the determination of

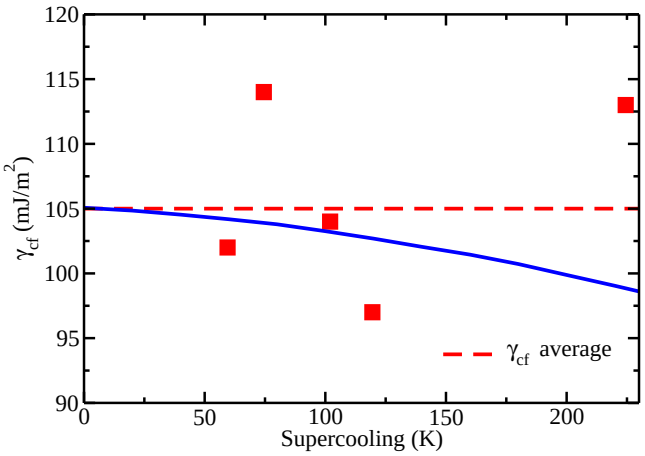

Figure 4.9: Interfacial free energy estimated via Eq. 4.6 for the critical clusters studied as a function of the supercooling. Within the accuracy of our data, γ_{cf} does not change with the supercooling. The dashed line is the average γ_{cf} and the solid line is the variation of γ_{cf} with temperature predicted by Turnbull.

T_c in our simulations raises the error in γ_{cf} up to 20 %.

4.6.6. Free energy barriers and nucleation rates

Once the interfacial free energy is calculated, we can obtain ΔG_c, the work needed to form a critical cluster in the metastable fluid, via Eq. 7.8. Then, we compute the attachment rate via Eq. 4.10 to finally obtain the nucleation rate from Eq. 4.8. To calculate the attachment rate via Eq. 4.10 we launch 10 trajectories at T_c from the equilibrated cluster (with N_c particles) and monitor N to obtain an average curve of $(N(t) - N_c)^2$. The slope of such curve, that should be a straight line in the regime in which the cluster diffuses on top of the barrier, is related to the attachment rate by Eq. 4.10. The time evolution of N in the ten trajectories and the resulting average $(N(t) - N_c)^2$ curve are shown in Fig. 4.10.

Note that, since the simulations are performed at T_c in some of the trajectories the cluster grows, in others it shrinks and in others it does not change its size. In table 4.4 we report our results for all quantities needed for the calculation of the nucleation barrier and the nucleation rate.

In Fig. 4.11 (a) and (b) we plot both the free-energy and the nucleation rate. Data represented in square purples are our results from the seeding technique, whereas red dots are data from Ref.[32]. Our seeding data have been obtained for milder supercooling than those of Ref.[32], but both data sets seem to be consistent at first sight. In Fig. 4.11(b) we also include the only available experimental data for the nucleation of NaCl

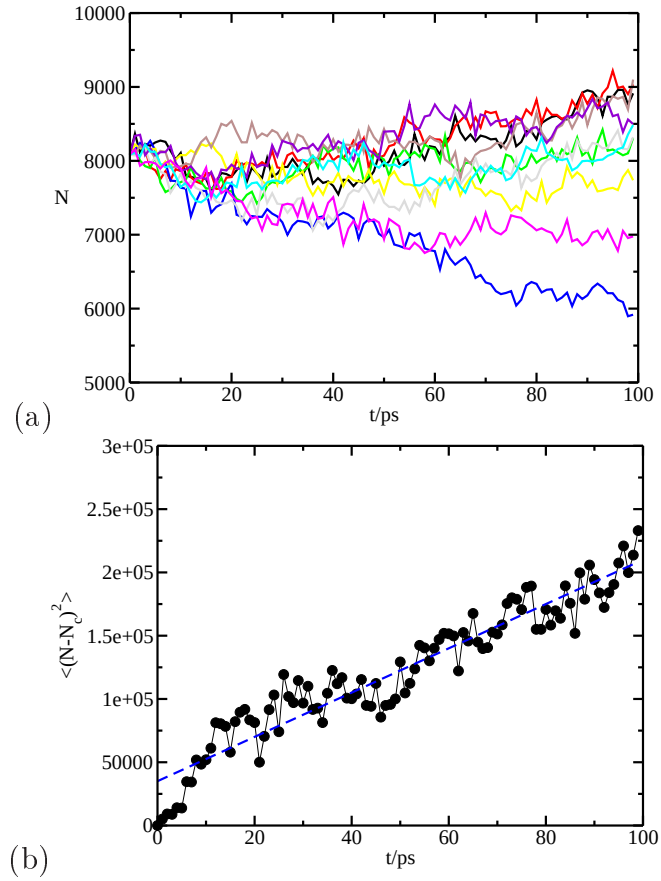

Figure 4.10: (a) N versus time for 10 trajectories launched at the temperature at which the cluster is critical ($T = 1007{,}5K$). (b) $< (N - N_c)^2 > (t)$ versus time, whose slope is related to the attachment rate by Eq. 4.10.

from its melt[34–36] (blue triangle). Remarkably, the experimental data is fully consistent with the predictions of the model.

From our seeding calculations we can estimate the whole dependence of ΔG_c and J with the supercooling. We use Eq. 7.8 to obtain ΔG_c at any temperature. The density of the solid as a function temperature is calculated by fitting several NpT simulations of the bulk solid. The fit thus obtained is $\rho_s(g/cm^3) = 2{,}259 - 0{,}00035811 \cdot T(K)$. As for the γ_{cf}, since it does not depend on T we can use the average value of 105 mJ/m^2. This gives the purple curve in Fig. 4.11 (a), that shows a good agreement with the points calculated in Ref.[32] by means of US. As expected, the free-energy barrier rapidly grows as the freezing point is approached (zero supercooling) and homogeneous nucleation becomes increasingly unlikely. To obtain J as a function of the supercooling we use Eq. 4.8. The density of the fluid is obtained via a linear fit of ρ_f versus T that we

N_c	T_c	$f^+/10^{14}$	$Z/10^{-3}$	$\kappa_p/10^{40}$	ΔG_c	$\log_{10}J$	λ
284	857.5	1,0	17	2,3	57	16	0.3
1152	962.5	4,2	5,9	3,1	111	-8	1.7
2322	980.0	6,0	3,8	3,2	188	-41	2.0
8084	1007.5	10	1,7	3,4	465	-162	1.1
11164	1022.5	20	1,3	3,5	506	-180	3.4

Table 4.4: Studied cluster sizes (N_c), temperature at which the cluster is founded to be critical ($T_c(K)$) and the corresponding values for the attachment rate (f^+, in s^{-1}); the Zeldovich factor (Z); the kinetic prefactor ($\kappa_p = \rho_f Z f^+$), in $m^{-3}s^{-1}$; the height of the nucleation free energy barrier (ΔG_c), in k_BT; the $\log_{10}$ of the nucleation rate (J) in $m^{-3}s^{-1}$; and the constant λ in Å.

obtain by performing NpT simulations at several supercoolings. The fit thus obtained is $\rho_f(g/cm^3) = 2{,}00776 - 0{,}0005702 \cdot T(K)$. The Zeldovich factor, Z, can be obtained at any temperature by using Eqs. 4.9 and 4.6 and assuming again a constant γ_{cf} of 105 mJ/m^2. The attachment rate, f^+, can also be estimated at any temperature with the aid of Eq. 7.5 using a λ averaged over all clusters ($< \lambda >= 1{,}7$Å), and an Arrhenius-like fit of $D(T)$ based o NpT simulations of the fluid ($\ln D(m^2/s) = -16{,}019 - 2886{,}1/T(K)$). It is a good approximation to use an average λ because, as shown in Table 4.4, λ does not change much with temperature and takes physically meaningful values of the order of one atomic diameter (the distance travelled by particles before attaching to the cluster). The curve of J versus supercooling thus obtained is shown in purple in Fig. 4.11 (b). The agreement with both the simulation of Ref.[32], and the experiment[34–36] is confirmed by the fit. Moreover, the fit works well even at very deep supercoolings, where we have estimated the rate by means of brute force simulations (black squares in Fig. 4.11 (b)). To obtain such rate estimates we simulate the fluid at a temperature, where the free energy barrier is low and nucleation is likely to happen spontaneously, and wait for the system to crystallize. The nucleation rate is estimated as $1/(< t > V)$, where V is the system's volume and $< t >$ is the average time the fluid takes to crystallize. To compute $< t >$ we perform 5 independent runs from the same initial configuration but with different Maxwellian momenta. The system size was 194920 ions for both 770 and 780 K and the nucleation time was 0.52 and 3.5 ns respectively. At 750 K a system with 21724 ions was used and the nucleation time was 0.53 ns. In summary, using our seeding results, we have obtained a curve that describes the dependency of the nucleation rate with the supercooling. The curve works well both at moderate supercoolings, where it coincides with experiments and previous simulations, and at deep supercoolings, where it is consistent with brute force simulations. The curve also provides nucleation rates for low supercoolings that have been up to date inaccessible to either simulations or

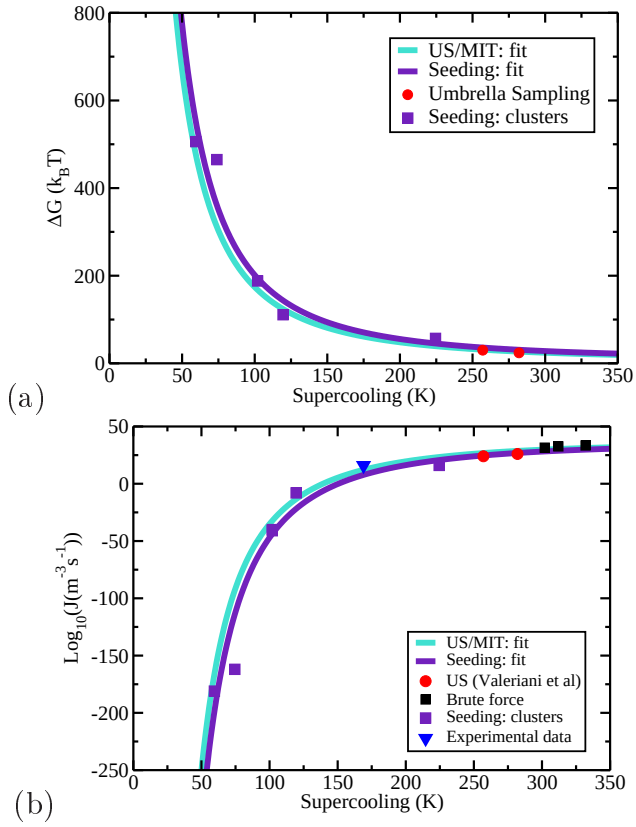

Figure 4.11: Free energy barrier height, (a), and nucleation rate, (b), as a function of the supercooling. Purple squares correspond to our seeding data, red circles are results from Ref.[32], the blue triangle is an experimental data from Refs.[34–36] and the black squares are our calculations of the nucleation rate from brute force MD calculations. The curves are fits based on the seeding data (purple) and on the estimates of γ_{cf} at coexistence by means of the MI method and US (cyan).

experiments.

4.7. Umbrella Sampling at coexistence

Umbrella Sampling (US) simulations[57] can be used to compute the free energy barrier associated with the formation of a crystal cluster in the supercooled fluid[58]. In Ref.[32], US was used to calculate the free energy barrier for the formation of NaCl crystallites at 800 and 825 K. From the height of the barriers obtained in Ref.[32] and using Eq. 4.6, γ_{cf} can be obtained. Such estimate requires assuming a particular shape for the critical cluster and can only be performed for temperatures below melting. US can also

be used to estimate γ_{cf} at coexistence[59]. To do that the free energy of formation of a crystal cluster ($\Delta G(N)$) is calculated under coexistence conditions. In this case $\Delta G(N)$ does not reach a maximum value since $\Delta\mu$ is 0, so γ_{cf} can not be obtained from the barrier height. However one can use Eq. 10.4 with $\Delta\mu = 0$ and, assuming a spherical shape for the cluster, obtain γ_{cf} as follows:

$$\gamma_{cf}(N) = \frac{\Delta G(N)}{(36\pi)^{1/3}}\rho_s^{2/3}N^{-2/3} \tag{4.12}$$

Note that this approach relies not only on the assumption on the cluster's shape, but also on the order parameter used to determine N.

This approach was followed in Ref.[33] to estimate γ_{cf} at coexistence. The coexistence temperature for the NaCl Tosi-Fumi model has been previously calculated and it ranges from 1060 to 1089K[15,29,30,39,60,61]. In Ref.[33] a value of 1060 K was used. However, in this work we consider that 1082 K is a more reliable value because it has obtained by different simulation methods[39]. Therefore, we repeat the calculations performed in Ref.[33] using 1082 K instead of 1060 K. We have divided the calculations in 20 US windows, using the same order parameter to compute N as in Ref.[32] (and the same used in this work for the seeding technique). For each window an NpT Monte Carlo simulation with bias potential $u_w = k(N - N_0)^2$ was performed (being k the bias constant $0{,}11264k_BT$ and N_0 the number of particles in the cluster around which the sampling window is centered). Our Monte Carlo simulations consisted of 5000 equilibration sweeps and 25000 production sweeps. (Each sweep consisted of two MC cycles in which a particle trial move and a volume trial move are attempted.) The configuration obtained at the end of a sweep is compared with that at the beginning of the sweep and accepted or rejected according to the Metropolis criterion with the bias potential above mentioned. Our results are compared to those of Ref.[33] in Fig. 4.12.

From $\Delta G(N)$ in Fig. 4.12 we can obtain $\gamma_{cf}(N)$ as explained above (Eq. 4.13). For clusters larger than ~ 80 particles the free energy reaches a plateau around 102 mJ/m^2. This value is very similar (about 3 mJ/m^2 higher) to that obtained in Ref.[33], so we can conclude that the effect of changing by about 20 K the melting temperature is very small.

With the seeding technique we concluded that, within the accuracy of our data, γ_{cf} did not depend on temperature (see Fig. 4.9). Since the interfacial entropy is the derivative of gamma with respect to T we concluded that the interfacial entropy was either zero or very small. We can double-check this statement by analysing our umbrella sampling data. By measuring the enthalpy of the system for each cluster size and subtracting the enthalpy of the liquid we obtain the enthalpy of cluster formation as a function of the cluster size N. Then, we subtract $N\Delta H_m$ to such enthalpy and divide by the cluster's surface area (assuming a spherical shape) to obtain the interfacial enthalpy H_{cf}. The interfacial entropy, S_{cf}, is finally obtained as $S = (H_{cf} - \gamma)/T$. In Fig. 4.14 we

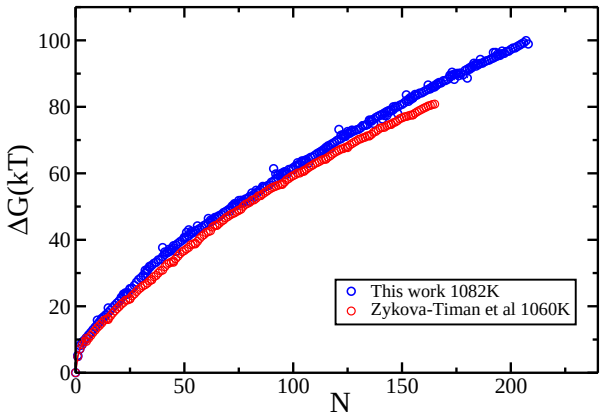

Figure 4.12: Free energy barriers (ΔG) as a function of N at coexistence (blue circles) and at 1060K (red ones), the latter from Ref.[33].

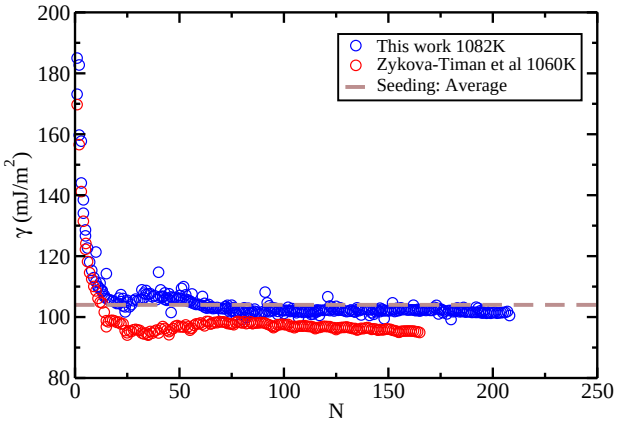

Figure 4.13: Interfacial free energy as a function of the cluster size assuming two different melting temperatures and from the seeding technique. The color code is the same as in Fig. 4.12

plot the interfacial free energy and the two terms that add up to it (H_{cf} and $-TS_{cf}$) as a function of the cluster size.

As the cluster becomes larger it is clear that γ_{cf} becomes increasingly dominated by the enthalpic term. For the largest simulated cluster (containing 210 particles) about 90 % of the interfacial free energy is enthalpic. For such cluster size the interfacial entropy is $S_{cf} = 0{,}01 mJ/m^2K$, so small that it would lead to a decrease of γ of only 3 mJ/m^2 for a supercooling of 300 K. Such decrease is smaller than our error bar in the seeding method. From Fig. 4.14 it seems that for large clusters convergence will be reached for $H_{cf} = \gamma$ and $S_{cf} = 0$. The fact that γ_{cf} for NaCl is mainly enthalpic

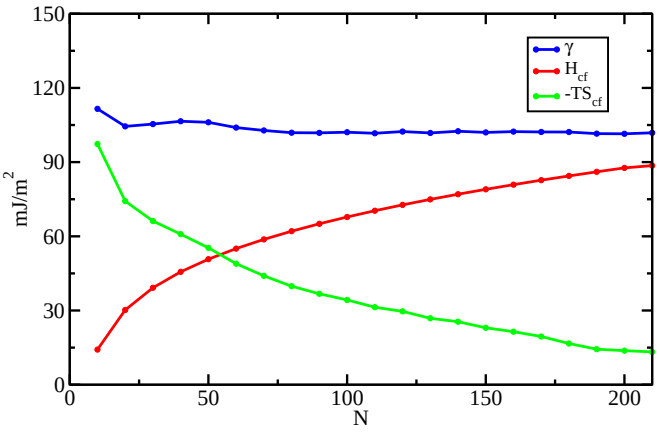

Figure 4.14: Interfacial free energy (blue), interfacial enthalpy (red) and interfacial entropy multiplied by -T (green) as a function of the cluster size N.

cannot be generalized to all systems. For instance, in water the cost to create the ice-fluid interface is entropic rather than enthalpic[62]. To conclude, the analysis performed from our umbrella sampling simulations confirms the conclusion drawn from the seeding technique that γ is either independent of T or varies very smoothly with it.

4.8. Discussion

The orientationaly averaged γ_{cf} obtained through the three different methodologies used in this work is about 100 mJ/m^2. This value is consistent with that obtained in Ref.[32] assuming a spherical cluster shape. The value is also similar, although about 10 % higher, to that recently obtained by means of an analysis of capillary wave fluctuations of the crystal-melt interface[48]. In order to get a good agreement between the γ_{cf} calculated for a planar interface (via MI or Capillary Fluctuations[48]) and that obtained from crystal clusters (seeding and US) we did not need to resort to corrections[63] to the simplest version of CNT. The value of 100 mN/m for γ_{cf} clashes with the 36 mN/m obtained in Refs.[14,31]. We suspect that the discrepancy may stem from finite size effects such as the comparable weight of surface and line tensions, arising when calculating contact angles with small droplets[64]. The good agreement between our results and those of Ref.[32] suggests that there are no irreducible size effects in the calculation of γ_{cf} using small NaCl crystal clusters[33].

The MI method gives γ_{cf} for different crystal orientations, whereas both seeding and US only provide an orientationaly averaged γ_{cf}. Moreover, both seeding and US are subject to an assumption on the cluster shape and to an order parameter that arbitrarily provides a value for the number of particles in the crystal cluster. The MI

method does not have these drawbacks, but only allows to obtain a γ_{cf} at coexistence. In order to get the dependence of γ_{cf} with temperature, seeding is the best option. US is in principle also valid for that purpose, but it is computationally very expensive to compute free energy barriers at low supercoolings, where the critical clusters contain thousands of particles. For NaCl we find that γ_{cf} does not depend on temperature (at constant pressure). This is not a general rule for all substances. For instance, recent studies for water show that γ_{cf} decreases when the temperature decreases[18,28,62,65]. Moreover, the seeding method permits the estimate of the nucleation rate as a function of temperature through the calculation of the attachment rate of particles to the critical cluster. The results are shown in Fig. 4.11(b) in purple squares and can be fitted using CNT (purple line in the same figure). The fit shows a good agreement with experimental data[34–36]. We have also used CNT to obtain a nucleation rate curve for US and MI. Since γ_{cf} does not depend on temperature one can take the average γ_{cf} calculated at coexistence with these techniques and use CNT as we did to fit the seeding data to obtain the cyan curve shown in Fig. 4.11. Both US and MI give the same curve because they yield the same average γ_{cf}. Of course, the curve is very close to that obtained with seeding because all methods give very similar γ_{cf} (and γ_{cf} does not depend on T). Obtaining a nucleation curve from MI or US at coexistence can only be attempted if γ_{cf} does not depend on T (which, according to the seeding data shown in Fig. 4.9, seems to be the case for NaCl).

In the seeding section of the paper we show that the shape of crystal clusters is spherical. Consequently, we have used the CNT expressions for a spherical cluster throughout the paper. With such expressions, seeding and US give the same result as the MI method. The latter method, as opposed to the other two, does not depend on any assumption on the cluster's shape. Therefore, both our shape analysis and the consistency of all techniques when clusters are assumed to be spherical indicate that NaCl clusters are indeed spherical. This result appears in principle contradictory with that of Ref.[32] where the clusters were reported to be cubic. In Ref.[32] the typical critical cluster size was of the order of 100 ions. In Fig. 4.8(c) we show a cluster of nearly 100 particles that has been obtained by taking the particles inside a sphere from the bulk crystal lattice. The cluster is cubic rather than spherical, which means that when dealing with such small NaCl clusters one can not see anything else than cubic clusters due to the impossibility of obtaining a spherical shape with a few nodes of a cubic lattice.

The kinetic prefactor for the nucleation rate of NaCl is of the order of $10^{40} m^{-3} s^{-1}$. This is about three orders of magnitude higher than that of realistic models of water (of the TIP4P family[66]) and of the same order of magnitude than that of the coarse-grain water model MW[67], for which water is seen like a single atom[18,28]. This suggests that the orientational degrees of freedom of water slow down by a factor of 1000 the attachment of particles to the critical cluster with respect to atomic systems.

4.9. Conclusions

The orientationaly averaged interfacial free energy of NaCl evaluated via three independent techniques is $\gamma_{cf} = 100 \pm 5 mJ/m^2$. All methods consistently give this result, which is in good agreement with Ref.[32]. The techniques employed have been the Mold Integration Method, that provides γ_{cf} for different crystal orientations, and the seeding and the umbrella sampling methods, that give an orientationaly averaged γ_{cf}. All studied orientations have a very similar γ_{cf} of around $100 mJ/m^2$, except the (111) plane, whose γ_{cf} is $114 \pm 1 mJ/m^2$. The seeding method also allows estimating γ_{cf} for different temperatures. We find that, within the accuracy of our calculations, γ_{cf} does not depend on temperature. Consistently, our Umbrella Sampling data at coexistence show that the work needed to form the crystal-fluid interface is mainly enthalpic rather than entropic.

An analysis of the shape of crystal clusters in the supercooled fluid reveals that these have a spherical shape. Small clusters –containing about 100 particles– look cubic simply because it is not possible to obtain a sphere with few nodes of a cubic lattice.

The seeding method also allows estimating free energy barriers and nucleation rates for several temperatures. Using Classical Nucleation Theory we obtain a fit for our nucleation rate data that is consistent with experiments[34–36] and that extrapolates well to high supercoolings, where we have evaluated the rate with brute force simulations.

Acknowledgments

All authors acknowledge the Spanish Ministry of Economy and Competitiveness for the financial support through the project FIS2013-43209-P and the RES for providing supercomputing facilities (project QCM-2015-1-0028). E. Sanz and J. R. Espinosa acknowledge financial support from the EU grant 322326-COSAAC-FP7-PEOPLE-2012-CIG. E. Sanz and C.Valeriani from a Spanish tenure track Ramon y Cajal. E. Sanz thanks useful discussions with L. G. MacDowell and J. Benet.

Bibliography

1. Boettinger, W., Coriell, S., Greer, A., Karma, A., Kurz, W., Rappaz, M. & Trivedi, R., Solidification microstructures: recent developments, future directions. *Acta Materialia* **48**, 43 – 70 (2000).

2. Woodruff, D. P., *The solid-liquid interface* (Cambridge University Press, Cambridge, 1973).

3. Kelton, K. F., *Crystal Nucleation in Liquids and Glasses*, vol. 45 (Academic Press, Boston, 1991).

4. Kelton, K. F., *Solid State Physics* (Academic Press, Dordrecht, 1991).

5. Volmer, M. & Weber, A. *Z. Phys. Chem.* **119**, 277 (1926).

6. Becker, R. & Doring, W. *Ann. Phys.* **24**, 719–752 (1935).

7. Farkas, L. *Z. Chem. Phys.* **125**, 236 (1927).

8. Gibbs, J. W. *The Scientific Papers of J. Willard Gibbs* **125**, Dover (1961).

9. Broughton, J. Q. & Gilmer, G. H., Molecular dynamics investigation of the crystal–fluid interface. vi. e xcess surface free energies of crystal–liquid systems. *J. Chem. Phys.* **84**, 5759–5768 (1986).

10. Hoyt, J. J., Asta, M. & Karma, A., Method for computing the anisotropy of the solid-liquid interfacial free energy. *Phys. Rev. Lett.* **86**, 5530–5533 (2001).

11. Laio, A. & Parrinello, M., Escaping free-energy minima. *Proc. Natl. Acad. Sci.* **99**, 12562 (2002).

12. Angioletti-Uberti, S., Ceriotti, M., Lee, P. D. & Finnis, M. W., Solid-liquid interface free energy through metadynamics simulations. *Phys. Rev. B* **81**, 125416 (2010).

13. Fernandez, L. A., Martin-Mayor, V., Seoane, B. & Verrocchio, P., Equilibrium fluid-solid coexistence of hard spheres. *Phys. Rev. Lett.* **108**, 165701 (2012).

14. Zykova-Timan, T., Ceresoli, D., Tartaglino, U. & Tosatti, E., Why are alkali halide surfaces not wetted by their own melt? *Phys. Rev. Lett.* **94**, 176105 (2005).

15. Zykova-Timan, T., Ceresoli, D., Tartaglino, U. & Tosatti, E. *J. Chem. Phys.* **125**, 164701 (2005).

16. Bai, X. M. & Li, M., Differences between solid superheating and liquid supercooling. *J. Chem. Phys.* **123**, 151102 (2005).

17. Knott, B. C., Molinero, V., Doherty, M. F. & Peters, B., Homogeneous nucleation of methane hydrates: Unrealistic under realistic conditions. *J. Am. Chem. Soc.* **134**, 19544–19547 (2012).

18. Sanz, E., Vega, C., Espinosa, J. R., Caballero-Bernal, R., Abascal, J. L. F. & Valeriani, C., Homogeneous ice nucleation at moderate supercooling from molecular simulation. *Journal of the American Chemical Society* **135**, 15008–15017 (2013).

19. Auer, S. & Frenkel, D., Prediction of absolute crystal-nucleation rate in hard-sphere colloids. *Nature* **409**, 1020 (2001).

20. Espinosa, J. R., Vega, C. & Sanz, E., The mold integration method for the calculation of the crystal-fluid interfacial free energy from simulations. *The Journal of Chemical Physics* **141**, 134709 (2014).

21. Davidchack, R. L. & Laird, B. B., Direct calculation of the crystal–melt interfacial free energies for continuous potentials: Application to the lennard-jones system. *J. Chem. Phys.* **118**, 7651–7657 (2003).

22. Benjamin, R. & Horbach, J., Crystal-liquid interfacial free energy via thermodynamic integration. *The Journal of Chemical Physics* **141**, 044715 (2014).

23. Davidchack, R. L., Hard spheres revisited: Accurate calculation of the solid–liquid interfacial free energy. *J. Chem. Phys.* **133**, 234701 (2010).

24. Mu, Y. & Song, X., Crystal-melt interfacial free energies of hard-dumbbell systems. *Phys. Rev. E* **74**, 031611 (2006).

25. Davidchack, R. L., Morris, J. R. & Laird, B. B., The anisotropic hard-sphere crystal-melt interfacial free energy from fluctuations. *J. Chem. Phys.* **125**, 094710 (2006).

26. Handel, R., Davidchack, R. L., Anwar, J. & Brukhno, A., Direct calculation of solid-liquid interfacial free energy for molecular systems: Tip4p ice-water interface. *Phys. Rev. Lett.* **100**, 036104 (2008).

27. Davidchack, R. L., Handel, R., Anwar, J. & Brukhno, A. V., Ice ih-water interfacial free energy of simple water models with full electrostatic interactions. *Journal of Chemical Theory and Computation* **8**, 2383–2390 (2012).

28. Espinosa, J. R., Sanz, E., Valeriani, C. & Vega, C., Homogeneous ice nucleation for several water models. *Journal of Chemical Physics* **141**, 18C529 (2014).

29. Fumi, F. & Tosi, M., Ionic sizes and born repulsive parameters in the NaCl-type alkali halides i. *Journal of Physics and Chemistry of Solids* **25**, 31–43 (1964).

30. Tosi, M. & Fumi, F., Ionic sizes and born repulsive parameters in the NaCl-type alkali halides II. *Journal of Physics and Chemistry of Solids* **25**, 45–52 (1964).

31. Zykova-Timan, T., Ceresoli, D., Tartaglino, U. & Tosatti, E., Physics of solid and liquid alkali halide surfaces near the melting point. *The Journal of Chemical Physics* **123**, 164701 (2005).

32. Valeriani, C., Sanz, E. & Frenkel, D., Rate of homogeneous crystal nucleation in molten NaCl. *J. Chem. Phys.* **122**, 194501 (2005).

33. Zykova-Timan, T., Valeriani, C., Sanz, E., Frenkel, D. & Tosatti, E., Irreducible finite-size effects in the surface free energy of nacl crystals from crystal-nucleation data. *Phys. Rev. Lett.* **100**, 036103 (2008).

34. Buckle, E. R. & Ubbelohde, A. R., Studies on the freezing of pure liquids. I. Critical supercooling in molten alkali halides. *Proceedings of the Royal Society of London. Series A. Mathematical and Physical Sciences* **259**, 325–340 (1960).

35. Buckle, E. R., Studies on the freezing of pure liquids. II. The kinetics of homogeneous nucleation in supercooled liquids. *Proceedings of the Royal Society of London. Series A. Mathematical and Physical Sciences* **261**, 189–196 (1961).

36. Buckle, E. R. & Ubbelohde, A. R., Studies on the freezing of pure liquids. III. Homogeneous nucleation in molten alkali halides. *Proceedings of the Royal Society of London. Series A. Mathematical and Physical Sciences* **261**, 197–206 (1961).

37. Dang, L. & Smith, D. E., Molecular dynamics simulations of aqueous ionic clusters using polarizable water. *J. Chem. Phys.* **99**, 6950 (1993).

38. Joung, I. S. & Cheatham, T. E., Determination of alkali and halide monovalent ion parameters for use in explicitly solvated biomolecular simulations. *The Journal of Physical Chemistry B* **112**, 9020–9041 (2008).

39. Aragones, J. L., Sanz, E., Valeriani, C. & Vega, C., Calculation of the melting point of alkali halides by means of computer simulations. *The Journal of Chemical Physics* **137**, 104507 (2012).

40. Essmann, U., Perera, L., Berkowitz, M. L., Darden, T., Lee, H. & Pedersen, L. G., A smooth particle mesh ewald method. *J. Chem. Phys.* **103**, 8577–8593 (1995).

41. Berendsen, H., van der Spoel, D. & van Drunen, R., Gromacs: A message passing parallel molecular dynamics implementation. *Computer Physics Communications* **91**, 43 – 56 (1995).

42. Hess, B., Kutzner, C., van der Spoel, D. & Lindahl, E., Gromacs 4: Algorithms for highly efficient, load-balanced, and scalable molecular simulation. *Journal of Chemical Theory and Computation* **4**, 435–447 (2008).

43. Bussi, G., Donadio, D. & Parrinello, M., Canonical sampling through velocity rescaling. *J. Chem. Phys.* **126**, 014101 (2007).

44. Parrinello, M. & Rahman, A., Polymorphic transitions in single crystals: A new Molecular Dynamics method. *J. Appl. Phys.* **52**, 7182–7190 (1981).

45. Schilling, T. & Schmid, F., Computing absolute free energies of disordered structures by molecular simulation. *The Journal of Chemical Physics* **131**, 231102 (2009).

46. Espinosa, J. R., Sanz, E., Valeriani, C. & Vega, C., On fluid-solid direct coexistence simulations: The pseudo-hard sphere model. *The Journal of Chemical Physics* **139**, 144502 (2013).

47. Tasker, P. W., The stability of ionic crystal surfaces. *Journal of Physics C: Solid State Physics* **12**, 4977 (1979).

48. Benet, J., MacDowell, L. G. & Sanz, E., Interfacial free energy of the nacl crystal-melt interface from capillary wave fluctuations. *The Journal of Chemical Physics* **142**, 134706 (2015).

49. Bai, X. M. & Li, M., Calculation of solid-liquid interfacial free energy: A classical nucleation theory based approach. *J. Chem. Phys.* **124**, 124707 (2006).

50. Pereyra, R. G., Szleifer, I. & Carignano, M. A. *J. Chem. Phys.* **135**, 034508 (2011).

51. Auer, S. & Frenkel, D., Numerical prediction of absolute crystallization rates in hard-sphere colloids. *J. Chem. Phys.* **120**, 3015–3029 (2004).

52. ten Wolde, P. R., Ruiz-Montero, M. J. & Frenkel, D., Numerical calculation of the rate of crystal nucleation in a Lennard-Jones system at moderate undercooling. *J. Chem. Phys.* **104**, 9932 (1996).

53. ten Wolde, P. R., Ruiz-Montero, M. J. & Frenkel, D., Numerical evidence for bcc ordering at the surface of a critical fcc nucleus. *Phys. Rev. Lett.* **75**, 2714 (1995).

54. Turnbull, D., Formation of crystal nuclei in liquid metals. *Journal of Applied Physics* **21**, 1022–1028 (1950).

55. Aga, R. S., Morris, J. R., Hoyt, J. J. & Mendelev, M., Quantitative parameter-free prediction of simulated crystal-nucleation times. *Phys. Rev. Lett.* **96**, 245701 (2006).

56. Peng, L. J., Morris, J. R. & Aga, R. S., A parameter-free prediction of simulated crystal nucleation times in the lennard-jones system: From the steady-state nucleation to the transient time regime. *The Journal of Chemical Physics* **133**, 084505 (2010).

57. Torrie, G. M. & Valleau, J. P., Nonphysical sampling distributions in Monte Carlo free-energy estimation: Umbrella sampling. *J. Comput. Phys.* **23**, 187 (1977).

58. ten Wolde, P. R. & Frenkel, D., Computer simulation study of gas-liquid nucleation in a Lennard-Jones system. *J. Chem. Phys.* **109**, 9901 (1998).

59. Cacciuto, A., Auer, S. & Frenkel, D., Solid-liquid interfacial free energy of small colloidal hard-sphere crystals. *J. Chem. Phys.* **119**, 7467 (2003).

60. Rowlinson, J. & Widom, B., *Molecular Theory of Capillarity*, Dover books on chemistry (Dover Publications, 2002).

61. Anwar, J., Frenkel, D. & Noro, M. G., Calculation of the melting point of NaCl by molecular simulation. *J. Chem. Phys.* **118**, 728 (2003).

62. Reinhardt, A. & Doye, J. P. K., Note: Homogeneous tip4p/2005 ice nucleation at low supercooling. *The Journal of Chemical Physics* **139**, 096102 (2013).

63. Prestipino, S., Laio, A. & Tosatti, E., Systematic improvement of classical nucleation theory. *Phys. Rev. Lett.* **108**, 225701 (2012).

64. MacDowell, L. G., Müller, M. & Binder, K., How do droplets on a surface depend on the system size? **206**, 277–291 (2002).

65. Ickes, L., Welti, A., Hoose, C. & Lohmann, U., Computing absolute free energies of disordered structures by molecular simulation. *Phys. Chem. Chem. Phys.* **17**, 5514 (2015).

66. Jorgensen, W. L., Chandrasekhar, J., Madura, J. D., Impey, R. W. & Klein, M. L., Comparison of simple potential functions for simulating liquid water. *J. Chem. Phys.* **79**, 926–935 (1983).

67. Molinero, V. & Moore, E. B., Water modeled as an intermediate element between carbon and silicon. *J. Phys. Chem. B* **113**, 4008–4016 (2009).

Results: Chapter 5

Seeding approach to crystal nucleation

Jorge R. Espinosa[†], *Carlos Vega*[†], *Chantal Valeriani*[†,‡], *Eduardo Sanz*[†]

[†]Departamento de Quimica Fisica I, Facultad de Ciencias Quimicas, Universidad Complutense de Madrid, 28040 Madrid, Spain.
[‡]Departamento de Fisica Aplicada I, Facultad de Ciencias Fisicas, Universidad Complutense de Madrid, 28040 Madrid, Spain.

5.1. Abstract

We present a study of homogeneous crystal nucleation from metastable fluids via the seeding technique for four different systems: mW water, Tosi-Fumi NaCl, Lennard-Jones and Hard Spheres. Combining simulations of spherical crystal seeds embedded in the metastable fluid with Classical Nucleation Theory we are able to successfully describe the nucleation rate for all systems in a wide range of metastability. The crystal-fluid interfacial free energy extrapolated to coexistence conditions is also in good agreement with direct calculations of such parameter. Our results show that seeding is a powerful technique to investigate crystal nucleation.

5.2. Introduction

The transition between a liquid and a crystal is a phenomenon of great importance in areas as diverse as biology (e. g. protein crystallization), climate change (crystallization in clouds), industry (e. g. drugs production), geology or optics. The emergence of a growing crystal nucleus in the fluid phase is the first step of the liquid-to-crystal transition[1]. The rate, size and structure with which such nucleus appears are fundamental parameters for the understanding and control of crystallization.

Whereas the nucleation rate can be measured experimentally[2–6], a microscopic description of the crystal nucleus remains elusive to current experimental techniques, due to the small size ($\sim$ nm) and short life ($\sim$ ns) of the nucleus[7]. To overcome this experimental shortcoming two different approaches are pursued. One is the use of colloidal systems as models for atomic and molecular systems[8]. Due to its big size ($\sim \mu m$), colloids can be seen and tracked in a microscope[9]. However, despite significant advances in the synthesis of colloidal particles[10], most investigations of crystal nucleation are restricted to spherical particles with isotropic interactions[9,11].

An alternative approach to the study of the mechanism of crystal nucleation is the use of computer simulations[12], that provide a detailed description of the system at a molecular level[13,14]. The main problem faced by simulations is that, for moderately supercooled fluids, the emergence of a crystal nucleus is a rare event and can not be directly probed in the size and time scales accessible to brute force Molecular Dynamics. Therefore, special rare event simulation methods like Umbrella Sampling (US)[15–17,17–29], Forward Flux Sampling (FFS)[20,21,29? –33], Metadynamics[34,35] or Transition Path Sampling[14,36,37] have to be employed. Although these methods artificially accelerate the appearance of the crystal nucleus they do not, in principle, alter the true crystallization mechanism. However, the use of these methods is quite demanding computationally, which restricts most studies to deeply metastable fluids, where the critical cluster is small (about 100-200 particles).

An approximate simulation approach, which we refer to as "seeding", has been used in the last few years to study nucleation in conditions of shallow metastability[38–44]. The technique is based in seeding the fluid with a crystal cluster. The microscopic information of the critical cluster obtained by means of simulations is combined with Classical Nucleation Theory (CNT)[1,45,46] to get estimates of the nucleation rate. The seeding method is quite simple to implement and enables the estimation of the nucleation rate in a broad range of orders of magnitude[41–43]. However, the method is approximate because it relies on the validity of both an *a priori* conceived nucleation pathway (that going through the inserted seed) and of Classical Nucleation Theory. It is therefore important to assess the extent to which this powerful but approximate technique can be confidently used.

The first seeding simulations were not so encouraging in this respect, as they provided a value of the crystal-fluid interfacial free energy, γ, for the Lennard-Jones system of 0.30 ϵ/σ^2[38], that does not quite agree with values ranging from 0.35 to 0.37 ϵ/σ^2 obtained in direct calculations[47–50] (where ϵ and σ are the energy and length scales of the Lennard-Jones system respectively). Later on, the seeding method was used to estimate the nucleation rate of chlatrates[39], but the results were not compared against rigorous calculations. We have used the seeding technique to investigate homogeneous ice nucleation and realised that an extrapolation of our results for the mW model to high supercooling gives reasonable, although not entirely satisfactory, results[42]. We have also

recently studied NaCl[43], for which seeding seems to work particularly well. Very recently, the seeding technique has been even applied to crystal nucleation from solution[44] but, again, a quantitative comparison with rigorous techniques has not been performed. In summary, the ability of the seeding method to quantitatively predict crystal nucleation rates still remains unclear.

In this work we assess the validity of the seeding approach by comparing the nucleation rate and the interfacial free energy obtained by seeding to those calculated using more rigorous methods. We use four different models for that purpose: mW water, Tosi-Fumi NaCl, Lennard Jones and Hard Spheres. We conclude that the seeding method is successful in all cases within the accuracy of the calculations.

5.3. Models and Simulation Details

We use four different models to test the ability of the seeding technique to predict nucleation rates.

One is the mW water model[51]. All simulations for this model are performed at 1 bar. The melting temperature of the mW model at 1 bar is 274.6 K[51]. We use the LAMMPS package[52] to perform Molecular Dynamics simulations of mW water. Further details on our simulations of this system can be found in Ref.[42]. Although we have already reported seeding results for the mW model in Ref.[42] here we revisit and refine our previous calculations (see Discussion below).

We also study the truncated and shifted Lennard-Jones (LJ) potential in the form proposed by Broughton and Gilmer[53]. The depth of the interaction potential, ϵ, and the distance at which the interaction potential is zero, σ, are used as energy and distance units respectively. All simulations are performed at pressure -0.02 ϵ/σ^3, for which the melting temperature is $T = 0{,}617\epsilon/k_B$[47]. We use the GROMACS[54] implementation for Ar to simulate the LJ system, with $\sigma = 3{,}405$ Å , $\epsilon = 0{,}997 KJ/mol$ and atomic mass of $6.69{\cdot}10^{-26}$kg. The time unit for the LJ system is defined as $\tau = ((m\sigma^2)/(\epsilon))^{1/2}$. Pair interactions are truncated at 8.5 Å.

Moreover, we investigate the hard spheres (HS) model. For practical reasons we use the continuous version of the HS potential proposed in Ref.[55]. This potential has been shown to closely reproduce the equation of state[55], dynamics[55], phase diagram[56] and crystal-fluid interfacial free energy[48] of pure HS. In this work we show that the continuous model also reproduces the nucleation rate of pure HS. We use the same simulation details as in Refs.[48,56]. To report quantities pertaining to this system we use the particle diameter, σ, as unit of length and as unit of time $6D_l/\sigma^2$, where D_l is the self diffusion coefficient of the fluid. Pair interactions are truncated at 1.175 σ.

Finally, we also discuss for completeness the case of crystallization of the Tosi-Fumi (T-F) model[57,58] of NaCl at 1 bar, results we recently published in Ref.[43 57,58]. For this

model, the melting temperature at 1 bar is 1082 K[59]. Further details on the simulations of this system are given in Ref.[43]. We use Particle Mesh Ewald Summations[60] to deal with electrostatic interactions. The cut-off radious for dispersive interactions and for the real part of electrostatic interactions is 14 Å.

In the Molecular Dynamics simulations carried out in GROMACS (for the LJ, NaCl and (pseudo)HS systems) pressure is kept constant using an isotropic Parrinello-Rahman barostat[61] with a relaxation time of 0.5 ps. To fix the temperature we employ a velocity-rescale thermostat[62] with a relaxation time of 0.5 ps. The time step for the Verlet integration of the equations of motion is 2 fs in all cases. In the simulations for the mW model, carried out with the LAMMPS package, temperature is kept constant with the Nose-Hoover thermostat[63] and pressure with the Nose-Hoover barostat[64], implemented as described in Ref.[65]. The relaxation time for both the thermostat and the barostat is 0.5 ps. The time step for the integration of the equations of motion is 5 fs.

5.4. The seeding method

According to CNT, the appearance of a crystal cluster in a metastable fluid entails a Gibbs free energy change, ΔG given by:

$$\Delta G(N) = -N|\Delta\mu| + \gamma A \tag{5.1}$$

where N is the number of particles in the crystal cluster, $|\Delta\mu|$ is the chemical potential difference between the fluid and the crystal, A is the area of the cluster's surface, and γ is the crystal-fluid interfacial free energy. The two competing terms in the expression above give rise to a free energy barrier whose top corresponds to a cluster of critical size N_c. By maximizing Eq. 10.4 with respect to N one gets the height of the free energy barrier,

$$\Delta G_c = N_c|\Delta\mu|/2 \tag{5.2}$$

and, assuming a spherical cluster shape, a critical cluster size of:

$$N_c = \frac{32\pi\gamma^3}{3\rho_s^2|\Delta\mu|^3} \tag{5.3}$$

where ρ_s is the density of the solid cluster.

The number density of critical clusters is given by $\rho_f \exp[-\Delta G_c/(k_B T)]$ (where ρ_f is the density of the fluid). Such density, multiplied by a kinetic pre-factor, gives the following CNT expression for the nucleation rate, J:

$$J = \sqrt{\frac{|\Delta\mu|}{6\pi k_B T N_c}} f^+ \rho_f \exp[-\Delta G_c/(k_B T)]. \tag{5.4}$$

where f^+ is the attachment rate of particles to the critical cluster.

By inserting Eq. 5.2 in Eq. 5.4, it becomes evident that the four factors needed to obtain an estimate of J at a certain T are N_c, ρ_f, $|\Delta\mu|$ and f^+.

The evaluation of N_c is what gives the name "seeding" to the technique. It consists in inserting a cluster of a given shape with a given structure in the supercooled fluid. The way this configuration is prepared is described in detail in Ref.[43]. Starting from such configuration we monitor the number of particles in the cluster for different temperatures. If the temperature is higher than that that makes the inserted cluster critical, the cluster will melt, and viceversa. In such way one can identify the temperature T_c for which the inserted cluster is critical as that enclosed between the highest temperature at which the cluster grows and the lowest at which it melts. We have used this method to determine the critical size of ice[41,42] and NaCl clusters[43]. In Section 5.5 we show an example of the determination of a critical cluster size and discuss the way we determine the number of particles belonging to the crystal cluster. The latter is a crucial point in the seeding technique given that N_c directly affects the calculation of both the nucleation rate and the interfacial free energy.

In this work we consider spherical clusters with the structure of the equilibrium crystal phase for all investigated systems. In previous work we considered the possibility that clusters of NaCl and cubic ice (both structures with cubic unit cells) have a cubic shape, but we concluded that they are better represented by a sphere[43,66] (of course, the surface of the cluster is not smooth but is roughened by capillary fluctuations intrinsic to the crystal-fluid interface[67,68]). In what follows we show that spherical clusters do indeed a good job in the prediction of crystal nucleation rates for water, Lennard-Jones, NaCl and HS.

The density of the fluid ρ_f is trivially calculated from an ensemble average in an NpT simulation at the temperature at which the cluster is found to be critical. $|\Delta\mu|$ can be computed either by direct calculations of the chemical potential of the fluid and crystal phases like in Ref.[66], or by thermodynamic integration from the melting temperature as described in Ref.[42].

To obtain f^+ we follow the expression proposed by Auer and Frenkel[18,69]:

$$f^+ = \frac{< (N(t) - N_c)^2 >}{2t} \tag{5.5}$$

Computing f^+ requires monitoring the number of particles in the cluster, N, for several trajectories launched at the temperature at which the cluster is critical. We show this type of trajectories for NaCl and water in Refs.[43] and[41,42] respectively.

After having calculated N_c, ρ_f, $|\Delta\mu|$ and f^+, a value of J is derived from Eq. 5.4. This procedure is repeated for 3 or 4 different cluster sizes typically ranging from $\sim 10^3$ to $\sim 10^4$ molecules. In such way we have 3-4 (J,T) points at low supercoolings where the calculations with rigorous rare event techniques would be too demanding.

Once the nucleation rate is obtained for a few points, one can try to fit them with a CNT expression in order to get a $J(T)$ curve that can be extrapolated outside the temperature range where the seeding calculations were performed. This entails obtaining N_c, ρ_f, $|\Delta\mu|$ and f^+ as a function of temperature.

Directly fitting the obtained N_c's as a function of temperature is not a good choice because the critical size sharply drops in a non-linear fashion as the temperature decreases, so it is not possible to describe $N_c(T)$ with only 3 or 4 points. Instead, we use Eq. 5.3 to obtain γ for each simulated cluster. By contrast to $N_c(T)$, we find that $\gamma(T)$ is a smooth function (linear for both NaCl and water[41–43]). Once $\gamma(T)$ is known, we obtain $N_c(T)$ via Eq. 5.3.

In order to obtain $\rho_f(T)$ we simply perform NpT simulations of the fluid at several temperatures and fit the average density as a function of temperature to the simplest possible functional form (typically a second order polynomial function suffices). Regarding $|\Delta\mu|(T)$, it can be obtained in a straightforward manner by integrating the enthalpy difference between the crystal and the fluid from the melting temperature as shown in Ref.[42].

Finally, to obtain $f^+(T)$, we use the following CNT expression for f^+:

$$f^+(T) = \frac{24D(T)[N_c(T)]^{2/3}}{\lambda^2} \tag{5.6}$$

where D is the diffusion coefficient of the liquid and λ is the distance travelled by particles in the vicinity of the cluster to attach to the cluster's surface. $D(T)$ is obtained by fitting the diffussion coefficient of the fluid obtained in NpT Molecular Dynamics simulations at several temperatures. $N_c(T)$ is obtained through $\gamma(T)$ as explained in the previous paragraphs. For a given temperature, λ is obtained by equating Eq. 5.6 to the value of f^+ obtained via Eq. 5.5. As shown in Tables 8.1, 5.2, and 5.3 the value of λ thus calculated does not change much with temperature and takes values of the order of the molecular diameter. To obtain $f^+(T)$ via Eq. 5.6 we use λ averaged over all studied temperatures for a given model.

With N_c, ρ_f, $|\Delta\mu|$ and f^+ as a function of temperature we obtain $J(T)$ via Eq. 5.4. For the HS system it is not the temperature, but the pressure, that controls the freezing transition. Therefore, the same procedure is followed using pressure instead of temperature as independent variable.

5.5. Number of particles in the cluster

To determine the critical cluster size we look for the temperature that makes a given cluster size critical. In Fig. 5.1 we show the trajectories that are used to determine the temperature at which an ice cluster of 3202 mW molecules is critical. In view of

the trajectories shown in Fig. 5.1 we conclude that the inserted cluster is critical at a temperature $T_c = 252{,}5 \pm 2{,}5K$.

In order to monitor the number of particles in the crystal cluster we need to label particles as liquid or solid-like. This is done by evaluating for each particle a function (order parameter) sensitive to the degree of local order[17,70]. The threshold in the order parameter for labelling a particle either as liquid or as solid is chosen in such way that the probability of mislabelling particles in the bulk liquid as solid-like is the same as that of mislabelling particles in the bulk solid as liquid-like. The chosen order parameter is that that gives the lowest mislabelling probability.

To illustrate this procedure we follow on with the example of mW water. In Fig. 5.2 (a) we show ($\bar{q}_4$,$\bar{q}_6$) points for molecules in the bulk ice-Ih and liquid phases at T=254 K. For the calculation of the $\bar{q}_i$ order parameter we follow Ref.[70]. As it is evident from Fig. 5.2 (a), the $\bar{q}_6$ order parameter is able to discriminate between liquid and solid molecules whereas the $\bar{q}_4$ is not. In Fig. 5.2 (b) we plot the percentage of mislabelled bulk particles as a function of the threshold chosen for the $\bar{q}_6$ order parameter, $\bar{q}_{6,t}$. The crossing point between the mislabelling curves of the liquid and solid phases gives the optimal value for $\bar{q}_{6,t}$ at T=254 K. The optimal threshold smoothly changes with temperature, as shown in Fig. 5.2 (c). This means that, in principle, one should use a different $\bar{q}_{6,t}$ for each temperature. This is the procedure we follow for the mW model. For the LJ (HS) model $\bar{q}_{6,t}$ smoothly varies with temperature (pressure) and we have simply used the average $\bar{q}_{6,t}$ in the range of studied temperatures (pressures). The thresholds used for the LJ and HS models are $\bar{q}_{6,t} = 0{,}362$ and $\bar{q}_{6,t} = 0{,}372$ respectively. For the T-F NaCl model we use the order parameter described in Ref.[20] to distinguish liquid from solid-like particles.

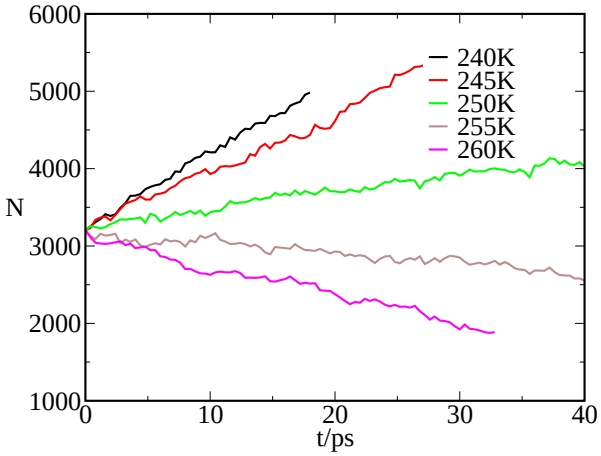

Figure 5.1: Number of particles in the cluster versus time for mW water at several temperatures (see legend) and 1 bar starting from a configuration with a cluster containing 3202 molecules.

5.6. Nucleation rate

In tables 8.1, 5.2, and 5.3 we report all variables leading to the calculation of the nucleation rate for mW water, LJ and HS respectively. With ΔT_c we refer to the supercooling corresponding to a given cluster, where the supercooling is defined as the difference between the melting temperature and the temperature of interest. For HS and LJ we report $|\Delta\mu|$ in k_BT per particle. We also report the total number of particles in the simulation box, N_T. The values for T-F NaCl are reported in Ref.[43].

N_c	N_T	$\Delta T_c/K$	$\lvert\Delta\mu\rvert/(kcal/mol)$	$\rho_f/(g/cm^3)$	$\gamma/(mJ/m^2)$	$(f^+/10^{14})/(s^{-1})$	λ/Å	$\Delta G_c/(k_BT)$	$\log_{10}(Jm^3s)$
688	22956	34.6	0.155	1.0040	30.4	0.7	2.51	112	-9
1916	77585	24.6	0.112	1.0037	30.7	1.9	2.38	216	-54
3202	77585	22.1	0.101	1.0035	32.7	2.5	2.54	321	-99
7247	183994	17.1	0.0783	1.0033	33.0	4.9	2.52	555	-201

Table 5.1: Values of the variables leading to the calculation of J for mW water via the seeding technique. See main text for the meaning of each variable.

N_c	N_T	$T_c/(\epsilon/k_B)$	$\rho_f/(\sigma^{-3})$	$\lvert\Delta\mu\rvert/(k_BT)$	$\gamma/(\epsilon/\sigma^2)$	f^+/τ	λ/σ	$\Delta G_c/(k_BT)$	$\log_{10}(J\sigma^3\tau)$
585	31901	0.534	0.868	0.246	0.33	40	1.15	72	-32
3794	87665	0.572	0.851	0.127	0.342	512	0.73	242	-106
12672	275758	0.587	0.843	0.084	0.348	650	1.00	533	-234

Table 5.2: Values of the variables leading to the calculation of J for LJ via the seeding technique. See main text for the meaning of each variable.

N_c	N_T	$p/((k_BT)/\sigma^3)$	$\lvert\Delta\mu\rvert/(k_BT)$	ϕ	$\gamma/(k_BT/\sigma^2)$	$f^+/(6D_l/\sigma^2)$	λ/σ	$\Delta G_c(k_BT)$	$\log_{10}[J/(6D_l/\sigma^5)]$
340	6819	14.5	0.285	0.518	0.658	1850	0.38	48	-19.5
547	23145	14.286	0.263	0.516	0.70	2110	0.36	70	-29
1075	23145	13.581	0.193	0.511	0.65	4294	0.31	104	-44
3814	107763	12.861	0.122	0.505	0.62	12397	0.28	232	-100
9066	202461	12.559	0.0914	0.502	0.61	39584	0.21	414	-178
39029	865074	12.220	0.0567	0.499	0.609	112120	0.20	1107	-479

Table 5.3: Values of the variables leading to the calculation of J for HS via the seeding technique. See main text for the meaning of each variable.

In Fig. 5.3 we show the decimal logarithm of the nucleation rate as a function of the supercooling for mW water, T-F NaCl and LJ, and as a function of the volume fraction occupied by spheres, $\phi = \pi/6\rho_f\sigma^3$, for HS. With symbols we show our seeding calculations (black circles) alongside calculations from other techniques as indicated in the legend. The seeding technique enables the estimation of the nucleation rate at

lower supercooling than any other technique. The technique that requires the largest supercooling is obviously "brute force", where nucleation takes place in the course of a standard NpT Molecular Dynamics simulation. Also note that with the seeding technique one can estimate the rate in a wide range of orders of magnitude whereas more rigorous methods are restricted to a narrower window because they are more demanding from a computational point of view. However, the seeding is an approximate method and has to be validated it by comparing it against rigorous approaches. For the case of mW there is one point for which we can make this comparison: for a supercooling of 34.5 K seeding and US[24] are in good agreement, which is quite encouraging.

To further test the ability of the seeding scheme to predict nucleation rates we fit our data with a CNT expression (see Sec. 5.4) and extrapolate our results to high supercooling, where we have a wealth of data from rigorous simulations to compare to. Such fits are shown by red dashed lines in Fig. 5.3. In all four systems the agreement between the CNT fit and more rigorous calculations is very good. Within 4 orders of magnitude (which is roughly the uncertainty of the fit) the CNT fit to the seeding data agrees with the calculations by Russo et al.[24], Haji-Akbari et al.[32], Moore et al.[71] and Li et al.[?] for the mW water model; by Valeriani et al.[20] and Espinosa et al.[43] for the T-F NaCl model; by Auer and Frenkel[18], and Filion et al.[21] for HS; and with our own brute force calculations for LJ. A zoom of Fig. 5.3 in the region where we compare the CNT fit to other data is shown in Fig. 5.4. Notice in Fig. 5.4 that for the mW model at $\Delta T = 39{,}5$ K there are two conflicting literature data. Both have been obtained with the FFS technique and differ by more than 6 orders of magnitude[32?] . We are uncertain about the origin of this discrepancy, but the value obtained from seeding is closer to that of Li et al.

Table 5.4: Interfacial free energy extrapolated to the equilibrium coexistence conditions (planar interface) from seeding calculations.

Model	γ
mW water	35.5(2.5) mJ/m^2
T-F NaCl	105(5) mJ/m^2
LJ	0.36(1) ϵ/σ^2
HS	0.58(3) k_BT/σ^2

5.7. Interfacial Free Energy

Using Eq. 5.3 we can obtain the interfacial free energy for each inserted cluster. Our seeding results are shown as black dots in Fig 5.5 for the four studied models. By linearly fitting our data we can extrapolate γ to coexistence conditions, where we can

compare to direct calculations of γ for a flat interface by contrasted methods like capillary wave fluctuations (CF)[72], cleaving (CL)[73] or mold integration[48]. When performing such comparison one should take into account that direct calculations provide γ for specific crystal orientations, whereas the γ obtained from spherical clusters is an average for all crystal orientations. Nevertheless, both approaches should yield similar values, as is the case for all four systems investigated. In fact, the γ extrapolated at coexistence from the seeding data is consistent with direct calculations by Limmer and Chandler[74] for mW water; by Espinosa et al.[43] for T-F NaCl; by Davidchack and Laird[47], Espinosa et al.[48], Agioletti-Uberti et al.[49], Morris and Song[75] and Benjamin and Horbach[50] for LJ; and by Davidchack and Laird[76,77], Espinosa et al.[48], Benjamin and Horbach[78] and Hartel et al.[79] for HS. Note that for the sake of clarity we have not included in Fig. 5.5 all data available in the literature. In summary, the seeding method is able to yield good estimates of the crystal-fluid interfacial free energy at coexistence for all studied systems. We summarize the values of γ at coexistence from our seeding simulations in Table 5.4.

In Fig. 5.5 we also compare our seeding results with literature data for conditions of metastability (below the melting temperature for mW water, T-F NaCl, and LJ, or above the coexistence pressure for HS). The only direct calculations of γ at such conditions that do not rely on CNT are those of Limmer and Chandler for mW water[74]. Their data are in reasonable agreement with ours. The other data available depend on CNT and can only be directly compared to ours if the same criterion to measure the size of the crystal nucleus is employed. This is the case only for T-F NaCl, for which we have a good agreement with the US simulations by Valeriani et al.[20]. For mW water and for HS we have a reasonable agreement with Li et al.[?] and Auer and Frenkel[18], although, as already mentioned, in these cases any discrepancy could be due to differences in the criterion with which the size of the cluster is determined.

5.8. Discussion

The results presented in this paper for mW water are somewhat different from those reported in Ref.[42]. Here, we report a value for the ice-water interfacial free energy at coexistence of 35.5± 2.5 mN/m, whereas in Ref.[42] we reported 29.5± 2.5 mN/m. Moreover, here we show in Fig. 5.5 that γ decreases as the supercooling increases, by contrast to Ref.[42] where we reported that γ does not depend on temperature for the mW model. Consequently, the curves of J versus temperature reported here and in Ref.[42] are not the same. The main reason for the discrepancy with our previous work is that in Ref.[42] we used as starting configurations for the seeding study of mW those prepared for the TIP4P/2005 model. These models give similar densities for the fluid phase, but not quite for the solid phase. Therefore, in retrospect, borrowing configurations from

the TIP4P/2005 model to study mW water was not a good idea. Moreover, we used the same order parameter as that used for TIP4P/2005 to determine the number of particles in the cluster. In the revisited calculations we have tuned the order parameter specifically for the mW model as described in Section 5.5 of this paper. With these improvements our results for mW are more consistent than before: γ at coexistence coincides with that reported by Limmer and Chandler[74], the extrapolation of J to high supercooling is consistent with previous calculations (see Fig. 5.3) and γ decreases as the supercooling increases, as observed for other water models[42]. Our mistake in the mW calculations highlights the importance of adequately generating the initial configuration in the seeding framework. We describe in detail how to generate initial configurations for seeding studies in Ref.[43].

In Fig. 5.3 we show that a seeding approach to crystal nucleation is successful in describing the nucleation rate for four different systems. It was unexpected to us that a simple theory like CNT was able to predict so well the nucleation rate up to very deep supercooling. In this work our approach relies on the assumption that the critical clusters are spherical and have the structure of the equilibrium crystal phase, which is the simplest a priori description one can conceive for the nucleation mechanism. By using rare event techniques that do not impose any a priori mechanism a more complex scenario may emerge for the structure of the critical nucleus[13,14,37].

Although from our results it seems that the correct nucleation rate can be obtained considering only spherical clusters with the equilibrium solid structure, this does not exclude that there are other independent nucleation pathways contributing to the rate. However, if there are not many alternative pathways and these are not faster than the path imposed in the seeding scheme, their contribution to the global nucleation rate would be within the error of the seeding method.

In any case, the seeding approach can also be used to calculate the nucleation rate for clusters with shapes other than spherical and structures different from that of the equilibrium crystal. For instance, in Ref.[66] we compare the ice nucleation rate via clusters with Ih and Ic structures and find that both paths have the same rate. Therefore, one can use the seeding approach to study the competition between freezing pathways going through any a priori conceivable critical cluster.

It should be added that the seeding method does not give information about the way the critical cluster is formed. Therefore, two-step mechanisms for the formation of the critical cluster[80–88] can not be inferred from seeding, where a CNT-like growth pathway is implicity assumed. However, as long as the critical cluster structure is correctly guessed, one can use seeding to predict nucleation rates if sub-critical nuclei are in quasi-equilibrim with the fluid (the reversible work needed to go from the fluid to the fluid containing the critical cluster does not depend of the specific pathway by which such cluster is formed).

It is fair to mention again that our CNT fit captures virtually all literature data

within an error bar of four orders of magnitude. This may seem a large uncertainty but there are two considerations warranted in this respect. One is that discrepancies of 3 orders of magnitude can be found for the calculation of the nucleation rate via several more rigorous rare event techniques[21]. And the other is that we are estimating the nucleation rate in a range of hundreds of orders of magnitude, which is way larger than the afore mentioned uncertainty. Due to their computational cost, rigorous rare event techniques typically provide results in a range limited to tens of orders of magnitude.

Another aspect worth discussing is that it is in principle safer to apply the seeding technique to large clusters for two reasons. One is that a macroscopic theory like CNT is expected to work better in the limit of large clusters. Another is that the relative error in the number of particles in the cluster, N, decreases as the cluster size increases. This is because the determination of N relies on order parameters trained to identify bulk particles. Therefore, if there were a mistake in determining N it would be mainly due to a wrong labelling of surface particles. As the fraction of surface particles goes as $N^{-1/3}$, it is more convenient to use large clusters. Nonetheless, we have obtained reasonable nucleation rates using the seeding method for a cluster as small as ~ 300 particles in the HS system. In any case, from our experience we recommend to use the seeding technique for large N_c (> 600 particles) and extrapolate the results to high supercooling with a CNT fit. With this procedure we have obtained nucleation rates consistent with the literature for the four models studied in this work.

5.9. Conclusions

These are the main conclusions we draw from our study of crystal nucleation via the seeding technique:

i) Using the seeding method the nucleation rate can be computed at lower supercooling than with rigorous rare event techniques.

ii) A fit to the seeding data based on Classical Nucleation Theory successfully compares to the data obtained at high supercooling with rigorous rare event methods. Such fit provides a reasonable estimate of the nucleation rate in a range of hundreds of orders of magnitude.

iii) The extrapolation the crystal-fluid interfacial free energy obtained from seeding to coexistence conditions is consistent with direct calculations of such quantity for all systems investigated.

iv) These results suggest that, to a good approximation, one can describe crystal nucleation for the systems here investigated in the simplest way: the nucleation of a spherical critical cluster with the structure of the stable crystal.

Acknowledgements

This work was funded by grants FIS2013/43209-P of the MEC, and by the Marie

Curie Career Integration Grant 322326-COSAAC-FP7-PEOPLE-2012-CIG. C.Valeriani and E. Sanz acknowledge financial support from a Ramon y Cajal Fellowship. J. R. Espinosa acknowledges financial support from the FPI grant BES-2014-067625. Calculations were carried out in the supercomputer facility Tirant from the Spanish Supercomputing Network (RES) (project QCM-2015-1-0028).

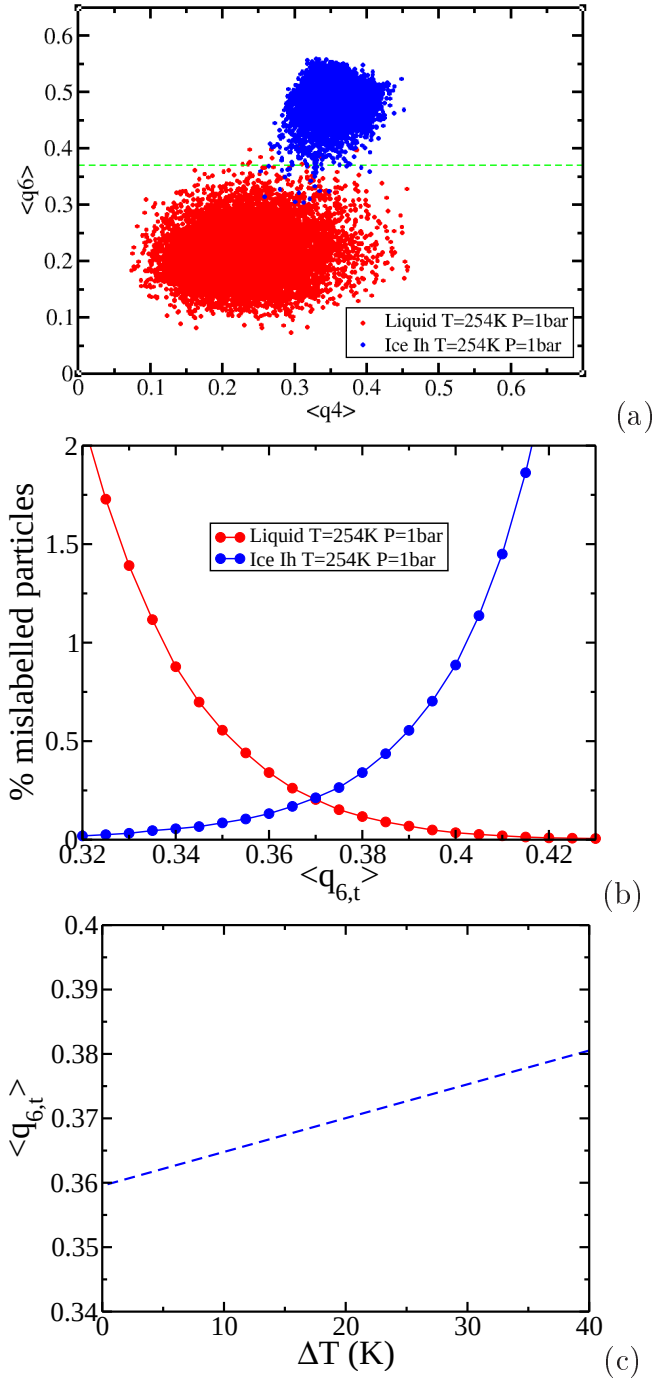

Figure 5.2: Procedure to distinguish liquid from solid-like molecules for mW water. (a) $\bar{q}_6$ versus $\bar{q}_4$ for 10000 liquid (red) and 10000 ice-Ih (blue) bulk molecules at 254 K. (b) Percentage of mislabelled bulk particles for each phase as a function of $\bar{q}_{6,t}$ at 254 K. (c) Dependence of the optimal $\bar{q}_{6,t}$ on the supercooling.

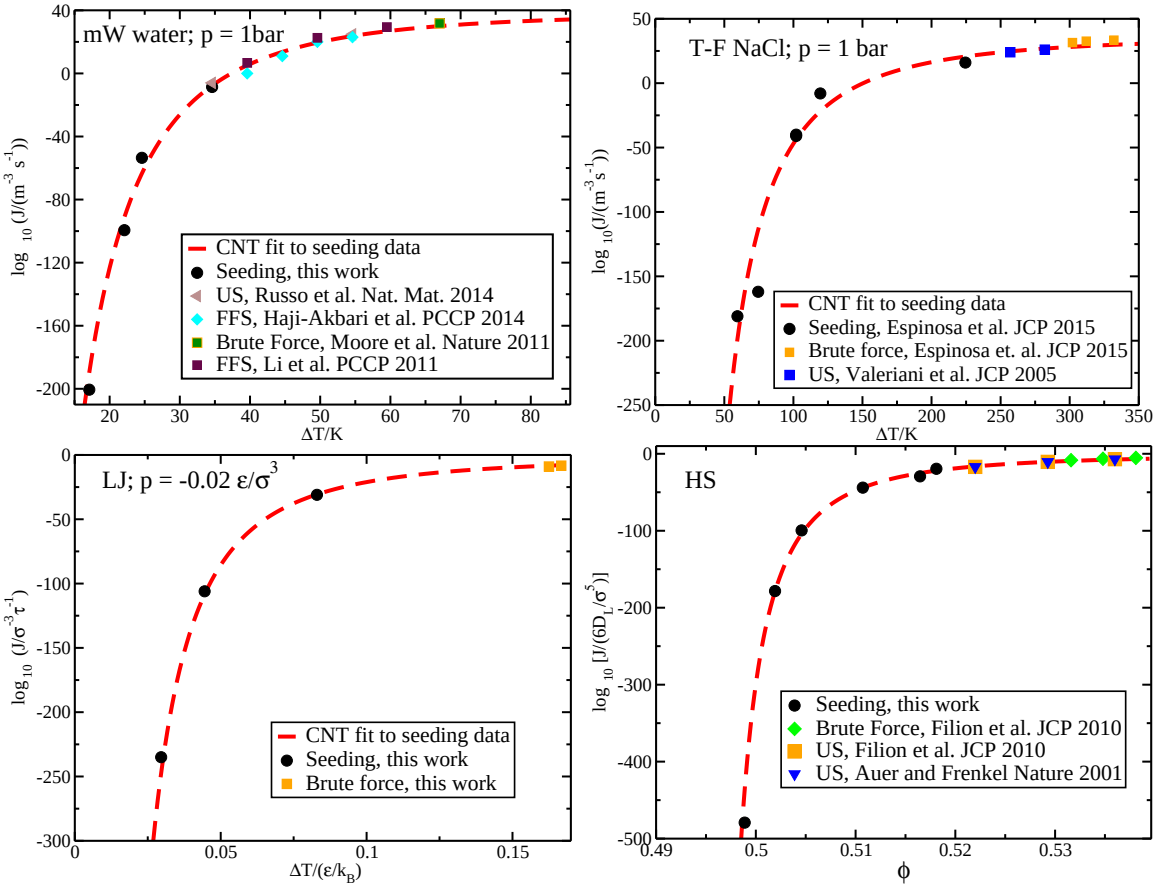

Figure 5.3: Top-left, top-right and bottom-left: logarithm of the nucleation rate as a function of the supercooling for the mW water model, the T-F NaCl model and the LJ model respectively. Bottom-right: logarithm of the nucleation rate as a function of the volume fraction of the parent fluid phase for the HS model. Symbols and curves as indicated in the legend.

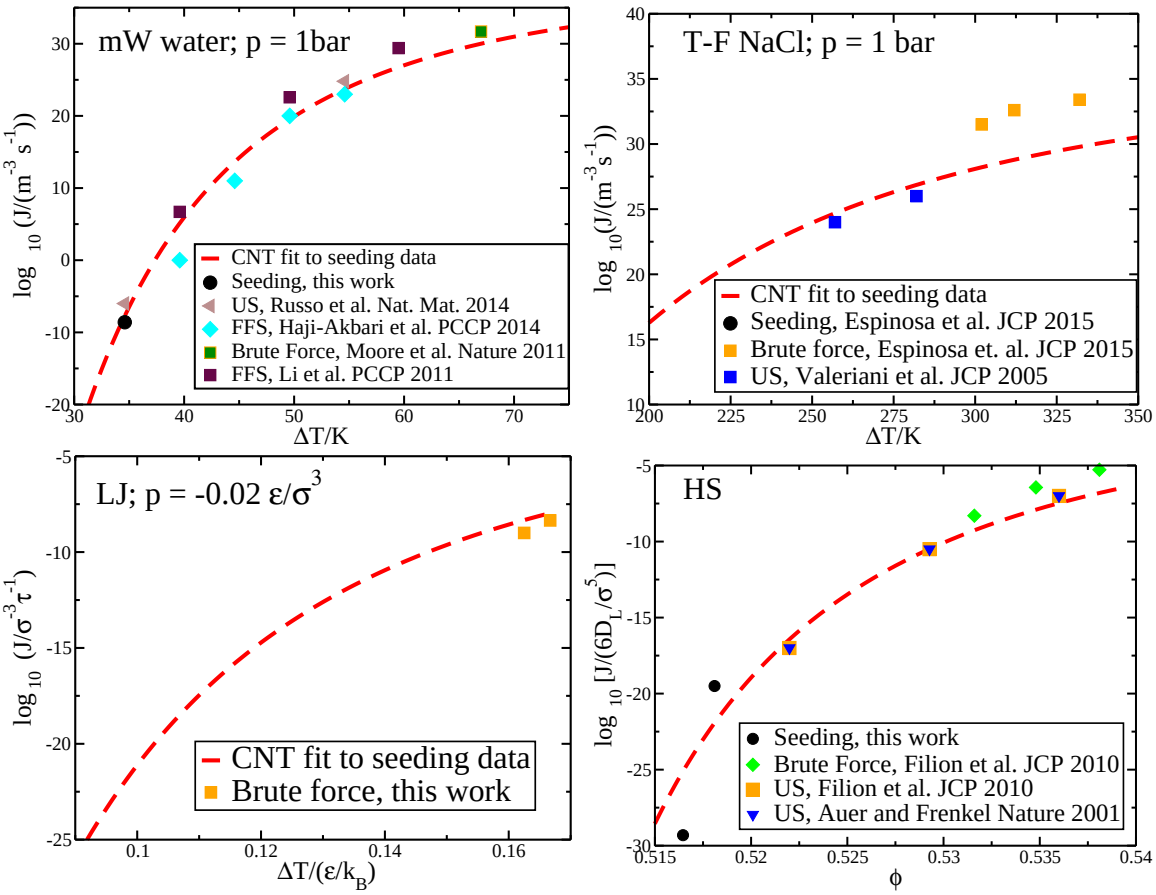

Figure 5.4: Zoom of the plots shown in Fig. 5.3 for the region where a comparison is established with literature data and our own brute force simulations for the LJ system.

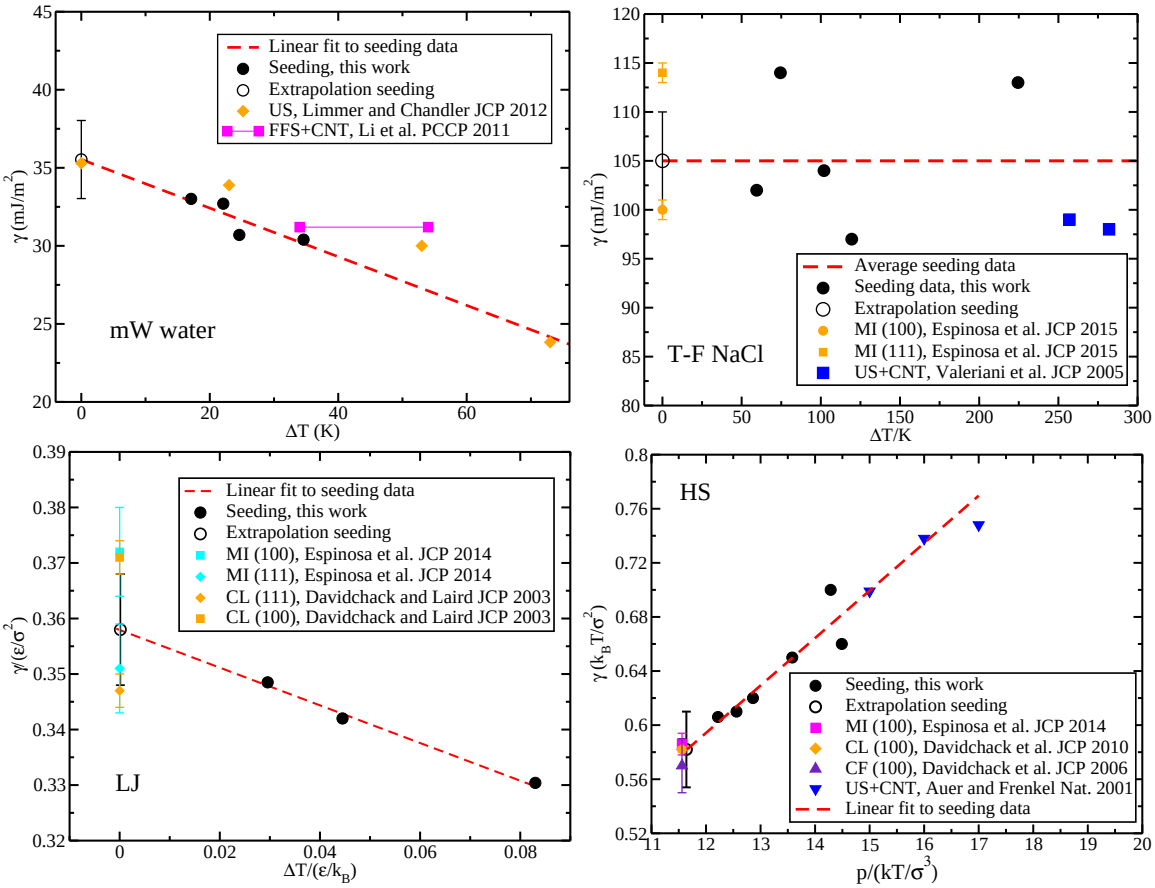

Figure 5.5: Crystal-melt interfacial free energy as a function of the supercooling/pressure. Top left, mW water model; top right, T-F NaCl model; bottom left, LJ model; bottom right, HS model. Symbols and dashed lines as indicated in the legend.

Bibliography

1. Kelton, K. F., *Crystal Nucleation in Liquids and Glasses* (Academic, Boston, 1991).

2. Buckle, E. R., Studies on the freezing of pure liquids. II. The kinetics of homogeneous nucleation in supercooled liquids. *Proceedings of the Royal Society of London. Series A. Mathematical and Physical Sciences* **261**, 189–196 (1961).

3. Pruppacher, H. R., A new look at homogeneous ice nucleation in supercooled water drops. *J. Atmosph. Sci.* **52**, 1924 (1995).

4. Murray, B. J., Broadley, S. L., Wilson, T. W., Bull, S. J., Wills, R. H., Christenson, H. K. & Murray, E. J., Kinetics of the homogeneous freezing of water. *Phys. Chem. Chem. Phys.* **12**, 10380 (2010).

5. Manka, A., Pathak, H., Tanimura, S., Wolk, J., Strey, R. & Wyslouzil, B. E., Freezing water in no man's land. *Phys. Chem. Chem. Phys.* **14**, 4505–4516 (2012).

6. Laksmono, H., McQueen, T. A., Sellberg, J. A., Loh, N. D., Huang, C., Schlesinger, D., Sierra, R. G., Hampton, C. Y., Nordlund, D., Beye, M., Martin, A. V., Barty, A., Seibert, M. M., Messerschmidt, M., Williams, G. J., Boutet, S., Amann-Winkel, K., Loerting, T., Pettersson, L. G. M., Bogan, M. J. & Nilsson, A., Anomalous behavior of the homogeneous ice nucleation rate in no-man's land. *The Journal of Physical Chemistry Letters* **6**, 2826–2832 (2015).

7. Ickes, L., Welti, A., Hoose, C. & Lohmann, U., Classical nucleation theory of homogeneous freezing of water: thermodynamic and kinetic parameters. *Phys. Chem. Chem. Phys.* **17**, 5514–5537 (2015).

8. Pusey, P. N. & van Megen, W., Phase behaviour of concentrated suspensions of nearly hard colloidal spheres. *Nature* **320**, 340 (1986).

9. Gasser, U., Weeks, E. R., Schofield, A., Pusey, P. N. & Weitz, D. A., Real-space imaging of nucleation and growth in colloidal crystallization. *Science* **292**, 258 (2001).

10. Glotzer, S. C. & Solomon, M. J., Anisotropy of building blocks and their assembly into complex structures. *Nat. Mat.* **6**, 557–562 (2007).

11. Harland, J. L. & van Megen, W., Crystallization kinetics of suspensions of hard colloidal spheres. *Phys. Rev. E* **55**, 3054 (1997).

12. van Duijneveldt, J. S. & Frenkel, D., Computer simulation study of free energy barriers in crystal nucleation. *J. Chem. Phys.* **96**, 4655 (1992).

13. ten Wolde, P. R., Ruiz-Montero, M. J. & Frenkel, D., Numerical evidence for bcc ordering at the surface of a critical fcc nucleus. *Phys. Rev. Lett.* **75**, 2714 (1995).

14. Moroni, D., ten Wolde, P. R. & Bolhuis, P. G., Interplay between structure and size in a critical crystal nucleus. *Phys. Rev. Lett.* **94**, 235703 (2005).

15. Torrie, G. & Valleau, J., Nonphysical sampling distributions in Monte Carlo free-energy estimation: Umbrella sampling. *Journal of Computational Physics* **23**, 187–199 (1977).

16. van Duijneveld, J. S. & Frenkel, D., Computer simulation study of free energy barriers in crystal nucleation. *J. Chem. Phys.* **96**, 4655 (1992).

17. ten Wolde, P. R., Ruiz-Montero, M. J. & Frenkel, D., Numerical calculation of the rate of crystal nucleation in a Lennard-Jones system at moderate undercooling. *J. Chem. Phys.* **104**, 9932 (1996).

18. Auer, S. & Frenkel, D., Prediction of absolute crystal-nucleation rate in hard-sphere colloids. *Nature* **409**, 1020 (2001).

19. Radhakrishnan, R. & Trout, B. L., Nucleation of hexagonal ice (Ih) in liquid water. *J. Am. Chem. Soc.* **125**, 7743 (2003).

20. Valeriani, C., Sanz, E. & Frenkel, D., Rate of homogeneous crystal nucleation in molten NaCl. *J. Chem. Phys.* **122**, 194501 (2005).

21. Filion, L., Hermes, M., Ni, R. & Dijkstra, M., Crystal nucleation of hard spheres using molecular dynamics, umbrella sampling, and forward flux sampling: A comparison of simulation techniques. *J. Chem. Phys.* **133**, 244115 (2010).

22. Cuetos, A. & Dijkstra, M., Kinetic pathways for the isotropic-nematic phase transition in a system of colloidal hard rods: A simulation study. *Phys. Rev. Lett.* **98**, 095701 (2007).

23. Reinhardt, A. & Doye, J. P. K., Free energy landscapes for homogeneous nucleation of ice for a monatomic water model. *J. Chem. Phys.* **136**, 054501 (2012).

24. Russo, J., Romano, F. & Tanaka, H., New metastable form of ice and its role in the homogeneous crystallization of water. *Nature Materials* **13**, 733 (2014).

25. Saika-Voivod, I., Romano, F. & Sciortino, F., Nucleation barriers in tetrahedral liquids spanning glassy and crystallizing regimes. *J. Chem. Phys.* **135**, 124506 (2011).

26. Buhariwalla, C., Bowles, R., Saika-Voivod, I., Sciortino, F. & Poole, P., Free energy of formation of small ice nuclei near the widom line in simulations of supercooled water. *Eur. Phys. J. E.* **38**, 39 (2015).

27. Brukhno, A. V., Anwar, J., Davidchack, R. & Handel, R., Challenges in molecular simulation of homogeneous ice nucleation. *Journal of Physics: Condensed Matter* **20**, 494243 (2008).

28. Geiger, P. & Dellago, C., Neural networks for local structure detection in polymorphic systems. *J. Chem. Phys.* **139**, 164105 (2013).

29. Haji-Akbari, A., DeFever, R. S., Sarupria, S. & Debenedetti, P. G., Suppression of sub-surface freezing in free-standing thin films of a coarse-grained model of water. *Phys. Chem. Chem. Phys.* **16**, 25916–25927 (2014).

30. Allen, R. J., Warren, P. B. & ten Wolde, P. R., Sampling rare switching events in biochemical networks. *Phys. Rev. Lett.* **94**, 018104 (2005).

31. Sanz, E., Valeriani, C., Frenkel, D. & Dijkstra, M., Evidence for out-of-equilibrium crystal nucleation in suspensions of oppositely charged colloids. *Phys. Rev. Lett.* **99**, 055501 (2007).

32. Haji-Akbari, A. & Debenedetti, P. G., Direct calculation of ice homogeneous nucleation rate for a molecular model of water. *Proceedings of the National Academy of Sciences* **112**, 10582–10588 (2015).

33. Li, T., Donadio, D., Russo, G. & Galli, G., Homogeneous ice nucleation from supercooled water. *Phys. Chem. Chem. Phys.* **13**, 19807–19813 (2011).

34. Laio, A. & Parrinello, M., Escaping free-energy minima. *Proc. Natl. Acad. Sci.* **99**, 12562 (2002).

35. Trudu, F., Donadio, D. & Parrinello, M., Freezing of a Lennard-Jones fluid: From nucleation to spinodal regime. *Phys. Rev. Lett.* **97**, 105701 (2006).

36. Bolhuis, P. G., Chandler, D., Dellago, C. & Geissler, P. L., Transition path sampling: Throwing ropes over rough mountain passes, in the dark. *Ann. Rev. Physical Chem.* **53**, 291 (2002).

37. Lechner, W., Dellago, C. & Bolhuis, P. G., Role of the prestructured surface cloud in crystal nucleation. *Phys. Rev. Lett.* **106**, 085701 (2011).

38. Bai, X.-M. & Li, M., Calculation of solid-liquid interfacial free energy: A classical nucleation theory based approach. *J. Chem. Phys.* **124**, 124707 (2006).

39. Knott, B. C., Molinero, V., Doherty, M. F. & Peters, B., Homogeneous nucleation of methane hydrates: Unrealistic under realistic conditions. *J. Am. Chem. Soc.* **134**, 19544–19547 (2012).

40. Pereyra, R. G., Szleifer, I. & Carignano, M. A., Temperature dependence of ice critical nucleus size. *J. Chem. Phys.* **135**, 034508 (2011).

41. Sanz, E., Vega, C., Espinosa, J. R., Caballero-Bernal, R., Abascal, J. L. F. & Valeriani, C., Homogeneous ice nucleation at moderate supercooling from molecular simulation. *Journal of the American Chemical Society* **135**, 15008–15017 (2013).

42. Espinosa, J. R., Sanz, E., Valeriani, C. & Vega, C., Homogeneous ice nucleation evaluated for several water models. *J. Chem. Phys.* **141**, 18C529 (2014).

43. Espinosa, J. R., Vega, C., Valeriani, C. & Sanz, E., The crystal-fluid interfacial free energy and nucleation rate of NaCl from different simulation methods. *J. Chem. Phys.* **142**, 194709 (2015).

44. Zimmermann, N. E. R., Vorselaars, B., Quigley, D. & Peters, B., Nucleation of NaCl from aqueous solution: Critical sizes, ion-attachment kinetics, and rates. *Journal of the American Chemical Society* **137**, 13352–13361 (2015).

45. Volmer, M. & Weber, A., Keimbildung in ubersattigten gebilden. *Z. Phys. Chem.* **119**, 277 (1926).

46. Becker, R. & Doring, W., Kinetische behandlung der keimbildung in ubersattigten dampfen. *Ann. Phys.* **416**, 719–752 (1935).

47. Davidchack, R. L. & Laird, B. B., Direct calculation of the crystal–melt interfacial free energies for continuous potentials: Application to the Lennard-Jones system. *J. Chem. Phys.* **118**, 7651–7657 (2003).

48. Espinosa, J. R., Vega, C. & Sanz, E., The mold integration method for the calculation of the crystal-fluid interfacial free energy from simulations. *J Chem. Phys.* **141**, 134709 (2014).

49. Angioletti-Uberti, S., Ceriotti, M., Lee, P. D. & Finnis, M. W., Solid-liquid interface free energy through metadynamics simulations. *Phys. Rev. B* **81**, 125416 (2010).

50. Benjamin, R. & Horbach, J., Crystal-liquid interfacial free energy via thermodynamic integration. *The Journal of Chemical Physics* **141**, 044715 (2014).

51. V. Molinero, and E. B. Moore, Water modeled as an intermediate element between carbon and silicon. *The Journal of Physical Chemistry B* **113**, 4008–4016 (2009).

52. Plimpton, S. *J. Comput. Phys.* **117**, 1 (1995).

53. Broughton, J. & Gilmer, G., Surface free energy and stress of a Lennard-Jones crystal. *Acta Metallurgica* **31**, 845 – 851 (1983).

54. Lindahl, E., Hess, B. & van der Spoel, D., Gromacs 3.0: a package for molecular simulation and trajectory analysis. *J. Mol. Model.* **7**, 306 (2001).

55. Jover, J., Haslam, A. J., Galindo, A., Jackson, G. & Muller, E. A., Pseudo hard-sphere potential for use in continuous molecular-dynamics simulation of spherical and chain molecules. *The Journal of Chemical Physics* **137**, 144505 (2012).

56. Espinosa, J. R., Sanz, E., Valeriani, C. & Vega, C., On fluid-solid direct coexistence simulations: The pseudo-hard sphere model. *The Journal of Chemical Physics* **139**, 144502 (2013).

57. Fumi, F. & Tosi, M., Ionic sizes and born repulsive parameters in the NaCl-type alkali halides I. *Journal of Physics and Chemistry of Solids* **25**, 31–43 (1964).

58. Tosi, M. & Fumi, F., Ionic sizes and born repulsive parameters in the NaCl-type alkali halides II. *Journal of Physics and Chemistry of Solids* **25**, 45–52 (1964).

59. Aragones, J. L., Sanz, E., Valeriani, C. & Vega, C., Calculation of the melting point of alkali halides by means of computer simulations. *J. Chem. Phys.* **137**, 104507 (2012).

60. Wheeler, D. R. & Newman, J., A less expensive ewald lattice sum. *Chem. Phys. Lett.* **366**, 537 (2002).

61. Parrinello, M. & Rahman, A., Polymorphic transitions in single crystals: A new Molecular Dynamics method. *J. App. Phys.* **52**, 7182–7190 (1981).

62. Bussi, G., Donadio, D. & Parrinello, M., Canonical sampling through velocity rescaling. *The Journal of Chemical Physics* **126**, 014101 (2007).

63. Hoover, W. G., Canonical dynamics: Equilibrium phase-space distributions **31**, 1695 (1985).

64. Hoover, W. G., Constant-pressure equations of motion. *Phys. Rev. A* **34**, 2499–2500 (1986).

65. Melchionna, S., Ciccotti, G. & Holian, B. L., Hoover npt dynamics for systems varying in shape and size. *Molecular Physics* **78**, 533–544 (1993).

66. Zaragoza, A., Conde, M. M., Espinosa, J. R., Valeriani, C., Vega, C. & Sanz, E., Competition between ices ih and ic in homogeneous water freezing. *The Journal of Chemical Physics* **143**, 134504 (2015).

67. Benet, J., MacDowell, L. G. & Sanz, E., Computer simulation study of surface wave dynamics at the crystal-melt interface. *The Journal of Chemical Physics* **141**, 034701 (2014).

68. Benet, J., MacDowell, L. G. & Sanz, E., A study of the ice-water interface using the TIP4P/2005 water model. *Phys. Chem. Chem. Phys.* **16**, 22159–22166 (2014).

69. Auer, S. & Frenkel, D., Numerical prediction of absolute crystallization rates in hard-sphere colloids. *J. Phys.:Condens. Matter* **120**, 3015 (2004).

70. Lechner, W. & Dellago, C., Accurate determination of crystal structures based on averaged local bond order parameters. *J. Chem. Phys.* **129**, 114707 (2008).

71. Moore, E. B. & Molinero, V., Structural transformation in supercooled water controls the crystallization rate of ice. *Nature* **479**, 506–508 (2011).

72. Hoyt, J. J., Asta, M. & Karma, A., Method for computing the anisotropy of the solid-liquid interfacial free energy. *Phys. Rev. Lett.* **86**, 5530–5533 (2001).

73. Broughton, J. Q. & Gilmer, G. H., Molecular dynamics investigation of the crystal–fluid interface. VI. Excess surface free energies of crystal–liquid systems. *J. Chem. Phys.* **84**, 5759–5768 (1986).

74. Limmer, D. T. & Chandler, D., Phase diagram of supercooled water confined to hydrophilic nanopores. *The Journal of Chemical Physics* **137**, 044509 (2012).

75. Morris, J. R. & Song, X., The anisotropic free energy of the Lennard-Jones crystal-melt interface. *J. Chem. Phys.* **119**, 3920 (2003).

76. Davidchack, R. L., Morris, J. R. & Laird, B. B., The anisotropic hard-sphere crystal-melt interfacial free energy from fluctuations. *J. Chem. Phys.* **125**, 094710 (2006).

77. Davidchack, R. L., Hard spheres revisited: Accurate calculation of the solid–liquid interfacial free energy. *J. Chem. Phys.* **133**, 234701 (2010).

78. Benjamin, R. & Horbach, J., Crystal-liquid interfacial free energy of hard spheres via a thermodynamic integration scheme. *Phys. Rev. E* **91**, 032410 (2015).

79. Härtel, A., Oettel, M., Rozas, R. E., Egelhaaf, S. U., Horbach, J. & Löwen, H., Tension and stiffness of the hard sphere crystal-fluid interface. *Phys. Rev. Lett.* **108**, 226101 (2012).

80. ten Wolde, P. R. & Frenkel., D. .

81. OÂ¿Malley, B. & Snook, I., Structure of hard-sphere fluid and precursor structures to crystallization. *The Journal of Chemical Physics* **123**, 054511 (2005).

82. Schöpe, H. J., Bryant, G. & van Megen, W., Two-step crystallization kinetics in colloidal hard-sphere systems. *Phys. Rev. Lett.* **96**, 175701 (2006).

83. Kawasaki, T. & Tanaka, H., Formation of a crystal nucleus from liquid. *Proceedings of the National Academy of Sciences* **107**, 14036–14041 (2010).

84. Schilling, T., Schöpe, H. J., Oettel, M., Opletal, G. & Snook, I., Precursor-mediated crystallization process in suspensions of hard spheres. *Phys. Rev. Lett.* **105**, 025701 (2010).

85. Shen, Y. C. & Oxtoby, D. W., Nucleation of lennard-jones fluids: A density functional approach. *The Journal of Chemical Physics* **105**, 6517–6524 (1996).

86. Lutsko, J. F. & Nicolis, G., Theoretical evidence for a dense fluid precursor to crystallization. *Phys. Rev. Lett.* **96**, 046102 (2006).

87. Kawasaki, T. & Tanaka, H., Structural origin of dynamic heterogeneity in three-dimensional colloidal glass formers and its link to crystal nucleation. *Journal of Physics: Condensed Matter* **22**, 232102 (2010).

88. Russo, J. & Tanaka, H., The microscopic pathway to crystallization in supercooled liquids. *Scientific Reports* **2**, 505 (2012).

Results: Chapter 6

Ice-Water Interfacial Free Energy for the TIP4P, TIP4P/2005, TIP4P/Ice and mW Models as Obtained from the Mold Integration Technique

Jorge R. Espinosa, *Carlos Vega and Eduardo Sanz*

Departamento de Química Física, Facultad de Ciencias Químicas, Universidad Complutense de Madrid, 28040 Madrid, Spain.

6.1. Abstract

The freezing of water is greatly influenced by the ice-water interfacial free energy. Yet, no consistent experimental measures of this thermodynamic parameter can be found. In this work we provide estimates for the ice Ih-water interfacial free energy at the normal melting temperature for different crystal planes (basal, primary prismatic and secondary prismatic) using some widely used water models: TIP4P, TIP4P/2005, TIP4P/Ice and mW. To compute the interfacial free energy we use the Mold Integration method. It consists in calculating the work needed to induce the formation of a crystal slab in the fluid at coexistence conditions with the aid of a mold of potential energy wells whose structure is that of the crystal plane under study. The basal plane has the lowest interfacial free energy in all models of the TIP4P family. For the mW model we could not resolve differences in interfacial free energy between different orientations. The interfacial free energies averaged over all crystal orientations we obtain are 27.2(8), 28.9(8), 29.8(8) and 34.9(8) mJ/m^2 for the TIP4P, TIP4P/2005, TIP4P/Ice and mW models respectively. The averaged interfacial free energy increases with both

the melting temperature and melting enthalpy of the model. Moreover, we compute the interfacial free energy for several crystal orientation of ice Ic using the TIP4P/Ice model and obtain, within the accuracy of our calculations, the same orientationally averaged interfacial free energy as that of ice Ih. Our results are in good agreement with previous estimates of the interfacial free energy based on a Classical Nucleation Theory analysis of simulations of spherical ice seeds embedded in supercooled water.

6.2. Introduction

The crystal nucleation rate and the shape and speed with which crystals grow are greatly affected by the free energy cost of forming an interface between the emerging crystal and the surrounding fluid. Therefore, obtaining accurate values of the crystal-fluid interfacial free energy is of central importance[1]. Yet, there are no reliable experimental techniques to measure such thermodynamic parameter. For instance for the ice-water interface values ranging from 25 to 35 mJ/m^2 have been reported[2,3]. A precise value for the ice-water interfacial free energy, γ_{iw}, is needed, for instance, to interpret measurements of the ice nucleation rate[2–14], a property that plays an important role in atmospheric physics and climate change models[15–17].

In the absence of reliable experimental values, estimates of γ_{iw} can be obtained from simulations of realistic water models. The first direct calculation of γ_{iw} was performed using an improved version of the cleaving method[18,19] for the TIP4P model[20]. In Ref.[21], such calculations were improved by including full electrostatic interactions and, in addition, values for the TIP4P-Ew and TIP5P-E models were also reported. By employing a method based on the analysis of capillary fluctuations[22], γ_{iw} was recently computed for the TIP4P/2005[23] and mW water models[24]. With the exception of Ref.[24], all the calculations of γ_{iw} previously mentioned correspond to the flat ice-water interface at the normal melting temperature of the model. To the best of our knowledge these are the only direct calculations of γ_{iw}. Given that the same model has not been studied by different groups, more work is needed to reach a consensus on the value of γ_{iw} for the most popular water models.

With the aim of establishing definite values for γ_{iw} for some widely used water models we perform direct calculations of γ_{iw} using the Mold Integration (MI) method[25] for the TIP4P[26], TIP4P/2005[27], TIP4P/Ice[28] and mW[29] models. Our results can also be useful to validate the analysis of simulation studies of ice nucleation[30–36,36–46] using Classical Nucleation Theory[47–51]. These studies provide estimates of γ_{iw} for a curved ice-water interface at temperatures below melting. The validity of such estimates can be assessed by extrapolating the results to coexistence conditions and comparing with direct calculations of γ_{iw}. By contrast to the estimates based on nucleation studies, where a γ_{iw} averaged over all crystal orientations is obtained, the method employed in

this work allows for the calculation of γ_{iw} for specific crystal orientations. We compute γ_{iw} for hexagonal ice, ice Ih, and three different crystal planes exposed to the fluid: basal, primary prismatic (pI) and secondary prismatic (pII). We also evaluate γ_{iw} for the (111), (100) and (110) planes of ice Ic. The comparison between the interfacial free energies of cubic (ice Ic) and hexagonal (ice Ih) ice can shed light in the role of these stacking polymorphs in the initial stages of ice nucleation and growth[10,32,37,40,41,52–60].

6.3. Simulation details

To simulate the TIP4P family models we use Molecular Dynamics with the GROMACS package[61]. All runs are performed at constant pressure of 1 bar. Pressure is only exerted along the direction perpendicular to the interface whose growth is induced within the MI scheme. In our coordinate system this is the x direction, so all runs are performed in the Np_xT ensemble. To avoid stress, the L_y and L_z edges of the simulation box are fixed to a value consistent with the equilibrium unit cell at coexistence conditions. All simulations are run at the constant pressure of $p = 1$ bar, using an anisotropic Parrinello-Rahman barostat[62] with a relaxation time of 0.5 ps. To fix the temperature we employ a velocity-rescale thermostat[63] with a relaxation time of 0.5 ps. The time step for the Verlet integration of the equations of motion is 1.5 fs. We use Particle Mesh Ewald Summations[64] to deal with electrostatic interactions. The cut-off radius for both dispersive interactions and the real part of electrostatic interactions is 14 Å. The interaction between the mold and the water molecules is provided to GROMACS in a tabular form.

To simulate the mW model we use a bespoke Monte Carlo code. Monte Carlo runs are performed at 1 bar and in the Np_xT ensemble. The shifts for the trial displacements and volume moves are tuned during equilibration to get an acceptance rate of 35-45 per cent. A Monte Carlo sweep consists in a trial displacement move per particle plus a trial volume move.

6.4. Mold Integration method

The MI method for the calculation of the crystal-fluid interfacial free energy has been recently proposed by us[25]. There are other methods to directly compute the interfacial free energy at coexistence[18,22,65–70], but MI is particularly suited for the present study because it can be combined with GROMACS and it does not require a large number of particles. The MI method was originally validated with the calculation of the interfacial free energy of the Lennard-Jones and Hard Spheres systems,[25] and later on applied to sodium chloride[71]. We refer the reader to these publications for a detailed

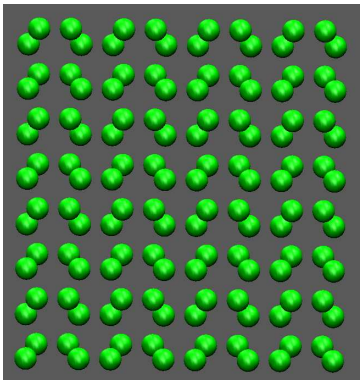

Figure 6.1: $y-z$ projection of a mold of 128 potential wells placed at the oxygen lattice positions of a pII plane at the TIP4P/Ice coexistence conditions (p=1bar, T=270 K).

description of the method. In brief, the MI method consists in computing the reversible work needed to induce the formation of a crystal slab in a fluid at coexistence conditions (at the normal melting temperature in our case, reported in Table 6.3 for the employed water models). Such work is a Gibbs free energy difference, ΔG, and is related to the interfacial free energy by:

$$\Delta G = 2A\gamma_{iw} \tag{6.1}$$

Where A is the area of the simulation box side in the diction perpendicular to the mold (the factor of two is due to the fact that two interfaces are generated). The formation of the crystal slab is induced by switching on an attractive interaction between a mold composed of potential energy wells and the fluid particles. The wells are placed in the equilibrium positions of the oxygen atoms of the ice lattice plane of interest at coexistence conditions. In Fig. 6.1 we show a mold for the pII plane and in Fig. 6.2 we show how such mold is able to induce the formation of an ice slab in liquid water at coexistence conditions. If the interaction between the wells and the oxygen atoms of the water model is square-well like (with maximum well-depth ϵ_m and well-radius r_w), γ_{iw} can be obtained as[25]:

$$\gamma_{iw}(r_w) = \frac{1}{2A}\left(\epsilon_m N_w - \int_0^{\epsilon_m} d\epsilon \left\langle N_{fw}(\epsilon)\right\rangle_{Np_xT}\right) \tag{6.2}$$

where N_w is the total number of wells, and $\langle N_{fw}(\epsilon)\rangle$ is the average number of filled wells obtained in the Np_xT ensemble for wells of depth ϵ. Basically, one has to perform thermodynamic integration along a path in which the depth of the wells is gradually increased to its maximum value, ϵ_m. The integration in Eq. 6.2 must be reversible. To ensure reversibility, the structure induced by the mold must quickly disappear when the interaction between the mold and the fluid is switched off. Therefore, one has to

make sure that the ice slab does not fully form in the integration. This is prevented by performing thermodynamic integration for wells whose radius is wider than a certain value r_w^o. In practise, $\gamma_{iw}(r_w)$ is estimated for several values of $r_w > r_w^o$ and then $\gamma_{iw}(r_w)$ is extrapolated to r_w^o, which is the well radius that gives the correct value of γ_{iw} (see Ref.[25]).

To implement the well-oxygen interaction, v_{wo}, in Molecular Dynamics we use a continuous version of the square-well potential[25]:

$$v_{wo} = -\frac{1}{2}\epsilon \left[1 - \quad \tanh\left(\frac{r - r_w}{\alpha}\right)\right], \tag{6.3}$$

where r is the distance between the well center and the oxygen atom with which the well interacts, and α is a parameter that controls the steepness of the well's walls. α can not be too large to avoid strong forces acting on the particles trapped inside the wells. We find that $\alpha = 0{,}017$ Åworks well for the case of water.

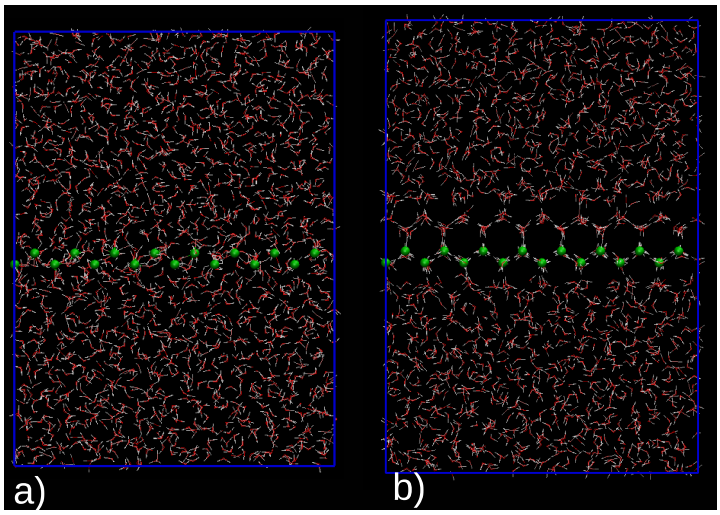

Figure 6.2: Snapshots of a TIP4P/Ice configuration at 1 bar pressure and 270 K (coexistence conditions). The mold of potential energy wells is represented by the green spheres. Its interaction with water molecules is switched off in (a) and on in (b). The radius of the mold's wells is 0.91 Åin this case.

6.5. Results

6.5.1. Determination of r_w^o

The first step is to make sure that one is indeed able to induce an ice slab using the selected mold. This should happen for small well radii. In Fig. 6.2 we show that using a pII mold with well radius = 0.91 Å an ice slab does grow from the fluid. Note that only the oxygen atoms interact with the mold. Once the mold is filled with oxygens the system is able to build up the hydrogen bond network on its own.

After having tested the ability of the molds to induce the formation of an ice slab, the next step is to find the optimal well radius, r_w^o (that for which the right γ_{iw} is obtained). This is done by performing several trajectories for different r_w's, all starting from a fluid configuration. The mold is fully switched on ($\epsilon = \epsilon_m$) at the beginning of each trajectory. If $r_w \leq r_w^o$, an ice slab should grow in all trajectories with no induction period given that there is no free energy barrier for the formation of the crystal. On the contrary, if $r_w > r_w^o$, a barrier must be overcome, which is reflected in some trajectories having an induction period before the slab grows, or even in no slab formation at all if r_w is too large[25]. To know if a crystal slab grows we monitor n_s, the number of molecules in the largest crystal cluster (to compute n_s we follow the procedure described in Ref.[30] that makes use of the order parameter proposed in Ref.[72]). The trajectories used to find r_w^o for the pII mold of Fig. 6.1 are shown in Fig. 6.3. The situation previously described for $r_w \leq r_w^o$ corresponds to the top panels (r_w = 0.919 and 0.953 Å), whereas that for $r_w > r_w^o$ corresponds to the bottom panels (r_w = 0.987, 1.022 and 1.192 Å). The largest r_w that does not show any run with an induction period is $r_w = 0{,}953$Å, and the smallest one in which at least one run shows induction period is $r_w = 0{,}987$Å. Therefore, we find $r_w^o = 0{,}97 \pm 0{,}05$Å. We acknowledge that the presence of trajectories with an induction period for $r_w = 0{,}987$ Å may not be entirely clear in view of Fig. 6.3. In order to be safe, the error bar we give for r_w^o includes cases where the absence/presence of trajectories with induction period is absolutely clear. The error in r_w^o is in fact the main source of uncertainty in our calculation of γ_{iw}.

In table 6.1 we report r_w^o for all crystal planes and water models studied in this work, along with the area of the simulation box side parallel to the mold, $L_y L_z$, the number of wells in the mold, N_w, and the number of water molecules used in the simulation, N. Note that r_w^o depends on the model and on the crystal plane. In all cases r_w^o takes the lowest value for the pI plane and the highest value for the pII plane.

6.5.2. Thermodynamic integration

Once r_w^o is known we compute the integral given in Eq. 6.2 for values of r_w larger than r_w^o. As an example, the integrand of Eq. 6.2 for the pII plane of the TIP4P/Ice

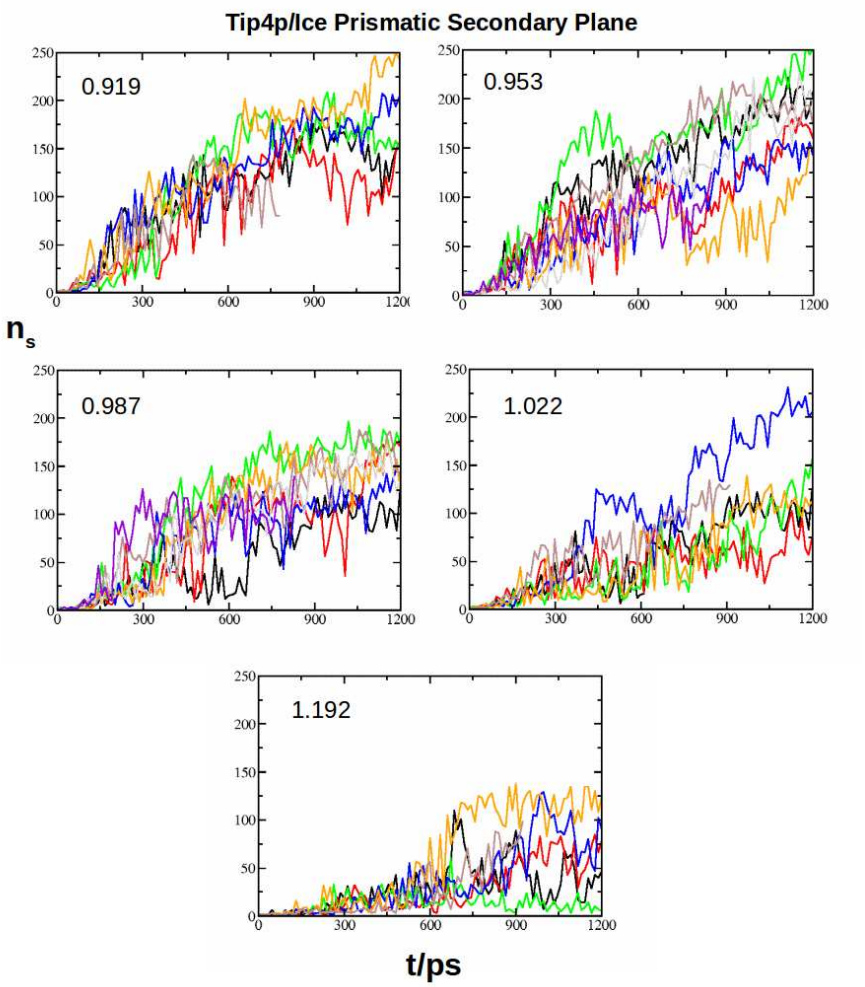

Figure 6.3: Number of particles in the largest crystal cluster, n_s, versus time for several trajectories and different well radii (as indicated in the legend in Å) for the pII plane of the TIP4P/Ice model. All simulations are performed at coexistence conditions (1 bar, 270 K). In all cases $\epsilon = \epsilon_m = 8k_BT$.

model is shown in Fig. 6.4. Each point corresponds to a different depth of the square well interaction between the wells and the oxygen atoms. The integrand reaches a plateau for large values of ϵ given that the average number of filled wells is nearly N_w beyond a certain value of the well depth. Once the plateau is reached the value of $\gamma(r_w)$ given by Eq. 6.2 does not almost depend on ϵ_m, which in our case is $8k_BT$.

To make sure that the thermodynamic integration is reversible it is advisable to check that n_s does not grow at any integration point. This kind of check is shown in Fig.

Model	Crystal Plane	$(L_y L_z)/^2$	N_w	N	$r_w^0/$	$\gamma_{iw}/(mJ/m^2)$	$\gamma_{iw}^{literature}/(mJ/m^2)$
TIP4P/Ice	basal (0001)	1141.2	128	1792	0.83(5)	27.2(8)	
TIP4P/Ice	pI ($10\bar{1}0$)	1075.9	128	1792	0.77(5)	31.6(8)	
TIP4P/Ice	pII ($11\bar{2}0$)	931.69	128	1280	0.97(5)	30.7(8)	
TIP4P/Ice	γ_0					29.8(8)	30.8(2.5)[31]
TIP4P/2005	basal	1128.7	128	1792	0.83(5)	27.2(8)	27(2)[23]
TIP4P/2005	pI	1064.1	128	1792	0.73(5)	29.5(8)	28(2)[23]
TIP4P/2005	pII	921.55	128	1280	0.94(5)	30.0(8)	28(2)[23]
TIP4P/2005	γ_0					28.9(8)	29.0(2.5)[31]
TIP4P	basal	1113.5	128	1792	0.83(5)	25.5(8)	24.5(6)[21]
TIP4P	pI	1049.8	128	1792	0.77(5)	28.2(8)	27.6(7)[21]
TIP4P	pII	909.09	128	1280	1.12(5)	28.0(8)	27.5(7)[21]
TIP4P	γ_0					27.2(8)	25.6(2.5)[31]
mW	basal	1084.4	128	1792	1.00(5)	34.5(8)	
mW	pI	1022.4	128	1792	0.63(5)	35.1(8)	
mW	pII	885.39	128	1280	1.00(5)	35.2(8)	
mW	γ_0					34.9(8)	35.2(2.5)[73], 35(2)[74]

Table 6.1: γ_{iw} for all water models and crystal orientations studied for ice Ih. We also report details on system size, and parameters used for the calculation (see main text). In the last column we also report for comparison results from other works.

6.5. For the r_w employed in this integration (1.3 Å) none of the runs shows a growing n_s. For the deepest wells ($\epsilon = 6{,}5$ and 8 k_BT) there is an incipient crystal slab forming and melting, as inferred from the large fluctuations in n_s. However, the incipient slab forms and re-dissolves quickly and thermodynamic integration can be safely performed. We further check the reversibility of the thermodynamic integration by looking at the impact of the initial configuration on the calculations. All the black points in Fig. 6.4 were obtained by using a fluid configuration as a starting point. We now use the final configuration of the simulation with the mold fully switched on ($\epsilon = \epsilon_m = 8K_BT$) to repeat the calculations. If a crystal slab had been irreversibly formed we would not obtain the same integrand. The test is satisfactory, though, and we obtain the red diamonds in Fig. 6.4.

For every model and crystal orientation we have performed thermodynamic integration for 3-4 different values of $r_w > r_w^o$. The resulting values of $\gamma_{iw}(r_w)$ are shown in Fig. 6.6 with solid symbols.

Crystal Plane	$(L_y L_z)/\text{Å}^2$	N_w	N	$r_w^0/$	$\gamma_{iw}/(mJ/m^2)$
(100)	1029.4	100	1800	0.90(5)	31.0(8)
(110)	1164.6	160	1920	0.99(5)	31.4(8)
(111)	931.69	128	1280	0.85(5)	26.9(8)

Table 6.2: γ_{iw} for ice Ic and several crystal orientations using the TIP4P/Ice model. We also report details on system size, and parameters used for the calculation (see main text).

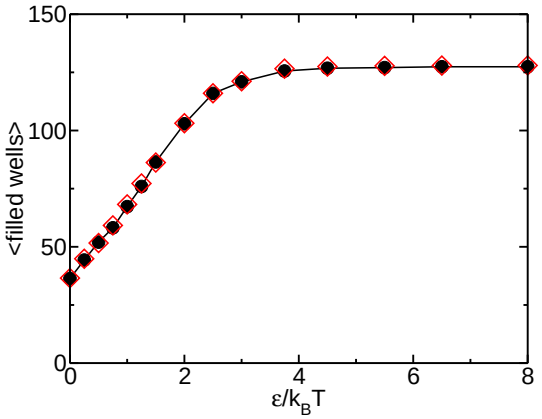

Figure 6.4: Average number of filled wells versus well depth (ϵ/k_BT) for the pII plane of the TIP4P/Ice model. The radius of the mold wells is 1.30 Å. All simulations are performed at 1 bar and 270 K. Each point corresponds to an Np_xT simulation with 0.5 ns of equilibration and 1 ns of production (for the mW model we performed for each integration point 10000 MC sweeps to equilibrate the system and an extra 40000 to obtain $< N_{fw} >$). Black circles (empty diamonds) correspond to simulations starting from an equilibrated configuration with the mold switched off (on).

6.5.3. Interfacial free energy, γ_{iw}

The $\gamma_{iw}(r_w)$ points corresponding to a given model and crystal plane are fitted to a straight line to extrapolate the results to r_w^o, where we read the definite value for γ_{iw} (shown with empty symbols in Fig. 6.6). Although we do not have a definite proof that the $\gamma_{iw}(r_w)$ dependence is linear, we have several indications to believe so. On the one hand, for all water models studied in this work and for the hard sphere, Lennard-Jones and NaCl models investigated in Refs.[25,71] we get a linear $\gamma_{iw}(r_w)$ dependence in the r_w range where the calculations were performed. On the other hand, the linear extrapolation to $r_w = r_w^o$ has given consistent results with direct calculations of the interfacial free energy using other methods for hard spheres, Lennard-Jones, NaCl (see Refs.[25,71]) and water (see below).

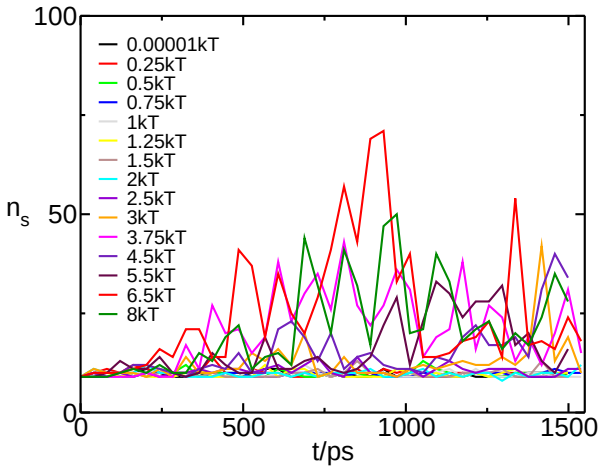

Figure 6.5: n_s versus time for all integration points shown in Fig. 6.4. Indicated in the legend is the well depth in k_BT.

The values of γ_{iw} linearly extrapolated to r_w^o for each water model and crystal orientation are reported in Table 6.1. For all models of the TIP4P family the basal plane has the lowest γ_{iw} and both prismatic planes have the same γ_{iw} within the error of our calculations. For mW we also obtain a lower γ_{iw} for the basal plane, although the error bar overlaps with those of the prismatic planes. Our results for the TIP4P, TIP4P/2005, and mW models are consistent with those of Refs.[21],[23] and[74] respectively, where γ_{iw} was directly computed at coexistence conditions. Our work improves the calculations reported in Refs.[23] and[74], though. On the one hand, our results for the TIP4P/2005 model are more accurate than those of Ref.[23], where the anisotropy of γ_{iw} with the crystal orientation could not be resolved using the capillary fluctuation method. We do see now that the basal plane has lower interfacial free energy than the prismatic planes. Regarding the mW model, in Ref.[74] it was not specified whether γ_{iw} was obtained for a spherical cluster or for a planar interface, whereas in this work we report the interfacial free energy for the three main orientations of the ice Ih lattice.

It is not obvious why the basal plane has a lower interfacial free energy than the prismatic ones, although here we provide a speculative explanation based on two previous observations. On the one hand, the penalty paid by creating the ice-water interface is entropic (the interfacial enthalpy is actually negative)[30,34]. On the other hand, it has been shown that the freedom to stack growing ice planes in two different positions confers some degree of disorder to the basal interface[23,75]. In particular, alternating patches of hexagonal and cubic ice have been observed in simulations of the basal interface, both at rest[23] and during ice growth[75] (in fact, the growth of the basal interface is delayed by the competition between such patches[75]). This mixed interfacial pattern may increase the

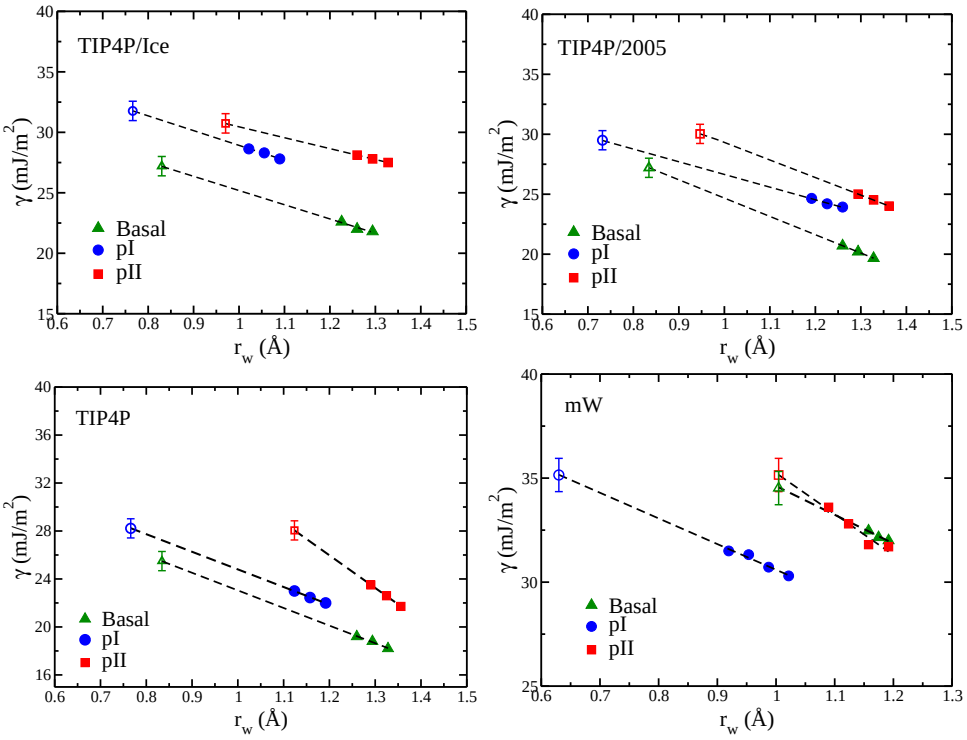

Figure 6.6: Filled symbols: Interfacial free energy for different values of the well radius and crystal orientations of ice Ih, as indicated in the legend (statistical errors have the size of the symbols). Dashed lines: linear fits to filled symbols. Empty symbols: extrapolation of the linear fits to the optimal well radius.

entropy of the basal interface and thus reduce the entropic cost of forming it. Because there is only one way of stacking a growing ice layer for both prismatic planes, these can not benefit from a disordered interfacial pattern. This kind of reasoning could also justify that the (111) plane in the hard sphere and Lennard-Jones systems has a lower interfacial free energy than the (100) one[25]. We are unable to explain, though, why the entropic stabilization of the basal plane is more noticeable for the TIP4P models than for mW.

We now focus the discussion on $\langle\gamma_{iw}\rangle$, the ice-water interfacial free energy averaged over all crystal orientations. The mW model has the highest $\langle\gamma_{iw}\rangle$, 34.9(8) mJ/m^2, then goes the TIP4P/Ice with 29.8(8) mJ/m^2, followed by the TIP4P/2005 and TIP4P with 28.9(8) mJ/m^2 and 27.2(9) mJ/m^2 respectively.

We have checked that the orientationally averaged interfacial free energy, γ_0, obtained from an expansion of γ_{iw} in spherical harmonics[76] (see table II of Ref.[23]) gives the arithmetic average of γ_{iw} for the three main crystal orientations, $\langle\gamma_{iw}\rangle$. Therefore,

we can compare our $\langle\gamma_{iw}\rangle$'s with those obtained from the seeding technique (a Classical Nucleation Theory analysis of simulations of spherical clusters embedded in the supercooled fluid[30,73,77–79]) for the TIP4P, TIP4P/Ice, TIP4P/2005[31] and mW[73] models. As shown in Table 6.1 the agreement between seeding and MI is quite good. Such consistency, alongside that reported for the Hard Spheres, Lennard-Jones and NaCl systems[73], supports that Classical Nucleation Theory[47–51] provides a good description of crystal nucleation.

In a recent publication we reported that the seeding method gives the same γ_{iw} for spherical ice Ic and ice Ih seeds[32]. To corroborate this finding we examine the interfacial free energy of different ice Ic planes for the TIP4P/Ice model. Details on the calculations are given in Table 6.2. Two of the ice Ic planes considered have the same inter-planar spacing as an ice Ih counterpart: the ice Ic (110) plane corresponds to the pII ice Ih plane, and the ice Ic (111) plane to the basal ice Ih plane. In fact, we obtain similar values of γ_{iw} for corresponding planes (see Tables 6.2 and 6.1). The ice Ic (111) and the ice Ih basal planes differ in the way hexagonal planes are stacked (ABC vs ABAB). Computing the impact on γ_{iw} of such stacking difference would require using molds with at least 3 hexagonal planes (we use 1 here to ensure reversibility in the thermodynamic integration). The effect of stacking is expected to be minor, though, as suggested both by the alternating cubic/hexagonal pattern of the basal interface[23] and by the stacking disorder often observed in ice growth simulations[41,60,75,80,81]. The (100) ice Ic plane does not have any ice Ih counterpart. Its γ_{iw} is similar to that of the prismatic ice Ih planes. With the values of γ_{iw} computed for three different orientations, and using an expansion of γ_{iw} in terms of cubic harmonics[82,83], we obtain $\gamma_0 = 30{,}1(8)$ mJ/m^2, which is similar to the value of $\gamma_0 = 29{,}8(8)$ mJ/m^2 obtained for ice Ih. This result is consistent with the observation reported in Ref.[32] that spherical seeds of ice Ih and ice Ic of the same size are critical at the same temperature.

Model	$\langle\gamma_{iw}\rangle$	T_m/K	ΔH_m	ΔS_m	$\rho_i/(g/cm^3)$	c_T	c_L
TIP4P	27.2	230[84]	1.05	4.56	0.940	0.37(2)	0.86(4)
TIP4P/2005	28.9	250[80,84,85]	1.16	4.64	0.921	0.37(2)	0.85(4)
TIP4P/Ice	29.8	270[86,87]	1.29	4.78	0.906	0.34(2)	0.82(4)
mW	34.9	274[29]	1.26	4.60	0.978	0.39(2)	0.90(4)

Table 6.3: Melting properties and Turnbull's and Laird's constants for the models studied in the work. The interfacial free energy, $\langle\gamma_{iw}\rangle$, is given in mJ/m^2, the melting enthalpy, ΔH_m, in kcal/mol, and the melting entropy, ΔS_m in cal/(mol K).

We finally seek a relation between the interfacial free energy and other thermodynamic parameters of the model. Turnbull empirically observed the following relation in

crystal nucleation studies[88]:

$$\frac{\gamma\rho^{-2/3}}{\Delta h_m} = c_T \tag{6.4}$$

where γ is the crystal-fluid interfacial free energy, ρ is the number of molecules per unit volume in the crystal (so $\rho^{-2/3}$ is an estimate of the mean area per molecule at the interface), Δh_m is the melting enthalpy per molecule, and c_T is a constant that Turnbull found to be 0.45 for many metals and 0.32 for water, Bi, Sn and Ge. Laird proposed an alternative relation by substituting Δh_m in Turnbull's expression by the thermal energy, $k_B T$, at the melting temperature, T_m[89]:

$$\frac{\gamma\rho^{-2/3}}{k_B T_m} = c_L \tag{6.5}$$

where c_L is a constant. This relation was found to work better than Turnbull's for the water models studied in Ref.[21] (TIP4P, TIP4P-Ew, TIP5P-E). We have checked if these relations hold for the water models studied in this work. The parameters involved in the calculation of c_T and c_L, and the constants themselves are reported in Table 6.3. Both relations seem to work well within the accuracy of our calculations, although the c_T and c_L constants for the mW seem to be a bit off perhaps because it does not belong to the TIP4P family. We would need to decrease the error bar in γ_{iw} in order to discriminate which relation works better. The fact that both relations work reasonably well suggests that Δh_m and T_m are correlated. The ratio between the melting enthalpy and the melting temperature is the melting entropy, that we report in Table 6.3. In fact, the melting entropy is quite similar for all studied models, which explains why both relations work similarly well. Substituting the density of the crystal by either the fluid density or an average fluid-crystal density does not improve the relations above.

6.6. Summary and Conclusions

We use the recently proposed Mold Integration method[25] to compute the ice-water interfacial free energy for different ice Ih crystal orientations (basal, primary prismatic and secondary prismatic) of some widely used water models: TIP4P, TIP4P/2005, TIP4P/Ice and mW.

The models of the TIP4P family predict a lower interfacial free energy for the basal plane than for the prismatic planes and a very similar one for both prismatic planes. For the mW model, we could not resolve differences in interfacial free energy between different crystal orientations. Our results for the interfacial free energies are summarized in Table 6.1.

The interfacial free energy averaged over all crystal orientations is consistent with that previously calculated by analyzing simulations of ice seeds in supercooled water

with Classical Nucleation Theory[30,31]. This consistency indirectly supports Classical Nucleation Theory as a good framework to understand crystal nucleation.

We also obtain the interfacial free energy of ice Ic for the (111), (110) and (100) planes using the TIP4P/Ice model. We find that ice Ic has the same orientationally averaged interfacial free energy as ice Ih, in agreement with our previous seeding work[32].

The interfacial free energy grows with the melting temperature and the melting enthalpy of the model, in agreement with Turnbull's[88] and Laird's[89] relations.

Acknowledgements

This work was funded by grants FIS2013/43209-P of the MEC, and by the Marie Curie Career Integration Grant 322326-COSAAC-FP7-PEOPLE-2012-CIG. E. Sanz acknowledges financial support from a Ramon y Cajal Fellowship. J. R. Espinosa acknowledges financial support from the FPI grant BES-2014-067625. Calculations were carried out in the supercomputer facility Tirant from the Spanish Supercomputing Network (RES) (project QCM-2015-1-0028).

Bibliography

1. Woodruff, D. P., *The solid-liquid interface* (Cambridge University Press, Cambridge, 1973).

2. Pruppacher, H. R., A new look at homogeneous ice nucleation in supercooled water drops. *J. Atmosph. Sci.* **52**, 1924 (1995).

3. Ickes, L., Welti, A., Hoose, C. & Lohmann, U., Classical nucleation theory of homogeneous freezing of water: thermodynamic and kinetic parameters. *Phys. Chem. Chem. Phys.* **17**, 5514–5537 (2015).

4. Hagen, D. E., Anderson, R. J. & Kassner-Jr., J. L., Homogeneous condensationÂ¿freezing nucleation rate measurements for small water droplets in an expansion cloud chamber. *J. Atmos. Sci.* **38**, 1236–1243 (1981).

5. Hage, W., Hallbrucker, A., Mayer, E. & Johari, G. P., Crystallization kinetics of water below 150 K. *The Journal of Chemical Physics* **100**, 2743–2747 (1994).

6. Huang, J. F. & Bartell, L. S., Kinetics of homogeneous nucleation in the freezing of large clusters. *J. Phys. Chem.* **99**, 3924 (1995).

7. Kramer, B., Hubner, O., Vortisch, H., Woste, L., Leisner, T., Schwell, M., Ruhl, E. & Baumgartel, H., Homogeneous nucleation rates of supercooled water measured in single levitated microdroplets. *J. Chem. Phys.* **111**, 6521–6527 (1999).

8. Stockel, P., Weidinger, I. M., Baumgartel, H. & Leisner, T., Rates of homogeneous ice nucleation in levitated H_2O and D_2O droplets. *The Journal of Physical Chemistry A* **109**, 2540–2546 (2005).

9. Stan, C. A., Schneider, G. F., Shevkoplyas, S. S., Hashimoto, M., Ibanescu, M., Wiley, B. J. & Whitesides, G. M., A microfluidic apparatus for the study of ice nucleation in supercooled water drops. *Lab Chip* **9**, 2293–2305 (2009).

10. Murray, B. J., Broadley, S. L., Wilson, T. W., Bull, S. J., Wills, R. H., Christenson, H. K. & Murray, E. J., Kinetics of the homogeneous freezing of water. *Phys. Chem. Chem. Phys.* **12**, 10380 (2010).

11. Manka, A., Pathak, H., Tanimura, S., Wolk, J., Strey, R. & Wyslouzil, B. E., Freezing water in no man's land. *Phys. Chem. Chem. Phys.* **14**, 4505–4516 (2012).

12. Bhabhe, A., Pathak, H. & Wyslouzil, B. E., Freezing of heavy water (D_2O) nanodroplets. *The Journal of Physical Chemistry A* **117**, 5472–5482 (2013).

13. Riechers, B., Wittbracht, F., Hutten, A. & Koop, T., The homogeneous ice nucleation rate of water droplets produced in a microfluidic device and the role of temperature uncertainty. *Phys. Chem. Chem. Phys.* **15**, 5873–5887 (2013).

14. Laksmono, H., McQueen, T. A., Sellberg, J. A., Loh, N. D., Huang, C., Schlesinger, D., Sierra, R. G., Hampton, C. Y., Nordlund, D., Beye, M., Martin, A. V., Barty, A., Seibert, M. M., Messerschmidt, M., Williams, G. J., Boutet, S., Amann-Winkel, K., Loerting, T., Pettersson, L. G. M., Bogan, M. J. & Nilsson, A., Anomalous behavior of the homogeneous ice nucleation rate in no-man's land. *The Journal of Physical Chemistry Letters* **6**, 2826–2832 (2015).

15. Baker, M. B., Cloud microphysics and climate. *Science* **276**, 1072–1078 (1997).

16. Cantrell, W. & Heymsfield, A., Production of ice in tropospheric clouds. *Bull. Amer. Meteor. Soc.* **86**, 795 (2005).

17. DeMott, P. J., Prenni, A. J., Liu, X., Kreidenweis, S. M., Petters, M. D., Twohy, C. H., Richardson, M. S., Eidhammer, T. & Rogers, D. C., Predicting global atmospheric ice nuclei distributions and their impacts on climate. *Proc. Natl. Acad. Sci.* **107**, 11217–11222 (2010).

18. Broughton, J. Q. & Gilmer, G. H., Molecular dynamics investigation of the crystal–fluid interface. VI. Excess surface free energies of crystal–liquid systems. *J. Chem. Phys.* **84**, 5759–5768 (1986).

19. Davidchack, R. L. & Laird, B. B., Direct calculation of the crystal–melt interfacial free energies for continuous potentials: Application to the Lennard-Jones system. *J. Chem. Phys.* **118**, 7651–7657 (2003).

20. Handel, R., Davidchack, R. L., Anwar, J. & Brukhno, A., Direct calculation of solid-liquid interfacial free energy for molecular systems: Tip4p ice-water interface. *Phys. Rev. Lett.* **100**, 036104 (2008).

21. Davidchack, R. L., Handel, R., Anwar, J. & Brukhno, A. V., Ice ih-water interfacial free energy of simple water models with full electrostatic interactions. *Journal of Chemical Theory and Computation* **8**, 2383–2390 (2012).

22. Hoyt, J. J., Asta, M. & Karma, A., Method for computing the anisotropy of the solid-liquid interfacial free energy. *Phys. Rev. Lett.* **86**, 5530–5533 (2001).

23. Benet, J., MacDowell, L. G. & Sanz, E., A study of the ice-water interface using the TIP4P/2005 water model. *Phys. Chem. Chem. Phys.* **16**, 22159–22166 (2014).

24. Limmer, D. T. & Chandler, D., Premelting, fluctuations, and coarse-graining of water-ice interfaces. *The Journal of Chemical Physics* **141**, 18C505 (2014).

25. Espinosa, J. R., Vega, C. & Sanz, E., The mold integration method for the calculation of the crystal-fluid interfacial free energy from simulations. *J Chem. Phys.* **141**, 134709 (2014).

26. Jorgensen, W. L., Chandrasekhar, J., Madura, J. D., Impey, R. W. & Klein, M. L., Comparison of simple potential functions for simulating liquid water. *J. Chem. Phys.* **79**, 926 (1983).

27. Abascal, J. L. F. & Vega, C., A general purpose model for the condensed phases of water: TIP4P/2005. *J. Chem. Phys.* **123**, 234505 (2005).

28. Abascal, J. L. F., Sanz, E., Fernandez, R. G. & Vega, C., A potential model for the study of ices and amorphous water: TIP4P/Ice. *J. Chem. Phys.* **122**, 234511 (2005).

29. V. Molinero, and E. B. Moore, Water modeled as an intermediate element between carbon and silicon. *The Journal of Physical Chemistry B* **113**, 4008–4016 (2009).

30. Sanz, E., Vega, C., Espinosa, J. R., Caballero-Bernal, R., Abascal, J. L. F. & Valeriani, C., Homogeneous ice nucleation at moderate supercooling from molecular simulation. *Journal of the American Chemical Society* **135**, 15008–15017 (2013).

31. Espinosa, J. R., Sanz, E., Valeriani, C. & Vega, C., Homogeneous ice nucleation evaluated for several water models. *J. Chem. Phys.* **141**, 18C529 (2014).

32. Zaragoza, A., Conde, M. M., Espinosa, J. R., Valeriani, C., Vega, C. & Sanz, E., Competition between ices ih and ic in homogeneous water freezing. *The Journal of Chemical Physics* **143**, 134504 (2015).

33. Reinhardt, A. & Doye, J. P. K., Free energy landscapes for homogeneous nucleation of ice for a monatomic water model. *J. Chem. Phys.* **136**, 054501 (2012).

34. Reinhardt, A. & Doye, J. P. K., Note: Homogeneous tip4p/2005 ice nucleation at low supercooling. *J. Chem. Phys.* **139**, 096102 (2013).

35. Svishchev, I. M. & Kusalik, P. G., Crystallization of liquid water in a molecular dynamics simulation. *Phys. Rev. Lett.* **73**, 975 (1994).

36. Quigley, D. & Rodger, P. M., Metadynamics simulations of ice nucleation and growth. *J. Chem. Phys.* **128**, 154518 (2008).

37. Li, T., Donadio, D., Russo, G. & Galli, G., Homogeneous ice nucleation from supercooled water. *Phys. Chem. Chem. Phys.* **13**, 19807–19813 (2011).

38. Buhariwalla, C., Bowles, R., Saika-Voivod, I., Sciortino, F. & Poole, P., Free energy of formation of small ice nuclei near the widom line in simulations of supercooled water. *Eur. Phys. J. E.* **38**, 39 (2015).

39. Geiger, P. & Dellago, C., Neural networks for local structure detection in polymorphic systems. *J. Chem. Phys.* **139**, 164105 (2013).

40. Malkin, T. L., Murray, B. J., Brukhno, A. V., Anwar, J. & Salzmann, C. G., Structure of ice crystallized from supercooled water. *Proceedings of the National Academy of Sciences* **109**, 1041–1045 (2012).

41. Moore, E. B. & Molinero, V., Is it cubic? ice crystallization from deeply supercooled water. *Phys. Chem. Chem. Phys.* **13**, 20008 (2011).

42. Moore, E. B. & Molinero, V., Structural transformation in supercooled water controls the crystallization rate of ice. *Nature* **479**, 506–508 (2011).

43. Russo, J., Romano, F. & Tanaka, H., New metastable form of ice and its role in the homogeneous crystallization of water. *Nature Materials* **13**, 733 (2014).

44. Radhakrishnan, R. & Trout, B. L., Nucleation of hexagonal ice (Ih) in liquid water. *J. Am. Chem. Soc.* **125**, 7743 (2003).

45. Cox, S. J., Kathmann, S. M., Slater, B. & Michaelides, A., Molecular simulations of heterogeneous ice nucleation. i. controlling ice nucleation through surface hydrophilicity. *J. Chem. Phys.* **142**, 184704 (2015).

46. Haji-Akbari, A. & Debenedetti, P. G., Direct calculation of ice homogeneous nucleation rate for a molecular model of water. *Proceedings of the National Academy of Sciences* **112**, 10582–10588 (2015).

47. Gibbs, J. W., On the equilibrium of heterogeneous substances. *Trans. Connect. Acad. Sci.* **3**, 108–248 (1876).

48. Gibbs, J. W., On the equilibrium of heterogeneous substances. *Trans. Connect. Acad. Sci.* **16**, 343–524 (1878).

49. Kelton, K. F., *Crystal Nucleation in Liquids and Glasses* (Academic, Boston, 1991).

50. Volmer, M. & Weber, A., Keimbildung in ubersattigten gebilden. *Z. Phys. Chem.* **119**, 277 (1926).

51. Becker, R. & Doring, W., Kinetische behandlung der keimbildung in ubersattigten dampfen. *Ann. Phys.* **416**, 719–752 (1935).

52. Murray, B. J., Knopf, D. A. & Bertram, A. K., The formation of cubic ice under conditions relevant to Earth's atmosphere. *Nature* **434**, 202–205 (2005).

53. Lisgarten, N. D. & Blackman, M., Cubic form of ice. *Nature* **178**, 39 (1956).

54. Shallcross, F. V. & Carpenter, G. B., X-ray diffraction study of the cubic phase of ice. *J. Chem. Phys.* **26**, 782 (1957).

55. Dowell, L. G. & Rinfret, A. P., Low-temperature forms of ice as studied by x-ray diffraction. *Nature* **188**, 1144 (1960).

56. Bertie, J. E. & Jacobs, S. M., Far-infrared absorption by ices ih and ic at 4.3 k and the powder diffraction pattern of ice ic. *J. Chem. Phys.* **67**, 2445 (1977).

57. Klotz, S., Besson, J. M., Hamel, G., Nelmes, R. J., Loveday, J. S. & Marshall, W. G., Metastable ice VII at low temperature and ambient pressure. *Nature* **398**, 681 (1999).

58. Klug, D. D., Handa, Y. P., Tse, J. S. & Whalley, E., Transformation of ice VIII to amorphous ice by melting at low temperature. *J. Chem. Phys.* **90**, 2390 (1989).

59. Kuhs, W. F., Sippel, C., Falenty, A. & Hansen, T. C., Extent and relevance of stacking disorder in ice Ic. *Proceedings of the National Academy of Sciences* **109**, 21259–21264 (2012).

60. Malkin, T. L., Murray, B. J., Salzmann, C. G., Molinero, V., Pickering, S. J. & Whale, T. F., Stacking disorder in ice i. *Phys. Chem. Chem. Phys.* **17**, 60–76 (2015).

61. Hess, B., Kutzner, C., van der Spoel, D. & Lindahl, E., Algorithms for highly efficient, load-balanced, and scalable molecular simulation. *J. Chem. Theory Comput.* **4**, 435–447 (2008).

62. Parrinello, M. & Rahman, A., Polymorphic transitions in single crystals: A new Molecular Dynamics method. *J. App. Phys.* **52**, 7182–7190 (1981).

63. Bussi, G., Donadio, D. & Parrinello, M., Canonical sampling through velocity rescaling. *The Journal of Chemical Physics* **126**, 014101 (2007).

64. Wheeler, D. R. & Newman, J., A less expensive ewald lattice sum. *Chem. Phys. Lett.* **366**, 537 (2002).

65. Angioletti-Uberti, S., Ceriotti, M., Lee, P. D. & Finnis, M. W., Solid-liquid interface free energy through metadynamics simulations. *Phys. Rev. B* **81**, 125416 (2010).

66. Fernandez, L. A., Martin-Mayor, V., Seoane, B. & Verrocchio, P., Equilibrium fluid-solid coexistence of hard spheres. *Phys. Rev. Lett.* **108**, 165701 (2012).

67. Zykova-Timan, T., Ceresoli, D., Tartaglino, U. & Tosatti, E., Why are alkali halide surfaces not wetted by their own melt? *Phys. Rev. Lett.* **94**, 176105 (2005).

68. Zykova-Timan, T., Ceresoli, D., Tartaglino, U. & Tosatti, E., Physics of solid and liquid alkali halide surfaces near the melting point. *The Journal of Chemical Physics* **123**, 164701 (2005).

69. Benjamin, R. & Horbach, J., Crystal-liquid interfacial free energy via thermodynamic integration. *The Journal of Chemical Physics* **141**, 044715 (2014).

70. Schmitz, F. & Virnau, P., The ensemble switch method for computing interfacial tensions. *The Journal of Chemical Physics* **142**, 144108 (2015).

71. Espinosa, J. R., Vega, C., Valeriani, C. & Sanz, E., The crystal-fluid interfacial free energy and nucleation rate of NaCl from different simulation methods. *J. Chem. Phys.* **142**, 194709 (2015).

72. Lechner, W. & Dellago, C., Accurate determination of crystal structures based on averaged local bond order parameters. *J. Chem. Phys.* **129**, 114707 (2008).

73. Espinosa, J. R., Vega, C., Valeriani, C. & Sanz, E., Seeding approach to crystal nucleation. *J. Chem. Phys.* **144**, 034501 (2016).

74. Limmer, D. T. & Chandler, D., Phase diagram of supercooled water confined to hydrophilic nanopores. *The Journal of Chemical Physics* **137**, 044509 (2012).

75. Seo, M., Jang, E., Kim, K., Choi, S. & Kim, J. S., Understanding anisotropic growth behavior of hexagonal ice on a molecular scale: A molecular dynamics simulation study. *The Journal of Chemical Physics* **137**, 154503 (2012).

76. Kara, M. & Kurki-Suonio, K., Symmetrized multipole analysis of orientational distributions. *Acta Crystallographica Section A* **37**, 201–210 (1981).

77. Bai, X.-M. & Li, M., Calculation of solid-liquid interfacial free energy: A classical nucleation theory based approach. *J. Chem. Phys.* **124**, 124707 (2006).

78. Pereyra, R. G., Szleifer, I. & Carignano, M. A., Temperature dependence of ice critical nucleus size. *J. Chem. Phys.* **135**, 034508 (2011).

79. Knott, B. C., Molinero, V., Doherty, M. F. & Peters, B., Homogeneous nucleation of methane hydrates: Unrealistic under realistic conditions. *J. Am. Chem. Soc.* **134**, 19544–19547 (2012).

80. Rozmanov, D. & Kusalik, P. G., Temperature dependence of crystal growth of hexagonal ice (ih). *Phys. Chem. Chem. Phys.* **13**, 15501–15511 (2011).

81. Carignano, M. A., Formation of stacking faults during ice growth on hexagonal and cubic substrates. *The Journal of Physical Chemistry C* **111**, 501–504 (2007).

82. Fehlner, W. R. & Vosko, S. H., A product representation for cubic harmonics and special directions for the determination of the fermi surface and related properties. *Canadian Journal of Physics* **54**, 2159–2169 (1976).

83. Benet, J., MacDowell, L. G. & Sanz, E., Interfacial free energy of the NaCl crystal-melt interface from capillary wave fluctuations. *The Journal of Chemical Physics* **142**, 134706 (2015).

84. Garcia-Fernandez, R., Abascal, J. L. F. & Vega, C., The melting point of ice ih for common water models calculated from direct coexistence of the solid-liquid interface. *The Journal of Chemical Physics* **124**, 144506 (2006).

85. Conde, M. M., Gonzalez, M. A., Abascal, J. L. F. & Vega, C., Determining the phase diagram of water from direct coexistence simulations: The phase diagram of the TIP4P/2005 model revisited. *The Journal of Chemical Physics* **139**, 154505 (2013).

86. Weiss, V. C., Rullich, M., KÃ¶hler, C. & Frauenheim, T., Kinetic aspects of the thermostatted growth of ice from supercooled water in simulations. *The Journal of Chemical Physics* **135**, 034701 (2011).

87. Yan, J. Y. & Patey, G. N., Molecular dynamics simulations of ice nucleation by electric fields. *The Journal of Physical Chemistry A* **116**, 7057–7064 (2012).

88. Turnbull, D., Formation of crystal nuclei in liquid metals. *J. Appl. Phys.* **21**, 1022–1028 (1950).

89. Laird, B. B., The solid-liquid interfacial free energy of close-packed metals: Hard-spheres and the turnbull coefficient. *The Journal of Chemical Physics* **115**, 2887–2888 (2001).

Results: Chapter 7

On the time required to freeze water

J. R. Espinosa, *C.Navarro, E.Sanz, C.Valeriani and C.Vega*

Departamento de Fisica Aplicada I , Facultad de Ciencias Fisicas, Universidad Complutense de Madrid, 28040 Madrid, Spain. Departamento de Fisica Aplicada I , Facultad de Ciencias Fisicas, Universidad Complutense de Madrid, 28040 Madrid, Spain.

7.1. Abstract

By using the seeding technique the nucleation rate for the formation of ice at room pressure will be estimated for the TIP4P/ICE model using longer runs and a smaller grid of temperatures than in previous work. The growth rate of ice will be determined for TIP4P/ICE and for the mW model of water. Although TIP4P/ICE and mW have a similar melting point and melting enthalpy they differ significantly in the dynamics of freezing. The nucleation rate of mW is lower than that of TIP4P/ICE due to its higher interfacial free energy. Experimental results for the nucleation rate of ice are between the predictions of these two models when obtained from the seeding technique, although closer to the predictions of TIP4P/ICE. The growth rate of ice for the mW model is four orders of magnitude larger than for TIP4P/ICE. Avrami's expression is used to estimate the crystallization time from the values of the nucleation and growth rates. For mW the minimum in the crystallization time is found at approximately 85K below the melting point and its value is of about a few ns, in agreement with the results obtained from brute force simulations by Moore and Molinero. For the TIP4P/ICE the minimum is found at about 55K below the melting point, but its value is about ten microseconds. This value is compatible with the minimum cooling rate required to avoid the formation of ice and obtaining a glass phase. The crossover from the nucleation controlled crystallization to the growth controlled crystallization will be discussed for systems of finite size. This crossover could explain the apparent discrepancy between

the values of J obtained by different experimental groups for temperatures below 230K and should be considered as an alternative hypothesis to the two previously suggested: internal pressure and/or surface freezing effects. A maximum in the compressibility was found for the TIP4P/ICE model in supercooled water. The relaxation time is much smaller than the crystallization time at the temperature at which this maximum occurs so this maximum is a real thermodynamic feature of the model. At the temperature of minimum crystallization time, the crystallization time is larger than the relaxation time by just two orders of magnitude.

7.2. Introduction

The formation of a solid phase from a metastable liquid is a process of particular interest, often occurring on the surface of small solid impurities[1,2] contained in the supercooled liquid. In the absence of impurities it is possible for the metastable liquid phase to survive for an arbitrarily long time until solid homogeneous nucleation takes place. In homogeneous nucleation a cluster of the solid phase has to reach a critical size and that requires overcoming a given free energy barrier.[3–7] Once this cluster is formed the new phase grows from this initial embryo.

Experimentally, since solids have well defined X-ray diffraction peaks, whose intensity is proportional to the amount of the solid phase, it is straightforward to determine when the system has frozen, and the time required to freeze it. τ is the time required to freeze the majority of the sample. τ depends on the supercooling (defined as the difference between the melting temperature and the temperature of interest). The value of τ is huge for temperatures slightly below the melting point and decreases significantly as the supercooling increases. However, τ is never zero. It reaches a minimum at a certain temperature and grows when increasing the supercooling. The existence of this minimum is crucial to the understanding of the formation of glasses. If the value of τ were zero at a certain temperature then the formation of the solid phase would be unavoidable.

However, glasses are indeed often found after a fast temperature quench of the liquid phase, indicating that τ must indeed have a minimum. In a celebrated paper published in the Journal of Chemical Physics almost 80 years ago Avrami[8,9] used a theoretical treatment showing that the time required to freeze a certain fraction ϕ of a sample depends both on the nucleation rate J (i.e the number of critical clusters formed per unit of volume and time) and on the growth rate of the solid phase u. This relation was found independently by other researches so the Avrami relation is sometimes denoted as the Kolmogorov-Johnson-Mehl-Avrami (KJMA) relation[8–11]. In his paper[8] Avrami relates the crystallization time to the (1/4) power of the inverse of the product of the nucleation rate J and the third power of the growth rate of the solid u obtaining

the following (approximate) expression for the crystallization time :

$$\tau_{Avrami} = ((3\phi)/(\pi J u^3))^{1/4} \tag{7.1}$$

where ϕ is the fraction of the sample that has frozen.

Since J increases with the supercooling and u decreases with the supercooling, a minimum in the crystallization time is indeed possible. The Avrami relation is often used in material science.

A system of particular interest is water. Understanding the freezing of water from the supercooled liquid is of great interest in climate science[12–14] (often small droplets of supercooled water are found in the clouds), microbiology[15],the food industry[16,17], materials science[18] and geology[19] . Also, controlling the freezing of water would have an impact in cryopreservation and food science[20,21]. For this reason it is of interest to determine the crystallization time for water. However this still constitutes a great challenge.

Experimental nucleation rates J for water are only available for temperatures between 232K and 245K[22–33]. Below 232K J is too high to be measured experimentally. Above 245K is too low. In the recent years it has been possible to determine J in the range from 205K to 230K[34–36]. However, different results were obtained by different groups and it is difficult to understand the origin of this discrepancy. Our knowledge of u is even more limited as it has been measured only for temperatures up to 10K below melting[37,38]. Simulations could be useful in providing some hints as to the value of the crystallization time for water.[39–45] However, on the one hand results should be taken with care as in computer simulations one must use an approximate description of the intermolecular interactions and therefore the results do not necessarily correspond to those of real water.[46–48] On the other hand, often τ can not be obtained from brute force simulations since usually it is much larger than the typical maximum length of a run (hundreds of ns). An interesting exception is the mW model of water[49] for which it has been possible to determine τ using brute force simulations for homogeneous[50] and heterogeneous nucleation[51–54]. For this model the value of τ at the minimum (at room pressure) was found to be of about a few nanoseconds. However for other water models[55–57] the value of τ at the minimum seems to be larger as can be inferred from the fact that ice is not obtained from brute force simulations. For temperatures far from the minimum it is not possible to determine τ unless one uses rare event techniques[58–61]. In this work our main goal is to estimate τ for the TIP4P/ICE model[56]. This model presents several advantages. It predicts rather well the phase diagram of water, especially at 1 bar[56,62]. Its melting point is quite close to the experimental value[56], and its melting enthalpy is only ten per cent lower that its experimental counterpart.

Estimating the crystallization time for TIP4P/ICE using Avrami's expression requires the estimation of the nucleation rate over a wide range of temperatures. We have

recently used an approximate technique denoted as seeding[63,64] to estimate J[65–69] showing that it provides reasonable estimates for hard spheres, LJ , NaCl and for the mW model of water[66] as compared to the values obtained from more rigorous techniques. The origin of the seeding technique can be traced back to the papers by Li et al.[63,64], Carignano et al.[70], Knott et al.[71] and Sanz et al.[65] among others. It consists in inserting a cluster of the solid phase and determining the temperature at which it becomes critical (i.e it has a 50 % probability of either growing or shrinking). After that one uses Classical Nucleation Theory[3,72,73] to determine the free energy barrier and runs from the critical cluster to estimate the kinetic term.

In this work we shall implement the seeding technique for TIP4P/ICE. In variance with previous work we shall increase the accuracy in determining the temperature at which the cluster is critical (by performing more runs for each temperature and by decreasing the window size of the temperatures considered). In addition we shall incorporate into the analysis the value of the interfacial ice-water free energy at the melting temperature which can be obtained independently (and rigorously) using the recently proposed Mold Integration technique[74]. After the values of J are estimated for this model, long runs are performed to determine the growth rate at high supercooling. By combining the values of J and u, the Avrami expression will be used to estimate the crystallization time. It is found that τ_{Avrami} has a minimum for temperatures of about 215K and at the minimum the crystallization time as estimated from Avrami's expression is of about ten microseconds. This value is consistent with experiments showing that to form glassy water the cooling rate should be larger than $5 \times 10^6 K/s$.[75–77]

We also estimated the relaxation time τ_r for supercooled water at room pressure and concluded that for the temperatures considered in this work the ratio of the crystallization and relaxation times is always a very large number except for the temperatures close to the minimum in the crystallization time where it is of the order of 100. Finally we discuss the expected variation of τ with supercooling for systems of different sizes and proposed a tentative explanation of this discrepancy in J found by different experimental groups at large supercoolings.

7.3. Computational details

All simulations in this work were performed with Gromacs[78] using a velocity-rescaling[79] thermostat and a Parrinello-Rahman barostat[80] with a relaxation time for both of about 2ps. The time step was always 2fs. The LJ term of the potential was truncated at 9 Å and long range corrections were added to account for the truncation of the LJ part. Ewald sums (with the PME technique[81]) were used to deal with the electrostatic interactions. The real part of the electrostatic potential was also truncated at 9 Å . The algorithm used to constraint the geometry of the molecule was LINCS.

Three type of simulations were performed. 1) Simulations aimed at determining the growth rate of ice, and/or the melting point were performed using 4000 molecules, located in an initial configuration consisting of 2000 molecules of ice in contact with 2000 molecules of liquid water. The dimensions of the box were approximately 3x3x9 (in nm) so that the slice of ice occupies about 4.5nm of the initial configuration. The barostat was anisotropic so that the dimensions of the simulation box L_x, L_y, L_z could be changed independently. Runs of about 200 ns were used at high temperatures, whereas runs of about 2 microseconds were used at the lowest temperatures. 2) Simulations aimed at determining the diffusion coefficient of water and the relaxation time used 2000 molecules in a cubic simulation box. In this case the barostat was isotropic (i.e the three dimensions of the box changed in the same way). Runs of about 200ns were used at high temperatures whereas runs of about 2 microseconds were used at the lowest temperatures. 3) Simulations used in the seeding technique. Three solid spherical crystalline clusters were prepared with about 8000,3000 and 600 molecules. The inserted clusters were spherical because we have checked in previous work that cubic clusters evolve very quickly into spherical ones[68]. One possible explanation to this fact is that the shape that minimizes the ratio area/volume (interfacial energetic penalty/driving force to nucleate) is the sphere. The clusters were inserted into a supercooled liquid having about 185000, 76000 and 23000 molecules respectively. The remaining details are identical to those of our previous work.[65,67] Simulations were performed in the NpT ensemble (using isotropic scaling). The typical length of the run was between 5 and 20 ns. To determine the temperature at which the cluster was critical we used a temperatures grid of about 2.5K. For some temperatures several independent runs were performed by changing the initial momenta of the particles. This is important due to the stochastic nature of the time evolution of clusters when their size is close to the critical one.

Ideally one should run as many trajectories as possible. However, the runs of the seeding technique are very expensive from a computational point of view and their number is limited. In the seeding technique we analyze the time evolution of the size of the solid cluster, identified by the q_6 proposed by Lechner and Dellago[82] as in our previous work[67]. We used the location of the oxygen atoms to define q_6 with a cut-off distance for identifying neighboring particles of roughly 3.5 Å corresponding to the distance of the first minimum of the oxygen-oxygen correlation function. For each molecule i we compute the value of $q_{6,i}$. When the value of $q_{6,i}$ was larger than a certain threshold value $q_{6,t}$ the molecule was labeled as solid and otherwise as liquid. Two solid particles were connected if their distance was smaller than 3.5 Å . In this way the size of the solid cluster was obtained as the size of the largest cluster of solid particles which are connected.

In our previous work, $q_{6,t}$ was constant and set to 0.358. In this work we tune the value of $q_{6,t}$ for every temperature. We shall use the mislabeling criteria to determine $q_{6,t}$[66,68,69]. At a given temperature we simulate bulk ice Ih and bulk water. The value of

$q_{6,t}$ was obtained as that for which the percentage of mislabeled particles in bulk ice (i.e those identified as liquid like) becomes identical to that of mislabeled particles in bulk water (i.e those identified as ice). Typically the value of mislabeled particles at $q_{6,t}$ was about 0.5 per cent and $q_{6,t}$ increases as the temperature decreases. This is due to the increasing tetrahedral order of the liquid phase when the temperature decreases.

7.4. Results

To determine τ_{Avrami} we need to determine J and u. Since we shall present the results as a function of the supercooling an accurate determination of the melting temperature is needed.

7.4.1. Melting temperature

The melting temperature of TIP4P/ICE should be determined with accuracy and using the same conditions (cutoff, constraints, time step, etc) that are used in the seeding technique. In the past we have reported a value of 272K from free energy calculations[56], 271K from the melting of the free surface of ice[83] and of 268K from the direct coexistence technique (using 864 particles)[84]. In this work we shall determine the melting point using the direct coexistence technique with 4000 molecules.

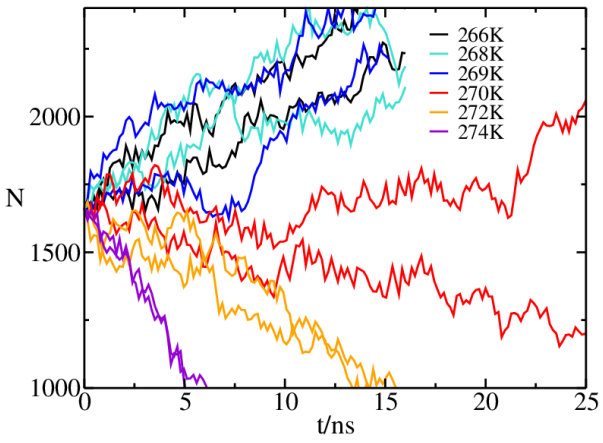

Figure 7.1: Direct coexistence runs for the ice-water interface at p=1bar and several temperatures of the TIP4P/ICE model. The evolution of the total number of solid particles N as a function of time (for different temperatures) is shown.

The results are shown in Fig.7.1. As can be seen the estimated melting point is 270(1)K. This is in agreement with another recent estimate obtained also from the direct

coexistence technique.[85] Notice that in our previous work dealing with the nucleation of ice for the TIP4P/ICE model we used the value of 272K for the melting temperature[65,67,68]. In this work the value of 270K will be used.

7.4.2. Growth rate

The growth rate was estimated from direct coexistence runs using the expression:

$$u = L_{growth}/(2\tau_{growth}) \tag{7.2}$$

where L_{growth} is the length of the ice slab that grows in a time τ_{growth}. We performed runs until the entire system had frozen. In this case L_{growth} is around half of the box size in the direction perpendicular to the interface (in the initial configuration half of the sample was ice and half was liquid water). The factor of 2 accounts for the fact that we have two interfaces.

The value of u depends on the plane considered. This has been studied in detail by Rozmanov and Kusalik for TIP4P/2005[86]. The value of the growth rate is large for prismatic planes (primary and secondary have similar growth rates) and smaller for the basal plane (the value of the growth rate for the basal plane is approximately 0.6 times that of the prismatic planes). In fact we computed u for the basal plane of the TIP4P/ICE model for three temperatures (245K,255K,260K) and found that its value was (within five per cent) 0.6 times the value of the secondary prismatic plane. In this work we obtain the the growth rate of the secondary prismatic plane u_{pII} (Table 7.1 and in Fig.7.2).

Table 7.1: Growth rate for the secondary prismatic plane u_{pII} as obtained in this work for the TIP4P/ICE and mW models.

Model	T/K	u_{pII}/(Å/ns)	Model	T/K	u_{pII}/(Å/ns)
TIP4P/ICE	215	0.006	mW	180	22
TIP4P/ICE	225	0.029	mW	190	60
TIP4P/ICE	235	0.169	mW	200	235
TIP4P/ICE	245	0.528	mW	210	300
TIP4P/ICE	250	0.633	mW	220	466
TIP4P/ICE	255	0.926	mW	230	512
TIP4P/ICE	257.5	0.803	mW	240	490
TIP4P/ICE	260	0.933	mW	250	375
			mW	260	266

Experimental results (only available for temperatures slightly below the melting point) are also shown[37,38]. The agreement between simulation results for the TIP4P/ICE

and experiments is very good. u has a maximum around 15 degrees below the melting point. A similar maximum was found by Rozmanov and Kusalik for the TIP4P/2005[87,88]. At the maximum the growth rate is about 1 Å per nanosecond.

We are interested in the value of u for spherical clusters (rather than for a planar ice-water interface). We shall estimate it as the average growth rate for the basal and the two prismatic planes, assuming that the value of the growth rate is the same for the two prismatic planes and that the value of the growth rate of the basal plane is 0.6 times the value of the prismatic planes. In practice this is equivalent to multiplying by 13/15 the value of the growth rate of the secondary prismatic plane ($u = (u_{p_{II}} + u_{p_I} + u_{basal})/3 \simeq (u_{p_{II}} + u_{p_{II}} + 0.6\ u_{p_{II}})/3$), so that we will approximate u for the spherical cluster as u=13/15 $u_{p_{II}}$ (Fig.2). We average the growth rates for these three different crystal orientations in the same way as previously done for the interfacial free energies of such planes in references[89–92]. For the case of the interfacial free energies, it was found that this type of average corresponds to γ_0 (as can be inferred from the results of Table II of Ref.[90] and taking into account that the values of ϵ_2 and ϵ_3 are rather small as shown in[91]) which is the zero order term of the expansion of γ into spherical harmonics and that the values of γ obtained from the seeding technique when extrapolated to the coexistence point yield values of γ close to γ_0[90–92]. In this case, we assume that the growth rate follows a similar dependence on the orientation to that of γ due to the resemblance of their trends (the growth rate and the interfacial free energies of p_{II} and p_I are quite similar and higher than those of the basal plane.) For this reason we shall also use this average to estimate the growth rate of a spherical cluster.

The values of u were fitted to the following expression (which works well for supercoolings $\Delta T = T_m - T$ larger than 15K)

$$\ln(u/(\ /ns)) = C_1 + C_2\Delta T + C_3(\Delta T)^2 \tag{7.3}$$

whose coefficients of the fit are given in Table 7.2.

Table 7.2: Coefficients of the fit for ln(u / (Å /ns)) for the TIP4P/ICE and mW models as a function of the supercooling. For TIP4P/ICE $T_m = 270K$. For mW $T_m = 274{,}6K$ These fits should be used for supercoolings larger than 15K only.

Model	C_1	C_2/K	C_3/K^2
TIP4P/ICE	-0.2597	0.028831	-0.002215
mW	4.1711	0.096266	-0.001148

We have also determined u_{pII} for the mW model of water. In this case we used the LAMMPS[93] package with a similar setup to that used for the TIP4P/ICE. Values of u_{pII} are presented in Fig.7.2. There is a maximum in the growth rate located around 40 K below the melting point of the model (i.e 274.6K). The value of the growth rate

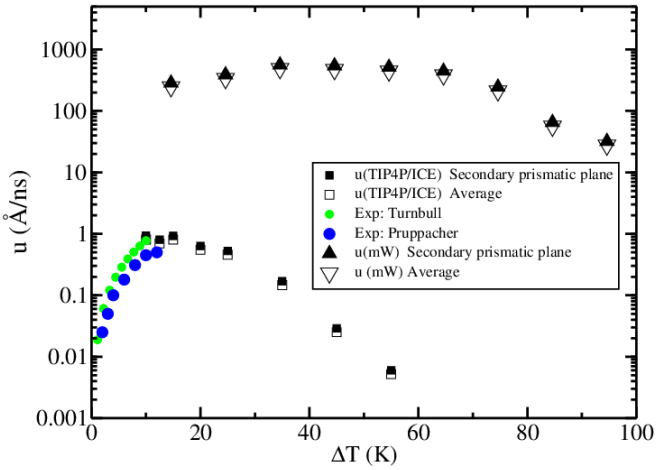

Figure 7.2: u_{pII} for the secondary prismatic plane of TIP4P/ICE and mW water models (black filled symbols). The average value u (for the two prismatic and the basal planes) (open symbols). and experimental values from Turnbull and Pruppacher are also shown[37,38].

at the maximum for the mW model is three orders of magnitude larger than for the TIP4P/ICE model. Also (in contrast to TIP4P/ICE) the decay of u_{pII} with temperature is very slow. For a supercooling of about 55K the growth rate of mW is around five orders of magnitude larger than that of TIP4P/ICE. The value of u for the spherical cluster of the mW model was also estimated as 13/15 of u_{pII} as for the TIP4P/ICE model.

7.4.3. Diffusion coefficients and results for the room pressure isobar

In Table 7.3 the values of the densities, diffusion coefficients and isothermal compressibilities of TIP4P/ICE are reported. The time required to diffuse one molecular diameter is also given ($\tau_r = \sigma^2/(6D) \simeq 10^2\ /(6D)$). This provides a rough idea of the relaxation time of the system. A more elaborate estimate of the relaxation time would be obtained from the decay of the self intermediate scattering function.[94–96] For instance at 230K, Haji-Akbari and Debenedetti[96] reported a relaxation time of 0.6ns for this model (to be compared with the one obtained here which is of about 1.5ns). The numbers are not identical, but are of the same order of magnitude, so that can be used as a rough guide for the relaxation time of the system.

In Fig. 7.3. the density of the TIP4P/ICE model along the room pressure isobar is shown. The model has a maximum in density located around $295K$ (in agreement with the results obtained via Monte Carlo runs few years ago[97]) and a minimum in

Table 7.3: Densities, diffusion coefficients and time required to diffuse one molecular diameter τ_r as obtained from NpT runs (for $p = 1$bar) for the TIP4P/ICE. The length of the runs was 100ns for temperatures above 270K, 500ns between 230K and 260K, and of the order of one or two microseconds for temperatures below 220K. The results of the isothermal compressibility as obtained from the volume fluctuations are also shown.

T/K	$\rho_f/(g/cm^3)$	$D/(m^2/s)$	τ_r/ns	$k_T \cdot 10^{10}/(J/m^3)$
320	0.989	$2.31 \cdot 10^{-9}$	0.006	4.53
310	0.991	$1.83 \cdot 10^{-9}$	0.008	4.55
300	0.992	$1.41 \cdot 10^{-9}$	0.010	4.66
290	0.992	$1.05 \cdot 10^{-9}$	0.013	4.87
280	0.991	$7.23 \cdot 10^{-10}$	0.02	5.19
270	0.988	$4.74 \cdot 10^{-10}$	0.03	5.54
260	0.982	$2.77 \cdot 10^{-10}$	0.06	6.14
250	0.972	$1.36 \cdot 10^{-10}$	0.11	6.77
240	0.958	$4.93 \cdot 10^{-11}$	0.31	6.95
230	0.942	$9.76 \cdot 10^{-12}$	1.48	6.11
220	0.929	$1.16 \cdot 10^{-12}$	13	4.77
210	0.923	$2.13 \cdot 10^{-13}$	80	2.77
200	0.923	$2.77 \cdot 10^{-14}$	550	1.69
190	0.925	$8.60 \cdot 10^{-15}$	2020	1.63

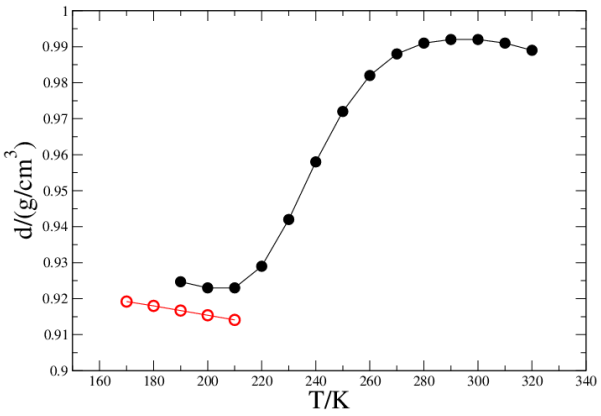

Figure 7.3: Mass density (d) of the liquid (filled circles) and ice Ih (open circles) of the TIP4P/ICE model of water as obtained along the $p = 1bar$ isobar.

density located at about $210K$. The density of ice Ih (and its potential energy) are always lower than those of the fluid phase. The behavior of the density curve is similar to that found[98] for TIP4P/2005 although the extrema are shifted by about 20K. In

Fig. 7.4. the isothermal compressibility (as obtained from volume fluctuations) along the room pressure isobar is presented and compared to experimental results[99–101] . The agreement with experiment is quite good. As can be seen it has a maximum located at about 245K. Again the location of the maximum is shifted by about 15-20K with respect to the maxima obtained with the TIP4P/2005 model.[102,103] At the temperature of the maximum, the equilibration time is of the order of half nanosecond (i.e the time require to diffuse one molecular diameter). Our runs lasted around 500ns so that each molecule moved around 1000 molecular diameters. At the temperature of the maximum in compressibility the crystallization time (see the discussion later in the paper) is of the order of seconds. Therefore the maximum in compressibility (which locates a point of the Widom line) is a real equilibrium feature of the model. It has been suggested by Limmer and Chandler[104–106] that these maxima may be due to the transient formation of ice and that generated some debate in the literature[107–109] but it seems that this is certainly not the case for the TIP4P/ICE model.

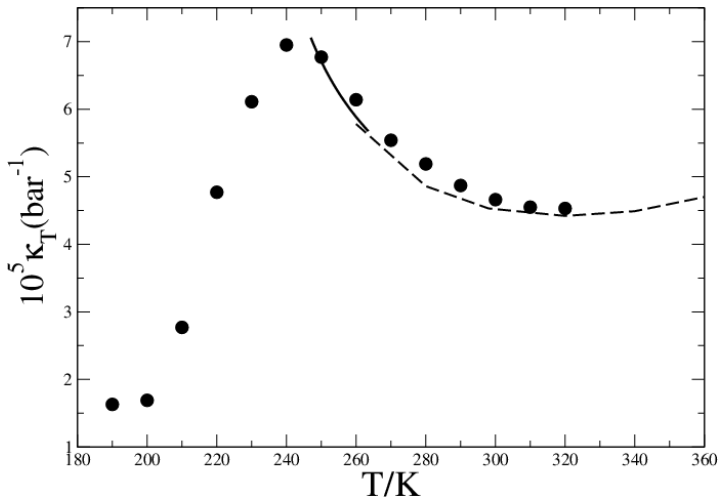

Figure 7.4: Isothermal compressibility of the TIP4P/ICE along the room pressure isobar as obtained from NpT simulations of the TIP4P/ICE model (symbols) and from experiments from Speedy and Angell at low temperatures[100] and from Kell[99] and Saul and Wagner[101] at moderate temperatures.

The results of the diffusion coefficient are shown in Fig. 7.5. for both the TIP4P/ICE and mW models. TIP4P/ICE underestimates the experimental[110] value of the diffusion coefficient (typically by a factor of two at moderate supercooling and by a factor of 4 at high supercooling) and mW overestimates it by 2-3 orders of magnitude. The value of D for the mW is hardly affected by the temperature whereas that of the TIP4P/ICE decreases significantly. The results of TIP4P/ICE are well described for temperatures

up to 230K by Mode Coupling Theory $D = D_0(T - T_{MCT})^{\alpha}$. The values obtained for T_{MCT} and α, 220.5K and 2.35, are in reasonable agreement with the experimental values, 221K and 2.2 respectively. The value of T_{MCT} for TIP4P/ICE is about 12K above that obtained for TIP4P/2005.[111] For temperatures below 230K the results are better described by an Arrhenius expression $D = D^* \exp(-E_a/(RT))$. This change in the variation of D with temperature is sometimes denoted as the fragile-strong transition[112]. For TIP4P/ICE this change seems to be located at 230K. The fragile to strong transition for supercooled water for TIP4P/2005 has been studied in detail recently by de Marzio et al.[94] and by Wong, Jahn, and Giovambattista[111]. The parameters of the fit for D of TIP4P/ICE (both for temperatures above 230K and for temperatures below) are shown in the inset of Fig.7.5

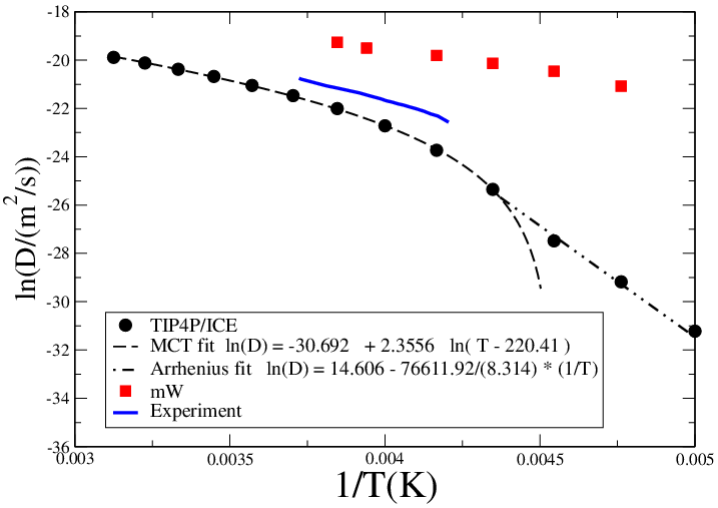

Figure 7.5: Diffusion coefficient D (in m^2/s) for the TIP4P/ICE and mW models of water. Experimental results have also been included.[110]

7.4.4. Estimating the nucleation rate J

The nucleation rate J will be estimated from the treatment of Becker and Doring[73] (often used when implementing the umbrella sampling technique[113–115])

$$J = \rho_f Z f^+ \exp(-\Delta G_c/(k_B T)) \tag{7.4}$$

where (ρ_f) is the number density of the fluid phase, Z is the Zeldovich factor, ΔG_c is the free energy barrier for the formation of the critical cluster and f^+ the attachment rate of particles to the critical cluster. The Zeldovich factor[3] is related to the curvature of the free energy surface on the top of the free energy barrier whose Classical Nucleation

Theory expression is $Z = \sqrt{|\Delta\mu|/(6\pi k_B T N_c)}$ where $\Delta\mu$ is the difference in chemical potential between the fluid and the solid phases at the temperature of interest. f^+ can be computed as a diffusion coefficient of the cluster size at the top of the barrier. We have recently shown that for a number of different systems (including water) f^+ is well described by the CNT expression[66,67,116]:

$$f^+ = \frac{24D(N_c)^{2/3}}{\lambda^2} \tag{7.5}$$

where N_c is the number of molecules of the critical cluster (so that $N_c^{2/3}$ is proportional to the number of molecules at the cluster's surface) and $\lambda^2/(6D)$ is the time required for a molecule to diffuse a given length λ (D being the self-diffusion coefficient of the supercooled liquid). Using a value of λ of the order of one molecule diameter gives a good estimate of f^+. Following our previous work[67] we use a value of λ of 3,8 Å for TIP4P/ICE and of 2,5 Å for the mW model of water. The values of the diffusion coefficient were obtained from this work (for TIP4P/ICE) and from our previous work for mW.[67]

The value of ΔG_c was obtained using the seeding technique is

$$\Delta G_c = N_c|\Delta\mu(T_c)|/2 \tag{7.6}$$

The value of $\Delta\mu$ is obtained by using thermodynamic integration[117] and the condition $\Delta\mu = 0$ at the melting point (270K for the TIP4P/ICE) model. For the TIP4P/ICE at 230K we obtained $\Delta\mu$ = 0,146 kcal/mol, in good agreement with the value 0,147 kcal/mol reported by Haji-Akbari and Debenedetti[96].

Finally, it is also possible to estimate the interfacial free energy γ from the expression (obtained from CNT):

$$\gamma^3 = N_c \frac{3\rho_s^2|\Delta\mu|^3}{32\pi} \tag{7.7}$$

where ρ_s is the number density of the solid phase. In Ref.[65–68] we have already presented all possible sources of errors coming from applying the seeding technique.

To compute N_c we considered three clusters having approximately 8000,3000 and 600 molecules inserted in the supercooled liquid. Results of the NpT runs for these three clusters for the TIP4P/ICE model are presented in Figs. 7.6 7.7 and 7.8 and in Table 7.4.

The values of γ (as obtained from Eq.7.7) are presented in Fig.7.9 and Table 7.4 together with γ for the planar interface at coexistence obtained using the mold integration technique[74,92] (the value presented corresponds to the average obtained for the two prismatics and the basal planes). Fitting the values of γ to a straight line, we find a slope of about -0.27mJ/(m^2K), similar to the slope used in Ref.[118] to reproduce the experimental values of J and consistent with the slope presented in figure 10 of

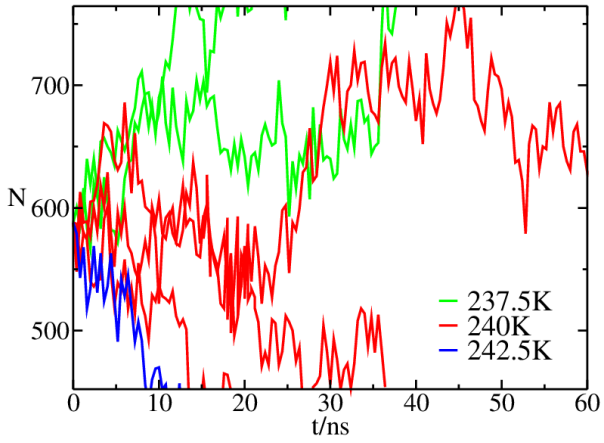

Figure 7.6: Time evolution of ice Ih cluster with 588 molecules for several temperatures. Different lines with the same color indicate trajectories with different initial velocities.

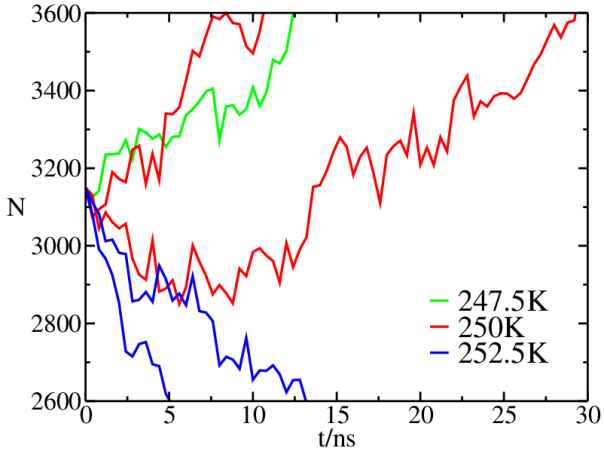

Figure 7.7: Time evolution of ice Ih cluster with 3150 molecules. Details as in Fig.7.6.

Ref.[22]. Fig.7.9 also represents the values of γ obtained from the seeding technique (for temperatures below the melting point) and from the mold integration technique for the mW model: they are larger than those of the TIP4P/ICE model and their decrease with the supercooling is less pronounced (the slope is -0.14mJ/(m^2K)). For the TIP4P/2005 model Reinhard and Doye[119] reported a value for the slope of -0.18(mJ/(m^2K) which is between the values obtained here for the TIP4P/ICE and mW models.

Now it is possible to obtain values of J for a wide range of temperatures by making use of a fit of the densities of the solid and fluid phases , a fit of the diffusion coefficient of liquid water, a fit of $\Delta\mu$ and a fit of γ as a function of T. The results of J for the TIP4P/ICE are shown in Fig.7.10, together with results for the mW model obtained from

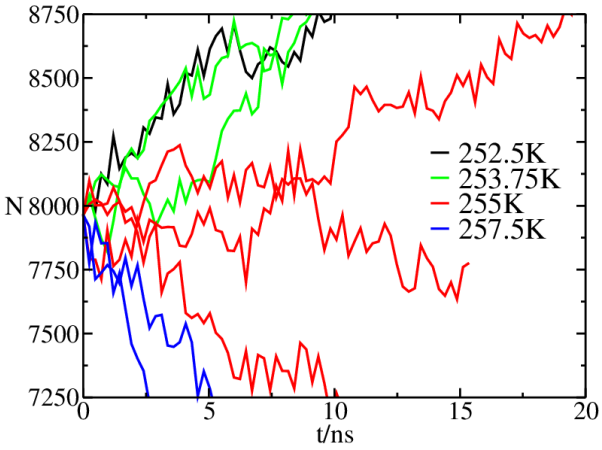

Figure 7.8: Time evolution of ice Ih cluster with 7964 molecules. Details as in Fig.7.6.

Table 7.4: Results for TIP4P/ICE model of water. N_c is the size of the solid cluster inserted in the liquid. N_{H_2O} is the total number of molecules of water used in the simulation, T_c is the temperature at which the cluster is critical, $q_{6,t}$ is the threshold value of the order parameter[82] used to distinguish liquid and solid particles (using the mislabeling criterion) and γ is the interfacial ice Ih-fluid free energy as obtained from Eq.7.7.

N_c	N_{H_2O}	T_c/K	$q_{6,t}$	$\gamma/(mJ/m^2)$
588	22712	238.75	0.372	21.4
3150	76781	251.25	0.364	24.2
7964	182585	255.0	0.361	26.9

the seeding technique in our previous work.[66] The values of J for a given supercooling are higher for TIP4P/ICE than for mW. Although the attachment rate f^+ is higher for mW (by about two to three orders of magnitude), its higher interfacial free energy causes a lower value of J.

Our results are qualitatively consistent with the results of Debenedetti and co-workers who computed J using forward flux sampling[120] for a supercooling of about 30K for both models[96,121] They found that the nucleation rate of TIP4P/ICE at 230K was about seven orders of magnitude larger than the nucleation rate of mW at 235K. However from a quantitative point of view the agreement is not so good, as the values of J for TIP4P/ICE at 230K from this work are about 14 orders of magnitude larger than those obtained by Haji-Akbari and Debenedetti from the more rigorous FFS technique. This certainly points out the approximate character of the seeding technique. However the deviation with respect to the results of Geiger and Dellago[122] goes in the opposite

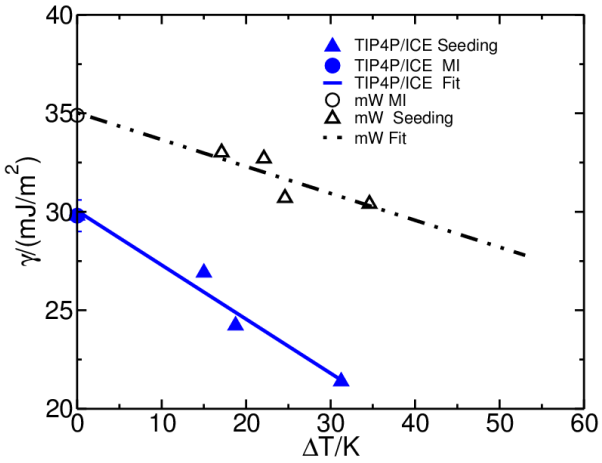

Figure 7.9: γ versus supercooling for the TIP4P/ICE and mW models of water as obtained from seeding (for temperatures below melting) and from mold integration (at the melting point). The fit to the results for the mW model is given by $\gamma(mJ/m^2) = 35{,}028 - 0{,}13648(274{,}6 - T)$. The fit for TIP4P/ICE model are $\gamma(mJ/m^2) = 30{,}044 - 0{,}27477(270 - T)$.

direction as in this case our work predicts a free energy barrier for nucleation at 235K of 56 k_BT which is higher than the value of 35 k_BT reported by Geiger and Dellago[122] at this temperature. Certainly further work is needed to clarify these discrepancies. In previous work[66,116] deviations of about 3-4 orders of magnitude between the predictions from seeding and those obtained from more rigorous techniques were found at high supercooling for systems as varied as hard spheres, LJ, NaCl and the mW model of water. The deviations found here for the TIP4P/ICE model are larger. Since there is only one result reported for J of the TIP4P/ICE obtained from the FFS technique and only one estimate of the free energy barrier it would be useful to have more values to compare with. This is especially relevant as, for the mW model, the values of J at 235K obtained from FFS may be as different as $10^{-1}/(m^3s)$[121] and $10^6/(m^3s)$[60] . It is also interesting to point out that even for the well studied hard spheres system the values of J at moderate saturation (i.e reduced pressure of 15) from FFS are about about 2-3 orders of magnitude lower than those obtained from umbrella sampling[114,123].

In Fig.7.11 we compare our values of J both for mW and TIP4P/ICE to the experimental results . The agreement of TIP4P/ICE with experiments is quite reasonable. The mW model seems to underestimate the experimental nucleation rate due to its large value of γ.

The agreement of the TIP4P/ICE model may be fortuitous as the seeding technique may be overestimating the nucleation rate of the TIP4P/ICE model (and this

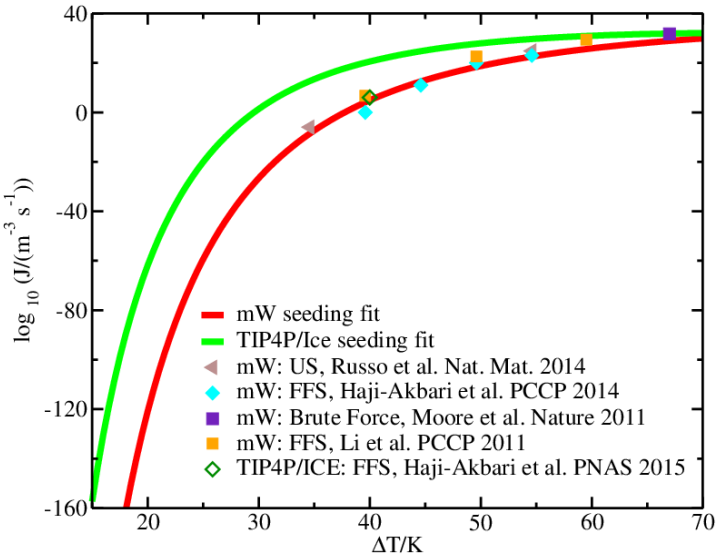

Figure 7.10: Values of the nucleation rate J for the TIP4P/ICE and mW models of water as obtained from seeding (solid lines). Results for seeding of TIP4P/ICE are from this work. Results for seeding of mW are from our previous work[66]. Results obtained from other works (symbols): mW by Russo et al.[61], Haji-Akbari et al.[121], Moore et al.[50], and Li et al.[60]; and TIP4P/ICE obtained from FFS by Haji-Akbari et al.[96].

issue should be clarified in future work). One reason to support the idea that the TIP4P/ICE can not reproduce the experimental results is the fact that its melting enthalpy (1,29kcal/mol) is about ten per cent lower than the experimental value of 1,44kcal/mol. Thus one may expect that the values of $\Delta\mu$ for the model (at a certain supercooling) may be about ten per cent lower. Since the driving force for nucleation in the model is lower than in experiments that would suggest lower nucleation rates. However $\Delta\mu$ is not the only variable that plays a role. The interfacial free energy γ also plays an important role[124–127]. According to the Turnbull rule the interfacial free energy at the melting point is correlated with the melting enthalpy. In fact for the TIP4P models (TIP4P,TIP4P/2005 and TIP4P/ICE) we have found that the value of γ increases with the melting enthalpy of the model. Thus it is possible that the value of γ for real water is higher than for the TIP4P/ICE model. Experimental values of γ between 26 and 35 mJ/m^2 have been reported[128,129] so this hypothesis can not be discarded. The free energy barrier for nucleation (from CNT) at a certain temperature is given by:

$$\Delta G_c = \frac{16\pi\gamma^3}{3\rho_s^2|\Delta\mu|^2}. \tag{7.8}$$

Therefore the free energy barrier for nucleation for real water could be ten per cent

higher than that found for the TIP4P/ICE model (notice that γ appears to the third power and $\Delta\mu$ to the second power). That could yield values of J for the model slightly larger than in experiments even though the melting enthalpy of the model is lower. This tentative explanation could justify why the values of J for the TIP4P/ICE model are slightly higher than those found in experiments as shown in Fig.7.11.

In any case, and even admitting that the good agreement with experiments shown by TIP4P/ICE can be due to a fortuitous cancellation of errors (i.e underestimates $\Delta\mu$ and γ) it is gratifying to see that a molecular approach can reproduce the experimental results so well over a broad range of temperatures. In contrast to empirical correlations of J[22,130], where it is difficult to test the validity of each term of the fit, here we present a molecular (although admittedly still incomplete) perspective.

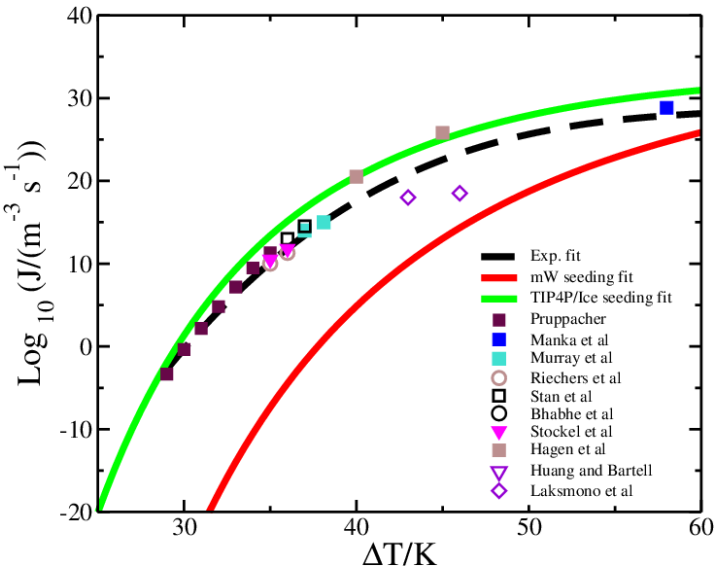

Figure 7.11: Values of logarithm of J for the TIP4P/ICE and for the mW model as obtained in this work from the seeding technique (solid lines) and from experimental results[22,24,25,29–32,34–36,131] (symbols). The experimental results (for $log_{10}(J/(m^3/s))$) were fitted to the following expression -154.59+8.5035 ΔT -0.13304$(\Delta T)^2$ +0.00070129$(\Delta T)^3$ where $\Delta T = 273{,}15 - T$ and they are shown as a dashed line. All experimental results (symbols) shown in this figure were included in the experimental fit.

Finally there is another issue that should be discussed. The experimental values for J shown in Fig.7.11 are quite similar for all temperatures above 232K. Below this temperature they are grouped in two families. The one with the results of Manka et al.[34] and Hagen et al.[31], and the ones with the results of Laksmono et al[131]. We shall return to this issue later in this paper.

7.4.5. Determining τ_{Avrami}

Once the values of u and J for the TIP4P/ICE and mW models have been determined it is time to determine τ_{Avrami} using Eq.7.1. Eq.7.1 is the linearized version of a more sophisticated expression that reads :

$$\phi = 1 - \exp\left(\frac{-\pi J u^3 \tau_{Avrami}^4}{3}\right) \tag{7.9}$$

For long times ϕ should go to one, and this is the case for the non-linearized version of the Avrami equation. In this work values of τ_{Avrami} will be obtained using $\phi = 0{,}7$. For this volume fraction the differences in τ_{Avrami} between both expressions are very small.

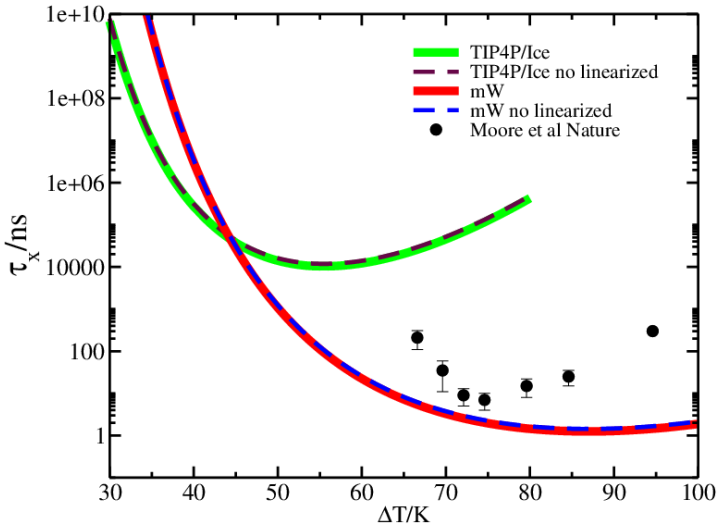

Figure 7.12: Crystallization time for $\phi = 0{,}7$ (lines) for mW and TIP4P/ICE models of water as obtained from the Avrami equation (both for the linearized Eq.7.1 and for non-linearized 7.9 expression). These plots are also denoted as time-temperature-transformation (TTT). The results of the seeding technique were used to estimate J. The growth rates were taken from this work. Simulations results (symbols) for τ from brute force simulations of Moore and Molinero[50] for the mW model of water (with about 4000 molecules and $\phi = 0{,}7$) are also shown.

In Fig.7.12 τ_{Avrami} for the TIP4P/ICE and mW models of water is shown. The value of τ_{Avrami} decreases as the supercooling increases, reaches a minimum and then increases again.[132] The reason is that J increases slowly at high supercoolings (even reaching a maximum) and u decreases very quickly. The fast decrease in u with the supercooling provokes the increase in τ_{Avrami}. For the mW model the minimum in τ_{Avrami}

is about one nanosecond. A comparison with the brute force simulations of Moore and Molinero[50] for τ is also shown in Fig.7.12. The minimum crystallization time found by Moore and Molinero is of about ten nanoseconds. The agreement although not perfect is reasonable. The Avrami expression is rather flat around the minimum when compared to the simulation results[50]. At the left of the minimum this can be explained taking into account that for the system size studied by Moore and Molinero the crystallization time corresponds to the nucleation time (this issue will be discussed more deeply in the next subsection when presenting the results of Fig.7.13). However, we do not have an explanation about the origin of the discrepancies on the right hand side of the minimum. Certainly further work is needed to clarify this issue. Most likely our estimates of J at these temperatures may have large errors since they were obtained by extrapolating the results obtained at moderate supercooling. It would also be interesting to test the validity of the assumptions behind Avrami expression and also performing simulations for larger system sizes.[133]. In any case the Avrami's expression used in this work is able to describe to within one order of magnitude the minimum of the crystallization time found by Moore and Molinero in their brute force simulations. For the TIP4P/Ice model the minimum in τ_{Avrami} is of about ten microseconds, four orders of magnitude higher than for mW.

To avoid the crystallization of the sample one should cross the region around the minimum (say 50K) in less than about 1/10 of the time of the minimum. For the mW model that yields a cooling rate of $50K/(1ns) = 5 \times 10^{10} K/s$. This is comparable with the cooling rate of $10^{10} K/s$ used by Moore and Molinero[50] for the mW model to avoid crystallization and to obtain a glass[50]. For TIP4P/ICE the results of this work suggest a minimum cooling rate of $50K/(1\mu s) = 5 \times 10^{7} K/s$ to obtain the glass. In real water the minimum cooling rate[75–77] to avoid crystallization is of about $10^{7} K/s$ in good agreement with the predictions of this work for TIP4P/ICE. The main reason for the difference of τ_{Avrami} at the minimum between mW and TIP4P/ICE is the large difference in u for both models which seems to be the dominant factor as it appears to the minus three fourths power in Avrami's expression as compared to J that appears to the minus one fourth power.

7.4.6. Nucleation versus Avrami time

Another interesting issue is that τ_{Avrami} as given by the Avrami expression (linearized or not) depends only on the intensive variables J and u. Therefore, the time required to freeze a certain fraction of a system does not depend on the system size. Could this be the case? Quite often to form the solid phase one must wait for a long time before a critical nucleus is formed: after that the growth of the solid phase is very fast. In this

case τ is not given by the Avrami expression but rather by the nucleation time τ_n

$$\tau = \tau_n = 1/(JV) \tag{7.10}$$

When τ is controlled by nucleation, it depends on the system size. The larger the system, the lower the time one has to wait to freeze a certain fraction of the sample. How to conciliate both descriptions (i.e the Avrami expression τ_{Avrami} which does not depend on the system size and τ_n which depends on the system size) ? Berg and co-workers[134] (among others[135,136]) addressed this issue some time ago. To illustrate the problem we shall present both τ_{Avrami} and τ_n for a system having the same number of water molecules as a spherical droplet with a radius of 5μm (a typical size in experiments). It should be pointed out that in our simulations we do not have droplets with a free surface since we are using periodic boundary conditions but there is no reason why we could not estimate τ_n for the TIP4P/ICE model for a system having a similar number of water molecules as that found in droplets of 5 μm of radius in real water.

In Fig.7.13 τ_{Avrami} and τ_n are presented for this droplet. As can be seen τ_n decreases very quickly as the supercooling increases and at a certain temperature which we shall denote as $\Delta T_J(N)$ it crosses the crystallization time given by the Avrami expression. An approximate picture of the problem is that for supercoolings smaller than $\Delta T_J(N)$, the crystallization is controlled by nucleation and τ can be approximated by τ_n, and for supercoolings larger than $\Delta T_J(N)$ the crystallization is controlled by the ice growth and τ is given approximately by τ_{Avrami} (even when using the Avrami expression the value of J matters, but since u appears elevated to the minus three fourths power it plays a crucial role so that it seems adequate to call this region the growth-controlled region). The notation $\Delta T_J(N)$ reminds us that the supercooling at which the crossover from nucleation-controlled to growth-controlled occurs depends on the system size. Let us now define τ_x as :

$$\tau_x = max(\tau_{Avrami}, \tau_n) \tag{7.11}$$

From the definition τ_x is given by τ_n for supercoolings up to ΔT_J and by τ_{Avrami} for higher supercoolings. τ_x is plotted in Fig.7.13 as thick solid lines. Therefore we suggest to approximate the crystallization time of water τ as :

$$\tau \simeq \tau_x \tag{7.12}$$

At this point it is pertinent to introduce a remark: the transition from the nucleation to the growth-controlled regime does not occur in an abrupt manner. Rather one should expect a smooth transition from τ_n to τ_{Avrami} for temperatures around $\Delta T_J(N)$ (some empirical suggestion has been proposed for obtaining such a smooth transition in Eq.(26.42) in the book by Kashchiev[135] , in Eq.(16) in the review of Li and Rutledge[136] or in the work of Berg and coworkers[134]).

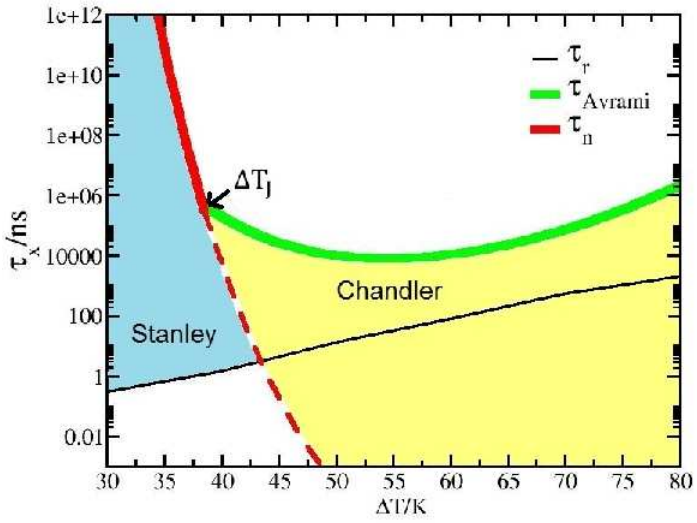

Figure 7.13: Crystallization time τ_x as defined in the main text (thick solid lines) as predicted for the TIP4P/ICE model of water for system containing the same number of water molecules as a droplet of water with a radius of 5μm. At high supercoolings τ_x is given by the Avrami expression (i.e Eq.7.1 with $\phi = 0{,}7$). At low supercoolings the crystallization is controlled by nucleation and τ_x is given by τ_n (i.e we neglect the time required for the growth of the solid phase after a critical cluster is formed). The black thin solid curve is the relaxation time τ_r , which was estimated as the time required for the molecules to move one molecular diameter. For the definition of Chandler's and Stanley's region, see the main text. ΔT_J is the supercooling at which the crossover from nucleation to growth controlled crystallization occurs.

However, and even taking into account that the transition from nucleation to growth-controlled crystallization should be smooth, our picture indicating that the transition should occur around $\Delta T_J(N)$ is qualitatively correct. From the results of this work for TIP4P/ICE (with J estimated from the seeding approach and u determined from direct coexistence simulations) it is clear that the transition from nucleation to growth-controlled crystallization for a droplet of 5μm occurs for a supercooling located around forty degrees. It is interesting to mention that $\Delta T_J(N)$ will move to lower/higher supercoolings as the size of the system becomes larger/smaller.

7.4.7. Can one use τ to estimate J?

We wish to propose an interesting question. Experimentally one determines τ which is the time required to freeze the majority of a sample. The question arises whether one

can use τ to determine the nucleation rate J.

The answer to this question is affirmative when for the conditions considered (system size and supercooling) crystallization is controlled by nucleation, but it is negative when the crystallization is controlled by crystal growth (one could in principle use Avrami's equation in this case but since the experimental value of u is in general completely unknown one can not determine J).

Of course the problem is that in general from experiments one simply gets τ but has no a priori information on whether one is in the nucleation or in the growth controlled regime. However, there is a simple experiment to test this. One could repeat the experiment using a system with say half the size of the initial sample. If one is in the nucleation-controlled regime the crystallization time τ should increases by a factor of two. If this is the case, one can indeed determine J from τ and besides J will be independent of the system size. Conversely, if the crystallization time does not change when the size of the system increases, one may suspect one is in the growth-controlled regime.

Another physical interpretation is that τ is given by Avrami's expression whenever for the system size considered there is already a critical cluster in the system for times much smaller than τ_{Avrami}.

7.4.8. Crossover from nucleation to growth-controlled crystallization

Let us now obtain a mathematical expression for the crossover radius, R as a function of ΔT_J. This is easily done by equating τ_n and τ_{Avrami}. We shall assume that we have a spherical droplet so that V is given by $4/3\pi R^3$. Then one obtains:

$$R = (\frac{3}{4})^{1/3}(\frac{1}{3\phi})^{1/12}(\frac{u(\Delta T)}{\pi J(\Delta T)})^{1/4} = 0{,}64(\frac{u(\Delta T)}{J(\Delta T)})^{1/4} \tag{7.13}$$

where we used $\phi = 0{,}7$ in the last expression.

We could implement this expression for the results of the TIP4P/ICE model. However since our aim is to provide a guide to experimentalist we shall use a hybrid approach. The value of J will be obtained from a fit to the experimental results of J, as shown in Fig.7.11 as a dashed line. For u we shall use the values obtained for the TIP4P/ICE model. After all they seem to agree well with experimental values, at least for small supercoolings.

In Fig.7.14 the value of R as a function of the supercooling ΔT is shown. For each supercooling τ is controlled by nucleation for a radius smaller than $R(\Delta T_J)$ and by growth for a radius larger than $R(\Delta T_J)$. Also one can state that for each radius there is a maximum supercooling where the crystallization is controlled by nucleation. Up to

this temperature it is correct to assume that τ is given by τ_n and to compute J from Eq.7.10. For supercoolings larger than this τ will be given by the Avrami expression and it is necessary to use the value of u to compute J correctly. In Fig.7.14 we have included the radius and supercoolings considered in different experimental works. As can be seen all of them fall into the nucleation controlled regime. The only exception are the results of Laksmono et al.[131] that fall into the growth controlled regime. As can be seen in the figure for a droplet of a radius of 5μ m (which is roughly the size considered by Laksmono et al.[131]) the maximum supercooling where crystallization is controlled by nucleation is about 41K, which corresponds to a temperature of about 232K. We would like to point out that we are by no means questioning the experiments nor the values reported for τ by Laksmono et al.[131]. We are just suggesting that their results may fall into the growth controlled regime so that it may not be possible to directly determine J from τ.

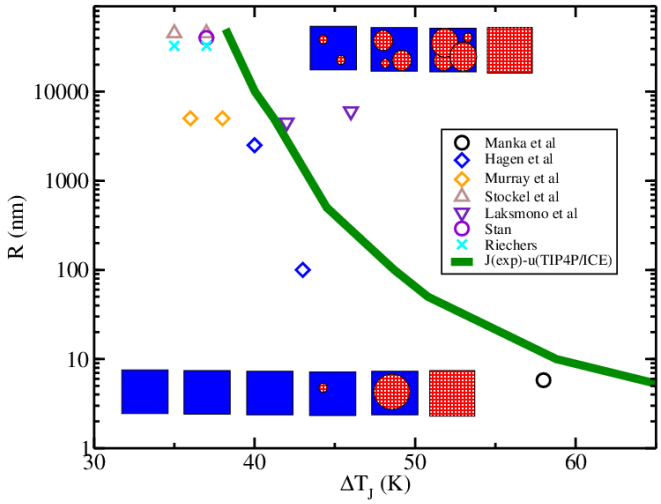

Figure 7.14: Radius R of the droplet where the crossover from nucleation to growth controlled crystallization occurs for a certain supercooling as given by Eq.7.13 using a fit to the experimental values of J and the values of u for the TIP4P/ICE model obtained in this work. The snapshots illustrate the two different mechanisms for crystallization. On the left side of the solid line, once a critical cluster is formed the system freezes very quickly since the growth rate of ice is very fast. On the right hand side critical clusters (which grow slowly) are formed steadily.

7.4.9. Possible role of the internal pressure versus heterogeneous nucleation in the small droplets

Since the value of J for a certain temperature should be unique it is necessary to provide an explanation of why different experimental values of J have been reported for a same supercooling (see the symbols in Fig.7.11). This is a problem for the entire community studying the nucleation of supercooled water.

The tentative hypothesis of this work is that for droplets of radius of $5\mu m$ it is possible to identify τ with τ_n only for temperatures up to 232K. For lower temperatures (i.e higher supercoolings) we suggest that one may fall into the growth controlled regime so that it may not be possible to obtain J from τ. However there are other possible explanations.

The first is that for small droplets (of size less than a few hundreds of nm) the internal pressure is high so that the results obtained do not correspond to room pressure. This is certainly true. However it is unlikely that this is sufficient to explain the large differences between the results of Laksmono[131] and those of Hagen et al.[31] and Manka et al.[34]. First, the internal pressure is never too large (about 500bar for the smallest drop of Manka et al.[34], which we included in Fig.7.11 and 15bar for the drops of Hagen et al.[31]) . Secondly, applying pressure should reduce J (and not to increase it) since the melting point of ice decreases with pressure so that for a certain value of T the supercooling would be lower. Besides this, the experimental results of Kanno, Speedy and Angell[137] show that pressure makes nucleation more difficult since the homogeneous nucleation temperature is more distant from the melting curve when pressure is applied and we have provided recently an explanation for that[69]. The results of Molinero and coworkers for nanometer droplets are also consistent with the idea that pressure decreases the nucleation rate.[138] In summary, if pressure were responsible one should expect that the values of J of Hagen et al.[31] and Manka et al.[34] should be lower than those of Laksmono[131].

The second possibility is that for small droplets the nucleation starts at the surface and that enhances the value of J in small droplets with respect to large droplets (i.e large surface to volume ratio). This is an interesting hypothesis that could indeed explain the discrepancies. If this were the case then the surface would dramatically enhance the nucleation rate. However Haji-Akbari et al.[121] have found for the mW model that the nucleation rate J in a system with a planar interface are slightly lower than those of a system without an interface. Vrbka and Jungwirth[139] found some indirect evidence of the opposite for a different water model although nucleation rates were not reported. The results obtained from seeding for the TIP4P/ICE model (for a system having no vapor-liquid interface) for J seem to be consistent with those obtained for small droplets suggesting that neither pressure nor surface play a dramatic role.

For the time being it is difficult to conclude which is the correct explanation for the

origin of the discrepancies in J from different groups (internal pressure, surface freezing or the crossover suggested in this work). Further work is needed to unravel this issue.

7.4.10. Can we equilibrate a liquid before it freezes?

An interesting question raised by Limmer and Chandler is if the liquid can be equilibrated before it freezes[104,106]. In Fig.7.13 the relaxation time τ_r (as given by the diffusion criteria) is also shown. As can be seen τ_x is always larger than τ_r. The difference is of many orders of magnitude at moderate supercooling and of just two orders of magnitude in the region where τ_x is minimum (in the Avrami region).

However we should distinguish two regions in this plot. In the so-called Chandler region, critical solid nuclei are formed steadily and they keep growing slowly. The system is indeed transient and it is not possible to determine the properties of the supercooled liquid in this region. Whereas in the so-called Stanley region no critical cluster is formed before the liquid equilibrates (although certainly some subcritical clusters will be formed[140,141] from time to time that could indeed be regarded as equilibrium fluctuations of the fluid phase), and since the crystallization time is much larger than the equilibration time it seems possible to determine the thermodynamic properties of the supercooled liquid.

These two regimes (Stanley's and Chandler's) are visible in the mean first passage time[142] plots of Moore and Molinero.[50] Notice that the sizes of the Stanley's and Chandler's regions depends on the system size as their border is given by τ_n which indeed depends on the system size (Eq.10). The red line shown in Fig.7.13 will move to the right for smaller systems and to the left for larger ones (the green and black lines in principle are not affected by the size of the system).

The reader may wonder how we estimated (in Fig.7.13) the relaxation time in the Chandler's region where the system is transient for droplets of 5 μm of radius. The explanation is that to estimate τ_r we used simulations results for a system having 2000 molecules of water so that for this small size the system is still in the Stanley's regime and is not transient. We also assume that the relaxation time is not size dependent (at least in the absence of critical solid clusters). The reason why the system is transient in the Chandler region of Fig.13 is not because the molecules do not have enough time to diffuse before they freeze but rather that critical clusters are formed in times comparable to the time required to diffuse. Notice also that all our seeding runs, were obtained in the region controlled by nucleation (i.e the Stanley region) so that the system was also not transient under these conditions.

Strictly speaking in the thermodynamic limit ΔT_J will go to zero. Thus the Chandler region will dominate all the behavior of the supercooled fluid. In fact in the thermodynamic limit the supercooled liquid is transient as there will always be critical solid clusters formed steadily and the system would evolve slowly to the solid phase.[143,144].

However, often experimentalists are able to measure thermodynamic properties of supercooled liquids.[145] This is so because real systems are always of limited size, so there will always be a Stanley region. The only way to push the Stanley region to the right (i.e to high supercoolings) is to decrease the size of the system. Not surprisingly and due to the extraordinary small system size used in computer simulations (by experimental standards) it was in computer simulations where it was possible to push the Stanley region to temperatures never explored before in experimental work and to learn about the extraordinary anomalous behavior of water in this region.[107,146–149]

7.5. Conclusions

In this work the seeding methodology is applied to the study of homogeneous nucleation of TIP4P/ICE water. We improved the accuracy of the calculations by using several runs for each temperature, using a smaller grid of temperatures and correcting the temperature of the melting point. The growth rate was also determined for the TIP4P/ICE and mW models to estimate the time required to freeze water. The main conclusions of this work can be summarized as follows:

- The values of the interfacial free energy γ obtained from seeding extrapolated to the melting point are consistent with those obtained from the rigorous mold integration technique. The value of γ of the mW model of water is higher than that of the TIP4P/ICE, even though both models have similar melting temperatures and enthalpies.

- Values of J for the mW model are lower than those of the TIP4P/ICE due to its higher interfacial free energy. The differences are higher at moderate supercooling and become smaller at high supercooling where the faster dynamics of the mW model (reflected in a higher attachment rate) partially compensate the higher interfacial free energy.

- The experimental values of J are located between those of the TIP4P/ICE and those of the mW models although they seem to be closer to those of the TIP4P/ICE model.

- The growth rate u of the mW model is between 3 (at moderate supercooling) and 5 (at high supercooling) orders of magnitude higher than that of TIP4P/ICE (when compared at the same supercooling). The growth rate obtained for the TIP4P/ICE is in reasonable agreement with the experimental results, at least for the temperatures at which it was possible to determine it experimentally.

- The minimum in the crystallization time obtained from the Avrami equation for mW is about a few ns, in agreement with the results obtained from brute force simulations[50]. For the TIP4P/ICE this minimum is of about ten microseconds. This value is consistent with the minimum cooling rate required to avoid crystallization and to form a glass phase in experiments[75–77]. The main reason for this difference in the minimum time for crystallization is the growth rate, since the differences in the values of J for these two models are not so large at high supercoolings.

- The compressibility of the TIP4P/ICE model for supercooled water presents a maximum. The relaxation time is much smaller than the crystallization time at the temperature at which this maximum occurs so that this maximum is a real thermodynamic feature of the model. The relaxation time increases with supercooling and it is always smaller than the crystallization time. However for the temperature at which the crystallization time reaches a minimum the difference is of only two orders of magnitude.

- Although the TIP4P/ICE is a simplification of water interactions and the seeding technique is an approximate route to J, we obtain a good overall description of the nucleation rates of real water. This may or may not be due to fortuitous cancelation of errors (approximate model and approximate technique).

- There is a system-size dependent crossover in the crystallization time from the region where it is controlled by nucleation to the region where it is controlled by growth. That could be at the origin of the discrepancies in the values of J reported by different experimental groups although other possibilities such as internal pressure or surface nucleation should not be discarded.

There has been significant progress in our understanding of the nucleation of ice in the recent years. This paper aims to show that simulations can be useful in interpreting the experimental results. However it is obvious that further work is needed. We hope that some of the issues raised in this paper can be clarified in the near future.

Acknowledgements

This work was funded by grants FIS2013/43209-P of the MEC, and by the Marie Curie Integration Grants COSAAC-FP7-PEOPLE-2012-CIG . C.Valeriani and E.Sanz acknowledge financial support from a Ramon y Cajal Fellowship. J. R. Espinosa acknowledges financial support from the FPI grant BES-2014-067625. Calculations were carried out thanks to the supercomputer facility Tirant in the Spanish Supercomputing Network (RES) (through project QCM-2015-1-0028). We thank Prof. Molinero for providing us with the input files to perform runs of the mW model of water using LAMMPS. We thank Dr.McBride for a critical reading of the manuscript and Prof.Abascal for helpful discussions.

Bibliography

1. Zielke, S. A., Bertram, A. K. & Patey, G. N., A molecular mechanism of ice nucleation on model agl surfaces. *J.Phys.Chem.B.* **119**, 9049 (2015).

2. Fraux, G. & Doye, J. P. K., Heterogeneous ice nucleation on silver-iodide-like surfaces. *J.Chem.Phys.* **141**, 216101 (2014).

3. Kelton, K. F., *Crystal Nucleation in Liquids and Glasses* (Academic, Boston, 1991).

4. Sosso, G. C., Chen, J., Cox, S. J., Fitzner, M., Pedevilla, P., Zen, A. & Michaelides, A., Crystal nucleation in liquids: Open questions and future challenges in molecular dynamics simulations. *Chem.Rev.* **116**, 7078 (2016).

5. Sear, R. P., The non classical nucleation of crystals: microscopic mechanisms and applications to molecular crystals, ice and calcium carbonate. *Internat. Materials Rev.* **57**, 328 (2012).

6. McBride, C., Vega, C., Sanz, E., MacDowell, L. G. & Abascal, J. L. F., The range of meta stability of ice-water melting for the TIP4P and SPC/E models. *Molec. Phys.* **103**, 1 (2005).

7. Sear, R. P., Nucleation: theory and applications to protein solutions and colloidal suspensions. *Journal of Physics: Condensed Matter* **19**, 033101 (2007).

8. Avrami, M., Kinetics of phase change. i general theory. *J. Chem. Phys.* **7**, 1103–1112 (1939).

9. Avrami, M., Kinetics of phase change. transformation¿time relations for random distribution of nuclei. *J. Chem. Phys.* **8**, 212 (1940).

10. Kolgomorov, A. N. *Bull. Acad. Sci. USSR, Phys. Ser.* **1**, 355 (1937).

11. Johnson, W. A. & Mehl, P. A. *Trans. Am. Inst. Mining and Metallurgical Engineers* **135**, 416 (1939).

12. Cantrell, W. & Heymsfield, A., Production of ice in tropospheric clouds. *Bull. Amer. Meteor. Soc.* **86**, 795 (2005).

13. Baker, M. B., Cloud microphysics and climate. *Science* **276**, 1072–1078 (1997).

14. DeMott, P. J., Prenni, A. J., Liu, X., Kreidenweis, S. M., Petters, M. D., Twohy, C. H., Richardson, M. S., Eidhammer, T. & Rogers, D. C., Predicting global atmospheric ice nuclei distributions and their impacts on climate. *Proc. Natl. Acad. Sci.* **107**, 11217–11222 (2010).

15. Hirano, S. S. & Upper, C. D., Bacteria in the leaf ecosystem with emphasis on pseudomonas syringae - a pathogen, ice nucleus, and epiphyte. *Microbiol. Molec. Biol. Rev.* **64**, 624 (2000).

16. Maki, L. R., Galyan, E. L., M.M., C. & Caldwell, D. R., Ice nucleation induced by pseudomonas-syringae. *Appl. Microbiol.* **28**, 456–459 (1974).

17. Li, J. K. & Lee, T. C., Bacterial ice nucleation and its potential application in the food-industry. *Trends in Food Sci. & Tech.* **6**, 259–265 (1995).

18. Michaelides, A. & Morgenstern, K., Ice nanoclusters at hydrophobic metal surfaces. *Nature Materials* **6**, 597–601 (2007).

19. Gerrard, A. G., *Rocks and Landforms* (Springer Netherlands, 1988).

20. Morris, G. J. & Acton, E., Controlled ice nucleation in cryopreservation–a review. *Cryobiology* **66**, 85 (2013).

21. Studer, D., High-pressure freezing system (2001), US Patent 6,269,649.

22. Pruppacher, H. R., A new look at homogeneous ice nucleation in supercooled water drops. *J. Atmosph. Sci.* **52**, 1924 (1995).

23. Taborek, P., Nucleation in emulsified supercooled water. *Phys. Rev. B* **32**, 5902–5906 (1985).

24. Stockel, P., Weldinger, I. M., Baumgartel, H. & Leisner, T., Rates of homogeneous ice nucleation in levitated h2o and d2o droplets. *J. Phys. Chem. A* **109**, 2540 (2005).

25. Murray, B. J., Broadley, S. L., Wilson, T. W., Bull, S. J., Wills, R. H., Christenson, H. K. & Murray, E. J., Kinetics of the homogeneous freezing of water. *Phys. Chem. Chem. Phys.* **12**, 10380 (2010).

26. Kuhs, W. F., Sippel, C., Falenty, A. & Hansen, T. C., Extent and relevance of stacking disorder in ice Ic. *Proceedings of the National Academy of Sciences* **109**, 21259–21264 (2012).

27. Malkin, T. L., Murray, B. J., Brukhno, A. V., Anwar, J. & Salzmann, C. G., Structure of ice crystallized from supercooled water. *Proceedings of the National Academy of Sciences* **109**, 1041–1045 (2012).

28. Malkin, T. L., Murray, B. J., Salzmann, C. G., Molinero, V., Pickering, S. J. & Whale, T. F., Stacking disorder in ice i. *Phys. Chem. Chem. Phys.* **17**, 60–76 (2015).

29. Riechers, B., Wittbracht, F., Hutten, A. & Koop, T., The homogeneous ice nucleation rate of water droplets produced in a microfluidic device and the role of temperature uncertainty. *Phys. Chem. Chem. Phys.* **15**, 5873–5887 (2013).

30. Stan, C. A., Schneider, G. F., Shevkoplyas, S. S., Hashimoto, M., Ibanescu, M., Wiley, B. J. & Whitesides, G. M., A microfluidic apparatus for the study of ice nucleation in supercooled water drops. *Lab Chip* **9**, 2293–2305 (2009).

31. Hagen, D. E., Anderson, R. J. & Kassner, J. L., Homogeneous condensation-freezing nucleation rate measurements for small water droplets in an expansion cloud chamber. *J. Atmos. Sci.* **38**, 1236–1243 (1981).

32. Kramer, B., Hubner, O., Vortisch, H., Woste, L., Leisner, T., Schwell, M., Ruhl, E. & Baumgartel, H., Homogeneous nucleation rates of supercooled water in single levitated microdroplets. *J. Chem. Phys.* **111**, 6521 (1999).

33. Mishima, O., Volume of supercooled water under pressure and the liquid-liquid critical point. *J. Chem. Phys.* **133**, 144503 (2010).

34. Manka, A., Pathak, H., Tanimura, S., Wolk, J., Strey, R. & Wyslouzil, B. E., Freezing water in no man's land. *Phys. Chem. Chem. Phys.* **14**, 4505–4516 (2012).

35. Huang, J. & Bartell, L. S., Kinetics of homogeneous nucleation in the freezing of large water clusters. *J. Phys. Chem.* **99**, 3924–3931 (1995).

36. Bhabhe, A., Pathak, H. & Wyslouzil, B. E., Freezing of heavy water (d2o) nanodroplets. *J. Phys. Chem. A* **117**, 5472–5482 (2013).

37. Pruppacher, H. R., Interpretation of experimentally determined growth rates of ice crystals in supercooled water. *J. Chem. Phys.* **47**, 1807–1813 (1967).

38. Turnbull, D., Under what conditions can a glass be formed? *Contemporary Physics* **10**, 473–488 (1969).

39. Matsumoto, M., Saito, S. & Ohmine, I., Molecular dynamics simulation of the ice nucleation and growth process leading to water freezing. *Nature* **416**, 409 (2002).

40. Radhakrishnan, R. & Trout, B., Nucleation of hexagonal ice (Ih) in liquid water. *J. Am. Chem. Soc* **125**, 7743–7747 (2003).

41. Radhakrishnan, R. & Trout, B. L., Nucleation of crystalline phases of water in homogeneous and inhomogeneous environments. *Phys. Rev. Lett.* **90**, 158301 (2003).

42. Perez, A. & Rubio, A., A molecular dynamics study of water nucleation using the tip4p/2005 model. *J. Chem. Phys.* **135**, 244505 (2011).

43. Brukhno, A. V., Anwar, J., Davidchack, R. & Handel, R. *J. Phys. Condens. Matter* **20**, 494243 (2008).

44. Quigley, D. & Rodger, P. M., Metadynamics simulations of ice nucleation and growth. *J. Chem. Phys.* **128**, 154518 (2008).

45. Buhariwalla, C., Bowles, R., Saika-Voivod, I., Sciortino, F. & Poole, P., Free energy of formation of small ice nuclei near the widom line in simulations of supercooled water. *Eur. Phys. J. E.* **38**, 39 (2015).

46. Guillot, B., A reappraisal of what we have learnt during three decades of computer simulations on water. *J. Molec. Liq.* **101**, 219–260 (2002).

47. Vega, C. & Abascal, J. L. F., Simulating water with rigid non-polarizable models: a general perspective. *Phys. Chem. Chem. Phys* **13**, 19663–19688 (2011).

48. Cisneros, G. A., Wikfeldt, K. T., Ojamae, L., Lu, J., Xu, Y., Torabifard, H., Bartok, A. P., Csanyi, G., Molinero, V. & Paesani, F., Modeling molecular interactions in water: From pairwise to many-body potential energy functions. *Chem. Rev.* **116**, 7501 (2016).

49. Molinero, E. B., Valeria und Moore, Water modeled as an intermediate element between carbon and silicon. *The Journal of Physical Chemistry B* **113**, 4008–4016 (2009).

50. Moore, E. B. & Molinero, V., Structural transformation in supercooled water controls the crystallization rate of ice. *Nature* **479**, 506 (2011).

51. Cox, S. J., Kathmann, S. M., Slater, B. & Michaelides, A., Molecular simulations of heterogeneous ice nucleation. i. controlling ice nucleation through surface hydrophilicity. *J. Chem. Phys.* **142**, 184704 (2015).

52. Cox, S. J., Kathmann, S. M., Slater, B. & Michaelides, A., Molecular simulations of heterogeneous ice nucleation. ii. peeling back the layers. *J. Chem. Phys.* **142**, 184705 (2015).

53. Cabriolu, R. & Li, T. S., Ice nucleation on carbon surface supports the classical theory for heterogeneous nucleation. *Phys.Rev.E* **91** (2015).

54. Fitzner, M., Sosso, G. C., Cox, S. J. & Michaelides, A., The many faces of heterogeneous ice nucleation: Interplay between surface morphology and hydrophobicity. *J.Am.Chem.Soc.* **137** (2015).

55. Abascal, J. L. F. & Vega, C. *J. Chem. Phys.* **123**, 234505 (2005).

56. Abascal, J. L. F., Sanz, E., Fernandez, R. G. & Vega, C. *J. Chem. Phys.* **122**, 234511 (2005).

57. Jorgensen, W. L., Chandrasekhar, J., Madura, J. D., Impey, R. W. & Klein, M. L., Comparison of simple potential functions for simulating liquid water. *J. Chem. Phys.* **79**, 926 (1983).

58. Bolhuis, P. G., Dellago, C., Geissler, P. L. & Chandler, D., Transition path sampling: throwing ropes over mountains in the dark. *J. Phys.:Condens. Matter* **12**, A147 (2000).

59. Auer, S. & Frenkel, D., Quantitative prediction of crystal-nucleation rates for spherical colloids: A computational approach. *Annu. Rev. Phys. Chem.* **55**, 333 (2004).

60. Li, T., Donadio, D., Russo, G. & Galli, G., Homogeneous ice nucleation from supercooled water. *Phys. Chem. Chem. Phys.* **13**, 19807–19813 (2011).

61. Russo, J., Romano, F. & Tanaka, H., New metastable form of ice and its role in the homogeneous crystallization of water. *Nature Materials* **13**, 733 (2014).

62. Abascal, J. L. F. & Vega, C., Dipole-quadrupole force ratios determine the ability of potential models to describe the phase diagram of water. *Phys. Rev. Lett.* **98**, 237801 (2007).

63. Bai, X.-M. & Li, M., Test of classical nucleation theory via molecular-dynamics simulation. *J. Chem. Phys.* **122**, 224510 (2005).

64. Bai, X.-M. & Li, M., Calculation of solid-liquid interfacial free energy: A classical nuclea tion theory based approach. *J. Chem. Phys.* **124**, 124707 (2006).

65. Sanz, E., Vega, C., Espinosa, J. R., Caballero-Bernal, R., Abascal, J. L. F. & Valeriani, C., Homogeneous ice nucleation at moderate supercooling from molecular simulation. *Journal of the American Chemical Society* **135**, 15008–15017 (2013).

66. Espinosa, J. R., Vega, C., Valeriani, C. & Sanz, E., Seeding approach to crystal nucleation. *J. Chem. Phys.* **144**, 034501 (2016).

67. Espinosa, J. R., Sanz, E., Valeriani, C. & Vega, C., Homogeneous ice nucleation evaluated for several water models. *J. Chem. Phys.* **141**, 18C529 (2014).

68. Zaragoza, A., Conde, M. M., Espinosa, J. R., Valeriani, C., Vega, C. & Sanz, E., Competition between ices ih and ic in homogeneous water freezing. *J. Chem. Phys.* **143**, 134504 (2015).

69. Espinosa, J. R., Zaragoza, A., Rosales-Pelaez, P., Navarro, C., Valeriani, C., Vega, C. & Sanz, E., Interfacial free energy as the key to the pressure-induced deceleration of ice nucleation. *Phys. Rev. Lett.* **117**, 135702 (2016).

70. Pereyra, R. G., Szleifer, I. & Carignano, M. A., Temperature dependence of ice critical nucleus size. *J. Chem. Phys.* **135**, 034508 (2011).

71. Knott, B. C., Molinero, V., Doherty, M. F. & Peters, B., Homogeneous nucleation of methane hydrates: Unrealistic under realistic conditions. *J. Am. Chem. Soc.* **134**, 19544–19547 (2012).

72. Volmer, M. & Weber, A., Keimbildung in ubersattigten gebilden. *Z. Phys. Chem.* **119**, 277 (1926).

73. Becker, R. & Doring, W., Kinetische behandlung der keimbildung in ubersattigten dampfen. *Ann. Phys.* **24**, 719–752 (1935).

74. Espinosa, J. R., Vega, C. & Sanz, E., The mold integration method for the calculation of the crystal-fluid interfacial free energy from simulations. *J Chem. Phys.* **141**, 134709 (2014).

75. Bruggeller, P. & Mayer, E., Complete vitrification in pure liquid water and dilute aqueous-solutions. *Nature* **288**, 569 (1980).

76. Debenedetti, P. G., Supercooled and glassy water. *J. Phys.:Condens. Matter* **15**, R1669–R1726 (2003).

77. Fuentes-Landete, V., Mitterdorfer, C., Handle, P. H., Ruiz, G. N., Bernard, J., Bogdan, A., Seidl, M., Amann-Winkel, K., Stern, J., Fuhrmann, S. & Loerting, T., Crystalline and amorphous ices. *Proceedings of the International School of Physics Enrico Fermi Course 187 Water: Fundamentals as the Basis for Understanding the Environment and Promoting Technology* **doi:10.3254/978-1-61499-507-4-173**, 173 (2015).

78. Lindahl, E., Hess, B. & van der Spoel, D., Gromacs 3.0: a package for molecular simulation and trajectory analysis. *J. Mol. Model.* **7**, 306 (2001).

79. Bussi, G., Donadio, D. & Parrinello, M., Canonical sampling through velocity rescaling. *The Journal of Chemical Physics* **126**, 014101 (2007).

80. Parrinello, M. & Rahman, A., Polymorphic transitions in single crystals: A new molecular dynamics method. *J. App. Phys.* **52**, 7182 (1981).

81. Essmann, U., Perera, L., Berkowitz, M. L., Darden, T., Lee, H. & Pedersen, L. G., A smooth particle mesh ewald method. *J. Chem. Phys.* **103**, 8577–8593 (1995).

82. Lechner, W. & Dellago, C. *J. Chem. Phys.* **129**, 114707 (2008).

83. Vega, C., Martin-Conde, M. & Patrykiejew, A., Absence of superheating for ice ih with a free surface: a new method for determining the melting point of different water models. *Mol. Phys.* **104**, 3583 (2006).

84. Fernandez, R. G., Abascal, J. L. F. & Vega, C., The melting point of ice ih for common water models calculated from direct coexistence of the solid-liquid interface. *J. Chem. Phys.* **124**, 144506 (2006).

85. Weiss, V. C., Rullich, M., KÃ¶hler, C. & Frauenheim, T., Kinetic aspects of the thermostatted growth of ice from supercooled water in simulations. *The Journal of Chemical Physics* **135**, 034701 (2011).

86. Rozmanov, D. & Kusalik, P. G., Anisotropy in the crystal growth of hexagonal ice, ih. *J. Chem. Phys.* **137**, 094702 (2012).

87. Rozmanov, D. & Kusalik, P. G., Temperature dependence of crystal grwth of hexagonal ice (ih). *Phys. Chem. Chem. Phys* **13**, 15501–15511 (2011).

88. Rozmanov, D. & Kusalik, P. G., Isoconfigurational molecular dynamics study of the kinetics of ice crystal growth. *Phys. Chem. Chem. Phys.* **14**, 13010 (2012).

89. Kara, M. & Kurki-Suonio, K., Symmetrized multipole analysis of orientational distributions. *Acta Crystallographica Section A* **37**, 201–210 (1981).

90. Benet, J., MacDowell, L. G. & Sanz, E., A study of the ice-water interface using the TIP4P/2005 water model. *Phys. Chem. Chem. Phys.* **16**, 22159–22166 (2014).

91. Sun, D. Y., Mendelev, M. I., Becker, C. A., Kudin, K., Haxhimali, T., Asta, M., Hoyt, J. J., Karma, A. & Srolovitz, D. J., Crystal-melt interfacial free energies in hcp metals: A molecular dynamics study of mg. *Phys. Rev. B* **73**, 024116 (2006).

92. Espinosa, J. R., Vega, C. & Sanz, E., Ice-water interfacial free energy for the tip4p, tip4p/2005 , tip4p/ice and mw models as obtained from the mold integration technique. *The Journal of Physical Chemistry C* **120**, 8068–8075 (2016).

93. Plimpton, S. *J. Comput. Phys.* **117**, 1 (1995).

94. Marzio, M. D., Camisasca, G., Rovere, M. & Gallo, P., Mode coupling theory and fragile to strong transition in supercooled tip4p/2005 wate. *J. Chem. Phys.* **144**, 074503 (2016).

95. Sciortino, F., Gallo, P., Tartaglia, P. & Chen, S.-H., Supercooled water and the kinetic glass transition. *Phys.Rev.E* **54** (1996).

96. Haji-Akbari, A. & Debenedetti, P. G., Direct calculation of ice homogeneous nucleation rate for a molecular model of water. *Proceedings of the National Academy of Sciences* **112**, 10582–10588 (2015).

97. Vega, C. & Abascal, J. L. F., Relation between melting temperature and temperature of maximum density for the most common models of water. *J. Chem. Phys.* **123**, 144504 (2005).

98. Pi, H. L., Aragones, J. L., Vega, C., Noya, E. G., Abascal, J. L. F., Gonzalez, M. A. & McBride, C., Anomalies in water as obtained from computer simulations of the tip4p/2005 model: density maxima, and density, isothermal compressibility and heat capacity minima. *Molec. Phys.* **107**, 365–374 (2009).

99. Kell, J. S., no se. *J. Chem. Eng. Data* **20**, 97 (1975).

100. Speedy, R. J. & Angell, C. A., Isothermal compressibility of supercooled water and evidence for a thermodynamic singularity at -45 degrees c. *J. Chem. Phys.* **65**, 851–858 (1976).

101. Wagner, W., Saul, A. & Pruβ, A., International equations for the pressure along the melting and along the sublimation curve of ordinary water substance. *J. Phys. Chem. Ref. Data* **23**, 515–527 (1994).

102. Abascal, J. L. F. & Vega, C., Eos supercooled. *J. Chem. Phys.* **134**, 186101 (2011).

103. Bresme, F., Biddle, J. W., Sengers, J. V. & Anisimov, M. A., Minimum in the thermal conductivity of supercooled water: A computer simulation study. *J. Chem. Phys.* **140**, 161104 (2014).

104. Limmer, D. T. & Chandler, D., The putative liquid-liquid transition is a liquid-solid transition in atomistic models of water. *J. Chem. Phys.* **135**, 134503 (2011).

105. Limmer, D. T. & Chandler, D., The putative liquid-liquid transition is a liquid-solid transition in atomistic. *J. Chem. Phys.* **138**, 214504 (2013).

106. Limmer, D. T. & Chandler, D., Time scales of supercooled water and implications for reversible polyamorphism. *Mol.Phys.* **113**, 2799 (2015).

107. Poole, P. H., Sciortino, F., Essmann, U. & Stanley, H. E., Phase behavior of metastable water. *Nature* **360**, 324 (1992).

108. Liu, Y., Palmer, J. C., Panagiotopoulos, A. Z. & Debenedetti, P. G., Liquid-liquid transition in st2 water. *J. Chem. Phys.* **137**, 214505 (2012).

109. Palmer, J., Martelli, F., Liu, Y., Car, R., Panagiotopoulos, A. Z. & Debenedetti, P. G., Metastable liquid-iquid transition in a molecular model of water. *Nature* **510**, 385 (2014).

110. Price, W. S., Ide, H. & Arata, Y. *J. Phys. Chem.* **103**, 448–450 (1999).

111. Wong, J., Jahn, D. A. & Giovambattista, N., Pressure-induced transformations in glassy water: A computer simulation study. *J. Chem. Phys.* **143**, 074501 (2015).

112. Faraone, A., Liu, L., Mou, C.-Y., Yen, C.-W. & Chen, S.-H., Fragile-to-strong liquid transition in deeply supercooled confined water. *J. Chem. Phys.* **121**, 10843 (2004).

113. Auer, S. & Frenkel, D., Numerical prediction of absolute crystallization rates in hard-sphere colloids. *J. Chem. Phys.* **120**, 3015–3029 (2004).

114. Auer, S. & Frenkel, D., Prediction of absolute crystal-nucleation rate in hard-sphere colloids. *Nature* **409**, 1020 (2001).

115. Valeriani, C., Sanz, E. & Frenkel, D., Rate of homogeneous crystal nucleation in molten nacl. *J. Chem. Phys.* **122**, 194501 (2005).

116. Espinosa, J. R., Vega, C., Valeriani, C. & Sanz, E., The crystal-fluid interfacial free energy and nucleation rate of NaCl from different simulation methods. *J. Chem. Phys.* **142**, 194709 (2015).

117. Vega, C., Sanz, E., Noya, E. G. & Abascal, J. L. F., Determination of phase diagrams via computer simulation: methodology and applications to water, electrolytes and proteins. *J. Phys. Condens. Matter* **20**, 153101 (2008).

118. Ickes, L., Welti, A., Hoose, C. & Lohmann, U., Classical nucleation theory of homogeneous freezing of water: thermodynamic and kinetic parameters. *Phys. Chem. Chem. Phys.* **17**, 5514–5537 (2015).

119. Reinhardt, A. & Doye, J. P. K., Note: Homogeneous tip4p/2005 ice nucleation at low supercooling. *J. Chem. Phys.* **139**, 096102 (2013).

120. Allen, R. J., Valeriani, C. & ten Volde, P. R., Forward flux sampling for rare event simulations. *J. Phys. Condens. Matter.* **21**, 463102 (2009).

121. Haji-Akbari, A., DeFever, R. S., Sarupria, S. & Debenedetti, P. G., Suppression of sub-surface freezing in free-standing thin films of a coarse-grained model of water. *Phys. Chem. Chem. Phys.* **16**, 25916–25927 (2014).

122. Geiger, P. & Dellago, C. *J. Chem. Phys.* **139**, 164105 (2013).

123. Filion, L., Hermes, M., Ni, R. & Dijkstra, M., Crystal nucleation of hard spheres using molecular dynamics, umbrella sampling, and forward flux sampling: A comparison of simulation techniques. *J. Chem. Phys.* **133**, 244115 (2010).

124. Davidchack, R. L., Handel, R., Anwar, J. & Brukhno, A. V. *J. Chem. Theory Comput.* **8**, 2383 (2012).

125. Handel, R., Davidchack, R. L., Anwar, J. & Brukhno, A. *Phys. Rev. Lett.* **100**, 036104 (2008).

126. Zobrist, B., Koop, T., Luo, B. P., Marcolli, C. & Peter, T., Heterogeneous ice nucleation rate coefficient of water droplets coated by a nonadecanol monolayer. *J. Phys. Chem. C* **111**, 2149–2155 (2007).

127. Alpert, P. A., Aller, J. Y. & Knopf, D. A., Initiation of the ice phase by marine biogenic surfaces in supersaturated gas and supercooled aqueous phases. *Phys. Chem. Chem. Phys.* **13**, 19882–19894 (2011).

128. Granasy, L., Pusztai, T. & James, P. F., Interfacial properties deduced from nucleation experiments: A cahn–hilliard analysis. *J. Chem. Phys.* **117**, 6157–6168 (2002).

129. Hardy, S. C. *Philos. Mag.* **35**, 471 (1977).

130. Jeffery, C. A. & Austin, P. H., Homogeneous nucleation of supercooled water: Results from a new equation of state. *J. Geophys. Research* **102**, 25269 (1997).

131. Laksmono, H., McQueen, T. A., Sellberg, J. A., Loh, N. D., Huang, C., Schlesinger, D., Sierra, R. G., Hampton, C. Y., Nordlund, D., Beye, M., Martin, A. V., Barty, A., Seibert, M. M., Messerschmidt, M., Williams, G. J., Boutet, S., Amann-Winkel, K., Loerting, T., Pettersson, L. G. M., Bogan, M. J. & Nilsson, A., Anomalous behavior of the homogeneous ice nucleation rate in ¿no-man¿s land¿. *The Journal of Physical Chemistry Letters* **6**, 2826–2832 (2015).

132. Yamada, M., Mossa, S., Stanley, H. E. & Sciortino, F., Interplay between time-temperature transformation and the liquid-liquid phase transition in water. *Phys. Rev. Lett.* **88**, 195701 (2002).

133. English, N. J. & Tse, J. S., Massively parallel molecular dynamics simulation of formation of ice-crystallite precursors in supercooled water: Incipient-nucleation behavior and role of system size. *Phys. Rev. E* **92**, 032132 (2015).

134. Berg, B. A. & Dubey, S., Finite volume kolmogorov-johnson-mehl-avrami theory. *Phys. Rev. Lett.* **100**, 165702 (2008).

135. Kashchiev, D., *Nucleation: Basic Theory with Applications* (Butterworth-Heinemann, Oxford, 2000).

136. Yi, P. & Rutledge, G. C., Molecular origins of homogeneous crystal nucleation. *Annu. Rev. Chem. Biomol.* **3**, 157 (2012).

137. Kanno, H., Speedy, R. J. & Angell, C. A., Supercooling of water to -92^{o}c under pressure. *Science* **189**, 880–881 (1975).

138. Johnston, J. C. & Molinero, V., Crystallization melting and structure of nanoparticles at atmospheric relevant temperatures. *J. Am. Chem. Soc.* **134**, 6650 (2012).

139. Vrbka, L. & Jungwirth, P., Homogeneous freezing of water starts in the subsurface. *J. Phys. Chem. B* **110**, 18126 (2006).

140. Overduin, S. D. & Patey, G. N., Fluctuations and local ice structure in model supercooled water. *J. Chem. Phys.* **143**, 094504 (2015).

141. Overduin, S. D. & Patey, G. N., An analysis of fluctuations in supercooled tip4p/2005 water. *J. Chem. Phys.* **138**, 184502 (2013).

142. Wedekind, J., Strey, R. & Reguera, D., New method to analyze simulations of activated processes. *J. Chem. Phys.* **126**, 134103 (2007).

143. Binder, K., Simulations clarify when supercooled water freezes into glassy structures. *Proceedings of the National Academy of Sciences* **111**, 9374 (2014).

144. Chandler, D., Metastability and no criticality. *Nature* **531**, E1 (2016).

145. Hare, D. E. & Sorensen, C. M., The density of supercooled water. ii. bulk samples cooled to the homogeneous nucleation limit. *J. Chem. Phys.* **87**, 4840 (1987).

146. Mishima, O. & Stanley, H. E., The relationship between liquid, supercooled and glassy water. *Nature* **396**, 329 (1998).

147. Gallo, P. & et. al, Water : A tale of two liquids. *Chem.Rev.* **116**, 7463 (2016).

148. Singh, R. S., Biddle, J. W., Debenedetti, P. G. & Anisimov, M. A., Two-state thermodynamics and the possibility of a liquid-liquid phase transition in supercooled tip4p/2005 water. *J. Chem. Phys.* **144**, 144504 (2016).

149. Ni, Y. & Skinner, J. L., Evidence for a liquid-liquid critical point in supercooled water within the e3b3 model and a possible interpretation of the kink in the homogeneous nucleation line. *J. Chem. Phys.* **144**, 214501 (2016).

Results: Chapter 8

Interfacial free energy as the key to the pressure-induced deceleration of ice nucleation

Jorge R. Espinosa[†], *Alberto Zaragoza*[†], *Pablo Rosales-Pelaez*[†], *Caridad Navarro*[†], *Chantal Valeriani*[†,‡], *Carlos Vega*[†] *and Eduardo Sanz*[†]

[†]Departamento de Quimica Fisica I, Facultad de Ciencias Quimicas, Universidad Complutense de Madrid, 28040 Madrid, Spain.
[‡]Departamento de Fisica Aplicada I, Facultad de Ciencias Fisicas, Universidad Complutense de Madrid, 28040 Madrid, Spain.

8.1. Abstract

The avoidance of water freezing is the holy grail in the cryopreservation of biologycal samples, food and organs. Fast cooling rates are used to beat ice nucleation and avoid cell damage. This strategy can be enhanced by applying high pressures to decrease the nucleation rate, but the physics behind this procedure has not been fully understood yet. We perform computer experiments to investigate ice nucleation at high pressures consisting in embedding ice seeds in supercooled water. We find that the slowing down of the nucleation rate is mainly due to an increase of the ice I-water interfacial free energy with pressure. Our work also clarifies the molecular mechanism of ice nucleation for a wide pressure range. This study is not only relevant to cryopreservation, but also to water amorphization and climate change modelling.

8.2. Introduction

In 1975 Kanno, Speedy and Angell[1] studied experimentally homogeneous ice nucleation (i.e. in the absence of surfaces and impurities) for pressures up to 2000 bar. By measuring the temperature at which microscopic emulsified water drops freeze when cooled at a rate of a few Kelvin per minute they established the so-called homogeneous nucleation line (HNL), whose slope is negative and larger than that of the melting line. Thus, they found that whereas water remains liquid for temperatures down to -38 Celsius at ambient pressure, at high pressures it is possible to have liquid water at temperatures as low as -92 Celsius. Therefore, applying pressure significantly increases the range of temperatures at which liquid water may exist. This important experimental result is the basis of state-of-the art coolers used for the preservation of biological samples[2,3]. Despite its importance, the experiment by Kanno et al. has long remained unexplained.

Using a combination of simulation methods to obtain nucleation rates and interfacial free energies[4–6] we find that the decelerating effect of pressure on ice nucleation is due to the increase of the ice I-water interfacial free energy. This conclusion is supported by both studied models: TIP4P/Ice[7] (main text) and the mW[8] (Supplementary Material, SM). These findings have implications in cryopreservation[2], water vitrification[9,10] and planetary and atmospheric science[11,12]. The importance and broad impact of simulation studies of crystal nucleation, and notably for water, are highlighted in a very recent review[13].

8.3. Results

To perform this research we use the seeding method[4,5,14,15], which is a computer experiment that consists in embedding an ice cluster in the supercooled fluid and following its evolution in a Molecular Dynamics simulation at constant pressure and temperature (see SM for simulation details) to determine the critical cluster size. In Fig. 8.1(a) we show the number of molecules in the critical cluster, N_c, as a function of the supercooling, ΔT (the difference between the melting temperature, T_m, and the temperature of interest), for 1 and 2000 bars. We insert spherical ice Ih clusters (according to our previous work we do not expect differences if ice Ic had been considered instead[16]). Clearly, the supercooling at which a certain cluster size is critical increases with pressure. This result already points to the experimental observation that pressure hinders ice nucleation.

In order to know for certain whether nucleation is slowed down with pressure one needs to evaluate the nucleation rate, J (the number of critical clusters that nucleate per unit time and volume). Classical Nucleation Theory (CNT)[20–22] gives the following

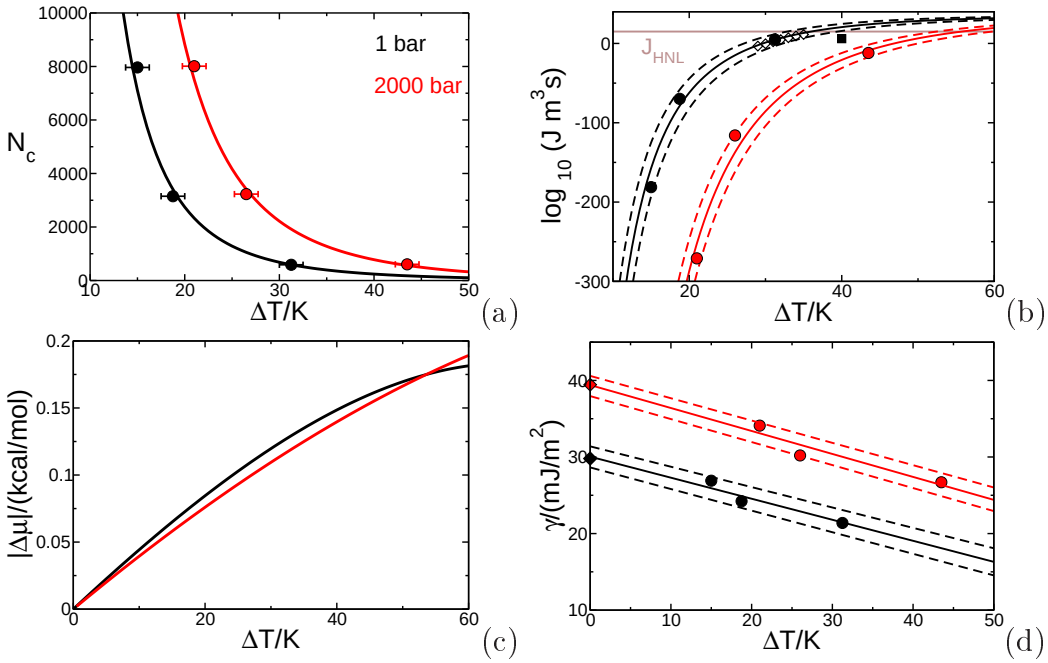

Figure 8.1: Plotted for 1(black) and 2000 bar (red) as a function of the supercooling: (a) number of particles in the ice Ih critical cluster; (b) decimal logarithm of the ice nucleation rate; (c) absolute value of the chemical potential difference between ice Ih and the liquid from thermodynamic integration[17]; (d) water-ice Ih interfacial free energy. In (a), (b) and (d): solid circles correspond to data obtained from inserted clusters and solid lines to fits (CNT-like in (a) and (b) as explained in Ref.[17], and linear in (d)). Diamonds in (d) correspond to the direct calculation of γ at coexistence (flat interface) from the MI method[6] (error is the size of the symbol). Dashed lines in (b) and (d) correspond to the boundaries of our statistical error (see SM). Black solid square in (b) corresponds to the Forward Flux Sampling calculation performed at 1 bar for TIP4P/Ice in Ref.[18]. Empty diamonds in (b) correspond to experimental measurements of J at 1 bar[19].

expression for the nucleation rate:

$$J = A\rho_f \exp[-\Delta G_c/(k_B T)] \tag{8.1}$$

where A is a kinetic pre-factor, ρ_f the fluid number density and $\Delta G_c/(k_B T)$ the free energy penalty associated to the appearance of the critical cluster ($\rho_f \exp[-\Delta G_c/(k_B T)$ is then the number density of critical clusters). In turn, $\Delta G_c/(k_B T)$, is given by two competing terms, a favourable one due to the lowering of the chemical potential when a liquid molecule incorporates into the crystal, and an unfavourable one due to the cost

of creating an interface between the liquid and the crystal:

$$\Delta G(N) = -N|\Delta\mu| + S(N)\gamma \tag{8.2}$$

where N is the number of molecules in the cluster, $|\Delta\mu|$ the ice-water chemical potential difference, S the area of the cluster surface, and γ is the water-ice interfacial free energy. ΔG_c, is derived by maximizing Eq. 10.4 with respect to N:

$$\Delta G_c = (N_c|\Delta\mu|)/2, \tag{8.3}$$

where N_c is the number of molecules in the critical cluster. The kinetic pre-factor is given by:

$$A = \sqrt{\frac{|\Delta\mu|}{6\pi k_B T N_c}} f^+ \tag{8.4}$$

where f^+ is the attachment rate of molecules to the critical cluster, calculated as the diffusion coefficient of the number of particles in the critical cluster[23]: $f^+ =< (N(t) - N_c)^2/(2t) >$.

In summary, to compute J one needs to obtain N_c, $|\Delta\mu|$, ρ_f and f^+ by simulation and combine them as in the equations above. Details on the way these variables are obtained are given in our previous work[4,5,17]. The obtained values of J as a function of the supercooling are plotted as filled circles in Fig. 8.1(b). The results for 1 bar have an improved accuracy with respect to our previous work[4,17]. The thermodynamic driving force for nucleation, $|\Delta\mu(T)|$, is plotted in Fig. 8.1(c).

To fit our J data we first obtain γ for the inserted clusters using the following CNT expression:

$$\gamma = \left(\frac{3N_c\rho_s^2|\Delta\mu|^3}{32\pi}\right)^{1/3}, \tag{8.5}$$

where ρ_s is the number density of the cluster. The values thus obtained are shown with circles in Fig. 8.1(d). We also compute γ at coexistence ($\Delta T = 0$) by means of the Mold Integration (MI) technique[6]. The results are shown with diamonds in Fig. 8.1(d) (the data for 1 bar was recently obtained by us in Ref.[24] and that for 2000 bar has been calculated in this work). By fitting $\gamma(T)$ to a straight line (combining both seeding and MI data), and $|\Delta\mu(T)|$ and $\rho_s(T)$ to a second degree polynomial, we obtain the dependency of ΔG_c with T as:

$$\frac{\Delta G_c(T)}{k_B T} = \frac{16\pi(\gamma(T))^3}{3(\rho_s(T))^2|\Delta\mu(T)|^2 k_B T} \tag{8.6}$$

On the other hand, we obtain $f^+(T)$ as described in Refs.[4,5,17] and combine it with $\Delta G_c(T)$ to obtain $J(T)$ via Eq. 9.4. The fits thus obtained are shown with solid curves

in Fig. 8.1 (b). The dashed lines correspond to the boundaries of our statistical error, which is mainly due to the the determination of the temperature for which the inserted clusters become critical (see SM for a detailed discussion on the error boundaries). We include experimental data, available only at 1 bar, in Fig. 8.1(b)(empty diamonds). For the sake of clarity we only show data from one group[19] in the figure but, within the uncertainty of our calculations, TIP4P/Ice predictions agree with most published measurements of J[25–30]. It is clear from Fig. 8.1(b) that the supercooling required to get a certain J increases with pressure, in qualitative agreement with the experimental trend[1,31].

We now aim at predicting the location of the HNL with the employed water model. In the experimental work where the HNL was reported, microscopic drops of volume V were cooled at a rate of $v = 3\mathrm{K/min}$ until ice formation was observed[1]. The time, τ, the sample spends at given temperature interval, ΔT, is $\Delta T/v$. Assuming that J is roughly constant in every temperature interval (small ΔT), the time needed for ice to nucleate when the droplet is at temperature $T \pm \Delta T/2$ is $\tau_N(T) = 1/(VJ(T))$. While τ is constant, $\tau_N(T)$ decreases upon cooling. When $\tau_N(T)$ equals τ ice formation is observed. Thus, by equating both times and taking $\Delta T = 1\mathrm{K}$ (the typical experimental temperature uncertainty) one can estimate the rate at which ice nucleates in Kanno's et al. experiments as $J_{HNL} = v/V$. This gives $J_{HNL} \approx 10^{15}\mathrm{m}^{-3}\mathrm{s}^{-1}$ for drops with $5\mu m$ radius. The homogeneous nucleation temperature at 1 bar is -38^oC[1]. At such thermodynamic conditions, the measured nucleation rate is $J = 10^{15}\mathrm{m}^{-3}\mathrm{s}^{-1}$ [27], which is consistent with the estimate above for J_{HNL}. Since neither v nor V are changed with pressure in the experiments by Kanno et al.[1], the HNL is an iso-nucleation rate line with $J = 10^{15}\mathrm{m}^{-3}\mathrm{s}^{-1}$.

Therefore, to obtain simulation predictions of the HNL we simply read from the fits given in Fig. 8.1(b) the temperature corresponding to such rate (given by the cross between the horizontal line and the solid curves in Fig. 8.1(b)). The points thus obtained are shown as red diamonds in Fig. 8.2(a). Their error bar is given by the cross between the horizontal line and the dashed curves in Fig. 8.1(b). The agreement between the experiment and the model is almost quantitative. According to the predictions by the TIP4P/Ice model the critical cluster contains between 300 (1 bar) and 200 (2000 bar) particles along the HNL. We show a snapshot of a critical cluster in the HNL at 1 bar in Fig. 8.2(b).

The question now is why is nucleation slowed down by pressure at constant supercooling. The natural logarithm of the nucleation rate is given by $\ln J = \ln(\rho_f A) - \Delta G_c/(k_B T)$. In Fig. 8.3(a) we plot the difference in $\ln J$ and in $-\Delta G_c/(k_B T)$ between both studied pressures as a function of ΔT. Clearly, the decrease of $\ln J$ with pressure at constant ΔT can be essentially ascribed to an increase of $\Delta G_c/(k_B T)$. In order to have a quantitative assessment of which variable contributes most to such increase we show in Fig. 8.3(b) the ratio between $\Delta G_c/(k_B T)$ at 2000 and 1 bar alongside all the factors that

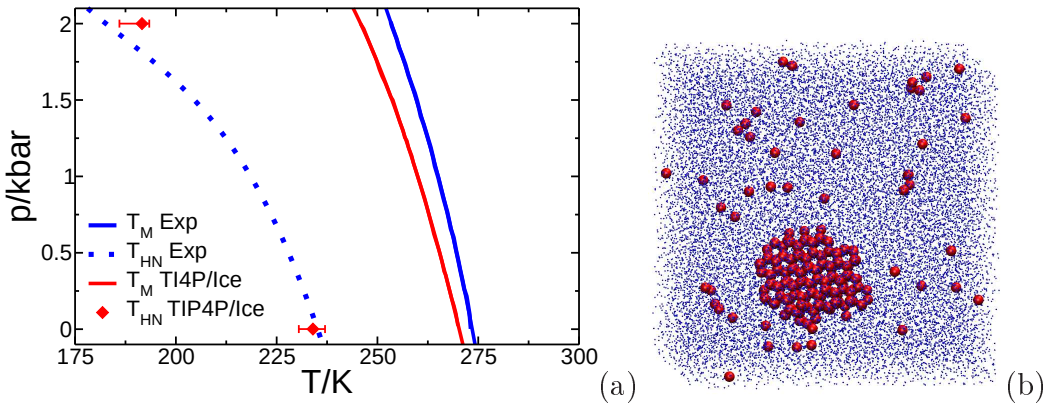

Figure 8.2: (a) The experimental HNL (dotted blue) has a larger negative slope than the melting line (solid blue). The TIP4P/Ice model, in red, captures this effect almost quantitatively. (b) Snapshot of a typical critical cluster embedded in the supercooled fluid at the experimental HNL at 1 bar. Particles with an ice-like environment are shown in red and those with a liquid-like environment in blue. The size of liquid-like particles has been scaled down to make the ice cluster visible.

contribute to such ratio (according to Eq. 8.6). $\Delta G_c/(k_B T)$ itself roughly increases by a factor of 2.5 (black curve). The ρ_s factor (green curve) has a minor contribution due to the solid incompressibility (being smaller than 1 because ρ_s increases with pressure and appears in the denominator of Eq. 8.6). The T factor (red curve) increases $\Delta G_c/(k_B T)$ roughly by ten per cent (slowing nucleation down) due to the decrease of the absolute temperature when pressure increases at constant ΔT, as a consequence of the negative slope of the melting line. The $|\Delta\mu|$ factor (blue curve) raises $\Delta G_c/(k_B T)$ by 25 per cent at low supercooling and slightly lowers it at deep supercooling. In fact, Fig. 8.1(c) shows that, for a given ΔT, increasing the pressure first decreases $|\Delta\mu|$ and then increases it at high supercooling. The γ factor (purple curve) multiplies by more than two $\Delta G_c/(k_B T)$ for all the supercooling range.

Therefore, the variable that accounts to a greater extent for the effect of pressure on ice nucleation is the water-ice interfacial free energy, γ. In Fig. 8.1(d) we show how γ notably increases with pressure for a given supercooling. Since it appears as a third power in the numerator of Eq. 8.6 its effect in raising the nucleation barrier (and therefore decreasing the nucleation rate) is quite important. Therefore, the increase of γ with pressure is the key to understand the slope of the HNL.

The dependence of γ with pressure is totally unknown experimentally. In fact, there is not even a consensus for the experimental value of γ at ambient pressure (there are reported values ranging from 25 to 35 mJ[32]). The increase of the solid-liquid interfacial

free energy along the coexistence line can not be seen as a water anomaly since it has also been reported for the Lennard-Jones system[33].

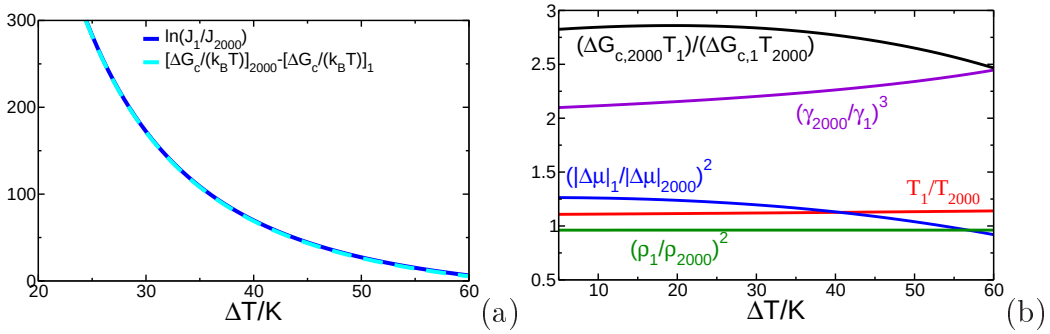

Figure 8.3: (a) Difference in $\ln J$ and $-\Delta G_c/(k_BT)$ between 2000 and 1 bar as a function of the supercooling. (b) Black curve, factor by which $\Delta G_c/(k_BT)$ increases in raising the pressure from 1 to 2000 bar as a function of the supercooling. Coloured curves, different factors that contribute to such increase, as indicated in the figure. The product of the coloured curves gives the black curve.

It is tempting to speculate that the observed increase of γ with pressure is due to the pressure-induced breakage of hydrogen bonds in the liquid phase, which is an effect that can be also observed by adding salt[34,35]. In fact, the diffusion coefficient of water, contrary to that of most liquids, increases with pressure. By breaking its hydrogen bonds, the liquid decreases its structural resemblance to ice and the interfacial free energy between both phases increases. This reasoning could also justify the temperature dependence of γ[36] (the liquid forms more hydrogen bonds on cooling and γ decreases).

The slope of the linear fits to $\gamma(\Delta T)$ in Fig. 8.1(d) provides an estimate of interfacial entropy $s_{int} = -(d\gamma/dT) = (d\gamma/d(\Delta T))$, which is -0.27±0.05 and -0.30±0.05 mJ/(m^{2}K) for 1 and 2000 bar respectively. The entropic contribution to γ, i. e. -T$_m s_{int}$, is, within our error bar, 73±10 mJ/m^2 for both pressures. The interfacial enthalpy can be obtained as $h_{int} = \gamma - \mathrm{T}_m s_{int}$, which gives -43±11 and -34±11 mJ/m^2 for 1 and 2000 bar respectively. Two comments are due in view of these figures:(i) in accordance with previous works[4,37], we observe that creating an ice-water interface is enthalpically favourable and entropically unfavourable. (ii) our data suggest that γ increases with pressure because forming the interface becomes enthalpically less favourable (this should be taken with caution, though, due to the large error bar in the slope of $\gamma(\Delta T)$).

In the mW water model the simulation HNL is parallel to the ice 0 melting line[38]. This has been interpreted as an evidence for ice 0 being the first crystal form to appear from the fluid[38]. Within this hypothesis, the mediation of ice 0 would explain the decelerating effect of pressure on ice nucleation. This new scenario could dramatically change

the interpretation of all nucleation rate measurements to date, based on the assumption that ice nucleates through an alternating stack of ice I polymorphs[39–41]. The ice 0 hypothesis of Ref.[38] implicitly assumes that $\Delta\mu$, T, ρ_s and γ are independent of pressure for a given ΔT. We show in this letter that this is not the case, particularly so for γ. In the SM we demonstrate that ice 0 is not involved in ice nucleation with the same water model used in Ref.[38]. Thus, our work not only explains the effect of pressure on ice nucleation, but also provides strong evidence regarding molecular aspects of the ice nucleation mechanism such as the structure (ice I) and shape (spherical) of the critical cluster.

The seeding method here used is approximate and relies on the validity of CNT. Therefore, one has to perform consistency checks to test the validity of the calculations. One such test consists in extrapolating the seeding results for γ to $\Delta T = 0$, where γ can be independently and directly computed using a rigorous method such as MI. In Fig. 8.1(d) we show that the test is passed for TIP4P/Ice at both pressures. In the SM we show that this point is also confirmed for the mW model. Another way to check the validity of seeding is to compare its results for the nucleation rate with those obtained by means of methods that do not rely on CNT[5]. Unfortunately, the nucleation rate predicted by us with seeding for TIP4P/Ice at 1 bar and $\Delta T = 40K$ is not consistent with a recent calculation by Haji-Akbari et al. using FFS (black square in Fig. 8.1(b)) even though they also see ice I clusters in their simulations[18]. For mW water at 1 bar, however, we[5] get consistent results with those obtained by Li et al.[42] with FFS and by Russo et al.[38] with Umbrella Sampling, but not fully consistent with those of Haji-Akbari et al. at $\Delta T = 40K$ with FFS[43]. For mW at 2000 and 5000 bar, we also get consistent results with our own brute force calculations of J at high supercooling (see SM). More work is needed to clarify the discrepancies between the different values of J reported for the mW and TIP4P/Ice water models. Another argument that strongly supports our approach is that it successfully predicts nucleation rates and interfacial free energies at coexistence for the well-characterised Hard Sphere, Lennard Jones and Tosi-Fumi Sodium Chloride models[5].

8.4. Conclusions

To conclude, we find that the increase of the ice I-water interfacial free energy is the main reason for the decelerating effect of pressure on ice nucleation (at least up to 2000 bar). Our work provides a physical explanation to the high pressure freezing techniques used in the preservation of food and biological samples[2,3] and may serve as guidance to experimentally obtain amorphous water[9,10,44] or to probe metastable supercooled water in no man's land[10,25,45]. Moreover, our work strongly supports that ice nucleates via ice I clusters[39–41], which is a crucial information to interpret ice nucleation experiments[27,32].

Acknowledgements

This work was funded by grants FIS2013/43209-P of the MEC, the Marie Curie Career Integration Grant 322326-COSAAC-FP7-PEOPLE-2012-CIG, and the UCM/Santander 910570. C.Valeriani and E. Sanz acknowledge financial support from a Ramon y Cajal Fellowship. J. R. Espinosa acknowledges financial support from the FPI grant BES-2014-067625. Calculations were carried out in the supercomputer facility Tirant from the Spanish Supercomputing Network (RES) (project QCM-2015-1-0028).

8.5. Appendix

8.5.1. Methods

Simulation details

We use the LAMMPS[46] and the GROMACS[47] Molecular Dynamics packages to simulate the mW[8] and TIP4P/Ice[7] models respectively. In GROMACS pressure is kept constant using an isotropic Parrinello-Rahman barostat[48] with a relaxation time of 0.5 ps. To fix the temperature we employ a velocity-rescale thermostat[49] with a relaxation time of 0.5 ps. The time step for the Verlet integration of the equations of motion is 3 fs. For the TIP4P/Ice model we use Particle Mesh Ewald Summations[50] to deal with electrostatic interactions. The cut-off radious for dispersive interactions and for the real part of electrostatic interactions is 9 Å. In LAMMPS temperature is kept constant with the Nose-Hoover thermostat[51] and pressure with the Nose-Hoover barostat[52], implemented as described in Ref.[53]. The relaxation time for both the thermostat and the barostat is 0.5 ps. The time step for the integration of the equations of motion is 5 fs.

Number of particles in the cluster

In order to compute the number of particles in the ice cluster we first identify particles with a solid-like environment and then find the largest cluster of such particles. To label particles as solid or liquid-like we use the local bond order parameters $\bar{q}_i$ proposed in Ref.[54] (i is the order of the spherical harmonics in $\bar{q}_i$). $\bar{q}_i$ is calculated with the coordinates of the tagged particle and those of its neighbors within a certain cut-off distance. A tagged particle is labelled as solid-like if its $\bar{q}_i$ is larger than a certain threshold, $\bar{q}_{i,t}$, and liquid-like otherwise. In order to chose $\bar{q}_{i,t}$ for a given thermodynamic state we compute the fraction of particles wrongly labelled in the bulk ice and liquid phase as a function of $\bar{q}_{i,t}$ and pick the value for which the fraction of mislabelled particles is the same in both phases. If such fraction is 0 for a certain range, we pick the middle value of the range. To distinguish liquid from ice Ih (ice 0) we use $i = 6$ ($i = 4$) and a cut-off distance of 3.5 Å (5 Å). The same cut-off distance has been considered to identify solid neighbors belonging to the same cluster. This procedure is explained in more detail in Refs.[4,5,16,17] for ice I. The value of the chosen $\bar{q}_{4,t}$ as a function of temperature to distinguish ice 0 from water for the mW model is shown in Fig. 8.4.

8.5.2. Error analysis of the main text results

The main error source in our calculations of the nucleation rate is the uncertainty in the temperature at which the inserted clusters are found to be critical. We have run

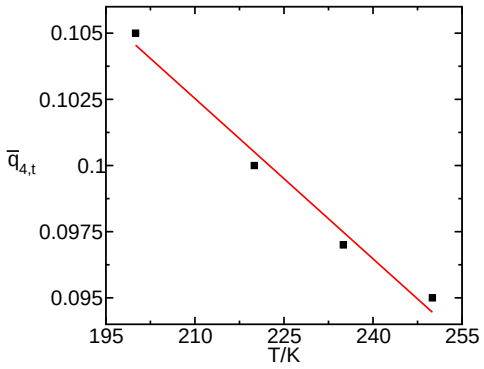

Figure 8.4: $\bar{q}_{4,t}$ threshold as a function of temperature to distinguish ice 0 from water at 1 bar for the mW model.

simulations for a 2.5 K temperature grid to enclose such temperature within a range of $\pm$ 1.25 K. In Fig. 8.5 we show in blue our seeding data ($\Delta T > 0$) for the interfacial free energy (triangles 1 bar and circles 2000 bar) and in magenta and green the corresponding values of γ if the clusters had found to be critical for a temperature 1.25 K higher and lower respectively. At $\Delta T = 0$ we plot in blue the value of γ obtained with the MI method[6,24] and in green and magenta the upper and lower boundaries of the error bar for such calculation respectively. To estimate an upper (lower) boundary for our linear fit to γ we take the green (magenta) points. The green fits, corresponding to high γ values, give rise to the lower boundary for J, indicated with a dashed line in Fig. 1(b) of the main text. On the other hand, the magenta $\gamma(T)$ fits give rise to the upper error boundary for J. The error bar for $J(\Delta T)$ is large for small ΔT because the slope of $J(\Delta T)$ is large for small supercooling. Dashed lines in Fig. 8.5 are linear fits that combine high values of γ at low ΔT with low values of γ at high ΔT or viceversa. The resulting fits are enclosed within the range defined by the fits to the green, i. e. high, and magenta, i. e. low, values of γ. Therefore, the most pessimistic estimate of the error bar for γ is given by the green and the magenta lines. Errors in γ have a strong effect in J since γ comes as a third power in $\Delta G_c/k_BT$ which, in turn, comes exponentially in J. Such functional dependency, along with the higher accuracy with which $|\Delta\mu(T)|$, $\rho_f(T)$, $\rho_s(T)$ and $f^+(T)$ are determined, causes that the impact of γ in the uncertainty of J is orders of magnitude higher that of the other variables affecting J.

The statistical error described above should be complemented with a systematic error coming from the fact that the true number of particles in the cluster could be different from that detected by the employed order parameter. Our order parameter works well for particles in the middle of the cluster and particles in the bulk liquid. However, interfacial particles can be ascribed to one phase or the other depending on

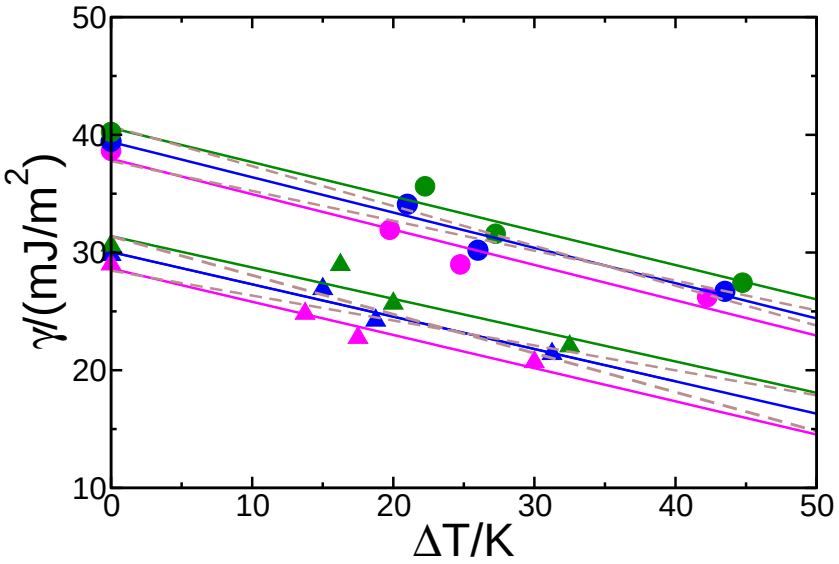

Figure 8.5: Interfacial free energy as a function of ΔT for TIP4P/Ice at 1 bar (triangles) and 2000 bar (circles). Results for $\Delta T > 0$ ($\Delta T = 0$) have been obtained with seeding (MI). Blue symbols are the γ values corresponding to the ΔT at which the inserted clusters were found to be critical. Magenta (green) symbols are the γ values that would have been obtained if the clusters had been found to be critical at a ΔT 1.25 K lower (higher). Solid lines are linear fits to the symbols with the same color as the line. Dashed lines are linear fits that combine high values of γ at low ΔT with low values of γ at high ΔT or viceversa.

subtle changes in the order parameter threshold. Since the number of particles in the surface goes as $N^{2/3}$, we use $N^{2/3}$ as an estimate for the error in the number of particles in the critical cluster. Taking this error source into account the uncertainty boundaries for $\gamma(T)$ broaden as shown in Fig. 8.6(a) with the dotted curves, that consider both systematic and statistical errors. The relative error in the number of particles in the cluster, $N^{-1/3}$, goes to zero as the number of particles in the cluster goes to infinity. Therefore, the systematic error will affect small clusters to a greater extent than large ones. This explains why the distance between dotted and the dashed lines is negligible at $\Delta T = 0$ and increases with ΔT. Using the $\gamma(T)$ dependence given by the dotted lines in Fig. 8.6(a) we obtain the combined systematic-statistical error boundaries for J, indicated by the dotted lines in Fig. 8.6(b). Not even taking the systematic error into account we are able to conceal our estimate of J with the calculation reported in Ref.[18]. The fact that for a given supercooling the nucleation rate decreases with pressure is captured for any ΔT outside the systematic+statistical error bars. However, in the

main text we deliberately do not include the systematic contribution to the error bar because our aim is to compare the nucleation rate for different pressures. A systematic error would affect both studied pressures in the same direction and including it would be deceptive when analysing the trend of J with pressure.

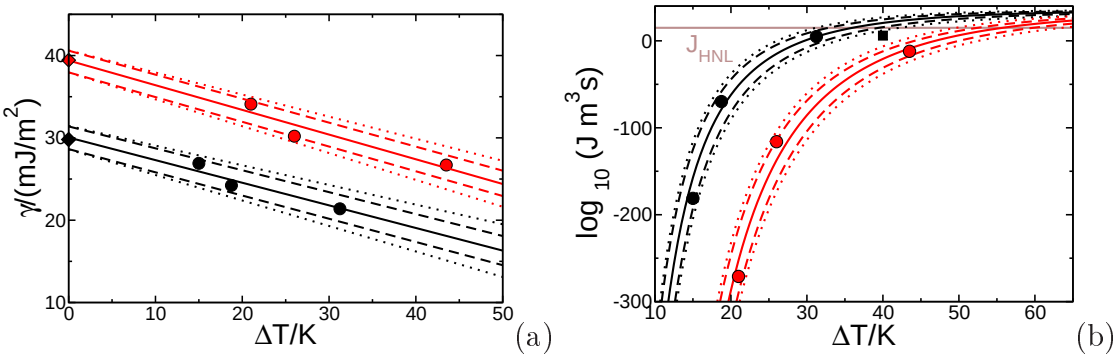

Figure 8.6: Same as Figs. 1 (d) and (b) in main text but with added dotted lines that include in the error bar possible systematic deviations from the true number of particles in the critical cluster.

8.5.3. Nucleation via ice Ih with mW

Here we show that the explanation we find for the slowing down of ice nucleation with pressure for the TIP4P/Ice model (an increase of γ with pressure) also holds for mW water. Moreover, we compare the performance of both models in predicting the behaviour of real water. In Table 8.1 we give details on our seeding calculations with mW using spherical ice Ih clusters.

p/bar	T/K	ΔT/K	N_c	$\Delta\mu/(\mathrm{kcal/mol})$	f^+/s^{-1}	$\rho_f/(\mathrm{g/cm}^3)$	$\rho_s/(\mathrm{g/cm}^3)$	$\gamma/(\mathrm{mJ/m}^2)$	$\Delta G_c/(k_BT)$	$\log_{10}(J\mathrm{m}^3\mathrm{s})$
2000	233.8	36.9	660	0.1630	$1{,}0\times10^{14}$	1.040	1.007	31.8	116	-8
2000	245.0	25.7	2334	0.1150	$3{,}1\times10^{14}$	1.039	1.006	34.3	276	-80
2000	252.5	18.2	6794	0.0822	$6{,}1\times10^{14}$	1.039	1.005	35.0	556	-202
5000	225.0	36.6	790	0.1560	$4{,}0\times10^{13}$	1.081	1.043	33.2	138	-20
5000	237.5	24.1	3034	0.1043	$1{,}2\times10^{14}$	1.078	1.042	34.8	335	-106
5000	242.5	19.1	7042	0.0839	$6{,}0\times10^{14}$	1.077	1.041	37.0	613	-226

Table 8.1: Variables involved in the calculation of the ice Ih nucleation rate and the water-ice Ih interfacial free energy of mW water. See main text for the meaning of all variables.

In Fig. 8.7(a) we show the ice nucleation rate as a function of the supercooling for different pressures. These curves were obtained by seeding the supercooled fluid with

an ice Ih spherical cluster. The prediction of mW is that for a given supercooling the nucleation rate decreases with pressure. Therefore, the model is in qualitative agreement with the experimental trend and with the predictions by the TIP4P/Ice model. In Fig. 8.7(b) we show a zoom of Fig. 8.7(a) in the region of high supercooling, where we can compare the seeding predictions to the nucleation rate computed by means of brute force (BF) simulations of spontaneous ice nucleation (from Ref.[55] at 1 bar and from this work at 2000 and 5000 bar). We obtain a satisfactory agreement between seeding and BF for all pressures, which strongly supports the validity of the approach followed in this work.

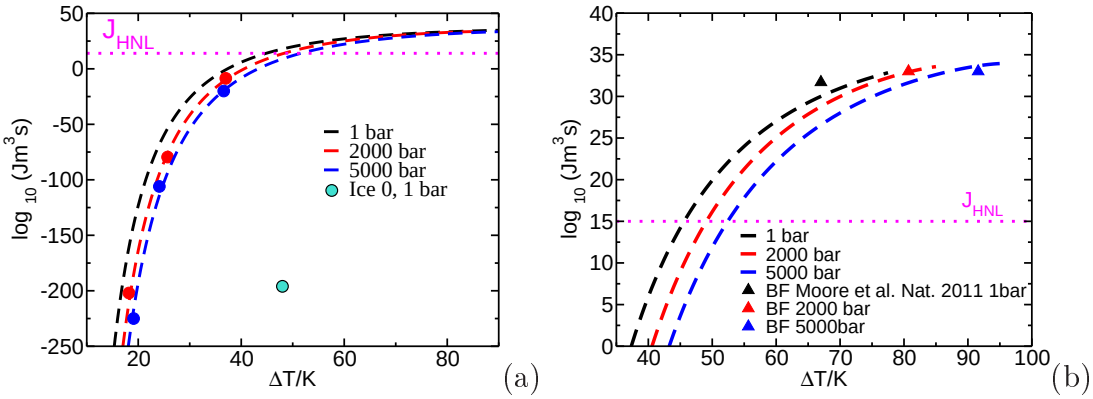

Figure 8.7: Decimal logarithm of the ice nucleation rate as a function of the supercooling for different pressures. Symbols are calculations from seeding simulations and curves are CNT fits done as described in Refs.[5,16,17,56]. The fit for 1 bar is taken from Ref.[17]. Fig. (b) is a zoom of Fig. (a) in the deep supercooling region where the seeding fits can be compared to brute force simulations (triangles). The horizontal dotted lines indicates the J associated to the HNL. All data correspond to ice Ih, except the cyan symbol that corresponds to ice 0 (note that ΔT refers to the ice Ih melting point).

In Fig. 8.8(a) we show the same as in Fig. 2 of the main text but including the mW data. Although mW qualitatively captures the experimental trend, the predictions made by the TIP4P/Ice model are in much better quantitative agreement with the experiment.

It is important to notice that the location of the HNL depends on the experimental set up. Specifically, it depends on the employed cooling rate, v, and on the volume of the system, V. Upon cooling, the time τ the sample spends at given temperature interval ΔT is the inverse of the cooling rate, v, times ΔT:

$$\tau = \frac{\Delta T}{v} \tag{8.7}$$

And, assuming that ΔT is small enough so that J is constant in the temperature interval, the time it takes for a critical nucleus to appear in the system in such temperature interval is:

$$\tau_N(T) = \frac{1}{VJ(T)}, \tag{8.8}$$

where T is the center of the temperature interval. The system will keep cooling down until $\tau_N(T)$ becomes smaller than τ. Thus, by equating both times and for $\Delta T = 1$K one gets the nucleation rate associated to the HNL is given by:

$$J(T_{HNL}) = \frac{v}{V} \tag{8.9}$$

As discussed in the main text, the experimental HNL defined in Ref.[1] is given by the points at which $\log_{10}(J\mathrm{m}^3\mathrm{s})$=15 (the rate associated to a cooling rate of 3K/min and microdroplets). The HNL defined in Ref.[38] is associated to a different nucleation rate given by: $J(T_{HNL}) = 1/(\tau_s V_s)$, where τ_s is the simulation time required to observe crystallization in a simulation box of volume V_s. Unfortunately, $J(T_{HNL})$ was not reported in Ref.[38], but typical values for $\log_{10}[J(T_{HNL})\mathrm{m}^3\mathrm{s}]$ in simulations are 32-33 (for simulations of a few nanoseconds for thousands of particles). In Fig. 8.8(b) we compare the simulation HNL defined in Ref.[38], HNLS, with the mW prediction of the experimental HNL, alongside the mW melting lines of ices 0 and I. The HNLS looks indeed parallel to the ice 0 melting line. However, the slope of the HNL depends on the nucleation rate with which it is associated. In fact, the mW prediction for the experimental HNL looks almost parallel to the ice I melting line rather than to the ice 0 one (although, as previously mentioned, the qualitative effect of the HNL having a larger negative slope than the ice Ih melting line is captured by the mW model). Therefore, no firm conclusions can be drawn from a HNL being parallel to a melting line and it is just a coincidence that the HNLS is parallel to the ice 0 melting line.

In seeking the main reason for the decrease of the nucleation rate with pressure at constant supercooling we also find for the mW model that the ice-water interfacial free energy is the main factor. In Fig. 8.9(a) we show that the kinetic prefactor is not responsible for the decrease of the nucleation rate and that the reason must be found in $\exp(\Delta G_c/(k_B T))$. Fig. 8.9(a) also shows that the slowing down of the nucleation rate for TIP4P/Ice is much more pronounced than for mW. In Fig. 8.9(b), we analyse the importance of the different factors contributing to the ratio between $\exp(\Delta G_c/(k_B T))$ at 2000 and 1 bar. Such ratio (black curve) is lower for mW than for TIP4P/Ice The temperature factor (red curve) is smaller for mW because the melting line of mW has a smaller negative slope. The density factor (green curve) accelerates nucleation more than it does for in TIP4P/Ice because ice is more compressible for mW. As in the TIP4P/Ice case, the interfacial free energy (purple curve) justifies most of the increase of the nucleation barrier with pressure.

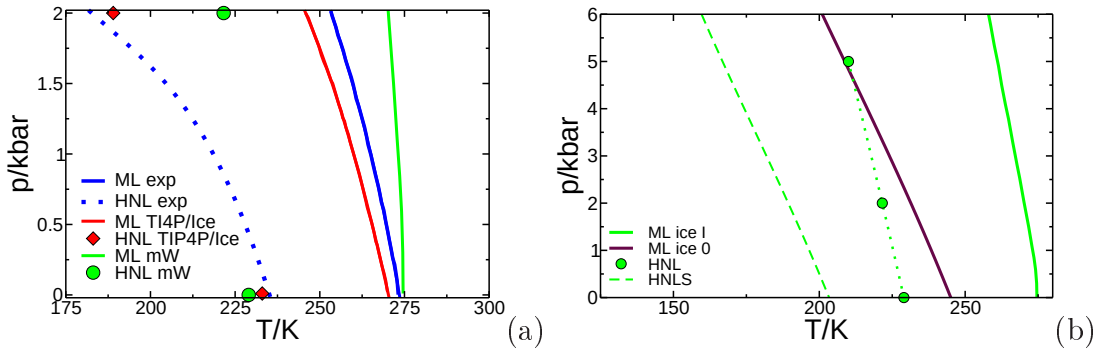

Figure 8.8: (a) Same as Fig. 2 in the main text but with the results for the mW model in green. (b) Results for the mW alone including the ice 0 melting line and the simulation HNL from Ref.[38], HNLS.

We show in Fig. 8.10(a) that γ indeed increases with pressure. Comparing this figure with Fig. 1(d) of the main text one can see that the predicted increase is lower for mW than for TIP4P/Ice. This is the main reason for the better quantitative performance of the TIP4P/Ice model shown in Fig. 8.8. We have double checked our estimation of γ by computing directly the interfacial free energy at coexistence with the MI method[6] (diamonds in Fig. 8.10(a)). For 1 bar we report the MI average value between the main crystal orientations (basal, primary prismatic and secondary prismatic)[24], whereas for 2000 and 5000 bar we report only the value for the basal plane. As for TIP4P/Ice, we find a good agreement between seeding and MI, confirming the validity of our approach.

8.5.4. Nucleation via Ice 0 with mW

In order to estimate the interfacial free energy for ice 0 we apply the seeding method to a spherical seed having ice 0 structure at 1 bar using the mW model. To illustrate how we find the temperature that makes the inserted cluster critical we show in Fig. 8.11 the number of particles in the cluster versus time for several temperatures. For temperatures higher than that at which the inserted cluster is critical, the cluster melts, whereas it grows for lower ones. Then, according to the results shown in Fig. 8.11, the inserted cluster is critical at T=226.5±2,5K. This is a supercooling of 18.5 K with respect to the ice 0 melting point of 245 K[38]. This result, alongside all variables needed for the calculation of the interfacial free energy, is reported in Table 8.2. The obtained interfacial free energy is plotted in Fig. 8.10 (a). By comparing the obtained value to the fit of the water-ice Ih interfacial free energy at 1 bar it becomes evident that ice 0 has a higher interfacial free energy. This result, together with the fact that the chemical potential difference between the liquid and ice 0 is smaller that that between

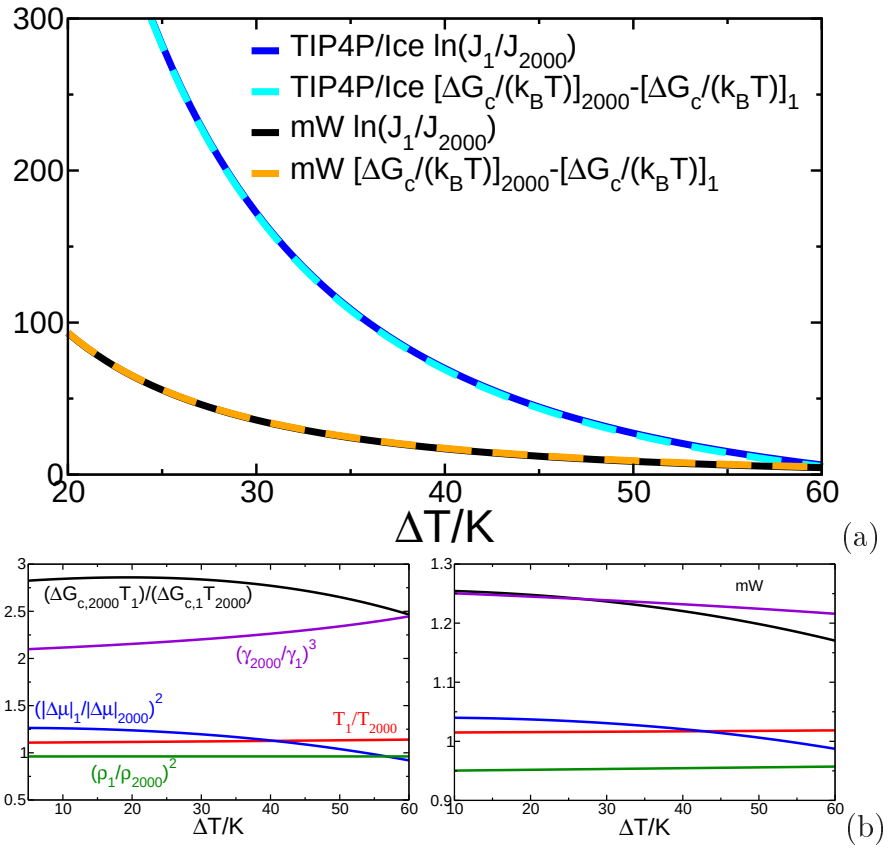

Figure 8.9: Same as Fig. 3 in the main text but for the mW model. We include also the TIP4P/Ice results from the main text to facilitate the comparison. Notice the different scale for the TIP4P/Ice and the mW figures.

the liquid and ice Ih (Fig. 8.10(b)), rules out any possible involvement of ice 0 in ice nucleation. Moreover, by measuring directly the interfacial free energy using the MI method at coexistence for a planar interface (1 bar and 245K) we obtain 35.4 mJ/m^2, which confirms the higher value of γ for ice 0 compared to ice Ih (see cyan diamond in figure 8.10 (a)).

From our seeding study we can also estimate the rate for the nucleation pathway going through a critical cluster with ice 0 structure. This is plotted in Fig. 8.7 with a cyan circle, to be compared with the black solid line corresponding to the nucleation rate at 1 bar for Ih spherical critical clusters. Because both $\Delta\mu$ and γ are less favourable for the nucleation of ice 0 than of ice I, the formation of an ice 0 critical cluster is about 200 orders of magnitude slower than that of an ice Ih one.

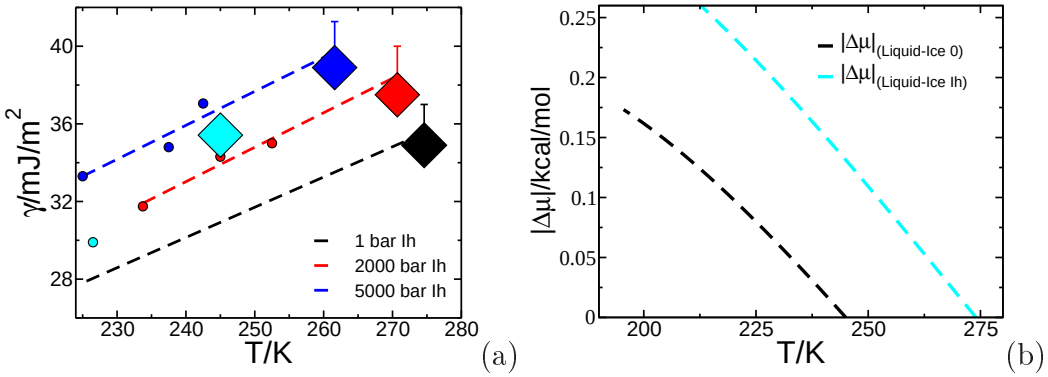

Figure 8.10: (a) Water-ice Ih interfacial free energy as a function of temperature for the mW model at different pressures. Circles are seeding data and straight lines linear fits. Diamonds are direct calculations of γ at coexistence with the MI method[6] (errors are the size of the symbol). Results for ice Ih at 1 bar are taken from Ref.[5,24]. All data correspond to ice Ih, except the cyan symbols that corresponds to ice 0 at 1 bar (circle and diamond from seeding and MI methods respectively). (b) Chemical potential difference between liquid and ices 0 and Ih as a function of temperature.

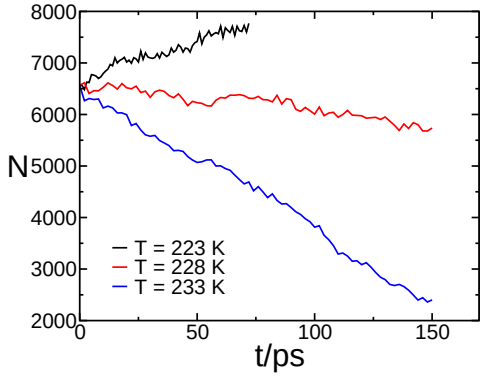

Figure 8.11: Number of particles in the ice 0 cluster versus time for several temperatures at 1 bar (as indicated in the legend).

p/bar	T/K	ΔT/K	N_c	$\Delta\mu$/(kcal/mol)	f^+/s^{-1}	ρ_f/(g/cm^3)	ρ_s/(g/cm^3)	γ/(mJ/m^2)	$\Delta G_c/(k_BT)$	$\log_{10}(J\mathrm{m}^3\mathrm{s})$
1	226.5	18.5	6583	0.074	$1{,}7 \times 10^{14}$	1.00	0.954	29.9	542	-196

Table 8.2: Variables involved in the calculation of the ice 0 nucleation rate and the water-ice 0 interfacial free energy of mW water. See main text for the meaning of all variables.

8.5.5. Surface structure of mW ice Ih clusters

In Ref.[38] critical clusters are found to have an ice I core surrounded by an ice 0 shell. This observation is not consistent with our result that the interfacial free energy of ice 0 with water is higher than that of ice I. We now look for ice 0 in the surface of our mW ice Ih seeds. Even though we initially insert an ice Ih seed, an ice 0 shell would develop when the cluster grows according to the mechanism proposed in Ref.[38]. We analyse a cluster of 8500 particles grown from a seed of 4500 particles at 1 bar and 245 K. We briefly explain first the way we look for ice 0 particles in such cluster. In Fig. 8.12(a) we show a $\bar{q}_4 - \bar{q}_6$ map for 5000 bulk particles of the liquid, ice Ih, ice 0 and ice Ic phases at 245 K. The cut-off to find neighbour particles for the calculation of both $\bar{q}_4$ and $\bar{q}_6$ was set to 5 Å. In Fig. 8.12(b) we show with brown dots the $\bar{q}_4 - \bar{q}_6$ map for all particles of the configuration of the grown cluster surrounded by the fluid. Distinct clouds for the fluid and ice Ih phases can be seen, as well as a 'bridge'joining both clouds. The bridge corresponds to interfacial particles having an order parameter in between that of the bulk phases. Only a couple of these particles falls in the order parameter region characteristic of bulk ice 0, indicated with a dashed ellipse in Fig. 8.12(b). In fact, the largest cluster of non-liquid particles in Fig. 8.12(c) shows only one ice 0 particle on its surface (in red). However, one could spuriously identify a shell of particles as ice 0 if, for the employed order parameter, the bridge of interfacial particles overlaps with the bulk ice 0 cloud. We illustrate this case in Figs. 8.12(d), (e) and (f), which correspond to a $\bar{q}_4 - \bar{q}_6$ order parameter with a cut-off distance of 4.6 Å instead of 5 Å. Both order parameters (5 and 4.6 Å) are equally valid to distinguish liquid from either ice Ih or ice 0 because the clouds of the different bulk phases do not overlap with each other (Fig. 8.12(d)). However, the order parameter of interfacial particles bridging the liquid and the ice Ih cluster clouds now overlaps with the ice 0 cloud (Fig. 8.12(d)). As a consequence, the largest cluster of non-liquid particles is surrounded by particles spuriously identified as ice 0 (in red) that in reality are interfacial particles with an order parameter intermediate between that of the ice Ih and the liquid clouds. We believe that the $W_4, \bar{q}_4$ order parameter employed in Ref.[38] may have the same shortcoming as the $\bar{q}_4 - \bar{q}_6$ used here with 4.6 Å cut-off. In fact, the ice 0 cloud shown in Fig. 6 of the Supplementary Material of Ref.[38] falls in between the liquid and the ice Ic clouds (the core of the clusters identified in Ref.[38] is mainly ice Ic).

In summary, this Supplementary Material on the one side confirms with the mW model the findings discussed in the main paper and on the other side dismisses the alternative explanation to the pressure effects on water freezing reported in Ref.[38]. Moreover, the results for the mW are a proof of concept for the seeding approach followed in our work: On the one hand, the nucleation rate predicted with seeding for high supercooling is consistent with brute force simulations. On the other hand, the extrapolation of the interfacial free energy obtained with seeding to 0 supercooling is consistent with direct

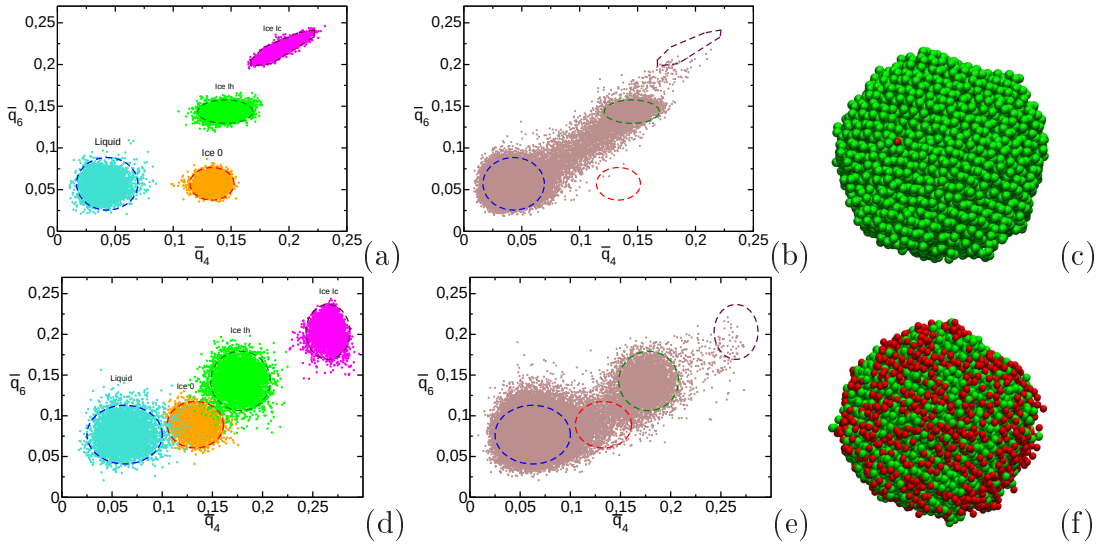

Figure 8.12: (a) $\bar{q}_4, \bar{q}_6$ map for 5000 bulk mW liquid, ice Ih, ice Ic and ice 0 particles at 245 K and 1 bar using a 5 Å cut-off distance to compute the order parameter. (b) $\bar{q}_4, \bar{q}_6$ map for a configuration at 245 K and 1 bar containing a growing ice Ih cluster. For visual aid dashed ellipses have been drawn limiting the area within which most particles of the corresponding bulk phase are enclosed. (c) largest cluster of non-liquid particles ($\bar{q}_4 > 0{,}095$) in the configuration of the growing ice Ih cluster. In red, particles whose order parameter is enclosed within the ellipse surrounding the ice 0 cloud. (d), (e) and (f): same as (a), (b) and (c) but with a cut-off of 4.6 Å and a threshold of $\bar{q}_4 > 0{,}108$ to label non-liquid particles.

calculations using the Mold Integration method.

We show that the mW qualitatively predicts the experimental observation that pressure slows ice nucleation. The quantitative agreement between mW and the experiment is not as good as that of the TIP4P/Ice model, though. As in the case of the TIP4P/Ice model, the slowing down of ice nucleation with pressure is due to a combined effect of the melting temperature, the chemical potential difference, the solid density and the ice I-water interfacial free energy, being the latter the predominant factor.

The interfacial free energy with the liquid is higher for ice 0 than for ice I. Therefore, ice 0 can not explain ice nucleation in mW. We argue that in Ref.[38] ice 0 was possibly mistaken with interfacial water.

Bibliography

1. Kanno, H., Speedy, R. J. & Angell, C. A., Supercooling of water to -92^{o}c under pressure. *Science* **189**, 880–881 (1975).

2. Morris, G. J. & Acton, E., Controlled ice nucleation in cryopreservation–a review. *Cryobiology* **66**, 85 (2013).

3. Studer, D., High-pressure freezing system (2001), US Patent 6,269,649.

4. Sanz, E., Vega, C., Espinosa, J. R., Caballero-Bernal, R., Abascal, J. L. F. & Valeriani, C., Homogeneous ice nucleation at moderate supercooling from molecular simulation. *Journal of the American Chemical Society* **135**, 15008–15017 (2013).

5. Espinosa, J. R., Vega, C., Valeriani, C. & Sanz, E., Seeding approach to crystal nucleation. *J. Chem. Phys.* **144**, 034501 (2016).

6. Espinosa, J. R., Vega, C. & Sanz, E., The mold integration method for the calculation of the crystal-fluid interfacial free energy from simulations. *J Chem. Phys.* **141**, 134709 (2014).

7. Abascal, J. L. F., Sanz, E., Fernandez, R. G. & Vega, C., A potential model for the study of ices and amorphous water: TIP4P/Ice. *J. Chem. Phys.* **122**, 234511 (2005).

8. V. Molinero, and E. B. Moore, Water modeled as an intermediate element between carbon and silicon. *The Journal of Physical Chemistry B* **113**, 4008–4016 (2009).

9. Loerting, T., Winkel, K., Seidl, M., Bauer, M., Mitterdorfer, C., Handle, P. H., Salzmann, C. G., Mayer, E., Finney, J. L. & Bowron, D. T., How many amorphous ices are there? *Phys. Chem. Chem. Phys.* **13**, 8783–8794 (2011).

10. Mishima, O. & Stanley, H. E., The relationship between liquid, supercooled and glassy water. *Nature* **396**, 329–335 (1998).

11. Jenniskens, P., F., B. D., Wilson, M. A. & Pohorille, A., High-Density Amorphous Ice, the Frost on Interstellar Grains. *The Astrophysical Journal* **455**, 389 (1995).

12. Cantrell, W. & Heymsfield, A., Production of ice in tropospheric clouds. *Bull. Amer. Meteor. Soc.* **86**, 795 (2005).

13. Sosso, G. C., Chen, J., Cox, S. J., Fitzner, M., Pedevilla, P., Zen, A. & Michaelides, A., Crystal nucleation in liquids: Open questions and future challenges in molecular dynamics simulations. *Chemical Reviews* **116**, 7078–7116 (2016).

14. Bai, X.-M. & Li, M., Calculation of solid-liquid interfacial free energy: A classical nucleation theory based approach. *J. Chem. Phys.* **124**, 124707 (2006).

15. Knott, B. C., Molinero, V., Doherty, M. F. & Peters, B., Homogeneous nucleation of methane hydrates: Unrealistic under realistic conditions. *J. Am. Chem. Soc.* **134**, 19544–19547 (2012).

16. Zaragoza, A., Conde, M. M., Espinosa, J. R., Valeriani, C., Vega, C. & Sanz, E., Competition between ices ih and ic in homogeneous water freezing. *The Journal of Chemical Physics* **143**, 134504 (2015).

17. Espinosa, J. R., Sanz, E., Valeriani, C. & Vega, C., Homogeneous ice nucleation evaluated for several water models. *J. Chem. Phys.* **141**, 18C529 (2014).

18. Haji-Akbari, A. & Debenedetti, P. G., Direct calculation of ice homogeneous nucleation rate for a molecular model of water. *Proceedings of the National Academy of Sciences* **112**, 10582–10588 (2015).

19. Pruppacher, H. R., A new look at homogeneous ice nucleation in supercooled water drops. *J. Atmosph. Sci.* **52**, 1924 (1995).

20. Kelton, K. F., *Crystal Nucleation in Liquids and Glasses* (Academic, Boston, 1991).

21. Volmer, M. & Weber, A., Keimbildung in ubersattigten gebilden. *Z. Phys. Chem.* **119**, 277 (1926).

22. Becker, R. & Doring, W., Kinetische behandlung der keimbildung in ubersattigten dampfen. *Ann. Phys.* **416**, 719–752 (1935).

23. Auer, S. & Frenkel, D., Prediction of absolute crystal-nucleation rate in hard-sphere colloids. *Nature* **409**, 1020 (2001).

24. Espinosa, J. R., Vega, C. & Sanz, E., Ice-water interfacial free energy for the tip4p, tip4p/2005, tip4p/ice and mw models as obtained from the mold integration technique. *The Journal of Physical Chemistry C* **120**, 8068–8075 (2016).

25. Manka, A., Pathak, H., Tanimura, S., Wolk, J., Strey, R. & Wyslouzil, B. E., Freezing water in no man's land. *Phys. Chem. Chem. Phys.* **14**, 4505–4516 (2012).

26. Hagen, D. E., Anderson, R. J. & Kassner-Jr., J. L., Homogeneous condensatio-nÂ¿freezing nucleation rate measurements for small water droplets in an expansion cloud chamber. *J. Atmos. Sci.* **38**, 1236–1243 (1981).

27. Murray, B. J., Broadley, S. L., Wilson, T. W., Bull, S. J., Wills, R. H., Christenson, H. K. & Murray, E. J., Kinetics of the homogeneous freezing of water. *Phys. Chem. Chem. Phys.* **12**, 10380 (2010).

28. Stockel, P., Weidinger, I. M., Baumgartel, H. & Leisner, T., Rates of homogeneous ice nucleation in levitated H_2O and D_2O droplets. *The Journal of Physical Chemistry A* **109**, 2540–2546 (2005).

29. Riechers, B., Wittbracht, F., Hutten, A. & Koop, T., The homogeneous ice nucleation rate of water droplets produced in a microfluidic device and the role of temperature uncertainty. *Phys. Chem. Chem. Phys.* **15**, 5873–5887 (2013).

30. Stan, C. A., Schneider, G. F., Shevkoplyas, S. S., Hashimoto, M., Ibanescu, M., Wiley, B. J. & Whitesides, G. M., A microfluidic apparatus for the study of ice nucleation in supercooled water drops. *Lab Chip* **9**, 2293–2305 (2009).

31. Debenedetti, P. G., Supercooled and glassy water. *J. Phys.:Condens. Matter* **15**, R1669–R1726 (2003).

32. Ickes, L., Welti, A., Hoose, C. & Lohmann, U., Classical nucleation theory of homogeneous freezing of water: thermodynamic and kinetic parameters. *Phys. Chem. Chem. Phys.* **17**, 5514–5537 (2015).

33. Laird, B. B., Davidchack, R. L., Yang, Y. & Asta, M., Determination of the solid-liquid interfacial free energy along a coexistence line by gibbs¿cahn integration. *The Journal of Chemical Physics* **131**, 114110 (2009).

34. Koop, T., Luo, B., Tsias, A. & Peter, T., Water activity as the determinant for homogeneous ice nucleation in aqueous solutions. *Nature* **406**, 611–614 (2000).

35. Kanno, H. & Angell, C. A., Homogeneous nucleation and glass formation in aqueous alkali halide solutions at high pressures. *The Journal of Physical Chemistry* **81**, 2639–2643 (1977).

36. Spaepen, F., *Homogeneous nucleation and the temperature dependence of the cystal-melt interfacial tension*, vol. 47, 1 (Academic Press, Boston, 1994).

37. Reinhardt, A. & Doye, J. P. K., Note: Homogeneous tip4p/2005 ice nucleation at low supercooling. *J. Chem. Phys.* **139**, 096102 (2013).

38. Russo, J., Romano, F. & Tanaka, H., New metastable form of ice and its role in the homogeneous crystallization of water. *Nature Materials* **13**, 733 (2014).

39. Kuhs, W. F., Sippel, C., Falenty, A. & Hansen, T. C., Extent and relevance of stacking disorder in ice Ic. *Proceedings of the National Academy of Sciences* **109**, 21259–21264 (2012).

40. Malkin, T. L., Murray, B. J., Brukhno, A. V., Anwar, J. & Salzmann, C. G., Structure of ice crystallized from supercooled water. *Proceedings of the National Academy of Sciences* **109**, 1041–1045 (2012).

41. Malkin, T. L., Murray, B. J., Salzmann, C. G., Molinero, V., Pickering, S. J. & Whale, T. F., Stacking disorder in ice i. *Phys. Chem. Chem. Phys.* **17**, 60–76 (2015).

42. Li, T., Donadio, D., Russo, G. & Galli, G., Homogeneous ice nucleation from supercooled water. *Phys. Chem. Chem. Phys.* **13**, 19807–19813 (2011).

43. Haji-Akbari, A., DeFever, R. S., Sarupria, S. & Debenedetti, P. G., Suppression of sub-surface freezing in free-standing thin films of a coarse-grained model of water. *Phys. Chem. Chem. Phys.* **16**, 25916–25927 (2014).

44. Fahy, G. M., Wowk, B., Wu, J., Phan, J., Rasch, C., Chang, A. & Zendejas, E., Cryopreservation of organs by vitrification: perspectives and recent advances. *Cryobiology* **48**, 157 – 178 (2004), special issue: Keynote papers from CRYOBIOMOL-2003.

45. Caupin, F., Escaping the no man's land: Recent experiments on metastable liquid water. *Journal of Non-Crystalline Solids* **407**, 441–448 (2015).

46. Plimpton, S. *J. Comput. Phys.* **117**, 1 (1995).

47. Lindahl, E., Hess, B. & van der Spoel, D., Gromacs 3.0: a package for molecular simulation and trajectory analysis. *J. Mol. Model.* **7**, 306 (2001).

48. Parrinello, M. & Rahman, A., Polymorphic transitions in single crystals: A new Molecular Dynamics method. *J. App. Phys.* **52**, 7182–7190 (1981).

49. Bussi, G., Donadio, D. & Parrinello, M., Canonical sampling through velocity rescaling. *The Journal of Chemical Physics* **126**, 014101 (2007).

50. Wheeler, D. R. & Newman, J., A less expensive ewald lattice sum. *Chem. Phys. Lett.* **366**, 537 (2002).

51. Hoover, W. G., Canonical dynamics: Equilibrium phase-space distributions **31**, 1695 (1985).

52. Hoover, W. G., Constant-pressure equations of motion. *Phys. Rev. A* **34**, 2499–2500 (1986).

53. Melchionna, S., Ciccotti, G. & Holian, B. L., Hoover npt dynamics for systems varying in shape and size. *Molecular Physics* **78**, 533–544 (1993).

54. Lechner, W. & Dellago, C., Accurate determination of crystal structures based on averaged local bond order parameters. *J. Chem. Phys.* **129**, 114707 (2008).

55. Moore, E. B. & Molinero, V., Structural transformation in supercooled water controls the crystallization rate of ice. *Nature* **479**, 506–508 (2011).

56. Espinosa, J. R., Vega, C., Valeriani, C. & Sanz, E., The crystal-fluid interfacial free energy and nucleation rate of NaCl from different simulation methods. *J. Chem. Phys.* **142**, 194709 (2015).

Results: Chapter 9

Lattice Mold technique for the calculation of crystal nucleation rates

Jorge R. Espinosa[†], *Pablo Sampedro*[†], *Chantal Valeriani*[†,‡], *Carlos Vega*[†] *and Eduardo Sanz*[†]

[†]Departamento de Quimica Fisica I, Facultad de Ciencias Quimicas, Universidad Complutense de Madrid, 28040 Madrid, Spain.
[‡]Departamento de Fisica Aplicada I, Facultad de Ciencias Fisicas, Universidad Complutense de Madrid, 28040 Madrid, Spain.

9.1. Abstract

We present a new simulation method for the calculation of crystal nucleation rates by computer simulation. The method is based in the use of molds to induce crystallization in state points where nucleation is a rare event. The mold is a cluster of potential energy wells placed in the lattice positions of the solid. The method has two distinct steps. In the first one the probability per unit volume of forming a sub-critical crystal cluster in the fluid is computed by means of thermodynamic integration. The thermodynamic route consists in gradually switching on an attractive interaction between the wells and the fluid particles. In the second step, the frequency with which such cluster becomes post-critical is computed in Molecular Dynamics simulations with the mold switched on. We validate our method with a continuous version of the hard sphere potential and with the sodium chloride Tosi-Fumi model. In all studied state points we obtain a good agreement with literature data obtained from other rare event simulation techniques. Our method is quite suitable for the study of both crystal nucleation of arbitrarily complex structures and the competition between different polymorphs in the nucleation stage.

9.2. Introduction

Below the melting temperature a crystalline solid is thermodynamically more stable than the fluid. However, many liquids, such as water, can be substantially supercooled in experiments where the presence of impurities is carefully avoided[1,2]. Fluids can be supercooled because the initial stage of the transition to the solid phase, called crystal nucleation, is a rare event. Crystal nucleation consists in a fluctuation of local order in the metastable liquid that gives rise to a crystalline nucleus whose size and structure are such that it can keep growing[3]. Fluctuations leading to small or poorly structured clusters are not successful in nucleating the crystal phase[4].

The nucleation stage determines in many cases the structure of the solid obtained by crystallization, which may or may not be that of the most stable crystal phase. In 1897 Ostwald published his famous "step rule" stating that the nucleating phase is that with closest free energy to the fluid[5]. This rule was reinterpreted in 1933 by Stranski and Totomanow, who claimed that nucleation follows the path with the lowest free energy barrier[6]. Be it as it may, it is quite important to control which solid phase is formed given that different polymorphs have different physical and chemical properties (solubility, melting temperature, bioavailability, catalytic activity, etc.). Therefore, the commercialization of crystalline solids, such as drugs, requires a precise control on polymorphic selection.

The importance of polymorphic selection has motivated an intense research activity aimed to understand crystal nucleation. Experimentally it is rather difficult to have access to molecular insight on such process. Due to its stochastic character, it is not possible to predict when and where in the sample it will take place. It may not occur for a long time but, when it happens, it develops quickly and involves only a small number of molecules. Nonetheless, important efforts have been devoted to observe nucleation experimentally. For instance, colloidal systems, whose constituents are visible with confocal microscopy, have been used to visualize crystal nucleation and growth[7]. With high-resolution *in situ* transmission electron microscopy (TEM) it has been recently possible to visualize crystal nuclei with an atomic scale[8–11]. Although promising[12], these experiments are still far from providing a detailed molecular description of the whole crystal nucleation process.

Computer simulations are an appealing alternative, given that they are cheap as compared to experiments and that they give information at the single-particle level. Although very important advancements have been made in computational studies of crystallization during the past two decades, the work performed so far is mostly limited to simple systems[13–15]. Rare event methods like Umbrella Sampling[16–18,18–30], Forward Flux Sampling[21,22,30–34], Metadynamics[35,36], or Path Sampling[4,37,38], have been used in combination with an order parameter[39–41] to simulate crystal nucleation. The order

parameter labels a tagged particle as solid or as fluid-like based on its local environment and it is required to monitor the growth of the crystal nucleus. This approach works well for solid structures like fcc[19], bcc[42] or diamond-like[43], where the local environment is the same for all particles. However, it is not easy to extend this approach to systems with complex symmetry like those typically encountered in industrial or technological applications. For instance ice polymorph ice-V has a monoclinic unit cell of 28 molecules and not all of them have the same environment. Devising a local-environment-based order parameter to study its nucleation with standard rare-event simulation techniques would be extremely complicated.

Here we propose a new methodology for the study of crystal nucleation that bypasses the local-bond order parameter problem. Our approach, which we call Lattice Mold (LM), is based on the use of molds to induce the formation of the crystal nucleus. We have recently shown that the crystal-fluid interfacial free energy can be computed by inducing the formation of a crystal slab in a fluid at coexistence conditions with the aid of a mold of potential energy wells[44–46]. We use a similar idea here to compute nucleation rates. We validate our method with two systems previously investigated: a system composed of pseudo-hard spheres[47] and sodium chloride modelled with the Tosi-Fumi interaction potential[48,49].

9.3. The Lattice Mold method

The main idea of our method, sketched in Fig. 9.1, is to use a mold to promote crystallization in a metastable fluid. The formation of a crystal cluster is induced with the aid of a mold formed by potential energy wells (represented by empty circles in Fig. 9.1). When the mold is turned off (wells drawn with dashed lines) particles do not feel the presence of the mold. When it is turned on (wells drawn with solid lines) there is one particle inside each well and a crystal cluster is formed.

By gradually switching on the mold, the reversible work to form the cluster can be computed. If the interaction between the particles and the wells is square-well like with well depth ϵ_m and well radius r_w, the free energy difference between the fluid and the fluid with the structure generated by the mold is given by[44]:

$$\Delta G^* = \epsilon_m N_w - \int_0^{\epsilon_m} d\epsilon \, \langle N_{fw}(\epsilon) \rangle \tag{9.1}$$

where N_w is the number of wells and $\langle N_{fw}(\epsilon) \rangle$ is the average number of filled wells for well depth equal to ϵ. This integral is computed numerically by calculating the integrand in several points by means of NpT simulations keeping fixed the mold position.

The asterisk in ΔG^* highlights the fact that both the orientation and the center of mass of the mold (and the cluster induced by it) are fixed. However, unconstrained

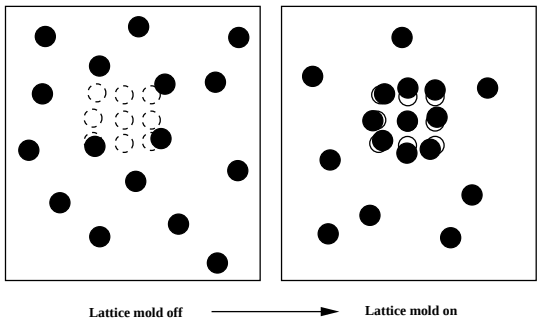

Figure 9.1: Schematic representation of how a mold of potential energy wells (circles) can induce the formation of a crystal cluster.

clusters are free to rotate and translate. We correct the effect of the constraint on the free energy difference as:

$$\Delta G/(k_B T) = \Delta G^*/(k_B T) - \ln(1/(\rho_f V_w)) - \ln(8\pi^2) \tag{9.2}$$

where k_B is the Boltzmann constant and the second and the third terms in the right hand side account for the translational and orientational free energies of the unconstrained cluster (ρ_f is the fluid number density and V_w the volume of a well, computed as $4/3\pi r_w^3$).

The probability per unit volume to find a crystal cluster in the fluid such as that generated by the mold is given by:

$$P = \rho_f e^{-\Delta G/(k_B T)}. \tag{9.3}$$

In our scheme it is crucial to choose the mold (N_w and r_w) in such way that the induced cluster is sub-critical. This implies that when the mold is fully switched on there is an induction period required for the system to crystallize, t. The average induction time, $\langle t \rangle$, can be obtained by averaging t over several independent NpT simulations with the mold fixed and fully switched on. Combining P with $\langle t \rangle$ we obtain the crystal nucleation rate J as:

$$J = P/\langle t \rangle \tag{9.4}$$

In the "Results" section we give more details on the way the method is implemented in practice by describing the calculation for one particular case.

9.4. Simulation Details

One of the models we use to test our method is the pseudo-hard spheres (PHS) potential, which is a continuous version of the hard sphere potential[47]. The PHS potential has been shown to closely reproduce the equation of state[47], dynamics[47], phase

diagram[50], crystal-fluid interfacial free energy[44] and crystal nucleation rate[19,22,51,52] of pure hard spheres. Here we use the same simulation details for PHS as in Refs.[44,50,51]. To report quantities pertaining to this system we use the particle diameter, σ, as unit of length and as unit of time $\sigma^2/(6D_l)$, where D_l is the self diffusion coefficient of the fluid. $\sigma^2/(6D_l)$ is then the "diffusive time", or the average time a particle takes to diffuse a distance of σ. Pair interactions are truncated at 1.175 σ.

We also validate our method with the Tosi-Fumi (T-F) model[48,49] for NaCl, whose nucleation rate has been previously calculated by Umbrella Sampling[21] and by seeding[46,51]. For this model, the melting temperature at 1 bar is 1082 K[53]. The simulations details for this system are the same as those given in Refs.[46,51]. We use Particle Mesh Ewald Summations[54] to deal with electrostatic interactions. The cut-off radious for dispersive interactions and for the real part of electrostatic interactions is 14 Å.

In the Molecular Dynamics simulations carried out in GROMACS[55] for the NaCl and PHS systems pressure is kept constant using an isotropic Parrinello-Rahman barostat[56] with a relaxation time of 0.5 ps. To fix the temperature we employ a velocity-rescale thermostat[57] with a relaxation time of 0.5 ps. The time step for the Verlet integration of the equations of motion is 2 fs in all cases.

To implement the well-particle interaction, v_{wp}, in Molecular Dynamics we use a continuous version of the square-well potential[44–46]:

$$v_{wp} = -\frac{1}{2}\epsilon \left[1 - \quad \tanh\left(\frac{r - r_w}{\alpha}\right)\right], \tag{9.5}$$

where r is the distance between the well and the particle centers, and α is a parameter that controls the steepness of the well's walls. α can not be too large to avoid strong forces acting on the particles trapped inside the wells. We use $\alpha = 0{,}017$ Å and $\alpha = 0{,}005$ σ for the NaCl and PHS systems respectively.

The number of particles used to simulate the PHS system was 5324, 2916 and 2048 for p=15, 16 and 17 k_BT/σ^3 respectively. For the NaCl system we run simulations with 4096 ions.

9.5. Results

We use the calculation of the nucleation rate for the PHS model at p=16 k_BT/σ^3 as a worked example to illustrate our method. For this system we use a mold with 32 wells placed in the lattice positions of a cluster taken from the equilibrium solid at p=16 k_BT/σ^3 (see Fig. 9.2). In Fig. 9.3 we show the integrand of equation 9.1 for three different well radii. Each point in figure 9.3 corresponds to an NpT Molecular Dynamics simulation of 33 diffusive times ($\sigma^2/(6D_l)$) in which the mold is kept fixed and interacts with the particles via the quasi-square well potential given in Eq. 9.5. Integrating these

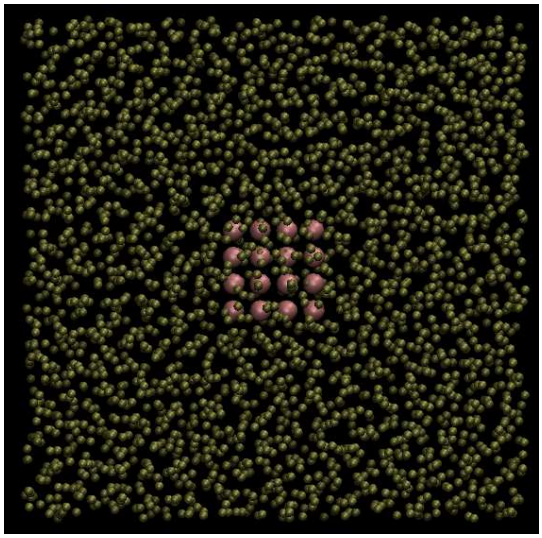

Figure 9.2: Big spheres: 32-well lattice mold used for the calculation of J in the PHS system at p=$16k_BT/\sigma^3$. Small spheres: fluid particles (scaled down to make the mold visible) of the fluid in which the mold is embedded.

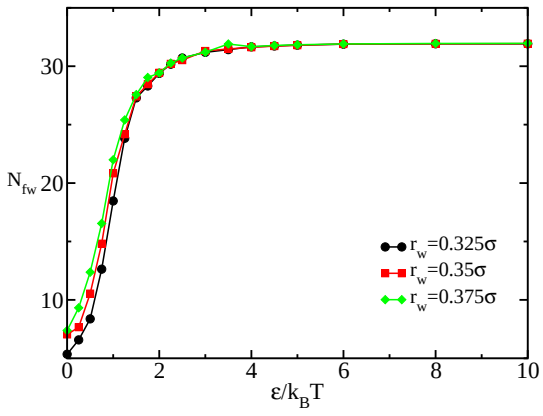

Figure 9.3: Number of filled wells (N_{fw}) versus the well depth (ϵ/k_BT) for the PHS model at p=16 k_BT/σ^3 and three different values of the well radius, r_w, as indicated in the legend.

curves and using Eqs. 9.1 and 9.2 we obtain ΔG for each well radius, as reported in Table 9.1. We then obtain $\langle t \rangle$ by running typically 10 NpT Molecular Dynamics simulations with the mold switched on with the wells at their maximum depth, ϵ_m. By monitoring the density we can easily identify the time at which each trajectory crystallizes to obtain

p	N_w	r/σ	$\Delta G/(k_BT)$	$\log_{10}[J/(6D_l/\sigma^5)]$	$\rho_f/(\sigma^{-3})$	$\langle t \rangle$
15	83	0.35	43.0	-22.2	1.02	3137
15	83	0.375	39.3	-20.9	1.02	6863
15	83	0.40	36.2	-20.1	1.02	22745
15		0.485		-16.6		
16	32	0.325	24.0	-13.2	1.01	664
16	32	0.35	22.0	-13.0	1.01	3140
16	32	0.375	19.8	-12.2	1.01	3568
16		0.485		-10.0		
17	14	0.33	10.4	-7.7	0.995	1008
17	14	0.34	10.1	-7.6	0.995	1734
17	14	0.35	10.0	-7.4	0.995	1585
17		0.485		-5.4		

Table 9.1: Nucleation rate, and variables involved in its calculation, for the PHS state points investigated in this work. Pressure p is given in (k_BT/σ^3) units and $\langle t \rangle$ in diffusive times, $\sigma^2/(6D_l)$. In the last row of each pressure we report the linear extrapolation of $\log_{10} J$ to r_w^e, which is the definite value of the LM method.

$\langle t \rangle$ as the average over all trajectories. The trajectories corresponding to p=16 k_BT/σ^3 and $r_w = 0{,}35\sigma$ are shown in Fig. 9.4. In this case we obtain a $\langle t \rangle$ of 3140 $\sigma^2/(6D_l)$, a much larger time than the 33 $\sigma^2/(6D_l)$ required to perform thermodynamic integration.

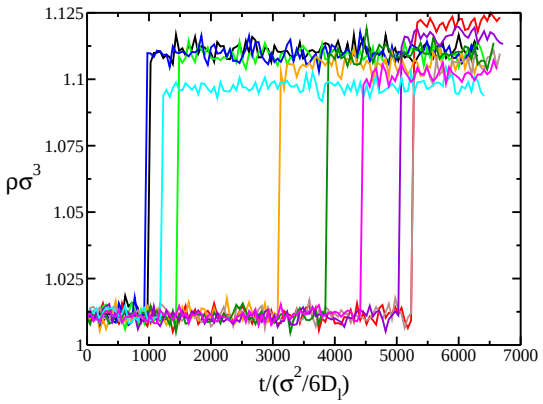

Figure 9.4: Density versus time for 10 NpT Molecular Dynamics simulations for the PHS system at p=16 k_BT/σ^3. A 32-well mold with $r_w = 0{,}35\sigma$ is permanently switched on with $\epsilon = \epsilon_m = 10k_BT$.

In order for the LM method to work the best $\langle t \rangle$ should be as long as one can afford in terms of computational time. In practice this means using molds with the smallest N_w and the largest r_w for which the system crystallizes in the longest time one can simulate. On the one hand, the longer the $\langle t \rangle$ the larger the free energy difference between the state induced by the mold and the top of the barrier separating the fluid from the crystal. Thus, the effect of constraining the crystallization path with a mold is reduced by increasing $\langle t \rangle$. On the other hand, $\langle t \rangle$ must be much larger than the time required to compute a point of the integrand in Eq. 9.1 so that thermodynamic integration can be safely performed without the interference of crystallization. One typically needs tens of diffusive times (1 diffusive time $= \sigma^2/(6D_l)$) to obtain an integrand point. As a rule of thumb we advice the use of molds for which $\langle t \rangle$ is 1 or 2 orders of magnitude larger. By tuning both N_w and r_w we could get molds that satisfy this requirement. As one can expect, molds with small N_w and large r_w give large $\langle t \rangle$'s, and viceversa.

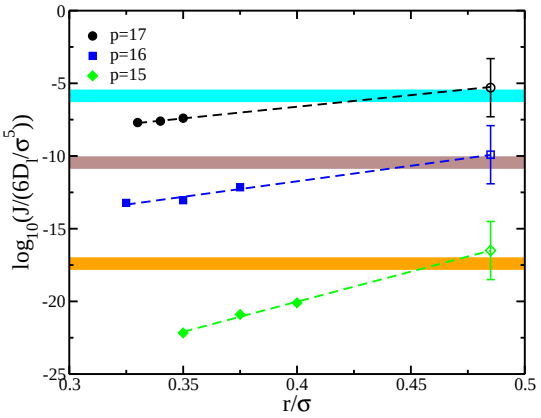

Figure 9.5: Solid symbols: nucleation rate computed for different r_w's for three different pressures of the PHS model as indicated in the legend. Dashed lines: linear fits to $\log_{10} J(r_w)$. Horizontal orange, brown and cyan lines: bibliographic values from US simulations for p=15, 16 and 17 k_BT/σ^3 respectively (tickness is comparable to the estimated error bar)[19,22,52]. Empty symbols with error bars correspond to our estimates of the nucleation rate. We give two order of magnitude error bars. One order comes from the arbitrariness in the determination of r_w^e and another one from the statistical uncertainty of our calculations and the extrapolation to $r_w = r_w^e$.

Once both ΔG and $\langle t \rangle$ have been obtained we compute J using Eq. 9.4. In Fig. 9.5 we show $\log_{10}(J)$ versus r_w for all pressures studied for the PHS model. The mold is the same for all r_w's of a given pressure, but different molds are used for different pressures (see Table 9.1). The larger the pressure the lower the nucleation free energy barrier and the smaller the mold required to induce crystallization. For all studied pressures

N_w	r_w/Å	$\Delta G/(k_BT)$	$\log_{10} J/(\mathrm{m}^{-3}\mathrm{s}^{-1})$	$\langle t\rangle$/ns
18	1.1917	15.0	29.9	12.8
18	1.2769	14.4	30.0	16.8
18	1.3620	13.4	30.2	35.4
18	1.4		30.2	

Table 9.2: Nucleation rate, and variables involved in its calculation, for the Tosi-Fumi NaCl model at 800 K and 1 bar (ρ_f= 3.345·10^{28} ions/m^3). In the last row we report the linear extrapolation of $\log_{10} J$ to r_w^e, which is the definite value of the LM method.

the logarithm of the nucleation rate increases with r_w and we obtain smaller rates than those predicted in the literature (see Fig. 9.5 and Table 9.1). This suggests that we need to extrapolate our results to a larger value of r_w, r_w^e. We try extrapolating to the largest r_w that can be used without having multiple occupancy in the wells. Thus, r_w^e will be given by half the distance at which the inter-particle interaction potential is ϵ_m ($10k_BT$). This gives r_w^e =0.485 σ for the PHS system. For $r_w > r_w^e$ two particles could gain energy by fitting into the same well. Directly calculating the rate at $r_w = r_w^e$ in order to avoid extrapolations would be prohibitively expensive using a 32-well mold given that $\langle t\rangle$ would be too long. We find that by linearly extrapolating our results to r_w^e we get a good agreement with previously reported values of J for the three studied pressures (see Fig. 9.5). The fact that we need to extrapolate our results suggests that for $r_w < r_w^e$ we are artificially restricting those nucleation paths that do not comply with the mold constraint. This does not happen at r_w^e, where we get the right nucleation rate. We acknowledge that the choice of r_w^e is somewhat arbitrary. However, it is worth noting from Fig. 9.5 that J changes by one order of magnitude (which is a typical error in calculations of the nucleation rate[21,22]) by changing r_w by 0.03σ. Therefore, we would have given a reasonable value of J by extrapolating to $0{,}47 < r_w^e < 0{,}50\sigma$. To compensate for the arbitrariness in the choice of r_w^e we increase by one order of magnitude our error bars in J. As discussed below, we also get good results for the Tosi-Fumi sodium chloride model using this criterion to establish r_w^e.

Following the same procedure we compute the nucleation rate for the Tosi-Fumi sodium chloride model at 800 K and 1 bar. The nucleation rate for such model at this thermodynamic state was previously computed in Ref.[21]. In Table 9.2 we give details on our calculation of J for this system. The runs for the computation of each integrand point in Eq. 9.1 lasted 1 ns. In Fig. 9.6 we show the nucleation rate as a function of r_w. The value we get for the nucleation rate at r_w^e (1.4 Å) is not in principle in agreement with that reported in Ref.[21], which is represented by a horizontal brown line in Fig. 9.6. There are about 4 orders of magnitude difference between both values, which is beyond

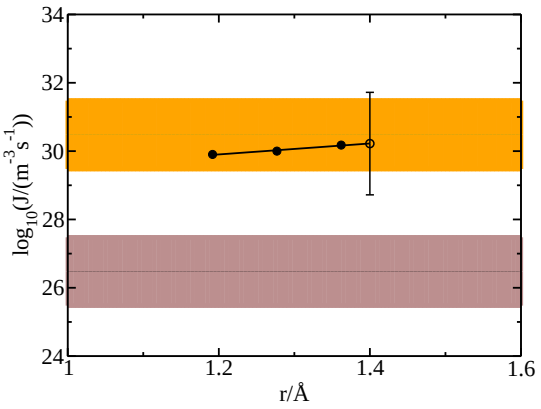

Figure 9.6: Solid symbols: nucleation rate computed for different r_w's for the Tosi-Fumi model of sodium chloride at 1 bar and 800 K. Black solid line: linear fit to $\log_{10} J(r_w)$. Horizontal brown line: bibliographic value (including the error bar) of the nucleation rate[21]. Horizontal orange line: bibliographic value corrected as discussed in the main text. Empty symbol with error bar corresponds to our estimate of the nucleation rate. We give 1.5 orders of magnitude error bar. 0.75 orders come from the arbitrariness in the determination of r_w^e and the rest from the statistical uncertainty of our calculations and the extrapolation to $r_w = r_w^e$.

the statistical uncertainty. The result of Ref.[21] was based on the method developed by Auer and Frenkel[58] that combines a calculation of the nucleation free energy barrier via Umbrella Sampling with that of the attachment rate of particles to the cluster, f^+, to obtain the kinetic prefactor. The free energy barrier reported in Ref.[21] has been recently corroborated in the context of a work that combines Hybrid Monte Carlo with Umbrella Sampling to compute nucleation free-energy barriers[59]. By inspecting the PhD thesis[58] that led to the publication of Ref.[21] we realised that f^+ is $1.3{\cdot}10^2 \mathrm{ps}^{-1}$ rather than $1.3{\cdot}10^{-2} \mathrm{ps}^{-1}$ as reported in Ref.[21] (see Fig. 4.5, Chapter 4, in Ref.[58]), which accounts for the 4 orders of magnitude difference. The value of Ref.[21] corrected by 4 orders of magnitude is shown with a horizontal orange line in Fig. 9.6. The agreement with our calculation is very satisfactory. Therefore, our method has served to correct the nucleation rate published in Ref.[21].

To summarize our results we show in Fig. 9.7 (a) and (b) the nucleation rate versus the volume fraction ϕ and the supercooling $\Delta T = T_{melting} - T$ for the PHS and the Tosi-Fumi NaCl systems respectively. We compare our nucleation rates with previously published results based on Umbrella Sampling (US)[19,22], Forward Flux Sampling (FFS)[21,22], Seeding[46,51] and brute force (BF) calculations[22,46]. Our results are in excellent agreement with either US or BF calculations in both cases. The seeding technique

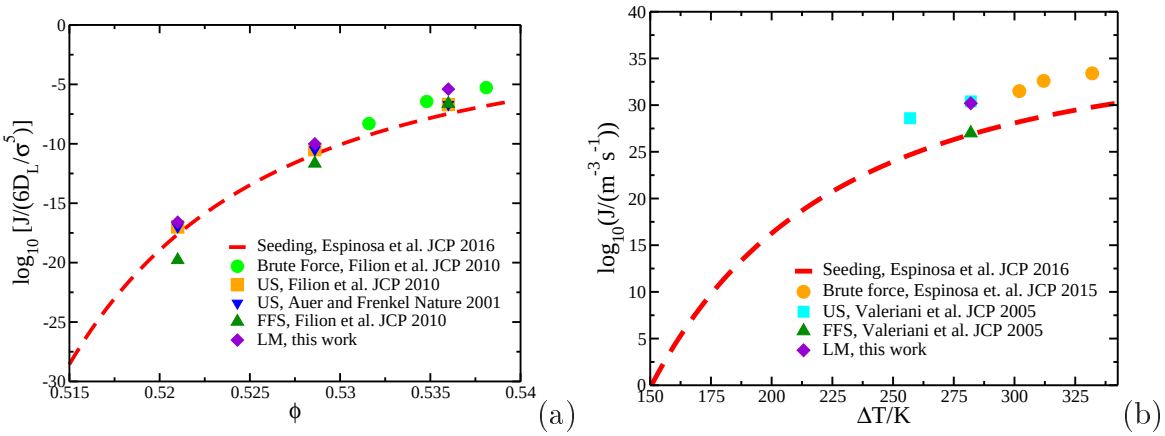

Figure 9.7: (a) Nucleation rate for the PHS (this work) and the hard sphere systems (other works as indicated in the legend) as a function of the volume fraction, ϕ. (b) Nucleation rate as a function of the supercooling for the Tosi-Fumi NaCl model at 800 K and 1 bar. The US value from Valeriani et al. has been corrected as explained in the main text.

(red dashed curve) provides a fit based on Classical Nucleation Theory to simulation data obtained by embedding a large crystal cluster in the fluid[51,60,61]. Despite being an approximate method it captures within 3 orders of magnitude all data from other rigorous techniques. The strength of the seeding method is that it provides an estimate of the nucleation rate over a range of hundreds of orders of magnitude[51]. FFS is in good agreement with US, BF and our method for hard spheres at high densities, but seems to underestimate J for low densities. Also for the NaCl system FFS seems to underestimate J with respect to US, BF and our method.

9.6. Summary and discussion

In this paper we propose a new method for the calculation of crystal nucleation rates in computer simulations. The method is based on the use of molds to induce crystallization in state points where crystal nucleation is a rare event. The method, which we call Lattice Mold, is divided in two steps. In the first step the probability per unit volume of forming a sub-critical crystal cluster in the metastable fluid is computed by means of thermodynamic integration. The thermodynamic route consists in gradually switching on an attractive interaction between the mold and the fluid particles. In the second step, the frequency with which such cluster becomes post-critical is computed in Molecular Dynamics simulations with the mold switched on. We validate our method

with a continuous version of the hard sphere potential and with the sodium chloride Tosi-Fumi model. In all studied state points we obtain a good agreement with literature data.

As discussed in the main text, the second step of the calculation is the most computationally demanding since simulations of hundreds/thousands of diffusive times are required. Such simulation times are rather accessible, particularly so because our method can be implemented in efficient Molecular Dynamics simulation packages like Gromacs. As an example, it took us five days to obtain the nucleation rate for a state point of the pseudo-hard sphere model using about 60 CPU nodes. The Lattice Mold is perhaps more demanding than Umbrella Sampling, particularly since it has been shown that the latter can be used in combination with Molecular Dynamics[59] instead of Monte Carlo. However, we expect Forward Flux Sampling to be more expensive than Lattice Mold, given the huge number of attempts required to estimate the probability to reach the critical cluster[22]. The Seeding method is the most efficient way to obtain the nucleation rate in a wide supercooling range[51], although, unlike Lattice Mold, Umbrella Sampling or Forward Flux Sampling, it relies on the validity of Classical Nucleation Theory.

In Umbrella Sampling simulations it has been observed that the structure of the cluster core is different from that of the interface in systems like Lennard-Jones or water[25,42]. This sort of effect could also be captured by the Lattice Mold method given that the induced cluster generates a crystalline halo in such way that the interfacial structure is not expected to be affected by the presence of the mold in the critical cluster's core. In this respect, it is desirable that the mold is significantly smaller than the critical cluster. For example, the mold used for the calculation of the nucleation rate of pseudo-hard spheres at reduced pressure of 16 contains 32 wells whereas the critical cluster is expected to have around 120 particles[19]. One knows that the employed mold is sufficiently small if it takes a long time to crystallize the system in the second step of the calculation (hundreds/thousands diffusive times).

In our approach the nucleation pathway is dictated by the mold structure. This issue may be seen as a drawback, but it actually has several advantages over other approaches that rely on the use of local-bond order parameters to detect the growth of crystal clusters. On the one hand, the use of molds enables the study of crystal nucleation through arbitrarily complex structures. It may be quite challenging to find local-bond order parameters for complex solid structures where the local environment changes between different positions of the unit cell. On the other hand, our method enables to rationalise polymorphic selection by comparing the nucleation rate with molds having the structure of all possible polymorphs. For instance, it would be interesting to compare the nucleation rate for fcc and bcc molds in the Lennard-Jones system given that US predicts bcc-like sub-critical nuclei, whereas the stable phase is fcc[18]. Also for the case of water there are different ice polymorphs (ice Ih, ice Ic and ice 0) whose role

in ice nucleation is currently under debate[25,62,63]. The Lattice Mold method is quite suitable to tackle this sort of problems. Of course, our method would fail in predicting nucleation paths through clusters whose structures are not conceivable a priori. In this work we have used molds with the equilibrium structure of the thermodynamically stable solid. The fact that we got a good agreement with other simulation methods suggests that this is a good approximation for the systems here investigated.

Methods like Umbrella Sampling or Forward Flux Sampling are not exempt of making a priori assumptions on the nucleation path either. These methods rely on a local-bond order parameter to identify particles belonging to the crystal phase. Such order parameter is able to discriminate between the fluid and a set of solid structures a priori considered as possible candidates for being responsible for crystal nucleation. In Umbrella Sampling or Forward Flux Sampling the structure with the highest nucleation rate among all those consistent with the selected order parameter emerges naturally in the calculations. However, this does not guarantee that it does not exist a faster nucleation path invisible to the order parameter.

Our work may inspire experimental groups interested in self-assembly or crystallization. Taking advantage of the fact that nano/micron-sized particles can be trapped by optical tweezers[64], small crystalline clusters of colloids have been built up with a lattice mold of optical traps[65]. Optical tweezers could play the role of the potential wells used in this paper to experimentally confine particles and induce crystal nucleation.

Acknowledgements

This work was funded by grants FIS2013/43209-P of the MEC, and by the Marie Curie Career Integration Grant 322326-COSAAC-FP7-PEOPLE-2012-CIG. C.Valeriani and E. Sanz acknowledge financial support from a Ramon y Cajal Fellowship. J. R. Espinosa acknowledges financial support from the FPI grant BES-2014-067625. Calculations were carried out in the supercomputer facility Tirant from the Spanish Supercomputing Network (RES) (project QCM-2015-1-0028).

Bibliography

1. Kanno, H., Speedy, R. J. & Angell, C. A., Supercooling of water to -92^{o}c under pressure. *Science* **189**, 880–881 (1975).

2. Manka, A., Pathak, H., Tanimura, S., Wolk, J., Strey, R. & Wyslouzil, B. E., Freezing water in no man's land. *Phys. Chem. Chem. Phys.* **14**, 4505–4516 (2012).

3. Kelton, K. F., *Crystal Nucleation in Liquids and Glasses* (Academic, Boston, 1991).

4. Moroni, D., ten Wolde, P. R. & Bolhuis, P. G., Interplay between structure and size in a critical crystal nucleus. *Phys. Rev. Lett.* **94**, 235703 (2005).

5. Ostwald, W. *Z. Phys. Chem.* **22**, 289 (1897).

6. Stranski, I. N. & Totomanow, D. *Z. Phys. Chem.* **163**, 399 (1933).

7. Gasser, U., Weeks, E. R., Schofield, A., Pusey, P. N. & Weitz, D. A., Real-space imaging of nucleation and growth in colloidal crystallization. *Science* **292**, 258 (2001).

8. Zheng, H., Smith, R. K., Jun, Y.-w., Kisielowski, C., Dahmen, U. & Alivisatos, A. P., Observation of single colloidal platinum nanocrystal growth trajectories. *Science* **324**, 1309–1312 (2009).

9. Harano, K., Homma, T., Niimi, Y., Koshino, M., Suenaga, K., Leibler, L. & Nakamura, E., Heterogeneous nucleation of organic crystals mediated by single-molecule templates. *Nature Materials* **11**, 877 (2011).

10. Smeets, P. J., Cho, K. R., Kempen, R. G., Sommerdijk, N. A. & De Yoreo, J. J., Calcium carbonate nucleation driven by ion binding in a biomimetic matrix revealed by in situ electron microscopy. *Nature Materials* **14**, 394–399 (2015).

11. Yuk, J. M., Park, J., Ercius, P., Kim, K., Hellebusch, D. J., Crommie, M. F., Lee, J. Y., Zettl, A. & Alivisatos, A. P., High-resolution em of colloidal nanocrystal growth using graphene liquid cells. *Science* **336**, 61–64 (2012).

12. Ross, F. M., Opportunities and challenges in liquid cell electron microscopy. *Science* **350** (2015).

13. Sear, R. P., Nucleation: theory and applications to protein solutions and colloidal suspensions. *Journal of Physics: Condensed Matter* **19**, 033101 (2007).

14. Anwar, J. & Zahn, D., Uncovering molecular processes in crystal nucleation and growth by using molecular simulation. *Angewandte Chemie International Edition* **50**, 1996–2013 (2011).

15. Sosso, G. C., Chen, J., Cox, S. J., Fitzner, M., Pedevilla, P., Zen, A. & Michaelides, A., Crystal nucleation in liquids: Open questions and future challenges in molecular dynamics simulations. *Chemical Reviews* **116**, 7078–7116 (2016).

16. Torrie, G. & Valleau, J., Nonphysical sampling distributions in Monte Carlo free-energy estimation: Umbrella sampling. *Journal of Computational Physics* **23**, 187–199 (1977).

17. van Duijneveld, J. S. & Frenkel, D., Computer simulation study of free energy barriers in crystal nucleation. *J. Chem. Phys.* **96**, 4655 (1992).

18. ten Wolde, P. R., Ruiz-Montero, M. J. & Frenkel, D., Numerical calculation of the rate of crystal nucleation in a Lennard-Jones system at moderate undercooling. *J. Chem. Phys.* **104**, 9932 (1996).

19. Auer, S. & Frenkel, D., Prediction of absolute crystal-nucleation rate in hard-sphere colloids. *Nature* **409**, 1020 (2001).

20. Radhakrishnan, R. & Trout, B. L., Nucleation of hexagonal ice (Ih) in liquid water. *J. Am. Chem. Soc.* **125**, 7743 (2003).

21. Valeriani, C., Sanz, E. & Frenkel, D., Rate of homogeneous crystal nucleation in molten NaCl. *J. Chem. Phys.* **122**, 194501 (2005).

22. Filion, L., Hermes, M., Ni, R. & Dijkstra, M., Crystal nucleation of hard spheres using molecular dynamics, umbrella sampling, and forward flux sampling: A comparison of simulation techniques. *J. Chem. Phys.* **133**, 244115 (2010).

23. Cuetos, A. & Dijkstra, M., Kinetic pathways for the isotropic-nematic phase transition in a system of colloidal hard rods: A simulation study. *Phys. Rev. Lett.* **98**, 095701 (2007).

24. Reinhardt, A. & Doye, J. P. K., Free energy landscapes for homogeneous nucleation of ice for a monatomic water model. *J. Chem. Phys.* **136**, 054501 (2012).

25. Russo, J., Romano, F. & Tanaka, H., New metastable form of ice and its role in the homogeneous crystallization of water. *Nature Materials* **13**, 733 (2014).

26. Saika-Voivod, I., Romano, F. & Sciortino, F., Nucleation barriers in tetrahedral liquids spanning glassy and crystallizing regimes. *J. Chem. Phys.* **135**, 124506 (2011).

27. Buhariwalla, C., Bowles, R., Saika-Voivod, I., Sciortino, F. & Poole, P., Free energy of formation of small ice nuclei near the widom line in simulations of supercooled water. *Eur. Phys. J. E.* **38**, 39 (2015).

28. Brukhno, A. V., Anwar, J., Davidchack, R. & Handel, R., Challenges in molecular simulation of homogeneous ice nucleation. *Journal of Physics: Condensed Matter* **20**, 494243 (2008).

29. Geiger, P. & Dellago, C., Neural networks for local structure detection in polymorphic systems. *J. Chem. Phys.* **139**, 164105 (2013).

30. Haji-Akbari, A., DeFever, R. S., Sarupria, S. & Debenedetti, P. G., Suppression of sub-surface freezing in free-standing thin films of a coarse-grained model of water. *Phys. Chem. Chem. Phys.* **16**, 25916–25927 (2014).

31. Allen, R. J., Warren, P. B. & ten Wolde, P. R., Sampling rare switching events in biochemical networks. *Phys. Rev. Lett.* **94**, 018104 (2005).

32. Sanz, E., Valeriani, C., Frenkel, D. & Dijkstra, M., Evidence for out-of-equilibrium crystal nucleation in suspensions of oppositely charged colloids. *Phys. Rev. Lett.* **99**, 055501 (2007).

33. Li, T., Donadio, D., Russo, G. & Galli, G., Homogeneous ice nucleation from supercooled water. *Phys. Chem. Chem. Phys.* **13**, 19807–19813 (2011).

34. Haji-Akbari, A. & Debenedetti, P. G., Direct calculation of ice homogeneous nucleation rate for a molecular model of water. *Proceedings of the National Academy of Sciences* **112**, 10582–10588 (2015).

35. Laio, A. & Parrinello, M., Escaping free-energy minima. *Proc. Natl. Acad. Sci.* **99**, 12562 (2002).

36. Trudu, F., Donadio, D. & Parrinello, M., Freezing of a Lennard-Jones fluid: From nucleation to spinodal regime. *Phys. Rev. Lett.* **97**, 105701 (2006).

37. Bolhuis, P. G., Chandler, D., Dellago, C. & Geissler, P. L., Transition path sampling: Throwing ropes over rough mountain passes, in the dark. *Ann. Rev. Physical Chem.* **53**, 291 (2002).

38. Lechner, W., Dellago, C. & Bolhuis, P. G., Role of the prestructured surface cloud in crystal nucleation. *Phys. Rev. Lett.* **106**, 085701 (2011).

39. Steinhardt, P. J., Nelson, D. R. & Ronchetti, M., Bond-orientational order in liquids and glasses. *Phys. Rev. B* **28**, 784–805 (1983).

40. Santiso, E. E. & Trout, B. L., A general set of order parameters for molecular crystals. *J. Chem. Phys.* **134**, 064109 (2011).

41. Lechner, W. & Dellago, C., Accurate determination of crystal structures based on averaged local bond order parameters. *J. Chem. Phys.* **129**, 114707 (2008).

42. ten Wolde, P. R., Ruiz-Montero, M. J. & Frenkel, D., Numerical evidence for bcc ordering at the surface of a critical fcc nucleus. *Phys. Rev. Lett.* **75**, 2714 (1995).

43. Zhang, Z., Chen, T. & Glotzer, S. C., Self-assembly of patchy particles into diamond structures through molecular mimicry. *Langmuir* **21**, 11547 (2006).

44. Espinosa, J. R., Vega, C. & Sanz, E., The mold integration method for the calculation of the crystal-fluid interfacial free energy from simulations. *J Chem. Phys.* **141**, 134709 (2014).

45. Espinosa, J. R., Vega, C. & Sanz, E., Ice-water interfacial free energy for the tip4p, tip4p/2005, tip4p/ice and mw models as obtained from the mold integration technique. *The Journal of Physical Chemistry C* **120**, 8068–8075 (2016).

46. Espinosa, J. R., Vega, C., Valeriani, C. & Sanz, E., The crystal-fluid interfacial free energy and nucleation rate of NaCl from different simulation methods. *J. Chem. Phys.* **142**, 194709 (2015).

47. Jover, J., Haslam, A. J., Galindo, A., Jackson, G. & Muller, E. A., Pseudo hard-sphere potential for use in continuous molecular-dynamics simulation of spherical and chain molecules. *The Journal of Chemical Physics* **137**, 144505 (2012).

48. Fumi, F. & Tosi, M., Ionic sizes and born repulsive parameters in the NaCl-type alkali halides I. *Journal of Physics and Chemistry of Solids* **25**, 31–43 (1964).

49. Tosi, M. & Fumi, F., Ionic sizes and born repulsive parameters in the NaCl-type alkali halides II. *Journal of Physics and Chemistry of Solids* **25**, 45–52 (1964).

50. Espinosa, J. R., Sanz, E., Valeriani, C. & Vega, C., On fluid-solid direct coexistence simulations: The pseudo-hard sphere model. *The Journal of Chemical Physics* **139**, 144502 (2013).

51. Espinosa, J. R., Vega, C., Valeriani, C. & Sanz, E., Seeding approach to crystal nucleation. *J. Chem. Phys.* **144**, 034501 (2016).

52. Auer, S. & Frenkel, D., Numerical prediction of absolute crystallization rates in hard-sphere colloids. *J. Phys.:Condens. Matter* **120**, 3015 (2004).

53. Aragones, J. L., Sanz, E., Valeriani, C. & Vega, C., Calculation of the melting point of alkali halides by means of computer simulations. *J. Chem. Phys.* **137**, 104507 (2012).

54. Wheeler, D. R. & Newman, J., A less expensive ewald lattice sum. *Chem. Phys. Lett.* **366**, 537 (2002).

55. Hess, B., Kutzner, C., van der Spoel, D. & Lindahl, E., Algorithms for highly efficient, load-balanced, and scalable molecular simulation. *J. Chem. Theory Comput.* **4**, 435–447 (2008).

56. Parrinello, M. & Rahman, A., Polymorphic transitions in single crystals: A new Molecular Dynamics method. *J. App. Phys.* **52**, 7182–7190 (1981).

57. Bussi, G., Donadio, D. & Parrinello, M., Canonical sampling through velocity rescaling. *The Journal of Chemical Physics* **126**, 014101 (2007).

58. Valeriani, C., *Numerical studies of nucleation pathways of ordered and disordered phases*, PhD thesis, University of Amsterdam (2007).

59. Gonzalez, M. A., Sanz, E., McBride, C., Abascal, J. L. F., Vega, C. & Valeriani, C., Nucleation free-energy barriers with hybrid monte-carlo/umbrella sampling. *Phys. Chem. Chem. Phys.* **16**, 24913–24919 (2014).

60. Knott, B. C., Molinero, V., Doherty, M. F. & Peters, B., Homogeneous nucleation of methane hydrates: Unrealistic under realistic conditions. *J. Am. Chem. Soc.* **134**, 19544–19547 (2012).

61. Sanz, E., Vega, C., Espinosa, J. R., Caballero-Bernal, R., Abascal, J. L. F. & Valeriani, C., Homogeneous ice nucleation at moderate supercooling from molecular simulation. *Journal of the American Chemical Society* **135**, 15008–15017 (2013).

62. Murray, B. J., Broadley, S. L., Wilson, T. W., Bull, S. J., Wills, R. H., Christenson, H. K. & Murray, E. J., Kinetics of the homogeneous freezing of water. *Phys. Chem. Chem. Phys.* **12**, 10380 (2010).

63. Zaragoza, A., Conde, M. M., Espinosa, J. R., Valeriani, C., Vega, C. & Sanz, E., Competition between ices ih and ic in homogeneous water freezing. *The Journal of Chemical Physics* **143**, 134504 (2015).

64. Grier, D. G., A revolution in optical manipulation. *Nature Photonics* **424**, 810–816 (2003).

65. Hermes, M., Vermolen, E. C. M., Leunissen, M. E., Vossen, D. L. J., van Oostrum, P. D. J., Dijkstra, M. & van Blaaderen, A., Nucleation of colloidal crystals on configurable seed structures. *Soft Matter* **7**, 4623–4628 (2011).

Results: Chapter 10

A simulation study of homogeneous ice nucleation in supercooled salty water

Guiomar D. Soria[†], **Jorge R. Espinosa**[†], *Jorge Ramirez*[§],*Chantal Valeriani*[†,‡], *Carlos Vega*[†] *and Eduardo Sanz*[†]

[†]Departamento de Quimica Fisica I, Facultad de Ciencias Quimicas, Universidad Complutense de Madrid, 28040 Madrid, Spain.
[‡]Departamento de Fisica Aplicada I, Facultad de Ciencias Fisicas, Universidad Complutense de Madrid, 28040 Madrid, Spain.
[§] Departamento de Ingenieria Quimica Industrial y Medio Ambiente, Escuela Tecnica Superior de Ingenieros Industriales, Universidad Politecnica de Madrid, 28006 Madrid, Spain.

10.1. Abstract

We use computer simulations to investigate the effect of salt on homogeneous ice nucleation. The melting point of the employed solution model was obtained both by direct coexistence simulations and by thermodynamic integration from previous calculations of the water chemical potential. Using a Seeding approach, in which we simulate ice seeds embedded in a supercooled aqueous solution, we compute the nucleation rate as a function of temperature for a 1.85 NaCl mole per water kilogram solution at 1 bar. To improve the accuracy and reliability of our calculations we combine Seeding with the direct computation of the ice-solution interfacial free energy at coexistence using the Mold Integration method. We compare the results with previous simulation work on pure water to understand the effect caused by the solute. The model captures the experimental trend that the nucleation rate at a given supercooling decreases when adding salt. Despite the fact that the thermodynamic driving force for ice nucleation is higher for salty water for a given supercooling, the nucleation rate slows down with salt due to

a significant increase of the ice-fluid interfacial free energy. The salty water model predicts an ice nucleation rate that is in good agreement with experimental measurements, bringing confidence in the predictive ability of the model.

10.2. Introduction

The formation of ice from supercooled water is arguably the most important freezing transition on Earth. Such transition has important consequences in geology[1], food industry[2,3], or cryopreservation[4]. Most water on Earth contains dissolved salt. Therefore, understanding freezing in salty water is of out-most importance. In this work we focus on homogeneous nucleation, the case in which ice starts growing in the bulk supercooled liquid. Salt hinders ice formation both by decreasing its melting temperature, T_m, and by increasing the supercooling with respect to T_m required to observe freezing[5]. We aim at understanding the latter effect in this paper.

The first step of the freezing transition is the nucleation of a critical crystal cluster –one that has equal chances to melt or irreversibly grow[6]. The number of such critical clusters appearing per unit time and volume is the nucleation rate, J. There are several experimental works where J has been measured for ice in salty water[5,7]. While the homogeneous nucleation rate can be experimentally measured in careful experiments to avoid the presence of impurities, other relevant nucleation parameters such as the size or the structure of the cluster, or the ice-liquid interfacial free energy are difficult to obtain in experiments[8].

Molecular simulations are an excellent complement to experimental studies of the freezing transition because they have access to detailed information at the molecular scale[9]. There are many simulation studies of ice nucleation in pure water (e.g.[9–17]), and salt precipitation in supersaturated solutions[18–21], but not much work has been devoted to study freezing of salty water[22–24]. In the few existing studies, neither nucleation rates nor ice-solution interfacial free energies have been calculated.

Like salt, pressure is known to slow down ice nucleation[5,25]. After having studied the effect of applying high pressure on homogeneous ice nucleation[26], we performed a comparative study of the effects of pressure and salt where we concluded that both factors hinder ice nucleation by increasing the ice-liquid interfacial free energy[27]. In this paper we focus the discussion on the effect of salt alone and provide details of our study of homogeneous ice nucleation in salty solutions that were not given in Ref.[27].

We study ice nucleation in a 1.85 NaCl mole per water kilogram solution (1.85 m) aqueous solution using a model that combines TIP4P/2005 water[28] and the Joung Cheetham/SPC/E NaCl[29] model[30].

We attempt to rationalise the nucleation rate by examining the variables upon which it depends according to Classical Nucleation Theory[6,31,32]. First, we determine

the melting temperature of ice in a 1.85 m NaCl solution at normal pressure via two different routes, one based on direct coexistence simulations between both phases[33] and another based on calculations of the chemical potential of the bulk phases separately[30,34]. Using thermodynamic integration from the melting point[35] we compute the chemical potential difference between ice and water in solution. We then obtain via seeded simulations the size of critical ice clusters for three different temperatures[36]. By simulating a critical cluster we estimate the frequency with which molecules attach to it[37]. To improve the reliability of our calculations we also compute the interfacial free energy at coexistence (a thermodynamic parameter that cannot be reliably measured experimentally) with the Mold Integration method[38,39]. Combining the simulation results with Classical Nucleation Theory (the seeding method[36]) we estimate the nucleation rate and the interfacial free energy for a wide supercooling range. To rationalise the effect of salt on ice nucleation we compare these results with those previously obtained for homogeneous ice nucleation in pure water[17,40].

10.3. Model

We use the TIP4P/2005 model for water[28]. For NaCl we use the Joung Cheetham model parametrised for SPC/E water[29], although in this work we combine it with TIP4P/2005 water as in Ref.[30]. Notice that it would not be a good idea to use SPC/E water as solvent for this study because its melting point for pure water is about 215K (too far from from the experimental value) and besides the kinetics for the supercooling considered in this work (i.e up to 40K) would be terribly slow for this model. The ion-water cross interaction follows the Lorentz-Berthelot combination rules[41,42] for the Lennard-Jones part and the Coulomb law for the electrostatic part. The solubility limit for this brine solution force field at 1 bar and 298 K is 3.5 m (NaCl mol per H_2O kg)[30], somewhat smaller than the experimental value of 6.15 m[43].

10.4. Simulation details

All runs are performed at constant pressure of $p = 1$ bar and NaCl concentration of 1.85 m.

All our simulations are run with the Molecular Dynamics (MD) GROMACS package[44]. We use a Parrinello-Rahman barostat[45] with a relaxation time of 0.5 ps to fix the pressure. To keep the temperature constant we employ a velocity-rescale thermostat[46] with a relaxation time of 0.5 ps. The time step for the Verlet integration of the equations of motion is 2 fs. We use Particle Mesh Ewald Summations[47] to deal with electrostatic interactions. The cut-off radius for both dispersive interactions and the real part of

electrostatic interactions is 9 Å. The LINCS algorithm is used to fix the geometry of the water molecules[48,49].

10.5. Methods

To obtain the melting temperature for the selected water-ion force field we use two different approaches. On the one hand we use the so-called direct coexistence method[33]. Such method consists in simulating the solid in contact with the liquid at several temperatures[22,23]. Below the melting temperature, the solid grows at the expense of the fluid phase, and vice versa. In this way the melting temperature can be enclosed within a certain range. The method has been used in the past by some of us to obtain the melting temperature of pure water[50], hard spheres[51,52] or sodium chloride[53]. On the other hand, we perform thermodynamic integration[35] from previous calculations of the chemical potential of the solvent and the solute[30,34] and from the melting point of pure water[54] in order to find the melting temperature as that for which the chemical potential of water in ice and in solution coincide. The calculation of the chemical potential of the components of a solution is a difficult task that has recently received great attention in the context of the computation of crystal solubilities[55–60].

Ice nucleation at moderate supercooling is beyond the time scale of standard Molecular Dynamics simulations. Special techniques are needed to promote the nucleation (rare) event. In this work we use the seeding method, which has recently been carefully validated by us[36]. The seeding technique consists in inserting an ice cluster in the supercooled fluid (salty water) and then simulating the resulting equilibrated configuration at several temperatures to obtain the temperature at which the inserted cluster reaches a critical size. Such information, combined with Classical Nucleation Theory[6,31,32] provides estimates of important quantities for the nucleation process such as the ice-liquid interfacial free energy[61,62], the height of the nucleation free energy barrier[63,64] and the nucleation rate[17,26,40,65–67]. The latter requires launching MD trajectories from the critical cluster in order to get the kinetic prefactor.

To compute the ice-solution interfacial free energy at coexistence (for a flat interface) we use the Mold Integration method, that has been developed by some of us[38] and employed to study the crystal-fluid interface for NaCl and water[26,39,66]. The method consists in gradually inducing the formation of a crystal slab in the fluid at coexistence conditions with the aid of a mold of potential energy wells placed at the lattice sites of a crystal plane[38]. The work needed to form such slab can be obtained by thermodynamic integration and is directly related to the crystal-fluid interfacial free energy[38].

We refer the reader to Refs.[51] (direct coexistence),[36] (seeding) and[38] (Mold Integration) for a detailed description of the employed methods. Nevertheless, in the following section we briefly explain these methods as we present and discuss the results.

10.6. Results

10.6.1. Melting temperature

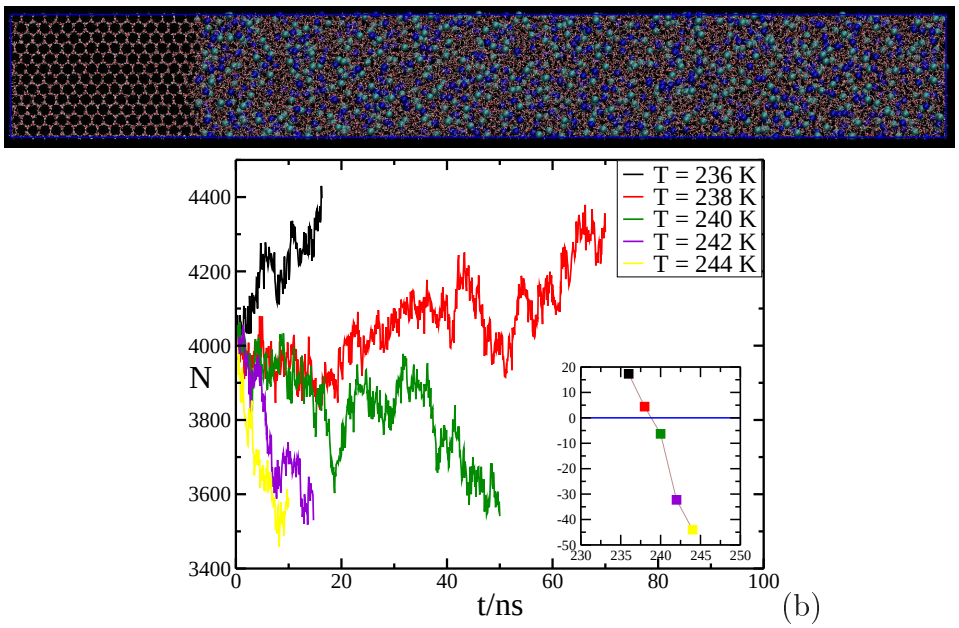

Figure 10.1: (a) Snapshot of the starting configuration used to evaluate the coexistence temperature between ice Ih and the NaCl aqueous solution. The solution is elongated in order to minimize concentration changes as the ice slab grows/shrinks.(b) Main: number of molecules belonging to the ice slab as a function of time at different temperatures. Inset: slope of a linear fit to the curves in the main panel as a function of temperature. The melting temperature is taken as that for which the interpolated slope is zero (239K).

To start with, we compute the melting temperature, T_m of ice in contact with the NaCl solution at the chosen NaCl concentration (1.85 m). We perform such calculation with two different methods: direct coexistence and and thermodynamic integration.

Direct coexistence

In the direct coexistence method an ice and a 1.85 m NaCl solution slab are put at contact as shown in Fig. 10.1 (a). Simulations are carried out in the anisotropic isothermic-isobaric NpT ensemble[52]. When the imposed temperature is below T_m the ice slab grows, and vice versa. In order to know whether the ice slab grows or melts we monitor N, the number of molecules in the ice phase (see appendix 10.9). In Fig.

10.1(b) we plot N versus time for different temperatures. At 238 K the number of ice-like particles grows whereas it decreases at 240 K: T_m is thus $239 \pm 1K$.

In order to use an unambiguous criterion to determine T_m we compute the slope of a linear fit to each $N(t)$ trajectory in Fig. 10.1(b). If the slope is positive, ice is growing and viceversa. Therefore, the temperature at which the slope is zero corresponds to T_m. The slope (in molecule/ns units) as a function of temperature is shown in the inset of Fig. 10.1(b). As announced, the slope becomes 0 at $T_m = 239K$.

When estimating T_m with the direct coexistence method, the salt concentration may change as water molecules are added/removed to/from the solution due the ice melt/growth. This is an undesirable finite size effect because we are interested in obtaining T_m for a specific value of the concentration (1.85 m). To alleviate such finite size effect we took three measures: (i) use a large system size (23100 water molecules, of which 4050 were in the ice phase + 638 NaCl) (ii) use a solution slab much larger than the ice slab (see Fig. 10.1 (a)) and (iii) determine whether ice grows or melts when only a few hundred water molecules melt or freeze. Proceeding with such caution we estimate that the NaCl concentration in solution never changes more than 1 % from its original value.

Thermodynamic integration

Another route to obtain the melting temperature is by finding the point at which the ice chemical potential (μ_w^i) equals the chemical potential of water in solution (μ_w^{sol}). To find such point we compute separately $\mu_w^i - \mu_w^0$ and $\mu_w^{sol} - \mu_w^0$, where μ_w^0 is the chemical potential of pure water. The temperature at which these two chemical potential differences become equal is the melting point. To obtain chemical potential differences we use the Gibbs-Helmholtz equation:

$$\left(\frac{\partial(\mu_w^\alpha/T)}{\partial T}\right)_p = -\frac{\bar{h}_w^\alpha}{T^2}, \tag{10.1}$$

Where the superscript α stands for a given phase (pure water, w, ice, i, or solution, sol).

$\bar{h}_w^\alpha$ is the water partial molar enthalpy which, for ice or pure water, is simply the molar enthalpy. For the solution, however, $\bar{h}_w^{sol}$ is defined as:

$$\bar{h}_w^{sol} = N_A \left(\frac{\partial H}{\partial N_w}\right)_{N_{NaCl},p,T} \approx N_A \left(\frac{\Delta H}{\Delta N_w}\right)_{N_{NaCl},p,T} \tag{10.2}$$

where N_A is the Avogadro's number and H is the system's enthalpy. We numerically evaluate the derivative above by computing the enthalpy for two different systems that have the same number of NaCl ion pairs and a different number of water molecules. It is important to make sure that the NaCl concentration in both systems (1.836 and 1.863

m in our case) narrowly encloses the concentration of interest (1.85 m). By dividing the enthalpy difference, ΔH, by the difference of the number of water molecules, ΔN_w, we get an estimate of $\bar{h}_w^{sol}$ at 1.85 m. Obtaining ΔH requires running long simulations (from 800 ns at 190 K to 100 ns at 300 K) because the enthalpy difference between both systems is very small. In Fig. 10.2 we plot h_w as a function of temperature for the solution (red dashed line) and the ice phases (black dashed line) and compare it with that of pure water (black solid line). As expected, the enthalpy of water in the ice phase is the lowest, whereas the enthalpy of pure water is lower than the partial molar enthalpy of water in the solution, reflecting the fact that the hydrogen bond network is disrupted by the ions.

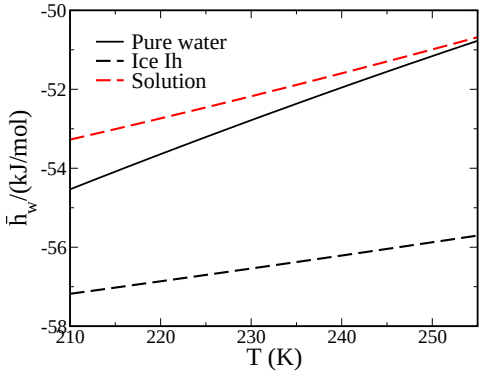

Figure 10.2: Molar enthalpies of ice, pure water, and partial molar enthalpy of water in the studied NaCl solution as a function of temperature.

Once the temperature dependence for the (partial) molar enthalpy is known, the water chemical potential difference between phases α and β at temperature T_B can be obtained by integrating Eq. 10.1 from T_A, a temperature of known chemical potential difference, to T_B:

$$\frac{\mu_w^\alpha(T_B) - \mu_w^\beta(T_B)}{T_B} = \frac{\mu_w^\alpha(T_A) - \mu_w^\beta(T_A)}{T_A} - \int_{T_A}^{T_B} \frac{\bar{h}_w^\alpha - \bar{h}_w^\beta}{T^2} dT \qquad (10.3)$$

For $\alpha = i$ and $\beta = 0$ (corresponding to ice and pure water) we use $T_A = T_m^0$, the melting temperature of pure water (250 K for TIP4P/2005), at which the chemical potential difference is 0. $\mu_w^i - \mu_w^0$ as a function of temperature is shown in Fig. 10.3 (black line) and has been previously reported by some of the authors[17,40].

For $\alpha = sol$ and $\beta = 0$ we use $T_A = 298K$, where the chemical potential difference $\mu_w^{sol} - \mu_w^0$ is equal to $RT \ln a_w(298K)$. The activity of water at 298 K, $a_w(298K)$, has been reported in Ref.[30] as a function of the concentration for the same solution model used here. The value we take for 1.85 m is 0.93. The red curve in Fig. 10.3 is $\mu_w^{sol} - \mu_w^0$.

The point where both curves in Fig. 10.3 cross corresponds to the melting temperature, 242 K. This value is different, but within the error bar, of that obtained by means of direct coexistence, 239 K. The error in the direct coexistence method comes from the stochasticity associated with the finite size of the system[52]. We have used the average value between direct coexistence and the chemical potential route, 240.5 K, as the melting temperature for all calculations in the paper.

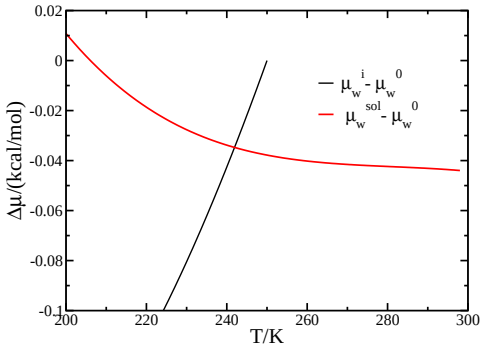

Figure 10.3: Chemical potential differences (see legend) as a function of temperature. The crossing point corresponds to the melting temperature.

10.6.2. Critical cluster size, Nc

The size of the critical clusters is determined simulating ice seeds embedded in a supercooled solution. All inserted seeds have spherical shape and ice-Ih structure. Spherical ice Ih clusters (or staking mixtures of ice-Ih and ice-Ic) seems to be the nucleation pathway followed in homogeneous ice nucleation from pure water[17,26,67]. We insert pure ice seeds with no ions in the crystal lattice. This approximation is inspired by the fact that the brine coexists with pure ice in the experimental phase diagram[68]. To check this approximation we have performed a 260 ns direct coexistence simulation below the melting temperature and computed the fraction of ions coming into the newly grown ice lattice. Such fraction was smaller than 0.2 per cent. This value, which is consistent with previous simulation work[22,24], is sufficiently small to justify the approximation of not including ions in the ice seeds.

In Ref.[66] (Fig. 7) we describe in some detail how to equilibrate an initial configuration of an embedded crystal seed into a supercooled fluid to start up the calculation. In Table 10.1 we give details on the three different initial configurations prepared ranging from a cluster of about 800 molecules up to one about 10 times larger. Starting from an equilibrated configuration with an ice cluster of N_c water molecules we launch several

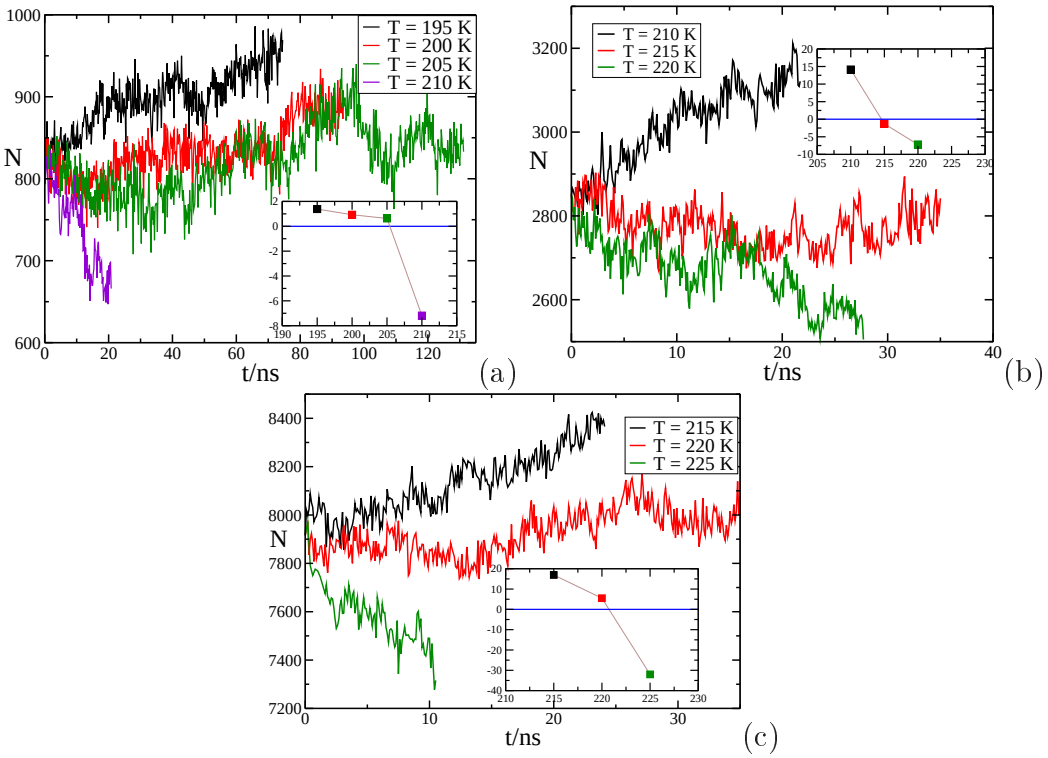

Figure 10.4: Time evolution of the number of particles in the ice cluster for different inserted clusters and temperatures. Inset: Slope of a linear fit of N(t) as a function of temperature. The temperature at which the inserted cluster is critical is taken as that at which the interpolated slope is zero. The size of the inserted clusters and the temperatures at which they are found to be critical are reported in table 10.1.

isotropic NpT simulations and monitor the number of ice molecules in the cluster, N. Such number is determined as explained in appendix 10.9. If N decreases, the inserted cluster is subcritical at the chosen temperature, whereas if N increases the cluster is post-critical. In such way we can determine the temperature at which the inserted cluster is critical. This is similar in spirit to the way the melting temperature is determined in direct coexistence simulations. Again, the large system sizes employed ensure that there are negligible concentration changes as the cluster grows or melts, which is the experimentally relevant case for ice nucleation in salty solutions at constant pressure and temperature.

In Figs. 10.4(a), (b) and (c) we show N versus time for the three simulated ice clusters at different temperatures. As for the determination of T_m, from the temperature at which the slopes of linear fits to $N(t)$ interpolate to 0 we determine the temperature at

System	N_c	T_c (K)	ΔT (K)	$\Delta\mu$ (kcal/mol)	$\rho_w/(\mathrm{g/cm^3})$	γ (mN/m)	$\Delta G_c/(k_BT)$	f^+/s^{-1}	$\log_{10}(\mathrm{J}(m^{-3}s^{-1}))$
Sol	794	205.5	35.0	0.145	0.980	28.6	141	$2{,}69x10^{10}$	-23
Sol	2850	214.5	26.0	0.111	0.982	33.4	371	$2{,}10x10^{11}$	-122
Sol	7916	220.5	20.0	0.087	0.983	36.8	784	$8{,}40x10^{11}$	-301
W	539	221.25	28.75	0.110	0.961	18.9	67	$1{,}30x10^{11}$	8
W	3117	232.5	17.5	0.071	0.974	21.9	240	$1{,}22x10^{12}$	-66
W	7900	237.0	13.0	0.055	0.978	23.0	461	$3{,}00x10^{12}$	-163

Table 10.1: Variables involved in the calculation of the ice Ih nucleation rate in pure and salty water. See main text for the meaning of all variables, whose values are reported with the corresponding units. The melting temperatures at 1 bar for pure water and the studied 1.85 m NaCl solution are 250 and 240.5 K, respectively.

which the inserted ice cluster is critical. The slope of $N(t)$ as a function of temperature is shown in the insets of Figs. 10.4(a), (b) and (c). The results for the temperature at which the clusters are found to be critical are reported in Table 10.1 and shown in Fig. 11.1(a) as a function of the supercooling, $\Delta T = T_m - T$. For comparison, we also include in the figure the results for pure water refined from our previous work with more statistics in the seeding simulations[17,40]. As shown in Fig. 11.1(a), for a given supercooling, the number of particles needed to form a critical cluster is larger in solution than in pure water. This suggests that, apart from the trivial effect of lowering T_m, the presence of salt hinders the nucleation of ice by changing the thermodynamic or the kinetic parameters that affect ice nucleation.

To make sure that the interface between the inserted ice cluster and the solution is properly equilibrated at the beginning of the simulations shown in Fig. 4 we examine the density profile of the ions along the radial distance from the ice cluster centre of mass. We analyse the trajectory corresponding to 215 K in Fig. 4(b) because the cluster size stayed roughly constant at about 2800 molecules throughout the run. In Fig. 10.6 we compare the ions density profile in the first nanosecond of the trajectory (turquoise curve) to that corresponding to the last 10 ns (black curve). The ion density profile is 0 in the interior of the cluster and increases at the interface up to the equilibrium bulk density: the ice cluster is characterised by a 3 nm radius and an interface width of nearly 1 nm. The ion density is surely equilibrated in the later period, starting at 25 ns of the trajectory, because the time required for ions to diffuse their own diameter at 215 K is about 2.5 ns. It is clear from Fig. 10.6 that both density profiles are quite similar, both at the interface and away from the ice cluster, which proves that we have started the trajectory from a configuration where the ice cluster is surrounded by an equilibrium distribution of ions.

10.6.3. Driving force for ice nucleation

According to Classical Nucleation Theory, the free energy change associated to the formation of a crystal cluster with N molecules is given by two competing terms:

$$\Delta G(N) = -N|\Delta\mu_w| + \gamma A \tag{10.4}$$

The first term favours the formation of the cluster and takes into account the fact that, below T_m, the chemical potential of water in ice is lower than in solution. Therefore, the chemical potential difference of water in both phases, $|\Delta\mu_w| = |\mu_w^i - \mu_w^{sol}|$ is the thermodynamic driving force for ice nucleation. The second term in the equation above hinders the nucleation of the crystal and is the product of the area of the cluster's surface, A, and the ice-solution interfacial free energy, γ.

To obtain $|\Delta\mu_w|$ as a function of temperature we use Eq. 10.3 with $\alpha = sol$, $\beta = i$ and $T_A = T_m = 240{,}5$ K, where $\mu_w^{sol} - \mu_w^i = 0$.

The chemical potential difference is plotted in Fig. 11.1(b), where we compare with our previous results for pure water. For a given supercooling, the thermodynamic driving force for the formation of ice is larger in solution (red) than in pure water (black), specially at high supercooling. This is consistent with the fact that the partial enthalpy of water in solution is higher than the enthalpy in pure water (Fig. 10.2). Therefore, the free energy gain when a fluid water molecule becomes part of the ice cluster is larger in solution than in pure water. According to $|\Delta\mu_w|$, then, the formation of ice in solution should be easier than in pure water, which is not consistent with Fig. 11.1(a), where we show that, for a given supercooling, larger clusters are required to nucleate ice in solution than in pure water. However, $|\Delta\mu_w|$ is not the full story. One also has to take into account the ice-solution interfacial free energy, γ, which is what we discuss in the following section.

10.6.4. Ice-solution interfacial free energy

By maximizing Eq. 10.4 and assuming a spherical cluster shape the following expression can be found for the interfacial free energy:

$$\gamma = \left(\frac{3N_c\rho_s^2|\Delta\mu_w|^3}{32\pi}\right)^{1/3}, \tag{10.5}$$

which depends on the number of particles in the critical cluster, N_c, the ice number density, ρ_s, and the ice-solution water chemical potential difference, $|\Delta\mu_w|$. In Table 10.1 we give the calculated values of γ for the three studied cluster sizes. Both in the table and in Fig. 11.1(c) we show that the ice-solution interfacial free energy is significantly larger than the ice-water one (for a given ΔT). Therefore, despite the fact that the

bulk free energy drop associated to the formation of an ice cluster is larger in solution than in pure water (Fig. 11.1(b)), the increase of surface free energy is higher for the solution (Fig. 11.1(c)), which explains why salt hinders the nucleation of ice clusters (Fig. 11.1(a)). In fact, once both γ and $\Delta\mu$ are known, the height of the nucleation free energy barrier can be evaluated according to CNT as:

$$\frac{\Delta G_c(T)}{k_B T} = \frac{16\pi(\gamma(T))^3}{3(\rho_s(T))^2|\Delta\mu_w(T)|^2 k_B T} \tag{10.6}$$

The calculated values are reported in Table 10.1 and plotted in Fig. 11.1(d). Clearly, for a given supercooling more work is required to reversibly grow an ice cluster in solution than in pure water. The responsible for such increase is the interfacial free energy, given that $\Delta\mu_w$ actually contributes to lower ΔG_c.

To make sure that γ increases when adding salt we also compute γ for a flat interface (at coexistence) using the Mold Integration method[38] that we have recently employed to compute the ice-water interfacial free energy for pure water at ambient[39] and high pressure[26]. In this method, which is only valid for coexistence conditions, a mold composed of square wells placed in the lattice sites of one or several crystal planes is gradually switched on to induce the formation of a solid slab in the fluid at coexistence conditions. The idea is sketched in Fig. 10.7. We note that the interfacial crystal halo generated by the mold is free to fluctuate and to incorporate and expel ions to reach its equilibrium structure. The free energy difference between the fluid and the fluid with the structure induced by the mold can be computed by integrating the average number of filled wells, $< N_{fw} >$, along such thermodynamic path:

$$\Delta G = N_w \epsilon_m - \int_0^{\epsilon_m} < N_{fw} > d\epsilon \tag{10.7}$$

where N_w is the number of wells in the mold, ϵ is the well depth and ϵ_m is the maximum well depth (10 $k_B T$ in our case). When the well radious, r_w, is equal to a certain "optimal" value, r_w^o, ΔG is equal to $2\gamma A$[38], where A is the area of the mold (the factor of 2 comes from the fact that two interfaces are generated). The position of the wells is fixed during the simulation and only the side of the simulation box perpendicular to the interface fluctuates to keep the pressure constant. Mold Integration can be easily implemented in GROMACS using a tabulated interaction potential between the mold and the fluid particles[38]. A cut-off of 14 Å is used for all interactions. The interfacial free energy of different crystal orientations can be obtained by using molds corresponding to different crystal planes[38,39]. In this work we study the basal, primary prismatic (pI) and secondary prismatic (pII) orientations. In table 10.2 we report details on our Mold Integration calculations such as N_w, A, r_w^o or the number of crystal planes in the mold, N_l, for each crystal orientation studied.

System	Plane	$(L_y L_z)/^2$	N_w	N_l	r_w^0/Å	$\gamma/(mJ/m^2)$
Sol	basal	1127.7	192	3	0.97(10)	43(2)
Sol	pI	1063.2	192	3	0.72(10)	49(3)
Sol	pII	920.73	192	3	0.85(10)	52(3)
Sol	γ_0					48(3)
W	basal	1128.7	128	2	0.83(5)	27.2(8)
W	pI	1064.1	128	2	0.73(5)	29.5(8)
W	pII	921.55	128	2	0.94(5)	30.0(8)
W	γ_0					28.9(8)

Table 10.2: Computational details of the Mold Integration calculations performed to obtain the ice-solution interfacial free energy for different crystal orientations. For comparison, we also report the results for pure water (W) from Ref.[39]. γ_0 is the average of the three orientations. N_l is the number of crystal layers in the mold.

In order to find r_w^o we run several simulations for different well radii monitoring the number of ice-like molecules. The simulations start from a configuration of the solution at coexistence conditions (1 bar and 240.5 K) and the mold is switched on at the beginning of the simulation. r_w^o is enclosed between the largest radious for which ice grows with no induction period and the smallest one for which ice either does not grow, or grows after some induction time[38]. Such runs for the pII plane are shown in Fig. 10.8(a). For $r_w = 0{,}7$Å (blue curves) or smaller (not shown) ice grows with no induction period in all trajectories, whereas for $r_w = 1$Å (green curves) or larger (not shown) ice does not grow. Thus, for this case we set $r_w^o = 0{,}85 \pm 0{,}10$Å.

Once we set a value for r_w^o we obtain ΔG from Eq. 10.7 for several values of r_w larger than r_w^o. The integrand of Eq. 10.7 for the pII orientation is shown in Fig. 10.8(b) for several r_w values. Each point in Fig. 10.8(b) is obtained in a simulation with well depth ϵ (indicated by the x-axis in the figure). By integrating these curves we obtain $\gamma(r_w) = \Delta G(r_w)/(2A)$, as shown in Fig. 10.8(c) for all studied orientations. Filled symbols correspond to our calculations for $r_w > r_w^o$ and empty ones to a linear extrapolation to $r_w = r_w^o$, that gives the value for γ. As in the case of pure water, the interfacial free energy of the prismatic planes is higher than that of the basal plane. In fact, the γ anisotropy is higher for salty than for pure water: in the case of pure water the interfacial free energy of the prismatic planes is about 2-3 mN/m higher than that of the basal plane, whereas for salty water the difference is about 6-9 mN/m. For all studied planes, the solid-fluid interfacial free energy is higher in the solution than in pure water. Therefore, the Mold Integration method confirms the seeding prediction that the ice-fluid interfacial free energy is larger for the solution. The orientationally averaged γ from the Mold Integration calculations is plotted alongside the seeding results in Fig.

11.1(c). Within our statistical uncertainty, the value from Mold Integration ($\Delta T = 0$) is consistent with the seeding calculations ($\Delta T > 0$).

10.6.5. Nucleation rate

We have already shown in Fig. 11.1(a) that, for a given ΔT, the size of critical ice clusters is larger in salty than in pure water. In the previous section we argue that this is due to the increase of the ice-liquid interfacial free energy. In the present section we aim at quantifying the extent to which ice nucleation is slowed down by adding salt. The speed of ice nucleation is measured by the nucleation rate, J, that is simply defined as the number of critical ice clusters appearing per unit time and volume. According to CNT J is given by:

$$J = Ae^{-\Delta G_c/(k_B T)}, \tag{10.8}$$

where ΔG_c has already been computed from Eq. 10.6 (see Fig. 11.1(d)). A, the kinetic pre-factor, is given by:

$$A = \rho_w \sqrt{\frac{|\Delta\mu_w|}{6\pi k_B T N_c}} f^+ \tag{10.9}$$

where ρ_w is the density of water in the solution and f^+ is the attachment rate, or the frequency with which new water molecules attach to the critical cluster, that can be calculated as[37]

$$f^+ =< (N(t) - N_c)^2/(2t) > \tag{10.10}$$

Computing f^+ requires performing several simulations of the critical cluster where N is monitored as a function of time, as shown in Fig. 10.9(a). By averaging $(N(t) - N_c)^2$ over all these trajectories we obtain a curve such as that shown in Fig. 10.9(b), whose slope is $2f^+$.

The calculation of f^+ is rather involving and we have only performed it as described above for the cluster containing $N_c = 2850$ molecules. For the other two studied clusters we have used the following expression for f^+ provided by CNT:

$$f^+ = \frac{24 D N_c^{2/3}}{\lambda^2} \tag{10.11}$$

where D is the diffusion coefficient of water in solution, which we plot as a function of temperature in Fig. 10.10, and λ is the distance travelled by particles in the vicinity of the cluster's surface to attach to the cluster. By equating the value of f^+ obtained via Eq. 10.10 for the cluster with 2850 molecules to Eq. 10.11 we obtain $\lambda = 6$Å, which is a reasonable value of the order of the molecular diameter. We use this value of λ combined with Eq. 10.11 to estimate f^+ for the other two studied clusters. The values of f^+ thus obtained are reported in Table 10.1.

We now have all factors required to compute the nucleation rate via Eq. 10.8. The results for the three studied clusters are reported in table 10.1 and plotted in Fig. 11.1(e) in comparison to those of pure water from Refs.[17,40]. For a given supercooling, the nucleation rate is lower in salty than in pure water, as expected from the result that the critical cluster size is larger in solution (Fig. 11.1(a)).

10.6.6. Decrease of J when adding salt

We now try to better rationalise which are the factors that contribute to the decrease of the nucleation rate when adding salt. To do that we first need to fit the data coming from the seeding simulations, which we do using the CNT expressions above[36,40]. In our fitting procedure we assume a linear temperature dependence of γ. We obtain the linear fit by combining seeding and Mold Integration data (see Fig. 11.1(c)). With $\gamma(T)$ and Eq. 10.5 we obtain $N(T)$ (solid lines in Fig. 11.1(a)). From $N(T)$, $\Delta\mu_w(T)$ and Eq. 10.6 we obtain CNT fits to $\Delta G_c(T)$ (solid lines in Fig. 11.1(d)). Finally, with the Arrhenius-like fit to $D(T)$, shown in Fig. 10.10, and Eqs. 10.11 and 10.8 we get the fits to J shown in Fig. 11.1(e).

Having the temperature dependence of the factors that affect the nucleation rate we can quantify and compare their variation when adding salt. We perform the comparison at constant supercooling rather than at absolute temperature to get rid of the trivial lowering in J caused by the decrease of the melting temperature. We compare first the extent to which the kinetic prefactor and $\Delta G_c/(k_BT)$ affect the drop in J. According to Eq. 10.8 the difference in $\ln(J)$ between pure (0) and salty (sol) water, $\ln(J_0/J_{sol})$, has two terms, one for the kinetic pre-factor, $\ln(A_0/A_{sol})$, and one for the free energy barrier height, $\Delta G_c^{sol}(T_{sol})/(k_BT_{sol}) - \Delta G_c^0(T_0)/(k_BT_0)$ (note that T_0 and T_{sol} are not the same because we compare at constant ΔT). The fact that $\ln(J_0/J_{sol})$ is equal to the difference in $\Delta G_c/(k_BT)$ (see Fig. 10.11(a)) means that the kinetic prefactor is not significantly affected by salt. It is then ratio between the free energy barrier height and the thermal energy that changes when adding salt. In Fig. 10.11(b), black curve, we show that $\Delta G_c/(k_BT)$ is between 4 and 5 times larger in the salty solution. According to Eq. 10.6 the factors that affect $\Delta G_c/(k_BT)$ are $\Delta\mu_w$, T, ρ_s and γ. In Fig. 10.11(b) we show the factor by which each of them contribute to the change of $\Delta G_c/(k_BT)$ when adding salt. The ice density and the temperature have a negligible effect on the change of the free energy barrier height (red and brown curves in Fig. 10.11(b)). The chemical potential difference does not change the barrier at low supercooling and lowers it about thirty per cent at high supercooling (green curve in Fig. 10.11(b)). As previously discussed, such lowering is a consequence of the fact that the partial molar enthalpy of water in solution is higher than in pure water. Therefore, $\Delta\mu_w$ aids ice nucleation when salt is added. However, the interfacial free energy largely compensates the modest effect of $\Delta\mu_w$, given that the increase of γ with salt multiplies by a factor of 5 the free energy

barrier (blue curve in Fig. 10.11(b)). The effect of the increase of γ on $\Delta G_c/(k_B T)$ is magnified by the fact that γ goes as a third power in Eq. 10.6. In summary, the driving force for ice nucleation, $\Delta\mu_w$, increases when adding salt, however γ, that hinders ice nucleation, increases to a greater extent, which causes the salt-induced deceleration of ice nucleation.

10.7. Discussion

10.7.1. Comparison with the experiment

Melting point depression

Experimentally, a 1.85 m NaCl solution freezes 6.6 K below the melting point of pure water[73]. The model captures that salt decreases the ice melting temperature, predicting a 9.5 K depression for a 1.85 m solution. Such depression is caused in experiments by a 2.6 m NaCl concentration[73]. Hence, the effect of salt on the melting point is larger in the model than in the experiment. This suggests that the NaCl model we are using causes a larger decrease in the chemical potential of TIP4P/2005 water than that caused by real NaCl in real water (see Fig. 4b of Ref.[30]).

To account for such enhanced effect of the model, it is interesting to compare model and experiment for the same activity of water in the solution coexisting with ice, a_w^i. We can compute a_w^i as:

$$a_w^i = \exp(\Delta\mu_0/(RT)) \tag{10.12}$$

where $\Delta\mu_0$ is the water chemical potential difference in ice and in pure liquid water at the ice-solution coexistence temperature (T_m =240.5K). We know $\Delta\mu_0$ from our previous work on homogeneous ice nucleation[17,40]. We obtain a_w^i =0.92. For such a_w^i, a melting point of $\sim$ 263 K can be interpolated from the experimental data reported in Ref.[7], which is about 10 K below the melting temperature of pure water. Such melting point depression of 10 K compares better with the 9.5 K obtained with our model. Therefore, when experiment and model are compared for a given water activity, a better agreement is obtained than when they are compared at a given concentration. In order to improve the employed model for NaCl aqueous solutions it is therefore necessary to modify the ion-water interactions in such way that a smaller water activity drop is caused by the ions.

Nucleation rate

It is experimentally known that the supercooling required to freeze microscopic salty water drops is larger than that required to freeze pure water drops[5,7,69]. Equivalently, for a given supercooling, the nucleation rate is higher in pure than in salty

water. In Fig. 11.1(e) we show that the model indeed captures the experimental trend. According to our results, such trend is due to an increase of the ice-solution interfacial free energy when adding salt. This simulation prediction is quite valuable considering the lack of accuracy in experimental measurements/estimates of the ice-liquid interfacial free energy[8].

According to the employed model (Fig. 11.1(e)), the nucleation rates in pure and salty water are quite similar at very high supercooling (about 60 K). The rate in such conditions can be measured using nanoscopic drops[72]. Consistently with the similarity of the rate, the interfacial free energy of pure water is also predicted to be similar to that of salty water at high supercooling (see Fig. 11.1(c)).

The model predictions for the nucleation rate in salty water, shown in Fig. 11.1(e), can be directly compared to experimental measurements by Alpert et al.[7] (empty symbols). The comparison can be made either for a solution with the same NaCl concentration (empty circle) or for one with the same water activity at the melting temperature, $a_w(T_m)$ (empty diamond). In either case the agreement between simulation and experiment is quite satisfactory.

10.8. Summary and Conclusions

We use computer simulations to investigate the effect of salt on homogeneous ice nucleation. To study the aqueous solution, we use the TIP4P/2005 model for water in combination with the Joung Cheetham NaCl model as parametrised for SPC/E water. To start with, we compute the ice melting point for the model using both direct coexistence and thermodynamic integration from previous calculations of the chemical potential of water in solution. The model predicts a larger cryoscopic depression than the experimental one for a given salt concentration. However, if we compare experiment and simulation for the same activity of water at coexistence we obtain a good agreement for the melting point drop. This suggests that the employed NaCl model is affecting the solute (water) to a greater extent than real NaCl does.

After computing the melting temperature we compute the size of critical ice clusters by embedding spherical ice Ih seeds in the supercooled solution and simulating trajectories at different temperatures. We compute the chemical potential difference of water in ice and in the solution using thermodynamic integration of the partial molar enthalpy from the melting temperature. With such chemical potential difference and the number of particles in the critical cluster we obtain the height of the ice nucleation free energy barrier and the ice-solution interfacial free energy using the expressions provided by Classical Nucleation Theory. We also compute the ice-solution interfacial free energy at coexistence using the Mold Integration method, that provides a thermodynamic route to reversibly grow an ice slab in the fluid at coexistence conditions. The interfacial

free energies obtained with seeding in supercooled conditions extrapolate linearly to the value at coexistence obtained with Mold Integration. This consistency test supports the validity of our approach. The interfacial free energy at any supercooling increases with respect to that of pure water (obtained in previous studies).

The kinetic pre-factor for the ice nucleation rate is obtained for one of the ice seeds by launching many trajectories and computing the mean squared displacement of the number of molecules in the cluster. The Classical Nucleation Theory expression for the kinetic pre-factor, which is proportional to the diffusion coefficient of water molecules in the liquid, is consistent with such calculation. Such consistency enabled us to use the diffusion coefficient of water as a function of temperature to get the temperature dependence of the kinetic pre-factor. That, combined with the temperature dependence obtained for the ice-solution chemical potential difference of water and for the interfacial free energy, gave us the temperature dependence of the nucleation rate for a wide range of orders of magnitude.

The model qualitatively captures the experimental trend that, for a given supercooling, the nucleation rate decreases by adding salt. Our model predicts that salt hinders ice nucleation despite the fact that the chemical potential difference between water in ice and in solution is larger when salt is added. This would in principle favour ice nucleation for a certain supercooling. However, the increase of the interfacial free energy largely compensates for the increase of the thermodynamic driving force for nucleation and the net effect is a deceleration of the ice nucleation process. The ice nucleation rate predicted by the salty water model is in good agreement with experimental measurements, which brings confidence in the predictions made by the model.

Acknowledgements

This work was funded by grants FIS2013/43209-P and FIS2016-78117-P FIS2016-78847-P of the MEC, and the UCM/Santander 910570 and PR26/16-10B-2. C.Valeriani and E. Sanz acknowledge financial support from a Ramon y Cajal Fellowship. J. R. Espinosa acknowledges financial support from the FPI grant BES-2014-067625. Calculations were carried out in the supercomputer facilities La Palma and Magerit from the Spanish Supercomputing Network (RES) (projects QCM-2015-3-0036 and QCM-2016-1-0039). The authors acknowledge the computer resources and technical assistance provided by the Centro de Supercomputacion y Visualizacion de Madrid (CeSViMa).

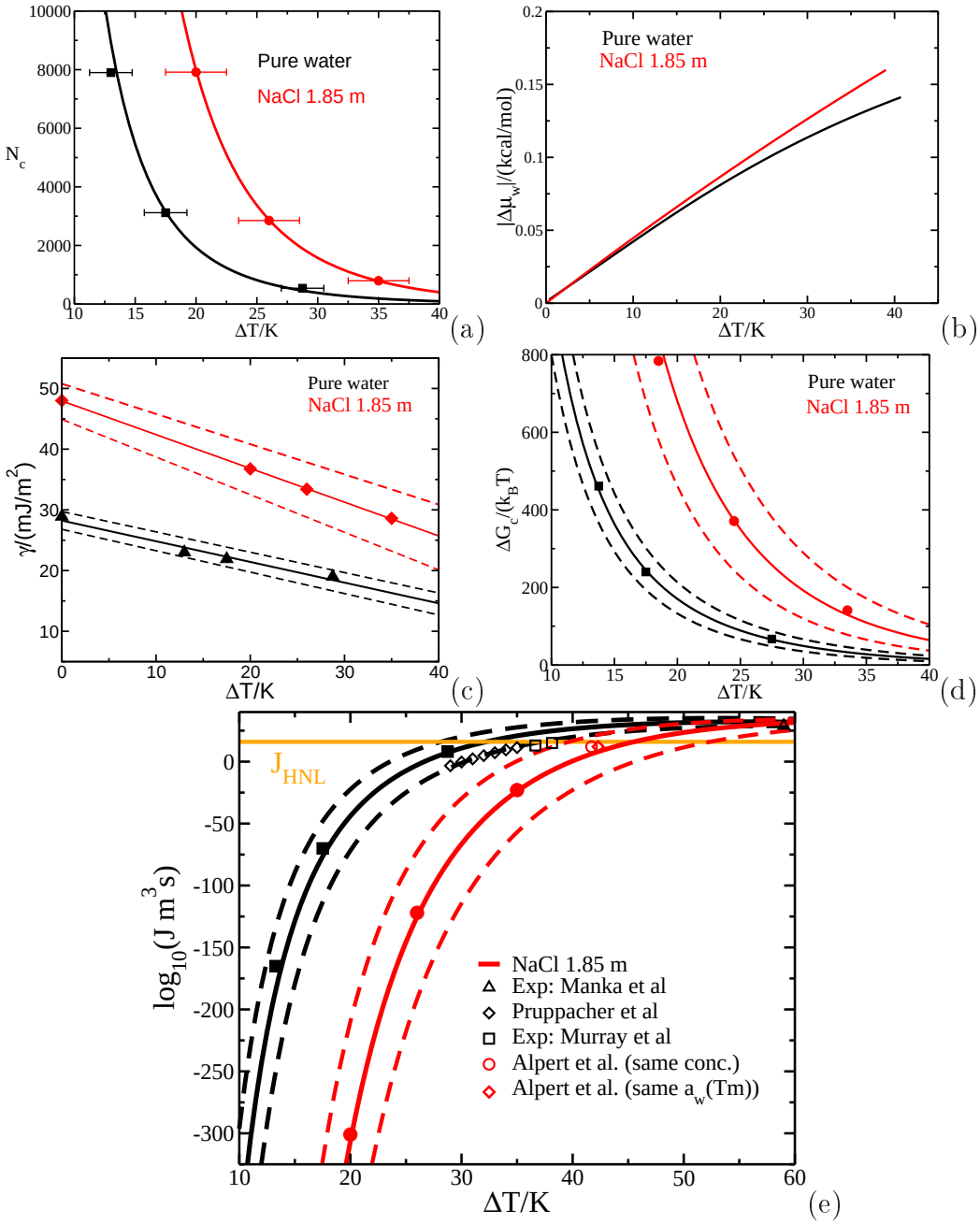

Figure 10.5: Plotted for pure (black) and 1.85 m salty water (red) as a function of the supercooling:(a) Number of particles in the critical cluster; (b) Water chemical potential difference between the liquid and the solid phases; (c) ice-water interfacial free energy; (d) height of the ice nucleation free energy barrier; (d) decimal logarithm of the nucleation rate for pure water and the 1.85 m NaCl solution. J_{HNL} is the homogeneous nucleation line corresponding to a rate of J=$10^{16} m^{-3} s^{-1}$ measured in typical experiments[69]. Solid symbols are our seeding results and empty symbols are experimental results by Pruppacher[70], Murray et al.[71], Alpert et al.[7] and Manka et al. (triangle at the top right of the figure)[72] as indicated in the legend.

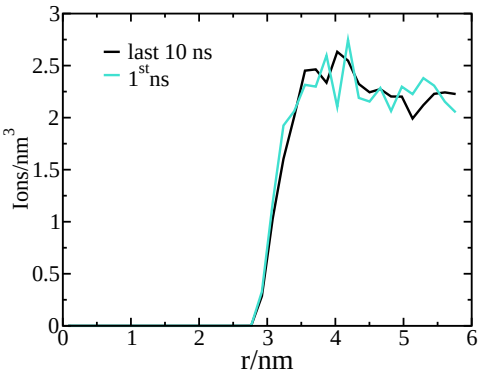

Figure 10.6: Ion density as a function of the radial distance from the center of mass of the ice cluster. Turquoise, density profile averaged over the first nanosecond of the trajectory in Fig. 10.4(b) corresponding to 215 K. Black, density profile averaged over the last 10 ns of the same trajectory.

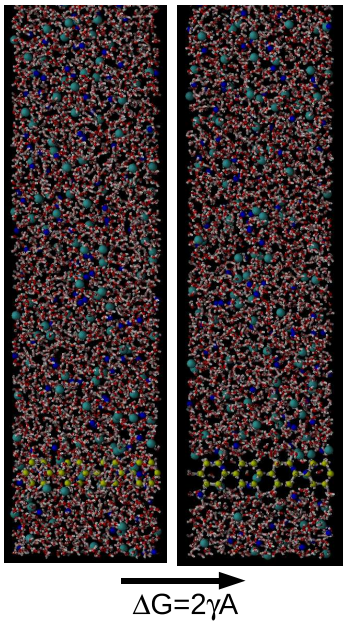

Figure 10.7: Snapshot of a 1.85 m NaCl solution configuration at the melting temperature at 1 bar. The square well-like interaction between the mold sites (yellow particles) and the oxygens of the water molecules is switched off in the left panel and on in the right panel. Note that the number for crystal planes in the mold, N_l, is three in this case.

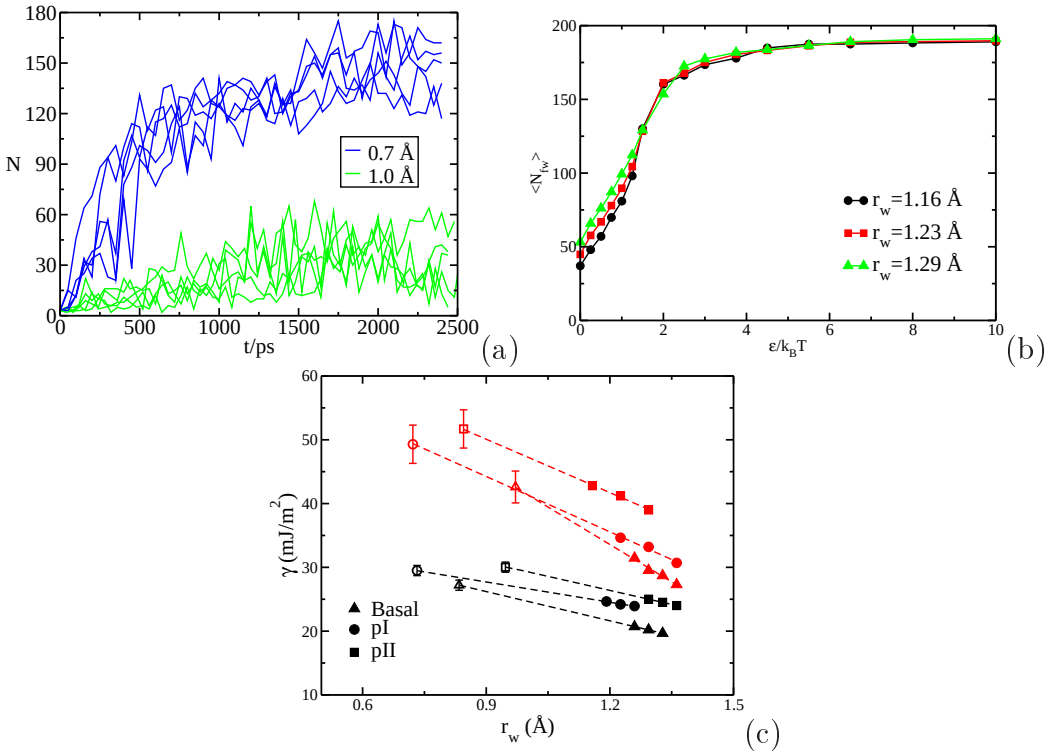

Figure 10.8: (a) Number of ice-like molecules growing from the mold as a function of time for several trajectories starting from the studied NaCl solution at coexistence conditions. The mold is switched on at the beginning of the simulation. The well radious r_w is 1 Å for the green curves and 0.7 Å for the blue ones. (b) Integrand of Eq. 10.7 for several r_w values, as indicated in the legend, for the secondary prismatic plane. (c) Ice-fluid interfacial free energy as a function of r_w for several crystal orientations as indicated in the legend. Red data correspond to the solution and black ones, from Ref.[39], to pure water. Filled symbols are the results of our calculations and empty ones are the extrapolation to the corresponding r_w^o, which give the final γ values.

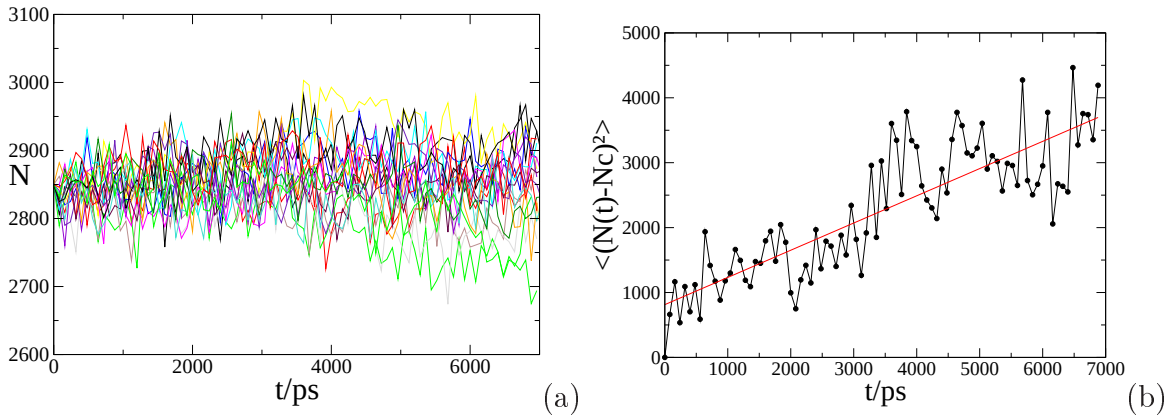

Figure 10.9: (a) Time evolution of the number of particles, N, in a critical ice cluster of $\sim$ 2850 molecules in salty water. Different trajectories correspond to runs launched with different velocity distributions. (b) Mean squared difference of the number of molecules in the cluster at time t and time 0 as a function of time.

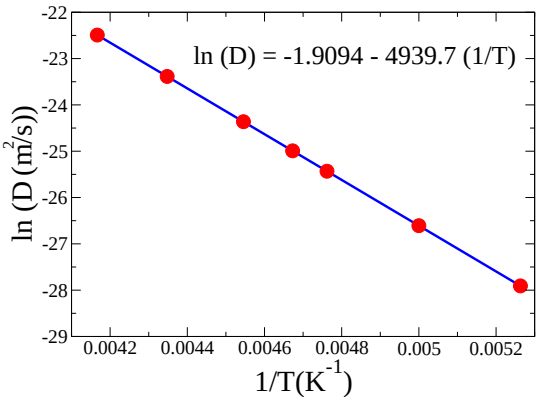

Figure 10.10: Diffussion coefficient of water in the salty solution as a function of the inverse temperature.

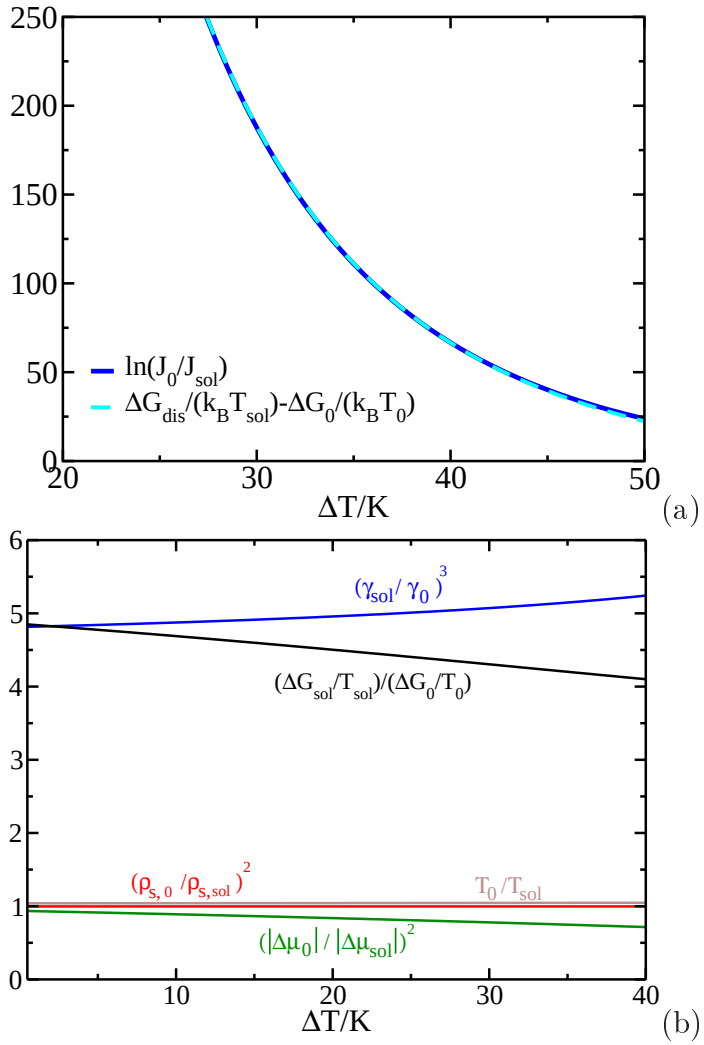

Figure 10.11: (a) Difference in $\ln J$ and $-\Delta G_c/(k_B T)$ between salty and pure water as a function of the supercooling. (b) Black curve, factor by which $\Delta G_c/(k_B T)$ increases in the salty solution with respect to pure water as a function of the supercooling. Coloured curves, different factors that contribute to such increase, as indicated in the figure. The product of the coloured curves gives the black curve.

10.9. Appendix: Determining N

To determine the number of particles in the ice phase (be it the ice slab in the direct coexistence simulations or the cluster in the seeding ones) we use the $\bar{q}_i$ rotationally invariant local-bond order parameter proposed in Ref.[74]. $\bar{q}_i$ is a scalar number whose value for a given particle depends on the relative positions of the tagged particle and its neighbors within a certain distance (3.5 Å, around the first minimum in the oxygen-oxygen radial distribution function of the liquid phase). We only use the oxygens for the calculation of $\bar{q}_i$. In Fig. 10.12 (a) we plot typical ($\bar{q}_4$,$\bar{q}_6$) values for ice (red) and solution (green) water molecules. Differently from $\bar{q}_4$, it is possible to establish a threshold for $\bar{q}_6$, $\bar{q}_{6,t}$, to discriminate between ice-like and solution-like water molecules (indicated with a horizontal dashed line in Fig. 10.12(a)). To establish the $\bar{q}_{6,t}$ value we look at the point at which the fraction of wrongly labelled particles in both phases coincide (see Fig. 10.12(b)). As shown in Fig. 10.12(c), the value of such threshold depends on temperature. For a given temperature, particles with $\bar{q}_6 > \bar{q}_{6,t}$ are labelled as solid-like. Having established all solid-like particles in the system, we cluster them using a neighbour cut-off distance of 3.5Å. N is the number of molecules in the largest detected cluster of solid-like molecules.

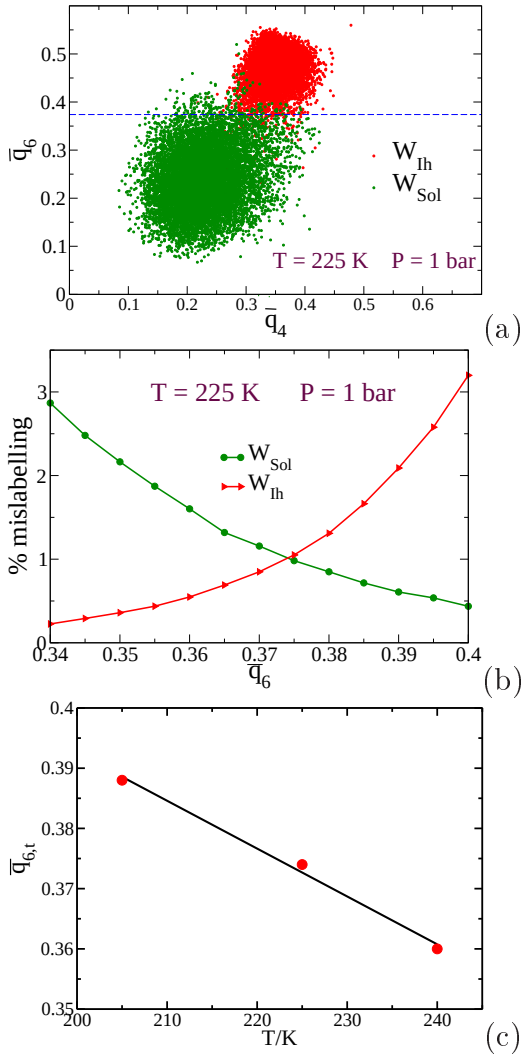

Figure 10.12: (a) $\bar{q}_6$ vs $\bar{q}_4$ for water in the salty solution (green) and water in ice Ih (red). (b) Fraction of mislabelled particles as a function of the $\bar{q}_6$ threshold for both phases at 225 K and 1 bar. The $\bar{q}_6$ threshold is chosen at the crossing point between both curves. (c) Selected $\bar{q}_6$ threshold, $\bar{q}_{6,t}$, as a function of temperature.

Bibliography

1. Gerrard, A. G., *Rocks and Landforms* (Springer Netherlands, 1988).

2. Li, J. K. & Lee, T. C., Bacterial ice nucleation and its potential application in the food-industry. *Trends in Food Sci. & Tech.* **6**, 259–265 (1995).

3. Maki, L. R., Galyan, E. L., M.M., C. & Caldwell, D. R., Ice nucleation induced by pseudomonas-syringae. *Appl. Microbiol.* **28**, 456–459 (1974).

4. Morris, G. J. & Acton, E., Controlled ice nucleation in cryopreservation–a review. *Cryobiology* **66**, 85 (2013).

5. Kanno, H. & Angell, C. A., Homogeneous nucleation and glass formation in aqueous alkali halide solutions at high pressures. *The Journal of Physical Chemistry* **81**, 2639–2643 (1977).

6. Kelton, K. F., *Crystal Nucleation in Liquids and Glasses* (Academic, Boston, 1991).

7. Alpert, P. A., Aller, J. Y. & Knopf, D. A., Ice nucleation from aqueous nacl droplets with and without marine diatoms. *Atmos. Chem. Phys.* **11**, 5539 (2011).

8. Ickes, L., Welti, A., Hoose, C. & Lohmann, U., Classical nucleation theory of homogeneous freezing of water: thermodynamic and kinetic parameters. *Phys. Chem. Chem. Phys.* **17**, 5514–5537 (2015).

9. Sosso, G. C., Chen, J., Cox, S. J., Fitzner, M., Pedevilla, P., Zen, A. & Michaelides, A., Crystal nucleation in liquids: Open questions and future challenges in molecular dynamics simulations. *Chemical Reviews* **116**, 7078–7116 (2016).

10. Radhakrishnan, R. & Trout, B. L., Nucleation of hexagonal ice (Ih) in liquid water. *J. Am. Chem. Soc.* **125**, 7743 (2003).

11. Quigley, D. & Rodger, P. M., Metadynamics simulations of ice nucleation and growth. *J. Chem. Phys.* **128**, 154518 (2008).

12. Geiger, P. & Dellago, C., Neural networks for local structure detection in polymorphic systems. *J. Chem. Phys.* **139**, 164105 (2013).

13. Moore, E. B. & Molinero, V., Is it cubic? ice crystallization from deeply supercooled water. *Phys. Chem. Chem. Phys.* **13**, 20008 (2011).

14. Malkin, T. L., Murray, B. J., Brukhno, A. V., Anwar, J. & Salzmann, C. G., Structure of ice crystallized from supercooled water. *Proceedings of the National Academy of Sciences* **109**, 1041–1045 (2012).

15. Li, T., Donadio, D., Russo, G. & Galli, G., Homogeneous ice nucleation from supercooled water. *Phys. Chem. Chem. Phys.* **13**, 19807–19813 (2011).

16. Haji-Akbari, A. & Debenedetti, P. G., Direct calculation of ice homogeneous nucleation rate for a molecular model of water. *Proceedings of the National Academy of Sciences* **112**, 10582–10588 (2015).

17. Sanz, E., Vega, C., Espinosa, J. R., Caballero-Bernal, R., Abascal, J. L. F. & Valeriani, C., Homogeneous ice nucleation at moderate supercooling from molecular simulation. *Journal of the American Chemical Society* **135**, 15008–15017 (2013).

18. Chakraborty, D. & Patey, G. N., How crystals nucleate and grow in aqueous nacl solution. *The Journal of Physical Chemistry Letters* **4**, 573–578 (2013).

19. Lanaro, G. & Patey, G. N., Birth of nacl crystals: Insights from molecular simulations. *The Journal of Physical Chemistry B* **120**, 9076–9087 (2016).

20. Zahn, D., Atomistic mechanism of NaCl nucleation from an aqueous solution. *Phys. Rev. Lett.* **92**, 040801 (2004).

21. Zimmermann, N. E. R., Vorselaars, B., Quigley, D. & Peters, B., Nucleation of NaCl from aqueous solution: Critical sizes, ion-attachment kinetics, and rates. *Journal of the American Chemical Society* **137**, 13352–13361 (2015).

22. Conde, M. M., Rovere, M. & Gallo, P., Spontaneous nacl-doped ice at seawater conditions: focus on the mechanisms of ion inclusion. *Phys. Chem. Chem. Phys.* **19**, 9566–9574 (2017).

23. Bullock, G. & Molinero, V., Low-density liquid water is the mother of ice: on the relation between mesostructure, thermodynamics and ice crystallization in solutions. *Faraday Discuss.* **167**, 371–388 (2013).

24. Bauerecker, S., Ulbig, P., Buch, V., Vrbka, L. & Jungwirth, P., Monitoring ice nucleation in pure and salty water via high-speed imaging and computer simulations. *The Journal of Physical Chemistry C* **112**, 7631–7636 (2008).

25. Kanno, H., Speedy, R. J. & Angell, C. A., Supercooling of water to -92^{o}c under pressure. *Science* **189**, 880–881 (1975).

26. Espinosa, J. R., Zaragoza, A., Rosales-Pelaez, P., Navarro, C., Valeriani, C., Vega, C. & Sanz, E., Interfacial free energy as the key to the pressure-induced deceleration of ice nucleation. *Phys. Rev. Lett.* **117**, 135702 (2016).

27. Espinosa, J. R., Soria, G. D., Ramirez, J., Valeriani, C., Vega, C. & Sanz, E., Role of salt, pressure, and water activity on homogeneous ice nucleation. *J. Phys. Chem. Lett.* **8**, 4486 (2017).

28. Abascal, J. L. F. & Vega, C., A general purpose model for the condensed phases of water: TIP4P/2005. *J. Chem. Phys.* **123**, 234505 (2005).

29. Joung, I. S. & Cheatham, T. E., Determination of alkali and halide monovalent ion parameters for use in explicitly solvated biomolecular simulations. *The Journal of Physical Chemistry B* **112**, 9020–9041 (2008).

30. Benavides, A. L., Aragones, J. L. & Vega, C., Consensus on the solubility of NaCl in water from computer simulations using the chemical potential route. *The Journal of Chemical Physics* **144**, 124504 (2016).

31. Volmer, M. & Weber, A., Keimbildung in ubersattigten gebilden. *Z. Phys. Chem.* **119**, 277 (1926).

32. Becker, R. & Doring, W., Kinetische behandlung der keimbildung in ubersattigten dampfen. *Ann. Phys.* **416**, 719–752 (1935).

33. Ladd, A. & Woodcock, L., Triple-point coexistence properties of the lennard-jones system. *Chemical Physics Letters* **51**, 155 – 159 (1977).

34. Sanz, E. & Vega, C., Solubility of KF and NaCl in water by molecular simulation. *J. Chem. Phys.* **126**, 014507 (2007).

35. Frenkel, D. & Smit, B., *Understanding Molecular Simulation* (Academic Press, London, 1996).

36. Espinosa, J. R., Vega, C., Valeriani, C. & Sanz, E., Seeding approach to crystal nucleation. *J. Chem. Phys.* **144**, 034501 (2016).

37. Auer, S. & Frenkel, D., Prediction of absolute crystal-nucleation rate in hard-sphere colloids. *Nature* **409**, 1020 (2001).

38. Espinosa, J. R., Vega, C. & Sanz, E., The mold integration method for the calculation of the crystal-fluid interfacial free energy from simulations. *J Chem. Phys.* **141**, 134709 (2014).

39. Espinosa, J. R., Vega, C. & Sanz, E., Ice-water interfacial free energy for the tip4p, tip4p/2005, tip4p/ice and mw models as obtained from the mold integration technique. *The Journal of Physical Chemistry C* **120**, 8068–8075 (2016).

40. Espinosa, J. R., Sanz, E., Valeriani, C. & Vega, C., Homogeneous ice nucleation evaluated for several water models. *J. Chem. Phys.* **141**, 18C529 (2014).

41. Lorentz, H. A., Ueber die anwendung des satzes vom virial in der kinetischen theorie der gase. *Annalen der Physik* **248**, 127–136 (1881).

42. Berthelot, D. *C. R. Acad. Sci.* **126**, 1713 (1898).

43. Hamer, W. J. & Wu, Y.-C., Osmotic coefficients and mean activity coefficients of uni¿univalent electrolytes in water at 25°c. *Journal of Physical and Chemical Reference Data* **1**, 1047–1100 (1972).

44. Hess, B., Kutzner, C., van der Spoel, D. & Lindahl, E., Algorithms for highly efficient, load-balanced, and scalable molecular simulation. *J. Chem. Theory Comput.* **4**, 435–447 (2008).

45. Parrinello, M. & Rahman, A., Polymorphic transitions in single crystals: A new Molecular Dynamics method. *J. App. Phys.* **52**, 7182–7190 (1981).

46. Bussi, G., Donadio, D. & Parrinello, M., Canonical sampling through velocity rescaling. *The Journal of Chemical Physics* **126**, 014101 (2007).

47. Wheeler, D. R. & Newman, J., A less expensive ewald lattice sum. *Chem. Phys. Lett.* **366**, 537 (2002).

48. Hess, B., Bekker, H., Berendsen, H. J. C. & Fraaije, J. G. E. M., Lincs: A linear constraint solver for molecular simulations. *J. Comput. Chem.* **18**, 1463–1472 (1997).

49. Hess, B., P-lincs:¿ a parallel linear constraint solver for molecular simulation. *Journal of Chemical Theory and Computation* **4**, 116–122 (2008).

50. Garcia-Fernandez, R., Abascal, J. L. F. & Vega, C., The melting point of ice ih for common water models calculated from direct coexistence of the solid-liquid interface. *The Journal of Chemical Physics* **124**, 144506 (2006).

51. Noya, E. G., Vega, C. & de Miguel, E., Determination of the melting point of hard spheres from direct coexistence simulation methods. *The Journal of Chemical Physics* **128**, 154507 (2008).

52. Espinosa, J. R., Sanz, E., Valeriani, C. & Vega, C., On fluid-solid direct coexistence simulations: The pseudo-hard sphere model. *The Journal of Chemical Physics* **139**, 144502 (2013).

53. Aragones, J. L., Sanz, E., Valeriani, C. & Vega, C., Calculation of the melting point of alkali halides by means of computer simulations. *J. Chem. Phys.* **137**, 104507 (2012).

54. Conde, M. M., Gonzalez, M. A., Abascal, J. L. F. & Vega, C., Determining the phase diagram of water from direct coexistence simulations: The phase diagram of the TIP4P/2005 model revisited. *The Journal of Chemical Physics* **139**, 154505 (2013).

55. Mester, Z. & Panagiotopoulos, A. Z., Temperature-dependent solubilities and mean ionic activity coefficients of alkali halides in water from molecular dynamics simulations. *The Journal of Chemical Physics* **143**, 044505 (2015).

56. Mester, Z. & Panagiotopoulos, A. Z., Mean ionic activity coefficients in aqueous nacl solutions from molecular dynamics simulations. *The Journal of Chemical Physics* **142**, 044507 (2015).

57. Paluch, A. S., Jayaraman, S., Shah, J. K. & Maginn, E. J., A method for computing the solubility limit of solids: Application to sodium chloride in water and alcohols. *The Journal of Chemical Physics* **133**, 124504 (2010).

58. Moucka, F., Lisal, M. & Smith, W. R., Molecular simulation of aqueous electrolyte solubility. 3. alkali-halide salts and their mixtures in water and in hydrochloric acid. *The Journal of Physical Chemistry B* **116**, 5468–5478 (2012).

59. Nezbeda, I., Moucka, F. & Smith, W. R., Recent progress in molecular simulation of aqueous electrolytes: force fields, chemical potentials and solubility. *Molecular Physics* **114**, 1665–1690 (2016).

60. Li, L., Totton, T. & Frenkel, D., Computational methodology for solubility prediction: Application to the sparingly soluble solutes. *The Journal of Chemical Physics* **146**, 214110 (2017).

61. Pereyra, R. G., Szleifer, I. & Carignano, M. A., Temperature dependence of ice critical nucleus size. *J. Chem. Phys.* **135**, 034508 (2011).

62. Bai, X.-M. & Li, M., Calculation of solid-liquid interfacial free energy: A classical nucleation theory based approach. *J. Chem. Phys.* **124**, 124707 (2006).

63. Hurtado, P. I., Marro, J. & Garrido, P. L., Demagnetization via nucleation of the non-equilibrium metastable phase in a model of disorder. *Journal of Statistical Physics* **133**, 29–58 (2008).

64. Jacobson, V., L.C.;Molinero, Can amorphous nuclei grow crystalline clathrates? the size and crystallinity of critical clathrate nuclei. *J.Am.Chem.Soc.* **133**, 6458 (2011).

65. Knott, B. C., Molinero, V., Doherty, M. F. & Peters, B., Homogeneous nucleation of methane hydrates: Unrealistic under realistic conditions. *J. Am. Chem. Soc.* **134**, 19544–19547 (2012).

66. Espinosa, J. R., Vega, C., Valeriani, C. & Sanz, E., The crystal-fluid interfacial free energy and nucleation rate of NaCl from different simulation methods. *J. Chem. Phys.* **142**, 194709 (2015).

67. Zaragoza, A., Conde, M. M., Espinosa, J. R., Valeriani, C., Vega, C. & Sanz, E., Competition between ices ih and ic in homogeneous water freezing. *The Journal of Chemical Physics* **143**, 134504 (2015).

68. Koop, T., Kapilashrami, A., Molina, L. T. & Molina, M. J., Phase transitions of sea-salt/water mixtures at low temperatures: Implications for ozone chemistry in the polar marine boundary layer. *Journal of Geophysical Research: Atmospheres* **105**, 26393–26402 (2000).

69. Koop, T., Luo, B., Tsias, A. & Peter, T., Water activity as the determinant for homogeneous ice nucleation in aqueous solutions. *Nature* **406**, 611–614 (2000).

70. Pruppacher, H. R., A new look at homogeneous ice nucleation in supercooled water drops. *J. Atmosph. Sci.* **52**, 1924 (1995).

71. Murray, B. J., Broadley, S. L., Wilson, T. W., Bull, S. J., Wills, R. H., Christenson, H. K. & Murray, E. J., Kinetics of the homogeneous freezing of water. *Phys. Chem. Chem. Phys.* **12**, 10380 (2010).

72. Manka, A., Pathak, H., Tanimura, S., Wolk, J., Strey, R. & Wyslouzil, B. E., Freezing water in no man's land. *Phys. Chem. Chem. Phys.* **14**, 4505–4516 (2012).

73. Potter, R. W., Clynne, M. A. & Brown, D. L., Freezing point depression of aqueous sodium chloride solutions. *Scientific Communications* **73**, 284–285 (1978).

74. Lechner, W. & Dellago, C., Accurate determination of crystal structures based on averaged local bond order parameters. *J. Chem. Phys.* **129**, 114707 (2008).

Results: Chapter 11

On the Role of Salt, Pressure and Water Activity on Homogeneous Ice Nucleation

Jorge R. Espinosa [†], *Guiomar D. Soria* [†], *Jorge Ramirez* [§], *Chantal Valeriani* [‡], *Carlos Vega* [†], *Eduardo Sanz* [†]

[†]Departamento de Quimica Fisica I, Facultad de Ciencias Quimicas, Universidad Complutense de Madrid, 28040 Madrid, Spain.
[‡]Departamento de Fisica Aplicada I, Facultad de Ciencias Fisicas, Universidad Complutense de Madrid, 28040 Madrid, Spain.
[§] Departamento de Ingenieria Quimica Industrial y Medio Ambiente, Escuela Tecnica Superior de Ingenieros Industriales, Universidad Politecnica de Madrid, 28006 Madrid, Spain.

11.1. Abstract

Pure water can be substantially supercooled below the melting temperature without transforming into ice. The achievable supercooling can be enhanced by adding solutes or by applying hydrostatic pressure. Avoiding ice formation is of great importance in the cryopreservation of food or biological samples. In this paper we investigate the similarity between the effects of pressure and salt on ice formation using a combination of state-of-the-art simulation techniques. We find that both hinder ice formation by increasing the energetic cost of creating the ice-fluid interface. Moreover, we examine the widely-accepted proposal that the ice nucleation rate for different pressures and solute concentrations can be mapped through the activity of water [Koop, Luo, Tsias, Peter, 406, 611, Nature, 2000]. We show that such proposal is not consistent with the nucleation rates predicted in our simulations because it does not include all parameters

affecting ice nucleation. Therefore, even though salt and pressure have a qualitatively similar effect on ice formation, they cannot be quantitatively mapped onto one another.

11.2. Introduction

The formation of ice from supercooled water is the most important freezing transition on Earth. Despite its relevance and ubiquity there are still many uncertainties about this phase transition. For instance, important issues such as the rate[1–3] and the mechanism[4,5] by which ice nucleates in supercooled water are still currently under debate[6].

The urge for understanding in detail water freezing comes from the fact that it has a central role in key industrial and environmental processes. For example, the content of ice in clouds has a strong impact on the Earth's albedo and, therefore, on climate change[7]. On the other hand, a successful cryopreservation crucially depends on avoiding water freezing, that can be deleterious for the cells[8].

A way to delay the formation of ice in cryopreservation protocols is to put the sample under hydrostatic pressure[9] to slow down ice nucleation[10]. Salt is also known to have a decelerating effect on ice nucleation[11].

In a seminal work Koop et al. compiled experimental data of the freezing of salty aqueous solutions at different concentrations and pressures. Quite remarkably, they were able to map the ice nucleation rate of all systems into a single curve that solely depends on the activity of water in solution[12]. This spectacular result, based on the parallelism between the effects of salt and pressure on ice nucleation, has had a great acceptance in the scientific community studying water freezing.

The goal of the present work is to investigate the analogy between the effects of pressure and salt on water freezing by means of computer simulations. By comparing the effects of salt and pressure we are able to assess the validity of the proposal by Koop et al. To achieve this we compare three systems: pure water at 1 bar, pure water at 2000 bar and an NaCl 1.85 m aqueous solution at 1 bar. State-of-the art simulations techniques are required to compute the ice nucleation rate and the interfacial free energy for these systems. We use the Seeding[13–15] and the Mold Integration[16] methods for that purpose. These techniques enable us to gain understanding on the parameters that affect the ice nucleation rate.

11.3. Results

We use the TIP4P/2005 water model[17] combined with the Joung Cheetham/SPC/E model for NaCl[18,19]. We perform Molecular Dynamics simulations at constant tempera-

ture and pressure with the GROMACS package[20]. We refer the reader to our previous work for further simulation details[3,21].

The Seeding Technique consists in simulating ice nuclei embedded in the supercooled fluid (either pure or salty water). We insert pure spherical ice Ih seeds as that shown in the graphical abstract. The embedded ice cluster configuration is equilibrated as described in Ref.[22]. We make sure the cluster interface is well equilibrated by looking at the ionic density profile[23]. Once we get an equilibrated configuration of an ice cluster embedded in the solution we monitor the evolution of the nucleus at different temperatures. For temperatures higher than that at which the inserted cluster is critical, the cluster melts, and viceversa.

In this way we obtain an estimate for the temperature at which the inserted cluster with N_c molecules is critical. We determine N_c using local-bond order parameters[24] as done in our previous work[14,15,25]. We use large system sizes to ensure that concentration changes are negligible as the cluster grows or melts in the brine solution[23]. In Fig. 11.1(a) we show N_c versus the supercooling, ΔT, which is the melting temperature, T_m, minus the temperature of interest (the model melting temperatures for pure ice in coexistence with pure water at 1 and 2000 bar[26] and with a 1.85 m NaCl aqueous solution at 1 bar[23] are 250, 227 and 240.5 K, respectively). Clearly, for a given ΔT, the number of molecules required to reach the critical size is larger in salty or compressed water than in pure water at normal pressure. This is consistent with the experimental observation that salt and pressure hinder ice nucleation[11].

To quantify the decelerating effect of salt and pressure on homogeneous ice nucleation we compute the nucleation rate, J. In the Seeding method, simulations are used to obtain the parameters on which the J expression given by Classical Nucleation Theory (CNT)[27–29] depends[14,15,30].

$$J = \sqrt{\frac{-\Delta\mu_w}{6\pi k_B T N_c}}\rho_f f^+ \exp\left(\frac{N_c \Delta\mu_w}{2k_B T}\right). \tag{11.1}$$

Such parameters are the fluid number density, ρ_f, the number of particles in the critical cluster N_c (Fig. 11.1(a)), the chemical potential difference of water in ice and in the liquid, $\Delta\mu_w = \mu_w^i - \mu_w$ (Fig. 11.1(b)), and the frequency with which particles attach to the critical cluster (the attachment rate). Further details on the calculation of these factors will be given in a forthcoming publication[23]. The nucleation rate as a function of the supercooling is plotted in Fig. 11.1(c) for the three systems under comparison. For a given supercooling, pure water at normal pressure (in black) has the highest nucleation rate. In other words, the supercooling required to freeze water increases when adding salt (in red) or applying pressure (in blue), in agreement with the experimental trend[10,11].

Since we have access to all variables required for the computation of J we can rationalise which is the main factor behind the pressure/salt-induced deceleration of

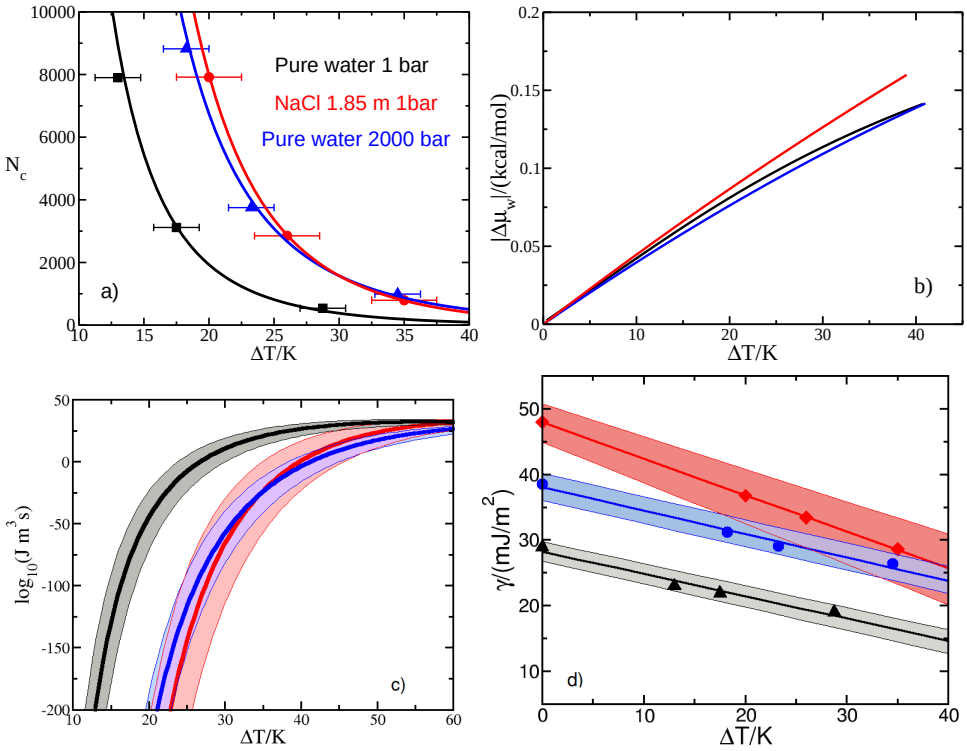

Figure 11.1: Plotted for pure (black), salty (red) and compressed water (blue) as a function of the supercooling:(a) Number of particles in the critical cluster; (b) Water chemical potential difference between the liquid and the solid phases; (c) decimal logarithm of the nucleation rate; (d) ice-water interfacial free energy. Symbols in (d) for $\Delta T = 0$ and $\Delta T > 0$ correspond to our calculations of γ with MI and Seeding, respectively. Shaded regions in (c) and (d) indicate the error bar.

ice nucleation. The nucleation rate is given by $J = Ae^{-\Delta G_c/(k_B T)}$ where A is a kinetic pre-factor and $\Delta G_c/(k_B T)$ is the Gibbs free energy barrier required to form a critical ice nucleus in the supercooled fuid. We have checked that A does not change by more than one or two orders of magnitude between different systems for a given supercooling, which is insignificant as compared to the large differences between the J curves in Fig. 11.1(c). The differences in J must be then ascribed to changes in $\Delta G_c/(k_B T)$. Within CNT, $\Delta G_c/(k_B T)$ is proportional to the third power of the ice-liquid interfacial free energy, γ, and inversely proportional to the second power of $|\Delta\mu_w|$. The latter does not significantly change from one system to another (see Fig. 11.1(b)). Therefore, the key to the decrease of J must be found in an increase of γ. This is in fact what we concluded in our recent study of ice nucleation under high pressure[31]. In Fig. 11.1(d) we represent γ versus the

supercooling for the three studied systems (the points for the supercooled fluid have been obtained with the Seeding method whereas those at coexistence, $\Delta T = 0$, with the Mold Integration method[16,21]). Indeed, the interfacial free energy increases when adding salt or applying pressure for a given supercooling. Therefore, both pressure and salt decelerate ice nucleation by increasing the ice-liquid interfacial free energy, which is one of the main conclusions of our work. This is a valuable simulation prediction given that there is no experimental consensus for the value of the ice-liquid interfacial free energy (not even for the case of pure water at 1 bar[32]).

The fact that pressure and salt hinder ice nucleation for the same reason is in principle consistent with the proposition that applying a certain pressure should have the same effect on ice nucleation as adding a given amount of salt[12]. Such proposal is the basis of the so-called water-activity-based ice nucleation theory (WAB-INT)[12,33]. The WAB-INT is based on an analysis of the freezing of salty water drops at different pressures and proposes that the nucleation rate depends only on the activity of water, a_w. This idea is extremely appealing because it enables to obtain the nucleation rate for any solution at any pressure with a fit solely depending on a measurable thermodynamic parameter such as the activity. Although the WAB-INT apparently works[12] it has never been carefully checked for three reasons: (i) a_w cannot be experimentally measured for deeply supercooled solutions due to the formation of ice (in fact, in many cases it is assumed to be independent of temperature[33]); (ii) the general character of the theory has not been tested since the J-range that can be measured is narrow (it is limited by the sample's volume and the cooling rate); (iii) the physical basis of the WAB-INT is unclear since many of the parameters that affect ice nucleation, like γ, N_c or $\Delta\mu_w$ for $T < T_m$, cannot be measured experimentally. Our simulations do not have these shortcomings and enable us to test the validity of the WAB-INT in a wide range of nucleation rates.

To start with, we evaluate the temperature dependence of a_w in the brine solution at 1 bar and with salt concentration $c = 1{,}85$ m via:

$$\mu_w(c, T, 1) = \mu_w(0, T, 1) + RT \ln[a_w(c, T, 1)] \tag{11.2}$$

In practise, the chemical potential difference with and without salt at 1 bar, $\mu_w(c, T, 1) - \mu_w(0, T, 1)$, is obtained as $\Delta\mu_w(0, T, 1) - \Delta\mu_w(c, T, 1)$, the difference between the black and the red curves in Fig. 11.1(b) (the chemical potential of water in ice cancels out when both $\Delta\mu_w$'s are subtracted). In Fig. 11.2 we plot $a_w(c, T, 1)$ as a function of the supercooling (red curve). To our knowledge, this is the first time that the temperature dependence of water activity is reported up to such deep supercooling either in simulations or experiments (there are simulation works that report activities as a function of concentration at constant temperature[34]). As explained below, the cross with the orange curve (activity of water coexisting with ice) corresponds to the melting temperature,

above which the water activity remains almost constant, in accordance with experimental observations for most simple ionic solutions[33]. By contrast, a_w sharply increases below the melting temperature.

The activity of pure water under pressure is in principle 1. However, in the framework of the WAB-INT, pure water under pressure p is effectively assigned the activity of a water solution at normal pressure having the same chemical potential difference with ice, $\Delta\mu_w$:

$$\mu_w(0,T,p) - \mu_w^i(0,T,p) = \tag{11.3}$$

$$\mu_w(0,T,1) + RT\ln a_w(c^{eff},T,1) - \mu_w^i(0,T,1) \tag{11.4}$$

where c^{eff} is the effective concentration required to satisfy the equality above. Thus, we can compute $a_w(c^{eff},T,1)$ as $\exp[(\Delta\mu_w(0,T,1) - \Delta\mu_w(0,T,p))/(RT)]$ (the exponent is obtained by subtracting the black and the blue curves in Fig. 11.1(b)). In Fig. 11.2 we show $a_w(c^{eff},T,1)$ as a function of temperature (blue curve). Again, the activity sharply raises below the melting temperature of compressed water, given by the crossing with the orange curve. Therefore, according to our simulations, the assumption that a_w does not depend on temperature for most ionic solutions[12,33] cannot be safely made, especially at low temperatures where water behaves anomalously[35,36].

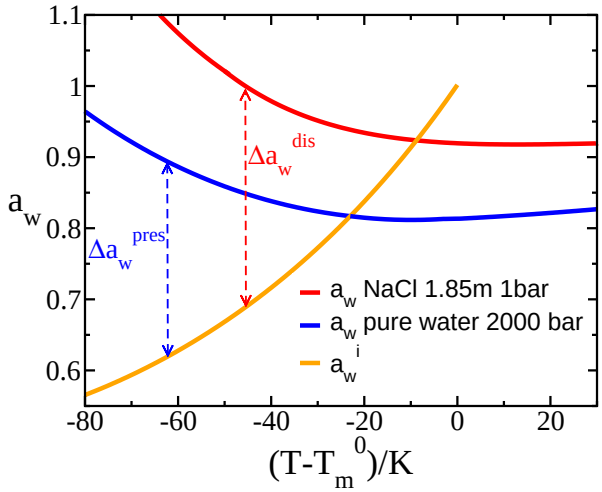

Figure 11.2: Water activity as a function of $T - T_m^0$, the difference between the temperature of interest and the melting temperature of pure water ($T_m^0 = 250$ K for the model). In red we plot the activity of water in the studied 1.85 m solution and in blue the effective activity for pure water at 2000 bar as defined in the main text. In orange we plot the activity of water coexisting with ice.

As pointed out in Ref.[33], the validity of the WAB-INT does not rely on whether or not a_w depends on temperature[12]. What the WAB-INT theory really proposes is that $J(\Delta a_w)$ is a universal curve for any pressure or concentration. Δa_w is the difference, for a given temperature, between the activity of water in the solution (or in compressed water) and the activity of water at coexistence with ice, a_w^i. The latter can be obtained through:

$$\mu_w^i(0,T,1) = \mu_w(0,T,1) + RT\ln[a_w^i(c,T,1)] \tag{11.5}$$

The chemical potential difference $\mu_w^i(0,T,1) - \mu_w(0,T,1)$ is simply $\Delta\mu_w$ for pure water at 1 bar (black curve in Fig. 11.1(b)). a_w^i is plotted in orange in Fig. 11.2 (at the melting point the orange and the red/blue curves cross because the activity of water becomes equal to a_w^i). Thus, to obtain Δa_w for the studied solution we have to subtract, for a given temperature, the red and the orange curves in Fig. 11.2, whereas for pure water under pressure we compute the difference between the blue and the orange curves (see red and blue arrows in Fig. 11.2, respectively). Knowing $\Delta a_w(T)$ and $J(T)$ (Fig. 11.1(c)) we obtain $J(\Delta a_w)$. In Fig. 11.3(a) we plot $J(\Delta a_w)$ for compressed and salty water. Both curves are not the same for every Δa_w. Therefore, the WAB-INT proposal of a universal $J(\Delta a_w)$ curve is not consistent with our simulation predictions. However, the $J(\Delta a_w)$ curves lie close to each other beyond the rate value measured in typical experiments, $J \sim 10^{16} m^{-3} s^{-1}$, given by the horizontal green line in Fig. 11.3(a). Thus, our results are compatible with the fact that the WAB-INT may seem to work when data of typical freezing experiments are analysed[12]. Why a theory that is not general may seemingly work at high values of Δa_w?

On the one hand, it is perhaps worth noting that the WAB-INT is not as neat as it may appear. In the publication where the WAB-INT was proposed variations of up to 15-20 K around the universal freezing curve can be clearly noticed[12]. In that temperature range there may be many orders of magnitude difference in the nucleation rate. On the other hand, the WAB-INT may be a particular case of CNT in certain limits. Since the WAB-INT solely depends on the activity of the solvent (chemical potential), it will be compatible with CNT if, for a given Δa_w, all other parameters that affect ice nucleation are the same. We check if this is the case for the ice-fluid interfacial free energy, a parameter that we have shown to be central in understanding the effect of salt (this work) and pressure (Ref.[31]) on homogeneous ice nucleation. Combining $\Delta a_w(T)$ and $\gamma(T)$ (Fig. 11.1(d)) we obtain $\gamma(\Delta a_w)$, shown in Fig. 11.3(b). Clearly, γ is not the same for salty and compressed water at low Δa_w and becomes increasingly similar as Δa_w increases. When both Δa_w and γ are similar, the WAB-INT may seem to work, but this is just a particular case of CNT. That γ becomes similar between different systems at high Δa_w may be related with the nucleation of ice clusters in solute-depleted regions when the critical cluster size becomes small[37]. With our analysis we conclude that CNT is a much more comprehensive theoretical framework than the WAB-INT to understand

ice nucleation and that the WAB-INT may only seemingly work as a particular case of CNT at high nucleation rates. The fact that the simulation approach employed in this work provides estimates of the nucleation rate in a much wider range than current experiments has clearly evidenced the deficiencies of the WAB-INT. We expect our work to inspire future attempts to derive phenomenological frameworks to describe ice nucleation that do not necessarily comply with the WAB-INT[38].

Our conclusions are based on the results obtained with a water model. One may wonder if our observations can be safely applied to real water as well. We argue that if WAB-INT had a strong physical foundation it should be able to explain ice nucleation both in real water and in any family of realistic water models. Our model is quite realistic because it closely reproduces the behaviour of real water for many thermodynamic and dynamic properties[39], including anomalies[40] and, most importantly, homogeneous ice nucleation in pure[14,30] and salty water[23]. Moreover, in this work we show that the model captures the experimentally observed deceleration of ice nucleation with pressure and salt[10,12] (Fig. 11.1(c)), as well as the fact that the WAB-INT may seemingly work in the range of nucleation rates typically accessible to experiments (see Fig. 11.3(a)). Furthermore, we do not need a perfect model for the NaCl ions to test the WAB-INT, as the theory should in principle work for a wide variety of solutes. So even if the simulated solute does not behave exactly as real dissolved NaCl, it can be taken as any arbitrary solute with which testing the WAB-INT. Be it as it may, we hope our work will motivate future experiments to definitely confirm our prediction. As a matter of fact, there have been already experiments reporting inconsistencies with the WAB-INT[41].

Our Seeding approach to ice nucleation relies on two assumptions: (i) the proposed structure of the critical cluster is the correct one, and (ii) the formation free energy of such cluster can be obtained via CNT. Our guess for the critical nucleus structure is that of a spherical pure ice Ih cluster. We use ice Ih because this structure, or stacking mixtures of ice Ic and Ih, has shown to be that of critical ice clusters at 1 bar[4,14,25,31,42]. We insert pure ice seeds disregarding the possibility that NaCl ions enter the ice lattice. This approximation is inspired by the experimental phase diagram, where the brine coexists with pure ice[43]. To make sure this is a good approximation we have performed a long (260 ns) direct coexistence simulation below the melting temperature and computed the fraction of ions incorporated into the grown ice lattice. Such fraction was smaller than 0.2 per cent, a value in agreement with previous simulation work[44,45] and sufficiently small to justify our approximation. We use spherical clusters, consistently with previous studies showing that the cluster's shape quickly equilibrates into a sphere[25] –with thermal fluctuations typical of a rough ice-fluid interface[46,47]. Assumption (ii), in turn, is expected to be satisfied for the large critical cluster sizes used in this work. Independent evidence of the validity of CNT to describe the free energy of crystal cluster formation can be found, e. g., in Ref.[48]. As long as conditions (i) and (ii) are satisfied, one can use seeding to obtain nucleation rates regardless the pathway leading to the formation of

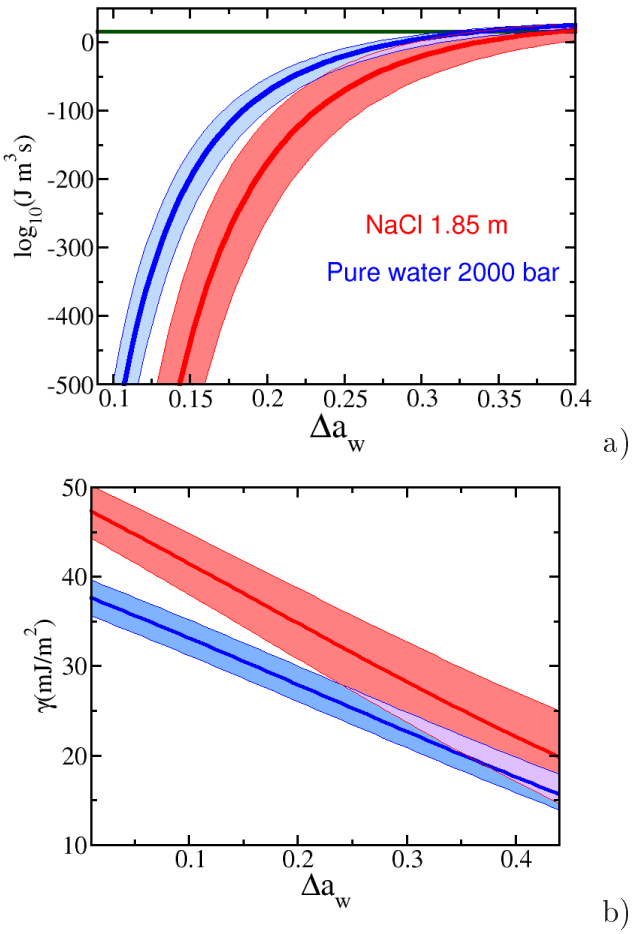

Figure 11.3: (a) Nucleation rate of salty (1.85 m NaCl) and compressed (2000 bar) water as a function of Δa_w. (b) Ice-fluid interfacial free energy as a function of Δa_w.

the critical cluster is CNT-like (a one-by-one addition of particles to a growing crystal cluster) or a more sophisticated one like composition fluctuations followed by the crystal cluster growth[37,49–51]. Thus, although seeding does not provide any information on the way the critical cluster is formed, it can be used to obtain nucleation rates[15], even in systems where the formation of the critical cluster has been reported to be two-step, like crystallization in hard spheres[52,53] or in mw-water[54]. In any case, since we are dealing with the crystallization of the solvent and with large critical clusters whose size exceeds that of typical composition fluctuations we do not expect the formation mechanism of the critical nucleus to be markedly two-step. It is also worth noting that seeding has been successful in predicting crystal nucleation rates in the Lennard Jones and the Tosi-

Fumi NaCl systems[15] as well, which gives further confidence in the predictions made in this paper. Moreover, in this work we find consistent values between the γ obtained at coexistence with Mold Integration, a method that does not rely on CNT and that does not suffer from strong finite size effects[16], and that obtained below the melting temperature with seeding (see Fig. 11.1(d)). This consistency test, and the considerations above mentioned, strongly support the validity of the approach followed in this work.

11.4. Conclusions

In summary, we compare the effects of pressure and salt on homogeneous ice nucleation. We find that both, pressure and salt, decelerate ice nucleation by increasing the ice-liquid interfacial free energy. Despite this qualitative similarity, it is not possible to quantitatively map ice nucleation rates of salty water onto those of compressed water through the activity of water. Our results question the validity of the so-called water-activity-based ice nucleation theory[12].

Understanding and quantifying the effect of salt on homogeneous ice nucleation can be useful to develop climate change models[7]. On the other hand, improving cryopreservation protocols, aimed at vitrifying biological samples by averting ice nucleation and growth upon cooling, requires deep understanding of the effect of freezing preventing factors like pressure, salt or combinations of both[8,9]. Our work may also have implications in the experimental search of the putative liquid-liquid transition of water[55–58], that in some cases uses pressure and solutes as strategies to approach the so-called no-man's-land[36,59,60].

Acknowledgements This work was funded by grants FIS2013/43209-P and FIS2016-78117-P FIS2016-78847-P of the MEC, and the UCM/Santander 910570 and PR26/16-10B-2. C.Valeriani and E. Sanz acknowledge financial support from a Ramon y Cajal Fellowship. J. R. Espinosa acknowledges financial support from the FPI grant BES-2014-067625. Calculations were carried out in the supercomputer facilities La Palma and Magerit from the Spanish Supercomputing Network (RES) (projects QCM-2015-3-0036 and QCM-2016-1-0039). The authors acknowledge the computer resources and technical assistance provided by the Centro de Supercomputacion y Visualizacion de Madrid (CeSViMa).

Bibliography

1. Laksmono, H., McQueen, T. A., Sellberg, J. A., Loh, N. D., Huang, C., Schlesinger, D., Sierra, R. G., Hampton, C. Y., Nordlund, D., Beye, M., Martin, A. V., Barty, A., Seibert, M. M., Messerschmidt, M., Williams, G. J., Boutet, S., Amann-Winkel, K., Loerting, T., Pettersson, L. G. M., Bogan, M. J. & Nilsson, A., Anomalous behavior of the homogeneous ice nucleation rate in no-man's land. *The Journal of Physical Chemistry Letters* **6**, 2826–2832 (2015).

2. Koop, T. & Murray, B. J., A physically constrained classical description of the homogeneous nucleation of ice in water. *The Journal of Chemical Physics* **145**, 211915 (2016).

3. Espinosa, J. R., Navarro, C., Sanz, E., Valeriani, C. & Vega, C., On the time required to freeze water. *The Journal of Chemical Physics* **145**, 211922 (2016).

4. Malkin, T. L., Murray, B. J., Brukhno, A. V., Anwar, J. & Salzmann, C. G., Structure of ice crystallized from supercooled water. *Proceedings of the National Academy of Sciences* **109**, 1041–1045 (2012).

5. Russo, J., Romano, F. & Tanaka, H., New metastable form of ice and its role in the homogeneous crystallization of water. *Nature Materials* **13**, 733 (2014).

6. Sosso, G. C., Chen, J., Cox, S. J., Fitzner, M., Pedevilla, P., Zen, A. & Michaelides, A., Crystal nucleation in liquids: Open questions and future challenges in molecular dynamics simulations. *Chemical Reviews* **116**, 7078–7116 (2016).

7. Cantrell, W. & Heymsfield, A., Production of ice in tropospheric clouds. *Bull. Amer. Meteor. Soc.* **86**, 795 (2005).

8. Morris, G. J. & Acton, E., Controlled ice nucleation in cryopreservation–a review. *Cryobiology* **66**, 85 (2013).

9. Studer, D., High-pressure freezing system (2001), US Patent 6,269,649.

10. Kanno, H., Speedy, R. J. & Angell, C. A., Supercooling of water to -92^{o}c under pressure. *Science* **189**, 880–881 (1975).

11. Kanno, H. & Angell, C. A., Homogeneous nucleation and glass formation in aqueous alkali halide solutions at high pressures. *The Journal of Physical Chemistry* **81**, 2639–2643 (1977).

12. Koop, T., Luo, B., Tsias, A. & Peter, T., Water activity as the determinant for homogeneous ice nucleation in aqueous solutions. *Nature* **406**, 611–614 (2000).

13. Knott, B. C., Molinero, V., Doherty, M. F. & Peters, B., Homogeneous nucleation of methane hydrates: Unrealistic under realistic conditions. *J. Am. Chem. Soc.* **134**, 19544–19547 (2012).

14. Sanz, E., Vega, C., Espinosa, J. R., Caballero-Bernal, R., Abascal, J. L. F. & Valeriani, C., Homogeneous ice nucleation at moderate supercooling from molecular simulation. *Journal of the American Chemical Society* **135**, 15008–15017 (2013).

15. Espinosa, J. R., Vega, C., Valeriani, C. & Sanz, E., Seeding approach to crystal nucleation. *J. Chem. Phys.* **144**, 034501 (2016).

16. Espinosa, J. R., Vega, C. & Sanz, E., The mold integration method for the calculation of the crystal-fluid interfacial free energy from simulations. *J Chem. Phys.* **141**, 134709 (2014).

17. Abascal, J. L. F. & Vega, C., A general purpose model for the condensed phases of water: TIP4P/2005. *J. Chem. Phys.* **123**, 234505 (2005).

18. Joung, I. S. & Cheatham, T. E., Determination of alkali and halide monovalent ion parameters for use in explicitly solvated biomolecular simulations. *The Journal of Physical Chemistry B* **112**, 9020–9041 (2008).

19. Benavides, A. L., Aragones, J. L. & Vega, C., Consensus on the solubility of NaCl in water from computer simulations using the chemical potential route. *The Journal of Chemical Physics* **144**, 124504 (2016).

20. Lindahl, E., Hess, B. & van der Spoel, D., Gromacs 3.0: a package for molecular simulation and trajectory analysis. *J. Mol. Model.* **7**, 306 (2001).

21. Espinosa, J. R., Vega, C. & Sanz, E., Ice-water interfacial free energy for the tip4p, tip4p/2005, tip4p/ice and mw models as obtained from the mold integration technique. *The Journal of Physical Chemistry C* **120**, 8068–8075 (2016).

22. Espinosa, J. R., Vega, C., Valeriani, C. & Sanz, E., The crystal-fluid interfacial free energy and nucleation rate of NaCl from different simulation methods. *J. Chem. Phys.* **142**, 194709 (2015).

23. Soria, G. D., Espinosa, J. R., Ramirez, J., Valeriani, C., Vega, C. & Sanz, E., A simulation study of homogeneous ice nucleation in supercooled salty water. *To be published* **-**, – (2017).

24. Lechner, W. & Dellago, C., Accurate determination of crystal structures based on averaged local bond order parameters. *J. Chem. Phys.* **129**, 114707 (2008).

25. Zaragoza, A., Conde, M. M., Espinosa, J. R., Valeriani, C., Vega, C. & Sanz, E., Competition between ices ih and ic in homogeneous water freezing. *The Journal of Chemical Physics* **143**, 134504 (2015).

26. Conde, M. M., Gonzalez, M. A., Abascal, J. L. F. & Vega, C., Determining the phase diagram of water from direct coexistence simulations: The phase diagram of the TIP4P/2005 model revisited. *The Journal of Chemical Physics* **139**, 154505 (2013).

27. Kelton, K. F., *Crystal Nucleation in Liquids and Glasses* (Academic, Boston, 1991).

28. Volmer, M. & Weber, A., Keimbildung in ubersattigten gebilden. *Z. Phys. Chem.* **119**, 277 (1926).

29. Becker, R. & Doring, W., Kinetische behandlung der keimbildung in ubersattigten dampfen. *Ann. Phys.* **416**, 719–752 (1935).

30. Espinosa, J. R., Sanz, E., Valeriani, C. & Vega, C., Homogeneous ice nucleation evaluated for several water models. *J. Chem. Phys.* **141**, 18C529 (2014).

31. Espinosa, J. R., Zaragoza, A., Rosales-Pelaez, P., Navarro, C., Valeriani, C., Vega, C. & Sanz, E., Interfacial free energy as the key to the pressure-induced deceleration of ice nucleation. *Phys. Rev. Lett.* **117**, 135702 (2016).

32. Ickes, L., Welti, A., Hoose, C. & Lohmann, U., Classical nucleation theory of homogeneous freezing of water: thermodynamic and kinetic parameters. *Phys. Chem. Chem. Phys.* **17**, 5514–5537 (2015).

33. Koop, T., Homogeneous ice nucleation in water and aqueous solutions. *Zeitschrift für Physikalische Chemie* **218**, 1231 (2004).

34. Mester, Z. & Panagiotopoulos, A. Z., Mean ionic activity coefficients in aqueous nacl solutions from molecular dynamics simulations. *The Journal of Chemical Physics* **142**, 044507 (2015).

35. Debenedetti, P. G., Supercooled and glassy water. *J. Phys.:Condens. Matter* **15**, R1669–R1726 (2003).

36. Gallo, P., Amann-Winkel, K., Angell, C. A., Anisimov, M. A., Caupin, F., Chakravarty, C., Lascaris, E., Loerting, T., Panagiotopoulos, A. Z., Russo, J., Sellberg, J. A., Stanley, H. E., Tanaka, H., Vega, C., Xu, L. & Pettersson, L. G. M., Water: A tale of two liquids. *Chemical Reviews* **116**, 7463–7500 (2016).

37. Bullock, G. & Molinero, V., Low-density liquid water is the mother of ice: on the relation between mesostructure, thermodynamics and ice crystallization in solutions. *Faraday Discuss.* **167**, 371–388 (2013).

38. Barahona, D., Analysis of the effect of water activity on ice formation using a new thermodynamic framework. *Atmos. Chem. Phys.* **14**, 7665–7680 (2014).

39. Vega, C. & Abascal, J. L. F., Simulating water with rigid non-polarizable models: a general perspective. *Phys. Chem. Chem. Phys.* **13**, 19663–19688 (2011).

40. Pi, H. L., Aragones, J. L., Vega, C., Noya, E. G., Abascal, J. L., Gonzalez, M. A. & McBride, C., Anomalies in water as obtained from computer simulations of the tip4p/2005 model: density maxima, and density, isothermal compressibility and heat capacity minima. *Molecular Physics* **107**, 365–374 (2009).

41. Swanson, B. D., How well does water activity determine homogeneous ice nucleation temperature in aqueous sulfuric acid and ammonium sulfate droplets? *Journal of the Atmospheric Sciences* **66**, 741–754 (2009).

42. Malkin, T. L., Murray, B. J., Salzmann, C. G., Molinero, V., Pickering, S. J. & Whale, T. F., Stacking disorder in ice i. *Phys. Chem. Chem. Phys.* **17**, 60–76 (2015).

43. Koop, T., Kapilashrami, A., Molina, L. T. & Molina, M. J., Phase transitions of sea-salt/water mixtures at low temperatures: Implications for ozone chemistry in the polar marine boundary layer. *Journal of Geophysical Research: Atmospheres* **105**, 26393–26402 (2000).

44. Conde, M. M., Rovere, M. & Gallo, P., Spontaneous nacl-doped ice at seawater conditions: focus on the mechanisms of ion inclusion. *Phys. Chem. Chem. Phys.* **19**, 9566–9574 (2017).

45. Bauerecker, S., Ulbig, P., Buch, V., Vrbka, L. & Jungwirth, P., Monitoring ice nucleation in pure and salty water via high-speed imaging and computer simulations. *The Journal of Physical Chemistry C* **112**, 7631–7636 (2008).

46. Benet, J., MacDowell, L. G. & Sanz, E., A study of the ice-water interface using the TIP4P/2005 water model. *Phys. Chem. Chem. Phys.* **16**, 22159–22166 (2014).

47. Benet, J., Llombart, P., Sanz, E. & MacDowell, L. G., Premelting-induced smoothening of the ice-vapor interface. *Phys. Rev. Lett.* **117**, 096101 (2016).

48. Koss, P., Statt, A., Virnau, P. & Binder, K., Free energy barriers for crystal nucleation from fluid phases. *arXiv* **-**, 1705.08216 (2017).

49. Agarwal, V. & Peters, B., *Solute Precipitate Nucleation: A Review of Theory and Simulation Advances*, 97–160 (John Wiley & Sons, Inc., 2014).

50. Vekilov, P. G., The two-step mechanism of nucleation of crystals in solution. *Nanoscale* **2**, 2346–2357 (2010).

51. Black, S., Simulating nucleation of molecular solids. *Proc. R. Soc. A* **463**, 2799–2811 (2007).

52. Schilling, T., Schöpe, H. J., Oettel, M., Opletal, G. & Snook, I., Precursor-mediated crystallization process in suspensions of hard spheres. *Phys. Rev. Lett.* **105**, 025701 (2010).

53. Russo, J. & Tanaka, H., The microscopic pathway to crystallization in supercooled liquids. *Scientific Reports* **2**, 505 (2012).

54. Moore, E. B. & Molinero, V., Structural transformation in supercooled water controls the crystallization rate of ice. *Nature* **479**, 506–508 (2011).

55. Poole, P. H., Sciortino, F., Essmann, U. & Stanley, H. E., Phase behavior of metastable water. *Nature* **360**, 324 (1992).

56. Mishima, O. & Stanley, H. E., The relationship between liquid, supercooled and glassy water. *Nature* **396**, 329–335 (1998).

57. Manka, A., Pathak, H., Tanimura, S., Wolk, J., Strey, R. & Wyslouzil, B. E., Freezing water in no man's land. *Phys. Chem. Chem. Phys.* **14**, 4505–4516 (2012).

58. Palmer, J. C., Martelli, F., Liu, Y., Car, R., Panagiotopoulos, A. Z. & Debenedetti, P. G., Metastable liquid-liquid transition in a molecular model of water. *Nature* **510**, 385–388 (2014).

59. Corradini, D., Rovere, M. & Gallo, P., A route to explain water anomalies from results on an aqueous solution of salt. *The Journal of Chemical Physics* **132**, 134508 (2010).

60. Caupin, F., Escaping the no man's land: Recent experiments on metastable liquid water. *Journal of Non-Crystalline Solids* **407**, 441–448 (2015).

Parte III

Conclusions

Conclusions

Computer simulations are a powerful tool for studying phenomena from a microscopic point of view and allow to understand the molecular mechanisms and the thermodynamic factors involved in many relevant process in nature. For the concrete case of nucleation, computer simulations are especially suitable, given that is possible to trace the formation of a nucleus of the stable phase within the metastable one, unlike in experiments. Understanding the mechanism by which the system nucleates and analysing the factors involved in such process are the keys for going forward in the comprehension of this phenomenon. Nonetheless studying nucleation by simulation is not an effortless task and it still requires much more work for reaching a full understanding. In that sense, developing new techniques for investigating it is needed. In this thesis, we have been working in that direction, developing new techniques and applying them from a priori simple systems to more complex ones. In what follows, we will summarize the main conclusions obtained during this work.

1. The Seeding technique is a powerful methodology for studying nucleation. Although it is an aproximate technique and its results have a higher uncertainty than those obtained by other rigorous techniques, it allows to evaluate interfacial free energies, nucleation barriers and nucleation rates in a range of metastability much wider than the accesible one by means of the other alternative techniques. We have validated the Seeding technique calculating nucleation rates and interfacial free energies for Hard-Spheres, Lennard-Jones, NaCl and mW water model (Chapter V), where in all cases, good agreement was obtained with previous results from other independent techniques.

2. The consistency of our Seeding results with independent estimates of γ and J by methods that do not rely on CNT, also implies that the CNT view of crystal nucleation, that of spherical critical clusters with the structure of the most stable polymorph nucleate, is a good approximation to describe crystal nucleation.

3. The crystal-fluid interfacial free energy is a very relevant magnitude for understanding nucleation. Experimentally, measuring this magnitude is quite difficult, and

for that reason, predictions from simulations are highly valuable. We have developed a novel technique, Mold Integration, for estimating γ in coexistence conditions (Chapter III). By means of MI we have been able to evaluate succesfully γ for several systems (and crystal orientations) such as Hard-Spheres, Lennard-Jones, NaCl and water. Moreover, coupling MI with Seeding, we can evaluate the dependence of γ from coexistence conditions to high metastabilities.

4. We have also developed a new technique for estimating nucleation rates that does not rely on any local order parameter nor it is based on the validity of Classical Nucleation Theory. This technique is Lattice Mold (Chapter IX) which we have used for calculating nucleation rates of monoatomic and ionic systems obtaining in all cases good agreement with previous results reported in literature, including the Seeding ones.

5. We evaluated for the Tosi-Fumi NaCl model the nucleation rate and the interfacial free energy from deep supercoolings to coexistence conditions by means of Seeding and MI (Chapter IV). We observed that γ is about $100 mJ/m^2$ and that remains practically constant in the whole range of supercooling. The nucleation rates computed were in agreement with the previous ones estimated by other techniques. We also clarified a discrepancy on the value of γ present in the literature. It was observed that the shape of the critical clusters was spherical despite of the fact that NaCl crystalline structure might suggest a cubic geometry for them. We explain this fact as the cluster minimizes the exposed area to the interface as much as possible for decreasing the energetic penalty of creating an interface, and therefore the spherical geometry is the most convenient one. This is a good example of how simulations can give an insight of the mechanisms that are inaccesible in experiments.

6. Homogeneous ice nucleation at normal pressure has been studied by means of Seeding. For that purpose we have used several water potential models such as TIP4P/2005, TIP4P/Ice, TIP4P y mW (Chapter I, II and VII). Although all of them predicted similar qualitative trends, TIP4P/2005 and TIP4P/Ice were the more accurate ones in reproducing the experimental behavior of supercooled water and the experimental nucleation rates. A linear negative dependence of γ with supercooling was predicted by every model. Also, for TIP4P/2005, TIP4P/Ice and mW, we evaluated the ice growth rate, u, as a function of the supercooling, finding again good agreement with the experimental measurements in both TIP4P/Ice and TIP4P/2005 and not so accurate for the case of mW. A combination of u and J, allowed us to estimate by means of the Avrami law, the time required to freeze a sample of water along the supercooling. Knowing this time, we also estimated the cooling rate needed for vitrifying a sample of water avoiding the formation

of ice, which is of about $10^7 K/s$ for the most realistic water models. Controlling this procedure would have many implications in cryopreservation and cryfixation of cells, tissues and food.

7. We calculated the interfacial free energy Ih-fluid at normal pressure for the different crystal orientations of ice Ih and for several water models: TIP4P, TIP4P/2005, TIP4P/Ice and mW (Chapter VI). For the most realistic models (TIP4P/Ice and TIP4P/2005), the average of γ over the different crystal planes, was of about $30 mJ/m^2$. Regarding to the anisotropy of the different crystal orientations, we observed that both prismatic planes (primary and secondary) have a 10 % higher γ than the basal face. We also evaluated the Ic-liquid γ for different crystal orientations, observing that the average of γ over the different crystal planes of both polymorphs (Ih and Ic) were the same within the uncertainty of our calculations. This fact supports previous Seeding estimations where both γ and J of ices Ic and Ih turned out to be similar, therefore indicating that ice I stacking disordered must be the nucleating phase at normal pressure.

8. By measuring both nucleation and growth rates, we put forward the hypothesis that a crossover between nucleation to growth-limited observation of ice formation explains current discrepancies between experimental measurements of ice nucleation rates (Chapter VII).

9. We investigated homogeneous ice nucleation at high pressures (2000 bar). We found a deceleration of the nucleation rate respect to the one at 1 bar for a given supercooling (Chapter VIII). Although experimentally it was already known that applying pressure on water hinders ice nucleation, the explanation of that fact remained still unclear. We discovered that the reason behind such decelaration of J is the increase of the interfacial free energy between water and ice respect to the one at 1 bar for a certain supercooling. We performed these calculations by Seeding and MI for the TIP4P/Ice model which predicted almost quantitatively the experimental values of J.

10. Ice nucleation rates from brine solutions at 1 bar (Chapter X) were evaluated by Seeding and MI. We observed an analogous effect to the one observed when compressing water, there was a considerable decrease in J respect to that of pure water. Analisying the factors on which J depends, we observed that the main responsible magnitude of such descent of J was γ, which was considerably higher than the one for pure water for a given supercooling. JC-TIP4P/2005 model was used for this study, and it reproduced reasonably well both the experimental cryoscopic decrease and the experimental values for the nucleation rate from brine solutions.

11. We tested the empirical conjecture Water Activity Based Ice Nucleation Conjecture (WAB-INC) that states that ice nucleation rates from different solutions or even from compressed water can be mapped through the variation of the water activity onto a universal curve of J. When applying the rule for our simulation predictions (Chapter XI) we did not observe that our curves of J overlap into a unique one. We noticed that for high nucleation rates ($\sim 10^{16} m^{-3} s^{-1}$), as the accesible ones in experiments, the rule seems to work, but is not general since for lower nucleation rates it fails. The only way for reconciling Classical Nucleation Theory with the WAB-INC would be if γ was function of the water activity difference between fluid-ice at coexistence and the fluid water at a certain supercooling, which only coincidentally happens for high nucleation rates. Therefore we conclude that this empirical conjecture is not general and that it seems not possible to find a pressure that affects water in the same way that a certain concentration of a given salt for a wide range of temperatures.

Therefore, once that the main conclusions of this thesis have been already discussed, it is worthy to mention as a general conclusion of this work that Classical Nucleation Theory has been able to describe nucleation succesfully in all cases, demonstrating its validity despite of its simplicity. Also using a combination of the three proposed techniques here, Seeding+MI+LM, it is possible to reach a full characterization of the nucleation phenomenon for a wide range of metastability evaluating the main factors needed for understanding in deep nucleation, such as the free energy barrier, the interfacial free energy and the nucleation rate. Applying this combination of techniques for studying nucleation from binary or ternary mixtures or even big molecules in solution, like pharmaceutical drugs, or predicting the nucleating polymorph in certain conditions, are the main goals that we would like to accomplish in the future.

Agradecimientos

Quiero expresar mi mayor gratitud a los dos principales artífices de que esta tesis haya sido posible, Edu y Carlos. Ambos me habéis guiado durante estos cinco años que llevamos trabajando juntos de manera excelente, y sois a los que realmente les corresponde todo el mérito de esta tesis doctoral. Muchas gracias a los dos, porque además de ser mis directores de tesis, habéis sido mis amigos y mi familia durante este tiempo, y espero que lo sigamos siendo por mucho más. Aparte del terreno científico, donde me habéis enseñado todo lo que sé, habéis convertido estos años de investigación predoctoral en una de la mejores etapas de mi vida, donde además de investigar hemos pasado muy buenos ratos, comidas, congresos, cervezas y muchísimas buenas experiencias.

También quiero agradecer especialmente a Chantal por toda su ayuda desde que llegué al grupo, siempre animándome a hacer más cosas y contagiándome su espíritu insaciable por seguir avanzando. Tu fuiste la que me "engañaste" para meterme en esto, y gracias a ti hoy estoy escribiendo estos agradecimientos.

Un agradecimiento importantísimo es para todos los demás miembros del equipo por haber estado siempre ahí al pie del cañón. Jose Luis (o más bien conocido como JLU), muchas gracias por aclararme tantas preguntas, por darme una perspectiva de la ciencia tan equilibrada y por todos estos años comiendo juntos donde hemos discutido tanto de ciencia así como de otros millones de anécdotas. También quiero expresar mi gratitud a Albertuch, un gran amigo del grupo de trabajo con el que siempre he podido contar para todo, tanto para cuestiones científicas como para tomarme unas cervezas y salir por ahí después de trabajar a relajar un poco el ambiente. Anibal, muchas gracias por ser un gran compañero de trabajo y un mejor amigo, siempre nos quedará Javea, e irte a visitar a Argentina donde seguro que te va a ir muy bien. También agradecer a Guiomar, por los dos años en el despacho donde además de reirnos mucho, trabajamos muy duro en el proyecto de las sales, que ha sido una parte fundamental de esta tesis. Pablo (R), gracias a ti también por estos años trabajando juntos, lo hemos pasado muy bien, en el trabajo y en el Bravas, tomando jarras en ese mítico bar de la noche universitaria madrileña. No me puedo olvidar tampoco de las generaciones más jovenes, como Víctor, (WC para los amigos) con el que he pasado dos años trabajando codo con codo y disfrutando de sus "historias" tanto en las comidas como en el despacho, Caridad que durante su proyecto de fin de grado trabajó muy duro y muchas de sus simulaciones hoy forman parte de esta tesis, o Pablo (M) y Marta con lo que he pasado muy buenos ratos también comiendo y cada vez que hemos salido. Un merecido agradecimiento es para Mac, gracias por resolver todas mis dudas en los inicios y por toda esa paciencia que tuviste conmigo. También quiero hacer una especial mención a Jorge Benet, por su gran generosidad cuando él estaba acabando la tesis para que yo pudiera empezar la mía. Te debo una sin duda, muchas gracias. María, todavía recuerdo aquella tarde que

después de llevar semanas intentando encontrar un error en un fichero, te pregunté a tí y después de diez minutos ya estaba solucionado. Gracias por ayudarme siempre que estuvimos compartiendo despacho. Lufi, a ti también muchas gracias por resolver mis primeras dudas cuando estaba empezando e instruirme con los asuntos informáticos. Así que en general, lo único que puedo decir sobre este grupo de simulación, es que habéis sido como una familia durante este tiempo donde siempre me he sentido muy a gusto.

Durante esta tesis he disfrutado de dos estancias de tres meses, la primera en Princeton en los grupos de Thanos Panagiotopoulos y Pablo Debenedetti, y la segunda en Cambridge en el grupo de Daan Frenkel. Quiero agradecerles a todos ellos, y a toda la gente de sus grupos (Andrew, Hao, Jeffrey, Antonia, Charlie, Aleks, Peter y todos los demás ...) por la magnífica acogida que me dieron y por todo lo que me han enseñado cuando he estado trabajando con ellos.

También quiero agradecer en esta tesis a Pablo Sampedro, juntos hemos pasado muchos años en esta facultad y también siempre que lo necesité me echaste un cable, sin importarte lo que fuera. Muchas gracias Pablo, lo pasamos genial con tus scripts mientras hacíamos el proyecto de Lattice Mold.

Otro muy buen amigo y colaborador al que quiero agradecer en esta tesis es a Jorge Ramírez, con el que trabajando, siempre han salido cosas muy interesantes. Muchas gracias también por todas las horas de Magerit que me has dejado, fundamentales para muchos de los proyectos de esta tesis. Además, eres otro gran atlético de corazón, y en el Matela, nuestro templo de reunión para ver los partidos del Atleti y comer las patatas rancias que nos pone Jose, siempre lo hemos pasado muy bien con Edu. Ya dicho lo cual, quiero aprovechar para agradecer al Cholo Simeone y al Mono Burgos por estas magníficas temporadas que nos han hecho vivir a todos los atléticos.

Un agradecimiento muy importante en esta tesis es para David, ya son muchos años liándola por el Escorial con la gente de allí y tocando la guitarra y la batería juntos. Muchas gracias por aguantar las chapas que te he dado todo este tiempo de tesis con mi dichosa nucleación de hielo y demás historias, y por siempre estar dispuesto a salir a tomar unas cervecitas y lo que caiga. También me quiero acordar en estos agradecimientos del resto del grupo de "música", Dave y Evert grandes genios del rock and roll y grandes amigos con los que me he relajado muchos fines de semana de la dura vida científica.

Alguien que merece un agradecimiento muy especial en esta tesis es Carmen, pasamos un par de años muy buenos durante el master y el inicio de esta tesis donde me apoyaste mucho con este trabajo y donde siempre que lo necesité estabas dándome buenos consejos. Muchas gracias por ello.

También agradezco al Estado español por la beca predoctoral (FPI) No. BES-2014-067625, y por la dotación económica de los proyectos No. FIS2013/43209-P (MEC) y Marie Curie Career Integration Grant No. 322326-COSAAC que han hecho posible la realización de esta tesis doctoral, al igual que la financiación para las dos estancias en

el extrajero por parte del MEC.

Por último quiero agradecer a toda mi familia por estar siempre conmigo pase lo que pase. A mi primo Andrés y Laura, a mis tíos Carlos y Teresa, a Inma y Rafa, y a mis tíos del Escorial, Pili, MariCarmen y Jose. También esto quiero dedicárselo a Sarita, Jesús y Mar con los que he pasado grandes momentos en Mazalinos, y que me han apoyado en momentos difíciles. A mis padres, que son los que siempre han tenido paciencia conmigo, y me han ayudado en todo lo que han podido y más. Y por último y muy en especial, a mis abuelos que siempre hicieron todo por mí. Esta tesis os la dedico a vosotros, Pilar, Mariano, Lola y Manuel.

Parte IV

Apéndice

Parámetros de orden

Un aspecto muy importante a tener en cuenta al describir las técnicas de nucleación es la definición de **parámetro de orden de nucleación**. Estos se utilizan típicamente para caracterizar la transición de fase y es función de la cual podemos representar la barrera de nucleación.

Los parámetros de orden suelen ser una función de las coordenadas de todas las partículas del sistema, y tienen las siguientes propiedades:

1. Nos permiten caracterizar de manera inequívoca tanto el estado metaestable inicial del sistema como el estado final, termodinámicamente estable.

2. Son una función monótona y creciente, desde el estado inicial hasta el estado final.

Los podemos clasificar a nivel general de la siguiente manera:

A. Parámetros de orden globales. Se utilizan generalmente si estudiamos la transición desde un punto de vista general y analizamos cambios en propiedades macroscópicas tales como la densidad o la energía interna las cuales serían nuestros parámetros de orden globlales.

B. Parámetros de orden locales. Si nos centramos en aspectos moleculares, como por ejemplo, el número de partículas que forman el núcleo más grande que está cristalizando en un líquido subenfriado o el tamaño de la burbuja más grande que esta creciendo en un líquido sobrecalentado, eso serían parámetros de orden locales.

En general, los parámetros de orden global son sencillos de calcular y seguir durante la transformación pero no ofrecen ninguna información sobre el mecanismo microscópico de nucleación. Por otro lado, los parámetros de orden locales sí que son capaces de describir este mecanismo pero su elección y definición no es tan secilla.

Generalmente las técnicas de eventos raros, como por ejemplo Umbrella Sampling[1,2], Forward Flux Sampling[3,4] o Transition Path Sampling[5,6], utilizan parámetros de orden locales para seguir la coordenada de reacción (habitualmente el tamaño del

clúster más grande), aunque sus resultados no dependen de ellos. En contraposición estas técnicas como se ha mencionado anteriormente, son muy costosas computacionalmente y solo permiten el cálculo de tasas y barreras de nucleaciñ para clústeres muy pequeños. El Seeding a diferencia de estas técnicas, aunque permite evaluar tasas de nucelación para un rango muy superior de sobresaturación y tamaños de clúster mucho más grandes con menor coste computacional, si que sus resultados dependen de la elección del parámetro de orden.

Es por ese motivo por el cual tiene una gran importancia definir un buen parámetro de orden que distinga apropiadamente entre las partículas pertenecientes al sólido y al líquido para poder determinar correctamente el tamaño del clúster insertado. A continuación vamos a describir los dos parámetros de orden que se han utilizado a lo largo de esta tesis doctoral.

Parametro de orden promedio $\bar{q}_l$

Conocer con exactitud el número de partículas sólidas del clúster crítico en el Seeding es fundamental si queremos obtener tasas de nucleación fiables y coherentes con las halladas por otras técnicas. Para ello hemos utilizado generalmente siempre los parametros de orden local propuestos por Lechner y Dellago[7] para distinguir entre partículas tipo-sólidas y tipo-líquidas. Este parámetro $\bar{q}_l(i)$ considera que una partícula i es sólida si excede un cierto umbral. La expresión para $\bar{q}_l(i)$ es la siguiente:

$$\bar{q}_l(i) = \sqrt{\frac{4\pi}{2l+1} \sum_{m=-l}^{l} |\bar{q}_{lm}(i)|^2} \tag{11.6}$$

donde

$$\bar{q}_{lm}(i) = \frac{1}{N_b(i)+1} \sum_{j=0}^{N_b(i)} q_{lm}(k) \tag{11.7}$$

y donde la partícula $j = 0$ es justamente la partícula central i

$$q_{lm}(i) = \frac{1}{N_b(i)} \sum_{j=1}^{N_b(i)} Y_{lm}(\vec{r}_{ij}) \tag{11.8}$$

donde $N_b(i)$ es el número de partículas vecinas a la partícula i dentro de una distancia r_c (cut-off), y $Y_{lm}(\vec{r_{ij}})$ son los esféricos armónicos de orden m del vector $\vec{r}_{ij}$ que une la partícula i con la partícula j.

Para definir cual es la mejor opción de parámetro de orden, se pueden calcular los valores de varios parámetros de orden tanto para la fase sólida pura como para la líquida pura en unas condiciones determinadas. En este trabajo generalmente se ha hecho para el $\bar{q}_4$ y $\bar{q}_6$. Por ejemplo para el caso del agua, como se puede ver en la Figura 11.4, el $\bar{q}_6$ es capaz de separar las nubes de puntos pertenecientes a fases sólidas (hielo hexagonal y cúbico) de la nube correspondiente a la fase líquida. Por el contrario si se deseara separar entre las fases cúbica y hexagonal se necesitaría emplear el $\bar{q}_4$.

El siguiente paso consiste en definir un umbral de $\bar{q}_{l,t}$ que permita separar de manera equitativa entre las dos fases de interés, que en nuestro caso van a ser la fase líquida y la sólida. Para ello vamos a considerar diferentes valores de $\bar{q}_{6,t}$ y vamos a evaluar el número de partículas maletiquetadas. Una partícula perteneciente a la fase pura líquida se va a considerar maletiquetada cuando su valor de $\bar{q}_6$ sea mayor que el del umbral, y viceversa, cuando una partícula de la fase sólida pura tenga un valor inferior de $\bar{q}_6$ que el umbral también se considerará maletiquetada. En la Figura 11.5 se representa el porcentaje de partículas maletiquetadas en función del umbral escogido $\bar{q}_{6,t}$ entre la fase hexagonal y el líquido y la fase cúbica y el líquido. Como se puede observar el mismo porcentaje de partículas maletiquetadas para diferentes fases es cuando las curvas se cruzan, en el caso entre la fase hexagonal de hielo y el líquido ocurre cuando $\bar{q}_{6,t} = 0{,}358$ y para la fase cúbica y el líquido a 0,38. Esto es lo que se conoce como *criterio de mislabelling*, establecer un umbral para distinguir entre partículas sólidas y líquidas donde el número de falsos positivos de una fase y la otra sean el mismo. Y ya finalmente cuando las partículas o moléculas han sido etiquetadas como sólidas o líquidas, se evalua con un algoritmo cual es el agregado más grande de partículas sólidas dentro de la distancia previamente establecida como cut-off.

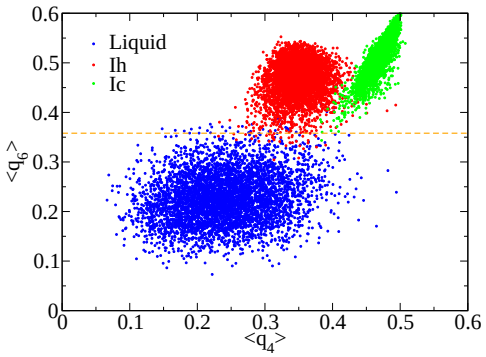

Figure 11.4: Representación bidimensional de los parámetros $\bar{q}_6$ and $\bar{q}_4{}^7$ para 5000 moleculas de una fase líquida pura (azul), hielo-Ih (rojo), y hielo-Ic (verde) para el modelo de agua TIP4P/2005 a 237 K y p=1bar.

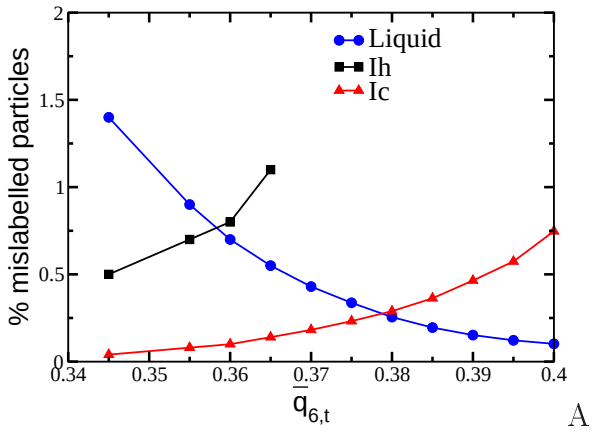

Figure 11.5: Porcentaje de partículas maletiquetadas para varias fases puras según se indica en la leyenda. Las curvas representadas han sido obtenidas a partir de las nubes de puntos mostradas en la Figura 11.4.

Los parámetros $\bar{q}_6$ y $\bar{q}_4$ son los que se han utilizado para prácticamente la mayoría de los estudios que se han hecho con Seeding, exceptuando el caso del NaCl (capítulo 4), en el cual se usó otro parámetro de orden local[8] con la intención de comparar directamente con la Referencia[4], donde se calcularon energías interfaciales y tasas de nucleación para el mismo modelo de NaCl con el cual se realizó nuestro estudio. A continuación se va a describir brevemente también este parámetro de orden.

Parametro de orden local de Steinhardt

Este parámetro de orden fue inicialmente introducido por Steinhardt *et al*[8] para describir el orden orientacional en líquidos y más adelante fue utilizado por van Duijneveldt *et al*[9] para calcular una barrera de energía libre en función de la cristalinidad global en un líquido metaestable. Posteriormente, fue refinado por Ten Wolde *et al*[10] para estudiar nucleación de un cristal a partir de un fluido subenfriado de Lennard-Jones.

En este parámetro lo primero es definir una lista de vecinos (partículas j) sobre la partícula i que están a una distancia más cercana que el primer mínimo de la función de distribución radial del sólido equilibrado en las condiciones de interés.

Sobre las partículas pertencientes a esta lista de vecinos, se va a calcular el siguiente vector complejo normalizado $\vec{q}_{l,m}$ para cada partícula i. Cada componente del vector viene dado por la siguiente expresión:

$$q_{l,m}(i) = \frac{\frac{1}{N_b(i)} \left(\sum_{j=1}^{N_b(i)} Y_{lm}(\theta_{ij,\phi_{ij}}) \right)}{\left(\sum_{m=-l}^{l} |\vec{q}_{l,m}(i)|^2 \right)^{1/2}} \tag{11.9}$$

donde $N_b(i)$ es el número de vecinos de la partícula i y $Y_{lm}(\theta, \phi)$ es la función de esféricos armónicos de orden l en coordenadas polares.

Para distinguir entre partículas tipo-líquido y tipo-sólido, Ten Wolde *et al*[11] propusieron una función invariante rotacional $d_l(i,j)$ que es el producto escalar entre el vector $\vec{q}_{l,m}(i)$ de la partícula i y el mismo vector complejo calculado para cada uno de sus vecinos:

$$d_l(i,j) = \sum_{m=-l}^{l} \vec{q}_{l,m}(i) \dot{\vec{q}}^*_{l,m}(j) \tag{11.10}$$

De modo que una vez calculado $d_l(i,j)$ para cada partícula i, podemos ya establecer un criterio para ver si dos partículas i y j están conectadas o no estableciendo un umbral d_c entre las distribuciones de probabilidad del líquido metaestable y el sólido.

Por último, se establece un criterio de número de conexiones mínimas que debe tener una partícula sólida para ser considerada como sólido

$$n_{con}(i) = \sum_{j=1}^{N_b(i)} H(d_l(i,j) - d_c) \tag{11.11}$$

donde $N_b(i)$ es el número de vecinos de la partícula i, H es una función de escalón de Heaviside y d_c el umbral para discriminar si dos partículas están conectadas o no. n_{con} es el número total de productos escalares d_l respecto de la partícula i que superan el umbral seleccionado d_c.

Así que representando la distribución de probabilidad para el número de conexiones que hay en el líquido puro y en el sólido puro (ver Figura 11.6) podemos establecer un número de conexiones umbral donde tengamos el mínimo solapamiento entre ambas distribuciones. Esto criterio nos permite discernir entre párticulas pertenecientes al sólido o al líquido, y ha sido el empleado en el estudio de nucleación de NaCl del Capítulo V.

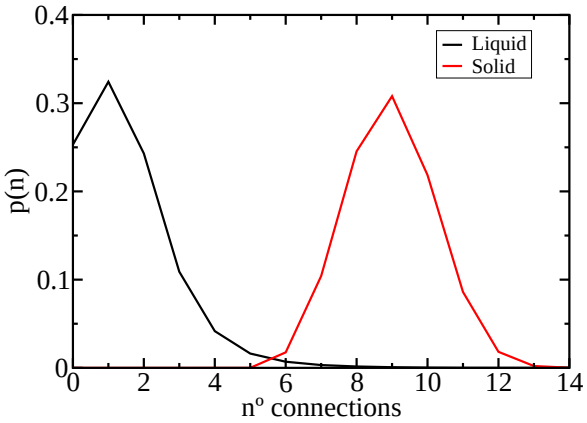

Figure 11.6: Distribución de probabilidad del número de conexiones por partícula para un líquido metaestable puro y para un sólido puro de NaCl a T=800K y p=1 bar.

Bibliografía

1. Torrie, G. & Valleau, J., Nonphysical sampling distributions in Monte Carlo free-energy estimation: Umbrella sampling. *Journal of Computational Physics* **23**, 187–199 (1977).

2. van Duijneveld, J. S. & Frenkel, D., Computer simulation study of free energy barriers in crystal nucleation. *J. Chem. Phys.* **96**, 4655 (1992).

3. Allen, R. J., Warren, P. B. & ten Wolde, P. R., Sampling rare switching events in biochemical networks. *Phys. Rev. Lett.* **94**, 018104 (2005).

4. Valeriani, C., Sanz, E. & Frenkel, D., Rate of homogeneous crystal nucleation in molten NaCl. *J. Chem. Phys.* **122**, 194501 (2005).

5. Bolhuis, P. G., Chandler, D., Dellago, C. & Geissler, P. L., Transition path sampling: Throwing ropes over rough mountain passes, in the dark. *Ann. Rev. Physical Chem.* **53**, 291 (2002).

6. Moroni, D., ten Wolde, P. R. & Bolhuis, P. G., Interplay between structure and size in a critical crystal nucleus. *Phys. Rev. Lett.* **94**, 235703 (2005).

7. Lechner, W. & Dellago, C., Accurate determination of crystal structures based on averaged local bond order parameters. *J. Chem. Phys.* **129**, 114707 (2008).

8. Steinhardt, P. J., Nelson, D. R. & Ronchetti, M., Bond-orientational order in liquids and glasses. *Phys. Rev. B* **28**, 784–805 (1983).

9. van Duijneveldt, J. S. & Frenkel, D., Computer simulation study of free energy barriers in crystal nucleation. *J. Chem. Phys.* **96**, 4655 (1992).

10. ten Wolde, P. R., Ruiz-Montero, M. J. & Frenkel, D., Numerical calculation of the rate of crystal nucleation in a Lennard-Jones system at moderate undercooling. *J. Chem. Phys.* **104**, 9932 (1996).

11. P. R. ten Wolde and M. J. Ruiz-Montero and D. Frenkel. *Faraday Discuss.* **104**, 93 (1996).